JAERI-M
8518

ENGINEERING ASPECTS OF THE JAERI PROPOSAL FOR INTOR (II)

November 1979

Fusion Research and Development Center

日本原子力研究所
Japan Atomic Energy Research Institute

この報告書は，日本原子力研究所がJAERI-Mレポートとして，不定期に刊行している研究報告書です．入手，複製などのお問合わせは，日本原子力研究所技術情報部（茨城県那珂郡東海村）あて，お申しこしください．

JAERI-M reports, issued irregularly, describe the results of research works carried out in JAERI. Inquiries about the availability of reports and their reproduction should be addressed to Division of Technical Information, Japan Atomic Energy Research Institute, Tokai-mura, Naka-gun, Ibaraki-ken, Japan.

Members of Design Team

Fusion Reactor System Laboratory, JAERI
K. SAKO, T. TONE, Y. SEKI, H. IIDA, K. MAKI[*1], T. YAMAMOTO[*2], A. MINATO[*3], H. SAKAMOTO[*4], K. SHINYA[*5], N. UEDA[*6]

Industries
(1) Hitachi, Ltd.
T. KASAHARA, I. NAGATA, S. ITOH, K. INOUE, M. NISHI, S. UCHIDA, T. KOBAYASHI, M. KITAMURA, M. KOIZUMI, S. ANDO, T. IWAMOTO, H. KOZAWA
(2) Kawasaki Heavy Industries, Ltd.
Y. TANAKA, M. TOKUMITSU, Y. NAKAI, T. AOTA, J. ADACHI, S. MORI, T. KURODA, M. NAKAGAWA
(3) Mitsubishi Group (Mitsubishi Electric Company, Mitsubishi Heavy Industries and Mitsubishi Atomic Power Industries)
T. SATOW, O. OGINO, T. YAMADA, R. SAITO, K. HIDA, Y. IMAMURA, N. ASAMI, M. NISHIKAWA, M. YAMADA, A. KAMEARI, S. NIIKURA, K. IOKI, T. NAITO
(4) Toshiba Corporation
K. EBISAWA, Y. GOMAY, T. HAMAJIMA, K. HASHIMOTO, T. HONDA, K. KITAMURA, T. MUNAKATA, M. NAGANUMA, Y. SAWADA, T. SUGAWARA, T. UCHIDA, M. YAMAGUCHI, H. YAMATO, M. YAMAUCHI[@]
@ Nippon Atomic Industry Group

---

*1 On leave from Hitachi, Ltd., Tokyo, Japan
*2 On leave from Fuji Electric Co. Ltd., Kawasaki, Japan
*3 On leave from Kawasaki Heavy Industries, Ltd., Tokyo, Japan
*4 On leave from Mitsubishi Heavy Industries, Ltd., Kobe, Japan
*5 On leave from Toshiba Corporation, Kawasaki, Japan
*6 On leave from Mitsubishi Atomic Power Industries Inc., Omiya, Japan

JAERI-M 8518

Engineering Aspects of the JAERI Proposal for INTOR (II)

Fusion Research and Development Center,
Tokai Research Establishment, JAERI

(Received October 2 , 1979)

To assess the data base for INTOR, a design study of the INTOR-J reactor system was carried out. Purpose of the study to evaluate the following five could be attained:

(1) validity of the guiding parameters (especially those related to reactor size),

(2) feasibility of a reactor with poloidal divertors,

(3) design problems and research/development items in respective components,

(4) possibility of repair and maintenance, and

(5) design of the test sections for tritium breeding and electric power generation.

Keywords ; INTOR-J, Tokamak Reactor, System Design, Poloidal Divertor, Repair, Maintenance, Guiding Parameter, Engineering Feasibility.

This report is presented at the Session III of IAEA INTOR Workshop held in Vienna, Oct., 1-19, 1979.

JAERI－M 8518

トカマク型核融合炉INTORの工学的諸問題の検討（Ⅱ）

日本原子力研究所東海研究所
核融合研究開発推進センター

（1979年10月2日受理）

INTORのデータベースを評価するために，INTOR－Jの詳細な設計研究を行った。この設計研究で目的とした以下の五項目の評価がなされた。

(1) ガイディング・パラメータの妥当性（特に炉の主要寸法の妥当性）。
(2) ポロイダルダイバータ付きトカマク炉の工学的実現可能性。
(3) 主要機器の設計上の問題点及び開発項目。
(4) 炉の分解補修法の実現可能性。
(5) トリチウム増殖試験及び発電試験のためのテストセクションの設計。

本報告書は1979年10月1日～19日にウィーンで行われたIAEA INTORワークショップの第3セッションに提出されたものである。

設計参加者

炉設計研究室

迫　　淳，　東　稔　達　三，　関　　泰，　飯　田　浩　正

外来研究員

真　木　紘　一[*1]，　山　本　　孝[*2]，　湊　　章　男[*3]，　坂　本　寛　己[*4]

新　谷　吉　郎[*5]，　上　田　憲　昭[*6]

日　立

笠　原　達　雄，　永　田　一　良，　伊　東　新　一，　井　上　孝太郎

西　　正　嗣，　内　田　俊　介，　小　林　朋　文，　喜多村　政　夫

小　泉　　真，　安　藤　司　文，　岩　本　太　郎，　小　沢　房　明

川崎重工

田　中　義　久，　徳　満　正　司，　中　井　保　夫，　青　田　利　一

安　達　潤　一，　森　　清　治，　黒　田　敏　公，　中　川　勝　文

三菱グループ（三菱電気，三菱重工，三菱原子力）

佐　藤　　隆，　荻　野　　治，　山　田　忠　利，　斉　藤　龍　太

飛　田　堅　三，　今　村　　豊，　浅　見　直　人，　西　川　正　名

山　田　政　男，　亀　有　昭　久，　新　倉　節　夫，　伊尾木　公　裕

内　藤　大　靖

東　芝

大　和　春　海，　五　明　由　夫，　菅　原　　亨，　橋　本　　清

本　多　　力，　沢　田　芳　夫，　山　口　　貢，　内　田　孝　穂

喜多村　和　憲，　浜　島　高太郎，　長　沼　正　光，　宗　像　　正

海老澤　克　之，　山　内　通　則（NAIG）

---

*1 日立製作所

*2 富士電機製造K.K.

*3 川崎重工業K.K.

*4 三菱重工業K.K.

*5 東京芝浦電気K.K.

*6 三菱原子力

CONTENTS

Appendices

目　　次

1. General

1.1 Objective of Design Study

In order to assess the INTOR design data base, consistent discussion based on a systematic reactor design is required. Isolated surveys for individual components tend to lack balance among them. Therefore we have performed a fairly detailed reactor design based on the guiding parameters which had gained a preliminary agreement in the second Workshop Session. The result of the design is presented in this report which we hope will be used as a reference in the Workshop Session III. The main objective of the study is to evaluate and assess the following five items.

(1) Validity of the guiding parameters (especially those related to reactor size),
(2) Feasibility of a reactor with poloidal divertors,
(3) Design problems and R&D items of each component,
(4) Feasibility of repair and maintenance, and
(5) Design of test sections for tritium breeding and electric power generation.

1.2 Design Process

Fusion Reactor System Laboratory of Japan Atomic Energy Research Institute (JAERI) conducted the overall system design and determined the design concept and fundamental specifications. For the technical feasibility study and detailed design of components, the cooperations of the inductries were obtained. The roles of the industries in the design are as follows:

(1) Hitachi Ltd. conducted (a) the design of poloidal divertors and relevant analysis such as magnetic field configuration designs for deciding conditions required for the divertor design, (b) repair and maintenance design of the divertor plate, (c) neutron and gamma flux calculation around divertor, and (d) non-breeding blanket structure design.

(2) Kawasaki Heavy Industries performed, (a) breeding and non-breeding blanket structure design, (b) cooling panel design, (c) design of cooling systems for blanket and cooling panel including electric power generating systems, and (d) blanket test section design.

(3) Mitsubishi Group carried out (a) the design of Modular Concept (Concept A) reactor structure and repair and maintenance, (b) magnet

design (Concept A), (c) shielding and vacuum vessel structure design, and (d) design of main vacuum pump.
(4) Toshiba conducted (a) the design of In-situ Concept (Concept B) reactor structure and repair and maintenance, (b) magnet design (Concept B), (c) NBI design, and (d) neutron streaming calculation through NBI ports.

The design study was initiated just after the Workshop Session II and this report was made in 2.5 months. Therefore there still exist inconsistencies between component designs and insufficiency in some investigations. However, many insights are obtained on the objectives (1) - (5) described in 1.1, and materials for discussions may be obtained from this report.

1.3 Extent of the Design

Based on the preliminary design study[1], and considering the agreements reached in the Workshop Session II, the design study of the following items are carried out. Design problems and R&D items were enumerated simultaneously with the design.

(1) Overall concept of reactor with poloidal divertor
(2) Neutronics design
(3) Blanket design (breeding and non-breeding)
(4) Shielding design
(5) Divertor design
(6) TF magnet design (for concept A and B)
(7) PF magnet design (for concept A and B)
(8) NBI design
(9) Main vacuum pump design
(10) Repair & maintenance of reactor, concept A and B
(11) Repair & maintenance of divertor
(12) Reactor cooling system
(13) Blanket test section

Based on the above design study, the evaluations of the following items are appended in the report.

(1) Tritium breeding blanket,
(2) Vacuum boundary of SCM,
(3) Reactor repair and maintenance,
(4) Structure of SCM,
(5) Minimum thickness of the inboard shield,
(6) Electric power generating system.

1.4 General Reactor Concept

Major design parameters related to this study are summarized in Table 1.4.1. Over view of INTOR-J is shown in Fig. 1.4.1. Vertical and horizontal cross-sections of the reactor are shown in Figs. 1.4.2 and 1.4.3, respectively. The reactor consists of six modules each of which has two toroidal coils. A dual purpose port for evacuation and neutral beam injection is placed on the outer side of a module. NBI's are installed on four of the six modules, and on the remaining two, blanket test sections are placed.

Blanket made of stainless steel cooled by water surrounds the plasma, and poloidal divertors are placed on the top and bottom. The divertor plate is made of copper tube panel, which will be replaced in case of failure by a manipulator inserted through the outside port in a reactor module.

In front of the blanket, cooling panels are installed. A TZM protection wall is placed in front of the panel to cope with plasma disruptions. Main structure material of the shielding is stainless steel. The inner portion of the shielding, where the nuclear heating rate is high, is made of stainless steel and the outer portion is made of heavy concrete. As the inboard shield material, the use of tungsten as a filling material for concrete was considered to enhance the radiation shielding effect. Vacuum vessel is on the inner surface of the shielding and bellows are used to obtain sufficient one turn electric resistance.

Both disk type and pancake type coil designs using Nb_3Sn superconductor are investigated for the toroidal magnets. For poloidal SC magnets, NbTi superconductor is used. Copper is always used as the stabilizer.

The concept for the repair & maintenance of blanket structure is one of the main design alternatives. The concept of withdrawing radially a module with two toroidal magnets (Concept A) and the concept of removing a part of the shielding in-situ and take out or access the blanket (Concept B) are both studied. In both concepts, the repair of magnets are also made to be feasible. In relation to the repair and maintenance design, the vacuum boundary of the magnets is investigated whereby the separated type and the belljar type are designed. The former is applied to the Concept A and the latter Concept B.

REFERENCE

(1) JAERI-M 8503, Engineering Aspects of the JAERI Proposal for INTOR(I), (1979)

Table 1.4.1 Main Design Parameters

basic parameters	
average neutron wall loading	1 MW/m^2
fusion power	395 MW
total thermal power	415 MW
burn time	200 s
dwell time (including start up & shut down)	50 s
availability	25 %
number of pulses during lifetime	3×10^5
major radius	5.0 m
aspect ratio	4.2
plasma radius	1.2 m
first wall radius	1.3 m
elongation	1.5
toroidal magnetic field at plasma center	5.0 T
field ripple	±0.75 %
plasma current	4.7 MA
neutral beam injector	
number of units	4
number of ion sources/unit	8
injection power	75 MW
beam energy	200 keV
duration	5 s
toroidal field coils	
number of coils	12
bore, height/width	9 m/6 m
cooling method	pool boiling
max. field	10∿11 T
magnetomotive force	10.4 MA/coil
conductor	Nb_3Sn
radiation dose	$\sim 1 \times 10^9$ rad (epoxy)
poloidal field coils (hybrid coil system)	
number of coils	24
location	outside of TF coils
max. field	8 T

(continued)

max. field rise	∿5T/0.1s ($t \leq 0.1$s)
	∿8T/5s ($0.1 \leq t \leq 5$s)
conductor	NbTi/Cu
OHC current ramp time	∿5 s
max. one turn voltage	∿100 V

vacuum vessel

location	inner surface of bulk shield
material	stainless steel
max. temperature	∿100°C
coolant	H_2O
toroidal loop resistance	0.2 mΩ

first wall

type	cooling panel with protection wall	
	protection wall	cooling panel
thickness/outer dia.	4 mm	2 mm/20 mm
material	low Z mat。 or low Z covered refractory metal	316 SS
coolant	none (by radiation)	H_2O pressure: 5 ata inlet temp. : 40°C outlet temp. : 90°C
max. temp. (structure)	∿1500°C	∿150°C
av。 neutron wall load (during burn)	1 MW/m^2	
av。 surface heat load	12.5W/cm^2	17.5W/cm^2
max. surface heat load	15 W/cm^2	21 W/cm^2
av。 nuclear heating rate		10 W/cc
max. nuclear heating rate		12 W/cc

blanket

number of modules	6
location	inboard & outboard
material	316 SS
coolant	H_2O
max. temp。 (structure)	∿150°C
thickness	0.3 m

(continued)

bulk shield	
inboard material	SS, W and heavy concrete
inboard thickness	0.5 m
outboard material	SS and heavy concrete
outboard thickness	1.0 m
coolant	H_2O/borated H_2O
max. temperature (structure)	$\sim$100°C

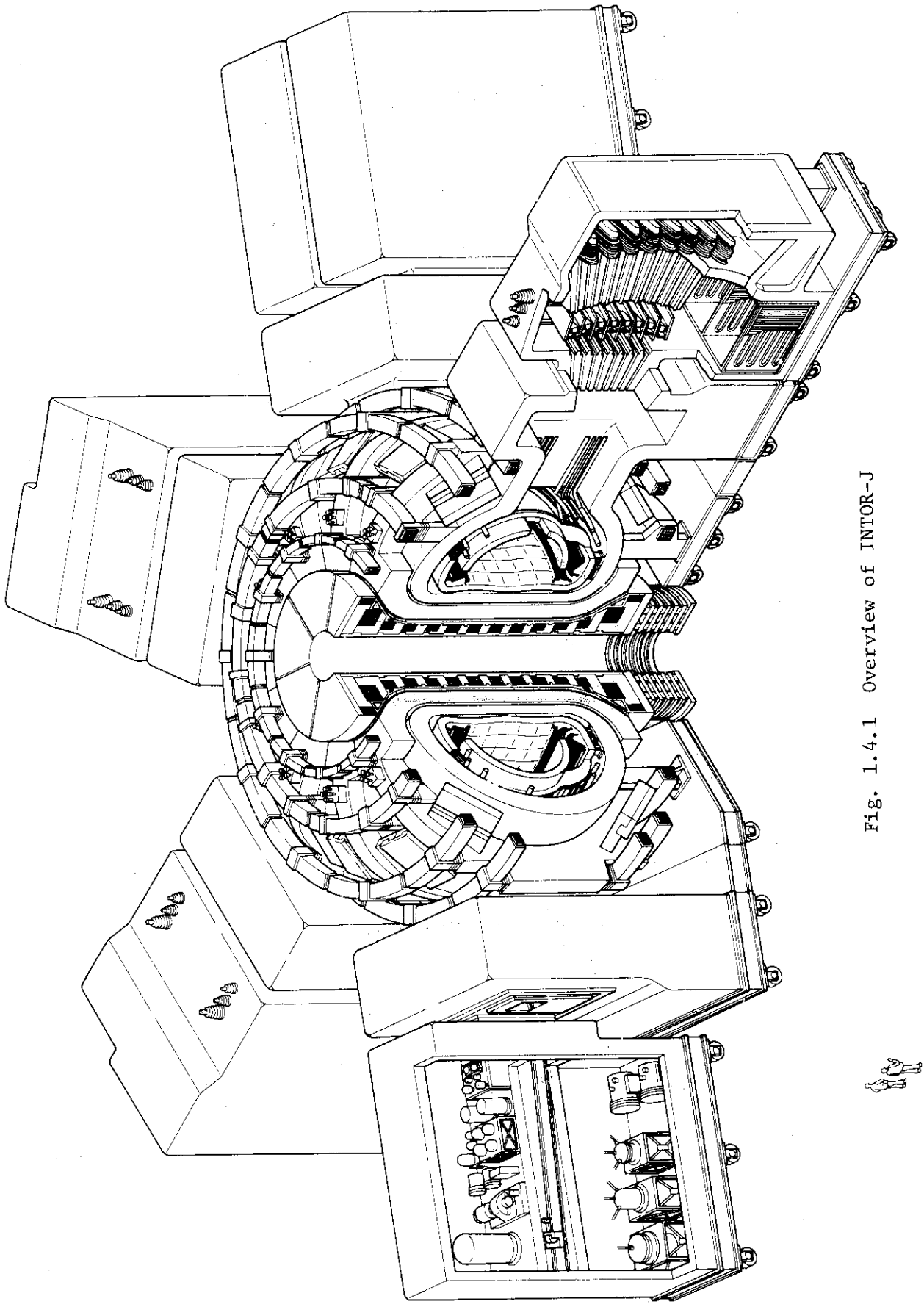

Fig. 1.4.1 Overview of INTOR-J

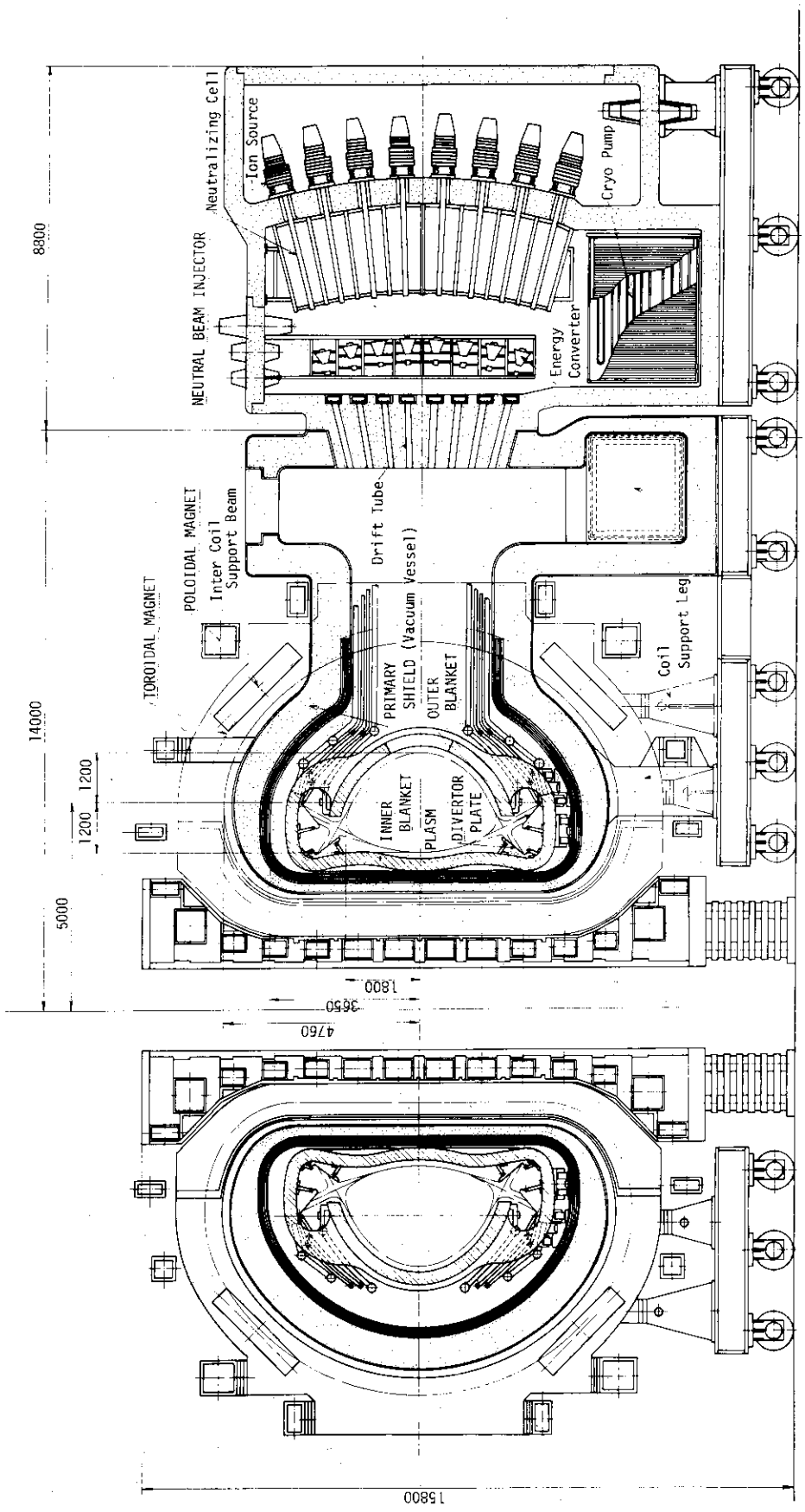

Fig. 1.4.2 General Reactor Concept of INTOR-J

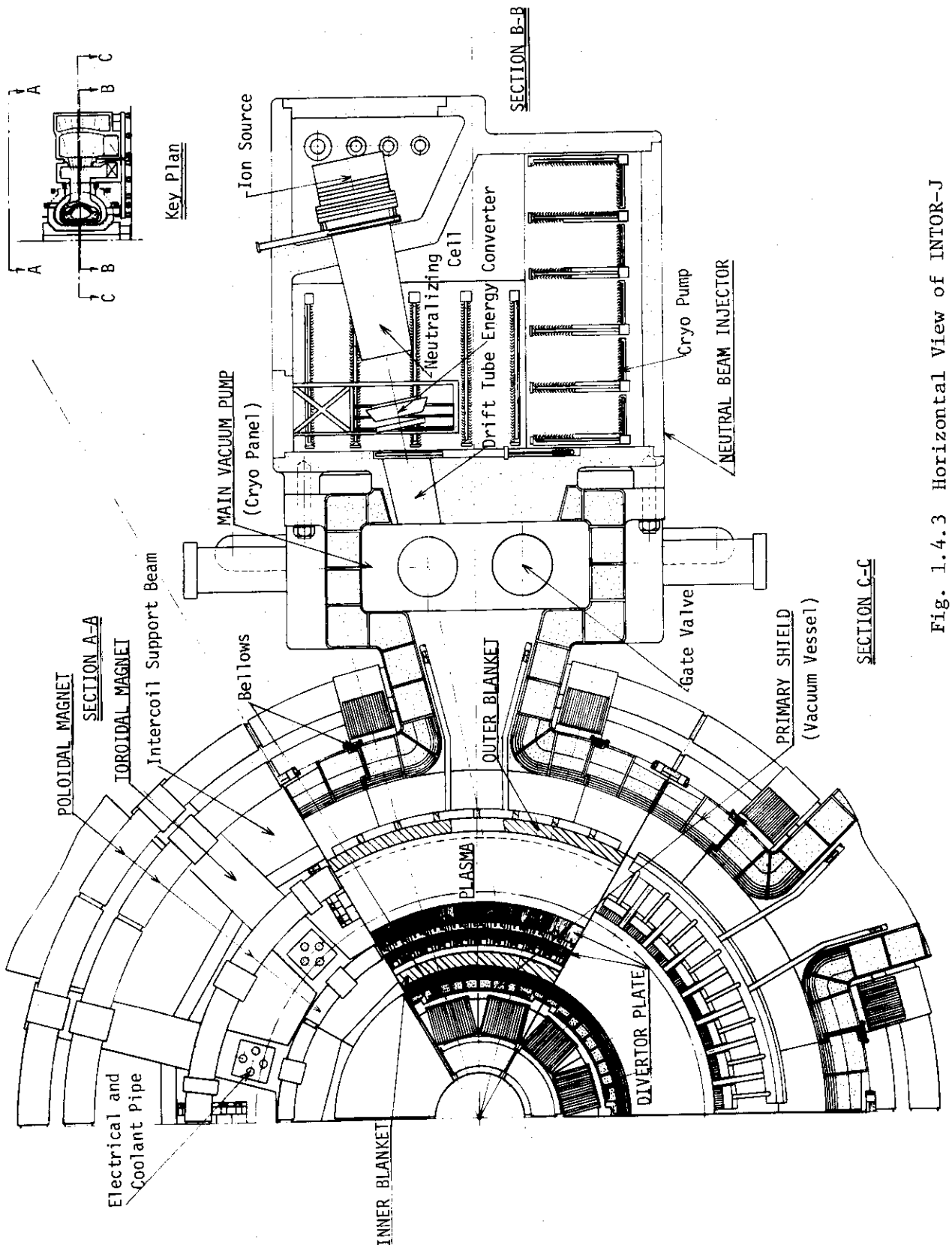

Fig. 1.4.3 Horizontal View of INTOR-J

1.5 Reactor Concept A

Reactor concept A is characterized by divertor and sector type structure. Plane and sectional view of the reactor concept A is shown in Fig. 1.5.1 and Fig. 1.5.2, respectively, and plan view is shown in Fig. 1.5.3. As shown in the figures, the reactor concept A is mainly composed of shield, toroidal field magnet, poloidal field magnet, movable base, belljar and cryopumps. Functions and structural characteristics of these components are summarized in Table 1.5.1 while the blanket is omitted here because of its common characteristics to concepts A and B.

Major characteristics of the reactor concept A is employment of belljar type vacuum chamber for superconducting magnets and following advantages are resultant.

1) Assembling and disassembling procedures and associated tools are simple and reliable.
2) Superconducting magnet structure is simple and cold support is easily possible.
3) Space factor of machine structure is high.

The second feature of the reactor concept A is large flexibility of repair and maintenance. Requirement for cooling and heating time of superconducting magnet is said to be a problem. But this problem might not be serious since preparation and rearrangement in repair and maintenance process is possible during the cooling and warming time.

Table 1.5.1 Functions and characteristics of main component of reactor Concept A

Component	Functions	Characteristics
Shield	(1) Attenuation of neutron and γ-ray radiation and protection of toroidal and poloidal magnets. (2) Vacuum barrier for plasma region. (3) Support for blanket.	(1) Layered structure of stainless steel-water and heavy concrete layers.
Toroidal field magnet	(1) Production of toroidal field. (2) Support of poloidal field coils.	(1) Nb_3Sn superconductor and liq. He pool cooling (2) Disc structure for hoop force, wedge structure for centripetal force and beam structure for overturning force. (3) Belljar type vacuum tank.
Poloidal field magnet	(1) Production of poloidal field.	(1) NbTi superconductor and SHE forced flow cooling. (2) Belljar type vacuum tank.
Movable base	(1) Support of machine (2) Transportation of machine	(1) Movable structure for assembling and dis-assembling
Belljar	(1) Vacuum barrier for superconducting magnet	(1) Cylinder and dome structure
Cryopumps	(1) Evacuation of plasma region	(1) Combination of cryosorption-panel for He and cryo-panel for other gasses

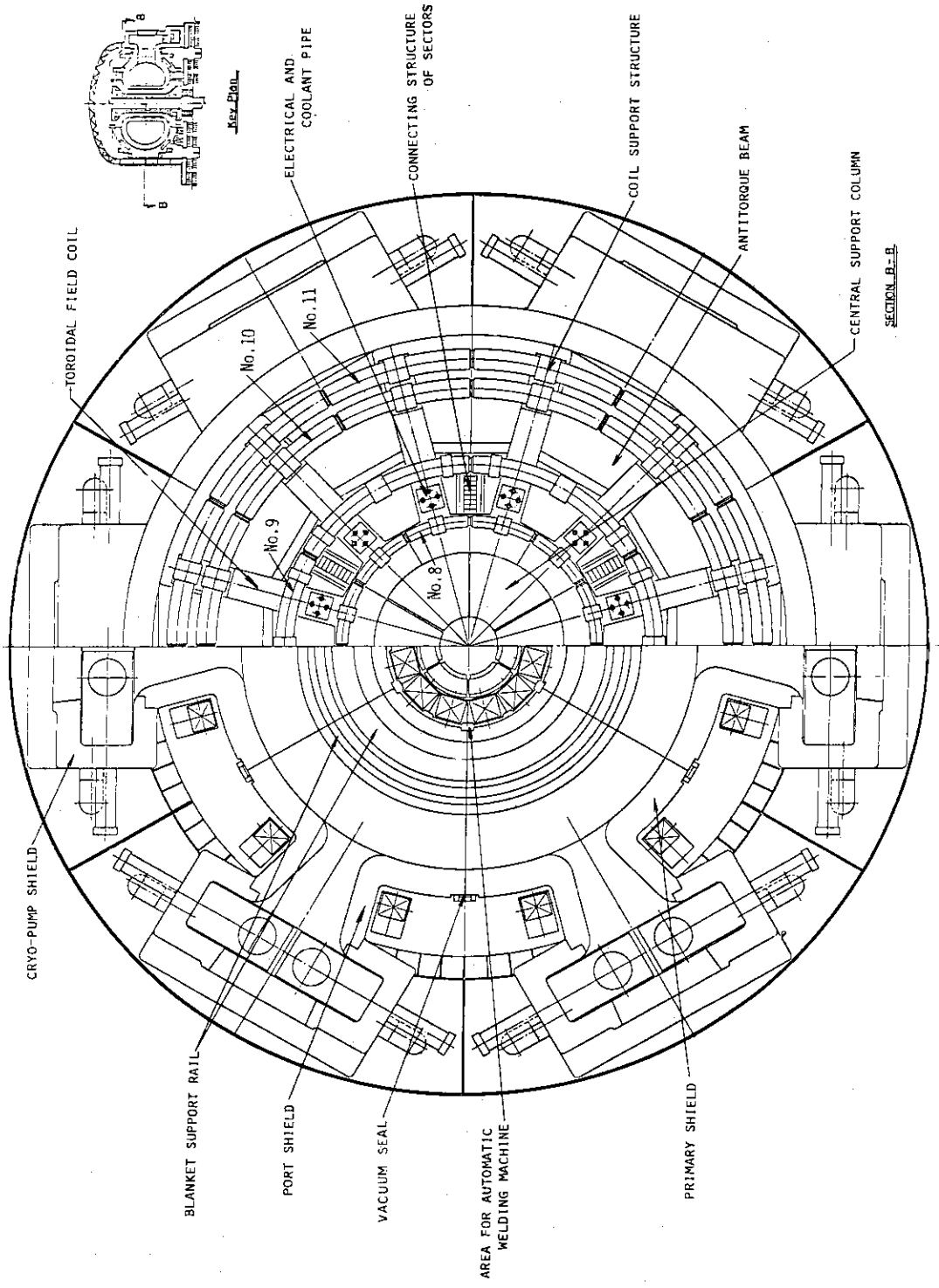

Fig. 1.5.1 Concept A Typical Plane

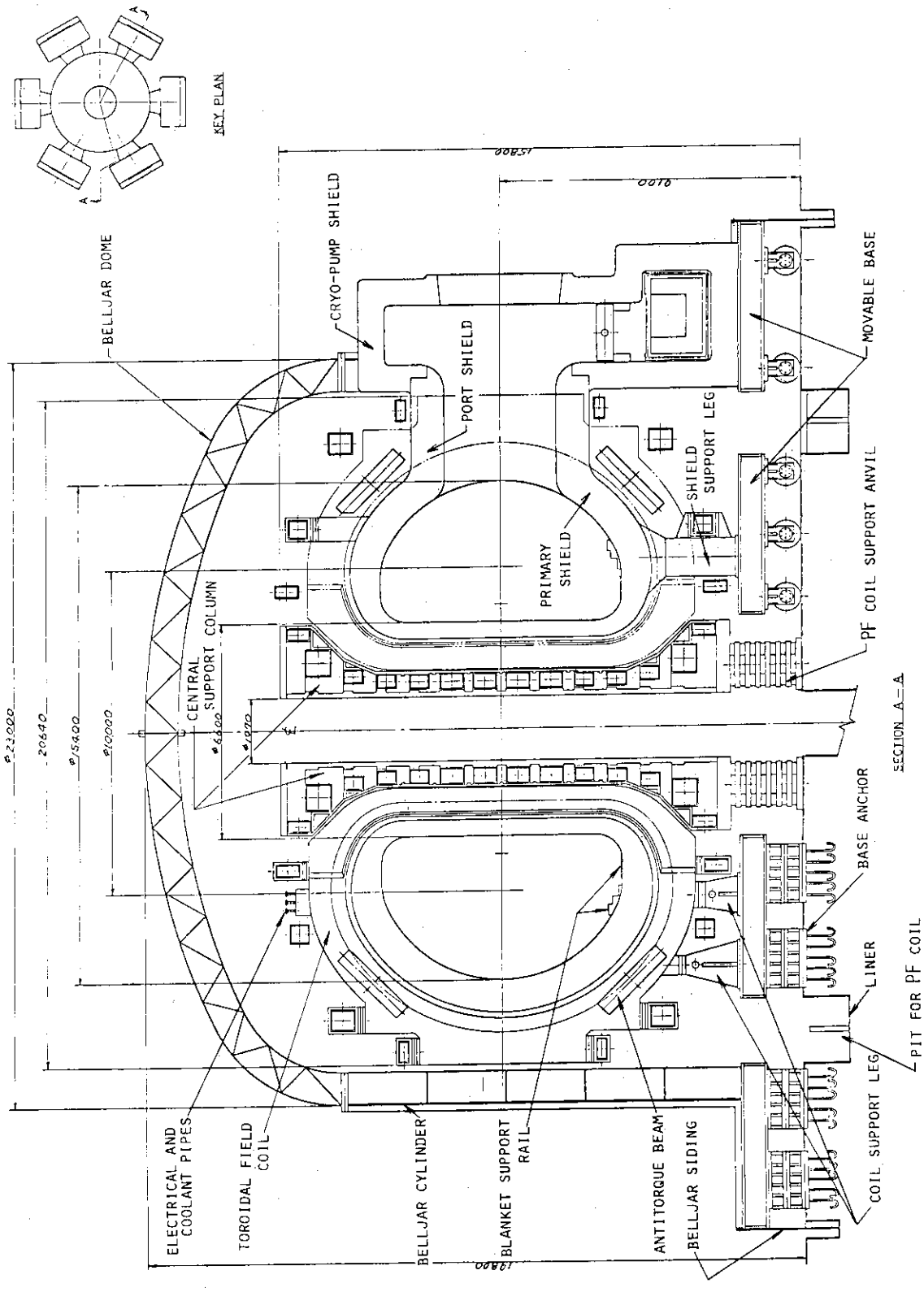

Fig. 1.5.2 Concept A Typical Section

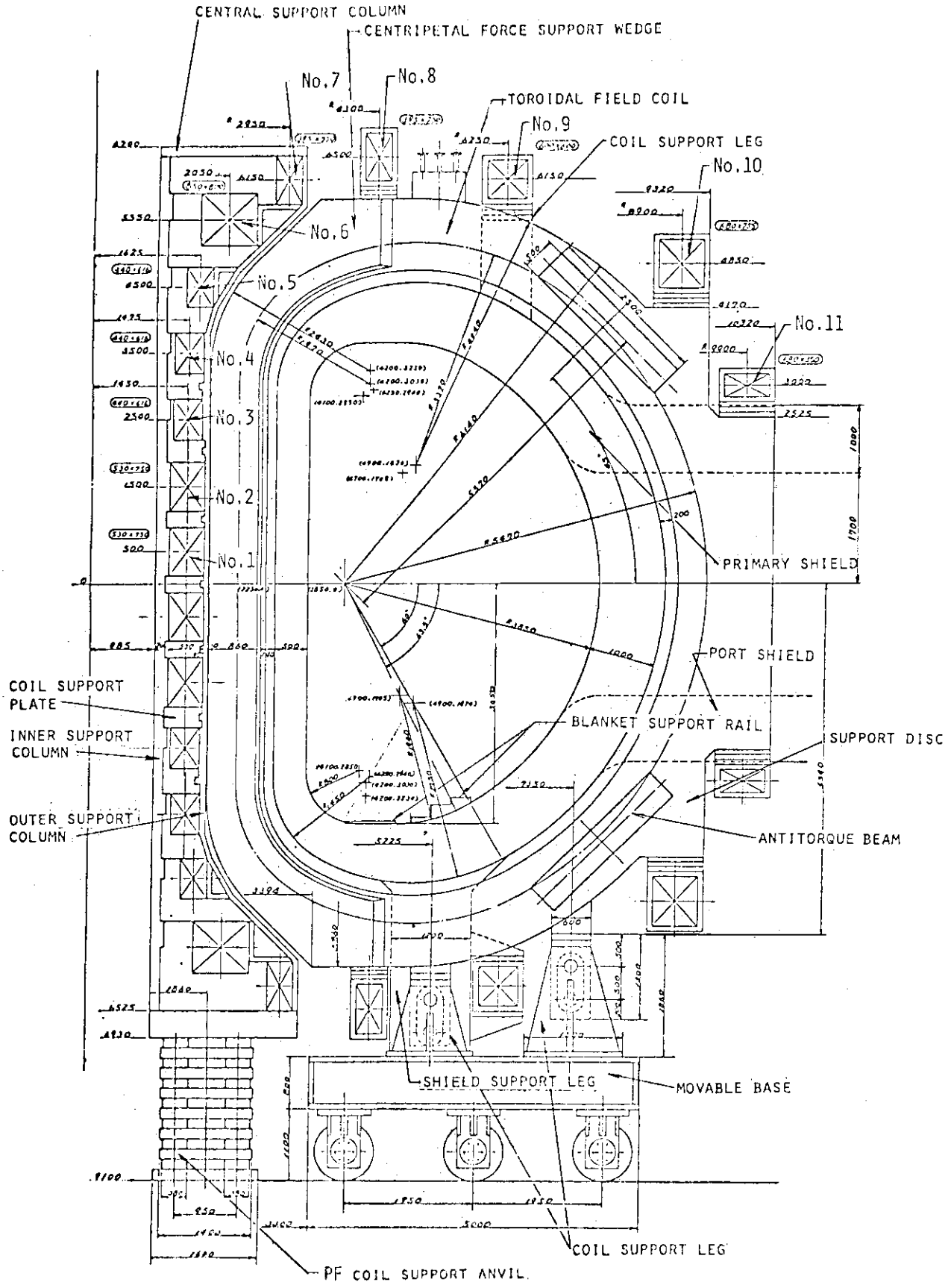

Fig. 1.5.3 Concept A Plan

1.6 Reactor Concept B

The main objective of this design study is to make a concept of maintenable reactor systems under the limitation of the INTOR design conditions. This includes: to choose structure design so that the major radius R can be 5 m; to develop structure design which accepts the easiest way to replace failure parts of reactor systems; and to make a concept of a reactor building of minimum space in view of reactor maintenance. Concerning the last two objectives, a removable blanket scheme has been studied in this design on behalf of the module extraction scheme which has been studied since the JAERI experimental Fusion Reactor (JXFR). The removable blanket scheme means that the blanket structure can be replaced without removing the toroidal field magnets and the shielding structure except for large hatches in the shielding structure located above the torus. The structure of the reactor concept B and NBI system is shown in Figs. 1.6.1 and 1.6.2. The characteristic features of this reactor system are summarized in this section.

To satisfy the design condition of R = 5 m, the following design concepts have been chosen.

(1) The centering force acting on the toroidal field magnets is supported by the pressure acting between the surfaces of wedge parts of the magnet cases which are located on the inner side in the major radius direction. The toroidal magnets are attached to the center pole in such a way that they can move inward in the major radius direction. Small wedge pieces are used so that the surface of the wedge parts of the magnet cases contacts each other firmly. Since the center pole is located inside the poloidal field magnet, the space necessary to support the centering force of the magnet is quite limited.

(2) The vacuum boundary of the plasma chamber is located on the inner side of the shielding structure, while the outer side of the shielding structure forms the vacuum boundary for the toroidal field magnets on the circumference near the center pole. Thus, no additional structure is necessary to form the vacuum boundary for superconducting magnets near the center pole.

The design features, which have been chosen to simplify maintenance procedure, are as follows.

(3) The blanket structures can be replaced from the upper side of the torus without removing the main vacuum system and the neutral beam injector and without recovering the liquid helium temperature of the superconducting magnets to room temperatures. The upper torus shielding structure has large hatches so that blanket handling machines located in the upper part of the reactor room can reach the blanket structures. The procedure to remove the blanket structures is described in detail.

(4) The blanket handling machines consist of manipulators to work on pipe cutting and welding, and cramp mechanisms to lift the blanket module and to slide the module radially in the toroidal direction. The blanket structure is supported to the shielding structure by screws which can be reached from the outside of the shielding structure. The vacuum boundary for the plasma chamber is located on the outside of the shielding structure in this part.

(5) The toroidal torsion force in the toroidal field magnets is supported by the thick cylinder formed by the wedge parts of the magnet cases and by the support structures between magnets. Strong support structures radially all around in minor cross-section are located in the sections without the neutral beam injectors. Strong structures are also located in all the bottom part of the magnet, thus the toroidal magnets form a strong annular cylinder to support the torsion force.

(6) The toroidal field magnets can be replaced in the reactor room by means of a carrier and the crane. The weight of the toroidal field magnet is supported on the base for the center pole. Thus the poloidal field magnets under the toroidal magnets can be replaced easily.

(7) The following two ideas are proposed to form the vacuum boundary for the toroidal magnets on the outer side in the major radius direction. First, each toroidal magnet has own vacuum chamber on the outer side in the major radius direction. This design has better accessibility to the shielding structure, but the space inside the vacuum chamber is limited and many places have to be cut when the toroidal magnet is disassembled. Second, every two toroidal magnets have a common vacuum chamber in the section where

no neutral beam injector is attached. This design gives more space inside the magnet vacuum chamber.

(8) The reactor room has four square spaces to draw back the neutral beam injectors and the main vacuum systems beyond circular area. Wide space for reactor maintenance can therefore be prepared around the torus without enlarging the reactor room. The reactor room has one large door where any single module in the reactor room can go through. Cranes and carriers with jacks can transport any module to storage areas which are located next to the reactor room.

The toroidal field magnet design of the reactor concept B is described in Sec. 6.2. The design concepts (1) and (2) allow the toroidal magnets to have the maximum cross-section under the condition of R = 5 m. The magnet shape has also been optimized so that the tension force in the magnet is uniform as far as possible. Stress analysis of the magnets however shows that the maximum stress in the toroidal magnet is still on the border of the limitation of acceptable stresses.

The poloidal field magnet design of this reactor system is reported in Sec. 7.2. The two poloidal magnets located above the torus are supported on the shielding structure so that they can be removed without recovering their cryogenic temperature considerably when the blanket structure is replaced. Since INTOR has the D-shaped divertor, some of the poloidal magnets are given a considerable amount of hoop force which requires larger magnet cross-section than usually expected.

Special emphasis in this design study is put on repair and maintenance of the reactor system which is reported in Chapter 11. Achievement of the removable blanket scheme described there depends on the possibility to find the way how to support the toroidal torsion force acting in the toroidal magnet system. It also depends on the possibility to realize the blanket handling machines. Although the detailed design study on these points has not been fulfilled yet, it appears that there is a great possibility to achieve this maintenance concept.

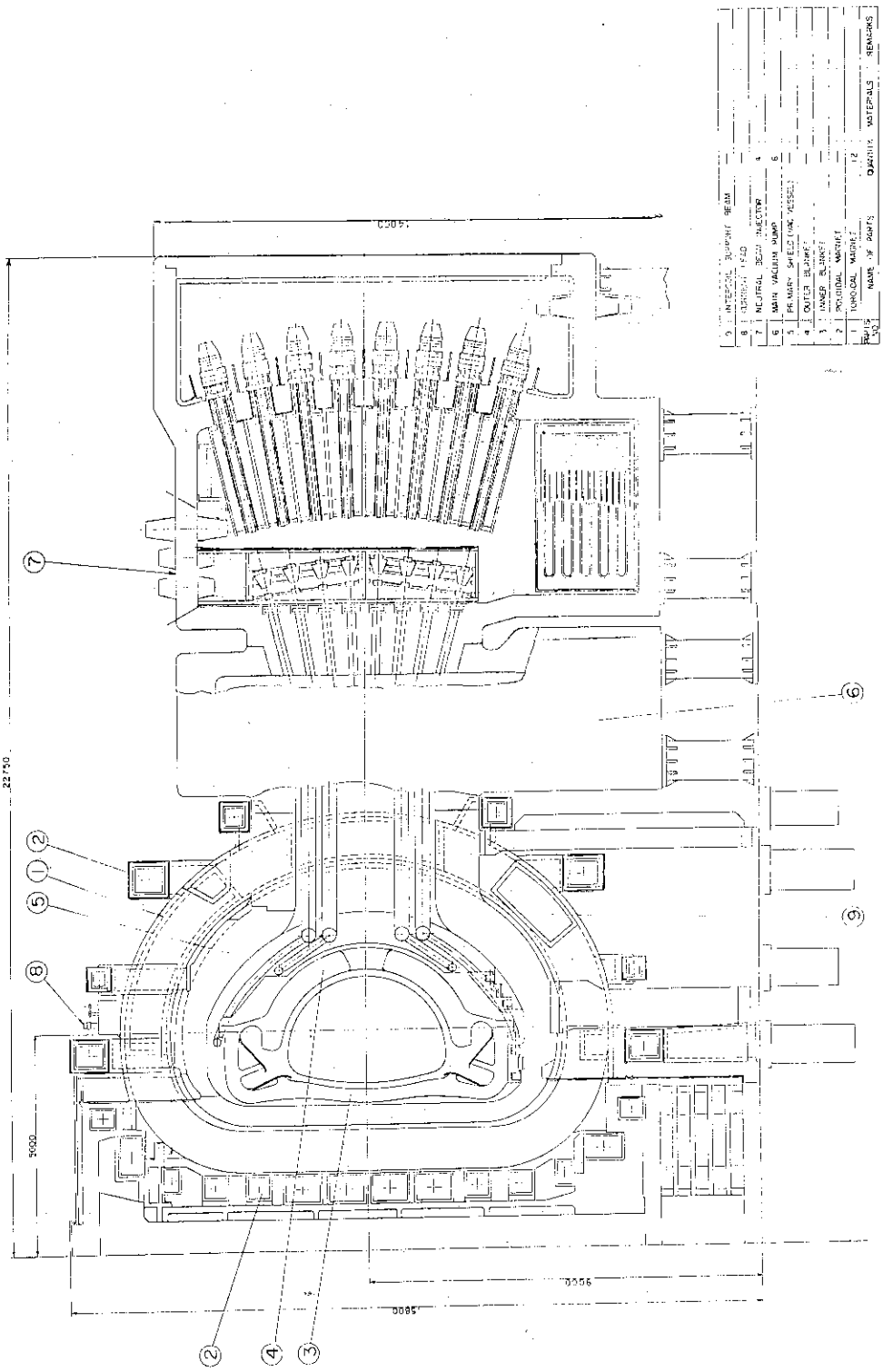

Fig. 1.6.1 Vertical Cross-Section of the Reactor Concept B and the Neutral Beam Injector

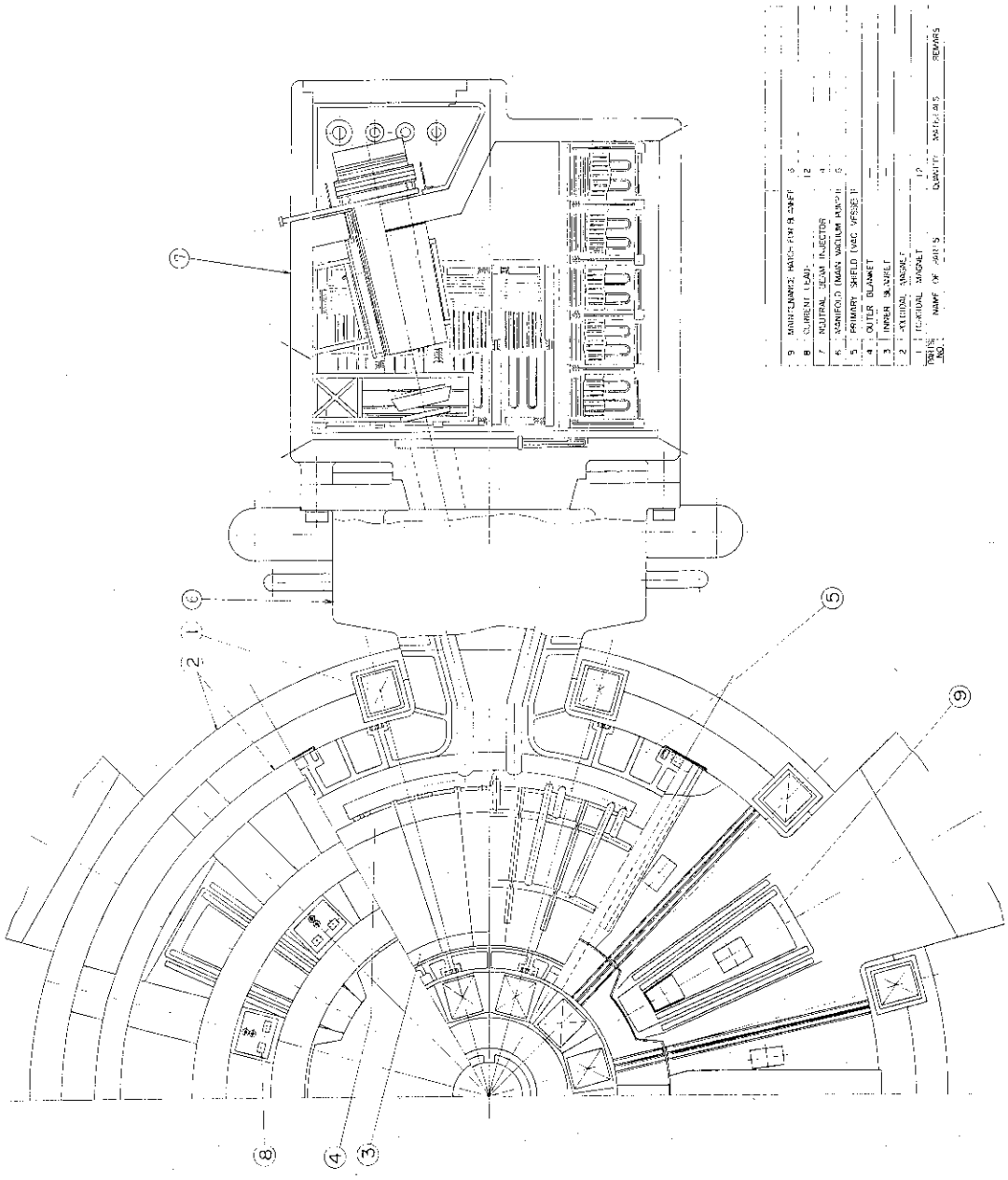

Fig. 1.6.2 Plane View of the Reactor Concept B and the Neutral Beam Injector

2. Neutronics

One dimensional (1D) S_N code ANISN[1], two dimensional (2D) S_N code DOT-3.5[2] and three-dimensional Monte Carlo code MORSE-I[3] were used in the INTOR neutronics calculations. In Section 2.1, calculated neutron and gamma-ray fluxes and nuclear heating obtained by the above three methods are presented. The 1D calculations are used in preliminary calculations and parametric surveys. The 2D calculations aimed at investigating the effect of neutron streaming through the divertor channel, and the 3D calculations, the poloidal distributions of nuclear effects in the first wall. Section 2.2 gives the spatial dose rate from induced activity, Section 2.3 the results of 1D shielding calculations. An albedo Monte Carlo method presently under development for the evaluation of neutron streaming through NBI ports is described in Section 2.4.

The blanket and shield models used in this neutronics design is not consistent. This is due to the fact that shielding structure and shielding material composition were not determined till the late stage of the design. Comparison of various outboard shield (or sometimes called outer shield) and the inboard shield (inner shield) are given in 2.2 and 2.3.1, respectively.

2.1 Neutron & Gamma-Ray Fluxes and Nuclear Heating

2.1.1 One dimensional calculation

The P_5 - S_8 approximation was used in the calculation of neutron and gamma-ray fluxes using the one-dimensional discrete ordinate transport code ANISN[1]. A 42 group-neutron, 21 group-gamma coupled cross-section library for 40 nuclides GICX40[4] was used. The nuclear data base of the GICX40 Library is ENDF/B-III and IV[5] for neutron data and POPOP4 Library[6] for gamma-ray production data.

Neutron and gamma-ray fluxes and nuclear heating rate distributions are calculated with the cylindrical models in Tables 2.1.1 and 2.1.2, respectively. These models are the ones proposed for INTOR in the Workshop Session II. Figures 2.1.1 and 2.1.2 show the neutron and gamma-ray fluxes for the inner and outer models, respectively. Radial distributions of total neutron flux, neutron flux with energy greater than 0.1 MeV, 14 MeV neutron flux and gamma-ray flux are shown. Their magnitudes are in the order written above in the first wall but the 14 MeV neutron flux attenuates below total gamma-ray flux just inside the blankets.

Nuclear heating rates in the inner and outer models are depicted in Figs. 2.1.3 and 2.1.4, respectively. Three curves for total nuclear heating rate, neutron and gamma heating rates are shown in the figures. Except for the blanket region in the outer model which includes lithium, gamma heating rate is always greater than neutron heating rate.

2.1.2 Two Dimensional Analysis of Radiation Shielding

1. Methods

(1) The analysis was performed by the two dimensional radiation transport calculation code DOT-3.5[2].

(2) The cylindrical calculation model is shown in Fig. 2.1.5. The calculation mesh interval was taken about 20 cm around the divertor plate. The number of the mesh intervals along R-axis and Z-axis were 42 and 31, respectively.

(3) The main compositions of the materials are shown in Table 2.1.3.

(4) The P_3-S_4 approximation was used.

(5) The cross-section library GICX40[4] (42 neutron groups and 21 gamma groups) was used.

2. Results

(1) The results obtained by the two dimensional calculation are compared with those by the one dimensional calculation in Table 2.1.4. The one dimensional calculation was performed with the same compositions and thickness along Z-axis.

(2) The fast neutron flux at the divertor plate calculated with the two dimensional code was about a half of that with the one dimensional code because of the decrease of scattering neutrons from the surroundings.

(3) The heating rate at the toroidal coil obtained by the two dimensional code was about two times as much as that by the one dimensional code because of the streaming effects through the divertor.

2.1.3 Three-dimensional calculation

Poloidal distributions of 14 MeV neutron flux, and helium production, displacement damage and nuclear heating rates in the first wall system are calculated using Monte Carlo transport code MORSE-I. The first wall system of INTOR-J consists of the closest part of blanket to plasma (the first wall) and a protection wall in front of it.

The blanket structure and the protection wall are made with stainless steel and molybdenum alloy, respectively. Figure 2.1.6 shows a

three-dimensional calculation model of INTOR-J. The neutron source distribution used in this calculation is shown in Fig. 2.1.7 (see Appendix A.2).

Both the protection wall and first wall are divided into eighteen regions as shown in Fig. 2.1.8. Neutron and gamma fluxes averaged in each region are calculated using track-length estimator. The fluxes and rates of helium production, displacement damage and nuclear heating are shown in Fig. 2.1.9 - 2.1.16.

Real curves in the figure are the least square fittings using 5th or 6th degree polynominal with the following limitations.

$$\frac{d}{d\theta} f(\theta) \Big/_{\theta=0^\circ} = 0$$

$$\frac{d}{d\theta} f(\theta) \Big/_{\theta=180^\circ} = 0$$

These limitations must be satisfied because a symmetrical boundary is assumed at the mid-plane. The peaking factors of 14 MeV neutron flux and helium production rate distributions are about 1.3 which is a little larger than those of DPA and nuclear heating rate distributions.

Because of the above limitations the fitting curves do not agree well with the original values at the innermost part ($\theta = 0^\circ$). It is necessary to make fractional standard deviations smaller for obtaining more accurate information about the flux at the innermost part. However it is practically impossible to follow more neutron histories because of increasing computational time.

The results of three-dimensional calculation are a little smaller than those of one-dimensional calculation. This may be caused by the overestimation of grazing component of particle flux in one dimensional calculation. Infinite cylinder approximation and uniform source distribution approximation overestimated the grazing component of particle flux.

Table 2.1.1 Inner model for the INTOR proposal

Region No., i	Region	Region Radius, r_i(cm)	Mesh No., j_i	$\sum_i j_i$	Mesh Width Δr_i(cm)
1.	Plasma	120.0	1	1	120.0
	Vacuum	133.5	1	2	13.5
2.	TZM protection wall	134.5	2	4	0.5
3.	SS tube wall	135.0	2	6	0.25
4.	SS(80%) + H_2O(20%)	145.0	5	11	2.0
5.	SS(90%) + H_2O(10%)	165.0	10	21	2.0
6.	Vacuum	170.0	1	22	5.0
7.	SS(30%) + W(40%) + Borated water	210.0	40	62	1.0
8.	Air	220.0	1	63	10.0
9.	SS cryostat vessel	225.0	2	65	2.5
10.	SCM, SS(60%) + Cu(28%) + Nb(7%)	310.0	40	105	2.125

Table 2.1.2 Outer model for the INTOR proposal

Region No., i	Region	Region Radius, r_i(cm)	Mesh No., j_i	$\sum_i j_i$	Mesh Width Δr_i(cm)
1.	Plasma	120.0	1	1	120
	Vacuum	133.5	1	2	13.5
2.	TZM protection wall	134.5	2	4	0.5
3.	SS tube + cell wall	137.0	2	6	1.25
4.	Li_2O(21.3%) + SS(4.74%) + He(21.3%)	155.0	6	12	3.0
5.	Li_2O(53.05%) + SS(20.15%) + He(10.5%)	181.6	16	28	1.66
6.	SS end wall	185.0	2	30	1.7
7.	Vacuum	270.0	1	31	85.0
8.	SS(90%) + Borated water(10%)	370.0	50	81	2.0
9.	Air	380.0	1	82	10.0
10.	SS cryostat vessel	385.0	2	84	2.5
11.	SCM, SS(60%) + Cu(28%) + Nb(7%)	480.0	40	124	2.375

Table 2.1.3 Material Composition

Regions	Materials	Density (g/m^3)	Composition (VOL %)
Plasma	Hydrogen	1.7×10^{11}	100
Neutralized Particle	Hydrogen	8.9×10^{12}	100
	SUS 316	7.98	87.9
Blanket	Water	1.0	7.6
	T Z M	10.1	4.5
	Tungsten	19.1	40
Shield	SUS 316	7.98	30
	Borated Water	1.0	30
	Copper	8.9	31.5
Toroidal Coil	Insulator	1.25	30.9
and	SUS 316	7.98	18.1
Poloidal Coil	Liquid Helium	0.417	8.9
	Bronze	8.7	6.4
	Nb_3Sn	8.4	4.2
Heavy Concrete	Magnetite	5.2	67
	Cement	3.0	21
	Water	1.0	12

Table 2.1.4 The Comparison of the Results of Two Dimensional Calculation with that of One Dimensional Calculation

		Neutron Flux ($\eta/cm^2.S$)				Nuclear Heating (w/cm^3)
		Fast Neutron (E_n>0.1MeV)	Intermediate Neutron (0.1MeV≦E_n<0.125)	Thermal Neutron (E_n≦0.215MeV)	Total	
Divertor Plate	1-D	2.9×10^{14}	1.4×10^{14}	4.2×10^{12}	4.4×10^{14}	1.2×10^{1}
	2-D	9.1×10^{13}	1.9×10^{13}	1.8×10^{0}	1.1×10^{14}	3.6×10^{0}
Toroidal Coil Surface	1-D	9.5×10^{6}	1.8×10^{6}	5.7×10^{0}	2.7×10^{7}	1.3×10^{-7}
	2-D	7.2×10^{6}	5.4×10^{7}	5.4×10^{5}	6.2×10^{7}	2.9×10^{-7}

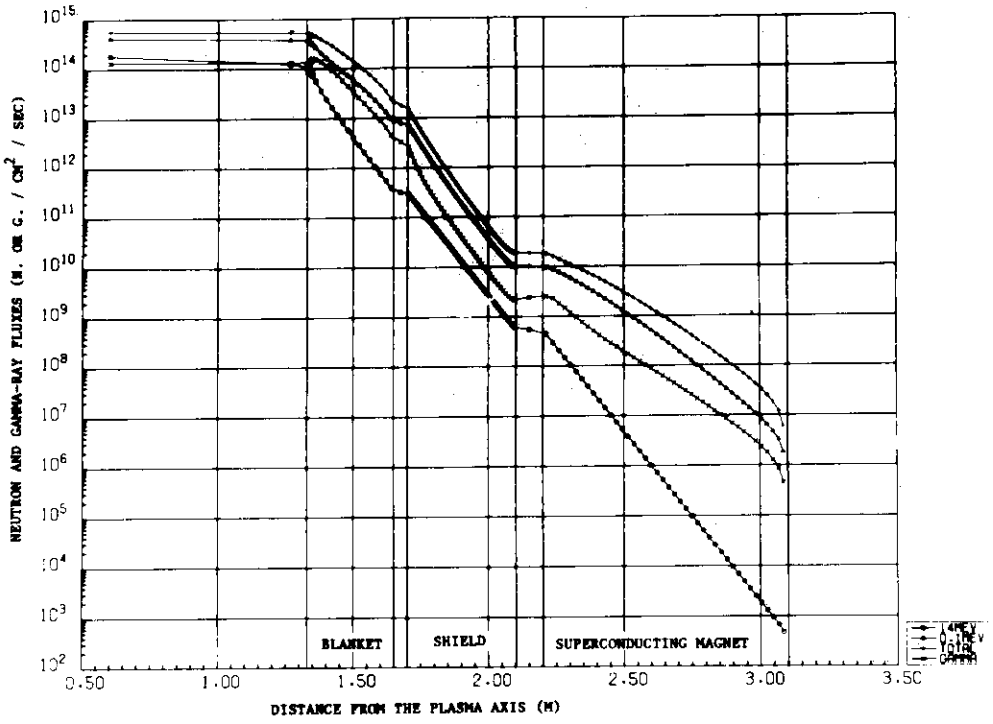

Fig. 2.1.1 Neutron and gamma-ray fluxes in the inner blanket, shield and toroidal field coil

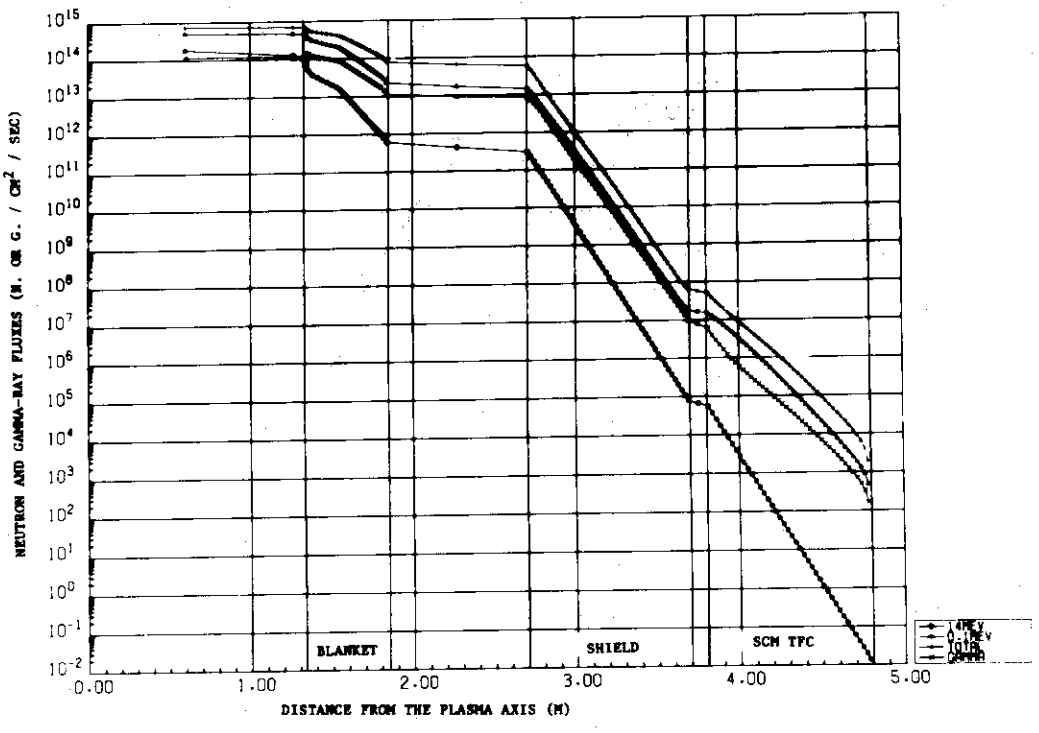

Fig. 2.1.2 Neutron and gamma-ray fluxes in the outer blanket, shield and toroidal field coil

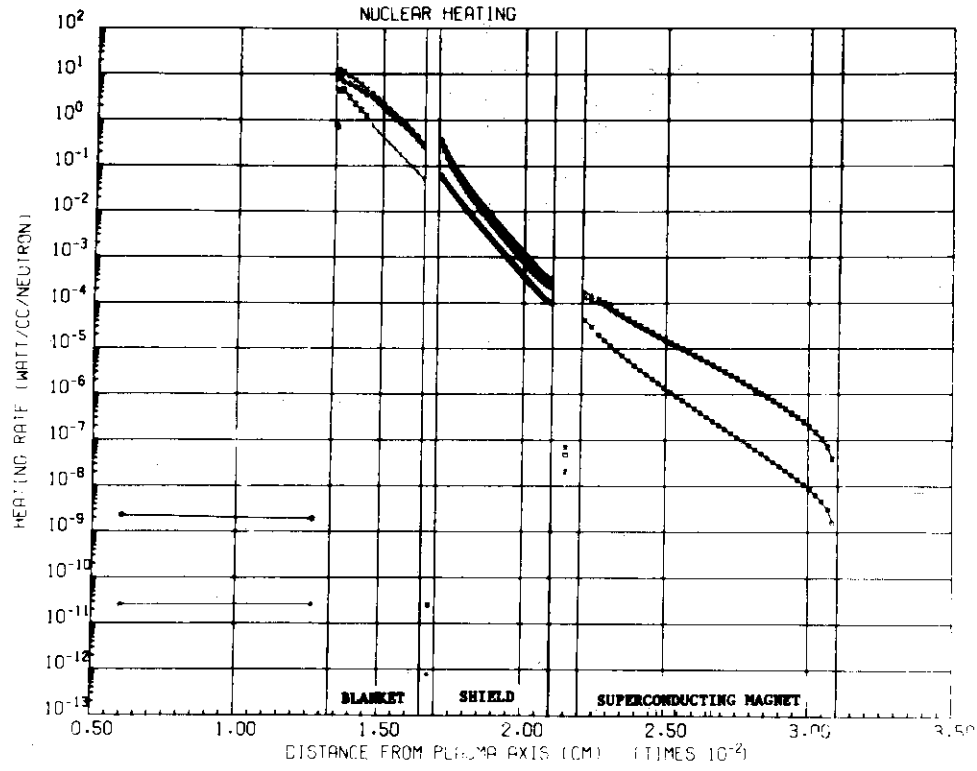

Fig. 2.1.3 Nuclear heating rate in the inner blanket, shield and toroidal field coil

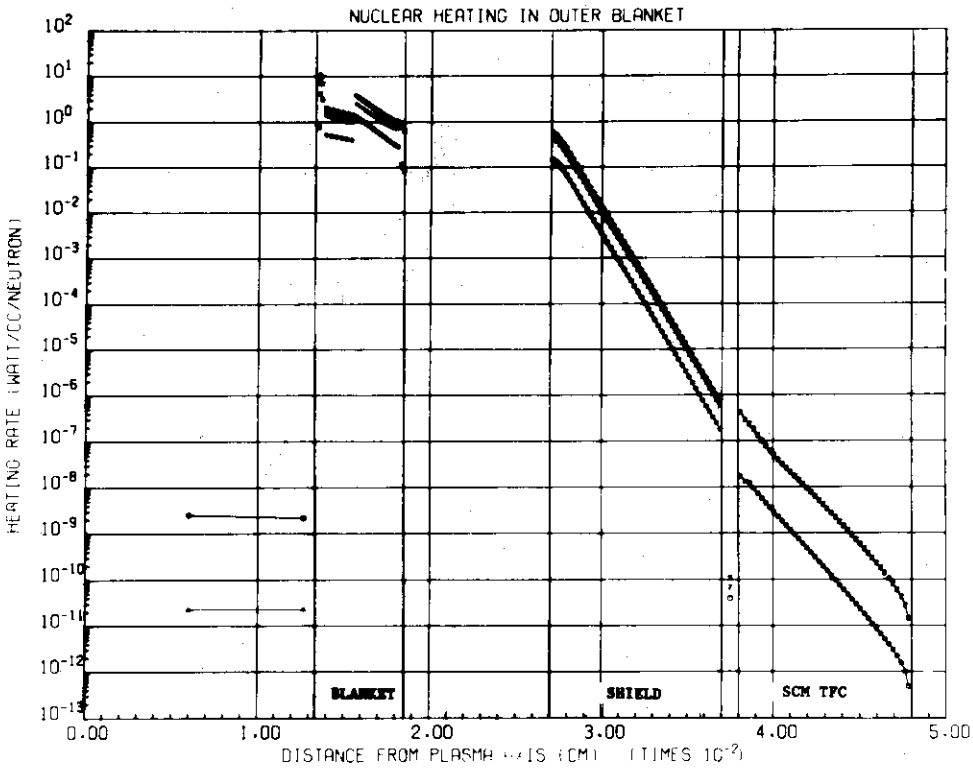

Fig. 2.1.4 Nuclear heating rate in the outer blanket, shield and toroidal field coil

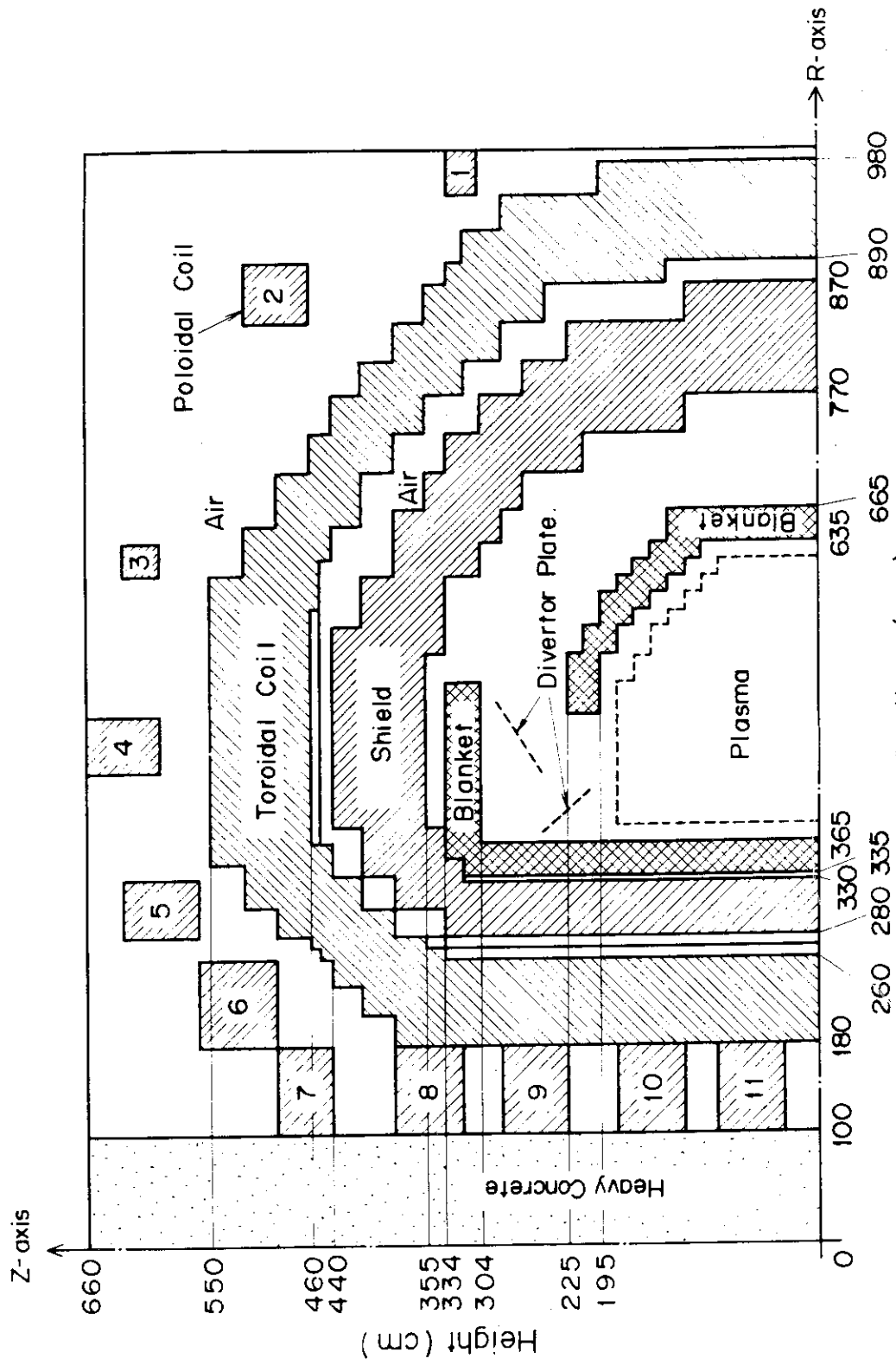

Fig. 2.1.5 Two Dimensional Calculation Model

1 Vacuum
2 Protection wall
3 First wall
4 S.S. (0.8) + H_2O (0.2)
5 S.S. (0.9) + H_2O (0.1)
6 Li_2O (0.213) + S.S. (0.047) + He (0.213)
7 Li_2O (0.5305) + S.S. (0.2015) + He (0.105)
8 End wall
9 Inner shield
10 Outer shield

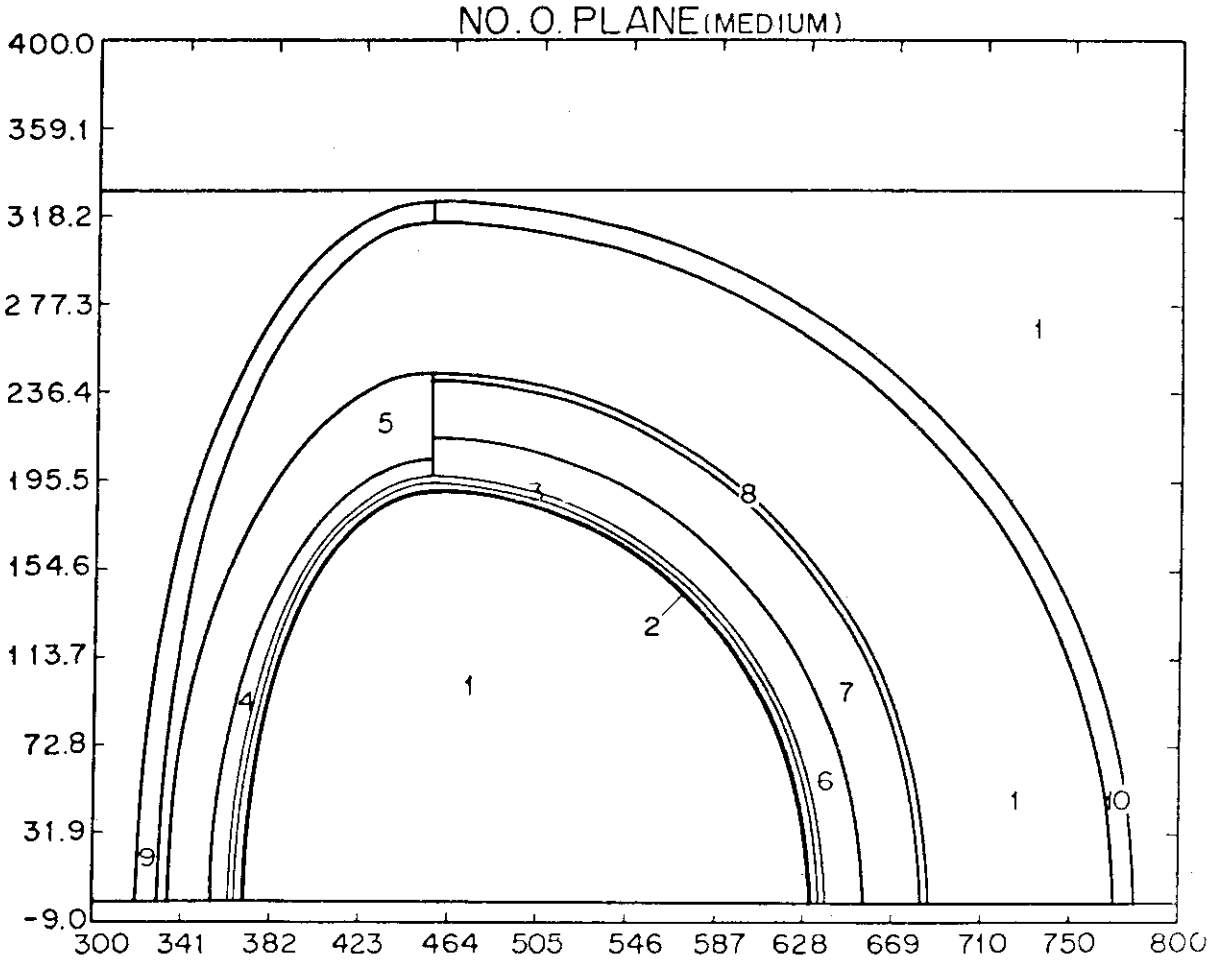

Fig. 2.1.6 Three-Dimensional Calculation Model of INTOR-J

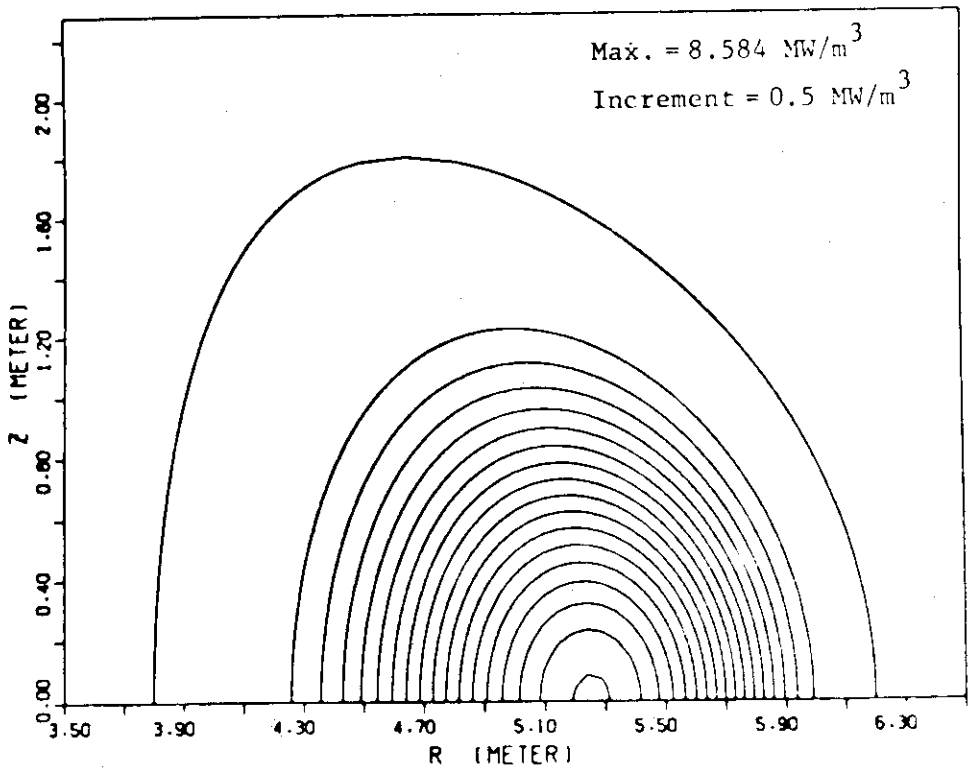

Fig. 2.1.7 Power Density Contour

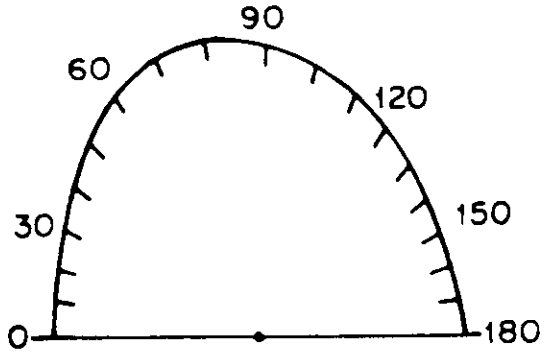

Fig. 2.1.8 Editing Region of the First Wall and the Protection Wall

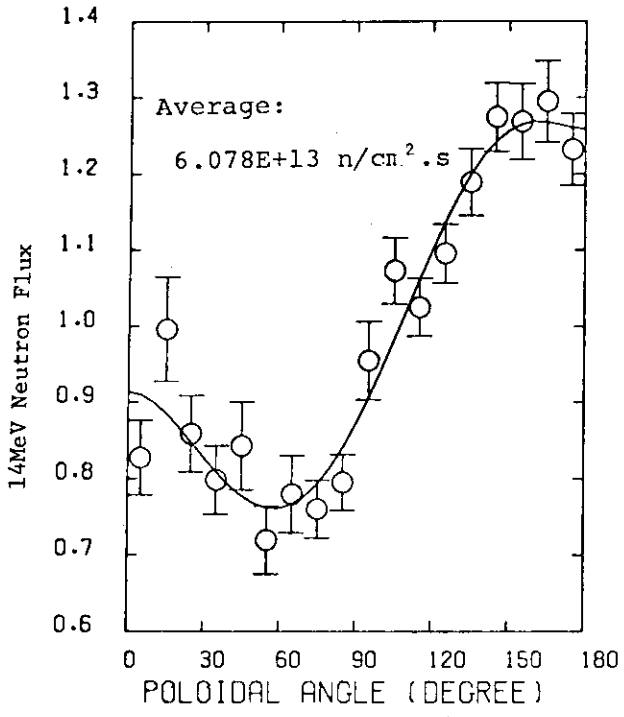

Fig. 2.1.9 Poloidal Distribution of 14 MeV Neutron Flux in the Protection Wall

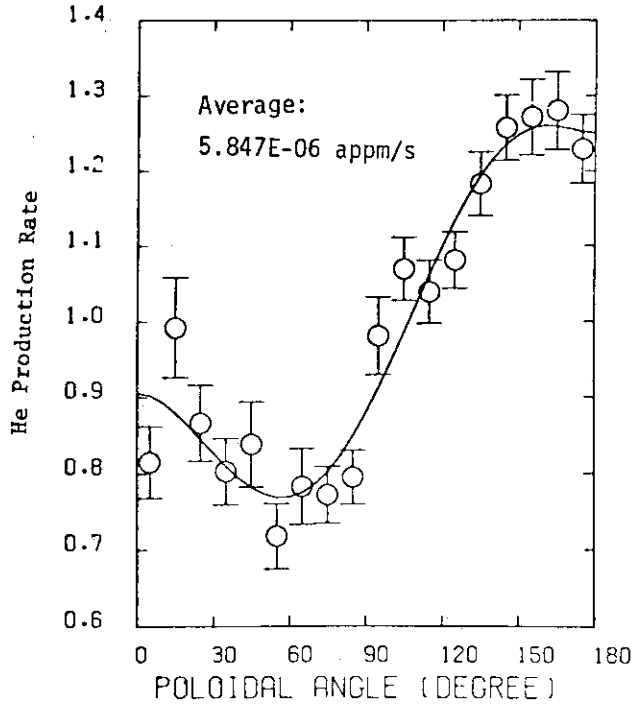

Fig. 2.1.10 Poloidal Distribution of Helium Production Rate in the Protection Wall

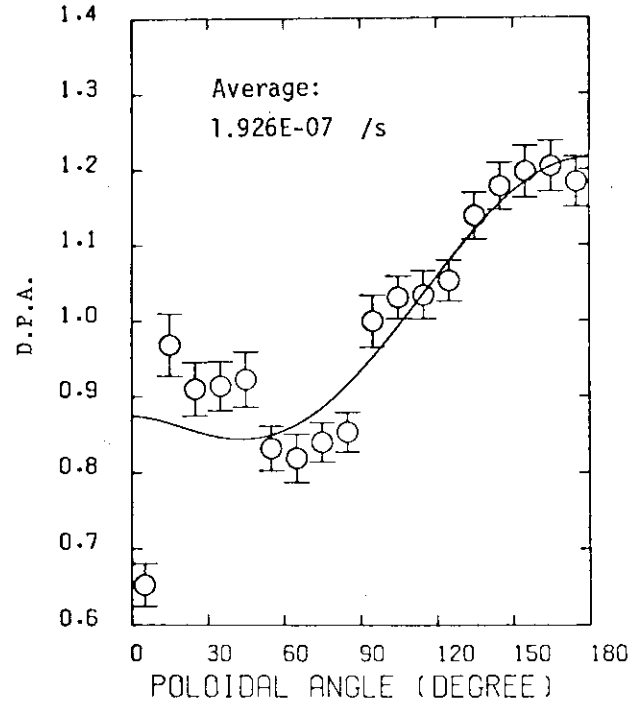

Fig. 2.1.11 Poloidal Distribution of D.P.A. in the Protection Wall

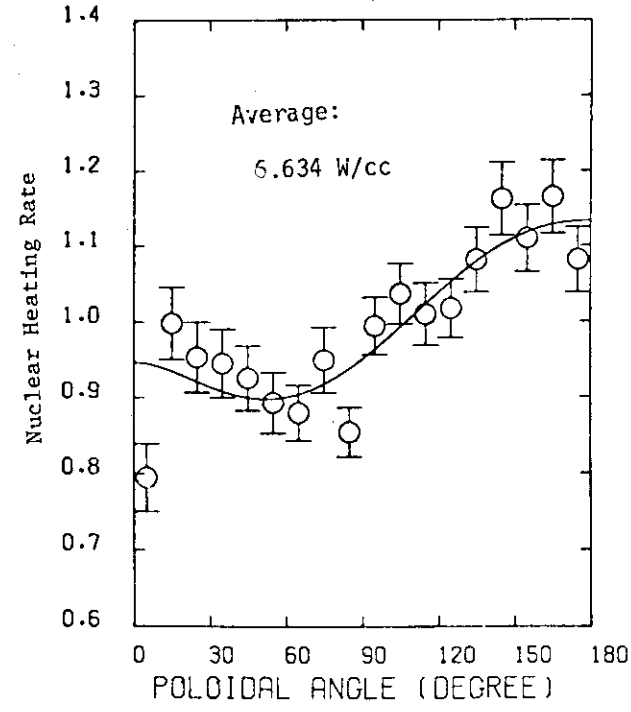

Fig. 2.1.12 Poloidal Distribution of Nuclear Heating Rate in the Protection Wall

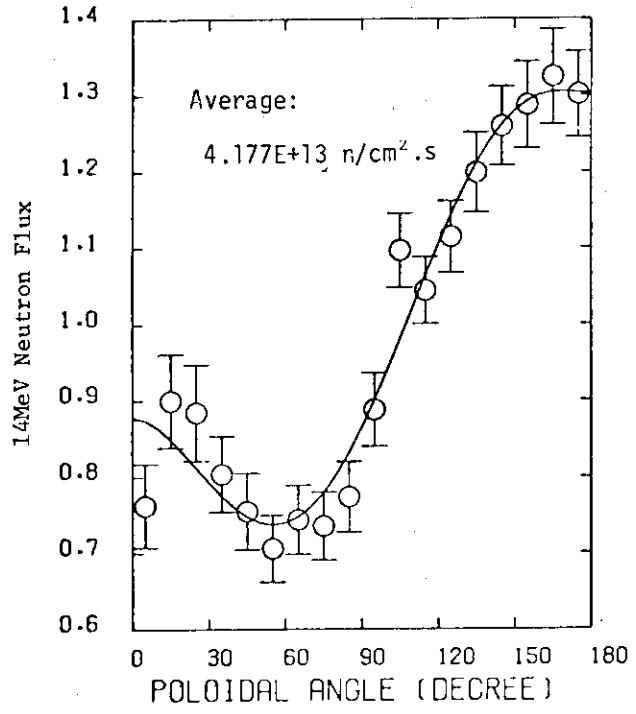

Fig. 2.1.13 Poloidal Distribution of 14 MeV Neutron Flux in the First Wall

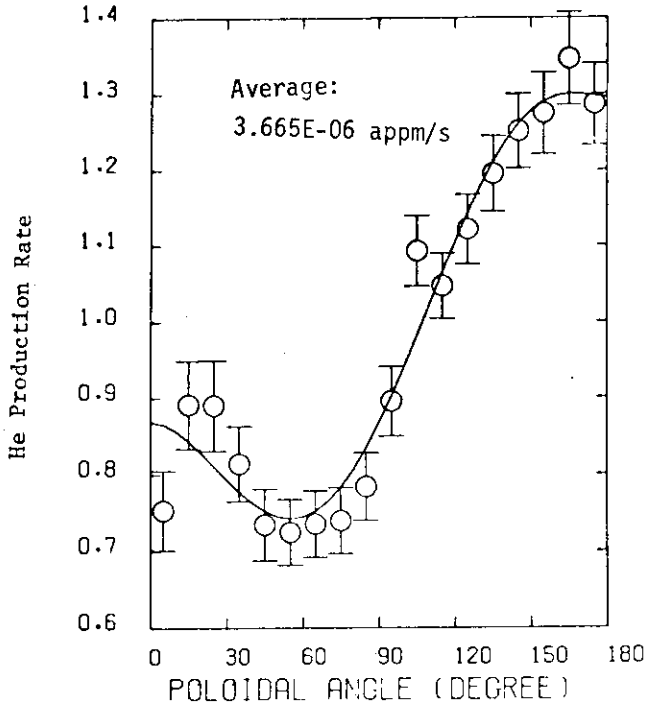

Fig. 2.1.14 Poloidal Distribution of Helium Production Rate in the First Wall

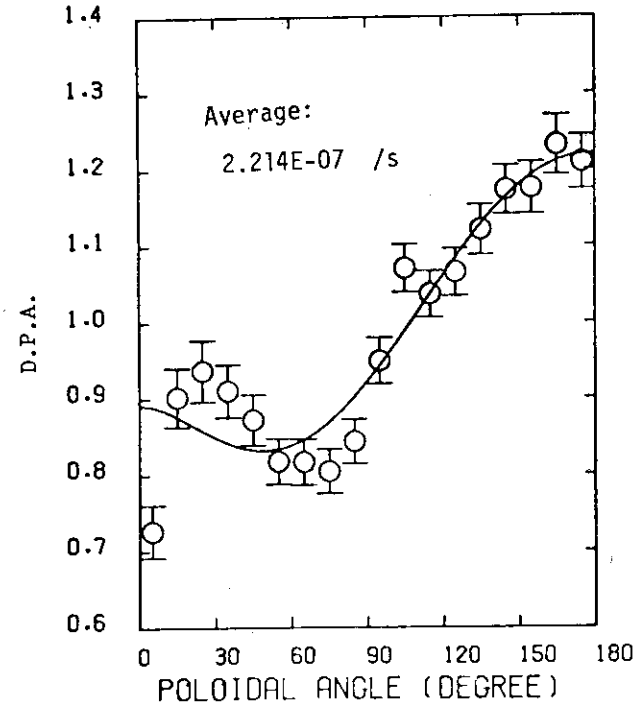

Fig. 2.1.15 Poloidal Distribution of D.P.A. in the First Wall

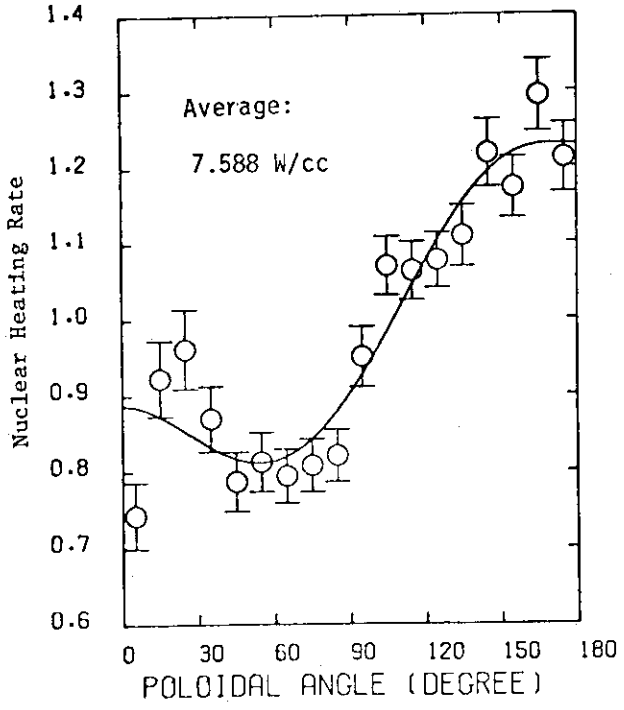

Fig. 2.1.16 Poloidal Distribution of Nuclear Heating Rate in the First Wall

2.2 Gamma dose rate after reactor shutdown

The thickness of the outboard shield will be determined by the requirement of supressing dose rate outside the shield after reactor shutdown. In the design of INTOR-J the target of the dose rate level is 2.5 mrem/h which allows almost free occupations of personnel in the reactor room.

Using THIDA code system, dose rates one day after shutdown are calculated. THIDA is a code system which calculates Transmutation, Hazard potential, Induced activity, Dose rate and After heat. It consists of the following: one- and two-dimensional discrete ordinate transport codes; induced activity calculation code; activation chain, activation cross section, radionuclide gamma-ray energy/intensity and gamma-ray group constant files; and gamma-ray flux to exposure dose rate conversion coefficients.

Figure 2.2.1 shows a schematic layout of an outboard calculational model of INTOR-J. Dose rates are calculated for two cases. The shields in the both cases have the same thickness but different compositions. Table 2.2.1 shows composition of the shields.

The major sources of gamma ray outside the shield are stainless steel structures of toroidal field coil when special materials such as tantalum are not used in the reactor. In this calculation iron, nickel and chromium are considered to be activated and become gamma-ray source.

Figures 2.2.2 and 2.2.3 show dose rates around the reactor one day after shutdown. In both cases the maximum dose rate outside the shield is larger than 10^2 mrem/h. The time for personnel to access the reactor is severely limited. The outboard shield of INTOR-J reference design is the combination of stainless steel cooled by water and heavy concrete. As the neutron attenuation by the reference design shield is expected to be smaller than the above two cases,it will be necessary to increase the thickness of the outboard shield.

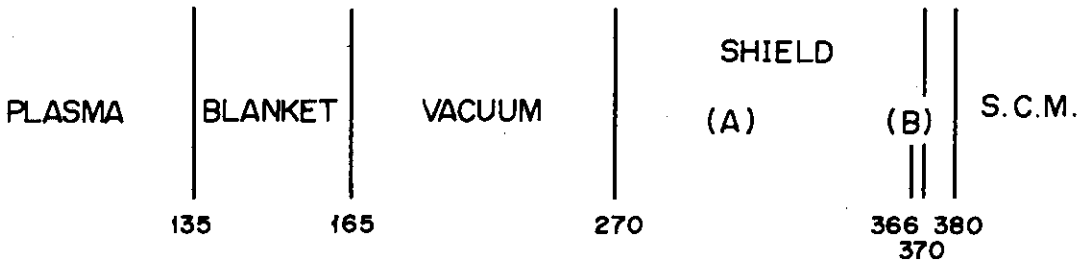

Fig. 2.2.1 Schematic Layout of an Outboard Calculation Model

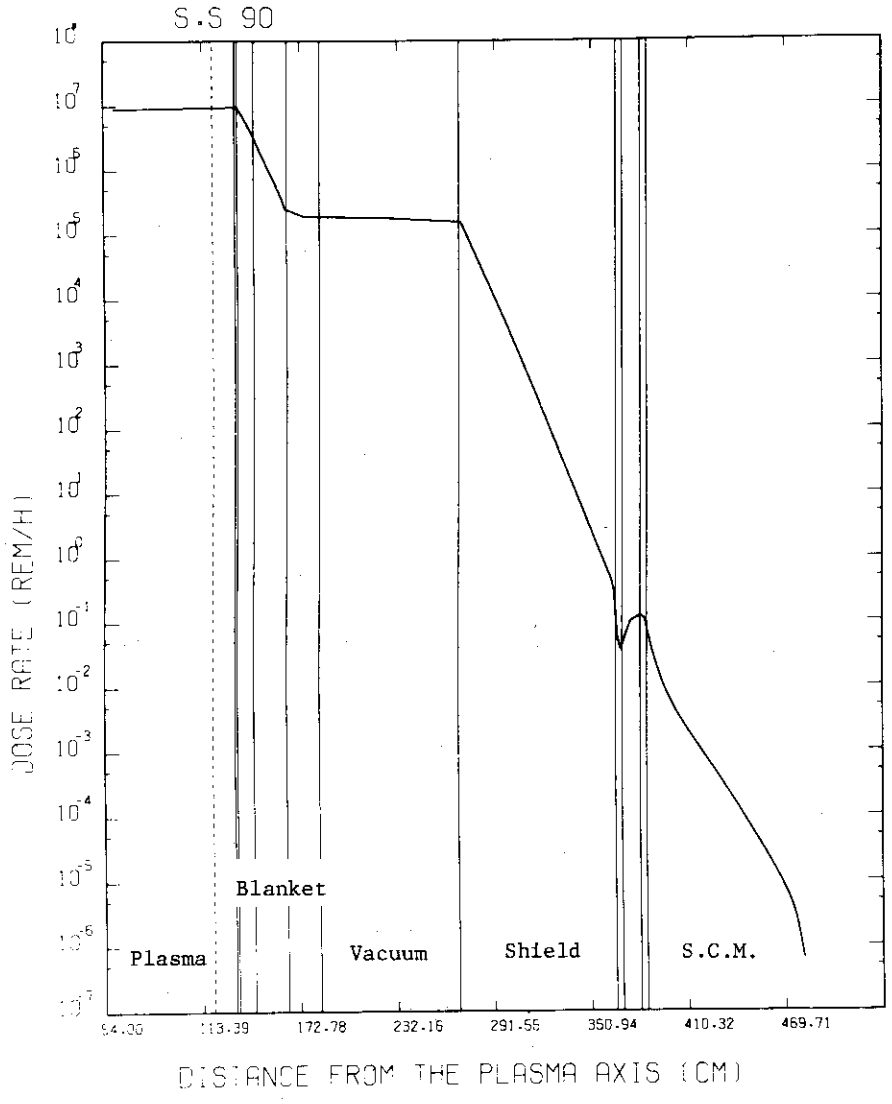

Fig. 2.2.2 Dose Rate Distribution of the Case 1

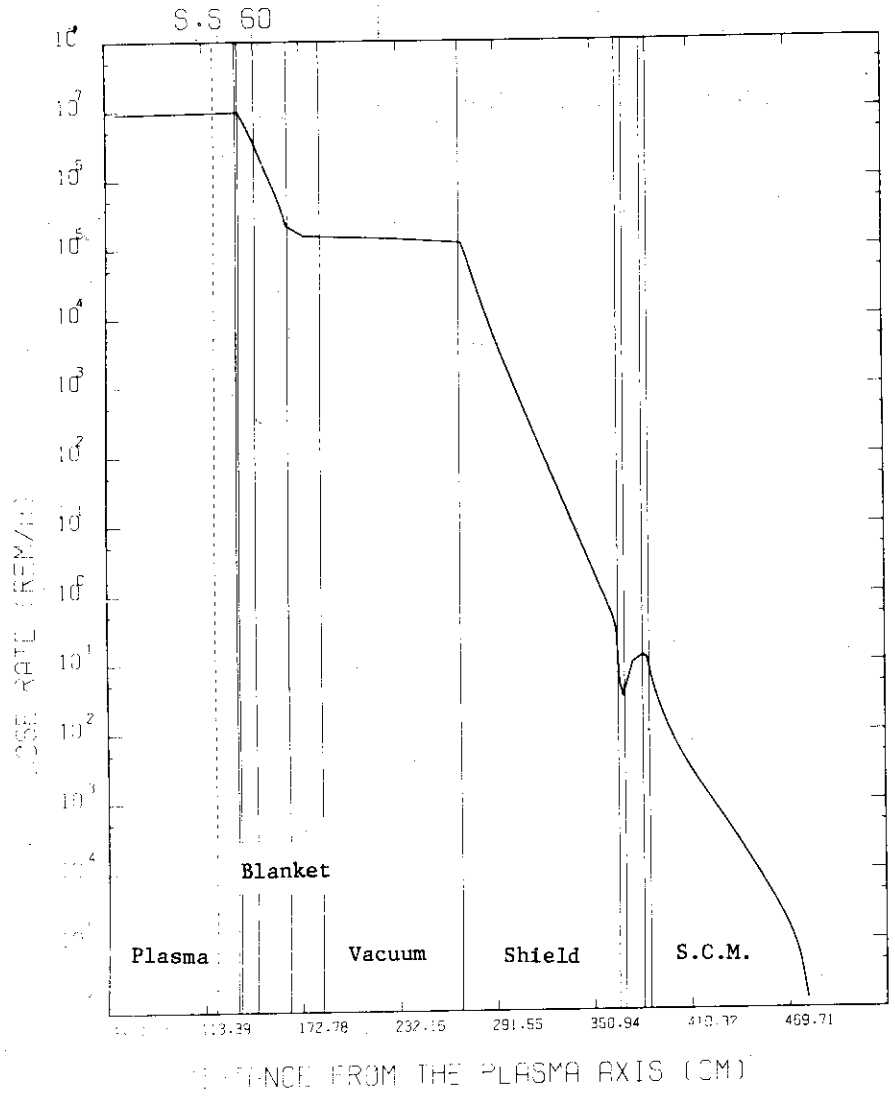

Fig. 2.2.3 Dose Rate Distribution of the Case 2

Table 2.2.1 Compositions of shielding

	Composition	
	(A)	(B)
Case 1	S.S.(0.90) H_2O(0.1)	Pb
Case 2	S.S.(0.60) H_2O(0.4)	Pb

2.3 Magnet Shielding

In this section, the results of two parametric surveys of inboard shield material change, radiation damage calculations and a summary discussion on the minimum shield thickness are given.

2.3.1 First parametric survey

An optimizing composition of the inboard shield was determined mainly from neutronics point of view and was presented to the Workshop Section II.

In the design of JAERI Experimental Fusion Reactor (JXFR)[7], an attempt was made to minimize the thickness of the inner shield[8] under the following three limitations; (1) Inner blanket will be cooled by helium gas and hence about 10% of the volume must be left for the coolant path. (2) Stainless steel structure will occupy at least 17% of the volume of the inner blanket. (3) Heavy concrete will be the main structural material for the inner shield.

As a result, the configuration shown in Table 2.3.1 was selected for the inner blanket and shield of JXFR. The total thickness of the bulk blanket and shield at mid-plane was 84.5 cm. It was found that stainless steel was effective in attenuating 14 MeV neutrons and that tungsten was excellent as the shield material for the fast neutrons with energies greater than 1 MeV.

Based on the result of the JXFR shielding design, an optimization of the inner shield material for INTOR was carried out. The limitations are as follows.

(1) The thickness of the blanket is 31.5 cm.
(2) The thickness of the shield is 40 cm.
(3) The coolant for the blanket was supposed to be helium in the beginning of the design but was changed to water at the later stage.
(4) Stainless steel is to be used as the structural material occupying more than 30% of the volume of both the blanket and shield.
(5) The displacement damage in copper stabilizer of the superconducting toroidal field magnet is the quantity to be minimized.

The choice of the copper displacement damage as the minimizing parameter arises from the fact that it was the critical quantity in the JXFR shielding design, and that the resistivity increase of copper by irradiation is better known experimentally than the critical dose for organic insulator, which is another important quantity. As an indicator of

radiation induced resistivity, neutron fluence listed in the INTOR guiding parameters is a poor one because the resistivity increase depends not only on the number of neutrons but also on their energy. DPA rate should be used instead of fluence. The maximum copper DPA rate in the toroidal coil for five configurations are shown in Table 2.3.2.

Among the first four cases with helium-cooled blanket, Case 3 with tungsten (W) volume ratio of 50% yielded the lowest DPA-rate. The volume ratio of 40% for tungsten was considered better because it uses less tungsten (which is quite expensive) with little increase in the DPA-rate (Case 4). By changing the blanket coolant from helium to water, further decrease of the DPA-rate was obtained as shown for Case 5, resulting in the value of 4.3×10^{-5} DPA per year under 25% availability condition. This means the toroidal field coil can be operated for more than two years without room temperature annealing under the assumed design condition of the magnet.

The composition of the inner blanket and shield adopted for further investigation is shown in Table 2.3.3.

Table 2.3.4 summarizes the tentative criteria and the results obtained from one-dimensional shielding calculations for the inner and outer superconducting magnets (SCM) of the INTOR proposal. Cumulative fluences are calculated assuming 25% availability and 10 years lifetime. Copper is supposed to be annealed to room temperature once every year. At the cumulative dose of 9.8×10^{-5} DPA for copper, the resistivity increase of copper becomes 2.5×10^{-8} ohm.cm at 4.2K and 12T field[9]. In the design of JXFR the above increase made the total resistivity at 4.2K, 12T to be 8×10^{-8}ohm.cm which was the design limit imposed by the magnet design.

As shown in Table 2.3.4, the inner model of Table 2.3.3 with the total bulk thickness of 71.5 cm satisfies all of the tentative criteria adopted for the SCM irradiation by a factor of two. This means the total shield thickness can be reduced a few centimeters if the present criteria proves to be reliable. But with the estimated error of the calculated result being a factor of 2, there is little sense in the reduction.

The minimum thickness of 71.5 cm is obtained under several limitations based on a thermal and structural analysis. By choosing the shield material considering only the shielding effectiveness, the shield thickness may be reduced another ten centimeters under the same tentative shielding requirement criteria. However 71.5 cm seems to be practical limit for a realistic design.

2.3.2 Second parametric survey

In the Workshop Session II, the annealing of toroidal magnets once every two years was considered to be too frequent because only a part of the defects in copper can be recovered by annealing. Therefore the inboard shield thickness was increased by 10 cm to make the total bulk shield thickness 81.5 cm.

Secondly, the composition of W(40%)+SS(30%)+Water(30%) was pointed out to be difficult to fabricate and also structurally inappropriate.

Thirdly, the additional cost and weight brought on by the use of tungsten and stainless steel was believed to be too large to offset the merit of making the reactor compact.

Considering the above three comments, four additional cases changing the composition of 50 cm bulk shield thickness in pair with the same 31.5 cm water cooled inner blanket were surveyed. The result of the calculations are summarized in Table 2.3.5. The composition of the Case W in the table is the same as the previous inner model of Table 2.3.3 with the thickness increased to 50 cm. The case W-HC, SS-HC and HC corresponds to more structurally feasible, fabricatable designs. The structure designs of the Cases W-HC and SS-HC are described in detail in Chapter 4 of this report. The result of Table 2.3.5 shows that with the Case W, there will be no need to anneal the magnet for 17 years, if the permissible accumulation is set at 9.8×10^{-5} DPA for copper. With the other three cases, the magnet must be annealed every 1.6 $\sim$ 2.5 years. Also the total neutron fluence and epoxy dose accumulation for the last three cases become close to the maximum allowable values listed in the second column of Table 2.3.4.

2.3.3 Radiation damage in the magnet

Distribution of copper DPA rate and epoxy dose rate in the Case W-HC inboard shield are shown in Figs. 2.3.1 and 2.3.2. The stainless steel DPA rate is also shown in Fig. 2.3.1. To obtain the copper DPA-rate per year,

$$10^{-24}(\mathrm{cm}^2/\mathrm{barn}) \times 5\times10^{16}(\mathrm{neutrons/s}) \times 3.15\times10^{7} \times 0.25(\mathrm{s/year}) = 0.394$$

must be multipled to the values in Fig. 2.3.1. Figure 2.3.2 shows that epoxy dose rate is predominantly due to neutron rather than gamma-rays in the magnet.

2.3.4 Summary

Although the inboard shield design was made more realistic from the viewpoint of structural design and fabrication technique, the neutronics characteristics of such designs were shown not to be satisfactory. In order to achieve the copper DPA rate less than 9.8×10^{-6} per year, either the thickness of the shield must be increased another 5 cm in the Case W-HC, 10 cm in the Cases SS-HC, or tungsten content must be increased.

Due to the short time allowed for this survey, only a limited range of material composition for the inboard shield has been investigated. There may be a better combination than the four listed in Table 2.3.5. Wider range of material composition together with iterations in the structure designs must be explored in order to obtain the optimum shield configuration.

Table 2.3.1 Composition of inner blanket and shield for JXFR[1]

Region No.	Region composition	Thickness(cm)
1.	Carbon coating	0.5
2.	Stainless steel (SS)	1.0
3.	Helium (He)	5.0
4.	SS	1.0
5.	SS(90%) + He(10%)	9.0
6.	SS(17%) + He(10%) + W(73%)	24.0
7.	SS	4.0
	Subtotal for the blanket	44.5
8.	Heavy concrete(90%) + Borated water(10%)	30.0
9.	SS(40%) + B_4C(40%) + H_2O(20%)	10.0
	Subtotal for the shield	40.0
	Total of the blanket and shield	84.5

Table 2.3.2 Optimization of inner blanket and shield

	Limitations	Case 1	Case 2	Case 3	Case 4	Case 5
Blanket	SS $\geq$ 30% Coolant $\geq$ 10% thickness 31.5cm	He-cooled	He-cooled	He-cooled	He-cooled	Water-cooled
Shield	SS $\geq$ 30% H_2O $\geq$ 10% thickness 40cm	SS 90% H_2O 10%	SS 30% H_2O 10% W 60%	SS 30% H_2O 20% W 50%	SS 30% H_2O 30% W 40%	SS 30% H_2O 30% W 40%
Cu-DPA [DPA/y]	10^{-4}*	3×10^{-4}	9×10^{-5}	5.5×10^{-5}	6.0×10^{-5}	4.3×10^{-5}

* If once a year annealing of the copper is allowed, the limit for the DPA-rate becomes ~10^{-4} DPA/year, corresponding to the resistivity increase of 2.5×10^{-8} Ω·cm.

Table 2.3.3 Composition of inner blanket and shield for the INTOR proposal

Region No.	Region composition	Thickness(cm)
1.	TZM protection wall	1.0
2.	SS tube wall	0.5
3.	SS(80%) + H_2O(20%)	10.0
4.	SS(90%) + H_2O(10%)	20.0
	Subtotal for the blanket	31.5
5.	SS(30%) + W(40%) + Borated water(30%)	40.0
	Subtotal for the shield	40.0
	Total of the blanket and shield	71.5

Table 2.3.4 Results of bulk shielding design calculations of superconducting magnets for the INTOR proposal

Items*)	Tentative design criteria	Values at inner SCM	Values at outer SCM**)
Maximum DPA in copper (DPA/year)	9.8×10^{-5}	4.3×10^{-5}	4.7×10^{-8}
Maximum neutron fluence (n/cm^2)	2.0×10^{18}	1.1×10^{18}	2.4×10^{15}
Maximum nuclear heating ($Watt/cm^3$)	10^{-3}	1.2×10^{-4}	2.4×10^{-7}
Maximum epoxy dose (rad)	2.4×10^{9}	1.2×10^{9}	1.5×10^{6}

*) Availability and the reactor lifetime are assumed to be 25% and 10 years, respectively.

**) The values at outer SCM surface should be multiplied by ~30 if the effect of neutron streaming through the injection ports are taken into account.

Table 2.3.5 Maximum nuclear characteristics value in the inner SC magnet for 4 types of inboard shield

Case name	W	W-HC	SS-HC	HC
Material composition	W 40% SS 30% Water 30% (Borated)	W 21.0% HC 21.0% SS 30.5% Water 27.5%	HC 21.0% SS 51.5% Water 27.5%	HC 42.0% SS 30.5% Water 27.5%
DPA in copper, DPA/year	5.78×10^{-6}	3.87×10^{-5}	5.72×10^{-5}	6.09×10^{-5}
Total neutron fluence, $n/(cm^2 \cdot 10years)$	2.26×10^{17}	1.45×10^{18}	2.02×10^{18}	1.74×10^{18}
Nuclear heating rate, $Watt/cm^3$	2.14×10^{-5}	1.07×10^{-4}	1.95×10^{-4}	2.29×10^{-4}
Epoxy dose, rad/10years	3.23×10^{8}	1.04×10^{9}	1.60×10^{9}	1.73×10^{9}

Availability and the reactor lifetime are assumed to be 25% and 10years, respectively.

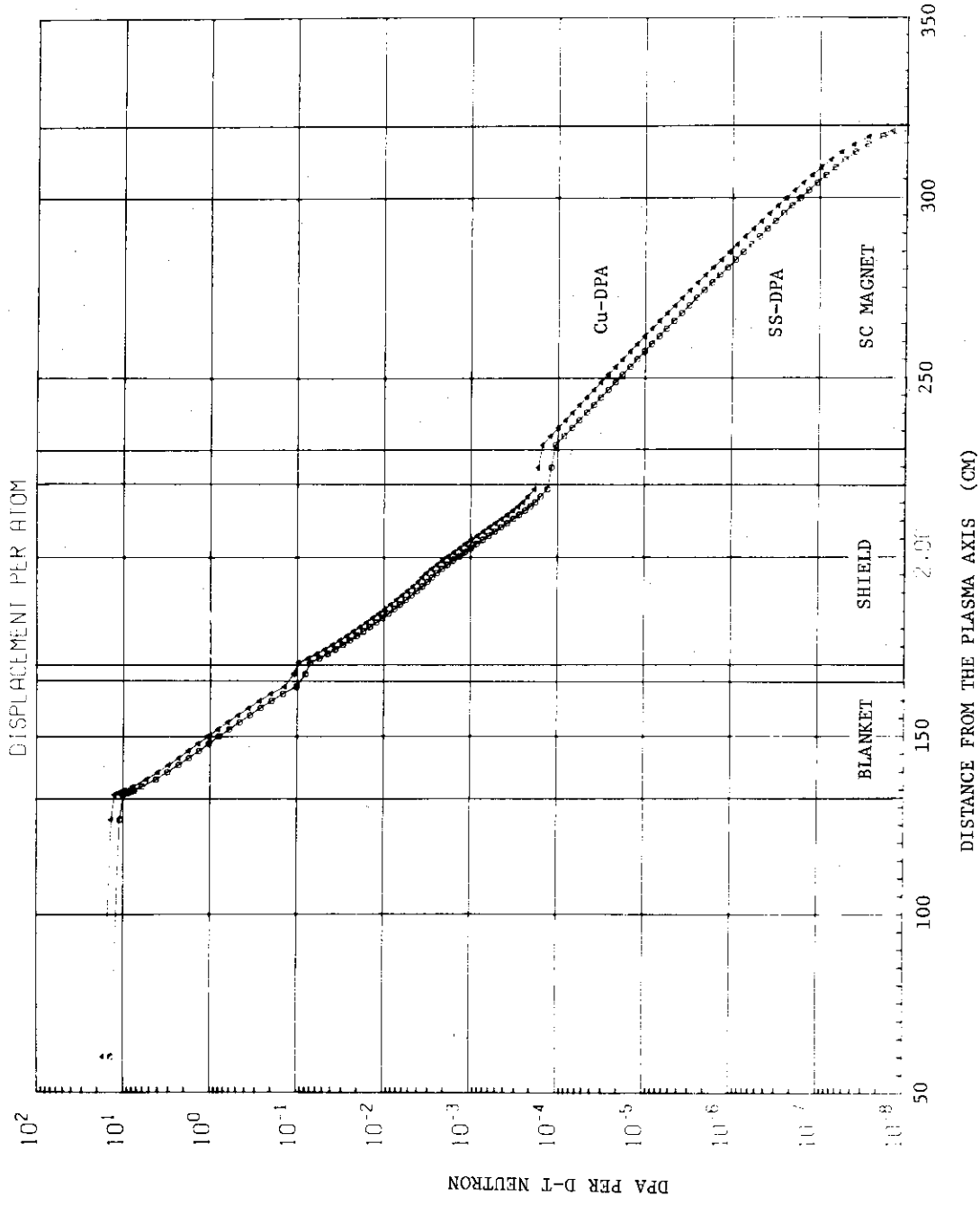

Fig. 2.3.1 DPA Rates of Stainless Steel and Copper in the Case W-HC Inboard Shield

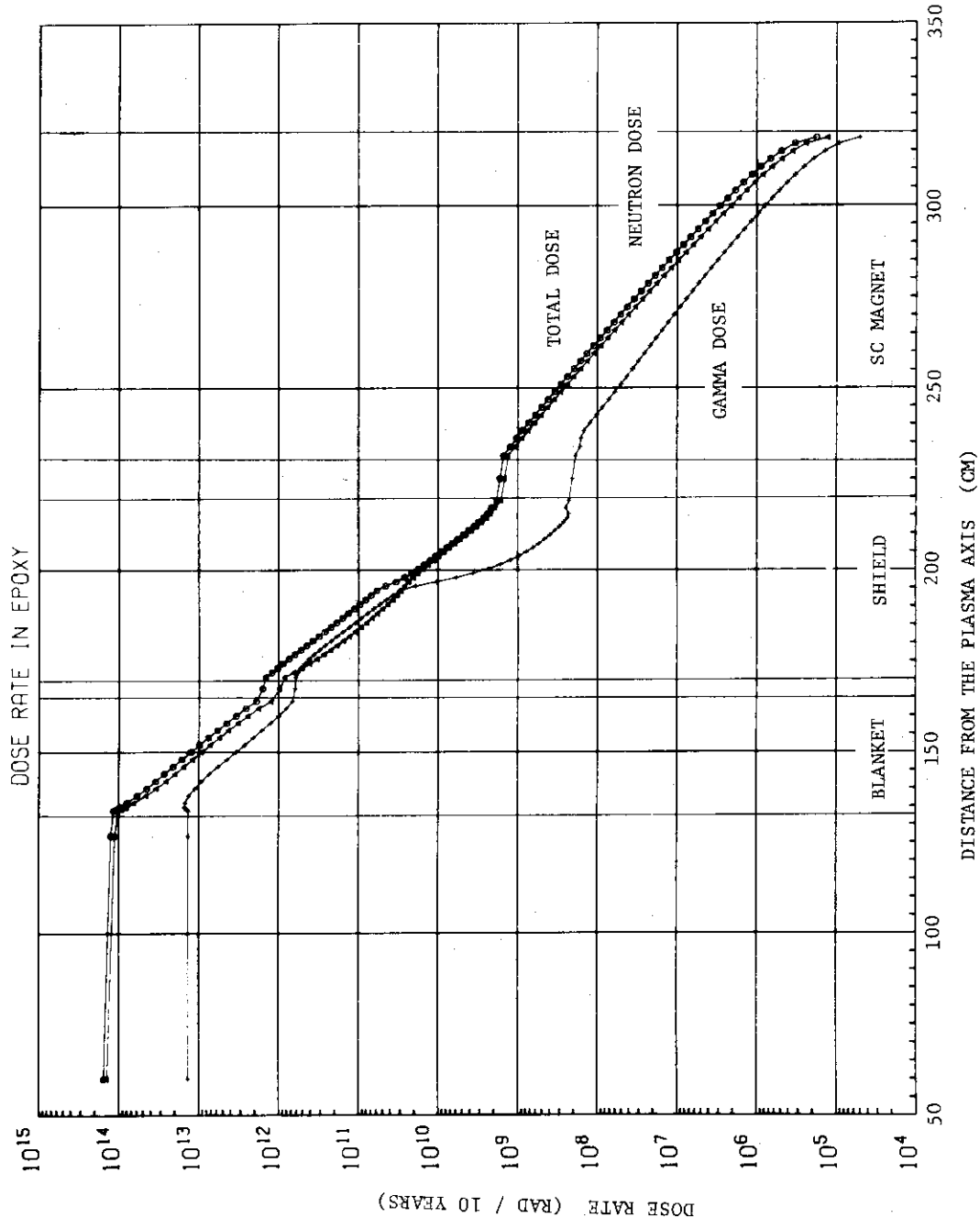

Fig. 2.3.2 Epoxy Dose Rate in the Case W-HC Inboard Shield

2.4 Neutron streaming through NBI port

Neutral Beam Injectors (NBI) are installed for plasma heating. As a path of neutral beam, a long vacuum duct region is constructed for each reactor module. Since neutral beam port directly connects ion source and a part of plasma which is the neutron source, the neutron which happens to proceed toward an ion source can easily reach the farthest portion of NBI. And this causes such nuisance as induced activity, radiation damage, nuclear heating and so on there. Therefore it becomes very important to estimate the magnitude of radiation which streams along NBI port.

Since NBI port has a very complicated configuration, it is almost impossible to estimate radiation streaming by Sn transport calculation. In the present work, an Albedo Monte Carlo (A.M.C.) method is used to obtain radiation streaming with reasonable computing time and core memory. An A.M.C. calculational method has been developed by improving the MORSE-I code[3] which is the revised version of the MORSE-GG code[10]. The code can treat torus geometry which is represented with biquadratic equation, as well as apply A.M.C. method which reduce computing time remarkably by omitting the calculation of particle random walk behind the albedo surface. Now the albedo data of stainless steel for the blanket plate, stainless steel with borated water for main shielding and heavy concrete for NBI shielding were prepared. And the A.M.C. calculation of NBI radiation streaming is now in progress. The object of this calculation is to obtain the following.

(1) Induced activity of ion source, neutralizing cell and cryo pump.
(2) Nuclear heating in cryo panels.
(3) Neutron and gamma-ray dose rates in ion source room.
(4) Required shielding thickness of NBI room.

REFERENCES

(1) Engle, W.W., Jr., "A User's Manual for ANISN, A One-Dimensional Discrete Ordinates Transport Code With Anisotropic Scattering", K-1693, Oak Ridge Gaseous Diffusion Plant (1967)

(2) RSIC Computer Code Collection, "DOT-3.5, Two Dimensional Discrete Ordinates Transport Code", CCC-276, Radiation Shielding Information Center, Oak Ridge National Laboratory (1976)

(3) Iida, H. and Yamauchi, M., Proc. 1978 Fall Meeting of the Atomic Energy Soc. of Japan, B35 (1978) (in Japanese)

(4) Seki, Y. et al., to be published.

(5) Drake, M.K., "Data Formats and Procedures for the ENDF Neutron Cross Section Library", BNL-50274 (T-601, TID-4500)(1970) Rev. 1974

(6) Ford, W.E., III., "The POPOP4 Library of Neutron-Induced Secondary Gamma-Ray Yield and Cross Section Data", CTC-42 (1970)

(7) Sako, K. et al., "First Preliminary Design of an Experimental Fusion Reactor", JAERI-M 7300 (1977)(in Japanese)

(8) Seki, Y., Iida, H. and Ide, T., "Evaluation of Shielding Design for Superconducting Magnets (III)", JAERI-M 6783 (1976)(in Japanese)

(9) Kulcinski, G.L. et al., "Wisconsin Tokamak Reactor Design", UWFDM-68 (1975)

(10) Straker, E.A., et al., "The MORSE Code - A Multigroup Neutron and Gamma-Ray Monte Carlo Transport Code", ORNL-4585 (1970).

3. Blanket

The design of the blanket has been carried out for the non-divertor system. In the case of the system with divertor, as the heat flux at the cooling panel is decreased by the amount of the heat flux to the divertor plate, there are some cases where the design of the cooling panel will be easy.

3.1 Design Conditions

(1) Outer Blanket
   a The coolant is water at 5 kgf/cm^2.
   b The coolant flows horizontally from one end of the outer blanket to the other.

(2) Inner Blanket
   a The coolant is water at 5 kgf/cm^2.
   b The coolant flows vertically from the lower side of the inner blanket to the upper side.

(3) Cooling Tube
   a The cooling tube which is provided at the plasma side on the inner and outer blanket is cooled by water at 5 kgf/cm^2.
   b The flow direction of the coolant is similar to the one of each blanket.

(4) Heat Flux and Nuclear Heating Rate
   a The maximum heat flux is 30 w/cm^2.
   b The maximum nuclear heating rate is 12 w/cc.

3.2 Blanket Structure

Non-breeding blanket which surrounds a plasma serves for a cooling and shielding purpose. It consists of six blanket modules, as shown in Figs. 3.2.1 and 3.2.2. Each module is formed with inner and outer blanket. The inner blanket is shown in Fig. 3.2.3 and the outer blanket is shown in Fig. 3.2.4. A cooling panel is provided at the plasma side of the blanket.

The inner blanket, which is 30 cm in thickness and is made of Type 316 stainless steel, consists of six modules. Each module is formed with 16 blanket blocks. Each block is formed with the layers of two plates that the cooling tube is sandwiched between the gap of the two semicircle. The gap between the inside of the plate and the outside of the cooling

tube will be brazed in order to increase the thermal conductivity.

The structure of the outer blanket is similar to the inner blanket.

The cooling panel is formed with a membrane wall structure which is assembled with a lot of fin-tubes having a small diameter made of Type 316 stainless steel.

A protection wall, which will be made of a semicircular TZM, is attached in a line at the plasma side of the cooling panel.

The inlet and outlet of each blanket and the cooling panel are collected with a common header and the coolant is transported to the cooling system being separated into two lines.

3.3 Design Analysis

3.3.1 Blanket Design Analysis

One dimensional steady state thermal analysis has been carried out to decide the cooling tube arrangement of the inner and outer blankets.

Using this configurations, thermal analysis with two dimension and transient thermal analysis with one dimension have been also carried out.

(1) One Dimensional Thermal Analysis

Fig. 3.3.1 and 3.3.2 shows the temperature distributions obtained from the following conditions.

$$q = q_0 e^{-0.105 \times}, \quad q_0 = 11 \text{ W/cc}$$

where $\times$ is a distance from the wall of the plasma side (cm).

Flow rate is 0.5 m/sec.

The coolant temperature is 90°C.

(2) Thermal Analysis with Two Dimensional Model

Fig. 3.3.3 shows the analytical model and Fig. 3.3.4 shows the results of the temperature distribution.

(3) Transient Thermal Analysis with One Dimensional Model

Fig. 3.3.5 shows the analytical model and Figs. 3.3.6 and 3.3.7 show the results.

3.3.2 Cooling Panel Design Analysis

Two types of water cooling panels have been considered.

(1) Cooling Panel Type A

Fig. 3.3.8 shows the analytical conditions of Type A. Fig. 3.3.9 shows the temperature distribution and Fig. 3.3.10 shows the transient temperature change.

(2) Cooling Panel Type B

Fig. 3.3.11 shows the analytical conditions of Type B. Figs. 3.3.12 and 3.3.13 show the temperature distributions. Fig. 3.3.14 and Fig. 3.3.15 show the transient temperature change.

3.3.3 Stress Analysis of Outer Blanket

The elastic thermal stress analysis of the outer blanket has been carried out under temperature distribution during operation which was already shown in Fig. 3.3.4.

Fig. 3.3.16 shows the analytical model of the outer blanket. An axisymmetrical finite element was employed for the stress analysis. The internal pressure in the cooling tube was not considered because the pressure is very small 0.05 kgf/mm^2).

The material properties of Type 316 stainless steel at 150°C were used and Young's modulus is 18,800 kgf/mm^2, Poisson's ratio ν is 0.3 and mean coefficient of thermal expansion α is 1.7×10^{-5}/°C, respectively.

The boundary conditions are as follows;

(1) the lower side in Fig. 3.3.16 is fixed in Z direction, but is free in R direction.

(2) the upper side in Fig. 3.3.16 is free in R and Z directions or is similar to the lower side.

In the above boundary condition (2), the former is named case 1 and the latter is named case 2.

Figs. 3.3.17-a and 3.3.17-b show the pre and post deformations of case 1 and case 2. Figs. 3.3.18-a and 3.3.18-b show the distributions of the stress intensities of case 1 and case 2.

In case 1, the maximum stress is generated at point A and the stress intensity is 9.8 kgf/mm^2. In case 2, the maximum stress is generated at point B and the stress intensity is 26.9 kgf/mm^2.

As the effect of the flange, which is provided to fix the outer blanket, was not considered for the above boundary conditions, it seems that the two values obtained from the stress analysis in this section.

The inner blanket is a similar shape to the outer blanket and has a similar temperature distribution during operation. Therefore, it seems that the stress which is similar to the outer blanket will generate.

Thermal cyclic fatigue of the blanket seems to be allowable from above results.

3.4 Alternative Design

When the first wall receives high heat flux from plasma, there will be a large temperature gradient which causes large deformation and/or thermal stress around it. One of the methods to avoid this problem is to use a cooling panel which consists of the SS cooling tubes covered with sleeves made of high thermal conductivity materials such as Cu, Al, Mo and their alloys. They can be attached by brazing.

TZM is chosen as the sleeve material in the thermal analysis. Special processing, for example using stripe type sleeve is necessary to reduce thermal stress and/or deformation caused by the difference in thermal expansion between SS and TZM. Stainless steel blanket structure and cooling panel are unificated by brazing in this design. High integrity brazing is necessary and special design consideration such as the use of block wise sleeves is also necessary. It is necessary to investigate the fabrication process to decide whether these panels can be separated from blanket structure or not. Such investigation is a future task. Thermal analysis is made under the conditions of the reactor with divertor. This structure is tolelable against higher heat load. Furthermore, it has the possibility to eliminate the use of protection walls.

(1) Conditions for Analysis

Heat Load

Radiation	15 W/cm^2 on the first wall (with divertor)
Neutron	15.6 W/cc around the first wall
Coolant	Water, 100°C, 10 kg/cm^2

(2) Structure

The cross section of a block is shown in Fig. 3.4.1

(3) Results of Analysis

Figure 3.4.2 shows steady state temperature distribution in the first layer of the inner blanket. Figure 3.4.3 shows steady state temperature distribution in the third layer of the inner blanket. Maximum temperature on the surface of the inner blanket is 149°C and temperature difference in the first layer is about 30°C. Therefore, cooling of the inner blanket presents no problem from thermal point of view.

3.5 Design Problem

3.5.1 Main Fabrication Technique

(1) Inner and Outer Blanket

Inner blanket consists of Type 316 block, cooling tube and header. In the fabrication of inner blanket, automatic orbital TIG welding technique of butt joint of small-sized tube (12 mm and 1 mm in outside diameter and wall thickness, respectively) and automatic brazing technique of this tube and block are considered to be main fabrication technique.

In the TIG welding of small-sized tube, it is clamped by the welding head specially desired and welded by automatically rotating electrode. In this welding procedure, it is designed due to close tube arrangement and its thin wall thickness that automatic high-integrity orbital TIG welding technique, such as, controlling technique of shield gas pressure is applied without filler metal by the special welding machine with very compact welding head.

Meanwhile, brazing foil material is wrapped uniformly around the tube, and then tube bundle is pressed by one pair of block with many semicircular grooves machined. Later, hydraulically internal pressure is applied to the tube so that brazing foil material wrapped around the tube come closely into contact with the groove surface. Brazing is performed automatically by feeding tube bundle and block into the furnace of inert gas atmosphere.

(2) Cooling Panel

Cooling panel consists of fin tube and protection wall. Straight fin tubes are joined with each other by fin-to-fin electron beam welder, and bent in the ambient temperature. Protection wall is completed by attaching semi-circular TZM piece continuously around the cooling tube.

The fin tube is produced by hot extrusion and following cold drawing. However, single cold drawing causes large tolerance on wall thickness around 50% which results from cross-sectional unsymmetry with respect to point. Therefore, fin tube should be produced by several times of cold drawing process.

This fin tube is joined to the stub which is welded to the header. This is the same technique as the automatic TIG welding of small-sized tube mentioned in inner blanket.

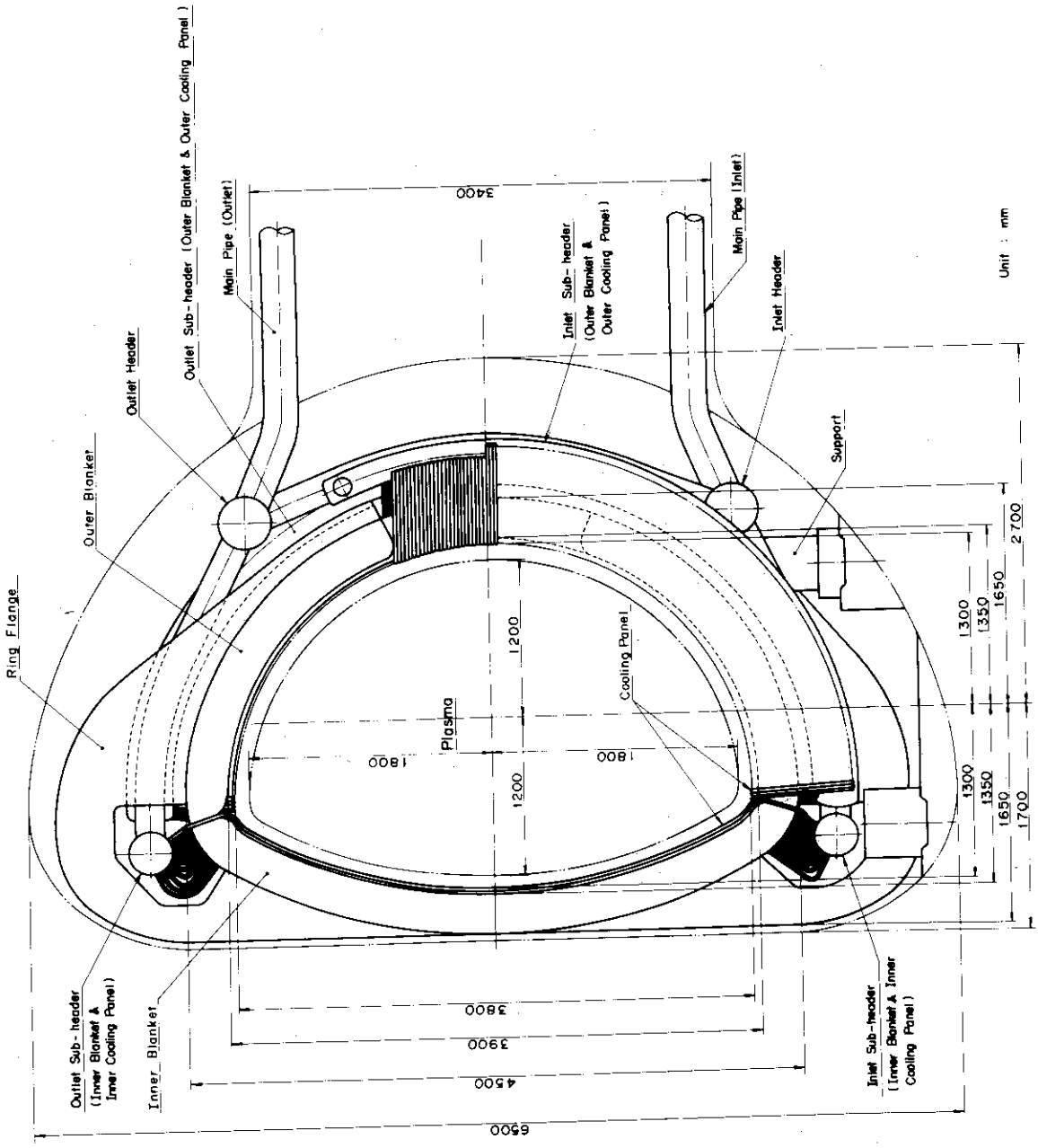

Fig. 3.2.1 Side View of Blanket Module

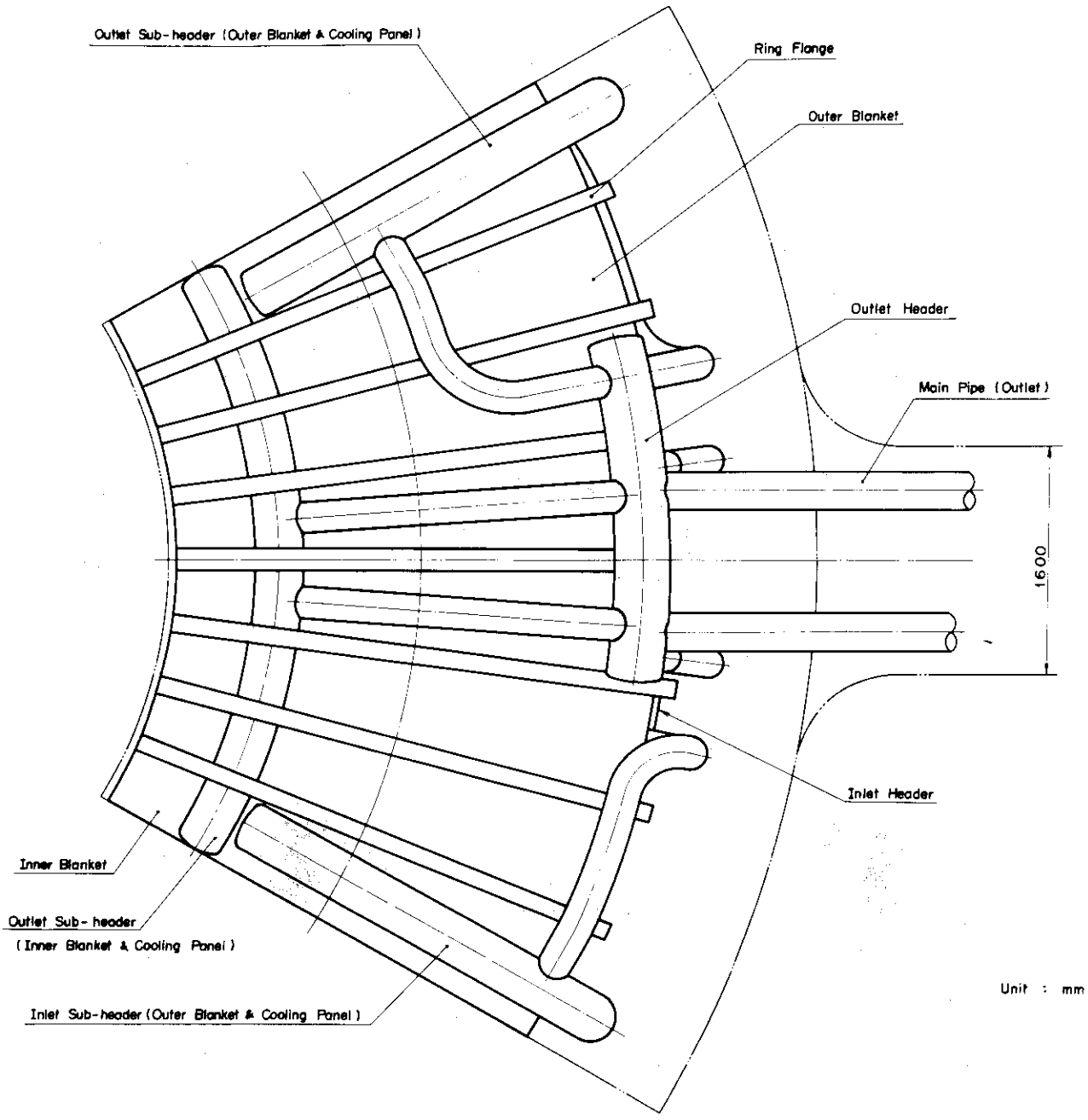

Fig. 3.2.2 Plane View of Blanket Module

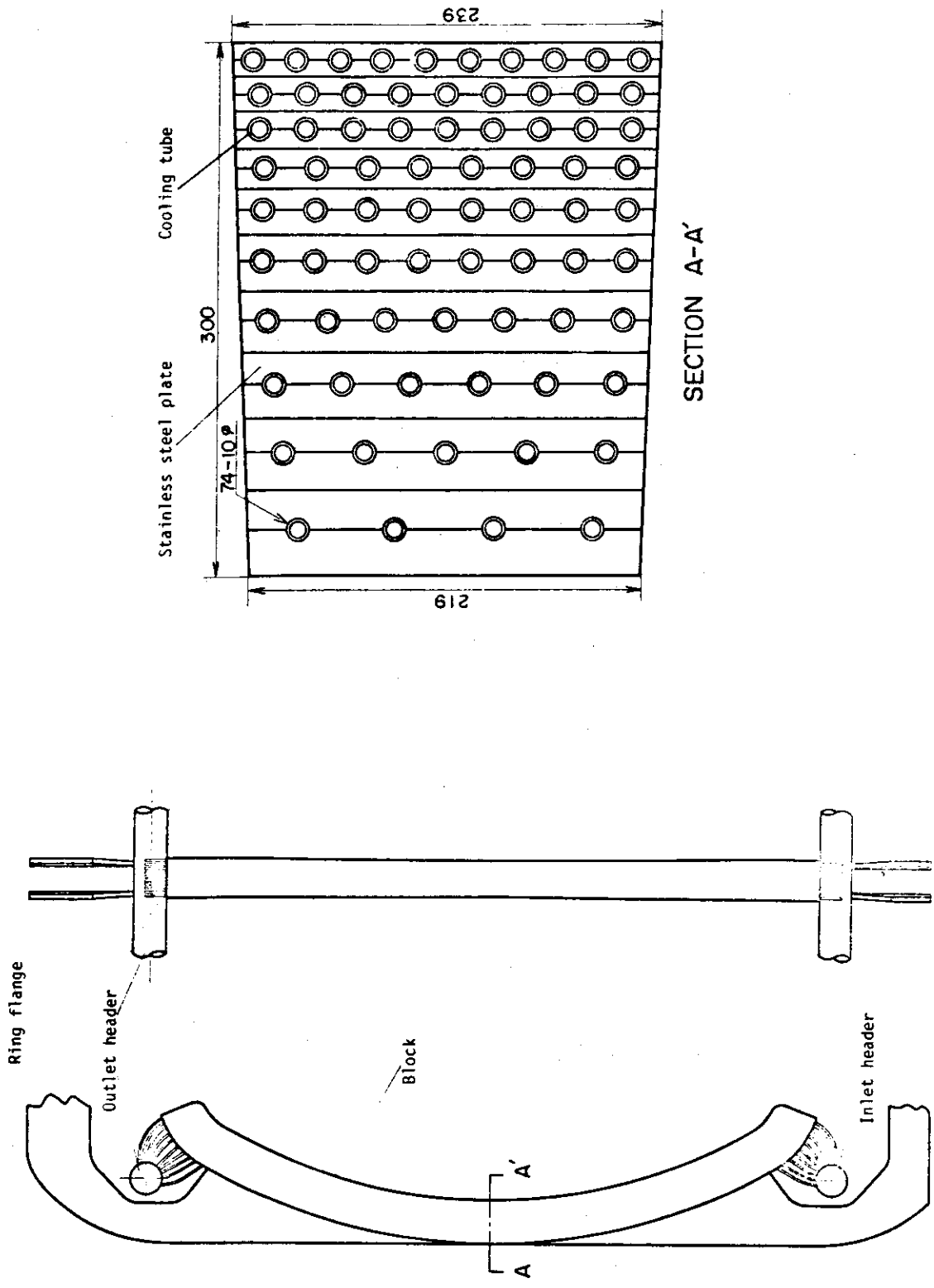

Fig. 3.2.3 Inner Blanket Ring

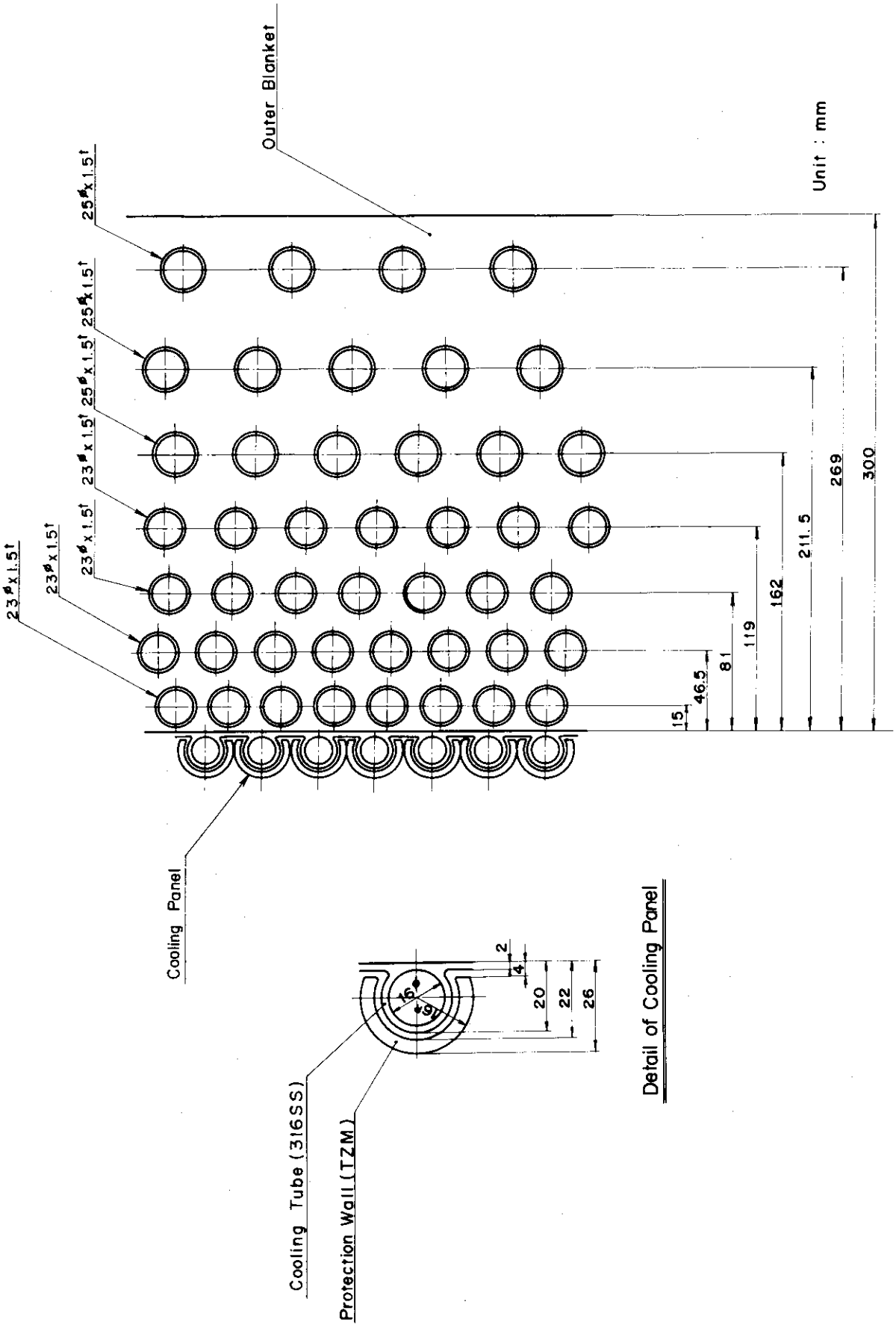

Fig. 3.2.4 Cross Section of Outer Blanket

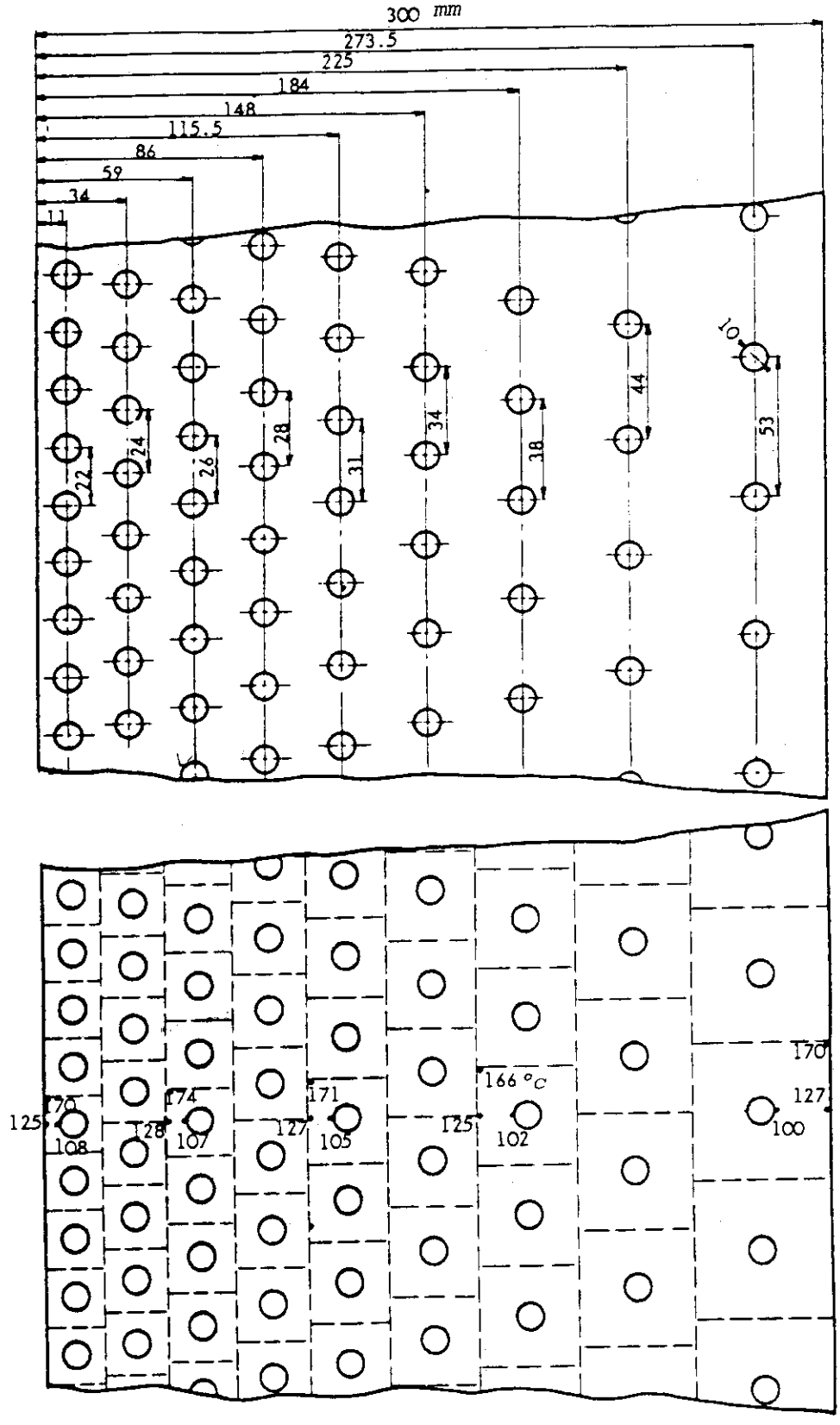

Numerical values show the temperatures (°C) at each point (•)

Fig. 3.3.1 Temperature Profile of Inner Blanket

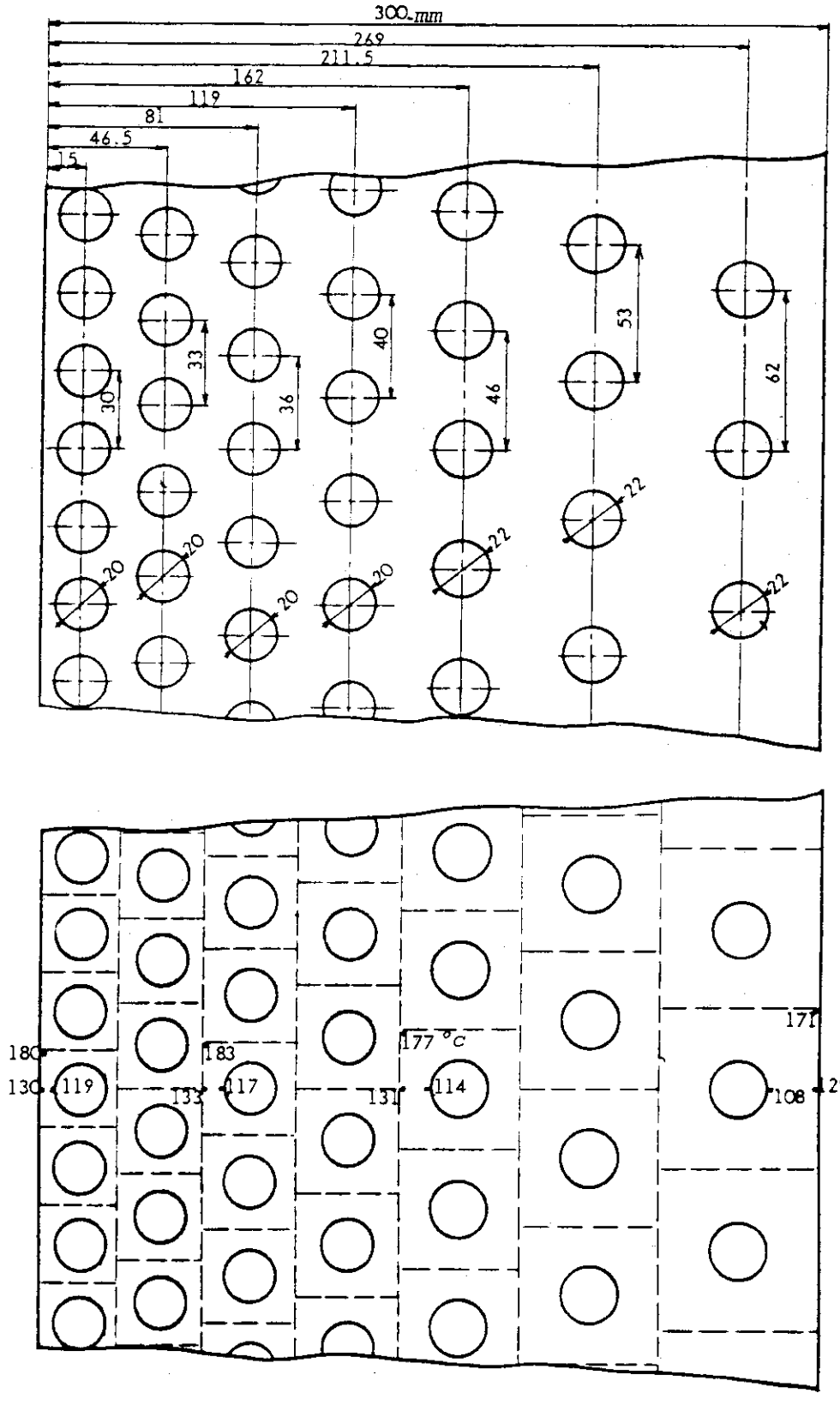

Fig. 3.3.2 Temperature Profile of Outer Blanket

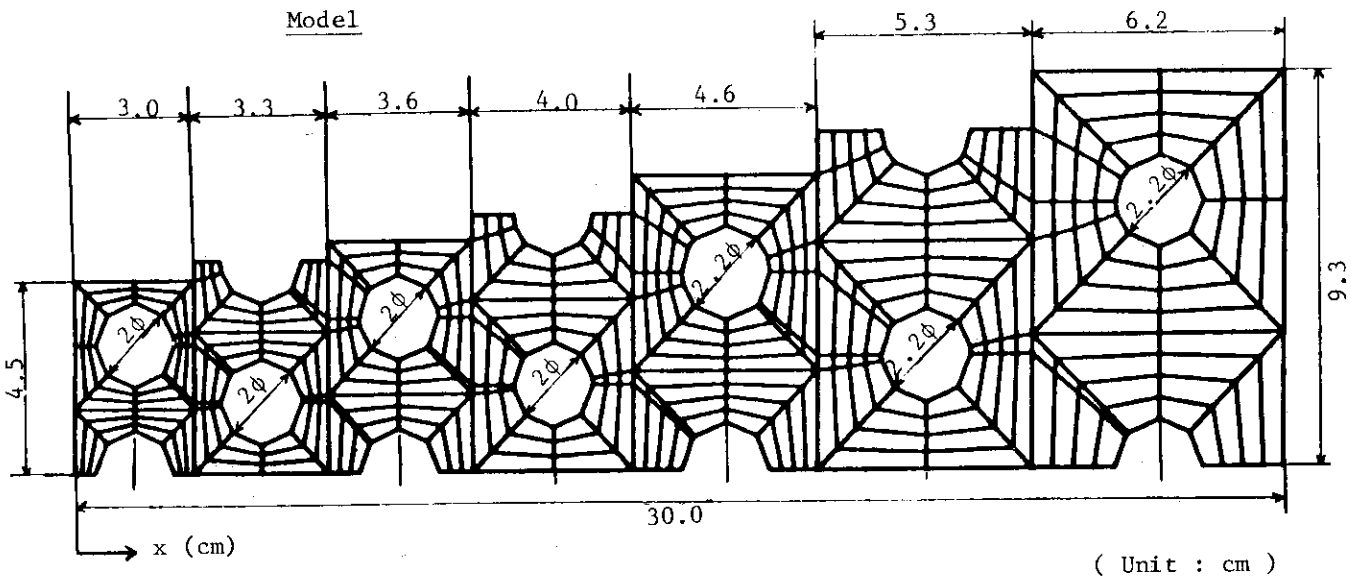

(Unit : cm)

Fig. 3.3.3 Analytical Model

Heat Generation Rate :

$11\ e^{-0.1x}$ W/cc

Thermal Conductivity :

0.036 cal/cm s °C

Coolant Temperature :

90 °C , H_2O

Heat Transfer Coefficient :

0.101 $cal/cm^2 s°C$ (2 cm dia.)

0.085 $cal/cm^2 s°C$ (2.2 cm dia.)

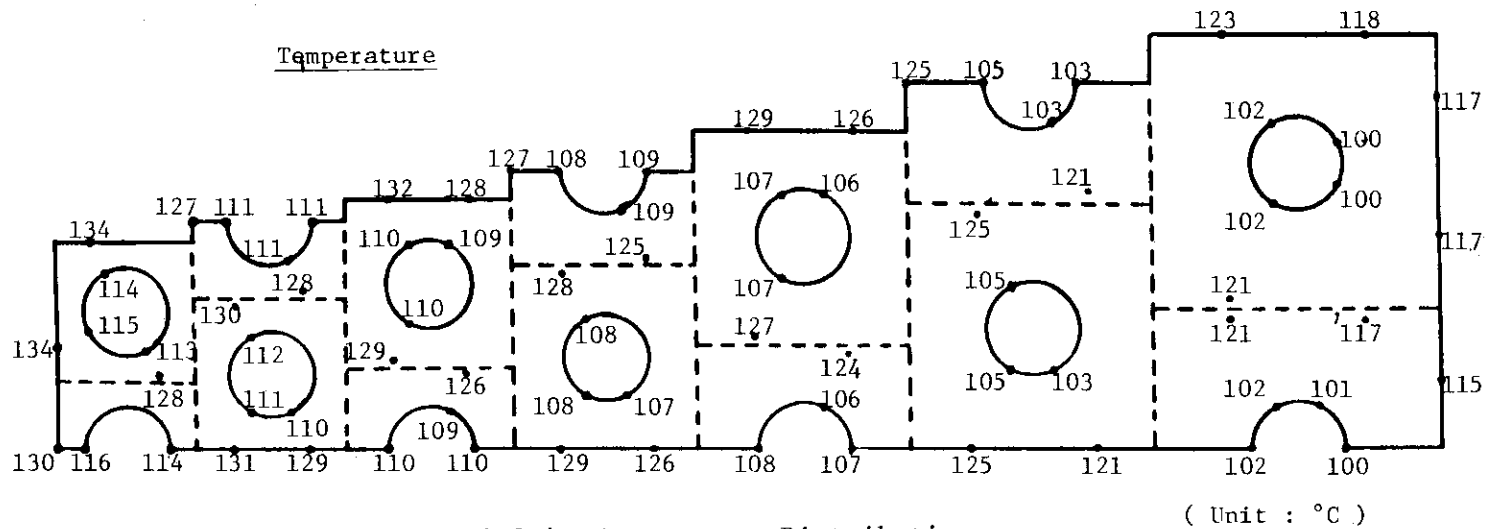

(Unit : °C)

Fig. 3.3.4 Temperature Distribution

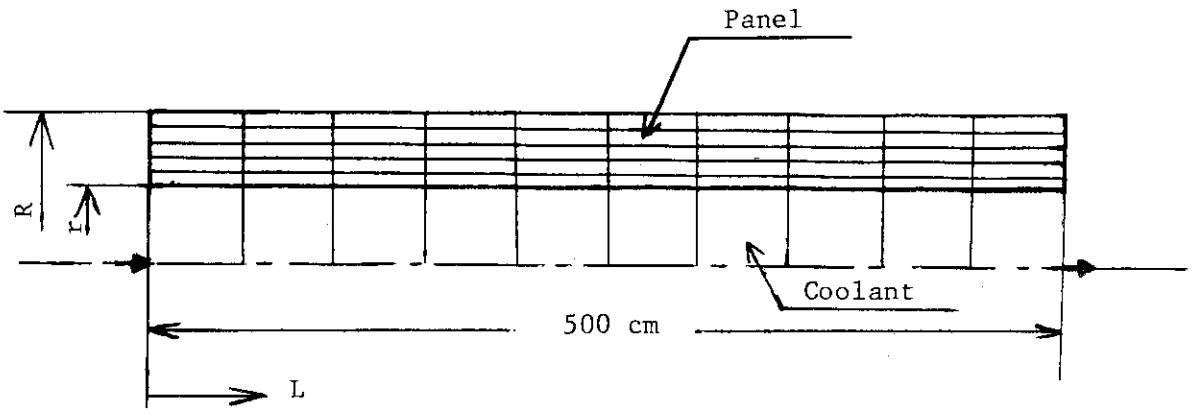

	Case 1	Case 2	Case 3
x (cm)	1.5	11.9	26.9
q (W/cc)	8.47	3.04	0.69
r (cm)	1.0	1.0	1.1
R (cm)	1.693	2.257	3.498
h (cal/cm^{2}s°C)	0.101	0.101	0.085

x : distance from top (see in Fig. 3.3.3)

q : heat generation rate $q = 11\ e^{-0.1x}$

r : inner radius

R : outer radius (equivalent)

h : heat transfer coefficient

Coolant ; H_2O

inlet temperature : 40 °C

flow rate : 161.5 g/s

Panel ; 316SS

thermal conductivity : 0.036 cal/cm s °C

heat capacity : 0.13 cal/g°C

density : 8.0 g/cc

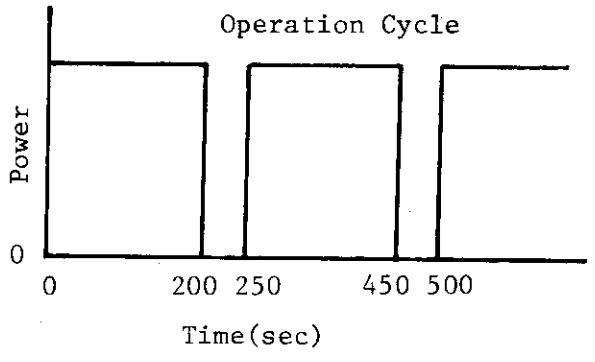

Fig.3.3.5 Analytical Model for Thermal Analysis

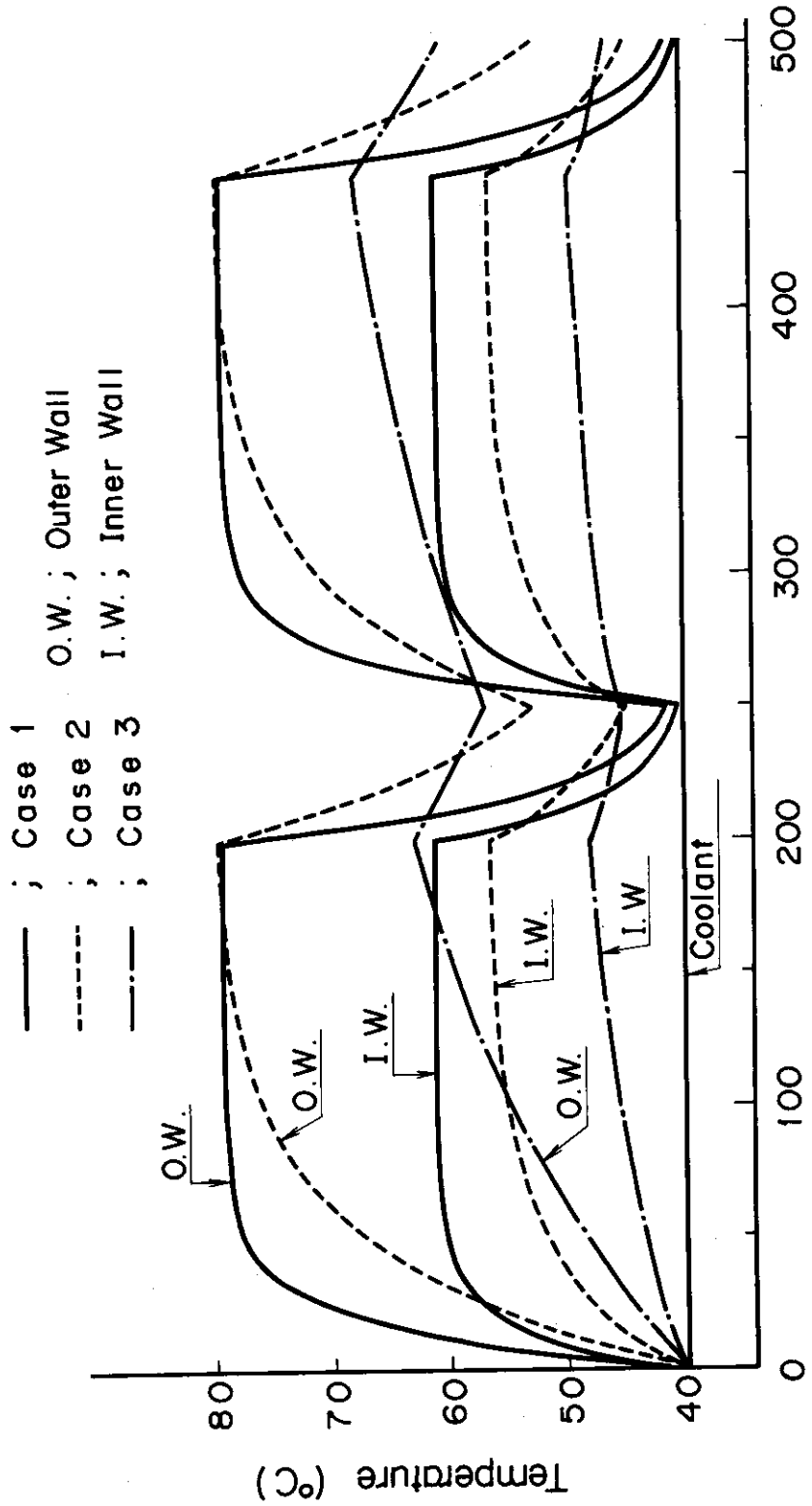

Fig. 3.3.6 Temperature Change at Coolant Inlet (L=0m)

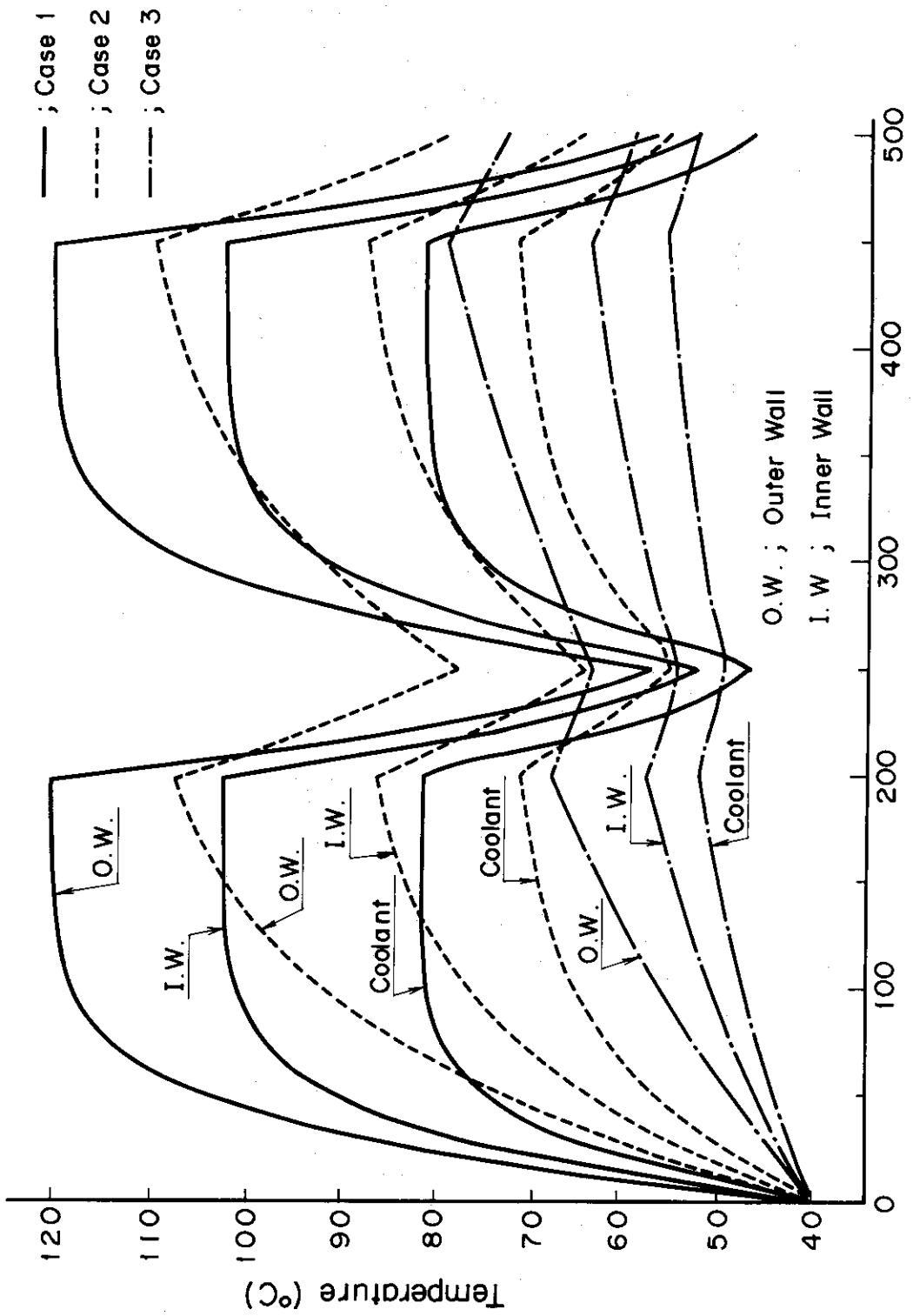

Fig. 3.3.7 Temperature Change at Coolant Outlet (L=5m)

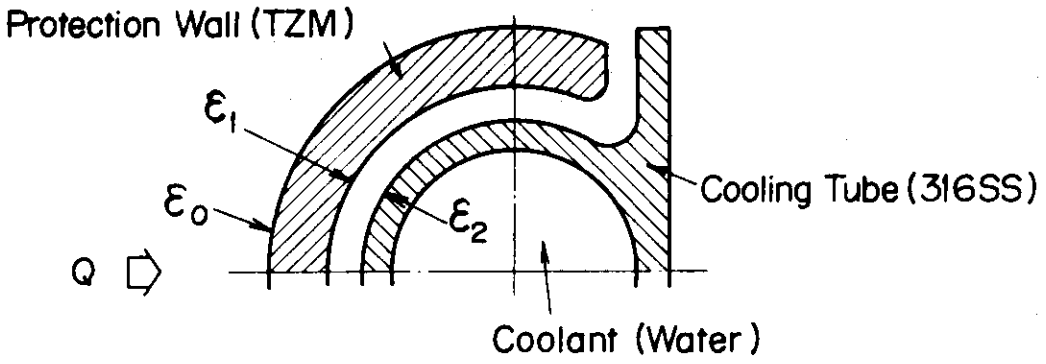

Souface Heat Flux: 30 W/cm^2(Flat top)

Heat Generation Rate: 12 W/cc(")

Radiation; $\varepsilon_0 = 0.4$ $\varepsilon_1 = 0.7$, $\varepsilon_2 = 0.7$

Coolant; H_2O
Temperature: 90°C, Flow Velocity: 5 m/s
Heat Transfer Coeff.: 0.65 cal/cm^{2}s°C

Material;	316SS	TZM
Thermal Conductivity(cal/cm s°C)	0.036	$0.34-9.09\times10^{-5}\cdot t$(t:°C)
Heat Capacity (cal/g°C)	0.13	0.068
Density (g/cc)	8.0	10.2

Fig. 3.3.8 Analytical Conditions of Type A

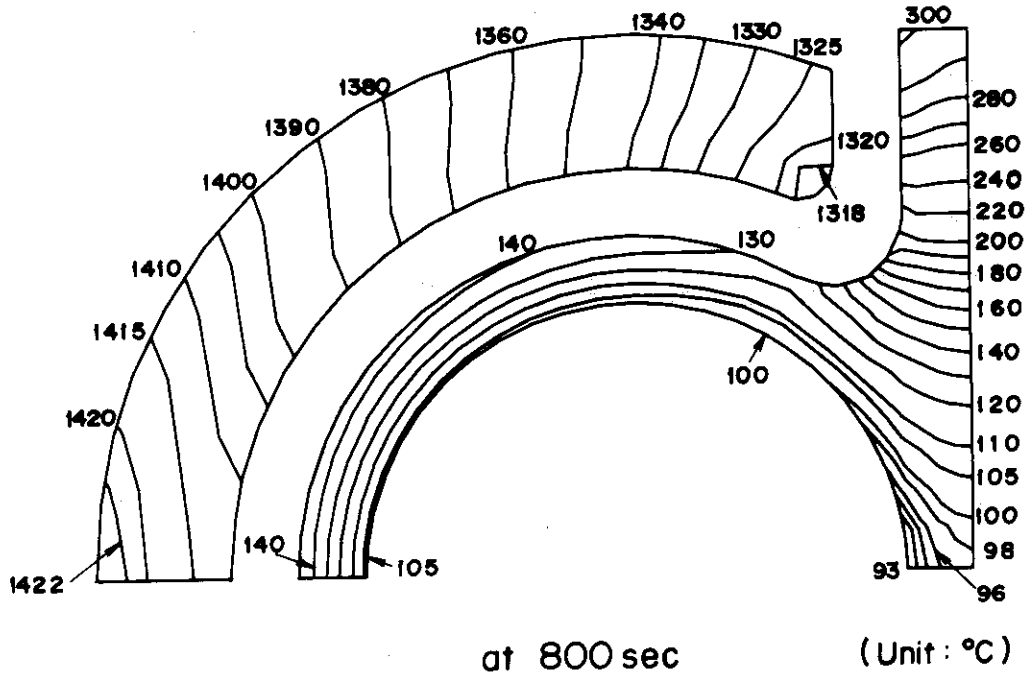

Fig. 3.3.9 Temperature Distribution

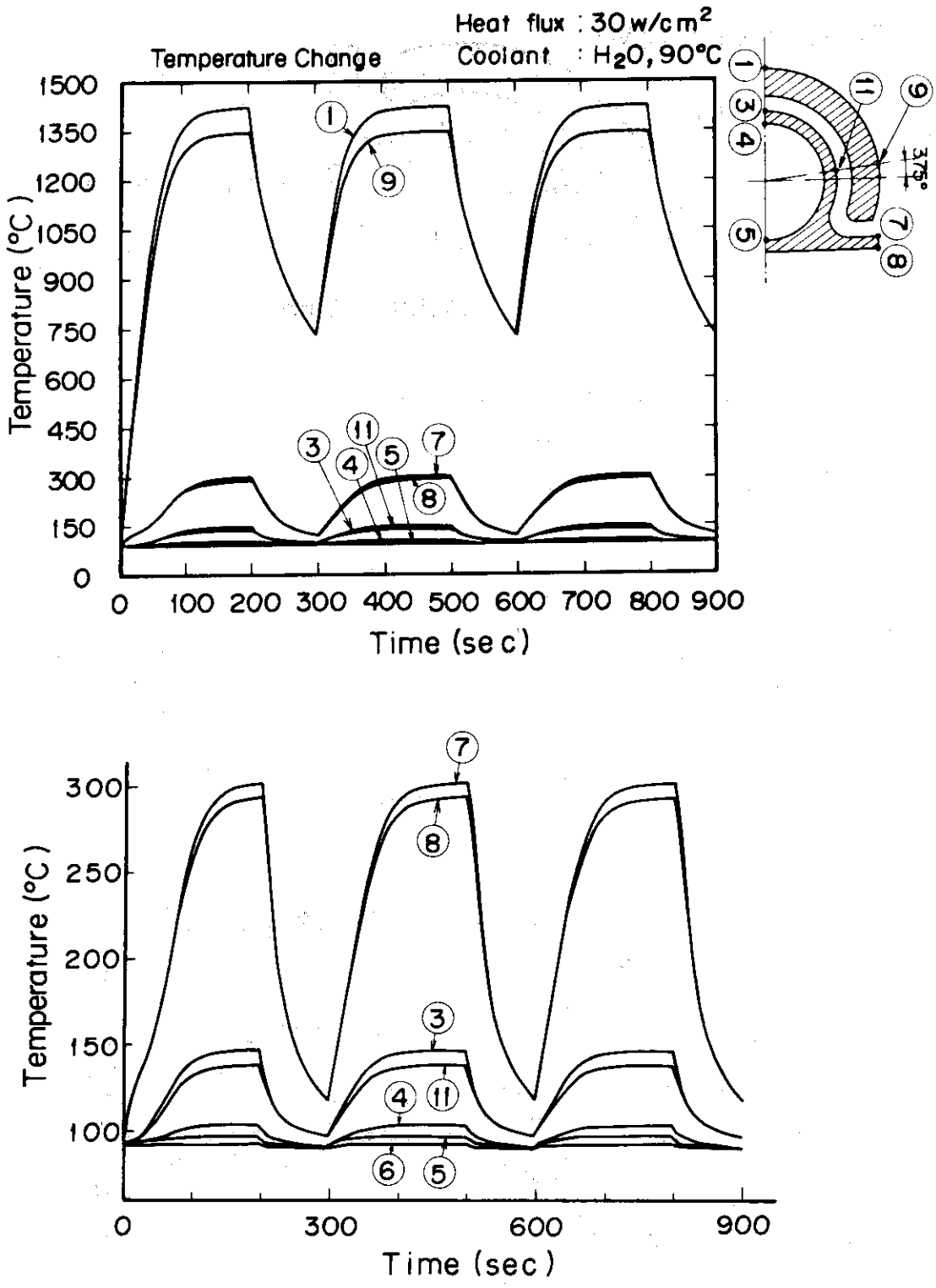

Fig. 3.3.10 Transient Temperature Change

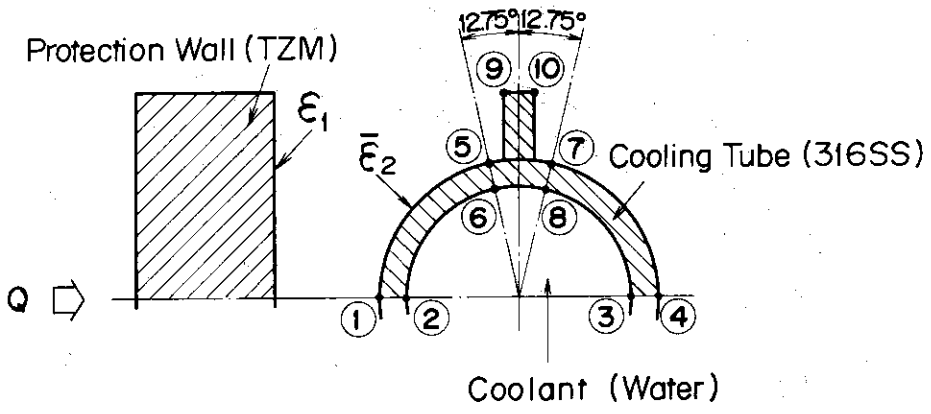

Surface Heat Flux: 30 W/cm^2(Flat top)

Heat Generation Rate: 12 W/cc(")

Radiation; ε_1 = 0.7, $\bar{\varepsilon}_2$ = 0.75 (P/D=1.25)

$\bar{\varepsilon}_2$ = 0.745(P/D=1.5)

Coolant; H_2O

Temperature: 90°C, Flow Velocity: 5 m/s

Heat Transfer Coeff.: 0.65 cal/cm^{2}s°C

Material;

	316SS	TZM
Thermal Conductivity(cal/cm s°C)	0.036	$0.34-9.09\times10^{-5}\cdot t(t:°C)$
Heat Capacity (cal/g°C)	0.13	0.068
Density (g/cc)	8.0	10.2

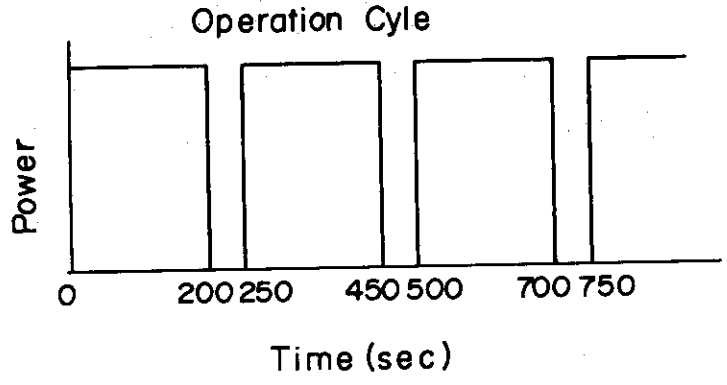

Fig. 3.3.11 Analytical Conditions of Type B

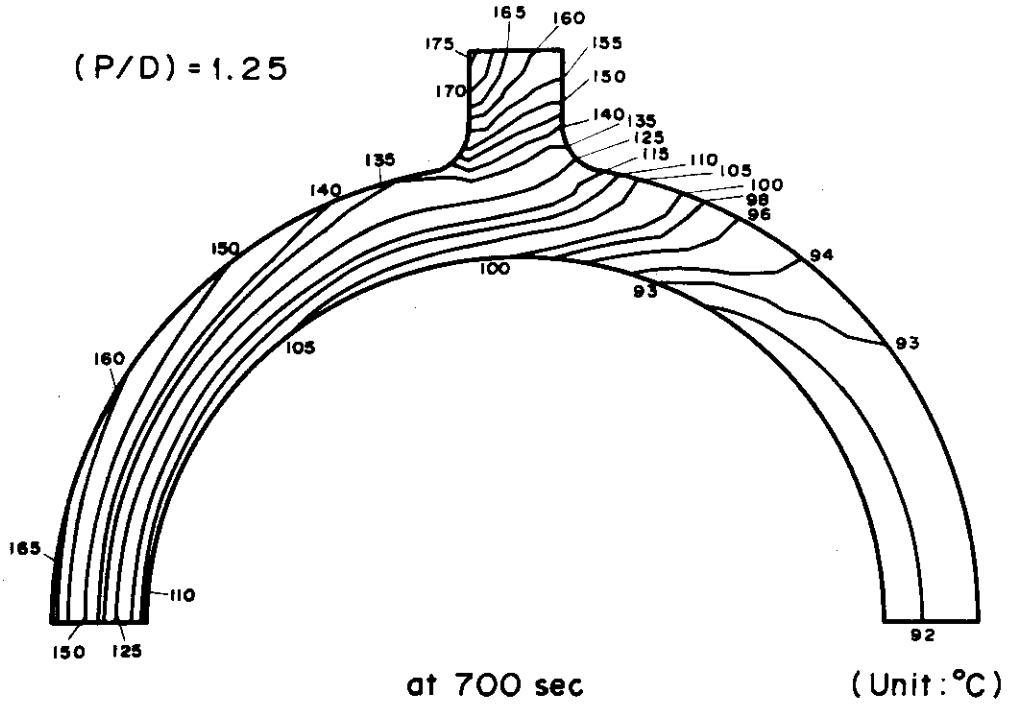

Fig.3.3.12 Temperature Distribution (P/D=1.25)

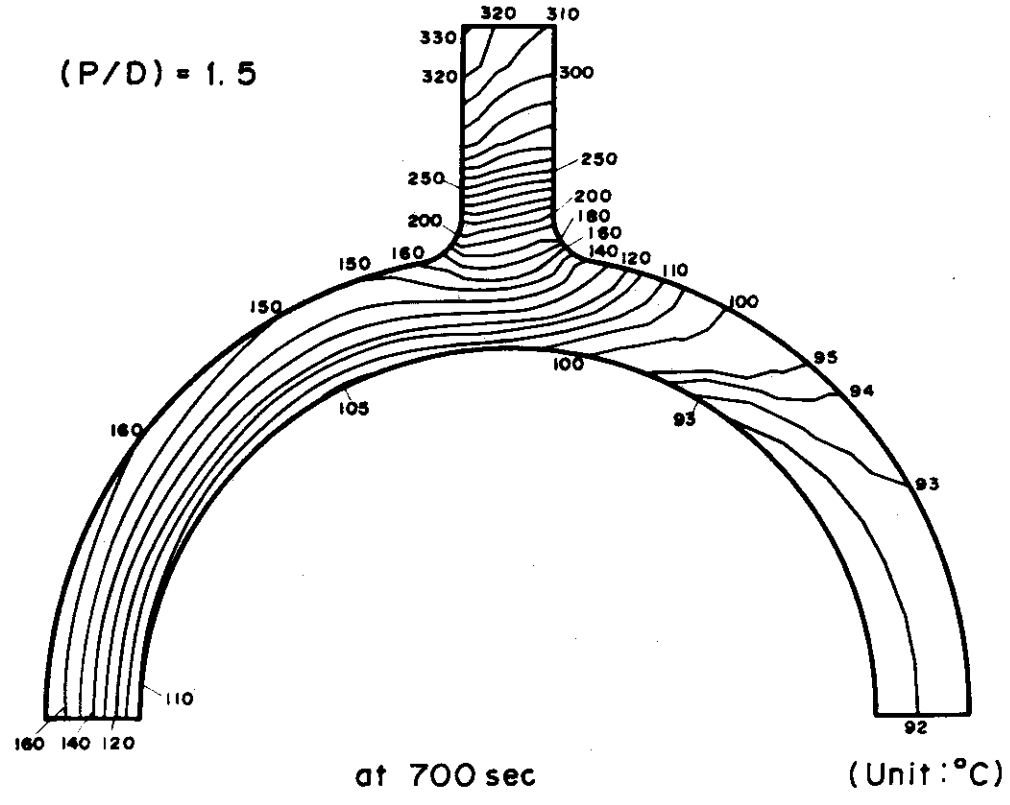

Fig.3.3.13 Temperature Distribution (P/D=1.5)

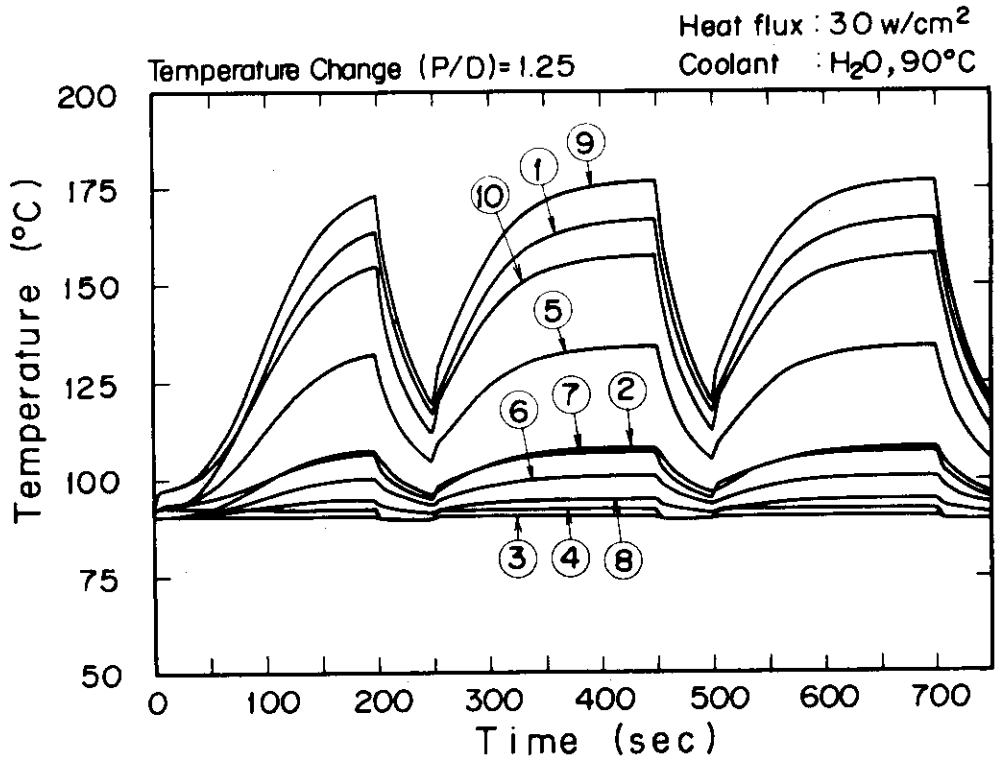

Fig. 3.3.14 Transient Temperature Change (P/D=1.25)

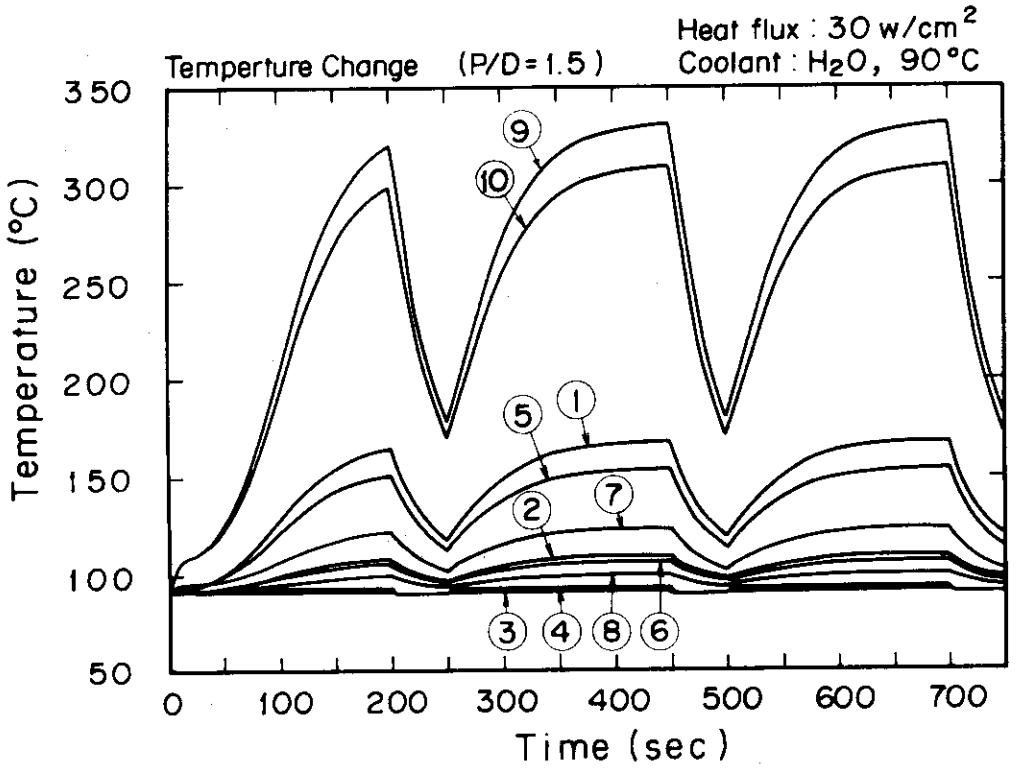

Fig. 3.3.15 Transient Temperature Change (P/D=1.5)

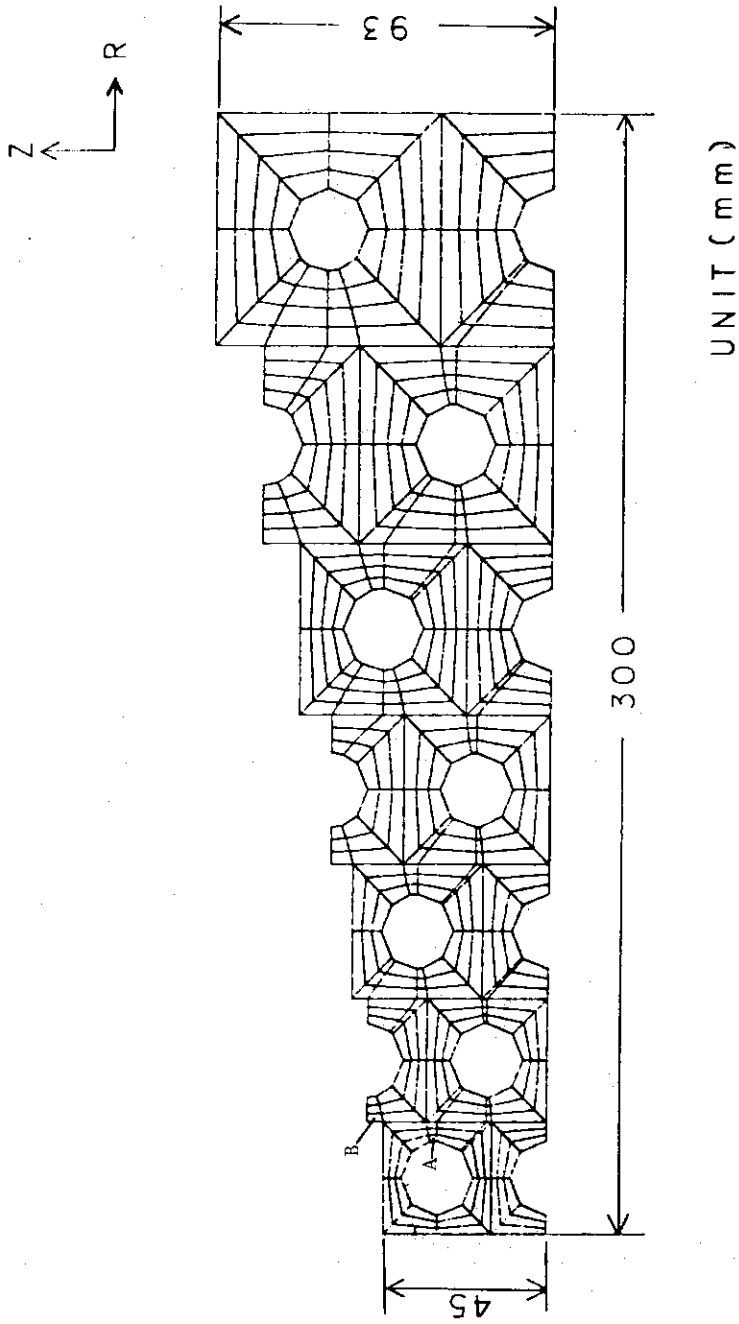

Fig. 3.3.16 Stress Analysis Model

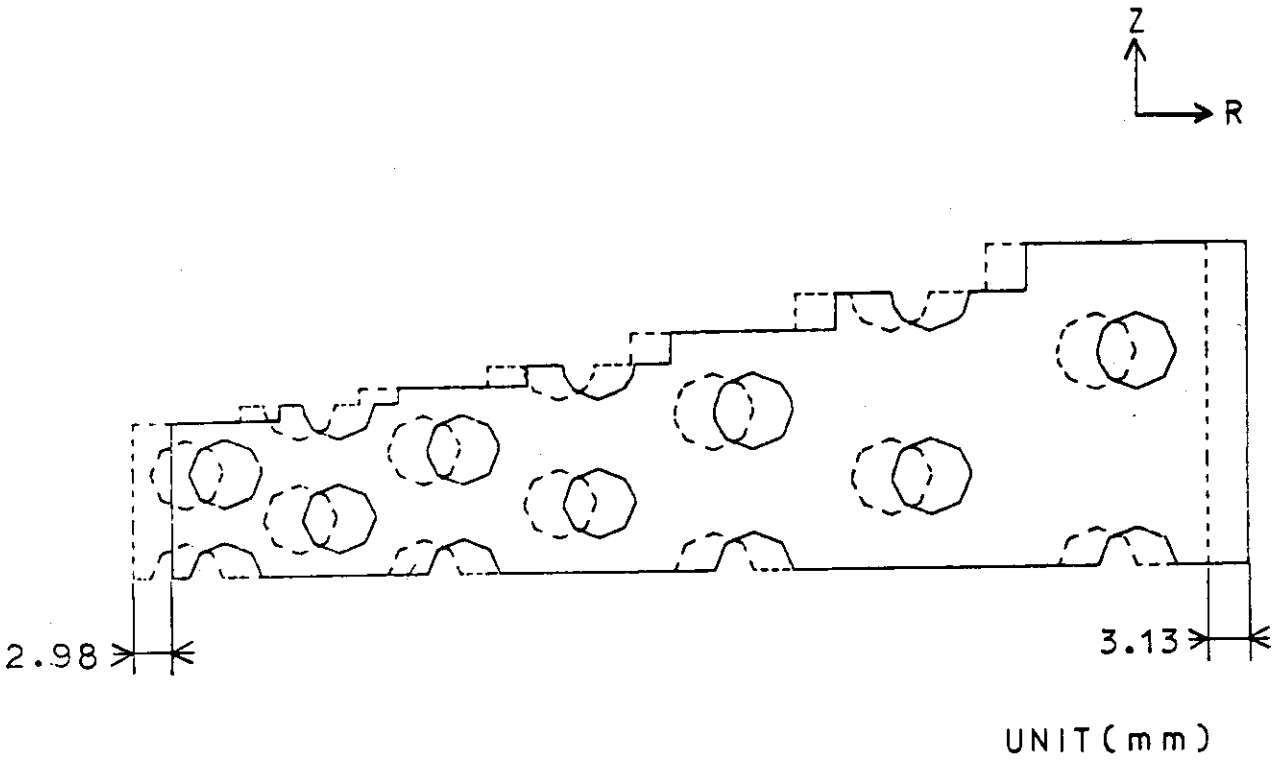

Fig. 3.3.17-a Shape of Pre and Post Deformation Case No. 1

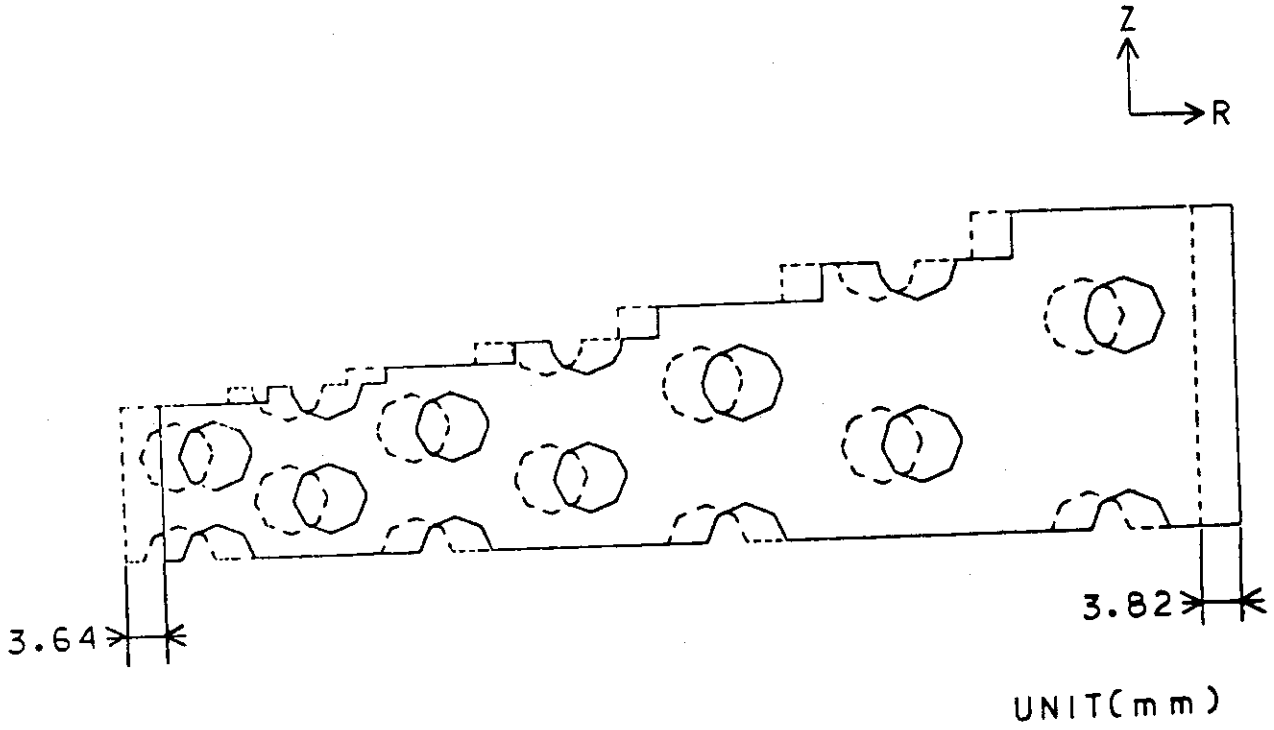

Fig. 3.3.17-b Shape of Pre and Post Deformation Case No. 2

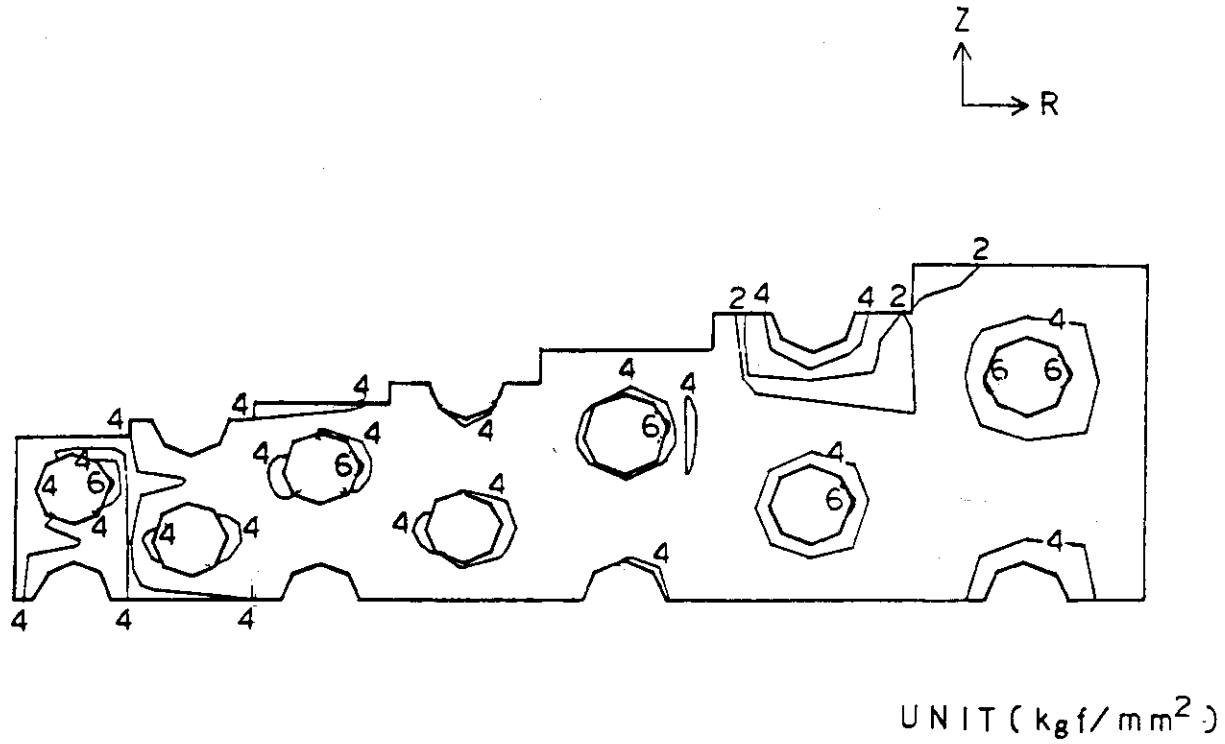

Fig. 3.3.18-a Distribution of Stress Intensity Case No. 1

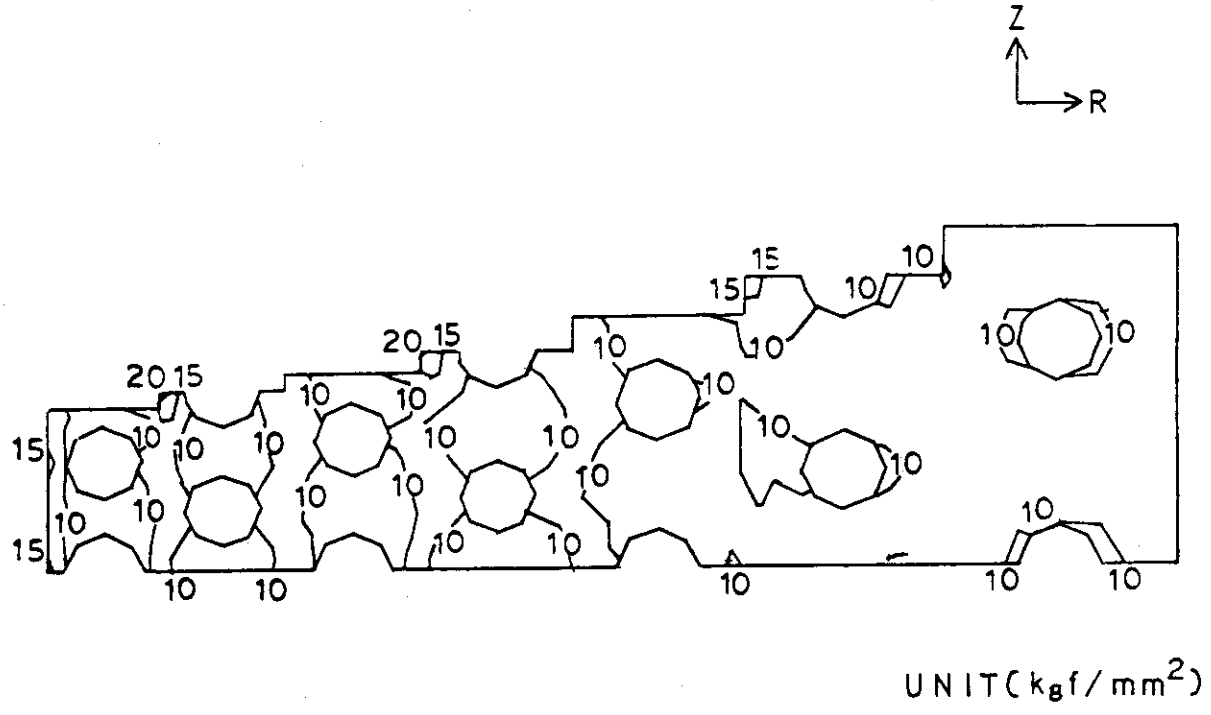

Fig. 3.3.18-b Distribution of Stress Intensity Case No. 2

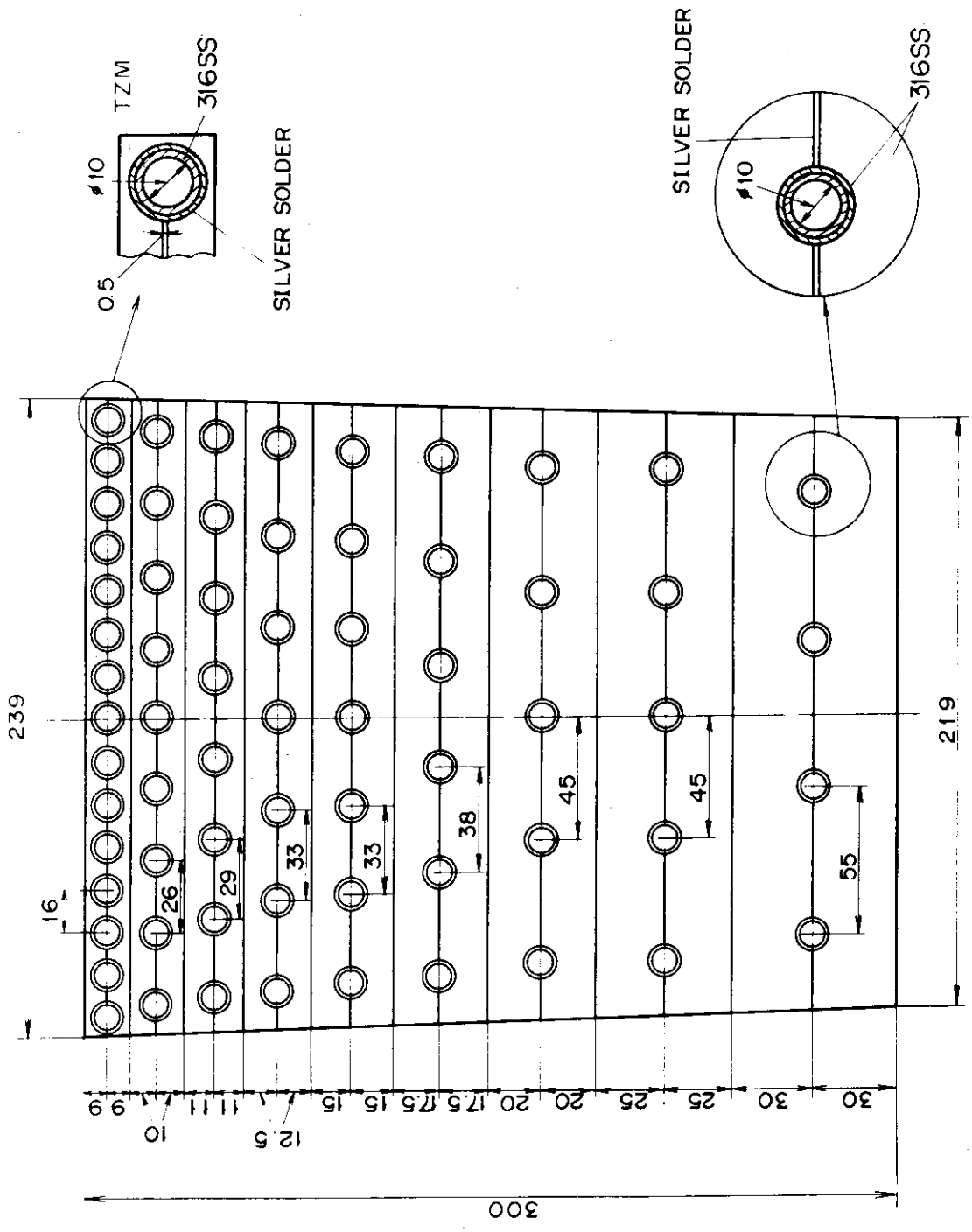

Fig. 3.4.1 Cross Section of a Blanket Block

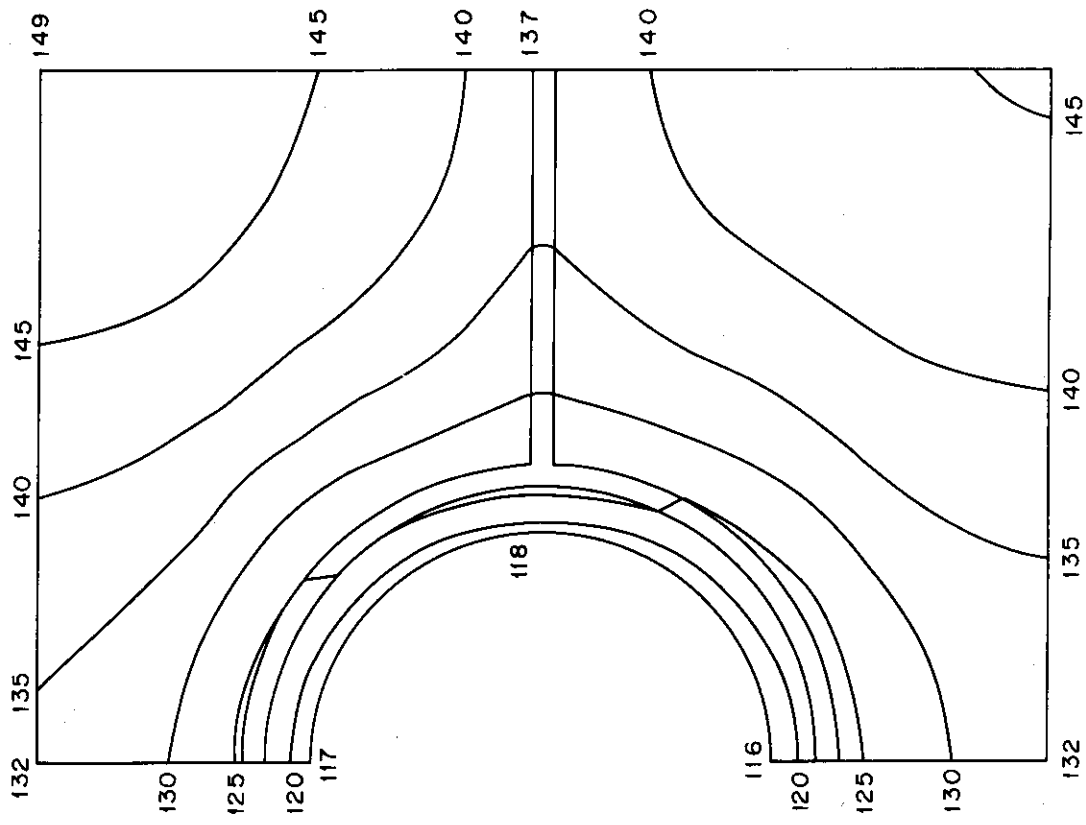

Fig. 3.4.3 Steady-State Temperature Distribution in the 3rd Layer

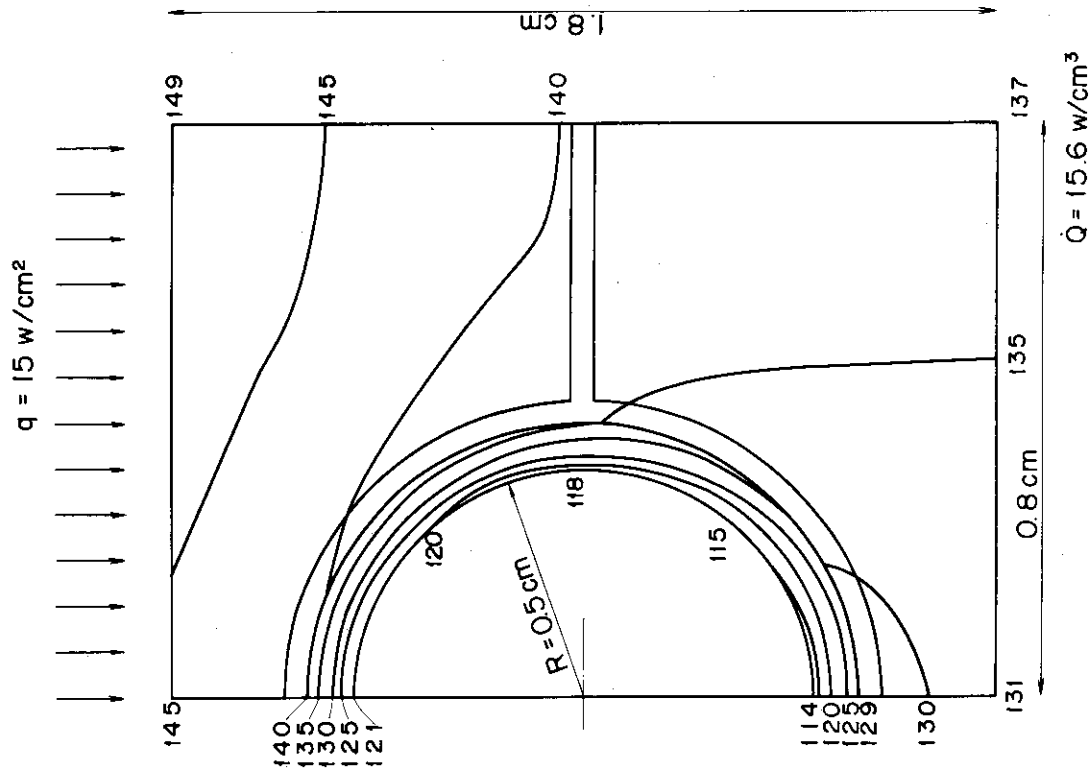

Fig. 3.4.2 Steady-State Temperature Distribution in the 1st Layer

4. Shield

Shield is required to protect the superconducting coils and other reactor components external to the shield from the effects of intense neutron radiation generated by burning plasma, and to provide a high quality vacuum boundary for plasma confinement.

The main characteristics of the shield is shown in Table 4.1.

Table 4.1 Main Characteristics of the Shield

	Whole Primary Shield	Inboard Shield	Outboard Shield	Others
Structure				
Number of sectors	6	-	-	-
Number of bellows/sector	2	-	-	-
Number of parts/sector	1	-	-	-
Structure	Multi-layered panel structure			
Layer structure		SS-water W-Heavy concrete SS	SS-water SS-Heavy concrete SS	Heavy-concrete
Dimensions				
Major radius	5 m	-	-	-
Inner diameter	$4.4^{W}\times7.3^{H}$m	-	-	-
Outer diameter	$5.9^{W}\times9.3^{H}$m	-	-	-
Total thickness	-	50 cm	100 cm	80 cm
SS-water layer	-	25 cm	25 cm	-
Concrete layer	-	21 cm	71 cm	80 cm
SS layer	-	4 cm	4 cm	-
Surface area				
Inner surface	660 m^2	-	-	-
Outer surface	800 m^2	-	-	-

Table 4.1 continued

	Whole Primary Shield	Inboard Shield	Outboard Shield	Others
Cooling				
Coolant	Water	-	-	-
Operation temperature		-	-	-
Composition				
		SS-Water layer SS: 55% Water: 45% Concrete layer W: 50% Heavy Concrete: 50% SS layer SS: 100%	SS-Water layer SS: 50% Water: 45% Concrete layer SS: 50% Heavy Concrete: 50% SS layer SS: 100%	Concrete layer SS: 10% Heavy Concrete: 90%
Electrical Resistance				
Per bellow	17 μ-ohm	-	-	-
Total	0.2 m-ohm	-	-	-
Weight				
Total	4200 ton	1150 ton	3050 ton	

* Heavy concrete: 40% SS containing concrete

4.1 Design Conditions

(1) Configuration

The configuration of shield of which shape is a hollow doughnut as a whole is determined as shown in Fig. 1.5.1 and Fig. 1.5.2 with consideration for the spacing with other components.

(2) Composition

The standard composition of the shield is shown as follows,

(i) INBOARD SHIELD

SS (36%) + W (21%) + Heavy Concrete (21%) + Water (22%)

(ii) OUTBOARD SHIELD

SS (53%) + Heavy Concrete (35%) + Water (12%)

(iii) OTHERS

SS (10%) + Heavy Concrete (89%) + Water (1%)

Lead shield is not considered in the present design, because necessity for lead shield has not been clarified by the neutronics analysis.

(3) Operating Temperature

less than 100°C

(4) Space for the Blanket

The blanket is installed within the primary shield. The shield leaves space necessary for the blanket (shown in Fig. 1.5.1 and Fig. 1.5.2) and the support leg for dead weight of the blanket. Maximum temperature of the blanket is assumed to be less than 150°C.

(5) Assembling and Disassembling

On account of the requirement for assembling and disassembling, the shield is divided into six sectors. Each sector is connected to adjacent ones by bolting at the flange, and is sealed by seal-welding.

It is possible to cut off a part of the shield for the automatic welding machine. However thickness of cut-off part is kept less than 100 mm.

(6) Electric Condition

The electrical resistance of the shield along the torus is higher than 200 μ-ohm.

(7) Vacuum Condition

The shield is required to provide a ultra high vacuum boundary. So the material of the shield of a vacuum side is stainless steel which is treated for high vacuum quality.

(8) Cooling Condition

The shield is cooled by water, and inlet temperature of cooling water is 35°C.

(9) Operating Condition

(a) The plasma burn and dwell times are 200 and 50 seconds, respectively.

(b) The Distributions of Neutron and Gamma Ray Flux and heating rate in the shielding are reported previously (JAERI-M 8503).

4.2 Shielding Structure

The reactor consists of six sectors along the torus. So the shield is divided into 1/6 sector similarly.

Fig. 4.2.1 shows the plane and section views of the whole shield. The shield consists of the layered structure of stainless steel-water shield and heavy concrete shield, from plasma side[1)].

Since there are two bellows parts in a 1/6 sector of the shield, each sector is divided into two outer blocks and one central block by bellows as shown in Fig. 4.2.2. The primary shield is divided into the inboard and the outboard shield, and the boundary is located at R = 5.0 m as shown in Fig. 4.2.3. The plane section of the bellows structure is shown in Fig. 4.2.4.

Note: 1) According to the design condition (2), lead layer is not set up. But addition of lead layer is not difficult from structural point of view.

2) The assembling procedure of the shield structure is shown in Fig. 10.2.1 and Fig. 10.2.2.

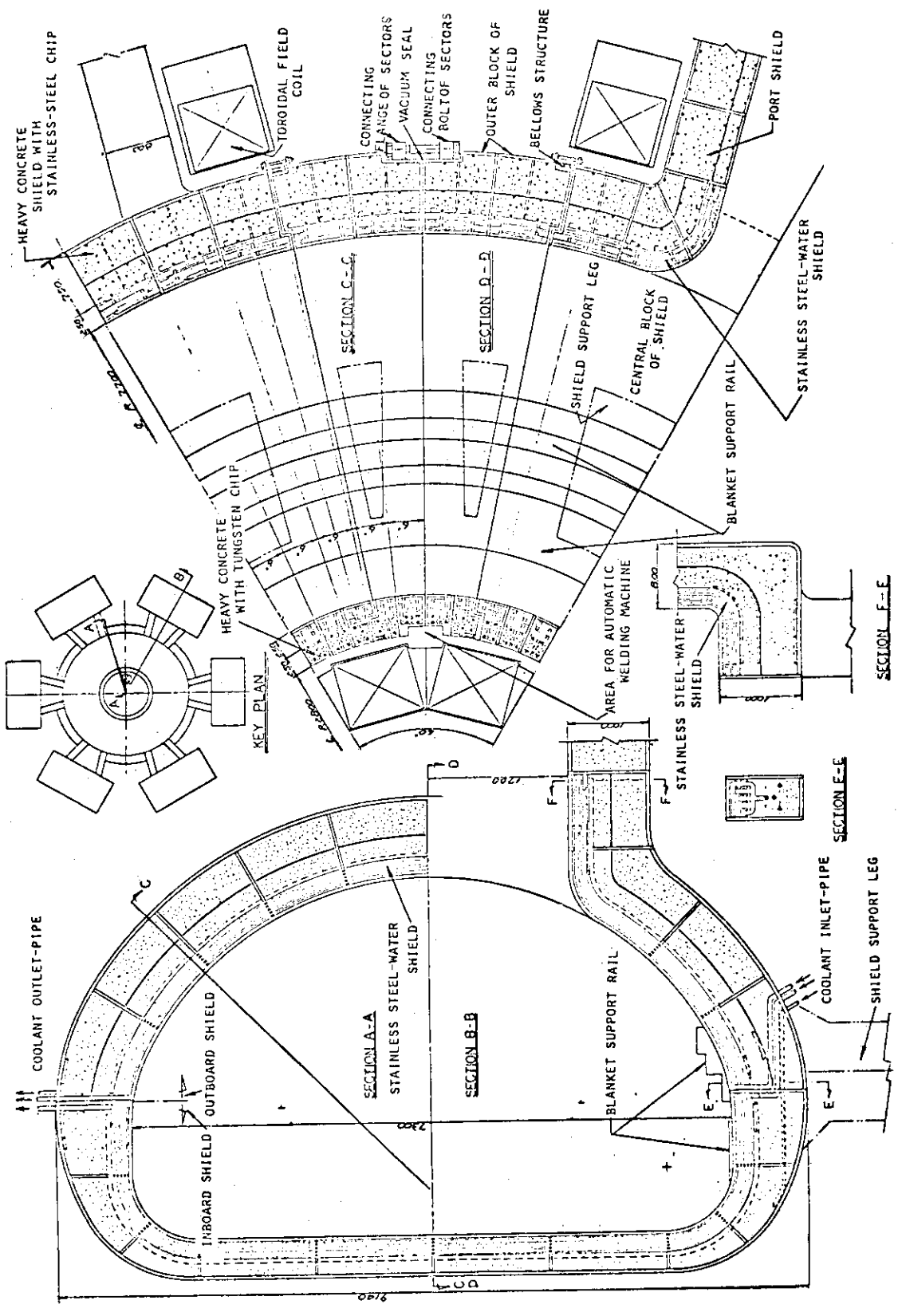

Fig.4.2.1 Primary shield structure

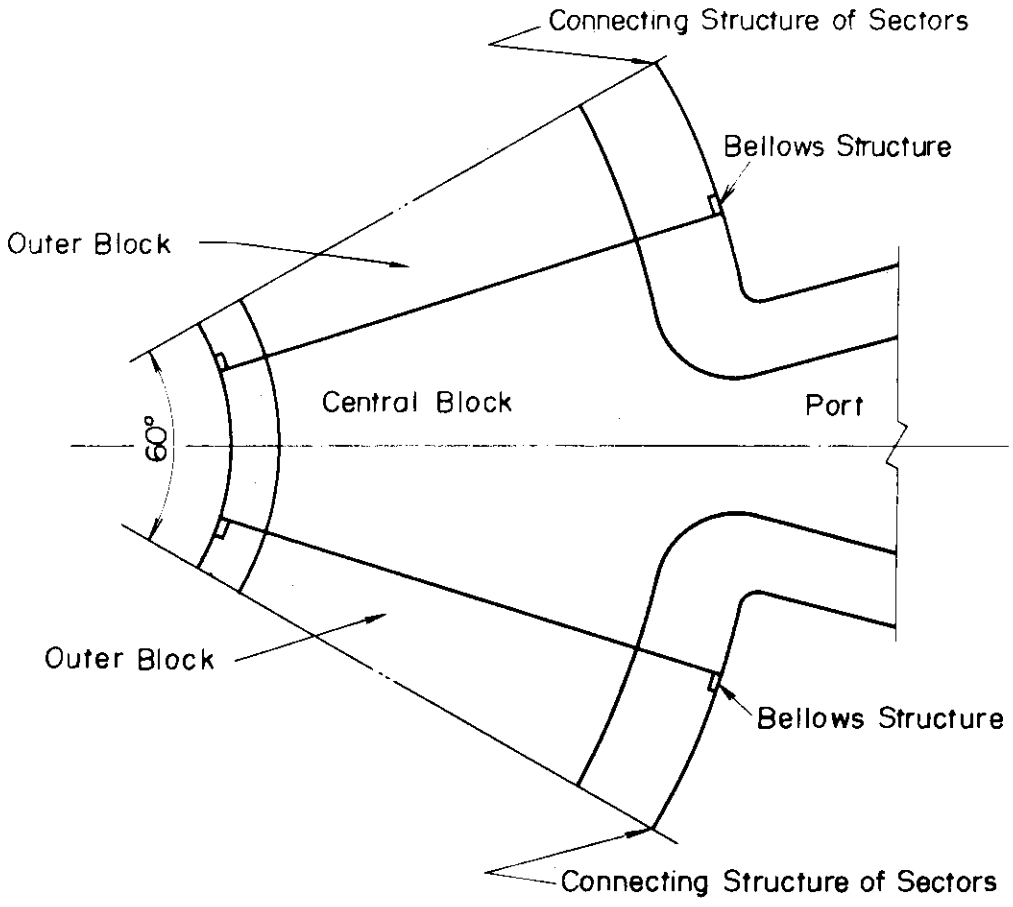

Fig. 4.2.2 Block of Shield Structure

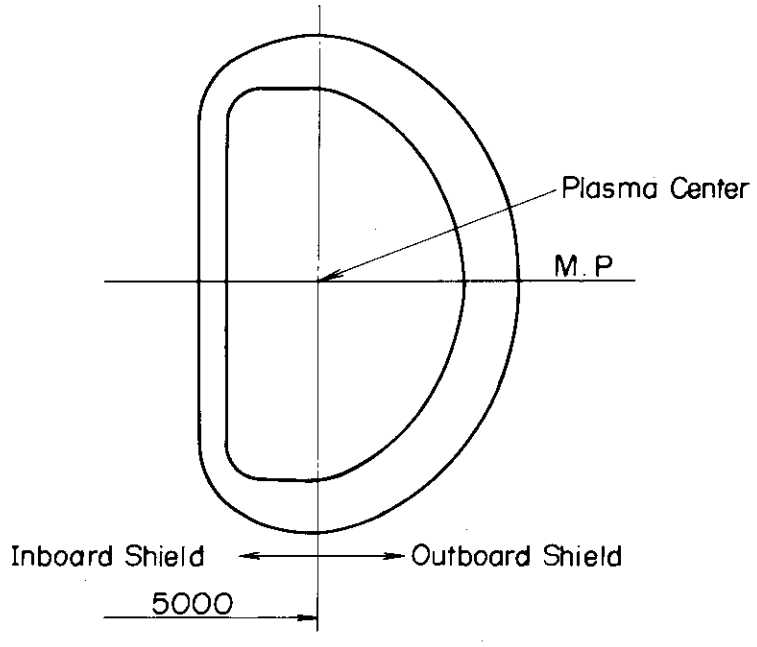

Fig. 4.2.3 Inboard and Outboard Shield

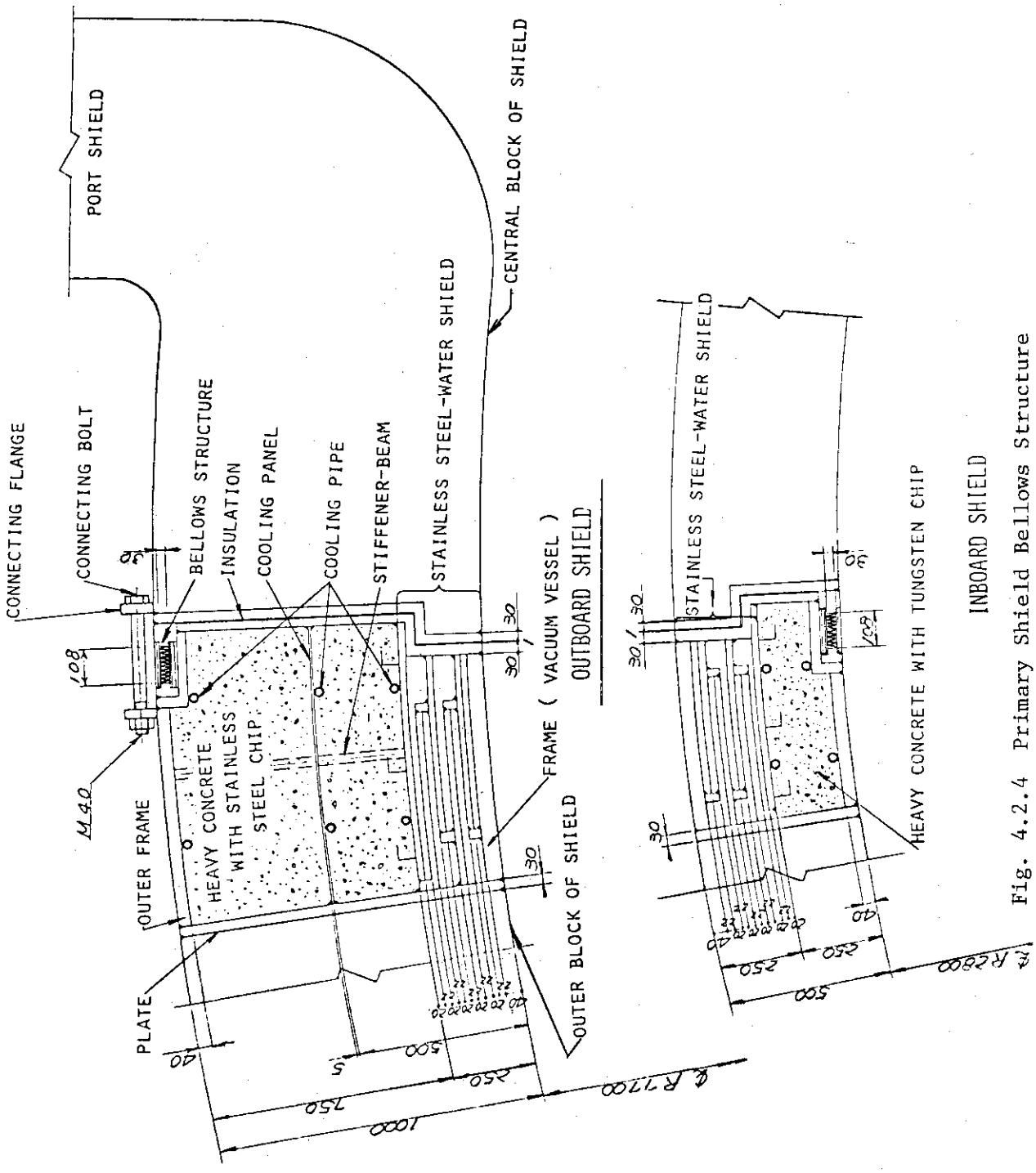

Fig. 4.2.4 Primary Shield Bellows Structure

(1) Stainless Steel - Water Shield

Since the heating rate in the shield structure near to the blanket is high, stainless steel-water shield with high cooling efficiency is installed at plasma side. The thickness of the stainless steel-water shield is designed to be 25 cm.

As assembling of the stainless steel-water shield, the frame of the shield is set up at first except outer frame. For next step the stainless steel plate divided along the poloidal direction is inserted from outside and is welded. This procedure is carried out from inner to outer. In this process, considering to insert from the outside of the shield, the length of one stainless steel plate along the torus is shorter than that of one division (Fig. 4.2.5). On the other hand, since the stainless steel plate near the port shield cannot be inserted from the outside of the shield, it is inserted from side of the shield (Fig. 4.2.6).

Cooling water flows in the inboard and the outboard shield independently.

Support rails for the blanket are set up on the inside of the shield. The rails are also used for the maintenance manipulator.

The inside frame of the shield also functions as vacuum boundary. The bellows and seal-welded parts function as vacuum boundary, too.

(2) Heavy Concrete Shield

Heavy concrete is used for outside shield. Tungsten chips are used in the inboard shield for aggregates, and stainless steel chips are used in the outboard shield.

In order to enhance the shielding effect, the ratio of aggregate is desired to be as high as possible. So the concrete shield by prepacked method using rough chips of about 20 $\sim$ 40 mm diameter is employed. In case of this method, it may be possible to increase the volume rate of rough chips up to about 50%. The heavy concrete of inboard shield is cooled through the stainless steel-water shield and the outer frame with cooling pipes. Because the outboard shield is thick, cooling panel is attached within heavy concrete to decrease the maximum temperature and its gradient in the heavy concrete to persimmible values.

(3) Bellows Structure

The bellows structure is shown in Fig. 4.2.4. Two bellow sections are set in one sector and twelve in total. The thickness, effective height, and pitch of bellows, are 1.5 mm, 2.0 mm, 6.0 mm, respectively.

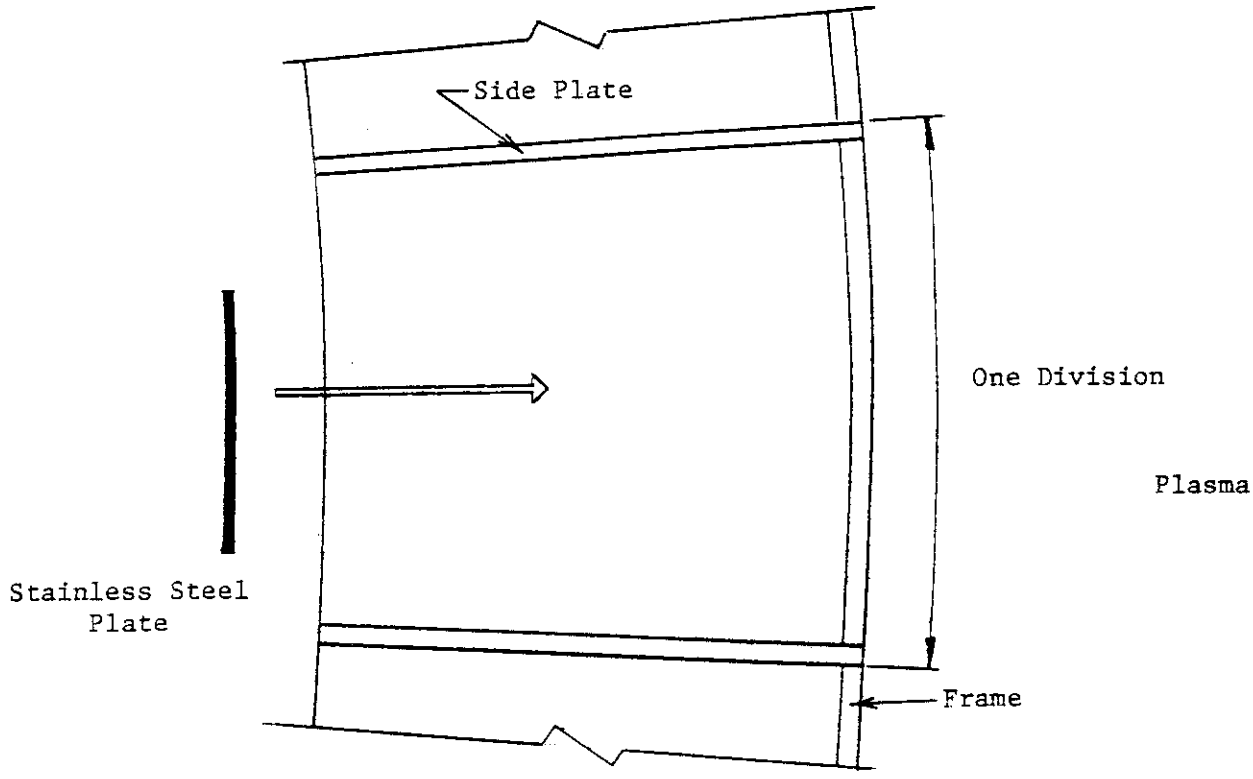

Fig.4.2.5 Assembling of Stainless Steel-Water Shield

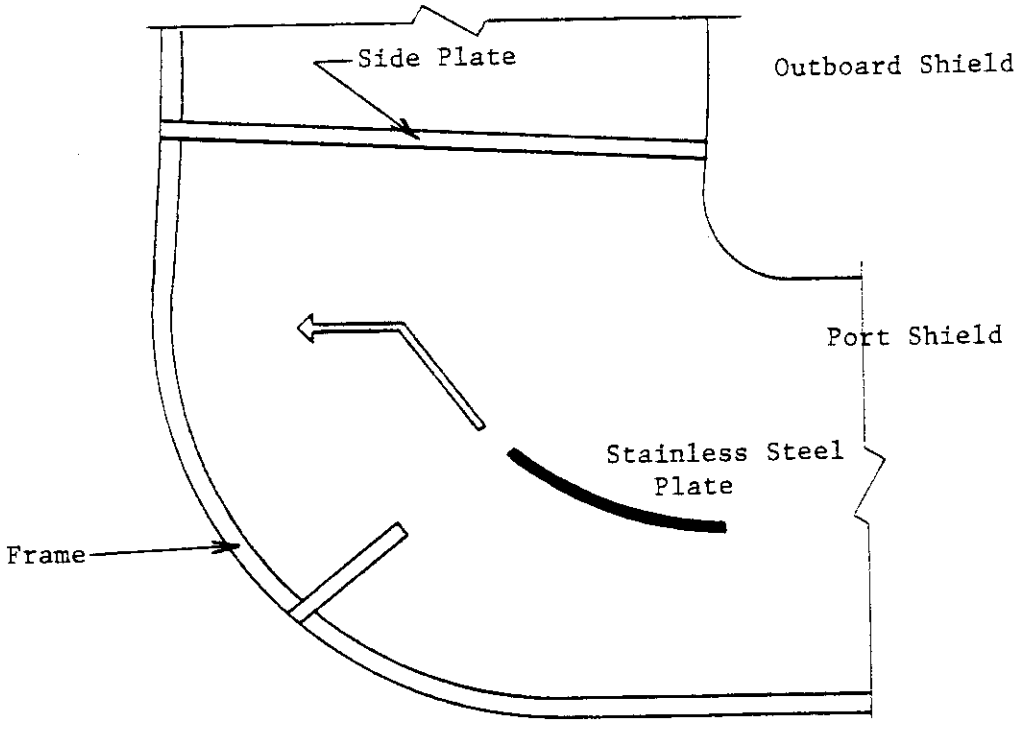

Fig.4.2.6 Assembling of Stainless Steel-Water Shield near Port Shield

Detonation coating of ceramics is applied to the walls of central and outer blocks facing each other. Between the blocks key structure is used in order to offset magnetic force mutually. At the outside the blocks are bolted each other. Since the space between the shield and the TF coils is narrow, bolting is only possible at the outside of the outboard shield and inside of the inboard shield. Tying at other places is under study.

(4) Port Shield

The port shield is constructed at the same time with the primary shield. The port shield consists of heavy concrete. Cooling panels are set on the port structure.

(5) Connecting Part of the Sectors

Sectors are automatically welded and bolted each other, A part of the shield is cut off for installation of the automatic welding machine. (Fig. 4.2.1 and Fig. 6.1.2)

(6) Cooling Path

The coolant inlet pipes are set at the bottom of the shield avoiding the shield support leg as shown in Fig. 4.2.1.

The coolant flows upwards along the poloidal direction in inboard and outboard shield independently, and flows out from outlet at the top of the shield.

4.3 Design Analysis

4.3.1 Thermal Analysis

1) The Maximum Temperature of the Stainless Steel-Water Shield

The highest heat load in the stainless steel-water shield is expected at the stainless steel plate facing the blanket. Therefore, one dimensional steady-state[1)] thermal analysis of the innermost plate is carried out.

Note 1) Since burn time is long enough (200 seconds) compared to dwell time (50 seconds), steady state analysis, which is more severe, is carried out.

Figure on the right shows the model of the analysis. Radiation from plasma and nuclear heating are considered as heat load. The temperature of the place which contacts with cooling water is assumed to be equal to that of water because heat flux is sufficientlly low.

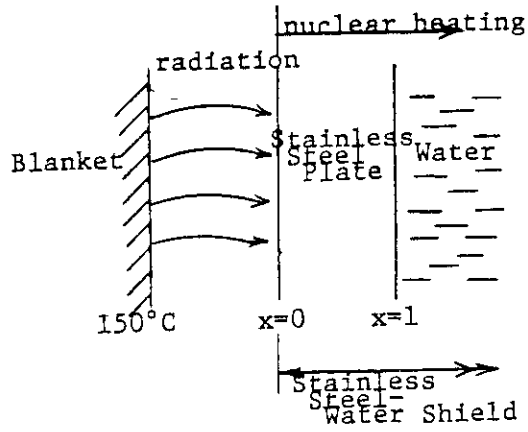

Model of Analysis

Basic equation:

$$\lambda\frac{\partial^2 T}{\partial x^2} + q_0 e^{-\mu x} = 0 \qquad (4.1)$$

Boundary condition:

$$\begin{cases} -\lambda\dfrac{\partial T}{\partial x} = q_1, & \text{at } x = 0 \\ T = Tw, & \text{at } x = \ell \end{cases} \qquad (4.2)$$

Here, T ; temperature

x ; distance from inside of the plate

λ ; thermal conductivity of stainless steel, 0.156 w/cm°C

$q_0 e^{-\mu x}$; term of nuclear heating

μ ; attenuation factor

q_1 ; thermal radiation from the blanket (assumed to be the infinite parallel plate)

$$q_1 = \sigma \frac{1}{\frac{1}{\varepsilon_1} + \frac{1}{\varepsilon_2} - 1} \{(273 + T_B)^4 - (273 + T_0)^4\} \qquad (4.3)$$

T_B ; surface temperature of the blanket

ε ; emissivity (assumed the stainless steel emissivity to be 0.4 and $\varepsilon_1 = \varepsilon_2$)

σ ; Stefan-Boltzmann's constant, 5.67×10^{-12} w/cm$^{2.0}$k^4

From (4.1) and (4.2) the temperature distribution of the stainless steel is expressed as

$$T = \frac{q_0}{\lambda\mu^2}(e^{-\mu\ell} - e^{-\mu x}) + (\frac{q_1}{\lambda} + \frac{q_2}{\mu\lambda})(\ell - x) + Tw \qquad (4.4)$$

The maximum temperature which is appeared at x = 0 is

$$Tmax = T_0 = -\frac{q_0}{\lambda\mu^2}(1 - e^{-\mu}) + (\frac{q_1}{\lambda} + \frac{q_2}{\mu\lambda})\ell + Tw \qquad (4.5)$$

We substitute q_0 = 0.4 W/cm^3, ℓ = 4 cm, Tw = 35°C into (4.3) and (4.5), and after iterative calculation, we get Tmax = 52.96°C.

2) The Maximum Temperature of the Heavy Concrete Shield

(1) Model of Analysis

One dimensional steady-state thermal analysis of the heavy concrete layer is carried out.

Figure on the right shows the model of the analysis. The heat load considered is nuclear heating in the heavy concrete layer. And the temperature at the place which contacts with cooling water is assumed to be equal to that of water because of low heat flux.

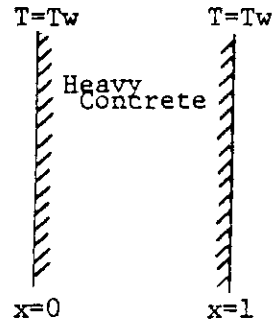

Model of Analysis

Basic equation:

$$\lambda\frac{\partial^2 T}{\partial x^2} + q_0 e^{-\mu x} = 0 \qquad (4.6)$$

Boundary condition:

$$\begin{cases} T = Tw, & \text{at } x = 0 \\ T = Tw, & \text{at } x = \ell \end{cases} \qquad (4.7)$$

Here, T ; temperature

x ; distance from inside of the concrete shielding

λ ; thermal conductivity of heavy concrete

$q_0 e^{-\mu x}$; term of nuclear heating

μ ; attenuation factor

From (4.6) and (4.7) the temperature distribution along the thickness of heavy concrete layer is expressed as

$$T = \frac{q_0}{\lambda\mu^2}\left(\frac{x}{\ell} e^{-\mu\ell} - e^{-\mu x} + 1 - \frac{x}{\ell}\right) + Tw \qquad (4.8)$$

Temperature gradient is

$$\frac{dT}{dx} = \frac{q_0}{\lambda\mu^2}\left(\frac{e^{-\mu\ell}}{\ell} + \mu e^{-\mu x} - \frac{1}{\ell}\right) \qquad (4.9)$$

The maximum temperature appears where $\frac{dT}{dx} = 0$, that is

$$x = -\frac{1}{\mu}\ell n \frac{1}{\mu\ell}\left(1 - e^{-\mu\ell}\right) \qquad (4.10)$$

The maximum temperature gradient appears at x = 0

(2) Estimation of the Thermal Conductivity of Heavy Concrete

The thermal conductivity of heavy concrete is 0.025 ∿ 0.030 w/cm-°C. In case of this design, since stainless steel and tungsten are used for aggregates, we estimate the thermal conductivity of the heavy concrete by the method to compute the thermal conductivity of filling layer. The effective thermal conductivity of filling layer is given as

$$\lambda_e{}^0 = \lambda_g \left\{ \varepsilon \left(1 + \frac{\alpha_{rv} \cdot D_p}{\lambda_g} \right) + \frac{1 - \varepsilon}{\dfrac{1}{\dfrac{1}{\phi} + \dfrac{\alpha_{rs} \cdot D_p}{\lambda_g}} + \dfrac{2\,\lambda_g}{3\,\lambda_s}} \right. \tag{4.11}$$

Here, λe^0 ; effective thermal conductivity of filling layer

λg ; thermal conductivity of mortar, ∿ 0.01 w/cm·°C

λs ; thermal conductivity of aggregates

{ SS : 0.151 w/cm·°C
{ W : 1.50 w/cm·°C

ε ; percent of mortar volume

Dp ; diameter of aggregate

α_{rv}, α_{rs} ; radiative heat transfer coefficient

In this case we omit radiation among aggregates and $\alpha_{rv} = \alpha_{rs} = 0$. The volumetric ratio of aggregates to mortar is 1 : 1.

Hence

material of aggregates	effective thermal conductivity
SS	0.03 w/cm·°C
W	0.06 w/cm·°C

(3) Thermal Calculation of the Inboard Heavy Concrete Shield

Because of uncertainty of thermal properties of heavy concrete, we consider two values for effective thermal conductivities of heavy concrete layer. One is λ = 0.06 w/cm·°C which is computed from the above method and another one is λ = 0.03 w/cm·°C, which is standard heavy concrete value. Numerical calculation of (4.8) ∿ (4.10) under following values is carried out.

{ μ = 0.173/cm
{ ℓ = 21 cm
{ q_0 = 0.015 w/cm^3
{ Tw = 35.0°C

The results are summarized in Table 4.3.1.

Table 4.3.1 Results of Thermal Analysis of the Inboard Heavy Concrete Shield

Effective thermal conductivity of heavy concrete w/cm·°C		0.06	0.03
Location of maximum temperature	cm *	7.61	7.61
Maximum temperature	°C	38.17	41.33
Maximum temperature gradient	°C/cm	1.06	2.12

* Distance from inside of heavy concrete

(4) Thermal Calculation of the Outboard Heavy Concrete Shield

In case of the outboard shield, cooling panel should be set among the heavy concrete layer of the outboard shield. So the temperature distribution within the heavy concrete is analyzed as a function of the position of cooling panel. Calculation is carried out under the following values.

$$\begin{cases} \mu = 0.138/\text{cm} \\ q_0 = 0.015\ \text{w/cm}^3 \\ \lambda = 0.03\ \text{w/cm·°C} \quad 1) \\ Tw = 35.0°\text{C} \end{cases}$$

The results for inner and outer heavy concrete layers are summarized in Table 4.3.2 and Table 4.3.3, respectively.

Table 4.3.2 Results of Thermal Analysis of the Outboard Heavy Concrete Shield (I)

Distance from inside of heavy concrete to cooling panel	cm	25	15	10
Location of maximum temperature *	cm	9.21	6.25	4.43
Maximum temperature	°C	44.52	40.61	38.30
Maximum temperature gradient	°C/cm	2.61	2.09	1.66

* Distance from inside of heavy concrete

Note 1) In this case, the thermal conductivity is 0.03 w/cm°C referring to 3.3 (2) (i) and standard heavy concrete's value.

Table 4.3.3 Results of Thermal Analysis of the Outboard Heavy Concrete Shield (II)

Distance from inside of heavy concrete to cooling panel	cm	25	15	10
Distance from cooling panel to outside of heavy concrete	cm	46	56	61
Location of maximum temperature *	cm	13.41	14.82	15.44
Maximum temperature	°C	35.97	36.59	37.20
Maximum temperature gradient	°C/cm	0.20	0.32	0.43

* Distance from cooling panel

(5) Summary

The design criteria of concrete structure are that the maximum temperature be lower than 70 ∿ 80°C and the maximum temperature gradient be lower than 1°C/cm.

In case of the inboard shield, the maximum temperature for both thermal conductivities satisfy the design criterion.

However, the maximum temperature gradient for both thermal conductivities are higher than the design criterion. But this criterion is applied to the concrete to which the strength is expected. Since the strength of concrete is unexpected in this design, higher thermal gradient might be permissible. But this argument should be confirmed through the research and development of thermal characteristic of concrete.

The outboard shield is under the same situation as the inboard shield, but temperature gradient of outboard shield depends on the location of cooling panel. The location of the cooling panel is decided as shown in Fig. 4.2.1 from the structural consideration. But this is not deterministic.

3) Temperature Rise of Coolant

Calculation of temperature difference between inlet and outlet coolant is carried out.

Following formula through energy balance is obtained.

$$SLA_o = Sw\ Vw\ \rho w\ Cw\ \Delta T \times 4.186 \qquad (4.12)$$

Here, S ; cross section area of the shield
L ; length of cooling path
Ao ; bulk heating value [1)]
Sw ; cross sectional area of cooling path
Vw ; velocity of coolant
ρw ; density of coolant
Cw ; specific heat of coolant
ΔT ; coolant's temperature difference between inlet and outlet

The temperature rises of coolant of the inboard and outboard shield are calculated as follows.

(i) Inboard shield ΔT = 4.86°C
(ii) Outboard shield at general part ΔT = 8.60°C
at port ΔT = 10.83°C

Consequently the temperature rise of coolant is not crucial.

4.3.2 Analysis of Electromagnetic Force for Vacuum Vessel

The electromagnetic load analysis of the vacuum vessel requires an evolution of currents induced in the vessel with the magnetic fields generated by the surrounding magnetic flux changing with time. The induced currents for an unintentional plasma disruption are much greater than those for the start up and shutdown situations.

In this analysis, a 10-msec disruption of a 4.7-MA plasma is assumed, and then induces a maximum current 1.91 MA in the vessel.

$$Ip = 4.7 \times \exp(-100t) \qquad (MA)$$

The method used for analyzing the transient behavior of the eddy currents induced in a vacuum vessel is based on the integro-differential equations with magnetic vector and electrostatic scalar potentials. The basis equations are as follows.

$$A(r, t) = A^{\circ}(r, t) + \frac{\mu_0}{4\pi}\int \frac{j(r', t)}{|r - r'|}\, dr'$$

$$\nabla^2 \phi = 0$$

Note 1) For simplification, the constant nuclear heating value within the shield is assumed to be the same to the value of innermost part. Therefore, the result is conservative enough.

$$\text{B.C.} \quad \left.\frac{\partial\phi}{\partial n}\right|_1 - \left.\frac{\partial\phi}{\partial n}\right|_2 = -\left(\frac{1}{\sigma_1} - \frac{1}{\sigma_2}\right) J_n$$

and

$$j = -\sigma\left(\frac{\partial A}{\partial t} + \nabla\phi\right)$$

where integration is over the region acting as the conducting medium and A° is the part of A due to all sources outside of this region. The boundary condition for the electrostatic scalar potential is a consequence of the continuity across the boundary for the normal components of the magnetic vector potential and current density. Subscripts 1 and 2 denote the shell sections composed of thick plates and the bellows composed of thin sheet, respectively. For thin conductors, which mean neglect of the eddy current distribution perpendicular to the conductor, the electrical conductivity σ_2 of the bellows is less than that of σ , by a few orders of magnitude.

The effective area conductivity is given as follows.

$$\sigma_\phi = \sigma_\tau = 8.333 \times 10^4 \quad (\Omega^{-1})$$

(at the shell section)

$$\sigma_\phi = 2.097 \times 10^3 \cdot R/7.7 \quad (\Omega^{-1})$$

$$\sigma_\tau = 4.092 \times 10^3 \cdot 7.7/R \quad (\Omega^{-1})$$

(at the bellows)

where R is the distance from the symmetric axis of the torus. The dependence of the effective area conductivity on R reflects the bending of the bellows in the toroidal direction.

The external magnetic field which induces the eddy currents in the vacuum vessel is produced by the line current at the major radius 5.0 m attenuated with a time constant of 10 mS, that is,

$$I_p = 4.7 \times \exp(-100t) \quad (\text{MA}).$$

The eddy currents in the vessel consist of a transit component which goes around the torus and is uniform in the direction of the symmetry axis, and a localized component which makes a closed circuit within each shell section. The latter is an axially non-symmetric component. Moreover, the transit component is resolved into three components. The first is the uniform component, which has a flat distribution in the transverse

cross-section, the second is the dipole component, which is distributed in proportion to cosθ (θ is the poloidal angle), and the last one is the quadrupole component and the residue of the transit component. The maximum values of the uniform, the dipole, the quadrupole component, and localized components are 1.91 MA at 15 mS, 330 kA at 7 mS, 276 kA at 8 mS, and 134 kA at 56 mS respectively.

Figure 4.3.1 shows the eddy current density distribution of the localized component and 54 mS and Fig. 4.3.2 shows the distribution of the electromagnetic force produced by the interaction of the toroidal fields and the eddy currents at the edge of the center block.

4.4 Design Problems

1. Heavy concrete
   (1) Thermal characteristics of heavy concrete
      o contraction at solidifing
      o dehydration of cement
      o suppression of temperature gradient
   (2) The construction of heavy concrete at narrow part
2. Part of electrical insulation
   (1) Fragility of bellows structure
   (2) Lack of bolting location
   (3) Material of thin electrical insulation
3. Connecting structure between sectors
4. Transport of the shield
5. Vacuum treatment
6. Nuclear characteristics

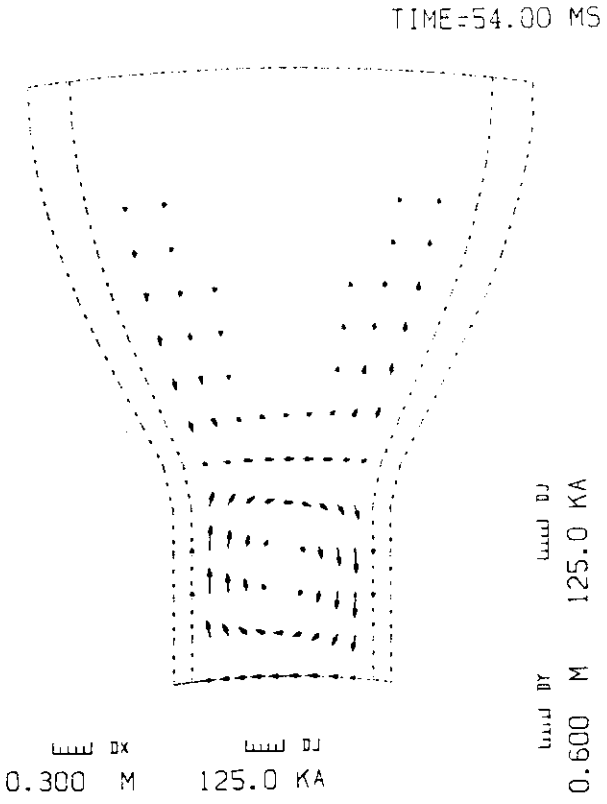

Fig. 4.3.1 Eddy Current Density Distribution of the Localized Component at 54 mS.

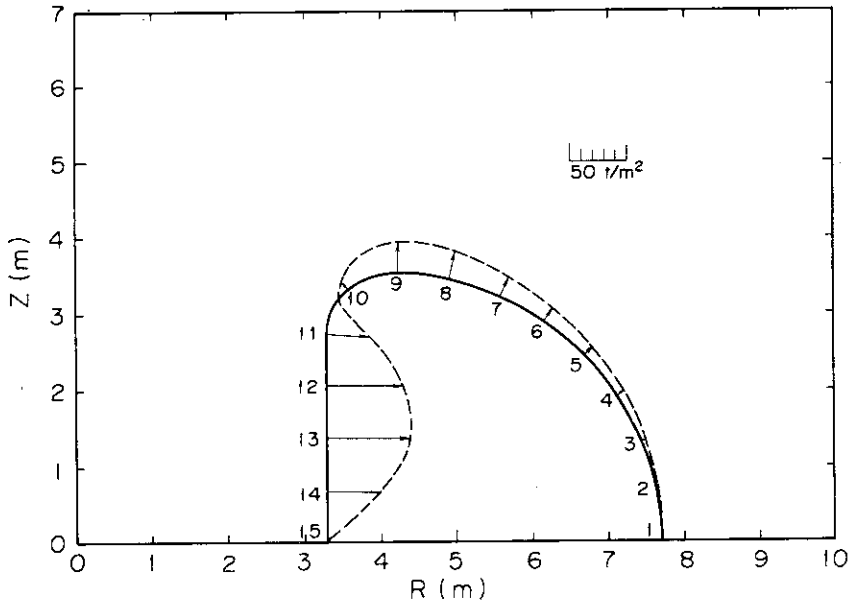

Fig. 4.3.2 Distribution of the Electromagnetic Force

5. Divertor

5.1 Design Conditions of the Divertor Plate

(1) Design Parameters

Material : Copper

Coolant : Water

Pressure temperature : 10 ata

inlet : 70°C

outlet : 90°C

Heat load 50 MW (total) due to ions and electrons

duration : 200 s

dwell time : 100 s

pulse shape: step function

distribution: Gaussian

FWHH 10 cm.

incident angle of particles to the toroidal direction 5°

(2) Magnetic Field Configuration

The axially symmetric MHD equilibria with arbitrary cross-section have been investigated by the method expanding the poloidal magnetic flux function ϕ with the orthogonal series of the first-order associated Legendre function in the spherical coordinates[1]. Ideal magnetohydrodynamic equilibria with axial symmetry are described by solution of the equation.

$$\frac{\partial^2\phi}{\partial R^2} - \frac{1}{R}\cdot\frac{\partial\phi}{\partial R} + \frac{\partial^2\phi}{\partial z^2} = -\mu_0 R J_\phi$$

for the flux function ϕ and

$$J_\phi = R\cdot\frac{dP}{d\phi} + \frac{1}{2R}\cdot\frac{dI^2}{d\phi}$$

where P is the plasma pressure, and I is the current stream function. Figure 5.1.1 shows that the desired MHD equibrium of the plasma realized by the configuration of the poloidal field coils arranged outside of the toroidal field coils.

(3) Arrangement of coolant channels

When the coolant path runs along the toroidal direction, the maximum

heat load along the coolant path becomes 9.3 MW/m^2. This amount of heat load exceeds the burn-out heat flux on the surface of the coolant channel. Furthermore, in arrangement of the above coolant path, it is very difficult to design coolant inlet and outlet structures which are compatible with demands of exchange of divertor plate by remote handling.

In order to reduce the heat flux on the divertor plate, it is desirable that the divertor plate is arranged nearly parallel to the beam line. The coolant pipe with cylindrical cross section cannot meet this condition, therefore, the surface of coolant pipe was flatened and tapered which faces the beam line.

(4) Numerical calculations of helium ash enrichment and exhaust by a simple divertor

A simple poloidal divertor which can enrich and exhaust helium ash has been proposed for the INTOR. Monte Carlo simulations are carried out to investigate the motion of DT fuel and He ash particles after they are re-injected from the divertor neutralizer plate. Helium ash exhaust was shown to be feasible with a modest pumping speed of 5×10^5 ℓ/s for most of the conceivable plasma particle containment conditions. Details are described in Appendix IV of Report of Group 3 Home Task presented to 3rd session of IAEA INTOR Workshop.

Reference

1) W. Feneberg, K. Lackner : Nucl. Fusion 13 (1973) 549

5.2 Structure

Figure 5.2.1 (a) and (b) show structure of the divertor plate.

(A) Sectional plan of the divertor room.
The divertor plate is installed so that the incident angle of the particle beam has an angle of 70° to the normal of the plate. It is supported by headers.

(B) Bird view of the divertor room.

(C) Arrangement of divertor plates in a block.
A module consists of 6 blocks.

(D) Cross section of a divertor plate.
The flat surface is subject to the heat load.
The left side in the figure is tapered with an angle of 7.5°.

5.3 Design Analysis

(1) Results of Thermal Analysis

Figure 5.3.1 shows temperature rise at the center of the divertor plate where the largest heat flux comes. The heat fluxes on the flat part and the tapered part are 1.6 MW/m^2 and 4 MW/m^2, respectively. The maximum temperature in the divertor plate is about 270°C.

The temperature difference between the surface (A) and the coolant channel wall (D) is 60°C. The thermal stress is below the proof stress of copper.

Figure 5.3.2 shows steady-state temperature distribution at the center of the divertor plate.

Figure 5.3.3 shows temperature rise at the center of the divertor plate when the separatrix is oscillated with frequency of 1 Hz. The full width of the oscillation is assumed to be 10 cm.

Figure 5.3.4 shows distribution of temperature rise in the divertor plate at 0.02s after start of irradiation.

Figure 5.3.5 shows deformation of the divertor plate due to thermal stress at 0.02s after start of irradiation.

Figure 5.3.6 shows distribution of thermal stress in the divertor plate at 0.02s after start of irradiation.

Figure 5.3.7 shows distribution of principal stress along the 'A-A' line in the divertor plate just after the start of operation of the divertor. "t" in the figure shows the time elapsed after the start.

(2) Electromagnetic Force for Divertor Plate

The interaction of the toroidal fields and the eddy currents induced in the divertor plate produces a vertical force. A 10-msec distruption of a 4.7-MA plasma applies the induction voltage of 1.4 volt in the divertor plate in consideration of the effect due to the eddy currents in the vacuum vessel which prevent the surrounding magnetic flux from changing with time. The interaction of the toroidal fields and the eddy currents in the divertor plate produces the vertical force of Max. 4.75 t/m in the divertor plate which is composed of copper and Max. 0.22 t/m in the divertor plate which is composed of copper pipe and stainless steel header

5.4 Summary of the Results

(1) The divertor plate can be cooled without any serious problem.

(2) Thermal stress in the divertor plate is below the proof stress of copper.

(3) Repetitive thermal stress due to pulsive operation of the reactor might lower the life time of the divertor plate to 3 to 4 months.

(4) Radiation damage of the plate due to 14-MeV-neutron irradiation, especially swelling of copper, could be a serious problem. But, it is difficult to evaluate its effect on the life time of the plate due to lack of data for radiation damage.

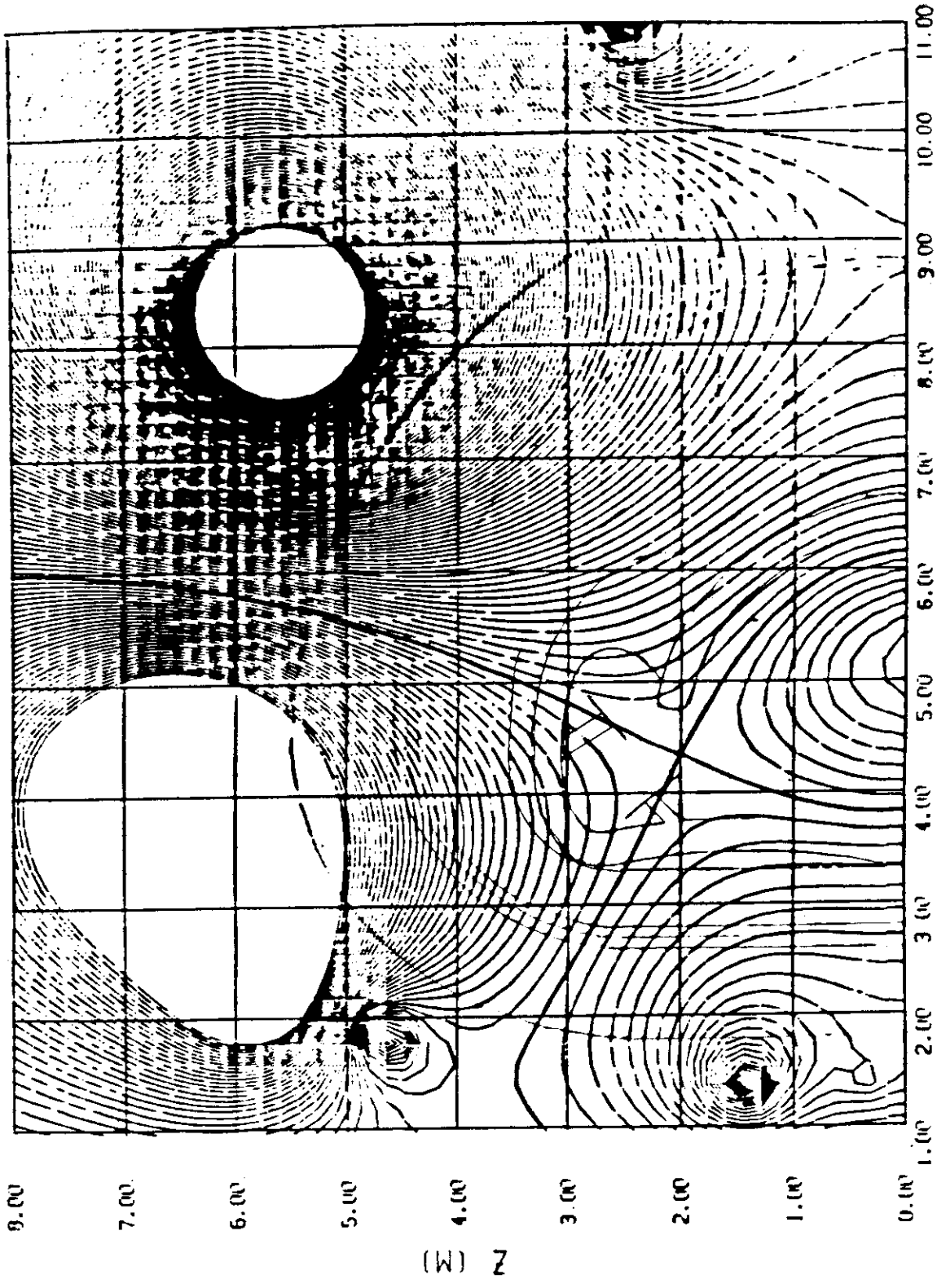

Fig. 5.1.1 Desired MHD Equibrium of the Plasma

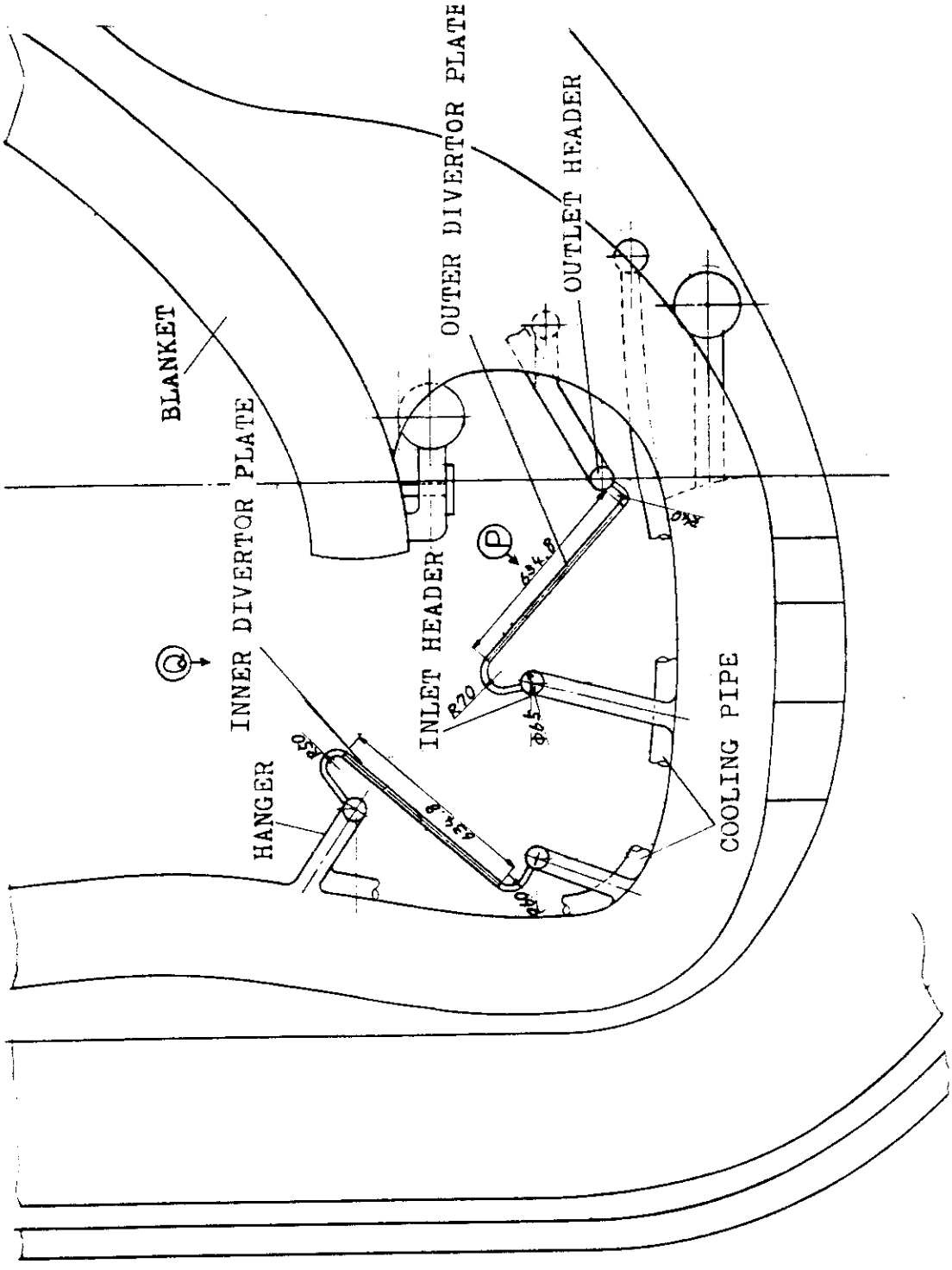

Fig. 5.2.1(a) Arrangement of Divertor Plate Room

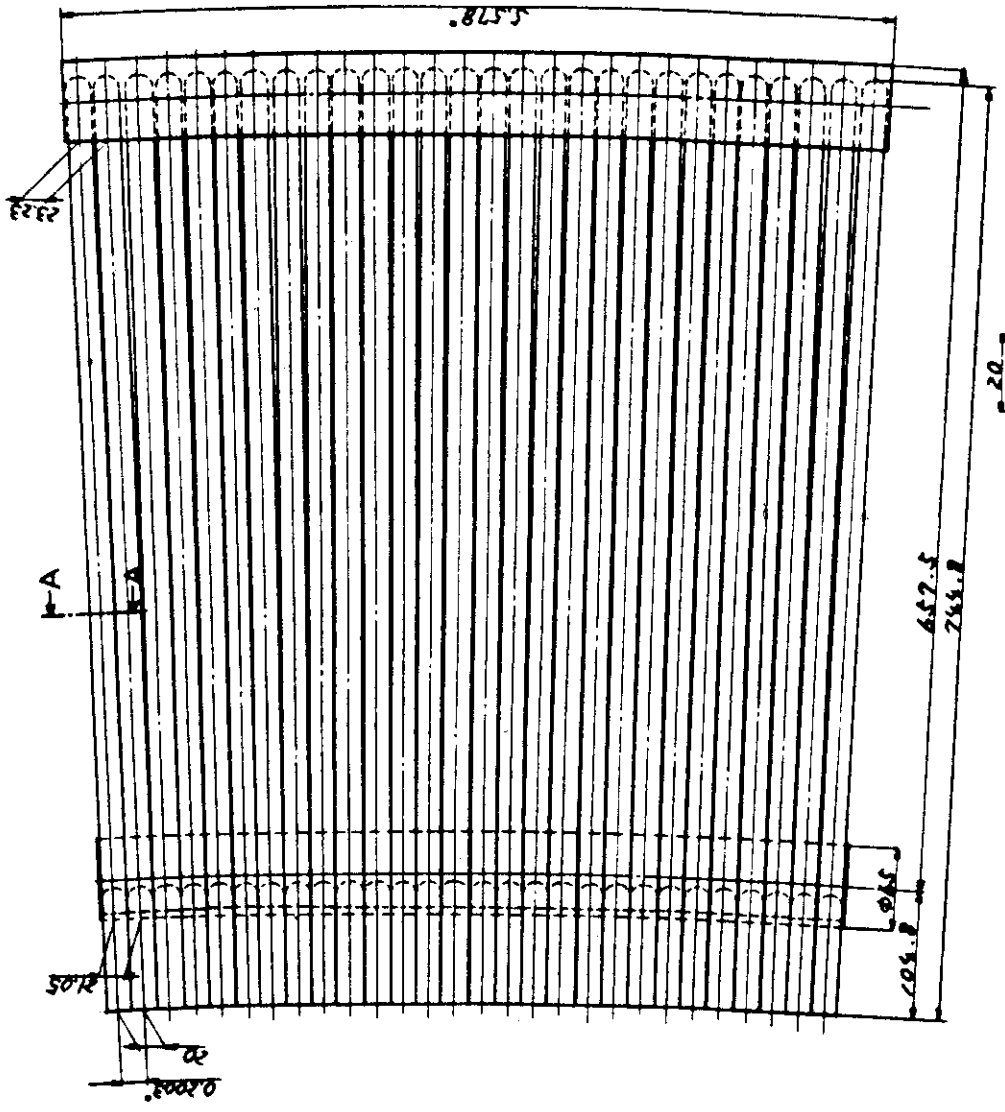

Fig. 5.2.1(b) A Block of Divertor Plate

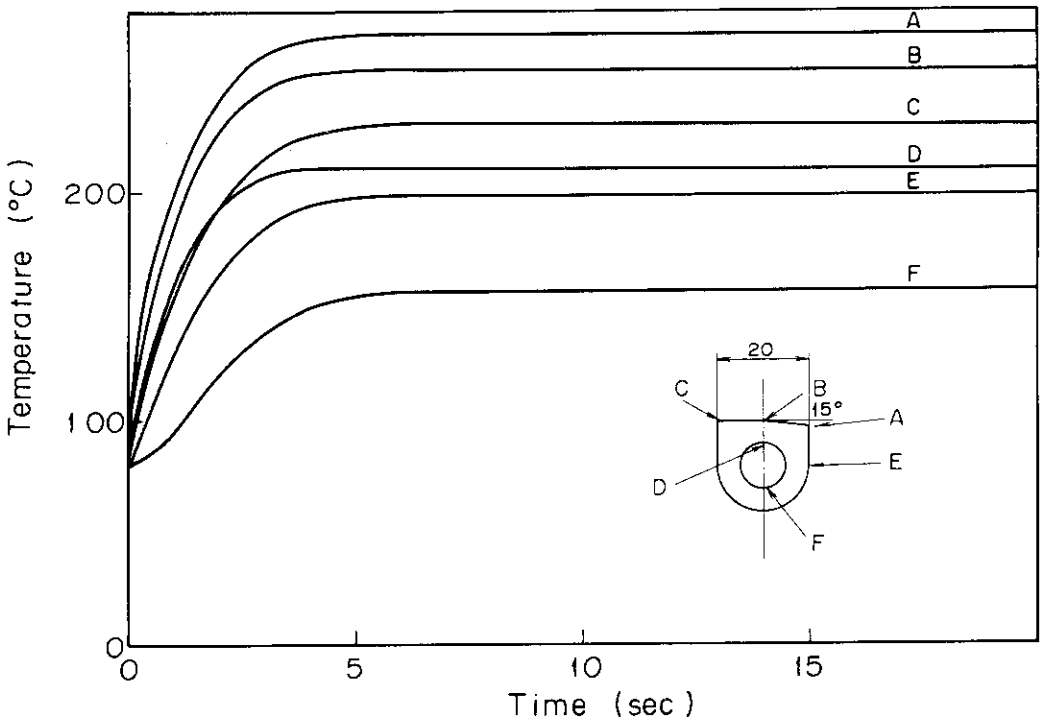

Fig. 5.3.1 Temperature Rise at the Center of the Divertor Plate Where the Largest Heat Flux Comes

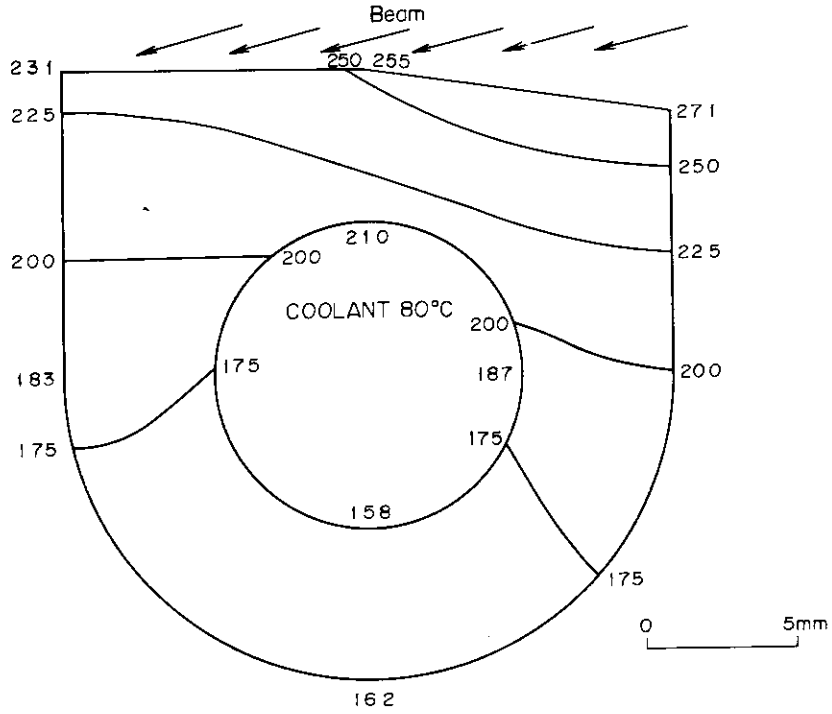

Fig. 5.3.2 Steady-State Temperature Distribution at the Center of the Divertor Plate

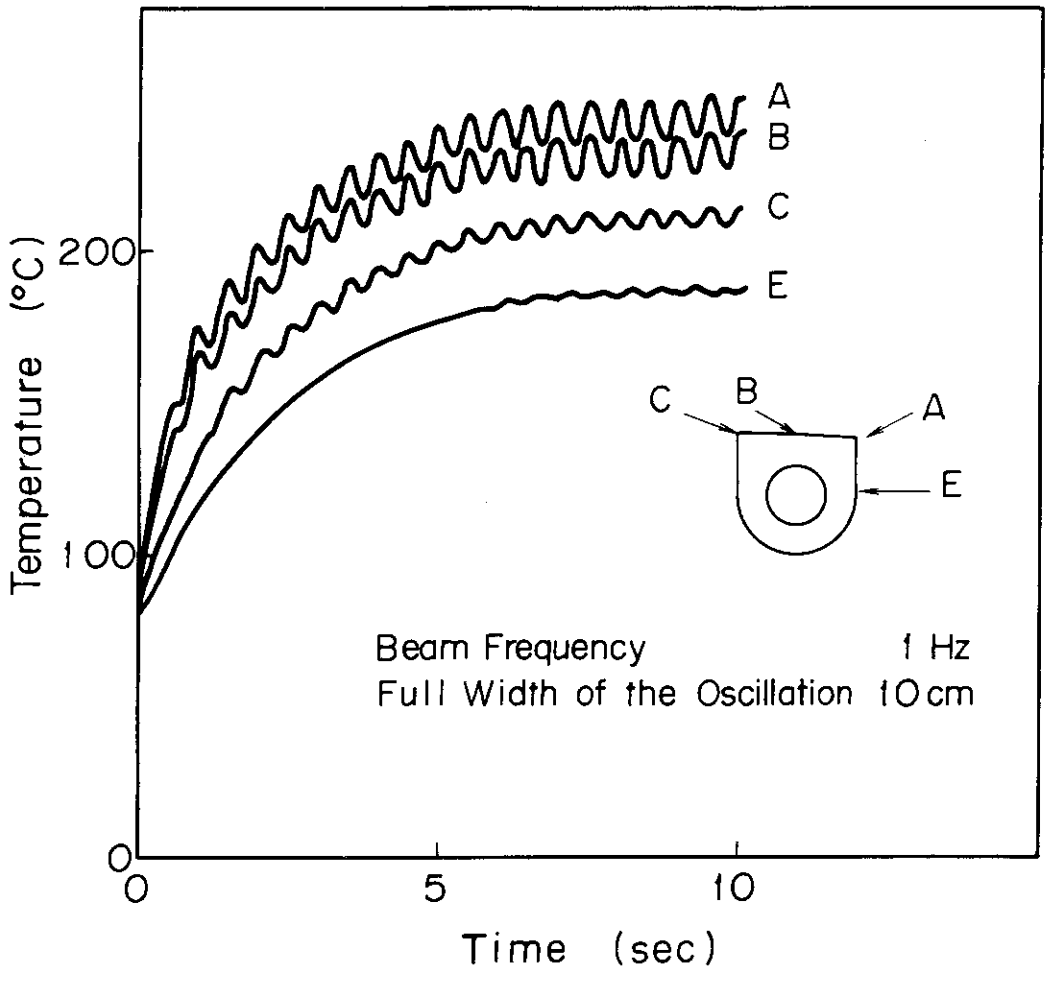

Fig. 5.3.3 Temperature Rise at the Center of the Divertor Plate When the Separatrix is oscillated with Frequency of 1 Hz. The Full Width of the Oscillation is assumed to be 10 cm.

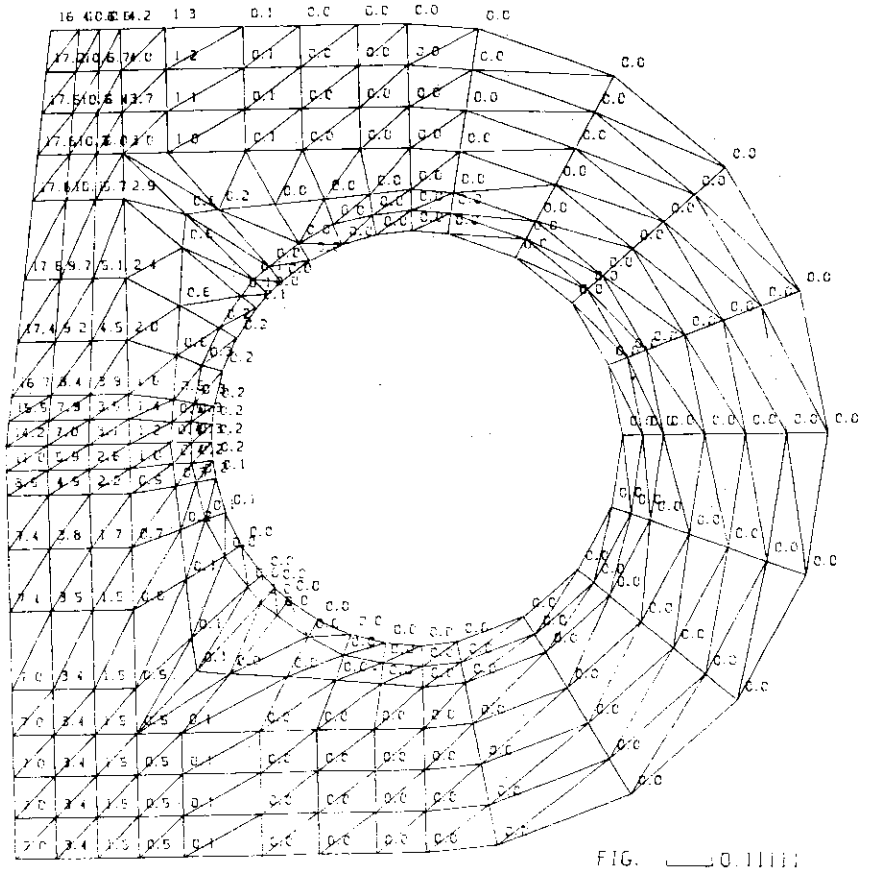

Fig. 5.3.4 Distribution of Temperature Rise in the Divertor Plate at 0.02S after Start of Irradiation

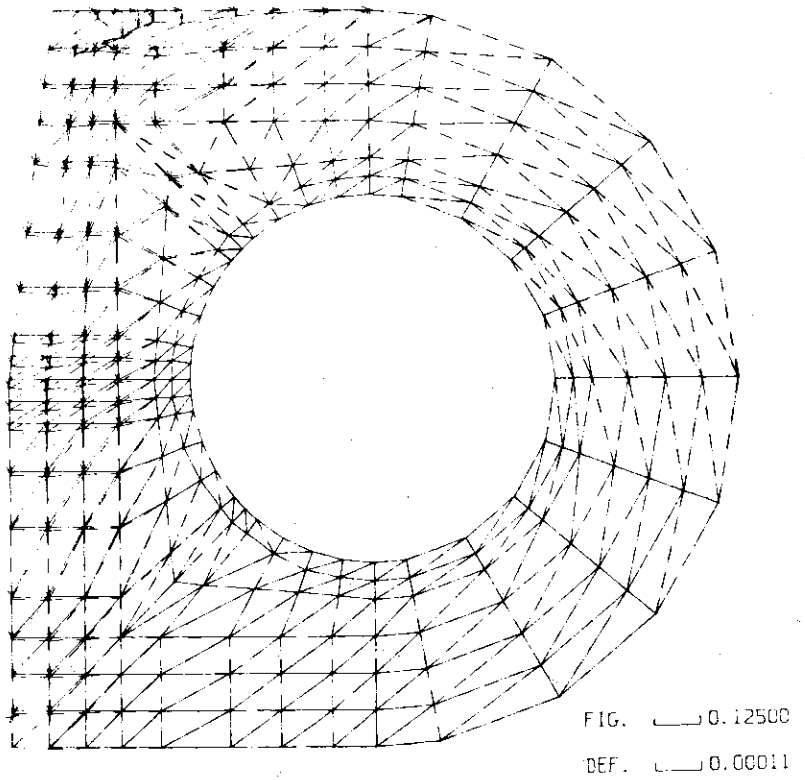

Fig. 5.3.5 Deformation of the Divertor Plate due to Thermal Stress at 0.02S after Start of Irradiation

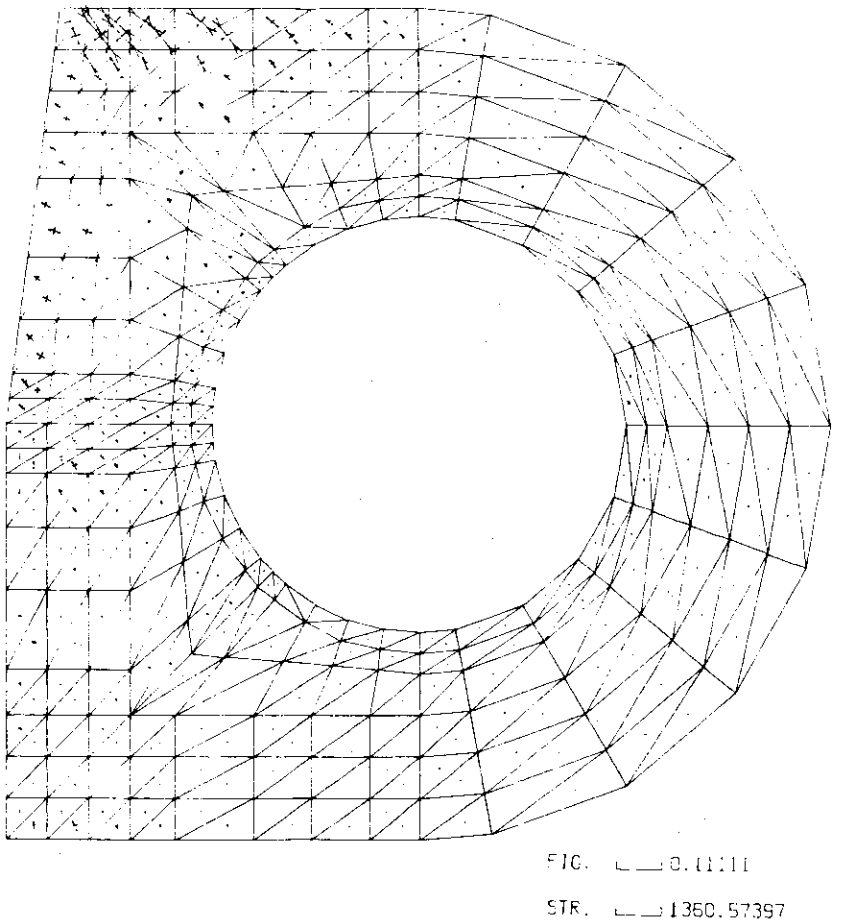

Fig. 5.3.6 Distribution of Thermal Stress in the Divertor Plate at 0.02S after Start of Irradiation

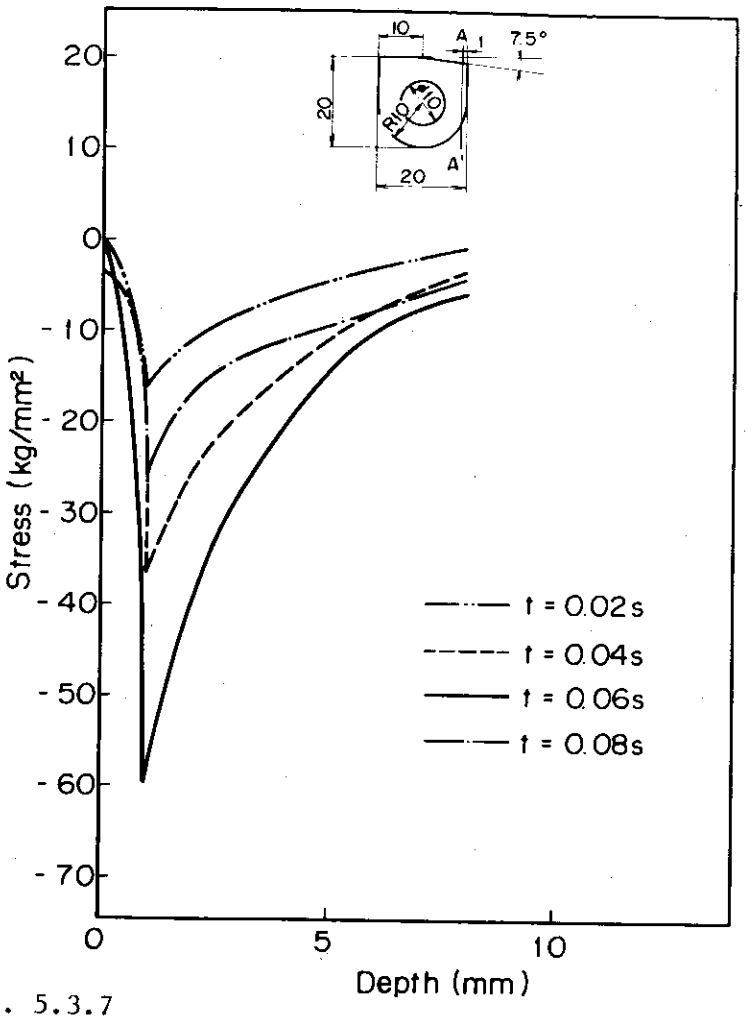

Fig. 5.3.7

Distribution of Principal Stress along the 'A-A' Line in the Divertor Plate just after the Start of Operation of the Divertor. "t" in the Figure shows the Time Elapsed after the Start.

6. Toroidal Field Magnet

6.1 Concept A

Design of the concept A toroidal field magnet of which main characteristics are shown in Table 6.1.1 corresponds to the concept A repair and maintenance of reactor. Therefore, it is supposed that a couple of coils are set on the one-sixth sector and that the sector moves radially for repair and maintenance.

Concept A toroidal field magnet is characterized by Nb_3Sn superconductor, liquid He pool boiling, disc structure for winding support and belljar type vacuum chamber.

Toroidal magnet with this type of vacuum chamber is sufficiently reinforced by cold structure since vacuum seal for these structure is not necessary.

Table 6.1.1 Main Characteristics of Toroidal Field Magnet

Structure	
Number of coil	12
Form of coil	D shape constant tension
Cable support	Disc
Number of discs per coil	36
Number of slots per disc	12
Number of conductors per slot	2 (double conductors)
Dimensions of Magnet	
Major radius	5 m
Inner diameter	$6.23^{W} \times 9.52^{H}$ m
Outer diameter	$8.44^{W} \times 11.72^{H}$ m
Magnetic Field	
Magnetic field at plasma center	5 T
Peak field at coil	10.3 T
Inductance	
Total	66 H
Stored Energy	
Total	19 GJ
Magnetomotive Force	
Total	125.00 MAT
Per coil	10.417 MAT
Magnetic Force	
Hoop force per coil	$\sim 9.6 \times 10^{3}$ ton
Centering force per coil	$\sim 3.0 \times 10^{4}$ ton
Dimensions of Coil	
Thickness	976 mm
Width	860 ∿ 1,350 mm
Length of straight section	6,060 mm
Stainless steel Disc	
Thickness	26 mm
Width	810 mm
Depth of slot	17 mm
Width of slot	29.44 mm
Depth of liq. He channel	8 mm
Width of liq. He channel	13 mm
Disc material	stainless steel
Number of Turns	
Total	5,184
Per coil	432
Per disc	12

Table 6.1.1 (continued)

Superconducting Cable	
Superconductor	Nb_3Sn
Stabilizer	Cu
Superconducting composite	Fine-multi twisted
Thickness	4.5 mm
Width	25-40 mm
Grades	4
Cu/SC ratio	49-15
Insulator	Epoxy glass fiber
Current	
Operational current	24.11 kA (12.06kA × 2 Double conductor)
Current Density	
At conductor	107.2 - 70.0 A/mm^2
Average at slot	48.9 - 32.2 A/mm^2
Average at disc	16.3 - 12.9 A/mm^2
Cooling	
Method	Liq. He pool boiling
Temperature	4.2°K
Vacuum chamber type	Belljar type
Head Load	
Superconductor loss	4.21 kW
Neutron and gamma ray heating	1.89 kW
Eddy current loss at structure material	0.15 kW
Cryostat loss	7.8 kW
Current lead loss	0.93 kW
Power Supply	
Number of suppliers	18
Excitation time	5 Hr
Length of Conductor	
Per turn (Average)	28.8 m
Total/coil	12.44 km
Weight	
Conductors of a disc	1.12 ton
Stainless steel disc (including conductors)	5.14 ton
Total/coil	370 ton

6.1.1 Magnet structure

The toroidal field magnet is composed of 12 Nb_3Sn pool boiling superconducting coils. Each coil is composed of superconducting cable, stainless steel discs, support discs, helium can, coil support legs, centripetal force support wedges, antitorque beams and thermal insulation.

1) Basic plan

Basic plans for concept A toroidal field magnet are as follows. Plans b) ∿ e) are essentially based on the previous studies for JXFR.

a) For 5T toroidal magnetic field at plasma center, 125 MAT of magnetomotive force is required. Therefore, magnetomotive force of a coil is 10.417 MAT.

b) Nb_3Sn superconductor cooled by pool boiling method is employed.

c) Operation current of cable is taken as about 25 kA supposing the soldering type double conductor cable. Combining this value with prescribed magnetomotive force operation current, total turn of magnet and turn per coil are determined as 24.11 kA, 5,184 and 432, respectively.

d) Hoop magnetic force is supported by disc structure which has higher ridgidity for hoop deformation.

e) Basic configuration of the coil is D shape constant tension to minimize the internal stress of coil.

2) Configuration

As previously noted, the basic configuration of the disc which support the hoop magnetic force is D shape constant tension. This configuration is determined from the radial position of coil and coil number. The radial position of coil on mid plane is determined as 1,825, 2,635 mm for nose and 8,915, 9,725 mm for outer branch from the view point of spatial relations with shield and poloidal magnet. Resulted configuration of the disc is shown in Fig. 6.1.1. Configuration of the support disc which fixed on both sides of assembled disc for coil reinforcement is deformed from simple D shape constant tension as shown in Fig. 6.1.1 to support poloidal coils No. 10 and No. 11.

3) Disc and relating structures

To support the hoop force and the weight of superconducting winding, disc type structure is used. Each disc has 12 slots for cable insertion and He channels on one side. Thickness of the disc is 26 mm and 36 discs are assembled to constitute a coil.

Slot distribution on disc as shown in Fig. 6.1.2, is determined from the view point of stability of superconductor. Superconducting cable is fastened to disc by small plate so that superconductor is sufficiently cooled by liq. He. Detail structure and liq. He flow pattern is shown in Fig. 6.1.3. On both sides of the assembled discs, support discs are settled to bundle discs and to strengthen the coil. Poloidal coil No. 8, 10 and 11 are fixed on the outer branch of the support discs. Thickness of the support disc is 60 mm. At the nose of the coil, the support disc is wedge shaped to support the centripetal force. By virtue of the wedge structure, the centripetal force of $\sim$ 30,000 tons/coil is supported. The support discs and wedges are tightened to assembled discs by tie bolts.

Between wedges of neighbouring coils, alignment pins are inserted as shown in Fig. 6.1.4. Facial pressure between wedges by centripetal force is less than 10 kg/mm^2. This wedge structure is also effective to support the overturning load at the inner branch of coil.

At outer branches, coils are mutually connected by antitorque beams to resist for overturning forces. Though the cross sectional area of beam in Fig. 6.1.1 is provisional, sufficient beam area is obtainable since each coil does not have each own vacuum chamber.

Assurance of mutual positions between discs and between disc and support discs or wedge structures is important for disc type coil. In this design, key structure is planned for this purpose, however, the detail design study and R & D are required.

Each coil has 2 legs to support dead weight. Considering the radial shrinkage of the coil and heat transfer from the base, double pendulum type leg is chosen. GFRP (glass fiber reinforced plastic) solid leg is now also studied.

Thermal insulation of which basic components are the vapor shield and super insulation is applied to the cold structures. At the area between poloidal and toroidal field coils, thermal insulation is not necessary.

Stress distribution within the D shape constant tension coil is only tension in ideal and is able to be estimated by following formula.

$$\sigma_t = \frac{\mu_o N i^2}{4\pi S}\left[\frac{P}{R}\left(1+\frac{1}{N}\cos\phi\right)+\frac{1}{N}\ell n\frac{1.284}{CN}R\right]$$

here, μ_o ; magnetic susceptibility of vacuum

N ; number of coils

i ; magnetomotive force of a coil

S ; effective crosssectional area of coil

P.R.ϕ ; curvature radius, radial position and angle of the representative position

C ; compensation factor

According to this formula, hoop stress of the disc is calculated as $\sim$ 26 kg/mm^2. Previous experience on JXFR design studies predicts maximum stress within the disc of this design may be in the range of 35 $\sim$ 40 kg/mm^2.

4) Belljar

Structure of the vacuum chamber largely affects on the repair and maintenance procedure. We have compared the following three types of vacuum chamber.

(a) Individual type vacuum chamber

(b) Hybrid type vacuum chamber

(c) Belljar type vacuum chamber

Though brief comparison of vacuum chamber shown in Table 6.1.2, belljar type vacuum chamber is employed. This type of vacuum chamber much simplifies the structure and assembling procedure of the magnet. Furthermore, space factor of the magnet is high and this fact agrees with compactness which is one of the guiding principle for INTOR.

Outline of the belljar of which diameter, height, volume are $\sim$ 23 m, $\sim$ 20 m, $\sim 10^4$ m^3, respectively, is shown in Fig. 6.1.5. The belljar is divided into dome, cylinder, siding and floor. Dome, cylinder and siding are designed as shell structure with vertical and horizontal ribs. The floor is composed of stainless steel liner. Corresponding to the one sixth sector of the machine, the belljar cylinder is divided into six segments along the torus. Some of the cylinder segments have air-lock entrance for man access and evacuation. Whole of the belljar is electrically insulated across the torus.

Table 6.1.2 Brief Comparison of Vacuum Tank for Toroidal Field Magnet

Item	Individual type	Hybrid type	Belljar type
Structure	Each coil has own exclusive vacuum chamber.	Each coil shares vacuum chamber between other coils and poloidal field coils.	Almost all the portion of the machine is enveloped by belljar.
Space factor of the magnet structure	Space factor is lower than other two types of vacuum chamber since each coil has its own chamber.	Space factor is intermediate.	Space factor is highest because no vacuum barrier near to coils.
Centripetal force support structure	The force should be supported through the vacuum tank. Therefore, cold support is impossible.	Cold support is possible.	Cold support is possible.
Assembling procedure of magnet	Vacuum seal process of the vacuum chamber through assembling is not necessary.	Vacuum seal process of the vacuum chamber through assembling is necessary. This process should be made by remote handling machine.	Vacuum seal process of the vacuum chamber of each coil is not necessary and direct aligning of coils is possible.

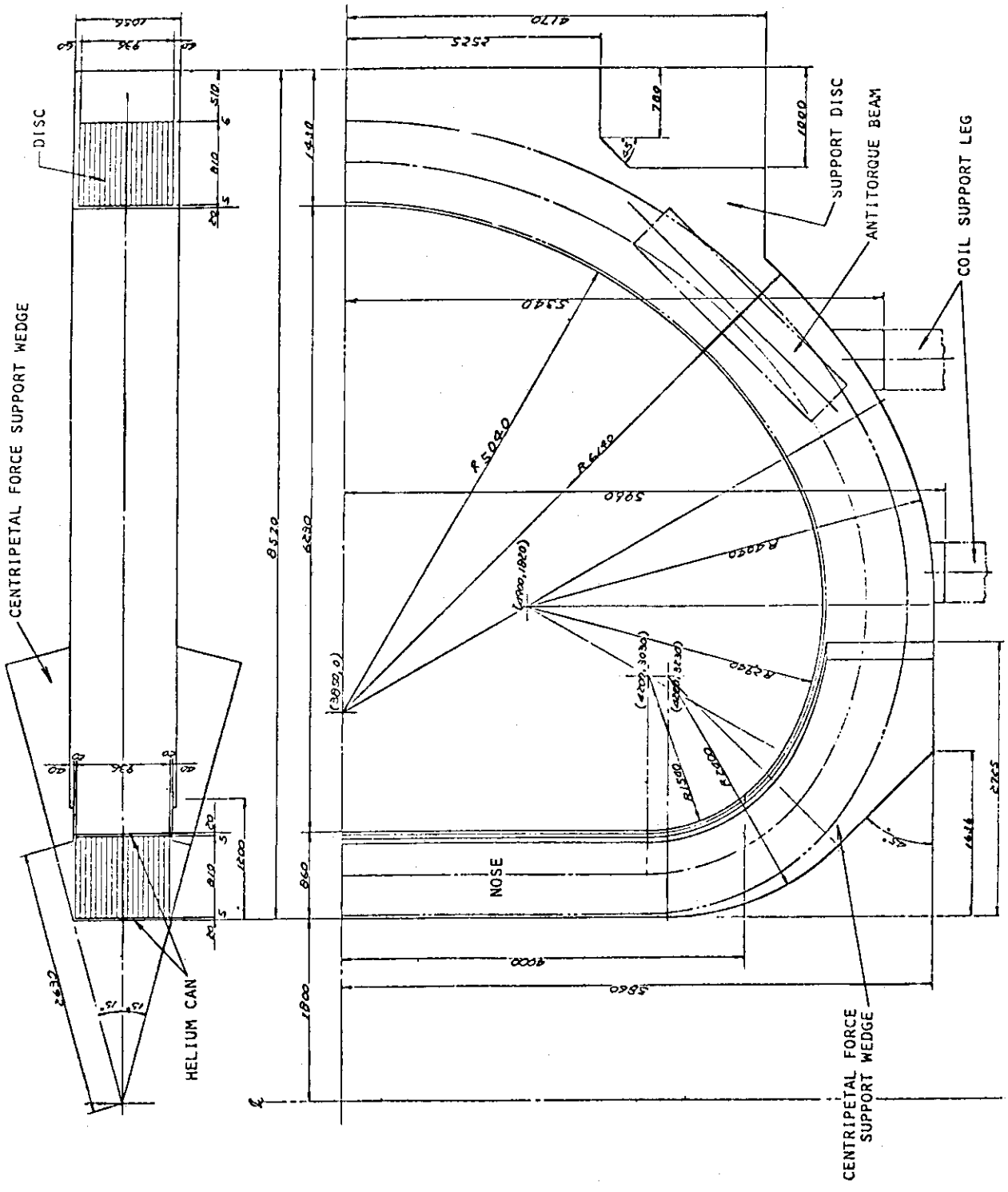

Fig.6.1.1 TF coil structure

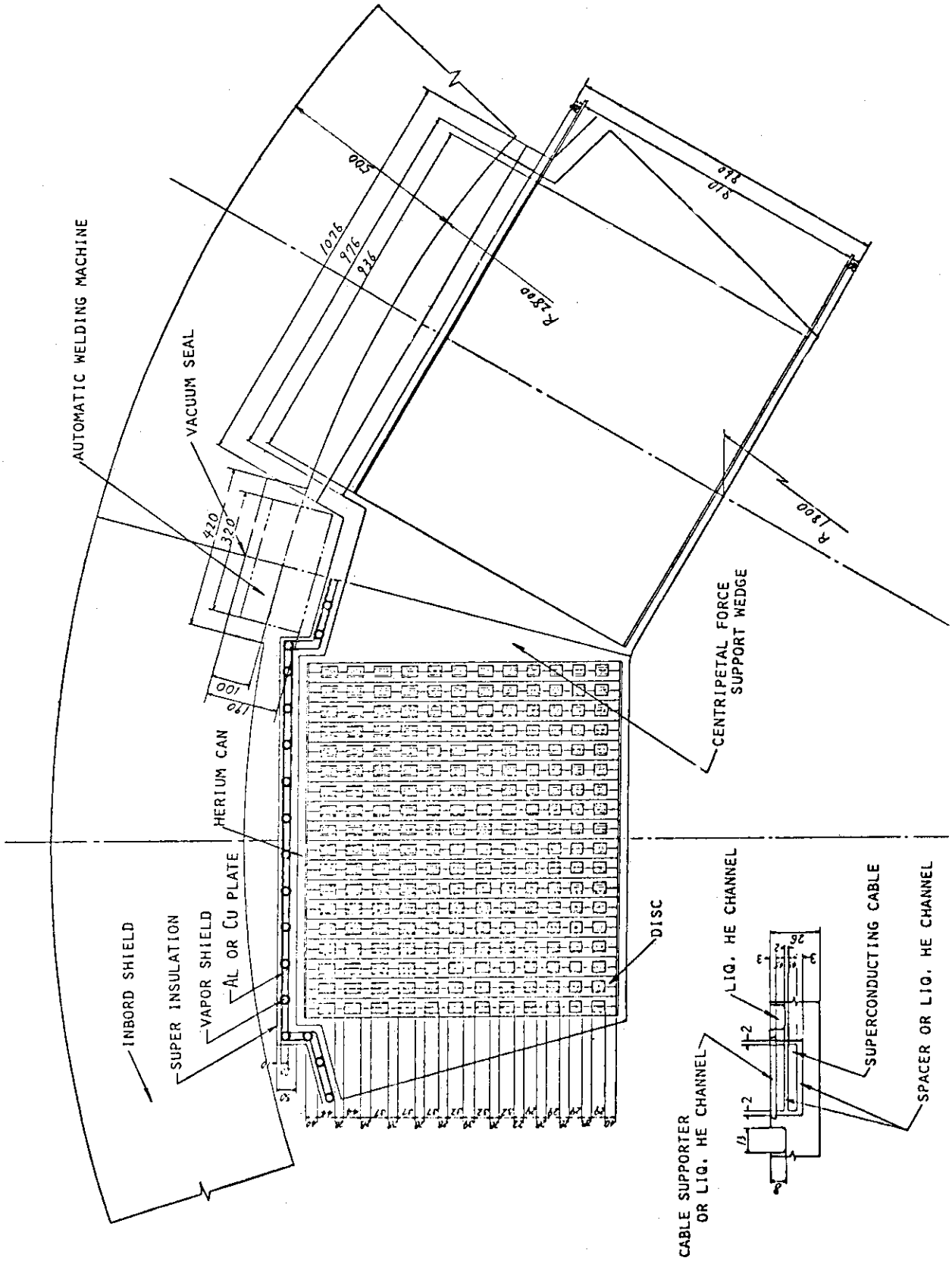

Fig. 6.1.2 TF Coil Nose Structure

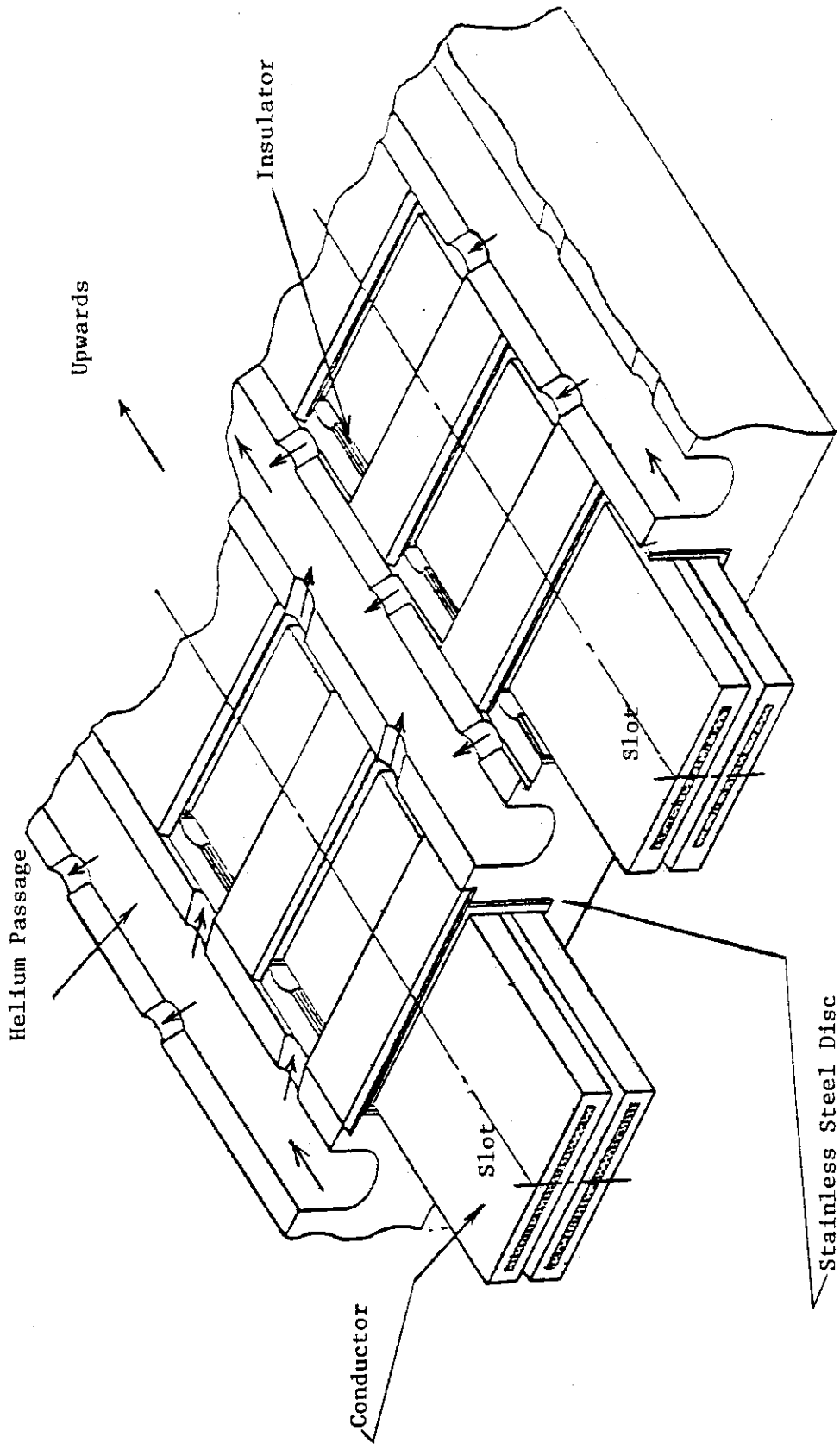

Fig. 6.1.3 Bird's-eye View of Super-Conductor Fixed to Slot and Liq. He Flow Pattern

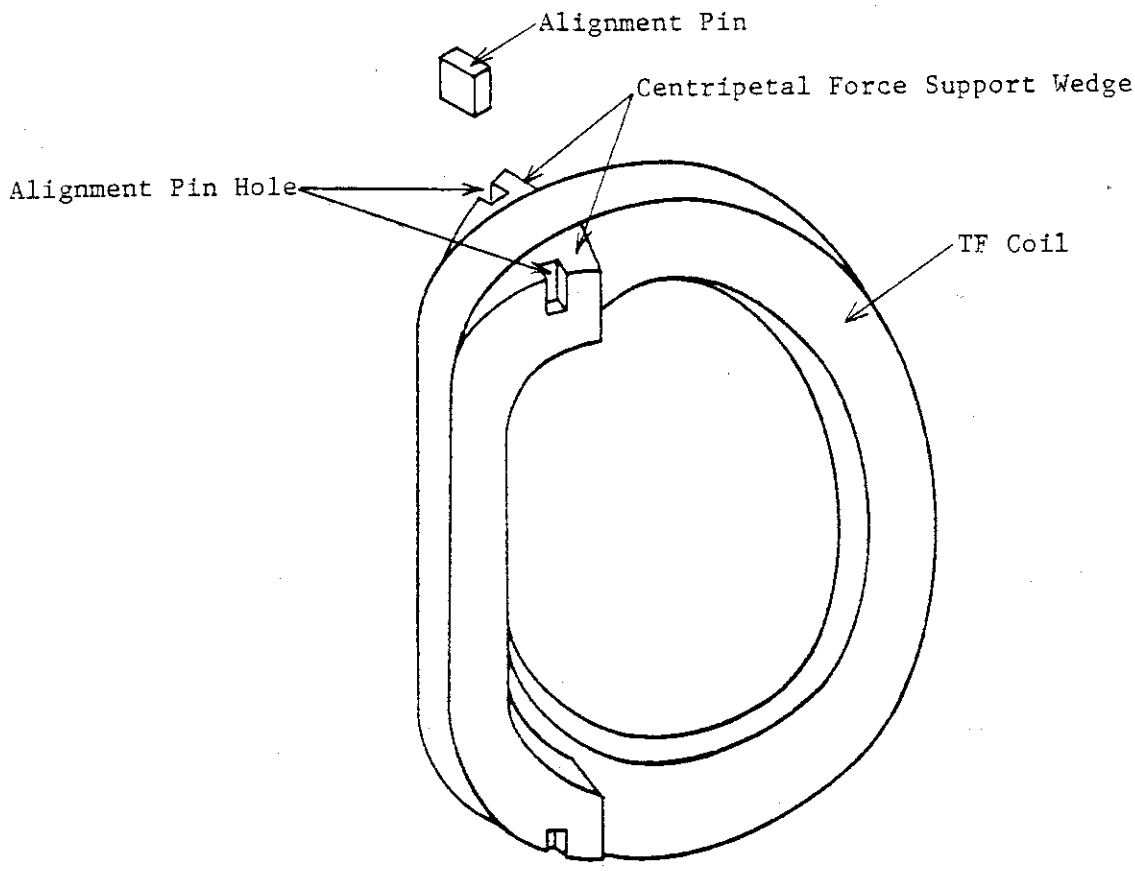

Fig. 6.1.4 Alignment Pin of TF Coil

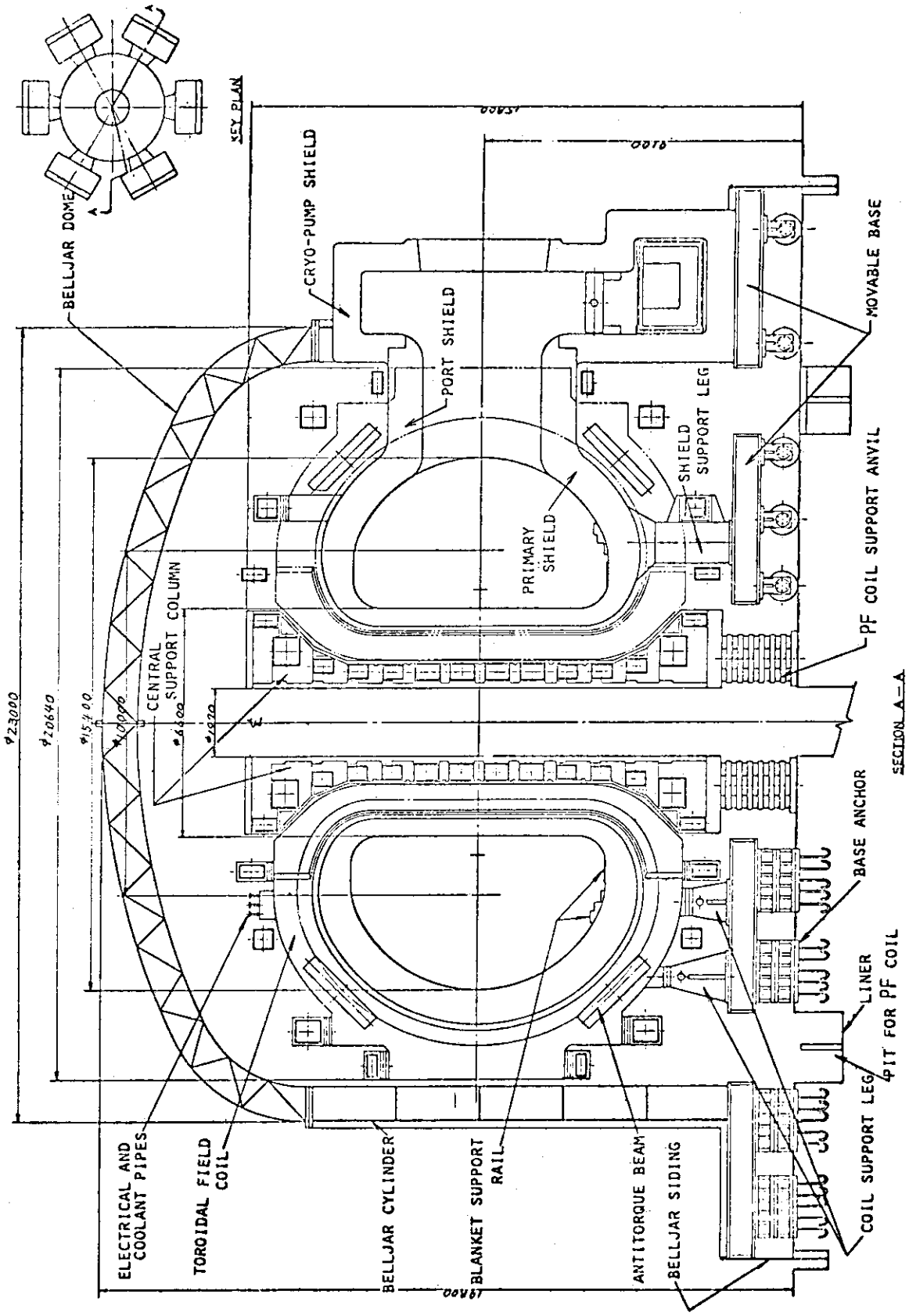

Fig. 6.1.5 Concept A Typical Section

6.1.2 Design Analysis

Structural design analysis is briefly described in Section 6.1.1. Conductor design and heat loss calculations including the same items for the poloidal field coils are described.

(1) Magnetic analysis

Magnetic analysis of the toroidal array consists of two main parts. The first is the determination of the peak magnetic field, the magnetic field as a function of radius and ampere turns per coil required to the desired field (B = 5 tesla at R = 5 m) with 12 toroidal coils. The second portion of the magnetic analysis is concerned with the calculation of forces acting on various parts of the toroidal field coils.

Determination of the peak magnetic field and spacial distribution of magnetic field was performed by using the magnetic field code, in which the coil winding and structure are treated as a homogeneous current carrying member.

Figure 6.1.6 shows the field plot for the coil array in Figure 6.1.1 on the condition, B = 5 tesla at $\bar{R}$ = 5 m. Each coil in the array has 10.42×10^6 ampere turns with a peak flux density of 10.02 tesla at the windings (2.615 meters from torus center). Considering the increased flux density in the area of the individual conductors, at the D shape straight corner, and the additional field of a poloidal field (perpendicular to a toroidal field), the peak field applied on the conductor is about 10.3 tesla.

The second requirement of magnetic field analysis is the determination of forces existing in the coil array. Forces acting on TF coils are as follows ; 1. hoop force/coil 2. centering force/coil (9.4×10^3 tons) 3. lateral force added from the poloidal magnetic field (3×10^4 tons).

(2) Selection of conductor coolant mode, conductor support structure type and conductor

In Table 6.1.3, selection of coolant mode, conductor support structure and conductor are shown with its brief reasons.

(3) Conductor design

Operational current of the toroidal field coils were decided to about 24 kA. In aspects of cryogenic stability of a conductor, the double conductors fixed in each slot, as shown in Figure 6.1.3, are chosen. Therefore, each conductor has a current of about 24/2 kA.

A conductor is the cable, the compacted soldered on the Cu substrate.

The conductor size was designed using the typical characteristics shown in Figure 6.1.7 ∿ Figure 6.1.10. Criteria for the cryogenic stabilization is "cold end stability (Maddock's method)". 4 gradings of the conductors were chosen, according to the magnetic fields applied on them.

Specifications of conductors and discs are briefly shown in Table 6.1.4.

(4) Heat load

Heat losses of the toroidal and poloidal field coils are shown in Table 6.1.5. The major parts of AC losses (field coupled hysteresis and eddy current loss) are superconductor loss.

Table 6.1.3 Selection of a conductor, support structure and cooling mode

([ ] : selected term)

	Selection Terms	Reasons of selection
Conductor	Nb-Ti Nb-Ti/Nb_3Sn [Nb_3Sn]	1. Peak field B max is about 10 tesla. 2. Under the condition of limited space of TF coil crosssection, high-Jc characteristics of Nb_3Sn will make structure design easier. 3. Nb-Ti/Nb_3Sn hybrid coil will have no merits in the future, when much Nb_3Sn conductor is used.
Support structure	[Disc] Pancake	1. Disc type support makes the stresses of Nb_3Sn composite conductor smaller.
Cooling mode	[Pool boiling] Forced flow SHE	1. Pool boiling coil system has more known engineering techniques, though vapor bubbles to traverse the conductor must be taken care of in its design.

Table 6.1.4 Brief Specifications of Conductors and Discs

Slot No.	Applied Field (T)	Cu-Substrate Width (mm)	Slot Width (mm)	Current Density (conductor) (A/mm^2)	Current Density (slot) (A/mm^2)	Current Density (disc) (A/mm^2)
1	2.7	25	29	107.2	48.9	16.3
2	2.7	25	29	107.2	48.9	16.3
3	3.1	25	29	107.2	48.9	16.3
4	4.0	25	29	107.2	48.9	16.3
5	4.6	28	32	95.7	44.3	15.5
6	5.3	28	32	95.7	44.3	15.5
7	6.0	28	32	95.7	44.3	15.5
8	6.6	33	37	81.1	38.3	14.3
9	7.3	33	37	81.1	38.3	14.3
10	8.0	33	37	81.1	38.3	14.3
11	9.2	40	44	70.0	32.2	12.9
12	10.3	40	44	70.0	32.2	12.9

* Nb_3Sn filament dia. 22 μmϕ

strand dia. 0.5 mmϕ

Table 6.1.5 Heat loads of toroidal and poloidal field coils

Heat load	Toroidal field coil (kW)	Poloidal field coil (kW)	note
Superconductor loss	4.21	12.0	4.5°K load
Nuclear heating	1.89	-	
Eddy current loss at structure material	0.15	-	
Current lead loss	0.93	3.2	
Cryostat loss	7.8		80°K load
Thermal shield*	10.5		
Thermal anchor*	5.9		

* Inlet temperature is 50°K.

6.1.3 Design problems

Design problems in toroidal field magnet are as follows.

1) Assurance of mutual position between discs, and between disc and wedge are important for disc type toroidal magnet. Therefore, we are now planning and evaluating to use key structure accompanying with other effects. However, there are possibilities of change in structure according to the comparative evaluation study. Settlement of support ring, tapering of discs, etc. are alternative concepts. Therefore, figures relating to this problems are not shown in detail at this stage.

2) Assurance of electrical insulation between disc and/or coils.

3) High stresses within the disc and superposition of cyclic load by poloidal fields.

4) Assurance of He bubble transport.

5) Alignment of coils.

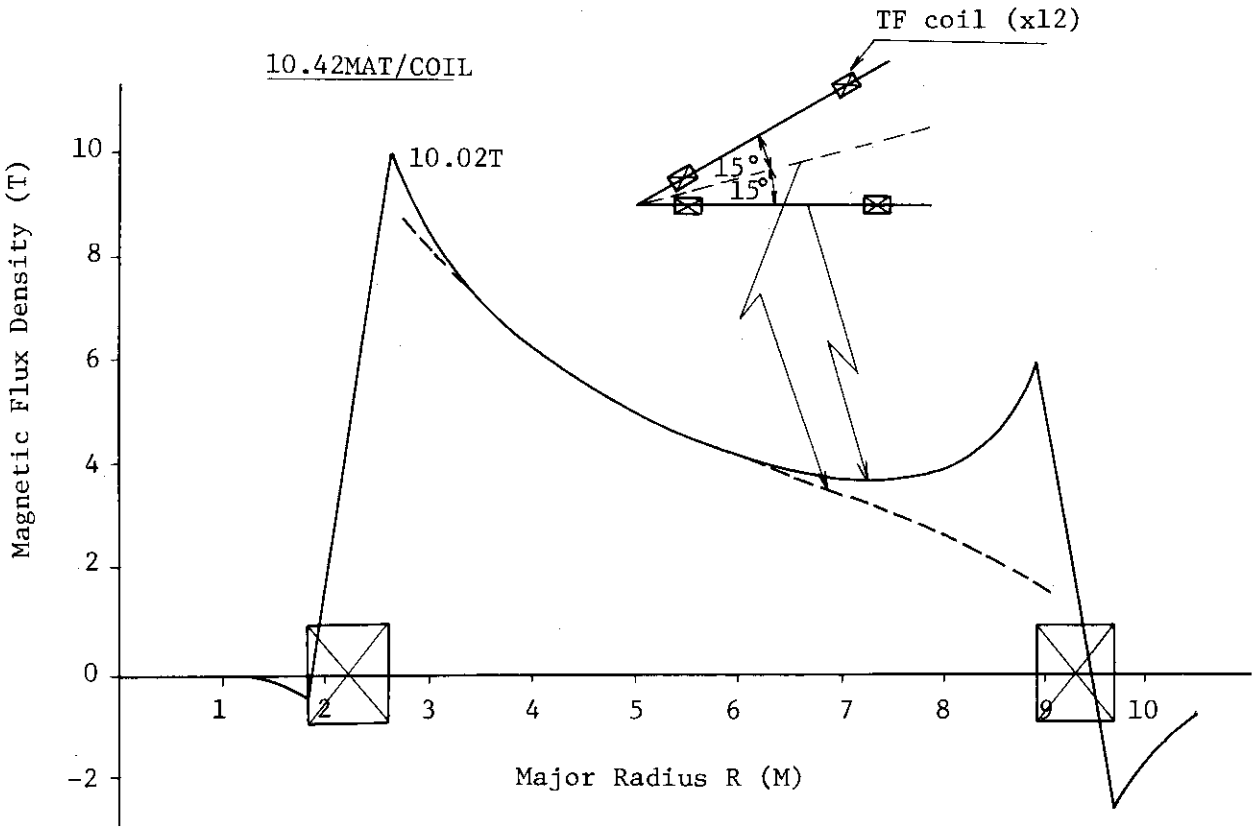

Fig. 6.1.6 Magnetic Flux Density v.s. Major Radius

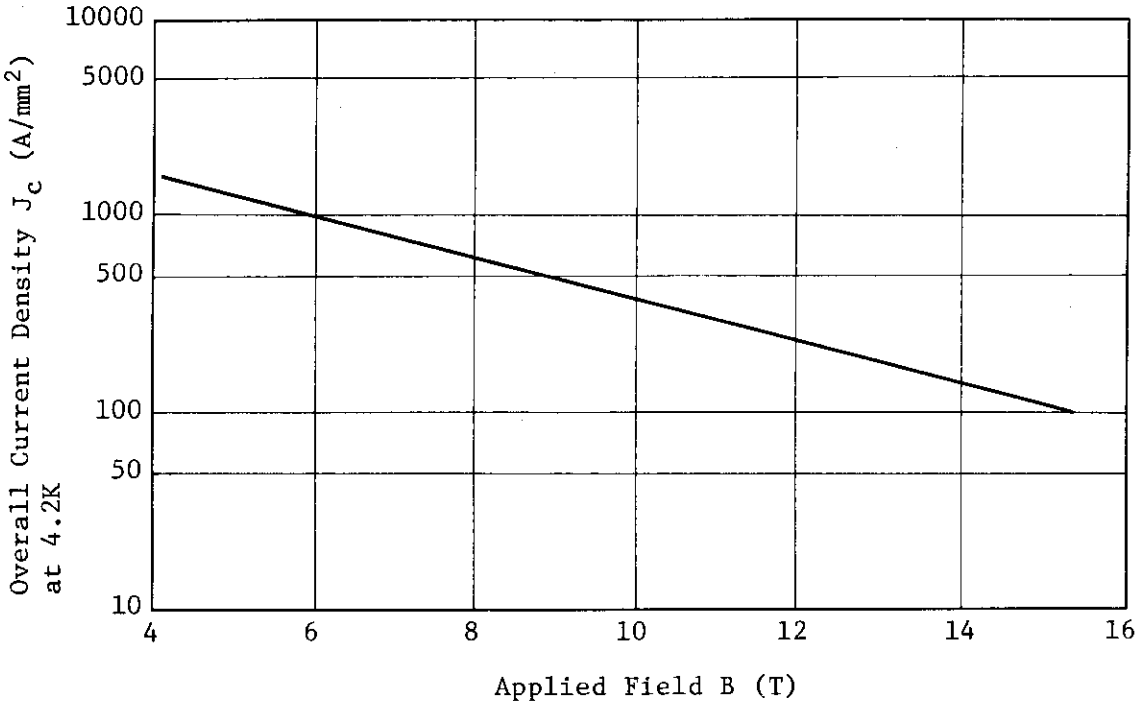

Fig. 6.1.7 Current Density v.s. Applied Field

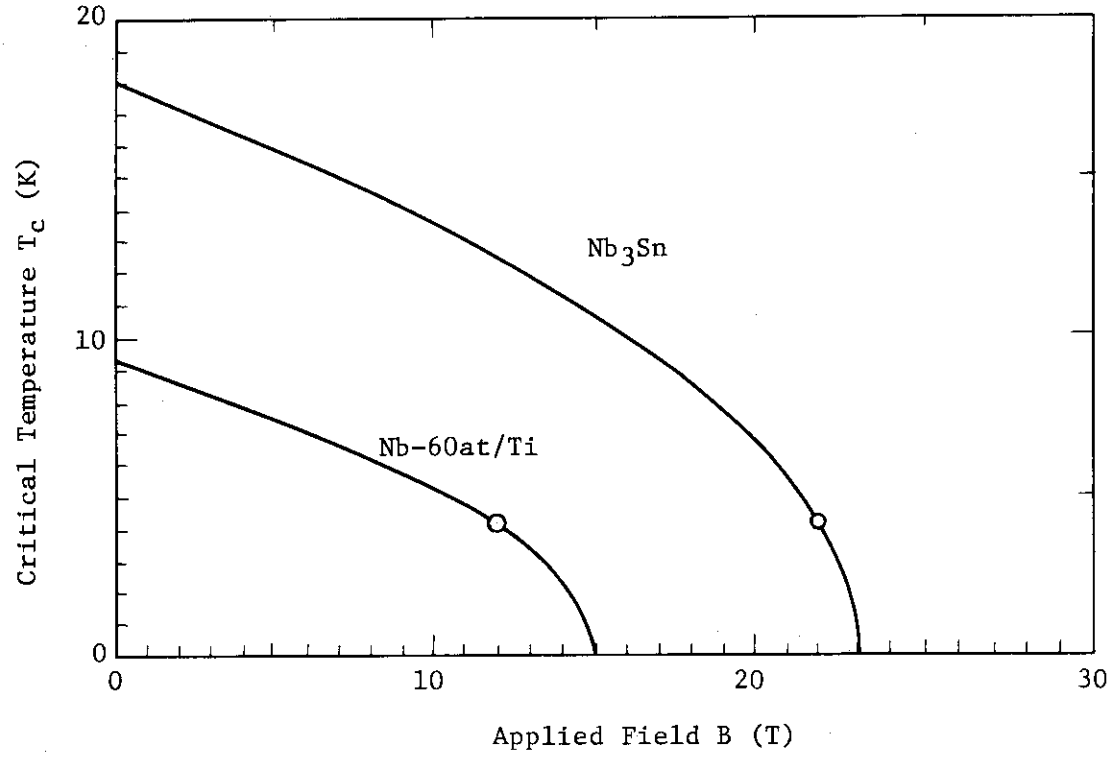

Fig. 6.1.8 Critical Temperature v.s. Applied Field

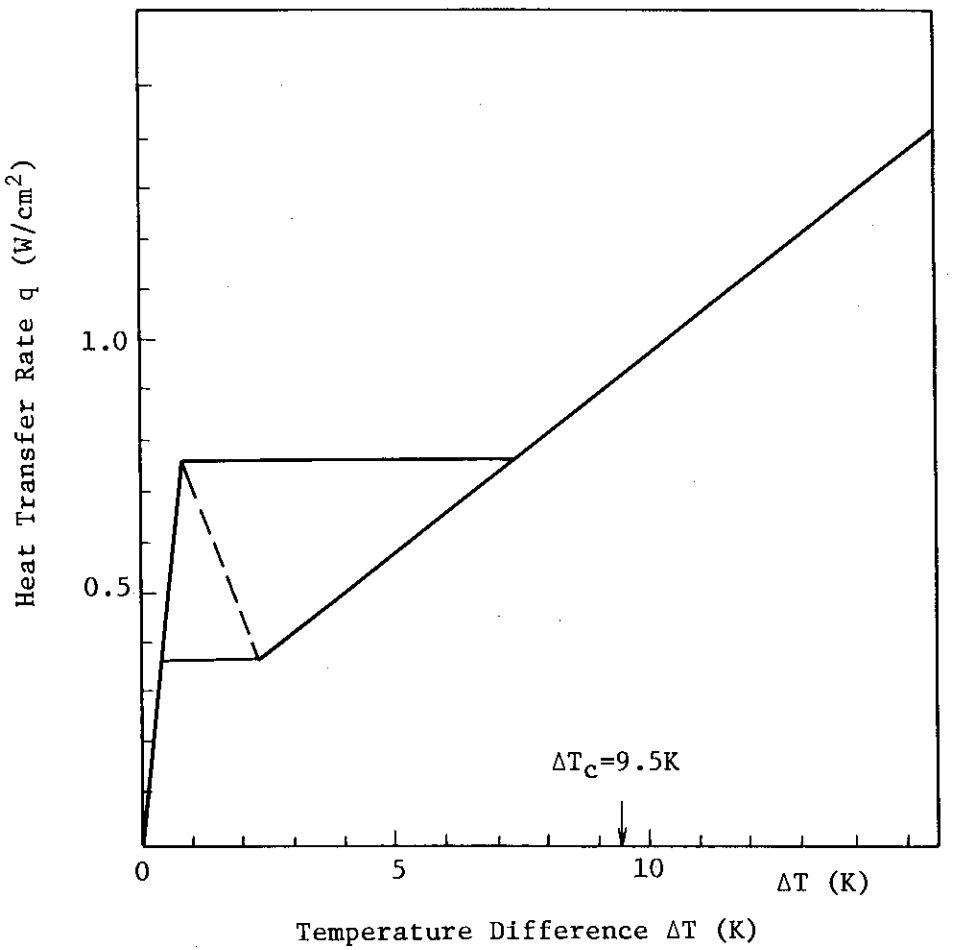

Fig. 6.1.9 Heat Flux of Rough Surface Conductor

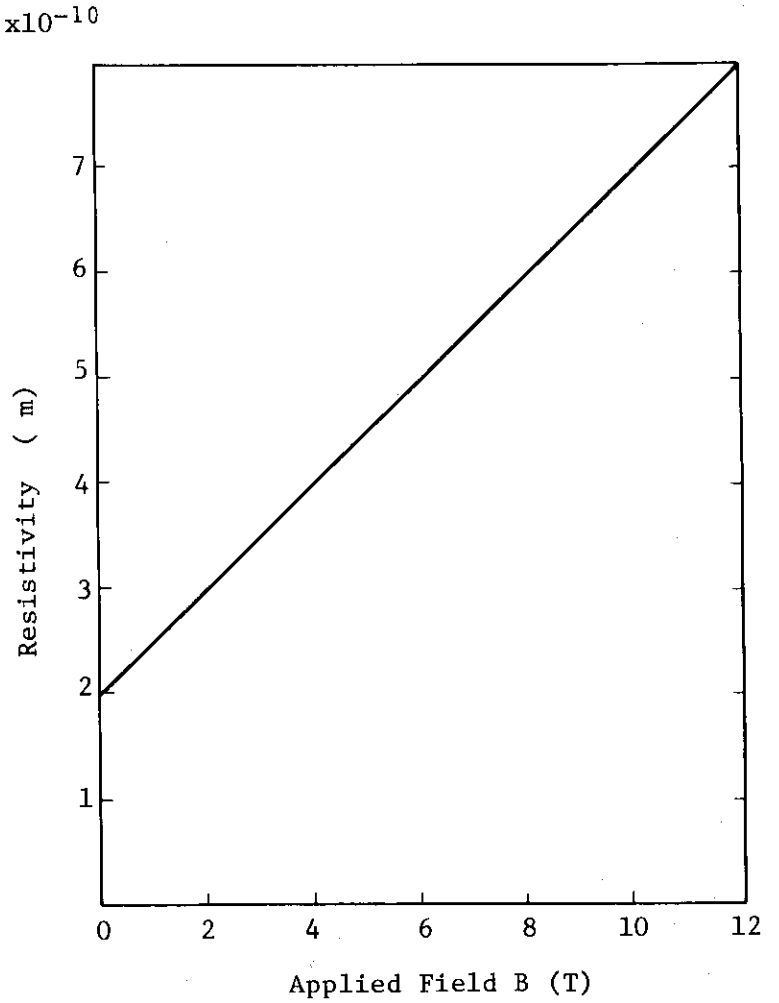

Fig. 6.1.10 Field Dependency of Cu resistivity

6.2 Concept B

The toroidal field (TF) coils are designed on the basis of the present and predictable technology. The coil characteristics of design B are listed in Table 6.2.1.

Table 6.2.1 TF Coil Characteristics

No. of coils	12
Cooling concept	Pool boiling
Windling concept	Pancake winding
Shape of coil	Constant tension D-shape
Superconductor	Multifilamentary Nb_3Sn
Stabilizer	OFHC hard copper
Peak field	11.0 T
Operating current	20,000 A
Average current density (in winding)	18.8 A/mm^2
Winding cavity	0.8 × 0.69 m^2
No. of turns	520 turns
No. of pancakes	13 double pancakes
No. of grading	3 (for 11 T, 8 T, 6 T)
Material of coil case	Stainless steel
Magnetic motive force	10.4 MAT/coil

6.2.1 Magnet structure

Conductor and Coil Winding: The conductor consists of multifilamentary Nb_3Sn and hard copper, and each conductor is reinforced with inserted stainless steel tape. The reinforcing tape which amounts to about 20% of the conductor is inserted so that the stress of the conductor can be acceptable. The conductor is designed to be cryostable in a pool boiling system. An aspect ratio of the conductor is about 2 and the both sides are longitudinally grooved to enlarge the cooled surface of the conductor.

Three conductor grades for operation at nominal fields of 11, 9, and 6 T have been designed in order to reduce the winding area and the cost. A pancake winding is selected in view of achievement of well ventilated helium channels. Pancake winding also produces well defined surfaces for transmission of radial forces. The scheme of the coil winding and the typical three graded conductors are illustrated in Fig. 6.2.1.

Structures: The shape of coil is made to be constant tension[1] as shown in Fig. 6.2.2, so as to optimize a stress distribution and minimize a bending stress of conductor and coil case. The coil bore is 6.1 × 9.2 m and the outer periphery of coil is 8 × 11.1 m. Cross sectional area of the coil is 0.83 m^2 (0.94 × 0.88 m) including coil case, and winding area is 0.55 m^2 (0.8 × 0.69 m), resulting in an overall current density of 12.6 A/mm^2. Both inner ring and outer ring are 50 mm thick and side plate is 75 mm thick except at the inner portion of the coil.

The length of the coil straight section is 5.74 m, and centering force (30,370 ton/coil) is supported by wedged portion of 12 coils. For this purpose, the wedges are inserted between coils, and connected with center cylinder by means of adjusting bolts as shown in Fig. 6.2.3.

The hoop force is supported by winding itself and coil case. The out-of-plane force causing overturning moment is supported by support structure attached between coils.

Total overturning moment (torsion) of toroidal magnet is supported by torsional rigidity of the whole toroidal magnet structure system. The gravity of all toroidal magnets is supported by center cylinder which is connected with all magnets by means of keyway and pins at top and bottom positions.

Vacuum chamber of toroidal magnet: A part of vacuum chamber of toroidal field coil is in common with the plasma vessel, which is placed at the shielding structure, on the inside of the torus in the major radius direction. The vacuum chamber of toroidal and poloidal inner magnets is in common at the inner portion of the torus. Moreover, as shown in Fig. 6.2.4, each separate vacuum chamber of toroidal coils is welded with the above-mentioned common chamber at the inner location of the torus.

REFERENCE

1) R.W. Moses, Jr. and W.C. Young; "Analytic Expression for Magnetic Forces on Sectored Toroidal Coils", Sixth Symposium on Engineering Problems of Fusion Research, (1975) 917.

6.2.2. Design Analysis

Field Analysis: A peak field which appears on the surface of the coil winding is calculated by using a field analysis programme. A field distribution including the peak field at the mid-plane is illustrated in Fig. 6.2.5.

Stability Analysis: The reliable operation of the coil requires the cryostability. Cryostable conductors are designed in such a way that the heat flux generated when transport current flows in the stabilizer is below allowable limits. The generated heat flux is given by

$$q_g = \frac{\rho I^2}{pA}$$

where, I is transport current, ρ is stabilizer resistivity, A is stabilizer cross section and p is cooled perimeter. Heat transfer characteristics indicates that the allowable heat flux removed from the surface of this 11 T conductor will be about 0.45 W/cm^2 which is over the generated heat flux. Further heat transfer improvement will be required in connecting with resistivity increase of copper due to neutron radiation.

Electromagnetic Force: The forces acting on TF coils are divided into the in-plane and out-of-plane forces. The in-plane forces which come from the interaction between TF coils, cause the hoop forces; the out-of-plane forces which come from the interaction between TF coils and PF coils cause the overturning moment. The in-plane forces acting on the each block of the TF coil are illustrated in Fig. 6.2.6. The centering forces moving toward the machine center are about 30,000 tons. The out-of-plane force distribution is illustrated in Fig. 6.2.7. In Fig. 6.2.7, the directions of the forces reverse near the top of the TF coil due to reverse of the shaping field.

Structural analysis: We carried out stress analysis of toroidal field coil against in-plane force as shown in Fig. 6.2.6 with two-dimensional plane stress analysis by finite element code SAPIV. Figure 6.2.8 shows the analysis model for toroidal field coil. In carrying out stress analysis of toroidal field coil, we assumed the followings,

(a) Treatment of inner ring and side plates

As winding tends to separate from inner ring during operation, we set up a gap between conductor and inner ring. We consider that the spacer between conductor and inner ring does not contribute as structure member during operation. We also treated spacers between conductor and side plate as mentioned above.

(b) Treatment of the spacer between conductor and outer ring.
The spacer between conductor and outer ring transmits the load only to normal direction, but not to shear direction, so that we used rod element to represent the spacer, taking account of interaction between conductor and outer ring.

(c) Material constant of conductor.
Since the winding is composite material consisting of copper, layer insulator and spacer, it is necessary to treat the winding as an anisotropic material. The resultant stress of the winding thus stands for mean stress of the winding composed of the three materials. We, therefore, need to transform the resultant stress to the stress in the copper portion by taking account of the difference of the physical properties in each portion. The equivalent Young's modulus, Poisson's ratio, and shear modulus were calculated in such a way that strain energy is not to be changed.

Calculation results: We carried out the stress analysis of toroidal field coil under the above-mentioned conditions. Figure 6.2.9 depicts the shape of the deformation and displacements of toroidal field coil. Figure 6.2.10 indicates the distribution of the stress intensity of toroidal field coil. The distribution of the stress intensity along the coil perimeter for each structure, (winding, inner ring, outer ring and side plate) are shown in Fig. 6.2.11 to Fig. 6.2.13.

It is found that the stress distribution at the element center near the central part of the winding is constant along the coil perimeter. But the stress distribution on the inner and outer surface of the winding is not constant. This is because of the influence of the winding thickness in radial direction. Accordingly, maximum stress intensities are 21.8 kg/mm^2 at the winding inner surface and 34.5 kg/mm^2 at the inner surface of the stainless steel inner ring. Here, the winding resultant stress is mean value. Transforming it to the stress in the copper part, the maximum stress intensity of stabilizing copper is 23.9 kg/mm^2.

If these stress intensities are taken for (P_L+P_b) in ASME Boiler and Pressure Vessel Code Section III, they must be smaller than 1.5 Sm. (Sm is an allowable stress and is 15 kg/mm^2 for hard copper at 4 K, and is 30 kg/mm^2 for stainless steel at 4 K, respectively). Therefore, coil case has an enough margin against failure. In contrast, it should be noted that the copper of the toroidal field coil is on the boarder of limitation of $1.5S_m$.

It can be said that the copper stress may become less, if the effect of conductor grading is considered. On the other hand, we have to take into account the mechanical strength of toroidal field coil against the out-of-plane force causing overturning moment as shown in Fig. 6.2.7. The maximum bending stresses of toroidal field coil are 4.1 kg/mm^2 of stabilizing copper, and 5.5 kg/mm^2 of coil case, respectively. Thus, the toroidal field magnet is in severe conditions in view of mechanical strength of the magnet.

6.2.3 Magnet type selection

The configuration of superconducting magnets greatly influences on both electrical and mechanical performances. There exists various choices in the selection of superconducting magnets. Some of those are such as the shape of conductor, cooling method, winding configuration, or type of conductor reinforcement. Considering the current technology of superconducting magnets, it seems that its engineering level is far below than required. We only assume that steady progress on research and development will make the choice narrow.

(a) Selection of conductor cooling method

Pool boiling was determined to be feasible for the toroidal field magnet for several reasons compared with the forced flow supercritical cooling. One of the advantages of the pool boiling is that it requires less electrical power to circulate the helium coolant. It also has more mature technology. On the other hand, the forced flow cooling needs considerable development of helium circulating pump. Another disadvantage is that the cooling pipes make the magnet structure and construction complicated. Also the stability criteria are not so clear as pool boiling.

(b) Conductor reinforcement

Though the shape of magnets was made to be constant tension type, it experiences pretty large stress. Therefore, the mechanical integrity of the coil play an important role for the reliable operation. The design of coil integrity has to be taken into account in connection with cooling methods. In case of pool boiling, coil integrity will be increased by either the adoption of grooved steel plate or the insertion of steel tape between turns. In this design B, the insertion of steel tape was preferably selected because the grooved steel plate is expensive in fabrication

and less effective to remove the vapor bubbles. It is noted that the coil integrity tends to decrease due to the fact that many cuts to three directions in the steel plate is necessary for the channel of vapor bubbles in case of pool boiling.

(c) Winding configuration

The pancake winding was adopted here because it has better cooling paths and easier fabrication than the layer winding.

(d) Superconductor

The copper stabilized Nb_3Sn conductor is the best choice for this magnet design. NbTi is no longer applicable to toroidal field magnets with the field of more than 11 T.

6.2.4 Design Problems

Conductor: The multifilamentary Nb_3Sn conductor is thought to be more suitable for the 11 T high field than the conventional NbTi conductor, though the technology of Nb_3Sn conductor applying to large magnets is premature. The fabrication of Nb_3Sn magnet has been extensively developed, and the characteristics have been investigated to some extent in these years, however, much more efforts need to be made.

The following researches and developments must be made in order to accomplish high field large superconducting toroidal magnets.

(1) Development of high field and large current Nb_3Sn conductor.
(2) Fabrication of large magnets made of Nb_3Sn conductor.
(3) Cryostabilization by pool boiling for large magnets and the improvement of heat transfer.
(4) Enhancement of mechanical strength of Nb_3Sn magnet.
(5) Power supply and protection system.

Mechanical Design: Reviewing the results obtained from stress analysis of toroidal field coil, it is considered that toroidal field coil (especially as for the stabilizing copper) is under severe situation.

Therefore, the rigidity of winding must be strengthened more by increasing the reinforced material in the winding or by using stronger reinforced materials.

Moreover, there are some problems to be studied in future as follows.

(1) Detailed stress analysis against out-of-plane force should be carried out.

(2) Both thermal stress analysis and heat conduction transient analysis for cool down and warm up should be carried out.

(3) Though we temporarily adopted ASME Boiler and Pressure Vessel Code Section III in this design, the new standards of evaluating stress must be determined at low temperature.

(4) Study for fabrication and manufacturing of coil should be carried out.

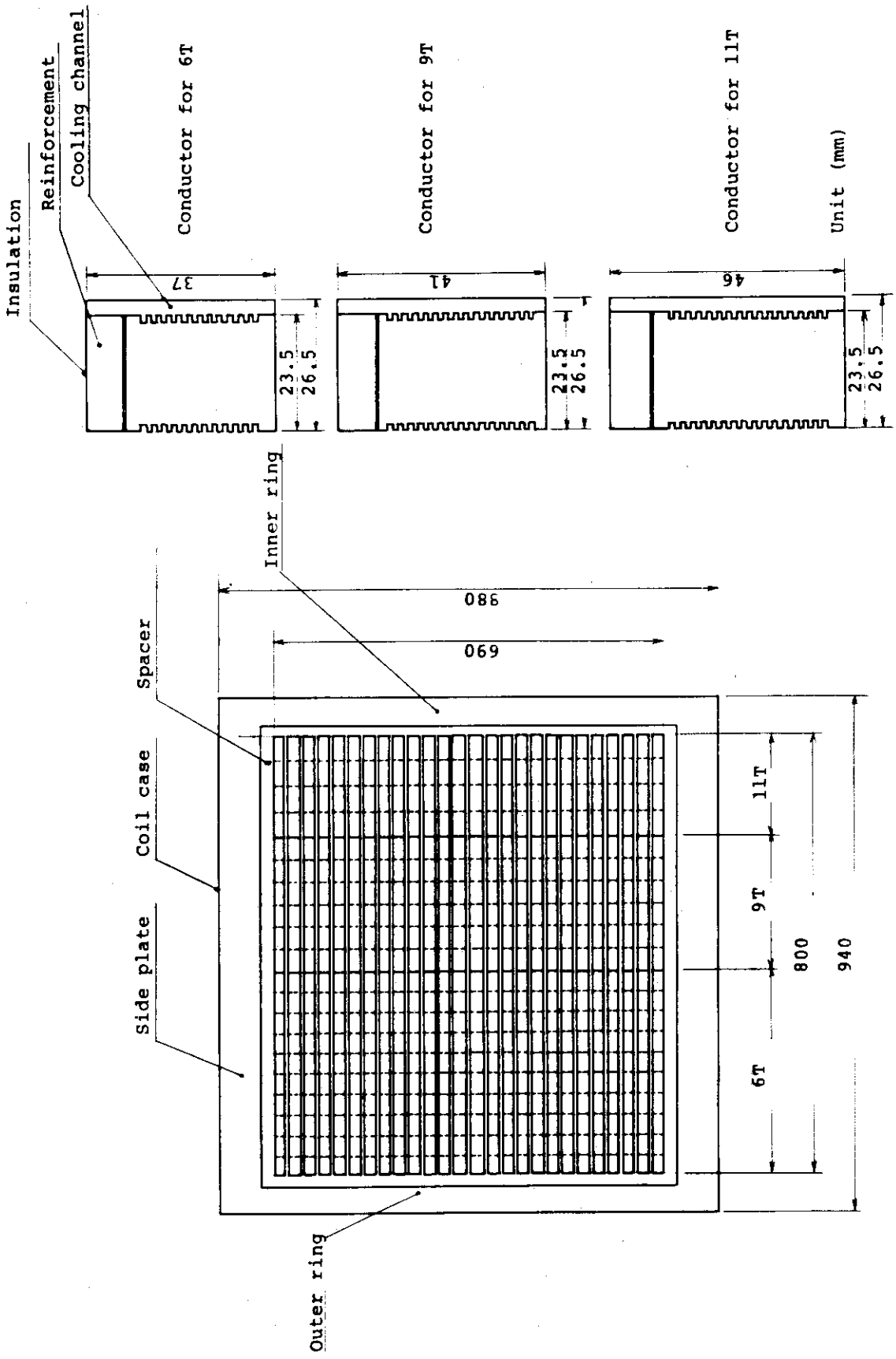

Fig. 6.2.1 Coil Cross-Section and Typical Conductors of TF Coil

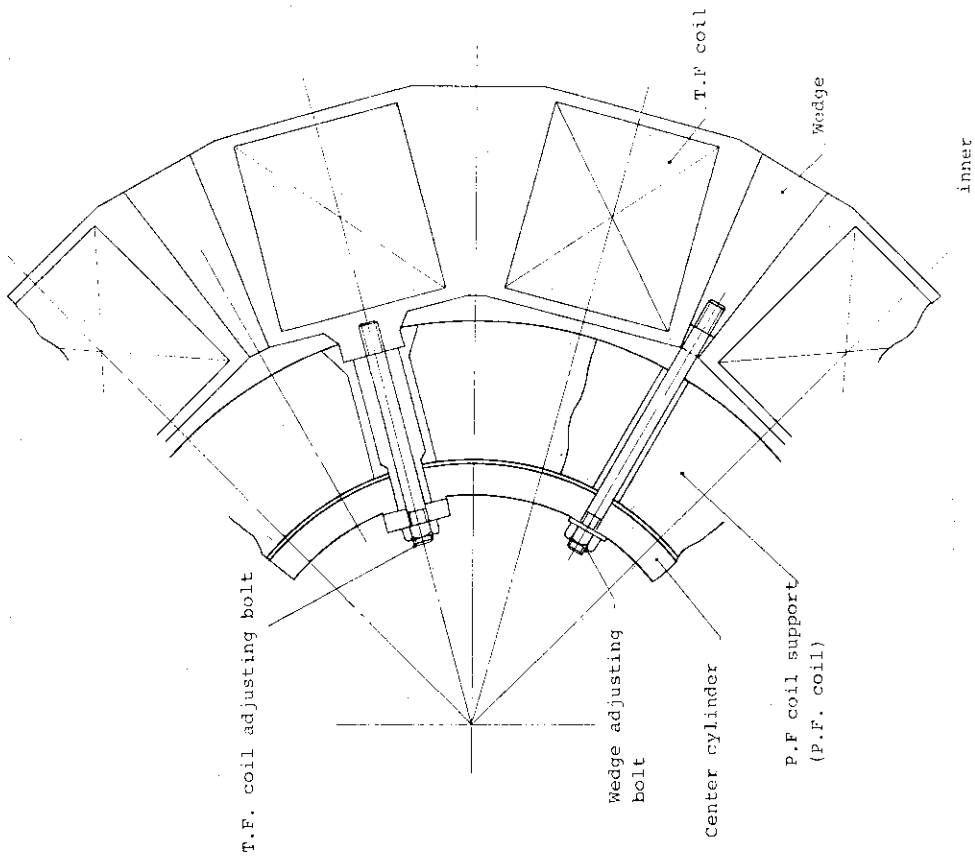

Fig. 6.2.3 Supporting Structure of TF Coil at the Inner Portion of Torus (Horizontal View)

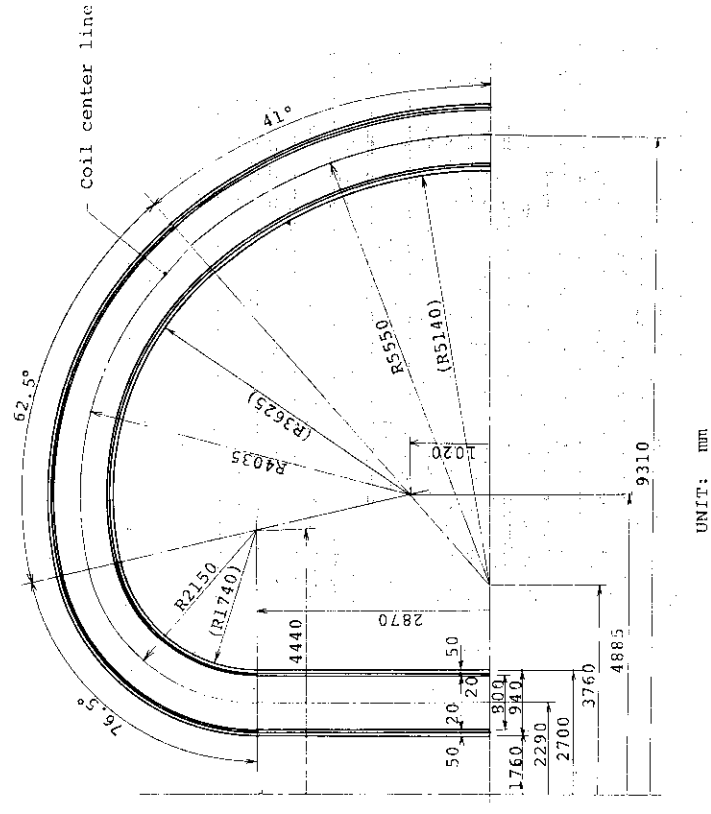

Fig. 6.2.2 Detailed Configuration of TF Coil

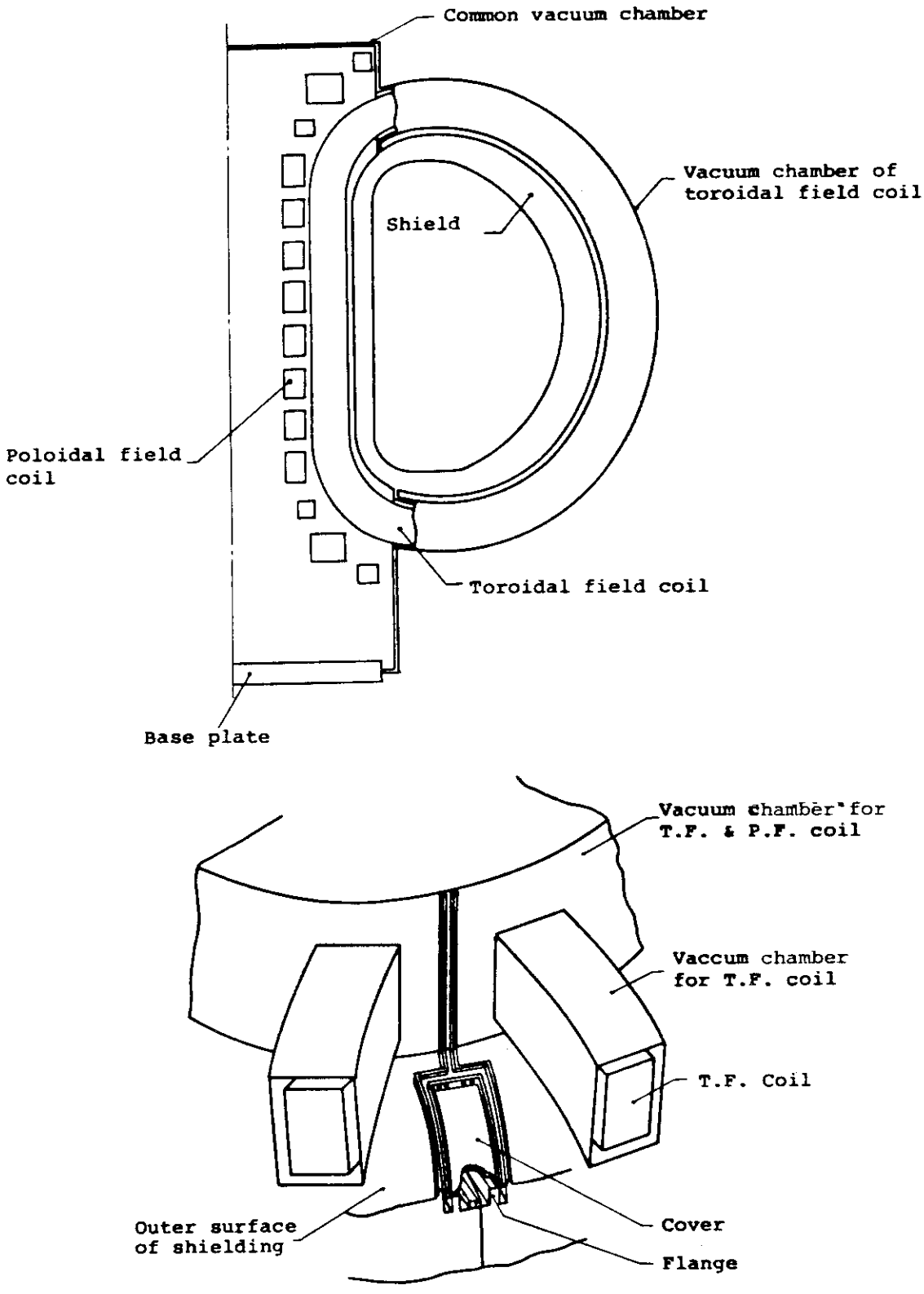

Fig. 6.2.4 Vacuum chamber of toroidal magnet

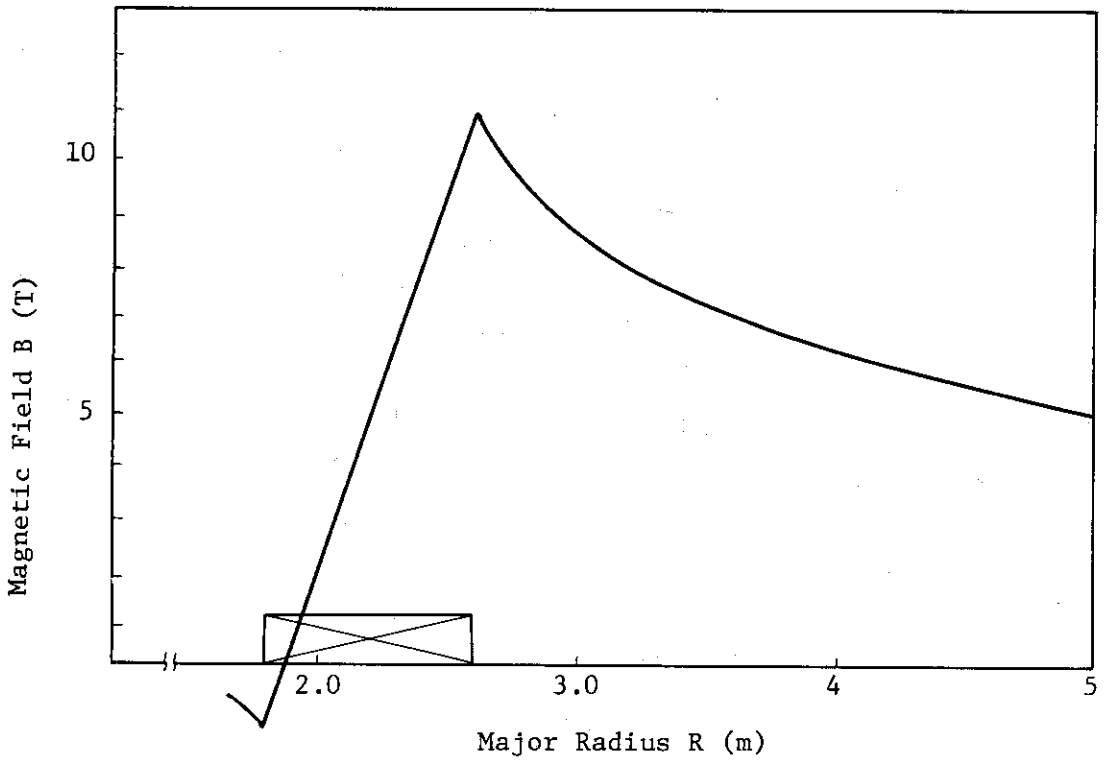

Fig. 6.2.5 Magnetic field distribution on a mid-plane

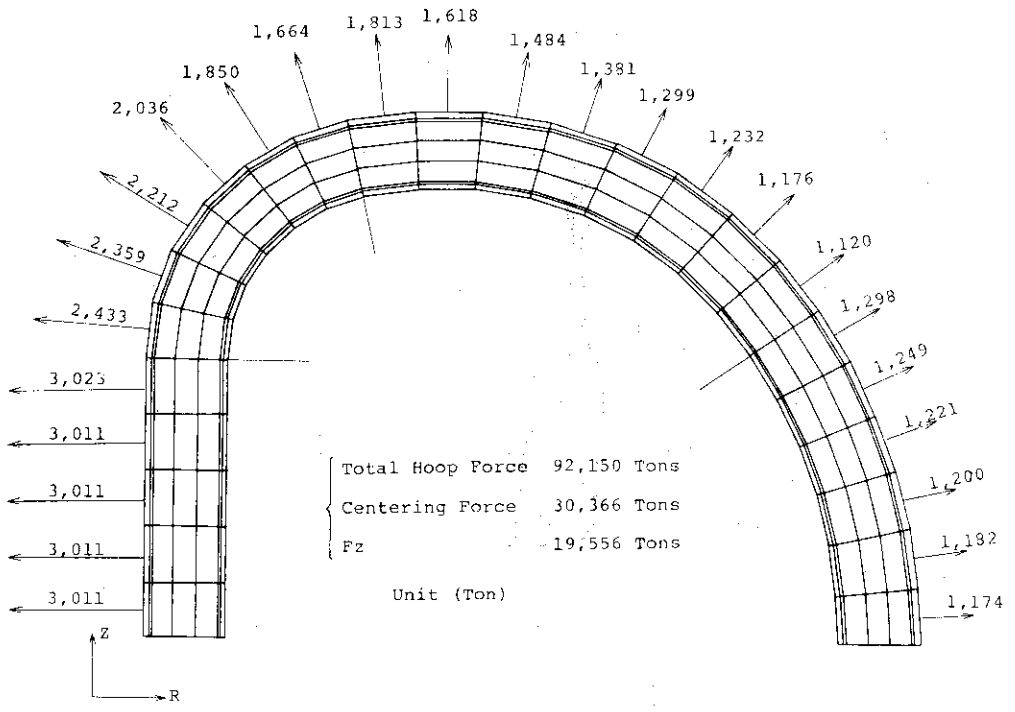

Fig. 6.2.6 Hoop Force Distribution of TF Coil

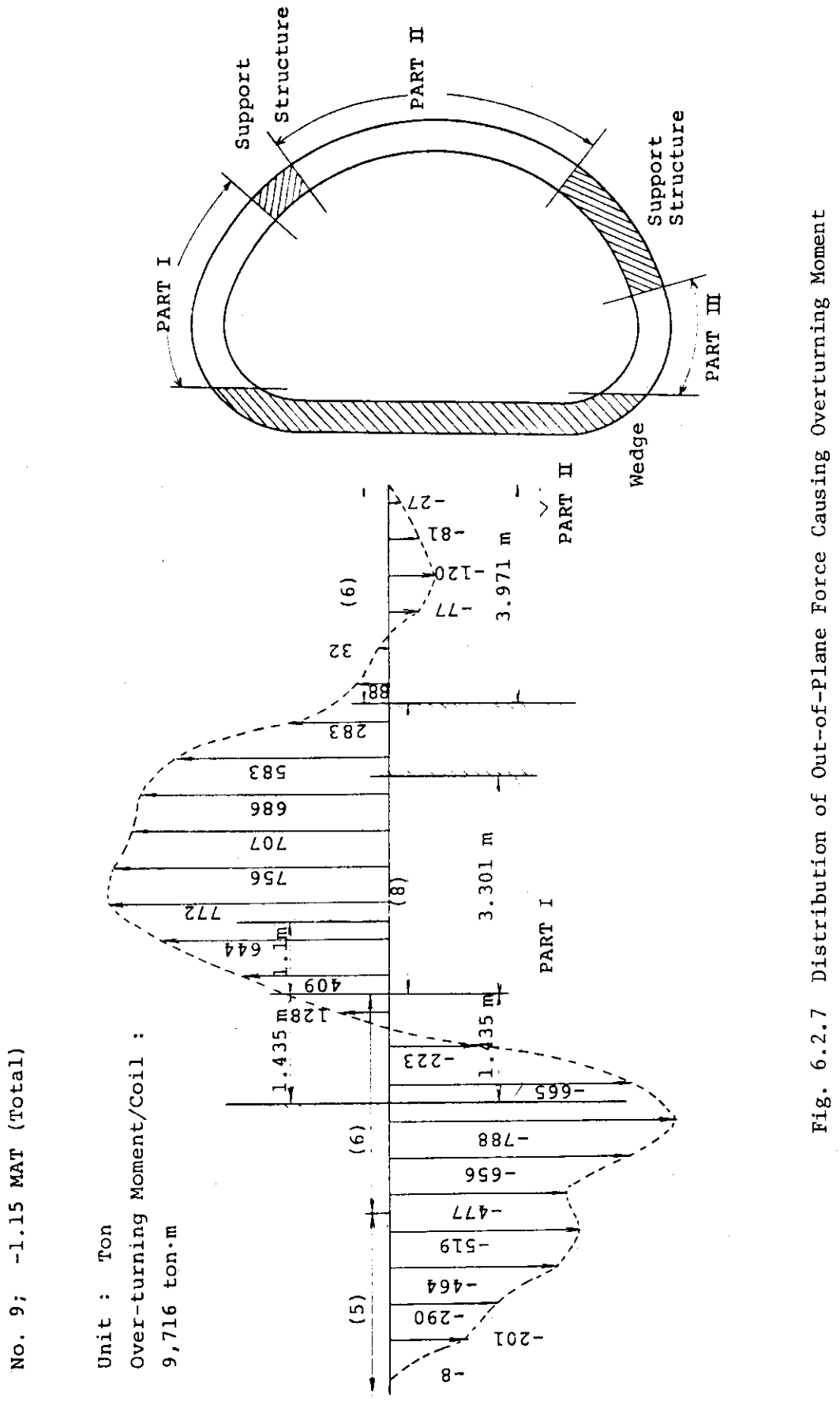

Fig. 6.2.7 Distribution of Out-of-Plane Force Causing Overturning Moment

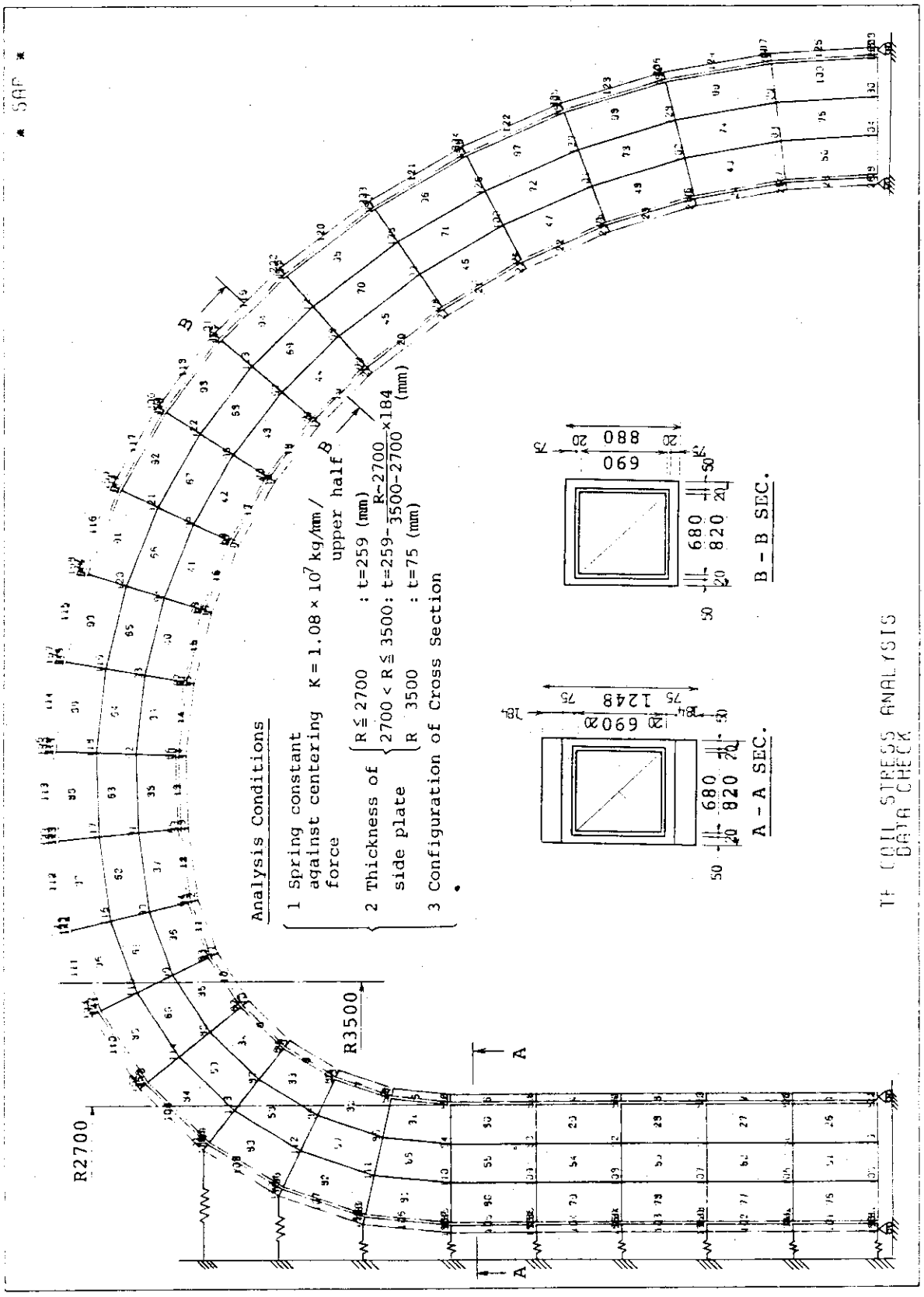

Fig. 6.2.8 Stress Analysis Model of a TF Coil

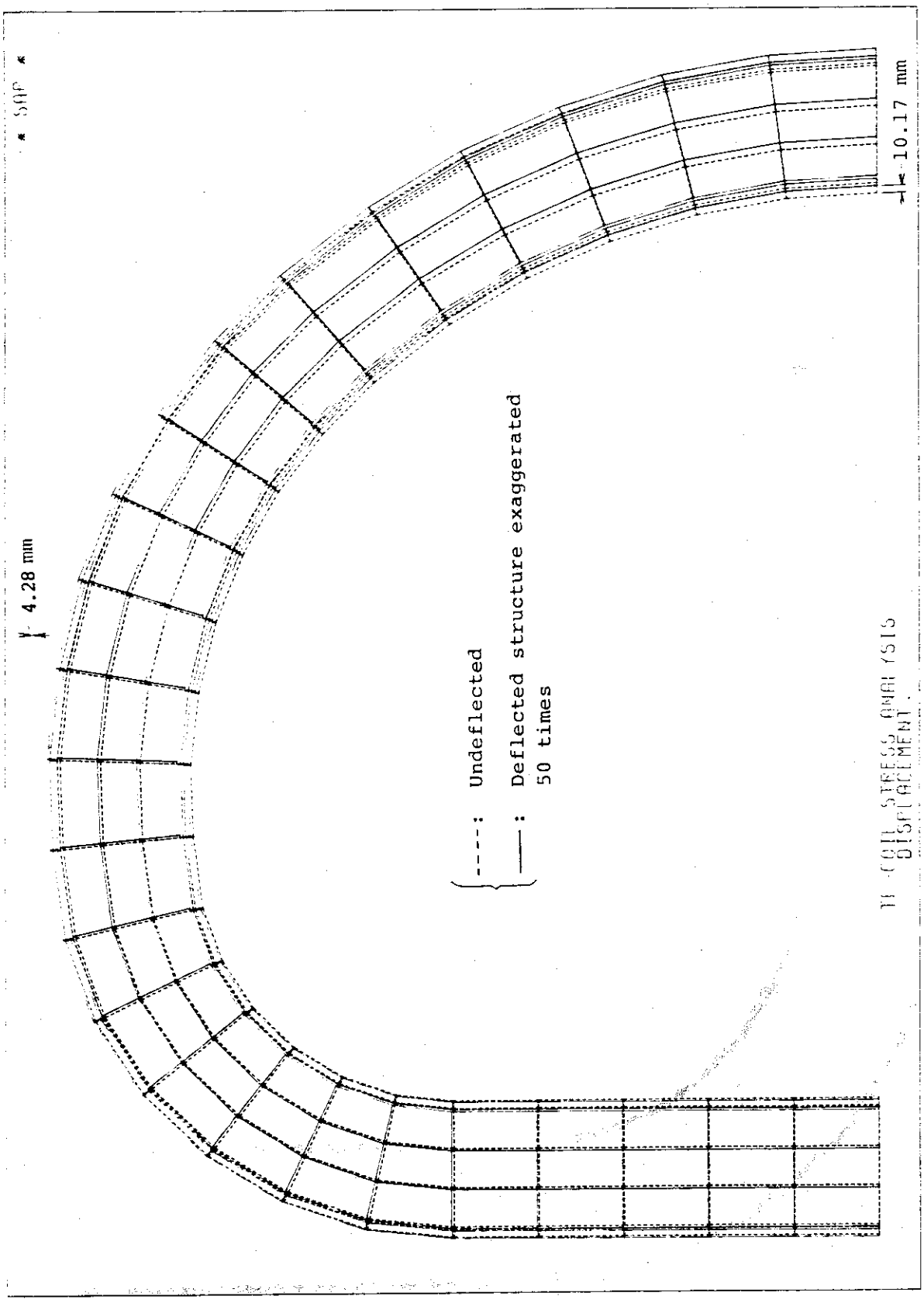

Fig. 6.2.9 The Deformation and the Displacement of a TF Coil

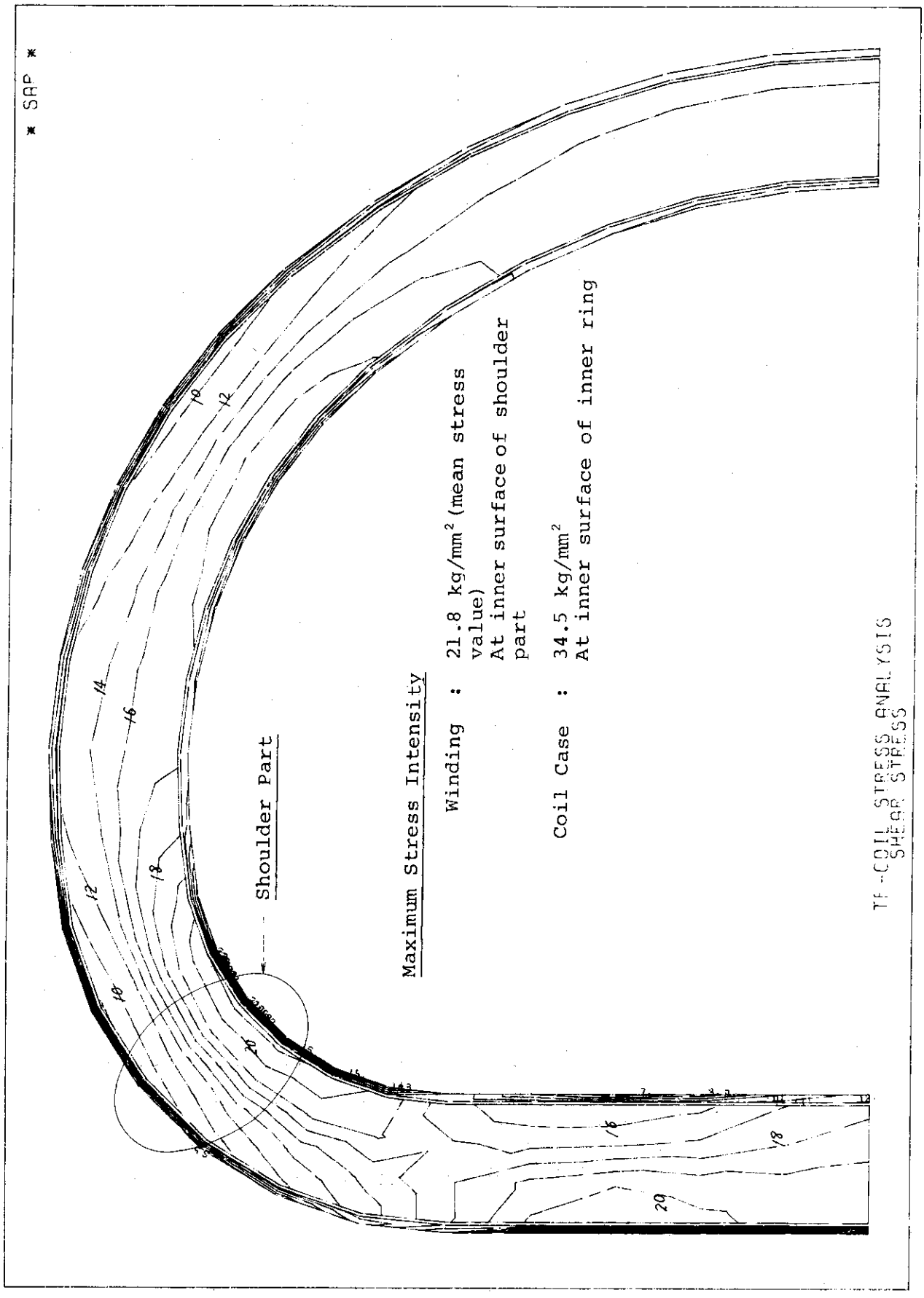

Fig. 6.2.10 Stress Distribution of a TF Coil

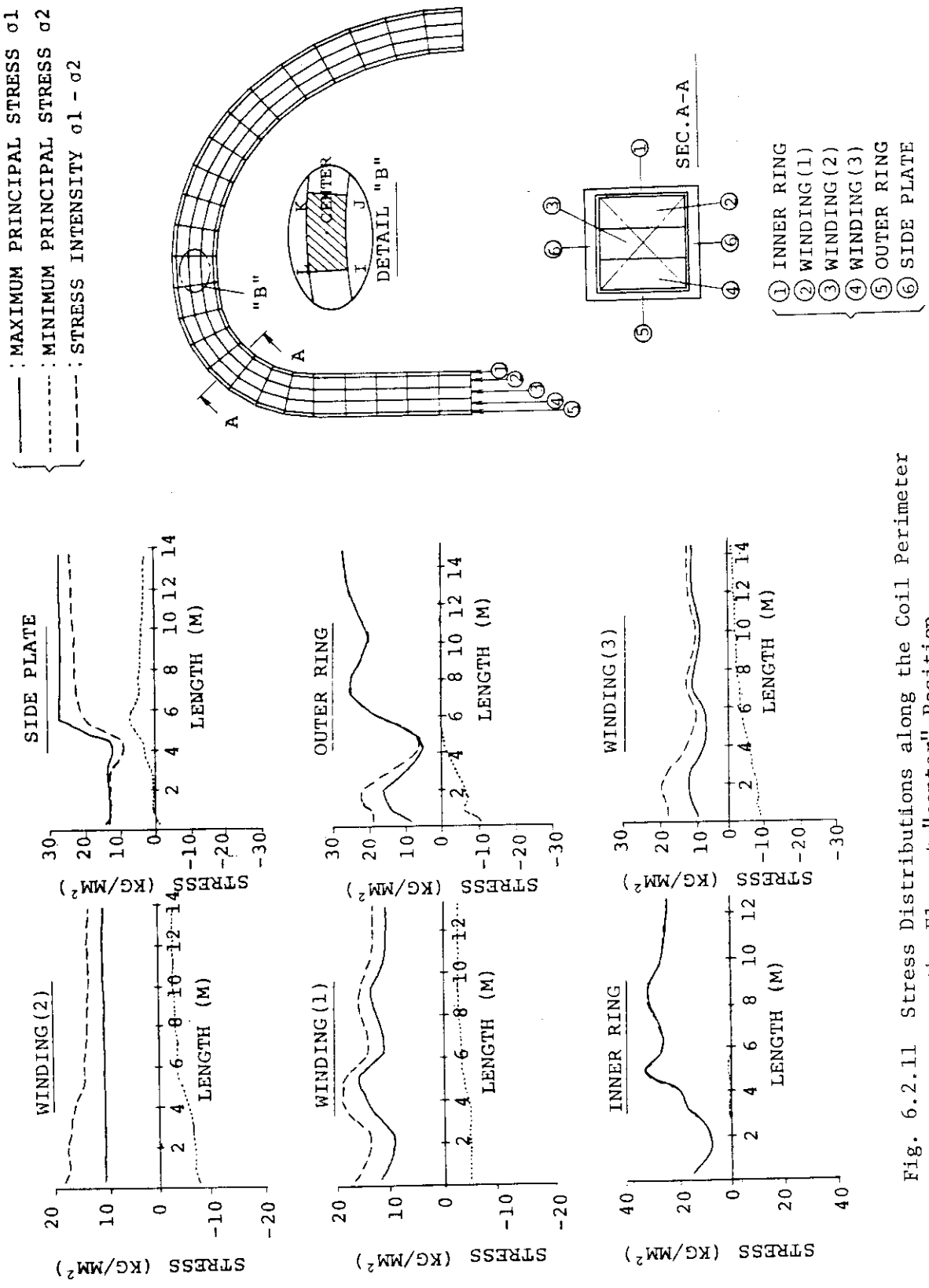

Fig. 6.2.11 Stress Distributions along the Coil Perimeter at the Element "center" Position

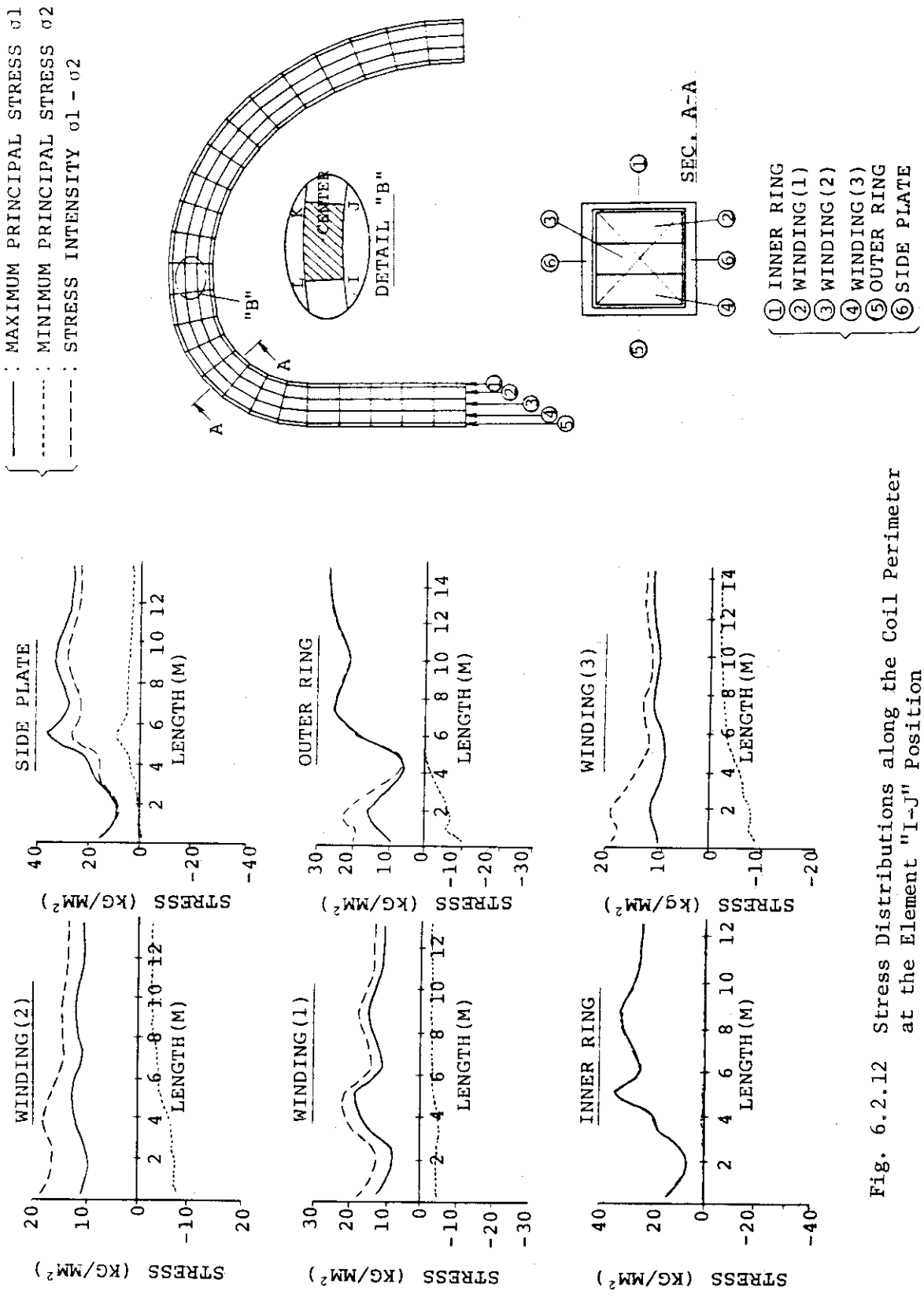

Fig. 6.2.12 Stress Distributions along the Coil Perimeter at the Element "I-J" Position

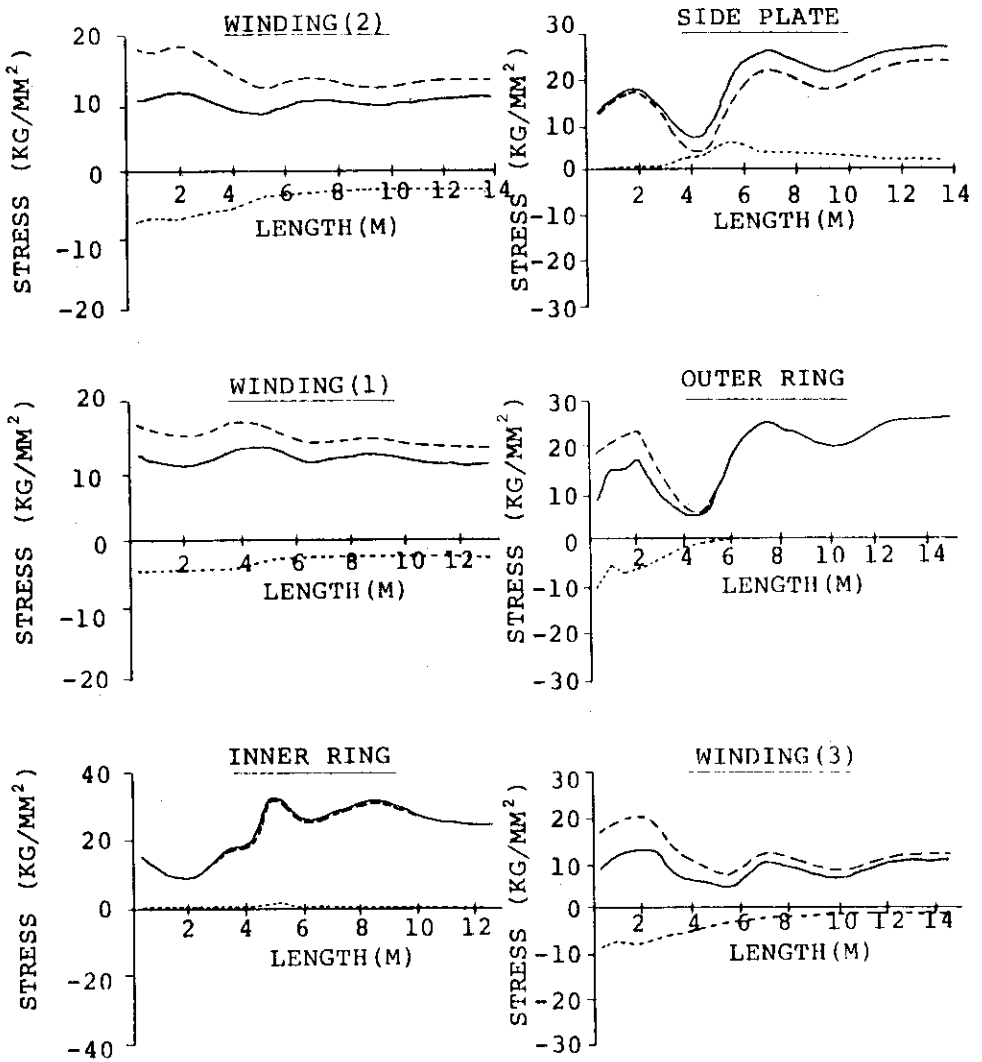

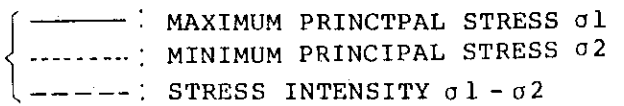

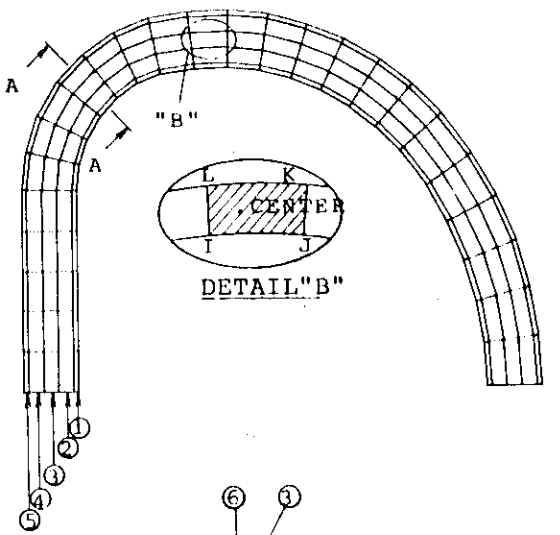

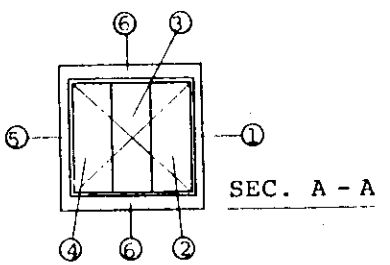

① INNER RING
② WINDING(1)
③ WINDING(2)
④ WINDING(3)
⑤ OUTER RING
⑥ SIDE PLATE

Fig. 6.2.13 Stress Distributions along the Coil Perimeter at the Element "K-L" Position

7. Poloidal Field Magnet

7.1 Concept A

Design of concept A poloidal field magnet of which are characteristics are shown in Table 7.1.1 corresponds to the concept A repair and maintenance of reactor. Therefore, the design is supposed that full turn of coils are removed or settled for repair and maintenance.

Concept A poloidal field magnet is characterized by NbTi superconductor and supercritical He forced flow cooling, except coil No. 9. Coil No. 9 is designed as demountable normal conducting coil from the view point of the assembling and disassembling.

Table 7.1.1 Main Characteristics of Poloidal Field Magnet

Structure	
(1) Structure	super conducting coils +normal conducting coils
(2) Number of coils	24
(3) Number of turns/coil	36 ∿ 140
Dimensions of coils	
(1) Major radius	1.45 ∿ 9.90 m
(2) Horizontal thickness	0.395 ∿ 0.68 m
(3) Vertical thickness	0.35 ∿ 0.80 m
Magnetic Field	
(1) Peak magnetic field at coil	8.0T
(2) Max. rate of magnetic field change	5T/0.1 sec. (0<t<0.1 sec.) 8T/5 sec. (0.1<t<5 sec.)
Magnetomotive Force	
(1) OH component/coil	-0.15 ∿ 3.68 MAT
(2) Plasma control component/coil	-5.17 ∿ 10.0 MAT

Table 7.1.1 (continued)

Magnetic Force	
(1) Max. hoop force	-2.0×10^4 ton
(2) Max. vertical force	-1.5×10^4 ton
Super conducting cable	
(1) Super conductor	NbTi
(2) Stabilizer	Cu
(3) Dimensions	$\sim$ 1800 mm^2
(4) Cu/SC ratio	$\sim$ 2
Normal conducting cable	
(1) Conductor	Ag-Cu
(2) Type	Hollow conductor
Current	
(1) Operation current/coil	-6.02 $\sim$ 10 MAT
(2) Operation current/cable	60 kA
Cooling	
(1) Method	Supercritical helium forced flow
(2) Path length	$\sim$ 200 m
Heat loss	see Table 6.1.5.
Weights	
(1) Cable/m	18.5 kg/m
(2) Cable/coil	16.9 93.1 ton/coil
(3) Cable/total	730 ton

7.1.1 Magnet structure

Poloidal magnet is composed of 11 sets of poloidal coils and each set of coils consist of 2 coils which are symmetric to mid plane. Configurations and maximum magnetomotive force of each coils shown in Table 7.1.2 are determined on the supposition of hybrid type current distribution. Magnetic forces for maximum coil current are summarized in Table 7.1.3. Each coils except coil No. 9 are composed of superconducting cable, support bundle and coil support structures.

Considering the insulation for surge voltage, maximum operation current of cable is normalized at 60 kA for every coils. Cross section of the super-conducting cable is shown in Fig. 7.1.1. Superconductor of the cable is NbTi according to later discussions. As for cooling, forced flow supercritical He is used since this type is rather superior to pool boiling in the one turn electrical insulation structure. Path length of coolant is roughly planed as $\sim$ 200 m and this fact is one of design problems. But this problem is soluble by appropriate arrangement of cable and coolant route. Turn number and stacking mode of the cable within each coils are determined from the total magnetomotive forces, electrical and cooling route, spacial relations to other components and facilities, assembling procedures, etc. and shown in Table 7.1.4. Cables taped by insulation are stacked into coil and bounded by stainless steel structure (support bundle) as shown in Fig. 7.1.1. Only coils No. 9 are water cooled normal conducting coil since they should be demountable. If lower No. 9 coil is undemountable, movable base structure has to be separated for assembling and such separation leads to lack of structural stability. On the other hand, upper No. 9 coil is full turn structure.

All the poloidal coils are enveloped in belljar type vacuum chamber that each coils are not necessary to have their own vacuum chamber. Therefore, cold structure of poloidal coils are only covered by thermal insulation. Poloidal coil support system is also simplified by the belljar type vacuum chamber. Vertical forces and self weight of the coils No. 1 $\sim$ No. 7 are supported by cold central support column. Basic structure of the central support column is a double cylinder (inner and outer support column) connected by horizontal plates.

Coils are settled within the area enclosed by double cylinders and plate. Coils No. 8, 10 and 11 are directly supported on toroidal field magnet's support disc. Upper and lower coils No. 9 are fastened on primary shield and shield leg, respectively, since these coils are

operated at normal temperature. All of these support structures are armed with the radial sliding mechanism for relative movement between coils and fixed portions. Magnetic forces, temperature difference through cooling process, etc. may be a cause of such relative movement. Fig. 7.1.1 ~ 7.1.3 illustrate these support structures.

Table 7.1.2 Configuration and Magnetomotive Force of Poloidal Coils

Coil Number	Coil position		Maximum Magneto-motive Force (MAT)
	R(m)	Z(m)	
1	1.475	0.500	-6.02
2	1.475	1.500	-6.02
3	1.475	2.500	-3.60
4	1.475	3.500	-3.60
5	1.625	4.500	-3.60
6	2.050	5.550	8.24
7	2.950	6.150	4.14
8	4.300	6.500	4.14
9	6.250	6.150	-3.15
10	8.900	4.850	-5.17
11	8.900	3.000	-2.13

Table 7.1.3 Magnetic Force for Maximum Coil Current

Coil Number	Magnetic Force (ton)	
	R direction	Z direction
1	15.5 $\times 10^3$	-0.7 $\times 10^3$
2	14.2	-3.5
3	6.3	-3.0
4	3.6	-3.7
5	-0.9	-9.1
6	26.0	15.4
7	3.6	-2.3
8	-10.2	-0.3
9	5.6	-1.8
10	18.2	-7.4
11	3.3	2.7

Table 7.1.4 Design Characteristics of PF Coils

Coil Number	Maximum Magneto motive Force (MAT)	Turn* staking (Radial × Vertical)	Size of cable* block (Radial × Vertical, mm)	Size of block *in cladding bundle (Radial × Vertical,mm)
1	-6.02	10 × 10	450 × 670	530 × 750
2	-6.02	10 × 10	450 × 670	530 × 750
3	-3.60	8 × 8	360 × 530	440 × 616
4	-3.60	8 × 8	360 × 530	440 × 616
5	-3.60	8 × 8	360 × 530	440 × 616
6	8.28	14 × 10	760 × 710	850 × 800
7	4.14	7 × 10	315 × 670	395 × 750
8	4.14	7 × 10	315 × 670	395 × 750
9	-3.15	-	-	600 × 600
10	-5.17	(3+3) × 15	600 × 675	680 × 755
11	-2.13	(3+3) × 15	600 × 270	680 × 350

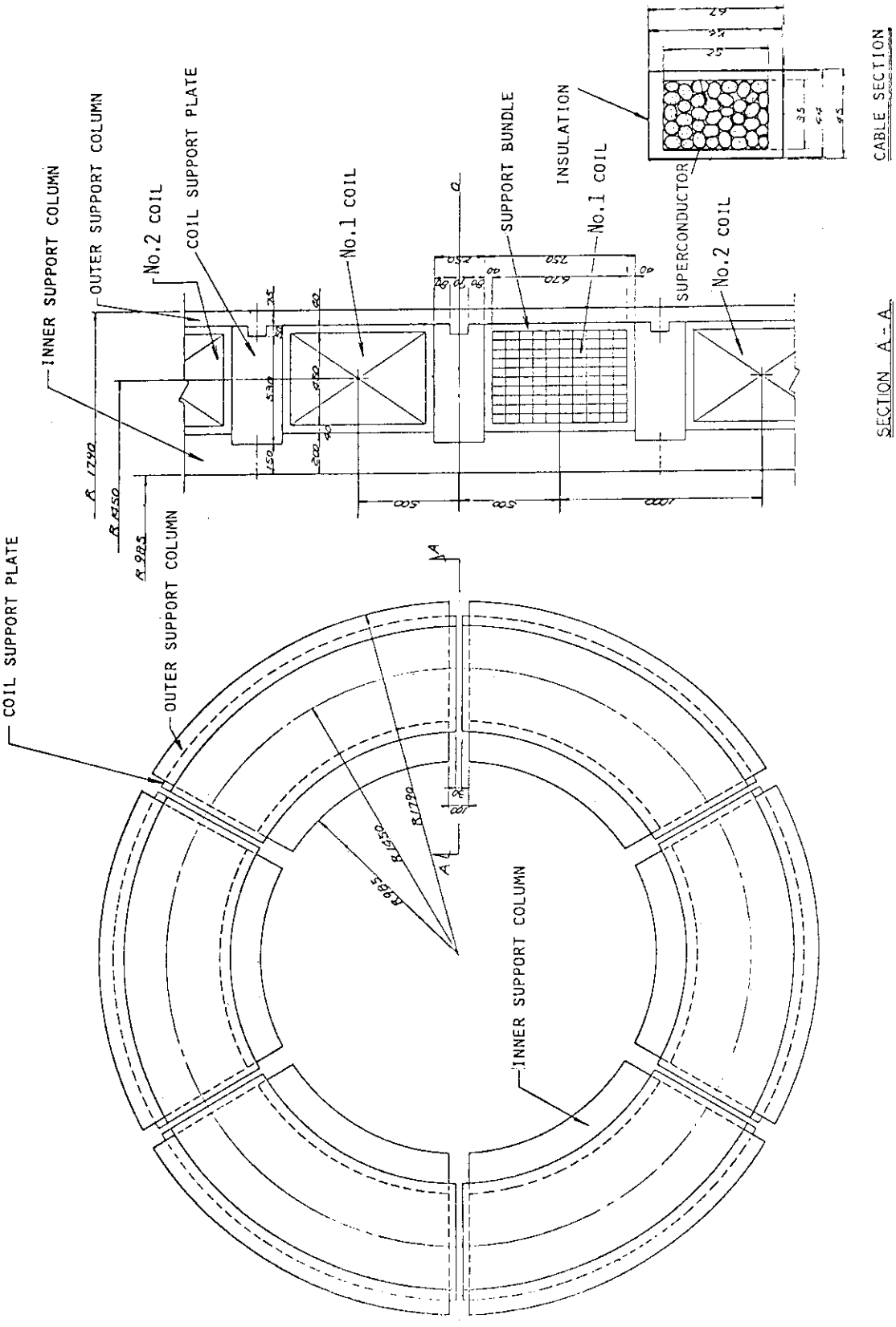

Fig. 7.1.1 PF Coil Structure

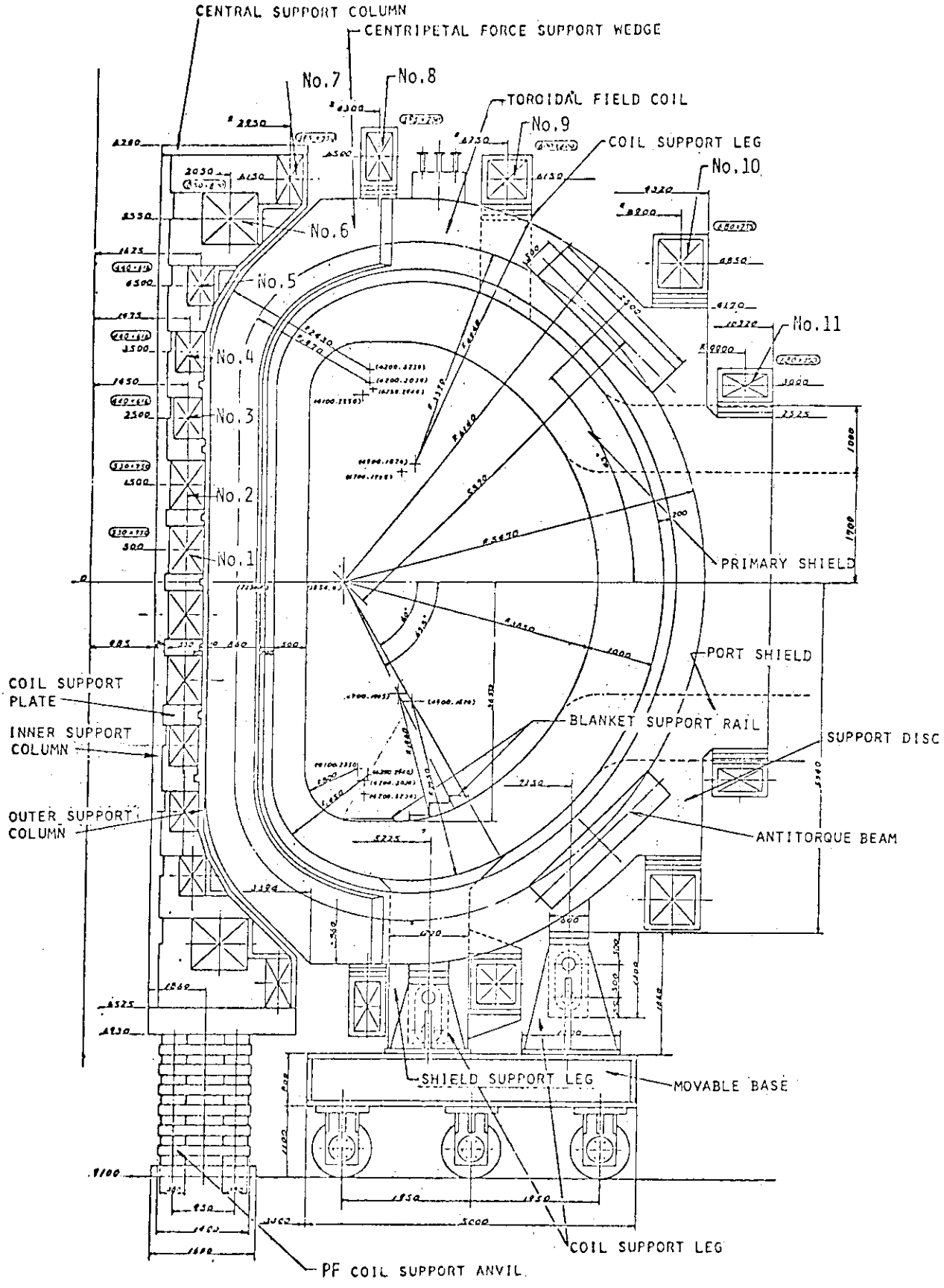

Fig. 7.1.2 Concept A Plan

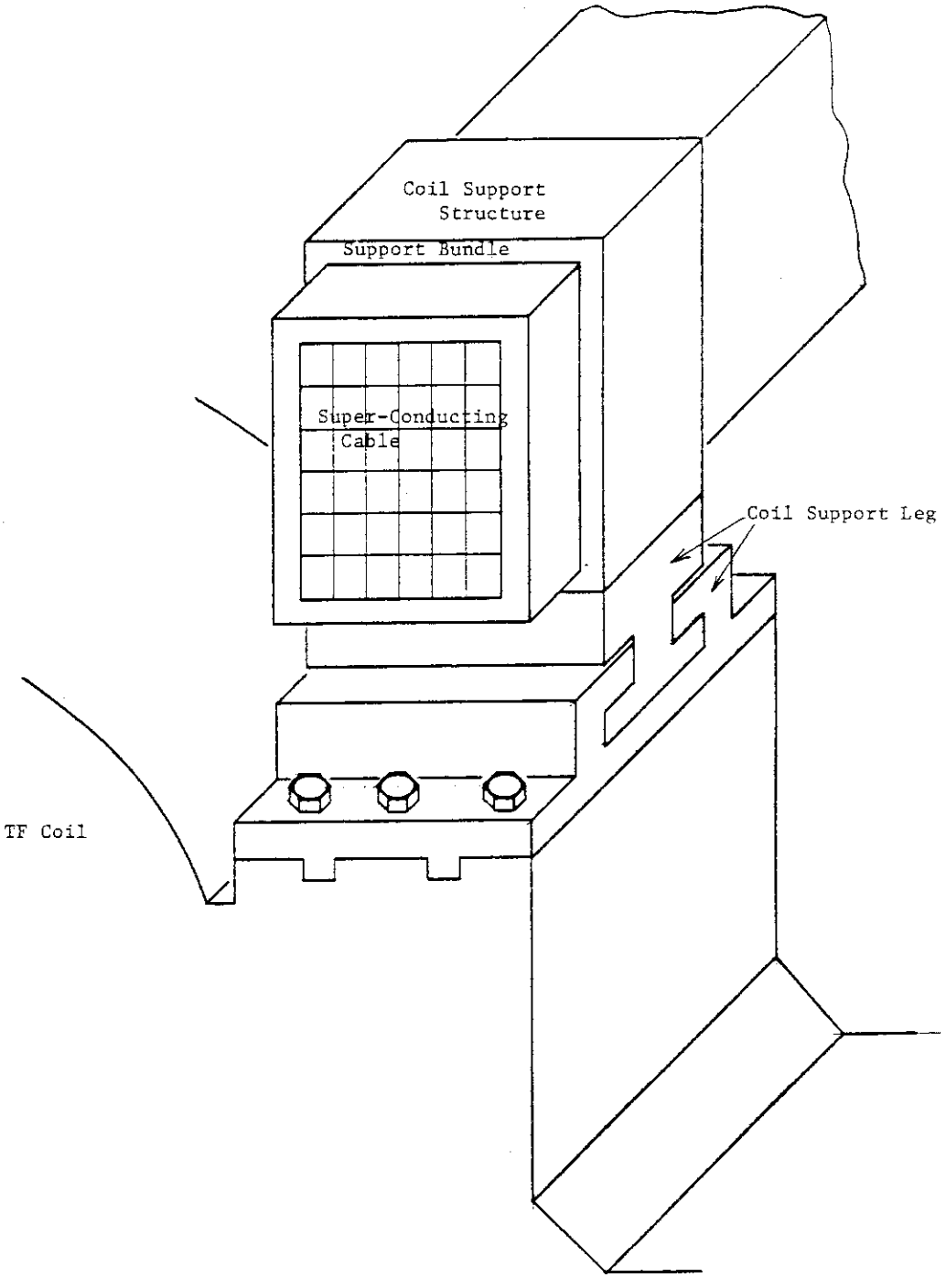

Fig. 7.1.3 Support Leg of PF Coil

7.1.2 Design Analysis

The peak field of each poloidal field coil is computed under the operating condition. Figure 7.1.4 shows that No. 6 coil has maximum peak field of 8 tesla. NbTi conductor was selected by the reason of the repeated stress, and the conductor coolant mode should be supercritical helium forced flow. Pool boiling method has two main design problems; (1) Electrical insulations of the helium cans at 4°K base for one turn loop, (2) Vapor bubble traversing in the horizontal direction.

Comparably large operating current (60 kA) was chosen, considering induced voltage between turns.

Specifications of the superconducting cable are shown in Table 7.1.5. AC losses for poloidal field coils are summarized in Table 6.1.5.

Table 7.1.5 Specifications of a conductor for poloidal field coils (8 tesla conductor)

Conductor	NbTi compacted cable
Cable dimension	45 mm × 67 mm (including support bundle)
Number of strands	3 × 7 × 46
Strand diameter	1.2 mm
Number of filaments per strand	533
Filament diameter	10 mm
Twist pitch	13 mm
o/o area for helium flow	- 40%

7.1.3 Design Problems

Design problems of poloidal field magnet are as follows.

1) Assurance of slide movement of support leg
2) Connecting structure of cables with electrical insulation
3) Cyclic load on cables and support structure
4) Large number of cooling pipes.

Coil No.	B peak (T)	Coil No.	B peak (T)
1	7.2	7	4.8
2	6.8	8	3.9
3	5.4	9	-
4	5.4	10	3.8
5	5.9	11	2.2
6	8.0		

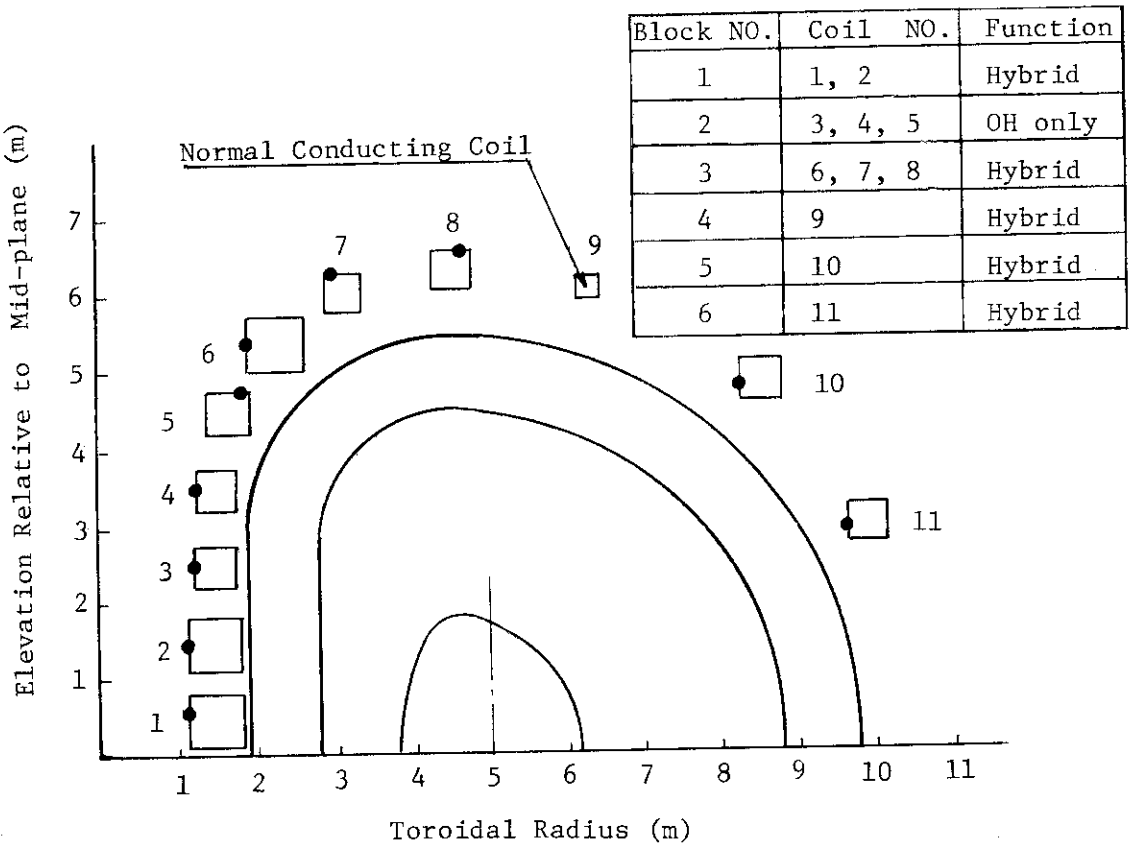

Block NO.	Coil NO.	Function
1	1, 2	Hybrid
2	3, 4, 5	OH only
3	6, 7, 8	Hybrid
4	9	Hybrid
5	10	Hybrid
6	11	Hybrid

Fig.7.1.4 B peak Location of Each Coil (dotted)

7.2 Concept B

Poloidal field magnet system is designed based on the following concepts. (Magnet location and maximum rating are listed in Table 7.2.1.)

(a) The design with reasonable certainty of feasibility.
(b) Easier manufacturing and repairing by remote handling.
(c) Reduction of electric power for the poloidal field magnets including the requirement of helium refrigeration.
(d) Reduction of heat dissipation due to the pulsive magnetic field in the superconductor as well as surrounding structures.

Those conditions imposed upon poloidal field magnets need to be satisfied but it would not be easily manageable to meet all of requirements. However, in this conceptual design of poloidal field magnets, the optimum approach was pursued through overall evaluations.

The features and design bases of poloidal field magnets are as follows.

(1) The pool boiling is employed for the advantage of easier cooling, less energy and mature technology.
(2) Overall current densities of superconducting magnets is set to be max. 19 A/mm^2 to fullfill stabilized operation of superconducting magnets.
(3) Hybrid coil system is selected based upon the consideration of limited available space.

7.2.1 Magnet Structure

Design conditions

(1) Both normal operating and fault conditions will be taken into account. Normal conditions mean all existing combinations of transformer magnets, shaping magnets, toroidal field magnets and plasma. Fault conditions include plasma disruption and failures of single or groups of poloidal field magnets.
(2) The loads that shall be considered include electromagnetic force, temperature-induced loads, seismic loads and dead-weight.
(3) The pulsive operation of poloidal field magnets calls for dynamic analysis in addition to static analysis.
(4) Magnet structures shall be designed in such a way that they are able to be disassembled and reassembled with minimal labor time by remote handling in case of repairing blanket.

Structure

A cross section of the superconducting poloidal magnet configuration is shown in Fig. 1.6.1. The system is composed of inner magnets and outer magnets. Magnet number 1 to 7 is defined to be inner magnets and they are installed in one common cryostat. Their weights and vertical motion is transmitted to the bottom supporting base which also sustains the toroidal field magnets. Outer magnets of magnets number from 8 to 11 are located along the periphery of toroidal field magnet and supported by either radiation shield or toroidal field magnet. Those magnets have individual cryostat.

Figure 7.2.1 depicts the details of magnet number 1. More detailed magnet structure is shown in Figs. 7.2.2 ∿ 7.2.5. The present poloidal field magnet design is summarized below.

(1) The magnet is composed of pancakes and cooled by pool boiling as shown in Figs. 7.2.1 and 7.2.2.
(2) The upper magnets of 8 and 9 are supported by the radiation shield for case of snaking out the blanket.
(3) The stranded NbTi wires constitute superconductors and they are placed in the stainless steel can which supports the electromagnetic force of the conductors as clear from Fig. 7.2.4.
(4) Punched cans, tilting spacers and plates with protrusions serve in such a way that the emerged vapor bubbles can move freely to any direction.
(5) Several turns as well as several magnets are connected in parallel to reduce the induced voltage as indicated in trimetric view of Fig. 7.2.5.
(6) The magnet and helium coolant is surrounded by the FRP case instead of thick stainless steel to avoid the excessive heat dissipation.

7.2.2 Design Analysis

The hybrid poloidal field coil system is designed to attain D-shape plasma equilibrium and to minimize error field at the plasma region. Consideration is also made on the heat dissipation in the superconducting magnets and the overturning moment acting on the toroidal field magnets. The magnet locations and magnetomotive forces of each coil are listed in Table 7.2.1.

Overall current densities of superconducting magnets are no more than 19 A/mm^2. This is enough to satisfy the equal area stabilization

criterion. Tables 7.2.2 and 7.2.3 summarize the magnetic field at the typical locations of each magnet. The maximum magnetic field of 8.8 T occurs at the bore of magnet 3. Electromagnetic forces acting on poloidal field magnets are summarized in Table 7.2.4 and they are shown schematically in Figs. 7.2.6 ∿ 7.2.10.

Inner magnets are at the tight situation competing with toroidal field magnets while outer magnets have more freedom. As the design will progress, the optimum compromise between poloidal field magnets and toroidal field magnets is necessarily required.

7.2.3 Magnet Type Selection

As for the selection of cooling method for the poloidal field magnets, pool boiling was chosen for the almost same reasons like toroidal field magnets. The forced flow cooling seems to be more desirable since it requires no FRP case. Also the magnets with forced flow cooling may be mechanically more reliable and could be designed in narrow space, and may be able to withstand high voltage which is generated by the abrupt change of the transformer component or by the plasma disruption.

However, the large pumping power and unmature technologies in the forced flow cooling are considered to be too serious to be adopted.

For winding configuration, the pancake type is employed since the layer winding pattern has the difficulties of coil support and manufacturing.

The superconductor is contained in the stainless steel can so that the radial force of the conductor can be sustained by the stainless steel. The magnetic field is not so high (no more than 9 T) that NbTi could serve well for this poloidal field magnets.

7.2.4 Design Problems

Though the design is at the conceptual stage and is now halfway, it is of value to note unnegligible design problems. They are summarized as follows.

(1) Heat Transfer

Heat transfer needs to be evaluated for the pool boiling. No experimental data have been obtained in particular for this kind of large horizontal magnets.

(2) Conductor

It is highly required to verify manufacturing of high current AC superconductor and to test AC stability and heat generation.

(3) FRP cryostat

Large size FRP cryostat backed with thin stainless steel needs to be developed.

(4) Ground insulation

Poloidal field magnets experience exceedingly high voltage despite the fact that conductors are bare. The reliable ground insulation system must be developed and on the other hand a way of reducing the voltage needs to be pursued coupled with the power supply system.

Table 7.2.1 INTOR Poloidal Field Coil Locations and Maximum Ratings

Magnet No.	Block No.	R (M)	Z (M)	Transformer Component (MAT)	Shaping Component (MAT)	Total (MAT)
1	1	1.4	0.5	-3.68	-2.34	-6.02
2	1	1.4	1.5	-3.68	-2.34	-6.02
3	2	1.5	2.5	-3.60	*****	-3.60
4	2	1.525	3.5	-3.60	*****	-3.60
5	2	1.675	4.5	-3.60	*****	-3.60
6	3	2.25	5.4	-1.72	10.0	8.28
7	3	3.1	6.05	-0.86	5.0	4.14
8	3	4.5	6.35	-0.86	5.0	4.14
9	4	6.25	6.1	-0.15	±1.0	+0.85 -1.15
10	5	8.5	4.85	-0.10	-5.17	-5.27
11	6	9.9	3.0	-0.15	-1.98	-2.13

with divertor

Table 7.2.2 Magnetic field at each magnet (PF No.9; 1 MAT)

unit; teslas

Magnet Number	Total		Transformer component		Shaping component	
	#1	#2	#1	#2	#1	#2
	#3	#4	#3	#4	#2	#4
1	8.19	4.31	5.33	2.79	2.85	1.57
	1.33	4.17	0.58	2.78	0.76	1.39
2	7.76	4.54	5.32	2.79	2.47	2.03
	1.63	3.75	0.59	2.77	1.12	0.97
3	8.84	3.79	5.81	3.31	0.83	0.90
	1.50	2.70	0.99	3.26	0.93	1.01
4	4.73	3.70	5.74	3.41	1.43	1.72
	2.24	1.98	1.00	3.19	1.44	1.23
5	3.09	5.28	5.24	3.63	3.25	4.03
	4.45	0.51	1.25	2.75	3.33	2.75
6	6.62	4.04	2.18	1.63	8.50	5.64
	2.61	6.00	0.36	0.63	2.63	6.44
7	3.49	3.41	1.13	1.08	4.57	4.45
	2.55	2.97	0.42	0.36	2.86	3.25
8	2.52	3.04	0.74	0.81	3.24	3.82
	3.55	3.16	0.58	0.46	4.10	3.60
9	0.54	1.09	0.11	0.20	0.44	1.20
	1.82	1.57	0.17	0.07	1.76	1.63
10	4.21	3.59	0.06	0.10	4.15	3.50
	2.88	2.98	0.08	0.03	2.80	2.95
11	2.34	1.77	0.14	0.14	2.19	1.62
	2.15	2.05	0.17	0.13	1.98	1.92

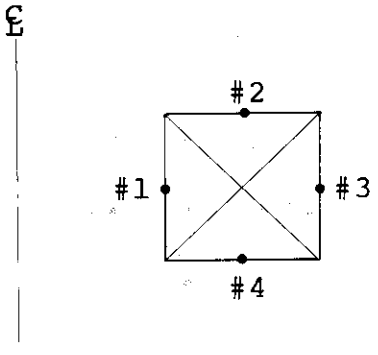

Table 7.2.3 Magnetic field at each magnet (PF No.9; -1 MAT)

unit; teslas

Magnet Number	Total		Transformer component		Shaping component	
	#1	#2	#1	#2	#1	#2
	#3	#4	#3	#4	#3	#4
1	8.34	4.42	5.33	2.79	2.99	1.66
	1.18	4.28	0.58	2.78	0.62	1.50
2	7.91	4.63	5.32	2.79	2.62	2.06
	1.49	3.88	0.59	2.77	1.00	1.10
3	6.01	3.87	5.81	3.31	0.82	0.84
	1.36	2.85	0.99	3.26	0.89	1.01
4	4.92	3.74	5.74	3.41	1.28	1.56
	2.06	2.13	1.00	3.19	1.31	1.10
5	3.25	5.21	5.24	3.63	3.06	3.84
	4.26	0.42	1.25	2.75	3.16	2.57
6	6.40	3.91	2.18	1.63	8.27	5.50
	2.80	5.92	0.36	0.63	2.84	6.34
7	3.23	3.36	1.13	1.08	4.32	4.39
	2.83	2.97	0.42	0.36	3.14	3.23
8	2.18	3.04	0.74	0.81	2.90	3.80
	3.95	3.26	0.58	0.46	4.50	3.69
9	2.33	1.76	0.11	0.20	2.24	1.65
	0.48	1.36	0.17	0.07	0.52	1.37
10	4.15	3.54	0.06	0.10	4.09	3.45
	2.92	3.02	0.08	0.03	2.84	2.99
11	2.33	1.75	0.14	0.14	2.19	1.60
	2.16	2.07	0.17	0.13	1.99	1.94

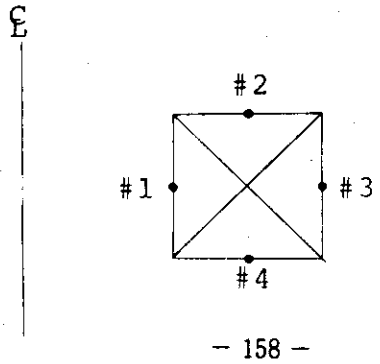

Table 7.2.4 Electromagnetic force

unit; tons

Magnet Number	Total		Transformer component		Shaping component	
	Fr	Fz	Fr	Fz	Fr	Fz
1	19.4	-0.9	7.96	-0.015	2.48	-0.35
	18.6	-0.94			2.16	-0.35
2	17.7	-4.0	7.93	-0.072	1.83	-1.5
	16.8	-4.0			1.48	-1.53
3	8.15	-3.2	7.98	-0.12	0	0
	7.56	-3.3				
4	5.08	-3.90	8.01	-0.36	0	0
	4.41	-3.96				
5	-2.16	-9.32	7.41	-1.80	0	0
	-2.99	-9.38				
6	22.5	16.2	2.08	-1.36	39.2	11.6
	25.3	16.3			42.7	11.8
7	0.66	-1.77	0.57	-0.66	4.14	-5.96
	2.86	-1.79			6.79	-5.99
8	-10.7	1.07	0.19	-0.43	-11.9	-1.24
	-6.39	0.58			-6.62	-1.82
9	5.74	-1.89	-0.02	-0.04	5.14	-1.36
	-3.68	1.37			-4.47	1.33
10	17.1	-7.84	-0.006	-0.018	18.6	-9.19
	18.7	-9.19			18.6	-8.09
11	0.99	2.18	-0.012	-0.007	1.10	1.92
	1.10	1.92			1.18	1.88

Note: No.9 PF magnet

-1 MAT
1 MAT

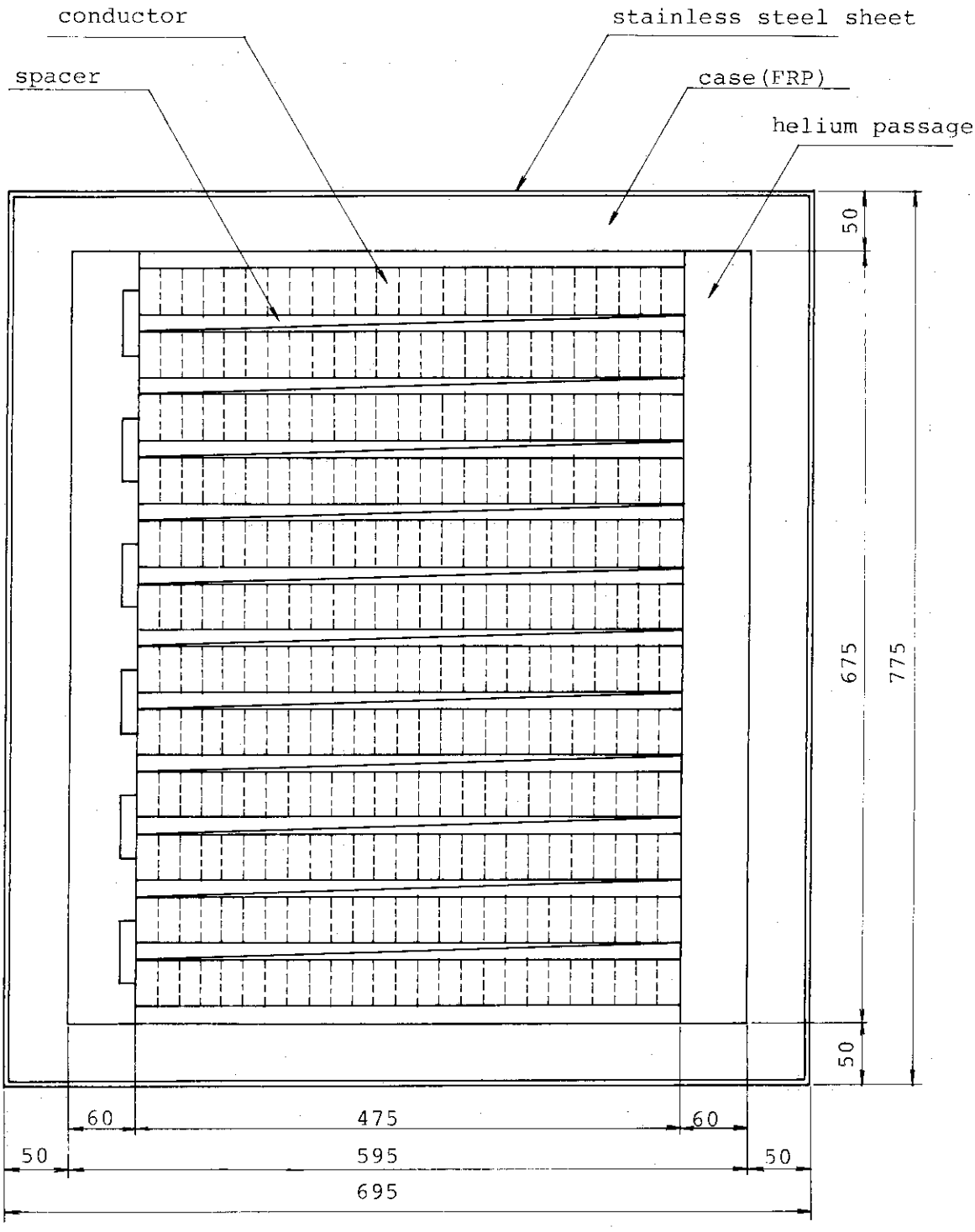

Fig. 7.2.1 Magnet Number 1

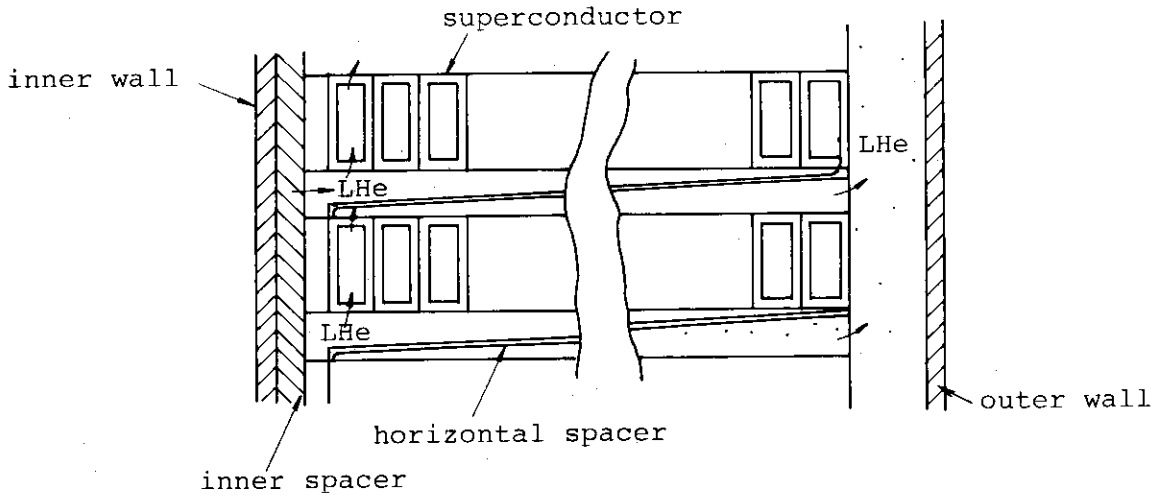

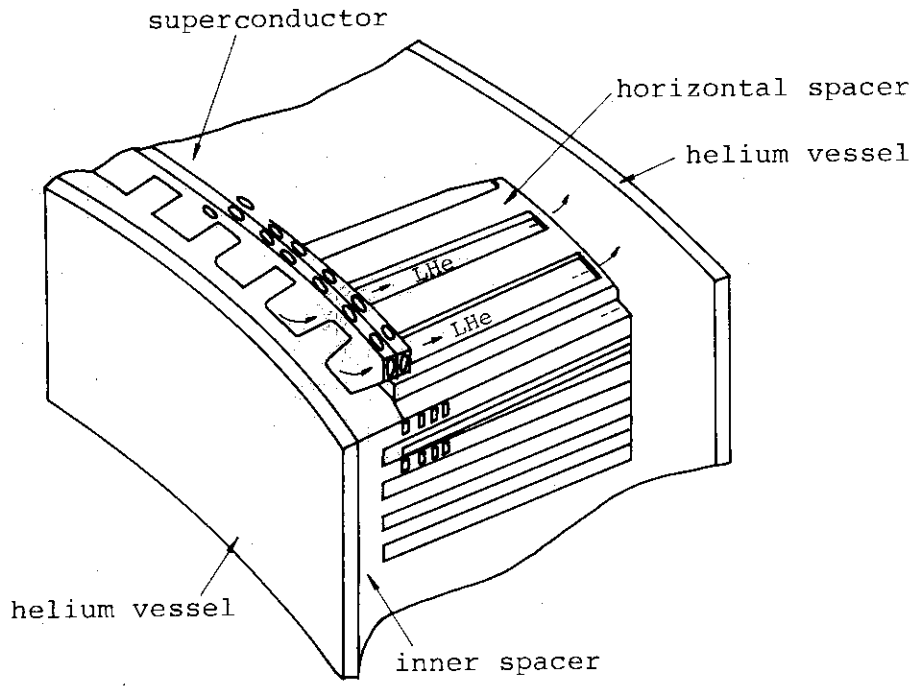

Fig. 7.2.2 Coil and Spacer for Cooling

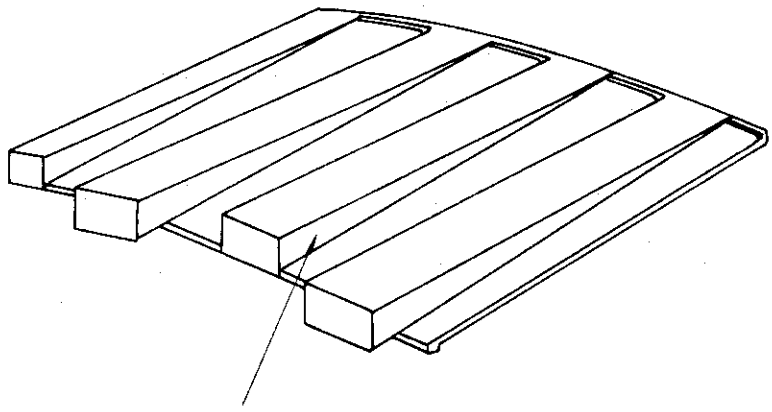

(a) A part of horizontal spacer for inner magnets

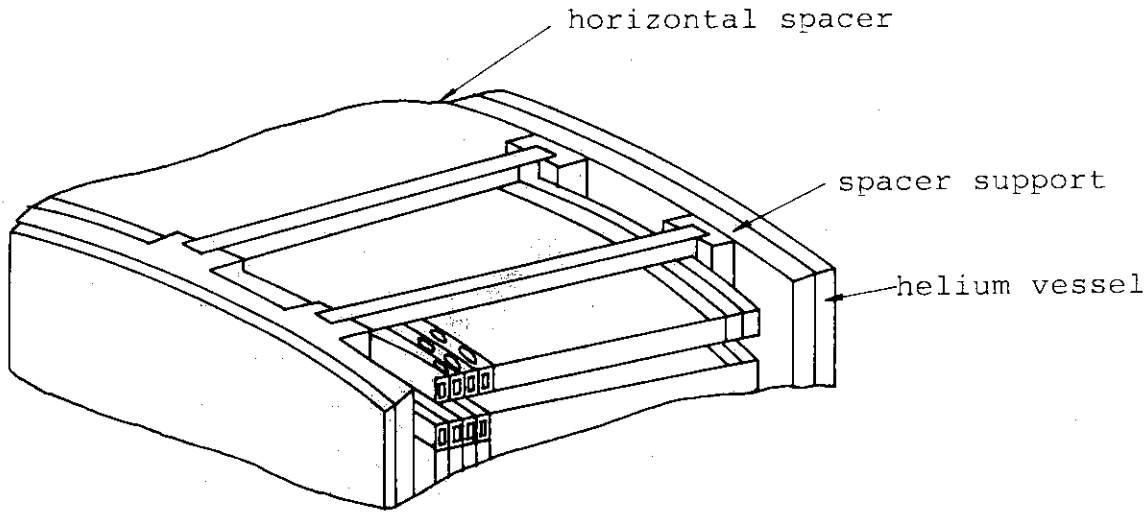

(b) spacer for outer magnets

Fig. 7.2.3 Spacer

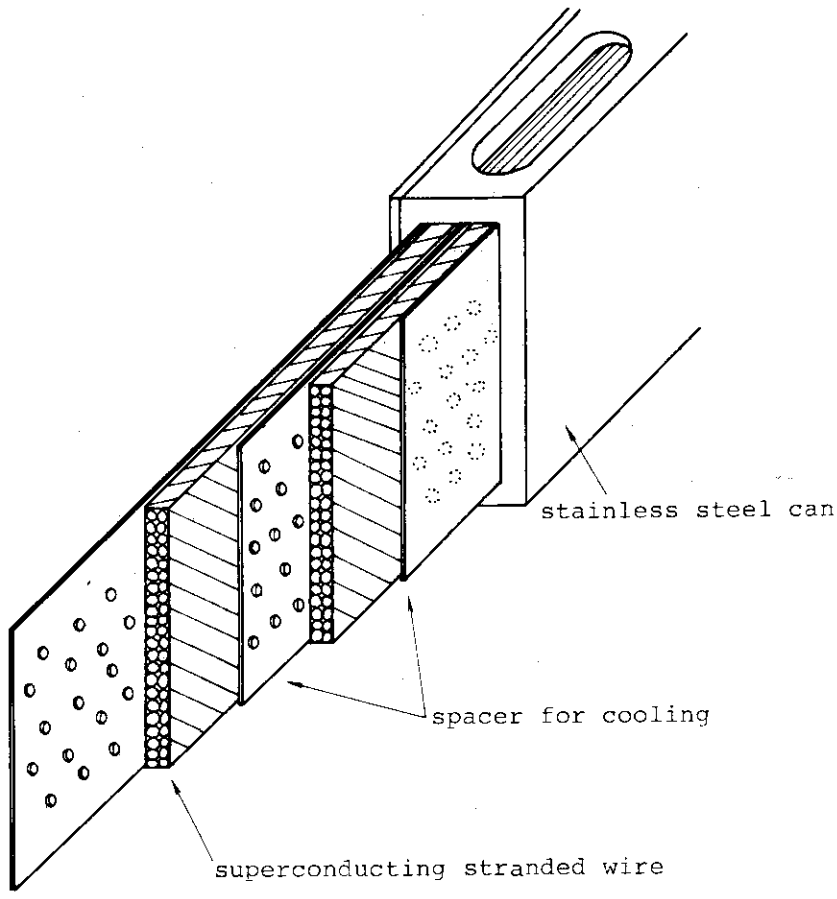

Fig. 7.2.4 Superconductor

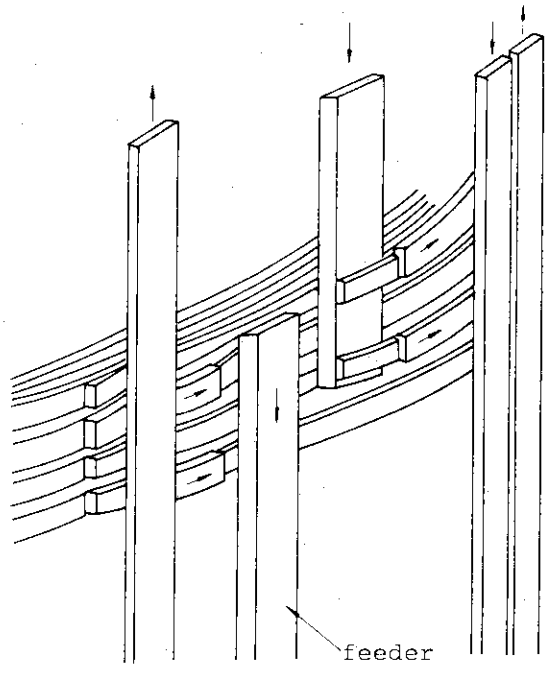

Fig. 7.2.5 Electrical Connection of Magnets

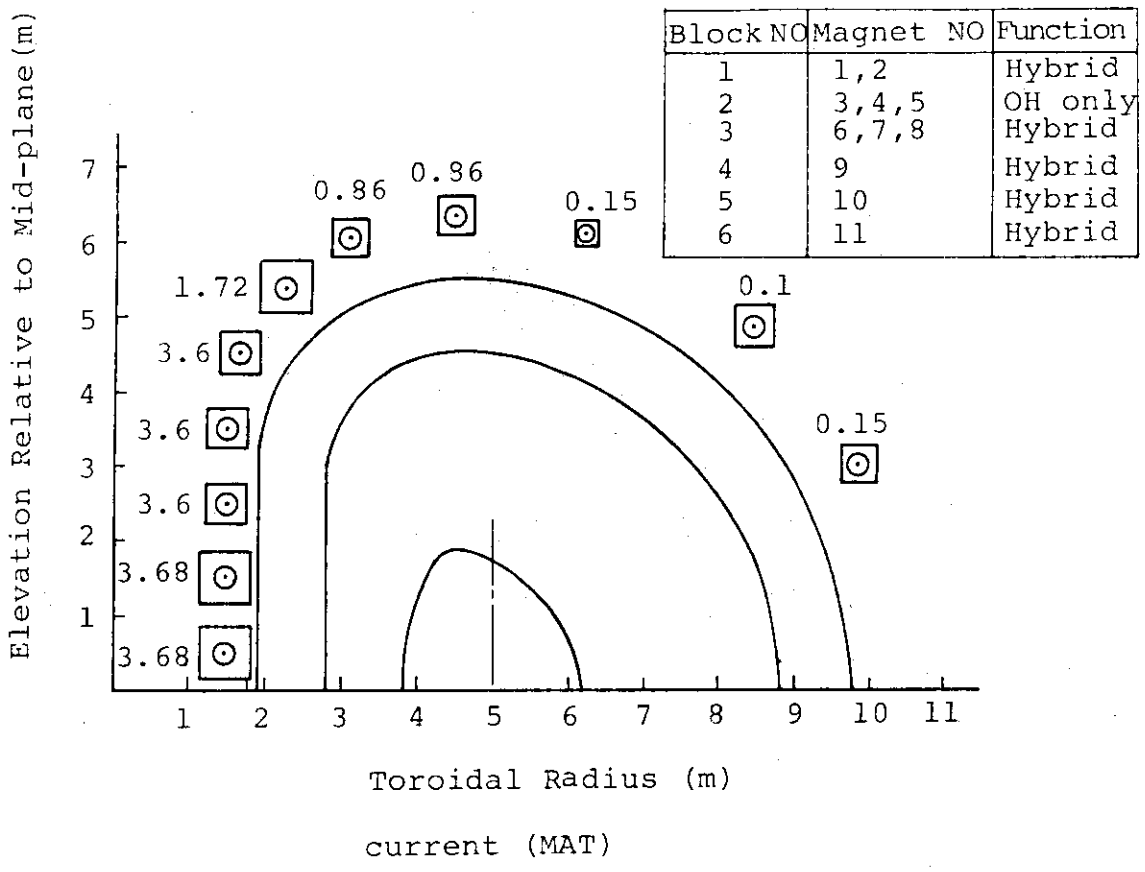

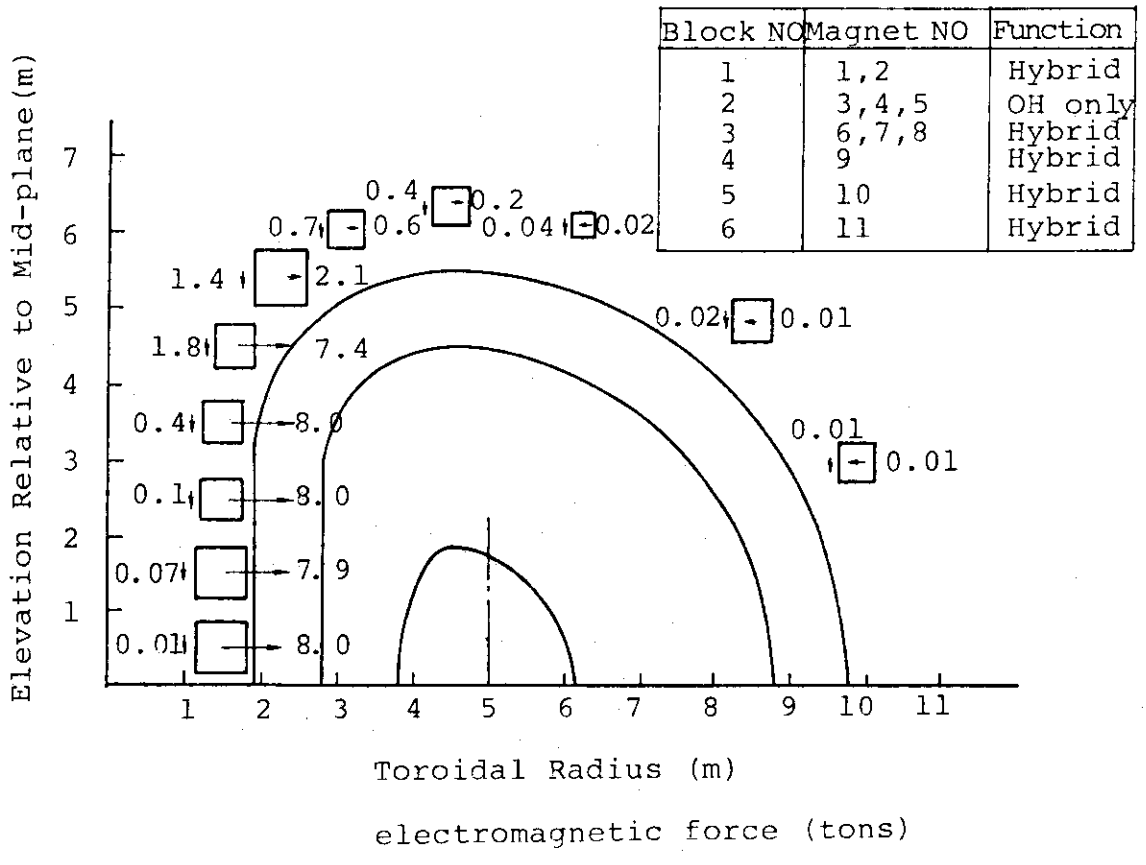

Fig. 7.2.6 Current and Force by Transformer Component

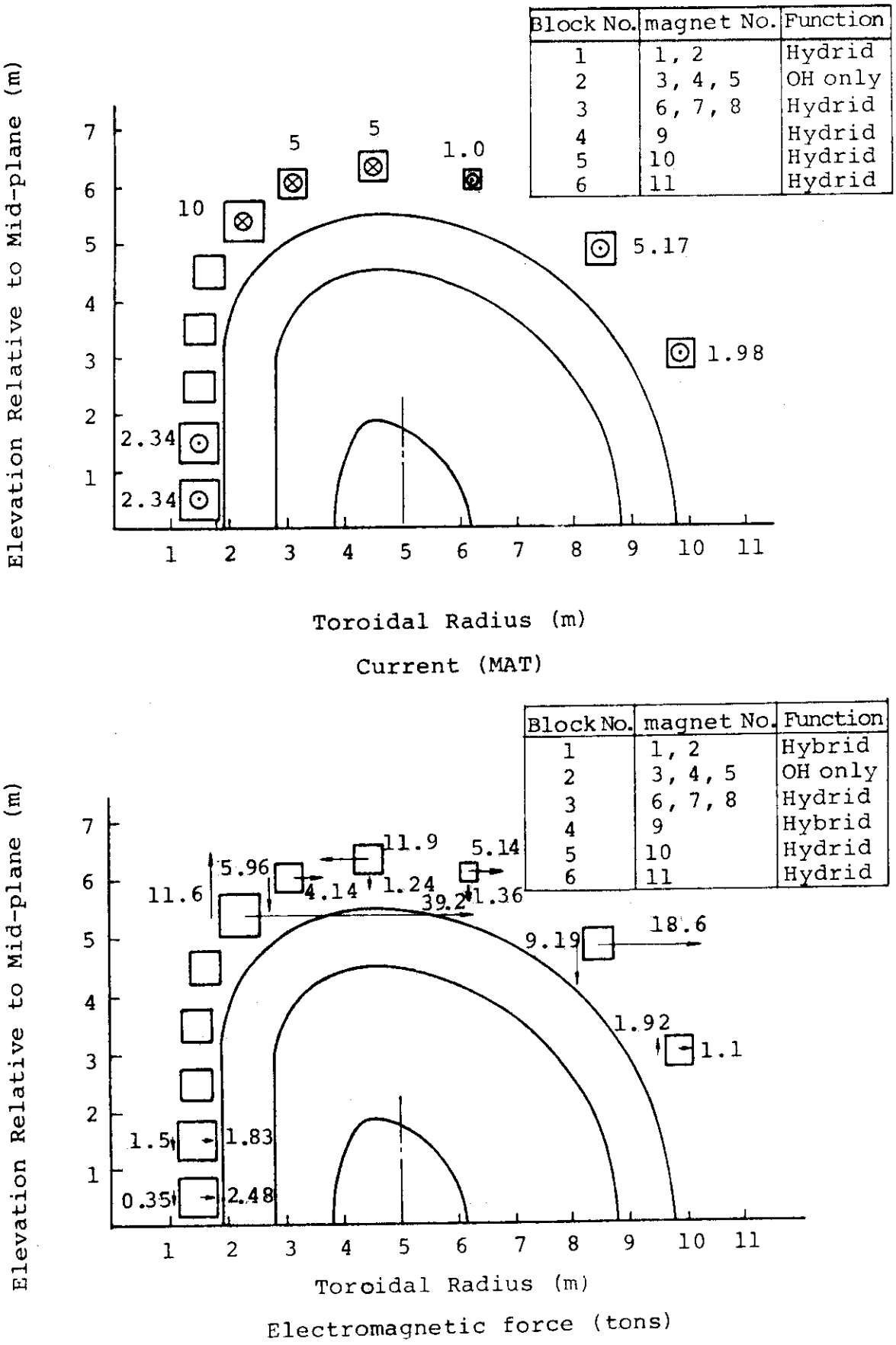

Fig. 7.2.7 Current and Force by Shaping Component (PF No. 9; -1 MAT)

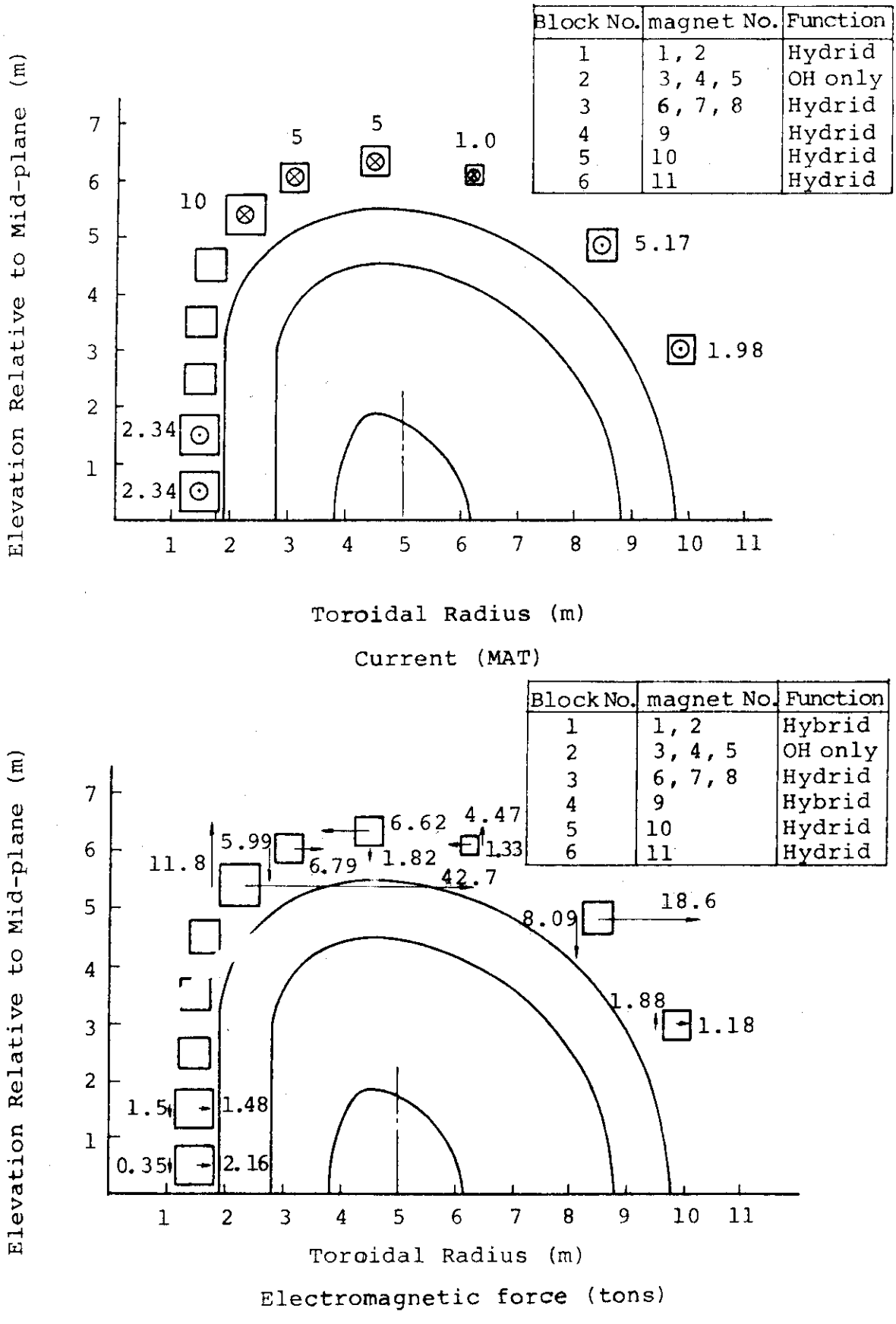

Fig. 7.2.8 Current and Force by Shaping Component (PF No. 9; 1 MAT)

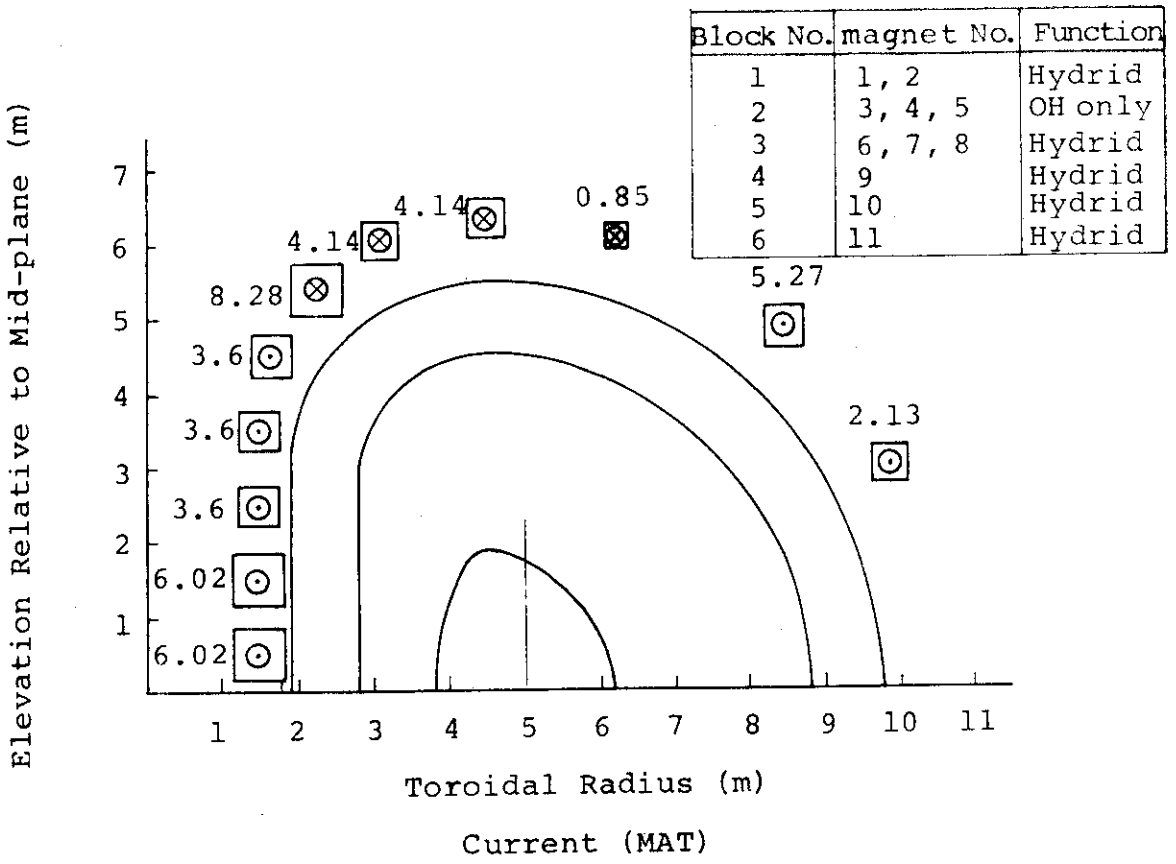

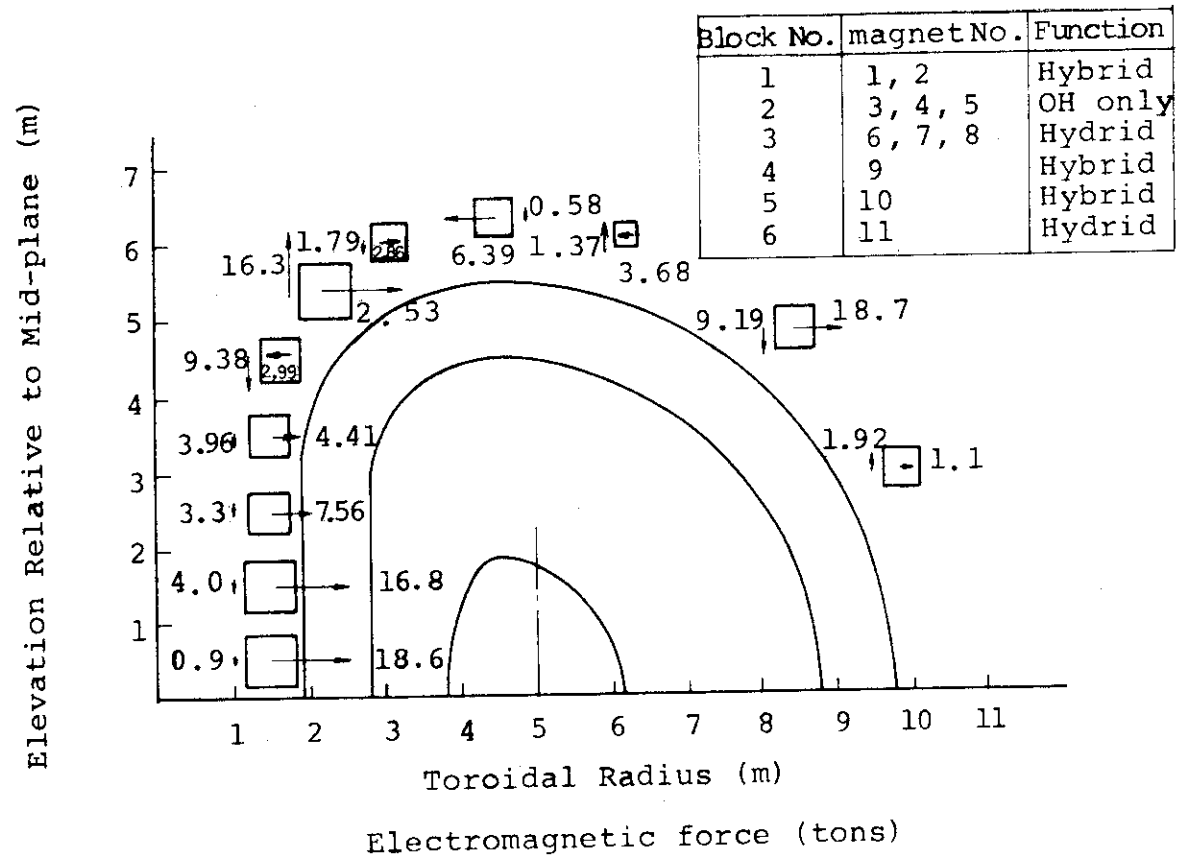

Fig. 7.2.9 The Total Current and Force (PF No. 9; 1 MAT)

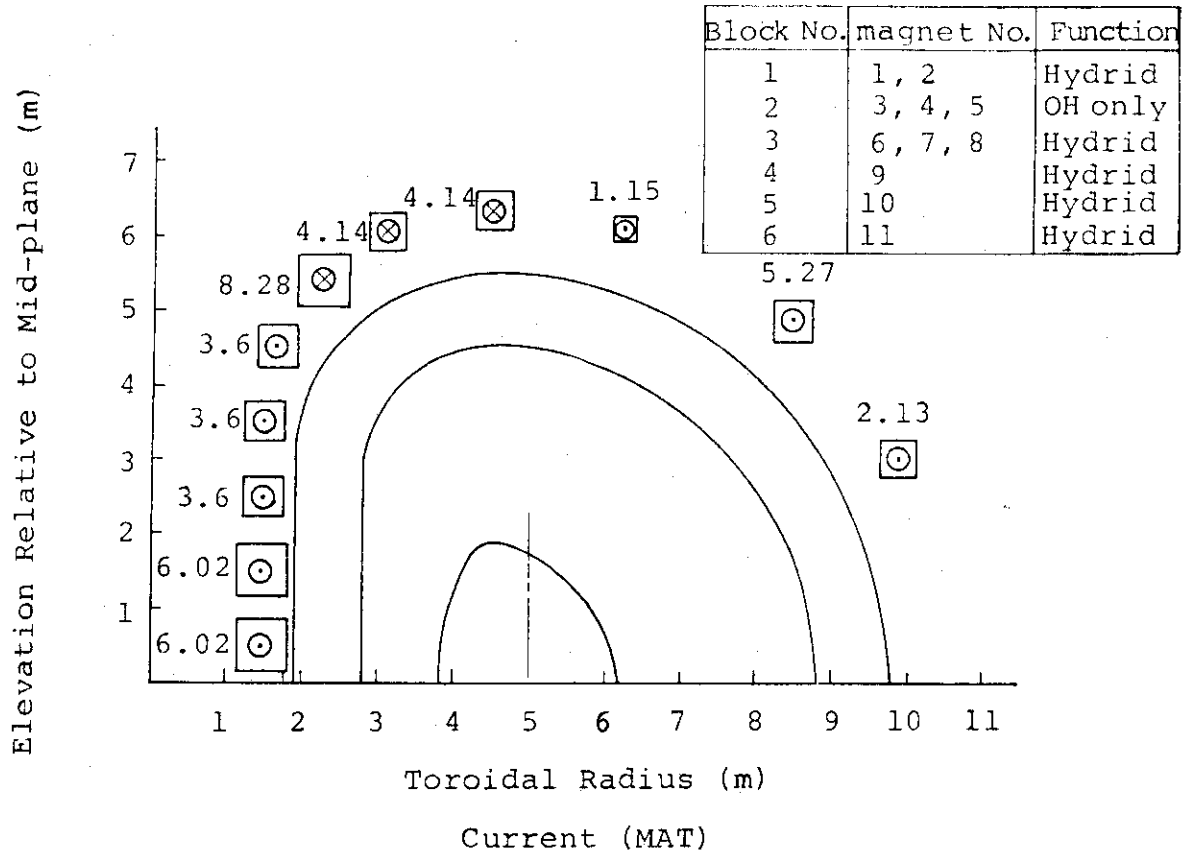

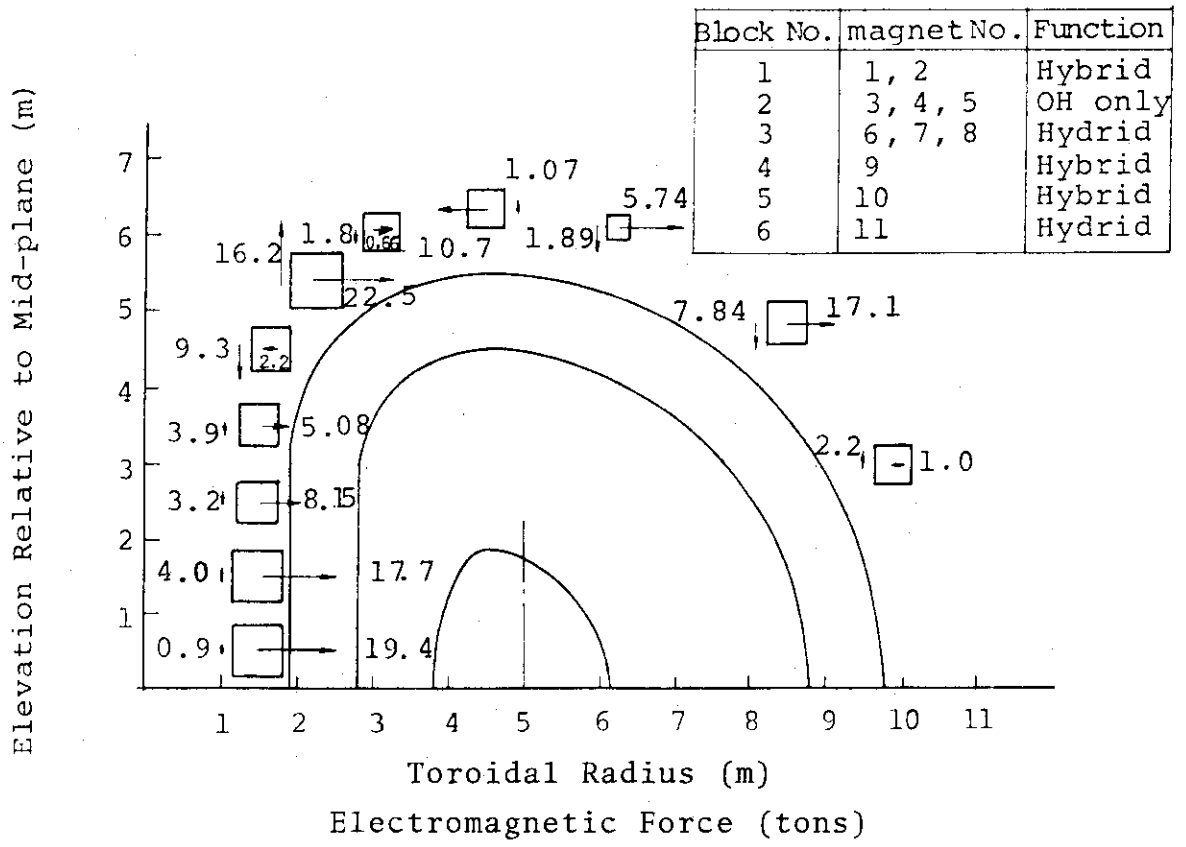

Fig. 7.2.10 The Total Current and Force (PF No. 9; -1 MAT)

8. Neutral Beam Injector

8.1 Design Conditions

The design conditions of the neutral beam injector (NBI) are as follows.

(1)	Injection power	75 MW
(2)	Injection energy	200 keV
(3)	Beam duration	5 sec
(4)	Angle to the plasma minor axis	15 degree
(5)	Injection ports in the torus	4

8.2 Component Structure

The NBI system shown in Fig. 8.1 ∿ 2 consists of the following main components: high current ion sources; neutralizers; direct energy converters; drift tubes; and cryopumps. The beam power per one ion source is 2.7 MW, and one injection port has 7 ion sources together with one spare source. Total length of beam line from the extraction grid of the ion source to the exit of the drift tubes is 7.5 m. The distance between the neutralizing cell and the drigt tube is 2.3 m, where the direct converter is located. The main design parameters are listed in table 8.1.

(1) Ion sources

The ion source with 98 A ion current extraction is chosen to hollow cathode type because of longer operation life, lower operation pressure (about 5.4×10^{-3} torr), and high gas efficiency (about 59%). Extraction system coinsists of four acceleration grids with an extraction area (11.1×127) cm^2. Acceleration voltages between the grids are 40, 50, 55 and 59, respectively, following -4 kV at the suppressor grid. These values are based on the equation $Vs = 6\times10^4\sqrt{d}$ obtained at Culham Lab.[1], where Vs and d are the acceleration voltage and the gap distance between extracted adjacent electrodes, respectively. The current density from the source plasma is 150 mA/cm^2, and the pressure at the entrance of the neutralizer is 2.6×10^{-3} torr. The pressure was chosen by estimating the heat load in the arc chamber due to electrons created by beam-gas interaction in the acceleration gaps.

(2) Neutralizer

The extracted iron beam is neutralized by the gas flowing in a rectangular duct which has beam limiters to form the beam shape. The power of shaped beam is 90% of that at the exit of the acceleration grids. The equilibrium neutral fraction of deuterium beam is shown in Fig. 8.3. Neutralization efficiency for 200 keV deuterium ion beam is about 20 percent. Gas thickness in a neutralizer is chosen to be 0.51 Torr-cm to provide 90% equilibrium. The cross sections of neutralization and ionization used in this estimation are 2.8×10^{-17} cm^2/molec. and 1.1×10^{-16} cm^2/molec., respectively, for 200 keV deuterium ion beam[3]. Since the neutralizer length is chosen to be 350 cm, some anount of gas needs to be fed into the neutralizer to get 0.51 Torr-cm in this length.

(3) Direct energy converter

Because of low efficiency of neutral atom production from positive ions at 200 keV, the power carried by unneutralized ion beam is very large. In this design, an in-line direct energy converter was chosen to handle those ions because of possibilities to make the system compact and to reduce the capacity of the power supply. The energy of the ion beam is recovered by decelerating the ions to a low energy and by collecting them on electrodes, thereby converting their kinetic energy back to electrical energy.

This converter is a space charge controlled type. There are two negative electrodes for electron suppression and one positive electrode for ion collection as shown in Fig. 8.4. In this design, the neutralizer is at ground potential, the collection electrode is at a positive high voltage V_{rec} (190 kV), and suppression electrodes are at $-V_{rep1}$ (-40 $\sim$ -50 kV) and $-V_{rep2}$ (-20 kV) before and after the collector, respectively.

It is expected that the beam width on the collector is 3 to 4 times that at the converter entrance, since the ion beam entering into the converter diverges because of its own space charge. The ion current density and beam width at the converter entrance are 50 mA/cm^2 and 12 cm, respectively. The pressure in the converter region is 5×10^{-5} Torr.

(4) Drift tube

Drift tubes are equipped to limit gas flow toward the torus. The tube cross-section is rectanguler and the dimension is listed in Table 8.1. The gate valves are equipped at the drift tube entrance to be used when cryopumps are regnerated.

(5) Cryopump

Gas flowing out of the neutralizer and the converter is evacuated by cryo-condensation pumps. The gas flow rate evacuated by the cryo-pump is 156 Torr.ℓ/sec. In order to keep the pressure in the coverter region at 5×10^{-5} Torr, the cryopump needs to have a pumping speed of 6.1×10^{6} ℓ/s. The pump entrance area of 40 m^2 is necessary to give this pumping speed, assuming that the pumping speed per pump entrance area is 15 $ℓ/cm^2$. sec. Cryopanels are placed on the sides and on the bottom of the vacuum chamber of NBI.

The gate valves located at the entrances of the drift tube and the neutralizer shown in Fig. 8.1 ∿ 2 are closed when the cryopanels are regenerated. It means that the NBI cannot be operated while the cryopumps are regenerated.

The interval between the terms of cryopump regeneration is decided by the explosion limit of deuterium gas in the NBI tank. The allowable deuterium gas amount is 1.75% of the air amount in the NBI tank at 1 atmoshere. Plasma operation of about 5,900 shots is possible within this limit.

8.3 Design Analysis

8.3.1 Heat load

(1) Electron back streaming in the acceleration grids.

In the extraction grids, secondary ions and electrons created by beam-gas interaction are accelerated by electric field and some of them cause grids to be heated. This heat load can be reduced by adjusting grid location carefully. However, the secondary particles that are not intercepted by the grids flow into the arc chamber or into the neutralizer. In order to estimate these heat load, the trajectories of secondary ions and electrons in the presence of the primary beam were calculated numerically.

The current generated over the primary beam path length, Δx, is

$$\Delta I = \sigma \cdot N_o \cdot \Delta x \cdot I_B$$

where N_o is the background density, I_B is the portion of the primary beam current flowing through the acceleration grids, and σ is mainly σ_i in the case of electron production and $(\sigma_i + \sigma_{10})$ in the case of ion production (σ_i; the ionization cross section of the background gas, and σ_{10}; electron capture cross section of the ion beam[3]). It was assumed that the local field, generated by the secondary particles, is too weak to perturb the primary beam. Typical secondary particle trajectories are shown in Fig. 8.5. (Using computer code IONORB[4], the potential distribution of the extractor region and the primary ion trajectories were calculated.) Thus, the heat load on the back streaming side of the arc chamber due to secondary electrons is estimated to be 2.7 kW/cm^2, when the pressure in the arc chember and at the entrance of the neutralizer are 5.4×10^{-3} Torr, and 2.6×10^{-3} Torr, respectively. Since this heat load is very large, it is necessary to equip a beam dump on the backstreaming side of the arc chamber.[2]

The power going into the neutralizer as the secondary ions is estimated to be about 26% of the primary beam power. The heat load on the neutralizer wall is about 80 W/cm^2, if all of the secondary ions and 10% of primary beam bombard the wall uniformly. A way to reduce the power due to secondary particles is to reduce the gas density in the grid gaps, which requires larger pumping speed, and thereby requires larger NBI systems.

(2) Coolector plate of the direct converter

In the direct converter, beam-gas interaction creates secondary electrons and ions, the latter of which yield secondary electrons on the electron suppressor electrode. The gas pressure in the direct converter systemr is decided to be 5×10^{-5} on the basis of power load resulting from acceleration and collection of these particles.

Secondary ion current, I_{Si}, produced by beam-gas interaction is is

$$I_{Si} = \int_o^L N_o(\ell)\sigma i\ (\ell) I_B\ d\ell$$

where I_B is the primary ion beam current, L is the effective length

of the beam in the converter, N_o is the neutral gas density and σ_i is the ion production cross section of the background gas. We assume that N_o is 1.7×10^{15} molec./cm^3 (5×10^{-5} Torr), L is 40 cm, the collector potential is 190 kV and the electric field strength, $\varepsilon = dV/d\ell$, is 190 kV/40 cm in the coverter. The ion production cross section, σ, is approximately

$$\sigma_i = \begin{cases} \sigma_{oi} & \text{from 10 keV to 30 keV} \\ \sigma_{oi}\left(\frac{Eo}{E}\right)^{0.7} & \text{from 30 keV to 200 keV} \end{cases}$$

where E is the ion beam energy, Eo is 30 keV, and σ_{oi} is 9×10^{-16} cm^2/molec.[3]

Thus, the heat load on the collector is about 400 ∿ 500 W/cm^2, when the ion current density at the entrance of the converter is taken to be 50 mA/cm^2. However, this estimation is based on the assumption of uniform heat loading. Computer analysis will be carried out to obtain the ion beam current density more accurately and to find correct shape of electrodes in future.

(3) Design consideration

Burn-out heat flux in a beam dump has been studied in detail at JAERI. It has been shown that the burn-out heat flux is 0.8 ∿ 1 kW/cm^2,[2] which is within the scatter of the results obtained in former heat transfer experiments. We think temporarily that permisible heat load on a plate is 500 W/cm^2 in this NBI design. The beam dump in the arc chamber and the collector of the direct converter will have to be disigned within this heat load.

8.3.2 Gas flow balance

In this section, we estimate gas flow rates into the torus, main vacuum system and NBI vacuum system. Gas flow conductance concerning these gas flow rates are listed in Table 8.2. The pumping speed of the main vacuum system is assumed to be 1×10^6 ℓ/s per port. In the plasma chamber, the pressure in the inside of the blanket structure is considered to be zero, because the plasma is an ideal pump. A considerable amount of gas may flow into the plasma through the diverter region, and some part of it may be ionized before it goes into the main plasma. The gas flow conductance through the divertor throats including ionization was

temporarily assumed to be 2×10^6 ℓ/s.

The gas flow rate thus obtained is shown in Fig. 8.6. The cryopump with the evacuating speed of 6.1×10^6 ℓ/s yields that the pressure near the direct converter is 5×10^{-5} Torr. The flow rate through the blanket NBI window is 0.2 Torr-ℓ/s per one window, and the flow rate through the diverter throat is 2.2 Torr-ℓ/s per one NBI port. Here the area of the blanket NBI window is chosen to be 65 × 100 cm which is enough for neutral beam transport.

8.3.3 Power efficiency

(1) Power recovery efficiency of the direct converter

power recovery efficiency of the direct converter, η_{rec}, is defined by the ratio of net recovered power to incident ion beam power

$$\eta_{rec} = \frac{Q_{th} + P_{pass} + P_{el}}{P_{ir}}$$

where P_{ir} is the power of ion beam entering the converter, Q_{th} is the power load on the electrodes due to the primary and secondary particles, P_{pass} is the power of ions which are not collected by the collector and Pel is electrical loss of the converter power supply.

P_{pass} and P_{el} is assumed to be

$$P_{pass}/P_{ir} = 10\%$$

$$P_{el}/P_{ir} = 5\%$$

The power load on the collector due to the decelerated primary ions and the secondary electrons emitted from the suppressor electrode by ion impinging is estimated to be 5% and 11% of P_{ir}, respectively. The power load on the suppressor due to the electrons generated by beam-gas interaction is 3.1%. Thus, Q_{th} becomes

$$Q_{th}/P_{ir} = 19\%$$

These values give us the power recovery efficiency

$$\eta_{rec} = 65\%$$

(2) Overall power efficiency

Overall power efficiency of the NBI system η is written in the

following way

$$\eta = \frac{\eta_I \cdot \eta_{div} \cdot \eta_N \cdot \eta_{RI}}{1-\eta_I \cdot \eta_{div} \cdot (1-\eta_N) \cdot \eta_{rec}}$$

where η_I is the power efficiency of ion source, η_{div} is the transmission efficiency through the neutralizer, η_N is the neutralization efficiency, η_{RI} is the beam fraction passing without reionization from the exit of the neutralizer to the blanket NBI window, and η_{rec} is the power recovery efficiency of the direct converter.

Each efficiency is defined as follows. The power efficiency of the ion source is

$$\eta_I = P_i/(P_i + P_s)$$

where P_i is the primary beam power extracted from the ion source and P_s is the power of the secondary particles produced by beam gas in the grid gaps. The value of (P_s/P_i) is estimated to be 0.33, which yields

$$\eta_I = 0.75$$

As is shown in 8.2 (1), 90% of the beam can pass the neutralizer, which means

$$\eta_{div} = 0.90$$

Since the gas thickness in the neutralizer is provided for 90% equilibrium, the neutralization efficiency is given as

$$\eta_N = 0.17$$

The neutral beam is decreased due to re-ionization from an exit of the neutralizer to the blanket NBI window. The re-ionization loss is estimated to be about 9% which means

$$\eta_{RI} = 0.91$$

Finally, the overall power efficiency is

$$\eta = 0.17$$

8.4 Repair and Maintenance

(1) Life estimation

The extraction grids, neutralizer wall and collector plate in the direct converter are bombarded by energetic ions, causing erosion of the plate by sputtering. The ion flux density at the extraction grids is estimated to be 3.8×10^{15} ions/cm^2/sec, assuming that the power intercepted by the extraction grid is about 0.1 per cent of the primary beam power, and that the ions are intercepted only by the first acceleration grid. The energy of the intercepted ions is about 50 keV. In the direct converter, the ions with the energy of 10 keV bombard the collector electrode. The ion flux density is estimated to be 7.8×10^{16} ions/cm^2/sec, assuming that the beam width on the collector is about 4 times that at the converter entrance.

The erosion thickness due to sputtering is estimated as shown in Table 8.3. Copper and molybdenum are the candidates of the electrode material. It is found that the erosion in 2×10^5 shots is negligibly small at the extraction grids and the collector even in the case of copper. The damage of the neutralizer due to sputtering is completely negligible. It means that scheduled replacement is not necessary in these parts, if erosion is caused only by sputtering. However, there are some other possible mechanism causing electrode erosion such as break down discharge between electrodes, blistering and etc. These effects can not be predicted because of the lack of experimental data. Erosion due to these effects is considered to be unexpected failure.

The life of the hollow cathode can be estimated by using the data of ion thrusters. It has been found that the corresponding tip erosion rate in the ion thruster is 5×10^{-5}mm/h at j_o/d_o=8A/mm,[5] where the arc current per one cathode, J_o, is taken to be 24 A, and the diameter of a cathode d_o is 3 mm. This errosion rate gives that the erosion thickness in the hollow cathode is 0.014 mm in 2×10^5 shots which is too small to affect the arc condition. We therefore consider that replacement of cathodes is needed only when any failure is found.

Aluminium oxide used for insulator in the ion source is irradiated by neutrons streaming out from the torus. Mechanical and electrical properties are degraded by neutron irradiation.

It has been found that the irradiation limit for degradation is 10^{21} neutrons.cm^{-2}.[6),7),8)] About 1% increase in volume has been measured over the dose range of 0.2 to 1.4 × 10^{21} neutrons.cm^{-2}.[8)] Neutron flux at the insulator of ion source may be less than 10^{10} neutrons/cm^2/sec, which will be estimated in detail in future. It means that more than 3 × 10^2 years are necessary to reach the dose limit.

(2) Failure indication

The hollow cathode, accelleration grids and the collector plates are replaced when any failure is indicated. The deterioration of hollow cathode can be found out by monitoring the change of voltage-current charecteristics of the arc. As for the extraction grids, the heat load on the neutralizer plate is increased by the damage of the extraction grids because of damage-induced beam divergence. Thus, the thermocouples located near the wall surface of the neutralizer can monitor the performance of the extraction grids. The damage in the direct converter can be found out by monitoring recovery current and heat load on the drift tube wall.

(3) Replacement procedure

In the NBI system, there are three easy replaceable portions such as the hollow cathodes in the ion source, acceleration grids and collector electrodes. The replacement procedures of these portions are shown in Fig. 8.7 ∿ Fig. 8.9 together with the time required for replacement. Figure 8.10 visualizes general idea how these replacements are carried out. Generally speaking, the replacement procedure is rather simple, therefore any replacement discussed here appears to be finished within one to three days.

The radiation shielding wall located on the back side of NBI is removed when the cathodes or the acceleration grids are replaced at present. Maintenance nachines are brought from the storage area when cathodes and grids are replaced. We may study *in-situ* maintenance machine in future to replace the cathodes without removing the radiation shielding wall.

8.5 Design Problems

We will have to study the following problems in future.

1) Estimation of the power recovery efficiency and the heat load on the

collector plate of the direct energy converter by numerical simulation. This estimation affects the pressure in the converter region, thereby it affects the evacuating system of NBI. The device size of NBI depends strongly on the evacuating system.

2) Better estimation of the life of the acceleration grids and the cathode. It appears that only experiments will give us this kind of information.

3) We should try to explore neutralization methods for fast ions other than gas cell method[2] because of the low neutralization efficiency in positive ions of higher energy. The capacity of the NBI evaluating system is mainly determined by the gas flow required for the gas cell concept.

4) Maintenance procedure needs to be considered again when the detailed structure design is carried out.

REFERENCES

1) J.R. Coupland, et al., "A Study of the Ion Beam Intensity and Divergence Obtained from a Single Aparture Three Electrode Extraction System", Rev. Sci. Instrum. 44 (1973)

2) Japan-INTOR group 4 report.

3) C.F. Barnet et al., "Atomic data for controlled fusion research", Vol. I and Vol. II, ORNL-5206, ORNL-5207 (1977)

4) S. Ohara, "Simulation Code for Beam Trajectories in an Ion Sources, INORB", (in Japanese) JAERI-M 6757 (1976)

5) H.R. Kaufman, "Technology of Electron-Bombardment Ion Thrusters", in Advances in Electronic and Electron Physics, Vol. 36, Academic Press (1974)

6) M.H. Van de Voorde and C. Restat, "Selection guide to organic materials for nuclear engineering", CERN 72-7 (1972)

7) Arthur A. Bauer et al., "An evaluation of electrical insulators for fusion reactors", BMI-1930 (1974)

8) G.W. Keilholtz et al., "Properties of Magnesium, Aluminium, and Beryllium Oxide Compacts Irradiated to Fast-Neutron Doses Greater than 10^{21} Neutrons cm^{-2} at 150, 800, and 1,100°C", in Proceeding of the conference an nuclear applications of nonfissionable ceramics,

Washington D.C. (1966)

9) L.C. Pittenger, UCRL-78501 (1976)

10) K.H. Berker et al., "Mixed Species in Intense Neutral Beams", Proceeding of 1st topical Meeting on Technology of Controlled Nuclear Fusion CONF-740402-PI 392 (1974)

Table 8.1 Design Parameters

Beam Lines		
Number of Injection Ports		4
Number of Ion Source per Port		7 + 1 spare
Length of Beamline (from exit of Ion Source to exit of Drift Tube)		750 cm
Length of Neutralizer		350 cm
Length of Drift Tube		170 cm
Ion Source		
Output power		19.6 MW
Acceleration Voltage		200 kV
Ion Current		98 A
Cathode Type		Hollow Cathode
Number of Acceleration Stages		4 (40, 50, 55, 59, -4kV)
Gas Efficiency		50 %
Operation Pressure	(Po)	5.4×10^{-3} Torr
Neutralizer		
Pressure : entrance	(P_1)	2.6×10^{-3} Torr
gas feed point	(P_2)	1.7×10^{-3} Torr
exit	(P_3)	5.0×10^{-5} Torr
Line Density of Gas Target		0.51 Torr-cm
Neutralization Efficiency		17.2 %
Beam divergence loss		9.8 %
Cross Sectional Area; entrance		127×11.1 cm^2
exit		112×12 cm^2

Table 8.1 (continued)

Drift Tube		
Cross Sectional Area ;	entrance	104×15 cm^2
	exit	97×18 cm^2
Pressure ;	entrance (P_3)	5×10^{-5} Torr
	exit (P_4)	2.6×10^{-6} Torr
Gas flow per port		2.9 Torr-ℓ/s
Direct Energy Converter		
Collector voltage		190 kV
Suppressor voltage		-50 kV
Pressure	(P_3)	5×10^{-5} Torr
Cryo Pump		
Pumping Speed		6.1×10^6 ℓ/s
Blanket window		
Cross Sectional Area		65×100 cm^2
Pressure	(P_5)	1×10^{-6} Torr

Table 8.2 Gas flow conductances

Part	Size		Conductance (ℓ/S)
Neutralizer	Cross sectional Area: Entrace	127 cm × 11.1 cm	5.02×10^3
	Exit	112 cm × 12 cm	
	Length	350 cm	
Drift tube	Cross sectional Area: Entrance	104 cm × 15 cm	1.55×10^4
	Exit	97 cm × 18 cm	
	Length	170 cm	
Pumping area between the neutralizer and drift tube		(190 cm × 550 cm) × 2	6.5×10^6
Radiation shield	Cross sectional Area	340 cm × 140 cm	1.5×10^6
Injection window of the blanket	Cross sectional Area	65 cm × 100 cm	2.03×10^5

Table 8.3 Electrode erosion due to ion sputtering

	Accel. Electrode		Converter Collector		Neutralizer
Ion flux (ions/cm sec)	3.75×10^{15}		7.8×10^{16}		2.8×10^{15}
Ion energy (keV)	50		10		170
Material	Mo	Cu	Mo	Cu	Cu
Sputtering ratio (atoms/ion)	10^{-2}	1.9×10^{-2}	6.3×10^{-3}	6.5×10^{-2}	3.8×10^{-3}
Errosion rate (cm/sec)	5.8×10^{-10}	8.4×10^{-10}	7.7×10^{-9}	6.0×10^{-8}	1.2×10^{-10}
Erosion after 2×10^5 shots (mm)	0.006	0.008	0.08	0.61	1.2×10^{-3}

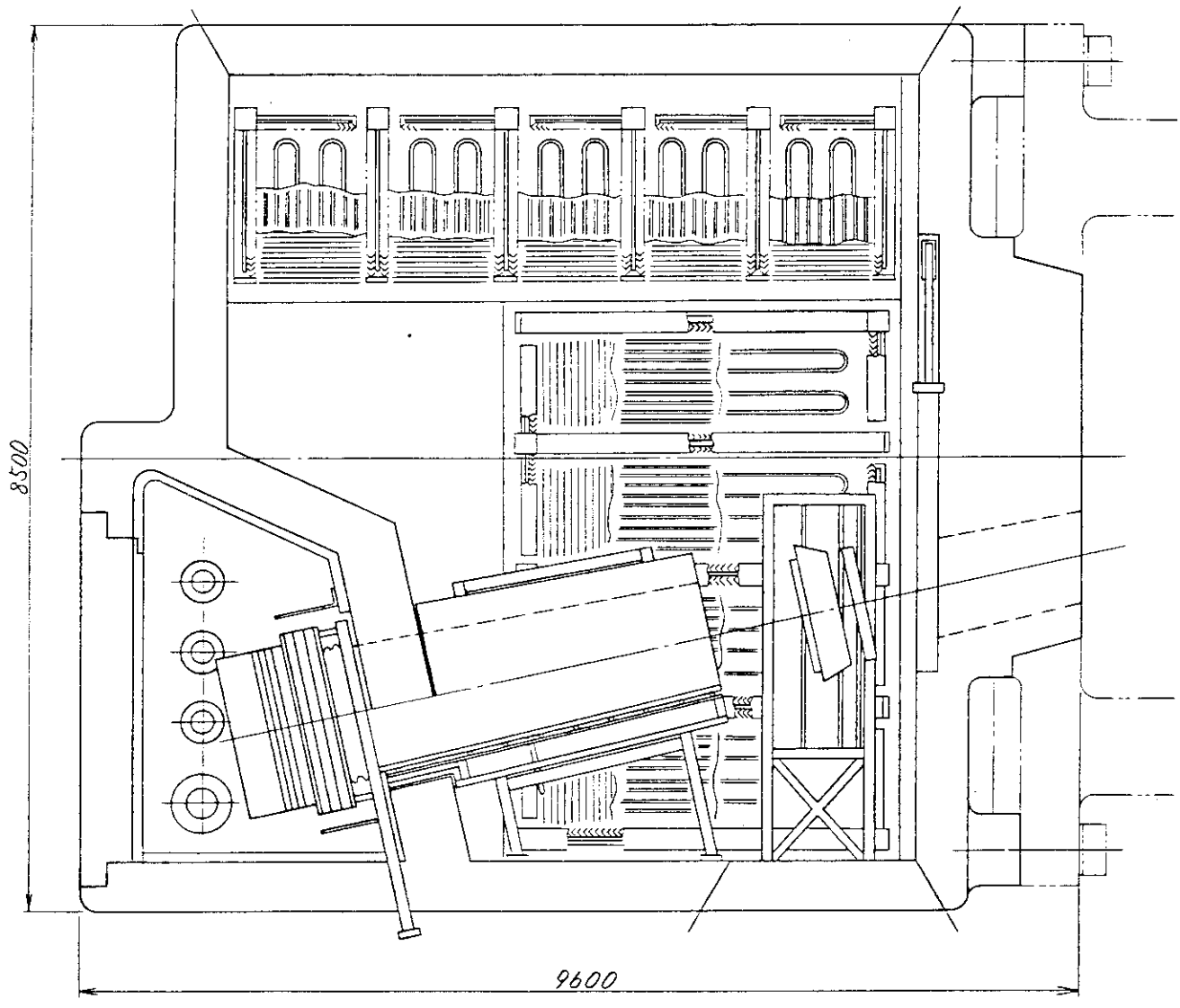

Fig. 8.1 Plane View of NBI System

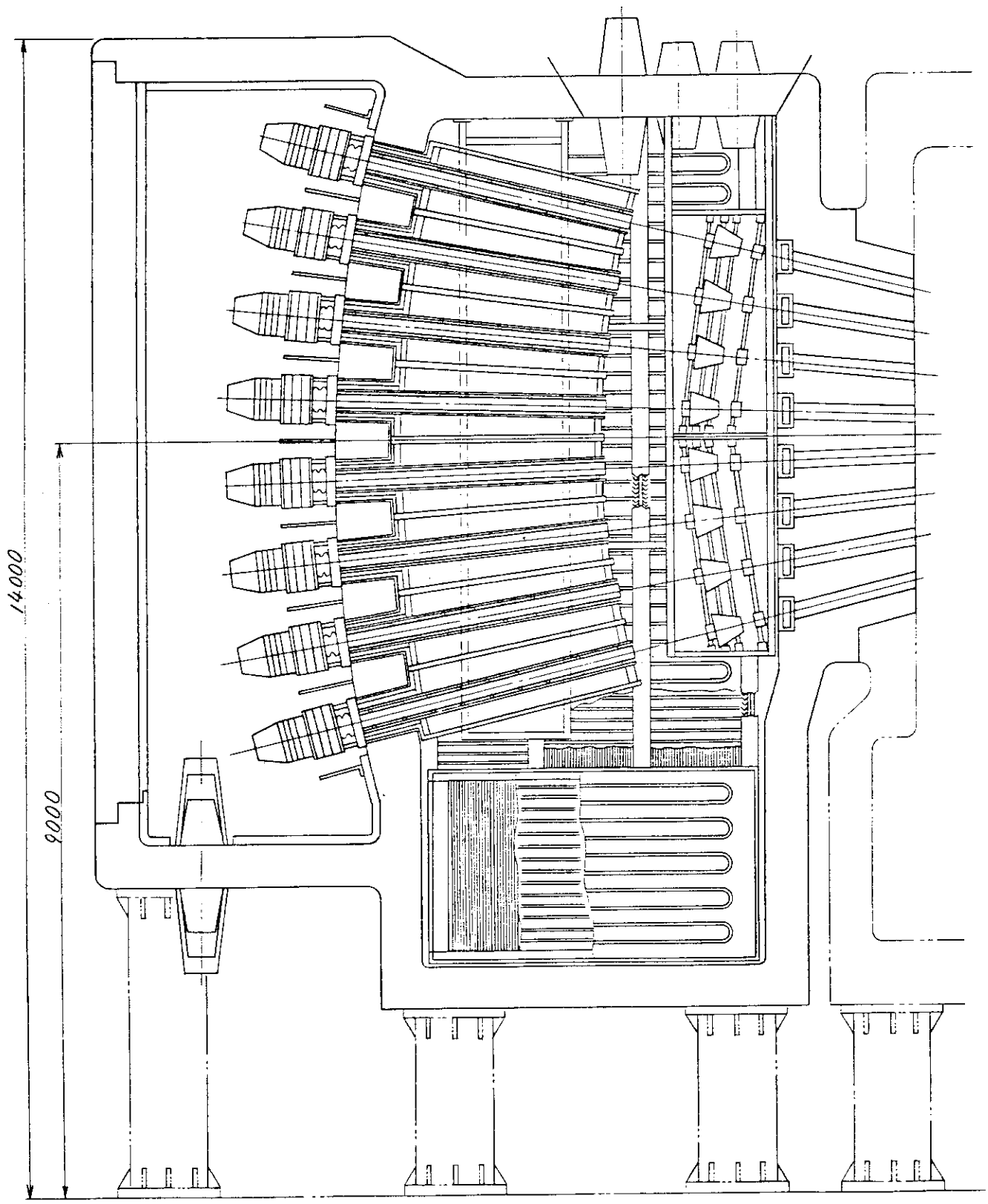

Fig. 8.2 Side View of NBI System

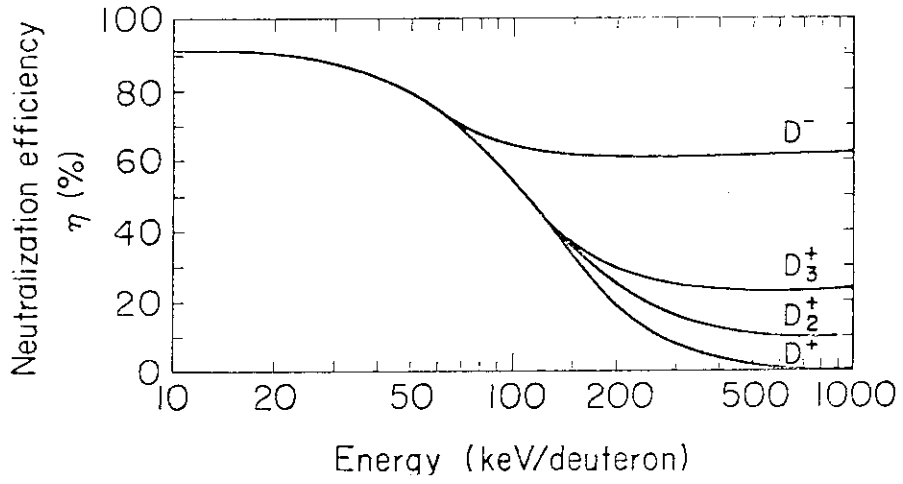

Fig. 8.3 Maximum Neutralization Efficiency in D vs. Beam Energy for Each of the Four Beams, D^+, D_2^+, D_3^+ and D^- [10]

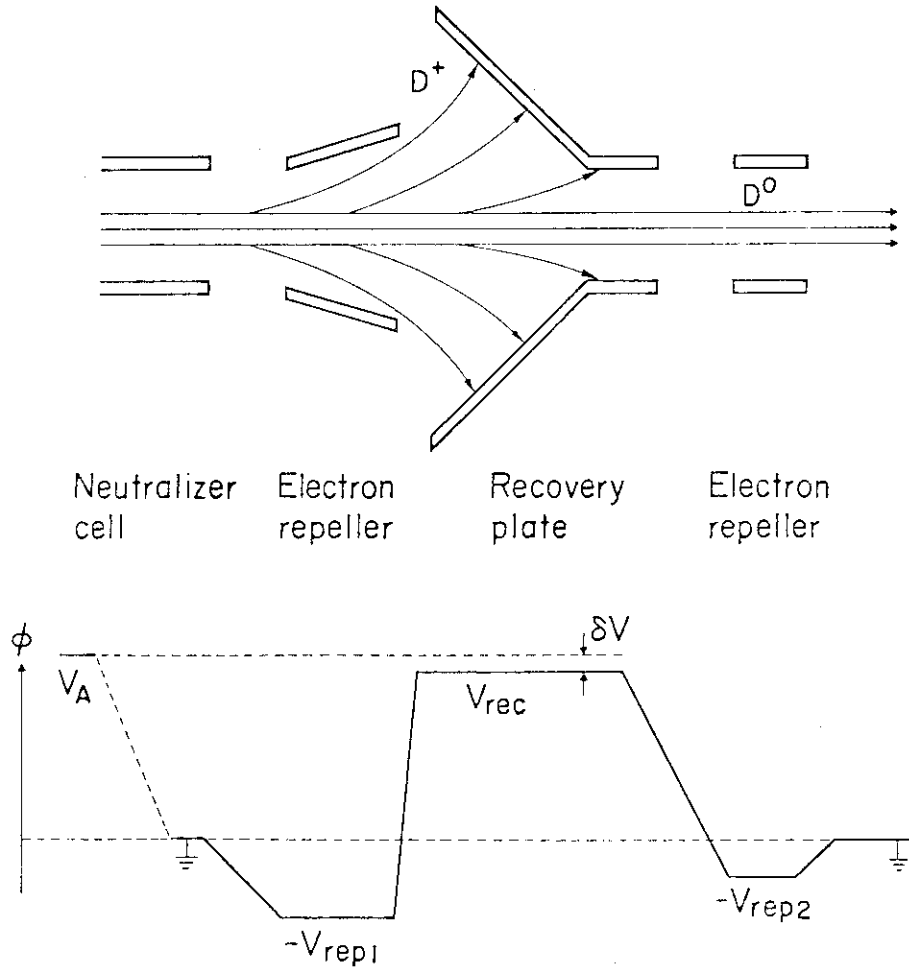

Fig. 8.4 Direct Energy Convertor

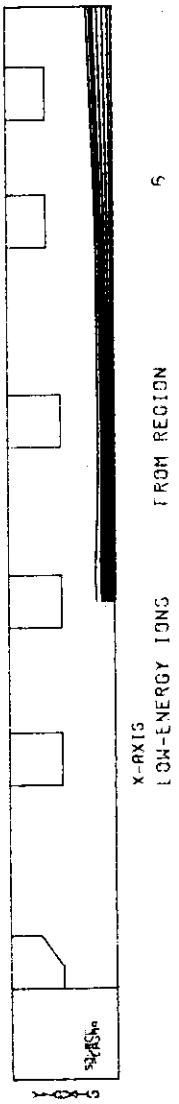

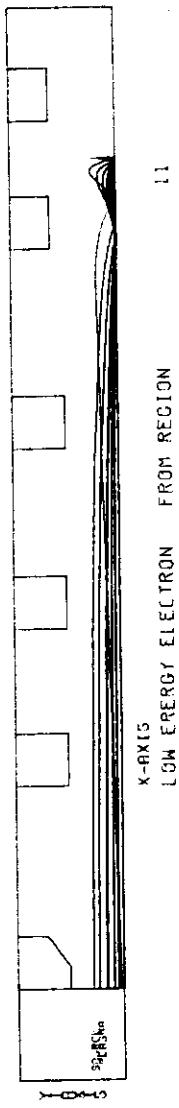

Fig. 8.5 Typical Trajectories of Secondary Particles

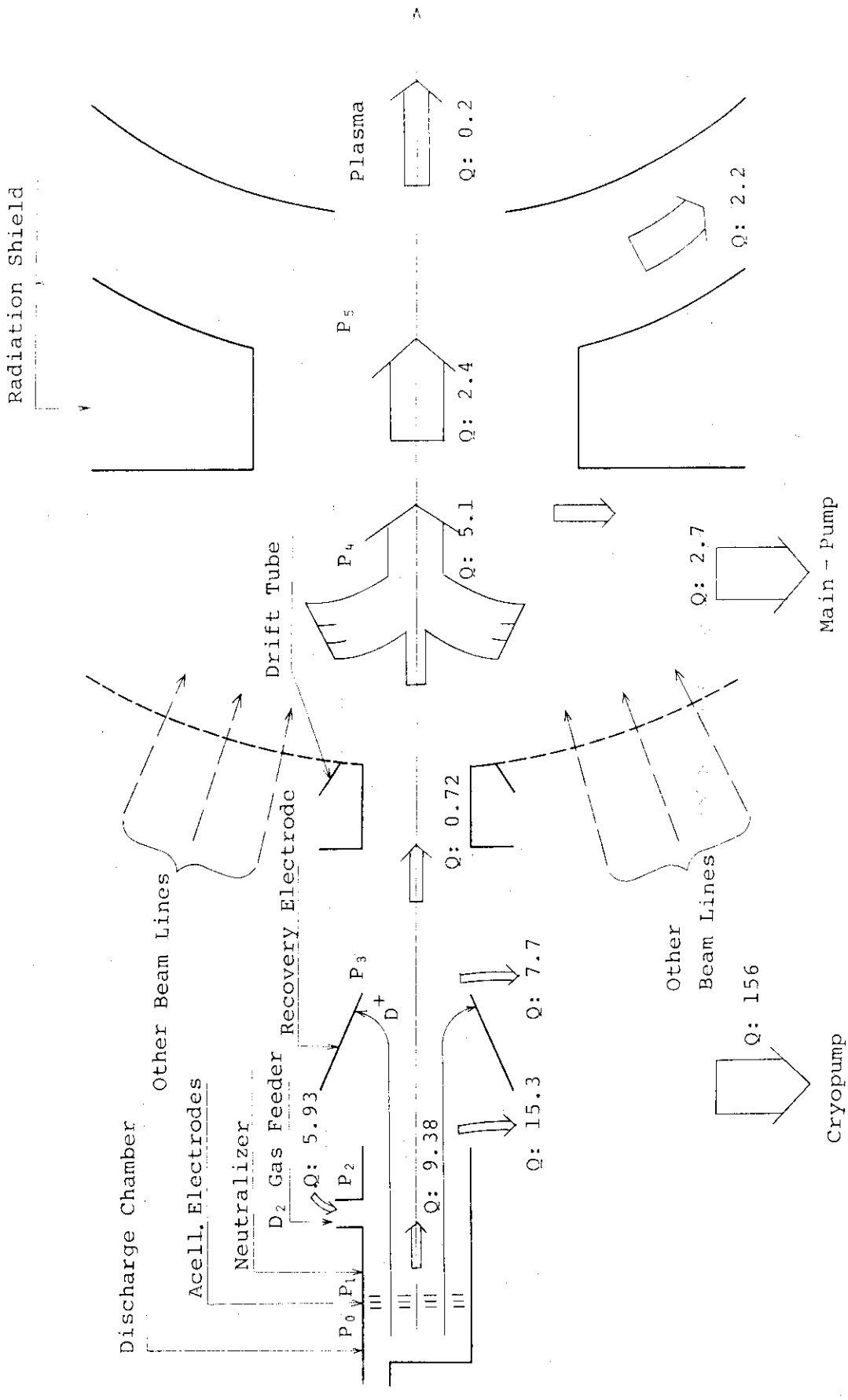

Fig. 8.6 Gas Flow of NBI System

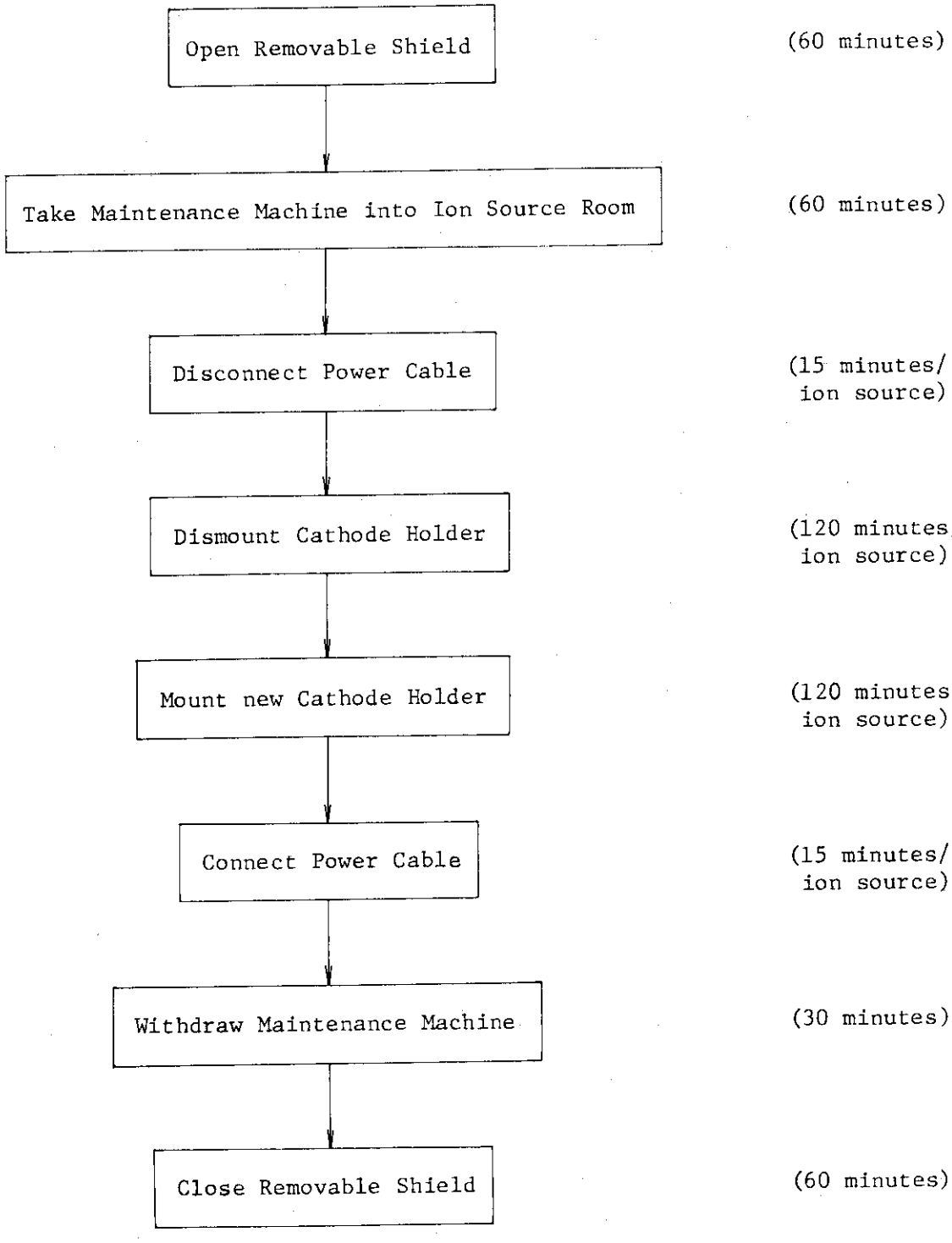

Fig. 8.7 Replacing Procedure of Cathodes

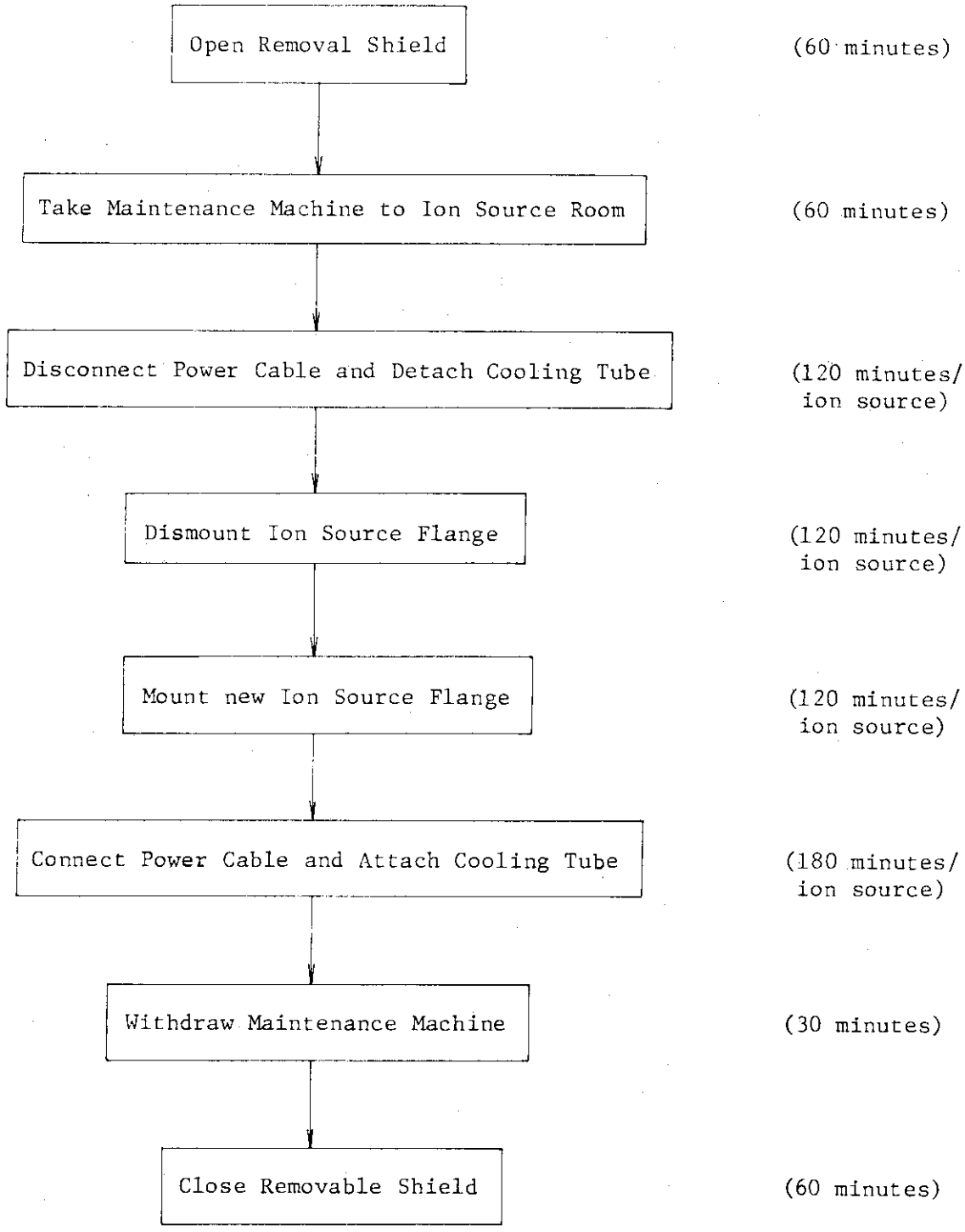

Fig. 8.8 Replacing Procedure of Acceleration Grids

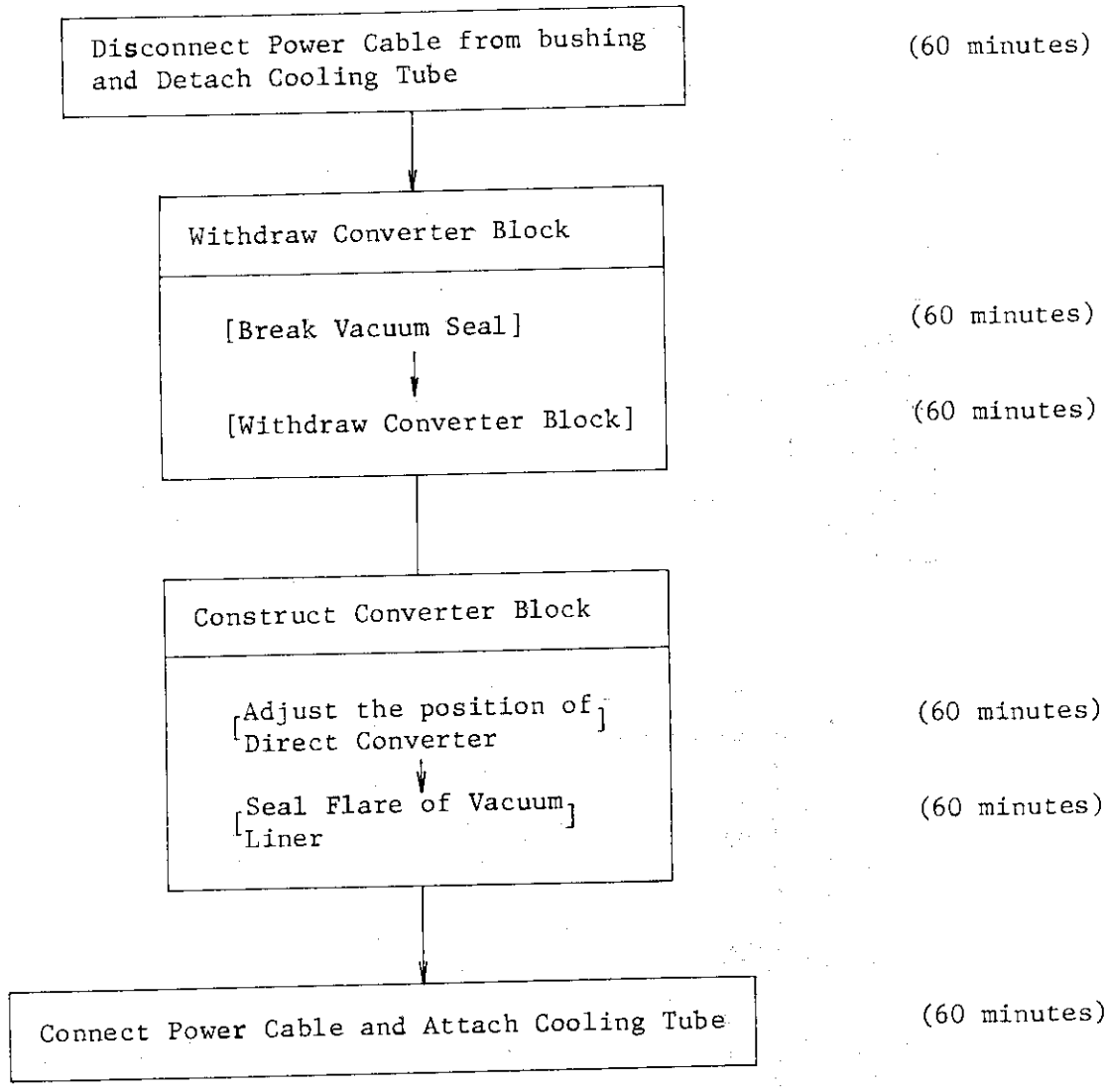

Fig. 8.9 Replacing Procedure of Direct Energy Convertors

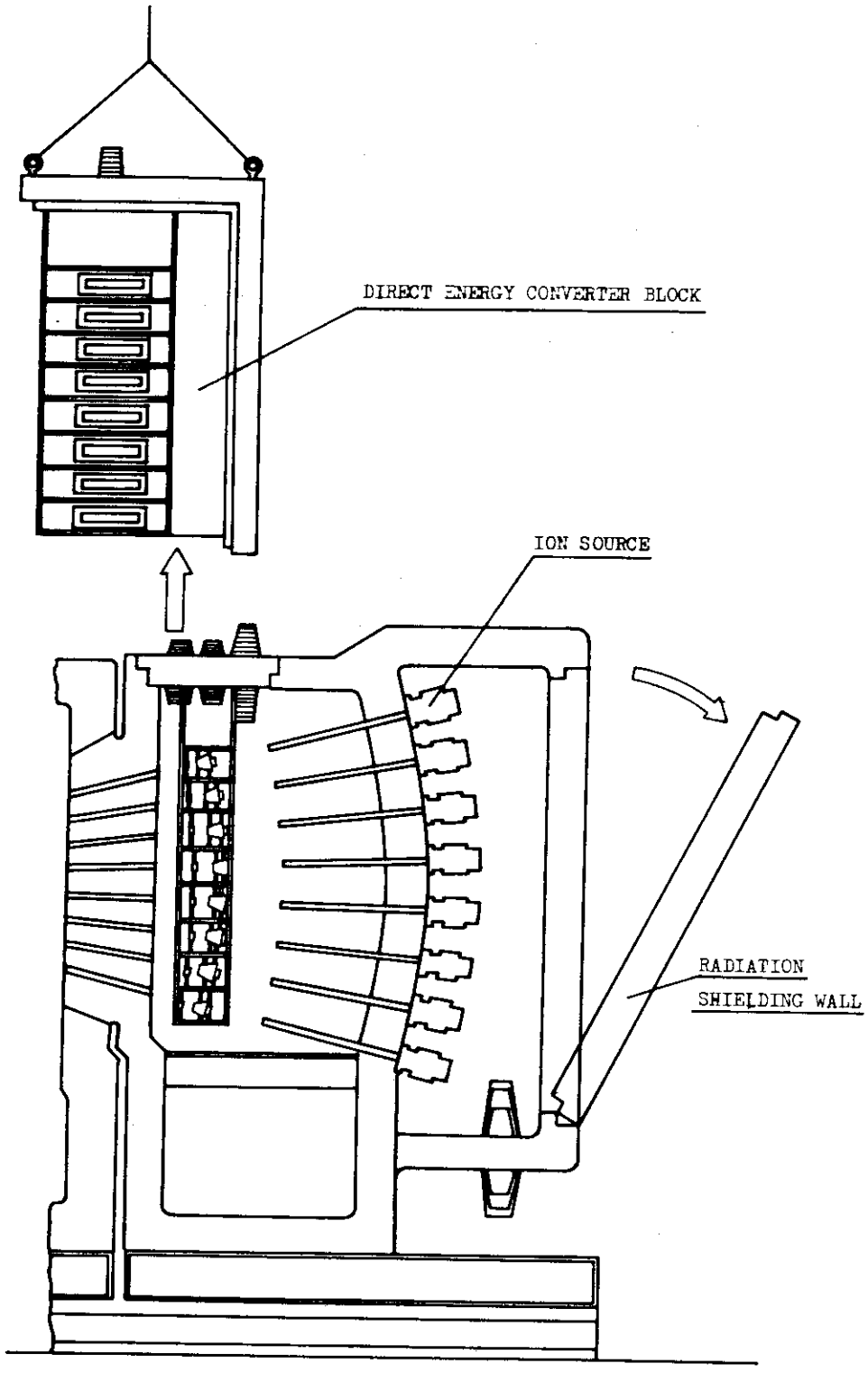

Fig. 8.10 Maintenance of NBI System

9. Main Vacuum Pump

The vacuum pumping system incorporates eight cryopumps located in four symmetrically oriented vacuum vessel below the neutral beam drift ducts. Each cryopump in cryopump room is isolated from the main vacuum region by 130 cm diameter gate valve when not operating. Cryocondensing panels are accomodated for fuel particles exhaust and behind these panels sorption panels are attached for ash exhaust.

Two cryopumps in one cryopump room are utilized with 50% duty cycles so that one system can be regenerated while the other is operating. Main characteristics of the vacuum pump are shown in Table 9.1.

9.1 Design Conditions

Following design conditions are considered,

i) Flux of 1.6×10^{20}/sec. ash particles to the pump are to be pumped out with realistic pumping speed.

ii) Some fraction of fuel particles ($\sim 2 \times 10^{21}$/sec. is assumed here) are also to be pumped out.

iii) Vacuum pumping system incorporates eight cryopumps located in four symmetrically oriented chambers below the neutral beam drift ducts and utilized with 50% duty cycles.

9.2 Design Analysis

Total conductance of the vacuum region is attainable about 7×10^5 ℓ/s for ash particles and 5×10^5 ℓ/s for fuel particles in the reference design of the vacuum system. Also the effective pumping speed is given by

$$S_{eff} = \Gamma kT/P \qquad (9.2.1)$$

where Γ is the flux of particles, P is the pressure of the vacuum duct, T is the temperature of particles and k is Boltzman constant.

Then using the conductance C and effective pumping speed S_{eff}, pumping speed is given by following relation.

$$\frac{1}{S_p} = \frac{1}{S_{eff}} - \frac{1}{C} \qquad (9.2.2)$$

and the results of required panel area are given for various pressure in Table 9.2.1. In the estimation of the required panel area, we used

the data for the effective pumping speed of the panel 6 ℓ/sec.cm^2 for deuterium, 5 ℓ/sec.cm^2 for tritium and 7 ℓ/sec.cm^2 for ash particles.

From the Table 9.2.1, pressure of 1.25×10^{-4} torr for ash and 2×10^{-4} torr for fuel particles are conservative and then required panel area is about 40 m^2. In the reference design of the cryopanel, area of about 100 m^2 is attainable. The design value of the panel area is larger than estimated value of 40 m^2. Configuration of the cryopump and gate valve is shown in Fig. 9.2.1.

9.3 Operation Mode

Two cryopumps in one room are utilized with 50% duty cycles so that one system can be regenerated while the other is operating. Considering of the regeneration of the cryopump, operation time per one cycle is longer the better. But it is required to limit the tritium inventory at some level, so 6 hr. is determined to be reasonable and then tritium inventory is about 140 gr.

9.4 Design Problems

Temperature of the cryopanel is not always known, so the effective pumping speed of the panel has some uncertainty. Also the data of effective pumping speed of the panel are few. Mechanical pump may be usable at this level of pumping speed.

Table 9.1 Main Vacuum Pump

Type	Cryopump
Number	
(1) Number of series	2
(2) Number of pumps/series	4
Evacuation speed (ℓ/sec.)	
(1) For He	3.2×10^6
(2) For other gases	2.7×10^6 for Tritium 3.3×10^6 for Deutrium
Panel area	
(1) Cryo-panel/pump	14 m^2
(2) Cryo sorption panel/pump	11 m^2
Operation	
(1) Operation pattern	2 series alternate
(2) Alternate cycle	6 hr.
Tritium inventory	
(1) Max. tritium inventory	∿ 140 gr.

Table 9.2.1 Pumping speed and required panel area

P_{He} (torr)	S^{He}_{eff} (ℓ/s)	S_p (ℓ/s)	Panel are (m^2)
1×10^{-5}	5.0×10^5	1.8×10^6	25
1.25×10^{-5}	4.0×10^5	9.4×10^5	13
1.5×10^{-5}	3.3×10^5	6.4×10^5	9
P_D (torr)	S^{D}_{eff} (ℓ/s)	S_p (ℓ/s)	Panel area (m^2)
1.5×10^{-4}	4.2×10^5	2.6×10^6	43
1.75×10^{-4}	3.6×10^5	1.3×10^6	22
2.0×10^{-4}	3.1×10^5	8.2×10^5	14
P_T (torr)	S^{T}_{eff} (ℓ/s)	S_p (ℓ/s)	Panel area (m^2)
1.5×10^{-4}	4.2×10^5	1.3×10^6	26
1.75×10^{-4}	3.6×10^5	8.8×10^5	18
2.0×10^{-4}	3.1×10^5	6.3×10^5	13

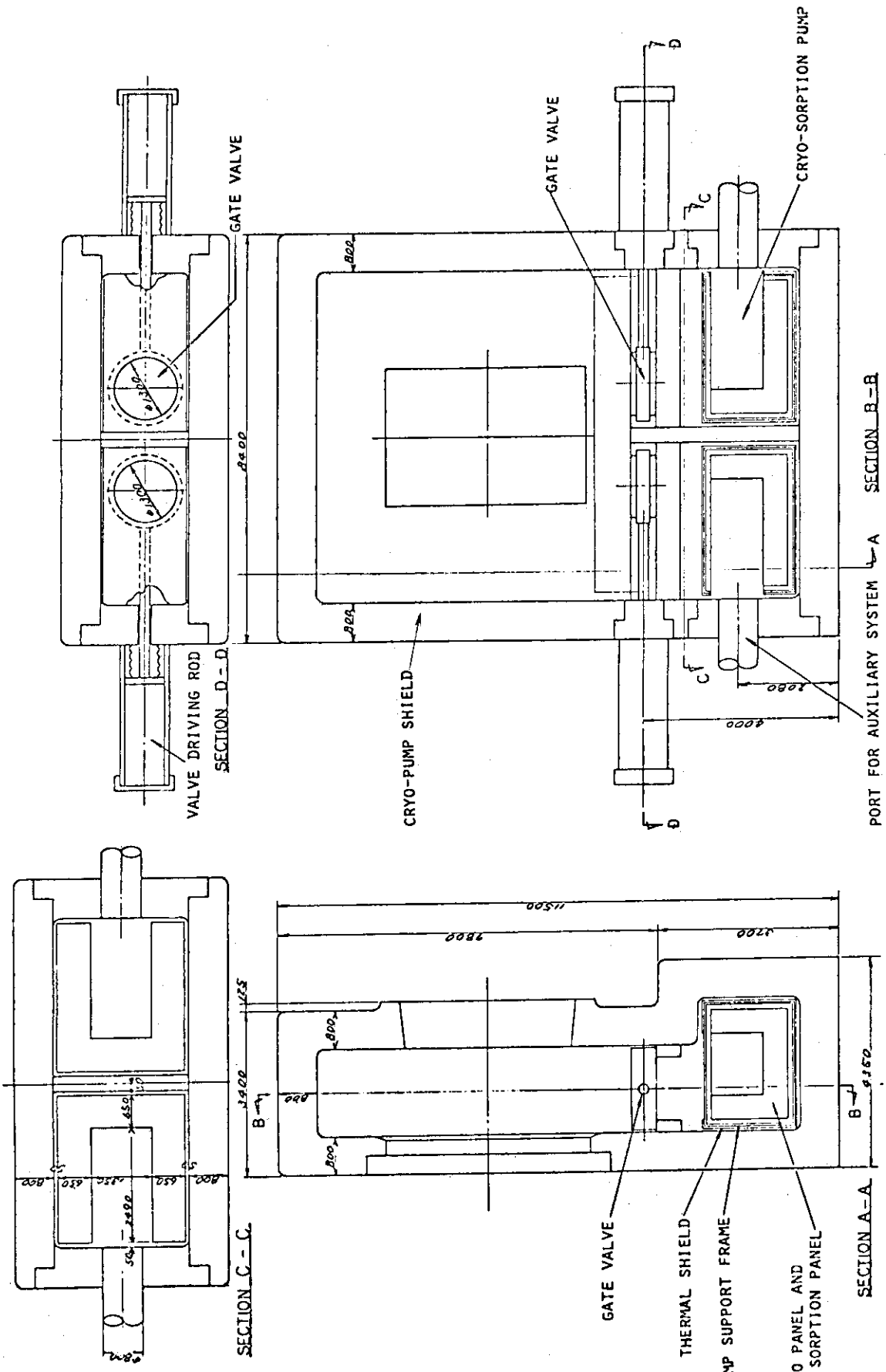

Fig.9.2.1 Cryo-sorption pump

10. Repair and Maintenance of Reactor (Concept A)

Repair and maintenance system are required for inspection and repair of any troubles, regular inspection, maintenance and reconstruction. The scheme of repair and maintenance must be designed in consideration of the following items.

(1) Contents and scopes of expected repairs
(2) Period of repairs
(3) Devices of remote handling, building and auxiliary systems
(4) Radiation flux level to workers

In this design stage, these requirements are not definitive, so we investigate two possible schemes in parallel. In one scheme, the machine is divided into sectors so that each sector can be separated to radial direction for repair and maintenance. In other scheme, toroidal and poloidal coils are not removed, only shield structures are removed partially and troubles are repaired in-situ.

In concept A, the former scheme is adopted.

10.1 Scheme of Repair and Maintenance

In this section, the scheme of repair and maintenance for Concept A is described.

The machine is divided into six unit sectors because of the axi-symmetry of sixth rotation of the machine. Each sector is composed of two toroidal coils, primary shield and blanket of 60° to toroidal direction and a set of main vacuum pumps and neutral beam injectors (and blanket test section). The superconducting poloidal coils are undemountable and do not interfere with other components in assembling and disassembling. Only the poloidal coils No. 9 can be demountable and are normal conductor because of interference with other components (movable base, mainly).

The structure of vacuum chamber of toroidal magnet cryostat influences upon the scheme of repair and maintenance. The following structures are compared for vacuum chamber.

1) Separate vacuum chamber; each vacuum chamber encloses one toroidal coil.
2) Hybrid vacuum chamber ; The vacuum chamber encloses toroidal magnet and poloidal coils supported by central support column.
3) Belljar ; The belljar encloses the whole machine.

As previously described (6.1.1), belljar is chosen for vacuum chamber in this design.

When the belljar is adopted to vacuum chamber of toroidal magnet cryostat, the scheme of disassembling and repair of the machine is little different from that of the present machines with normal conducting coils. Primary shield and blanket of 60° segment and two toroidal coils are set on 1/6 sector of movable base and removed to the radial direction in disassembling. The poloidal coils No. 1 to 8 are fixed on the central support column. The coils No. 9 are demountable normal conducting coils because of interference with movable base and the coils No. 10 and 11 are removed to upper and lower directions.

It is desirable to connect cryopump shields to primary shields and align these connected structures. But cryopump shields are connected to primary shields after aligning all sectors of primary shield in this design by following reason. It is impossible to lift up pit covers and lower poloidal coil No. 10 by main crane. And if poloidal coil No. 10 is jacked up, belljar base mat has complicated structures for vacuum seal. So it is decided to lift lower poloidal coil No. 10 by crane car. Cryopump shields and belljar cylinders interfere with crane car, if they are connected to primary shield before aligning these connected structures.

10.2 Procedure of Assembling and Disassembling

In this design, the procedure of disassembling is inverse to that of assembling basically. It is possible to disassemble partially according to the extent of repair or maintenance. In this section, the whole procedure of assembling is shown. The block diagram and figures of procedure of assembling are shown in Fig. 10.2.1 and Fig. 10.2.2. The correspondence between the number in Fig. 10.2.1 and those of Fig. 10.2.2 is shown in Table 10.2.1. The tasks of each step in Fig. 10.2.2 are summarized as follows.

1) Belljar base mat composed of base anchors and liners is laid. PF coil support anvil and inner support column are set up.

2) PF coils No. 1 ∿ 7 and coil support plates are set up on inner support column from lower part to upper part.

3) Outer support column is set up on coil support plates. Lower PF coils No. 10 and 11 are laid in pit and lower PF coil No. 8 is set up temporally on central support column.

4) Two toroidal coils and 1/6 sector of blanket, primary shield and lower PF coil No. 9 are fixed on movable base. 1/6 sectors on movable bases are aligned to prefixed positions.

5) Movable bases are fixed on base anchors. Sectors of vacuum vessel of primary shield are welded each other and connecting flanges are fastened by tie bolt. PF coils No. 8 and 10 are set up on TF coils and upper PF coil No. 9 is fixed on primary shield. Lower PF coils No. 9 is fixed on primary shield legs after the conductors are connected.

6) Cryopump, its shield and 1/6 belljar cylinder fastened to cryopump shield are aligned on cryopump movable base. Movable bases are set up on base anchors and cryopump shields are welded to port shields.

7) Upper and lower PF coils No. 11 are fixed on TF coils. Water cooling pipes of blanket are connected by remote handling within NBI port. Each segment of belljar cylinder is bolted up. Belljar sidings are connected to belljar cylinder and belljar liner. Belljar dome is connected on belljar cylinder.

Table 10.2.1 Correspondence between Fig. 10.2.2 and Fig. 10.2.1

Fig. 10.2.2	Fig. 10.2.1
1	1 ∿ 4
2	5
3	6 ∿ 9
4	10
5	11 ∿ 22
6	23 ∿ 25
7	26 ∿ 32

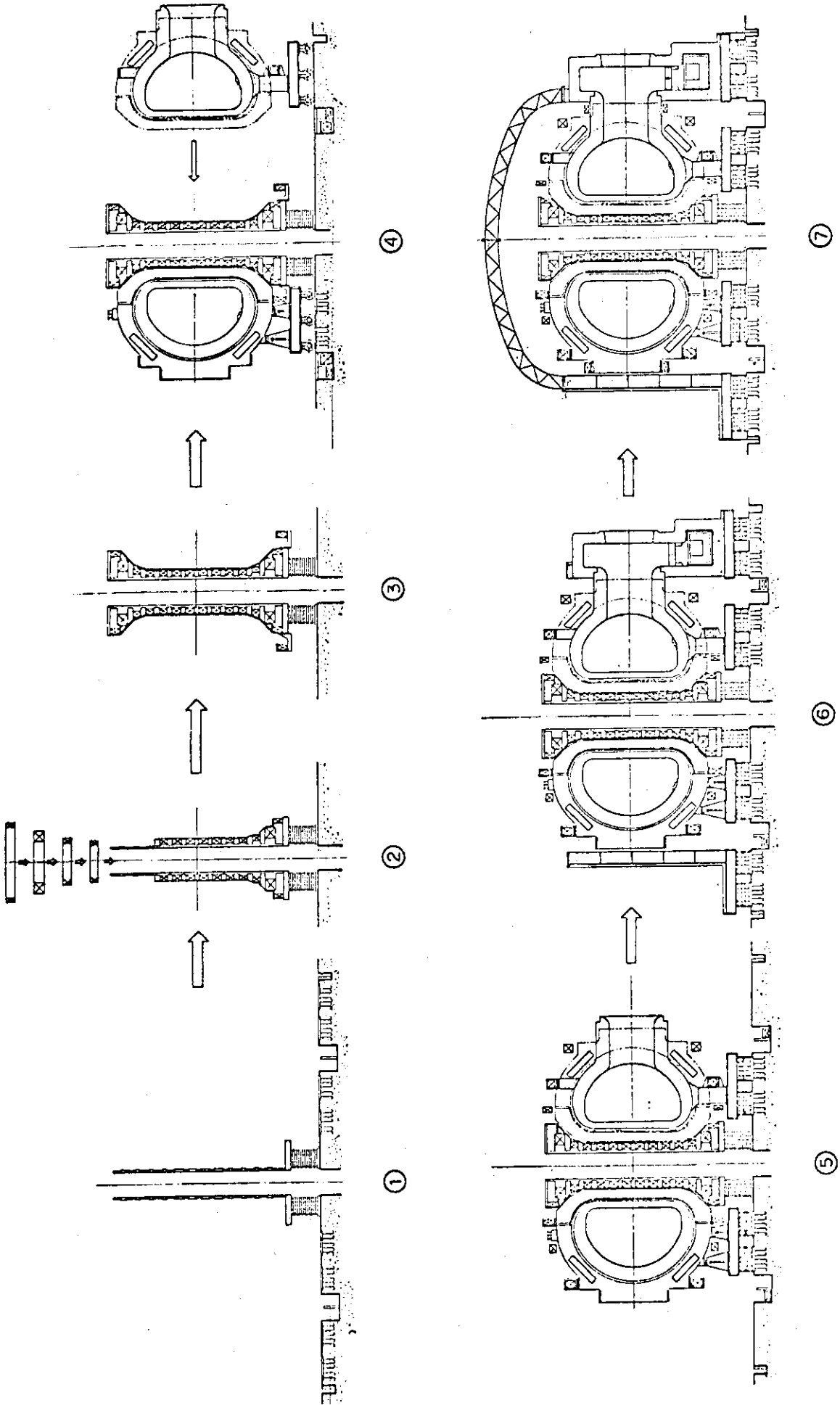

Fig. 10.2.1 Concept A Assemble Procedure

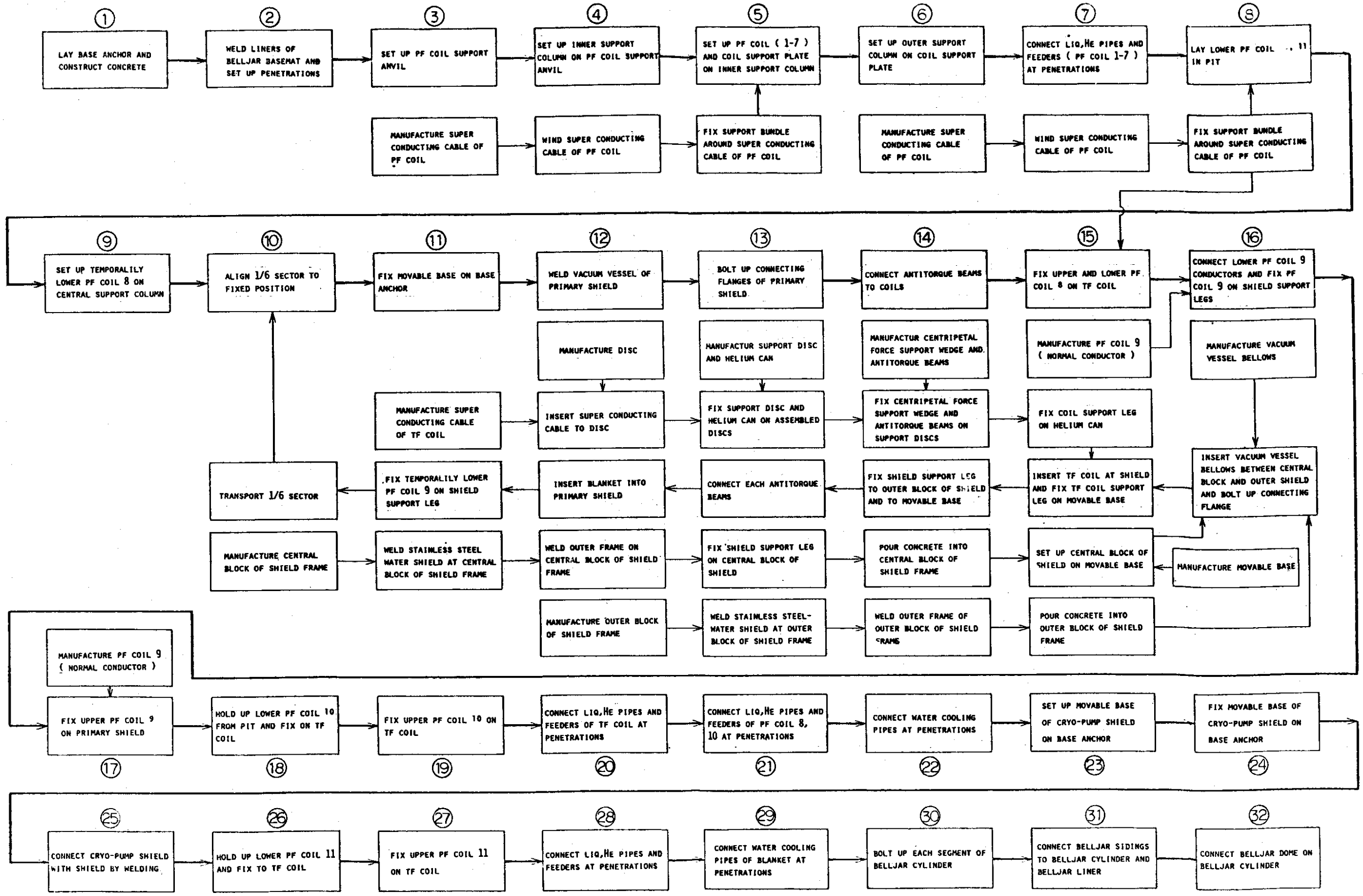

Fig. 10.2.2 Concept A Assembling Logic

10.3 Reactor Components

Structure for assembling and disassembling is shown as follows.

(1) Alignment pin of TF coil

The alignment pin to align and fix the neighbouring TF coils is inserted into alignment hole of contripetal force support wedge.
Structure of alignment pin is shown in Fig. 10.3.1.

(2) Connecting structure of anti-torque beam

Half-length anti-torque beams are prefixed on TF coil. In case of assembling, neighbouring half-length anti-torque beams are connected by connecting pad.
Structure of connecting pad is shown in Fig. 10.3.2.

(3) Rails for automatic welding machine of primary shield

The rails for automatic welding machine are located both edge of 1/6 sector primary shield. Rail of one side edge is for sustaining the welding machine and the other is only for guiding.
Structure of rails is shown in Fig. 10.3.3.

(4) Connecting flange of primary shield

Primary shield is connected by bolting at connecting flange.
The connecting flanges to connect primary shield are located both edge of 1/6 sector primary shield.
Structure of connecting flange is shown in Fig. 10.3.4.

(5) Support leg of PF coil

PF coils No. 8, and 11 are supported by support legs on TF coils.
Structure of support leg holds vertical magnetic force of PF coil but does not restrain the radial movement of coils.
Structure of support leg of PF coil is shown in Fig. 7.1.3.

(6) Tug barrow and rack and pinion driving system

Movable base is driven by electric tug barrow which moves by the rack and pinion system for effective transmission of driving force.

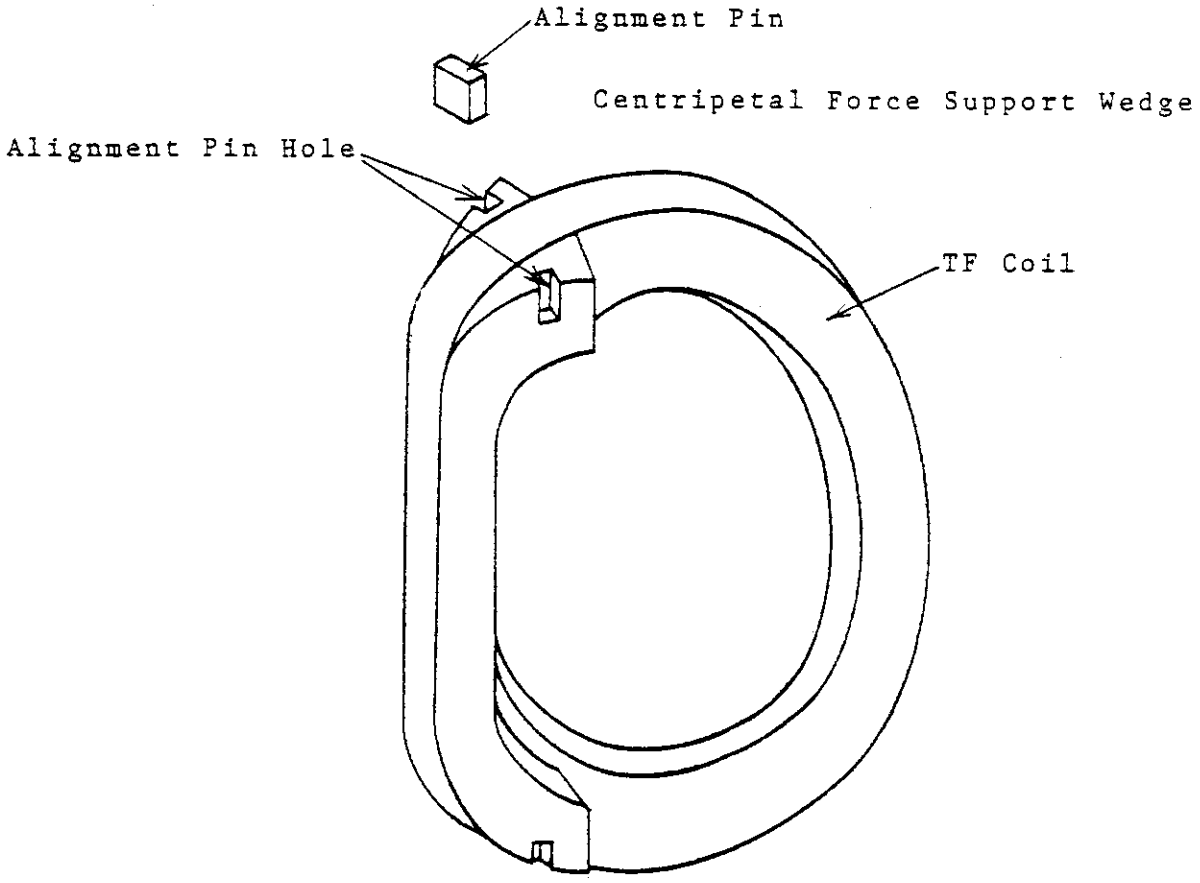

Fig. 10.3.1 Alignment Pin of TF Coil

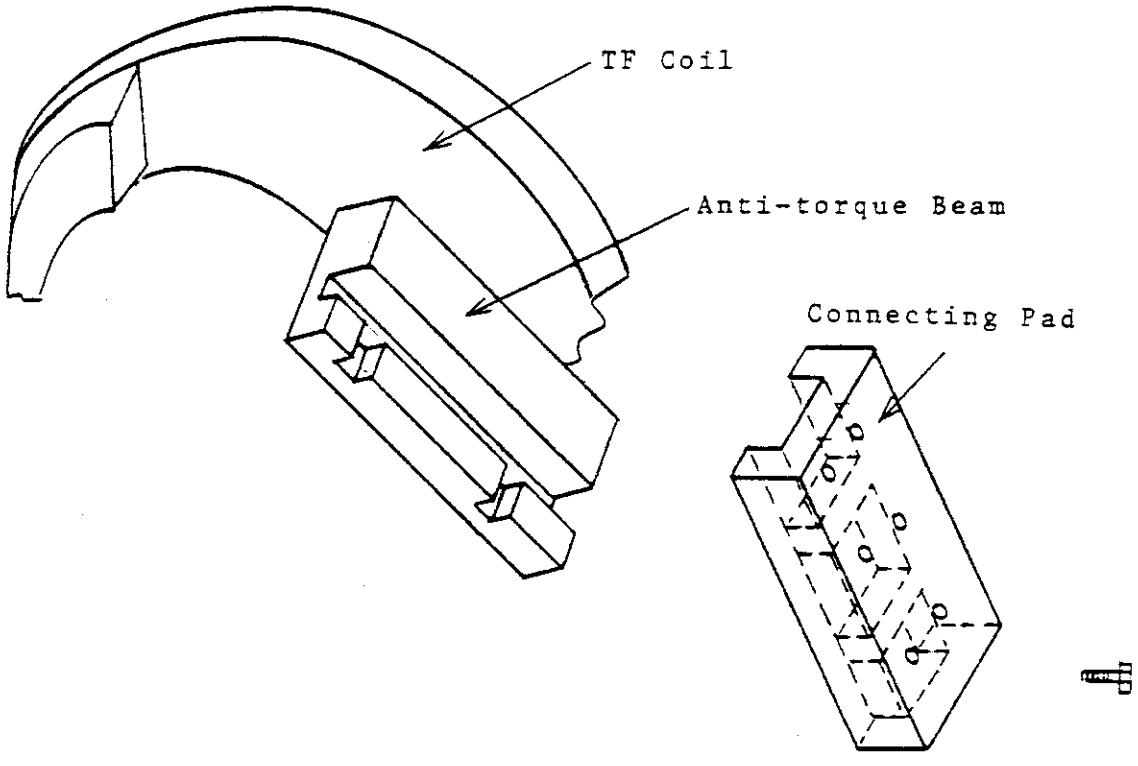

Fig. 10.3.2 Jointing Structure of Anti-Torque Beam

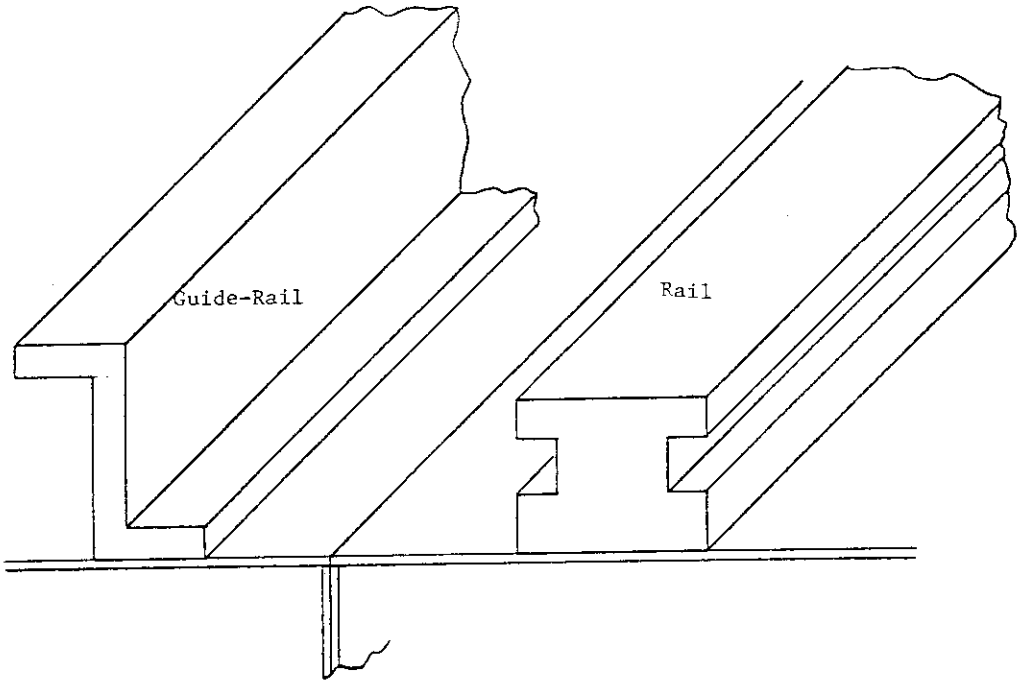

Fig. 10.3.3 Rail for Automatic Welding Machine

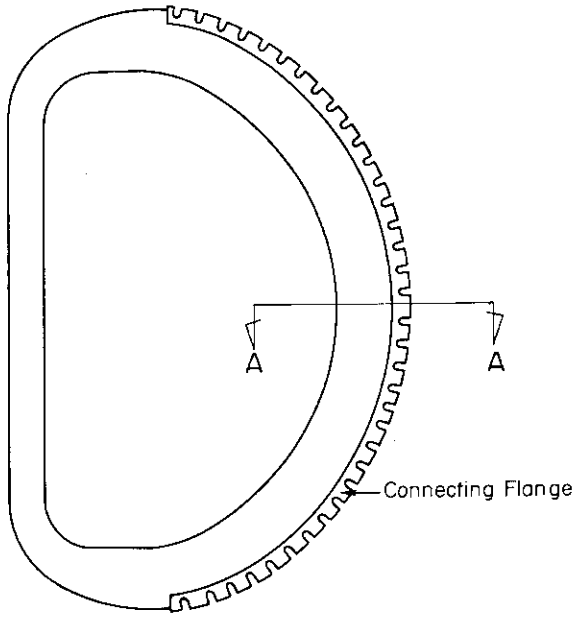

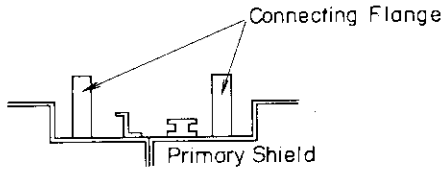

Fig. 10.3.4 Connecting Flange of Primary Shield

10.4 Maintenance Devices

Maintenance devices are classified into two types as follows.

1 Devices to assemble and disassemble.

2 Devices for inspection of the structures.

(1) Devices to assemble and disassemble

Assembling and disassembling require welding, cutting, lifting, bolting, unbolting, connecting, etc. Each of these procedures is made by devices for its exclusive use. They are summarized in Table 10.4.1.

(2) Devices for inspection of the structures

Structure is inspected by television camera, eddy current detector, helium leak detector, ultra-sonic inspection apparatus etc.
Main inspection devices are shown in Table 10.4.1.
Built-in monitoring systems such as thermometer, radiation counter, neutron counter, flow meter are excluded here.

Table 10.4.1 Devices to Assemble and Disassemble

Name	Objective component	Functions and characteristics
Automatic welding machine	Primary shield	1. Alignment of lips by wheels 2. Alignment of lips' height by cutter 3. Automatic welding of lips 4. Cutting of welded lips The automatic welding machine must be compact to increase TF coils and primary shield's space. Structure concept is shown in Fig. 10.4.1
Tug barrow	1. Movable base of TF coils and primary shield. 2. Movable base of cryopump shield.	1. Driving of main movable base 2. Driving of cryopump movable Movable base is driven by electric tug barrow which moves by the rack and pinion system for effective transmission of driving force.
Bolting machine	1. Anti-torque beam 2. Alignment pin 3. Support leg of PF coil 4. Primary shield 5. Conductor of PF coil No. 9	1. Fixing of object of machines.
Crane	1. PF coil 2. Belljar dome 3. Others	
Car mounted crane	1. lower PF coil No. 10 2. Pit cover 3. Others	Car mounted crane is necessary for lift lower PF coil No. 10 and pit cover, because main crane cannot access to the place beneath the primary shield.

Table 10.4.2 Devices for Inspection of the Structure

Name	Objective component	Functions
ITV	1. Sealed lips of primary shield 2. Connecting point of bolt joint 3. External appearance of damaged part	1. ITV is provided on automatic welding machine.
Eddy current detector	1. Helium can of TF coil 2. Primary shield 3. Cooling pipes	
Helium leak detector	1. Helium can of TF coil 2. Super conducting cable of PF coil 3. Belljar 4. Primary shield 5. Cooling pipes	
Ultra-sonic inspection apparatus	1. Belljar 2. Helium can of TF coil 3. Vacuum vessel	
Mass spectro-meter	1. Belljar 2. TF coil 3. PF coil 4. Vacuum vessel 5. Primary shield	The following inspections are possible through the analysis of gas composition in the belljar. 1. Belljar has leakage when oxygen and nitrogen are detected. 2. TF coil or PF coil has leakage when helium is detected. 3. Vacuum vessel has leakage when deuterium and tritium are detected. 4. PF coil No. 9 or primary shield has leakage when water is detected.

Table 10.4.2 (continued)

Name	Objective component	Functions
	6 Cryo pump	The following inspections are possible through the analysis of gas composition in the cryo-pump. 1. Degradation of sorption pump when helium is detected to increase in quantity.

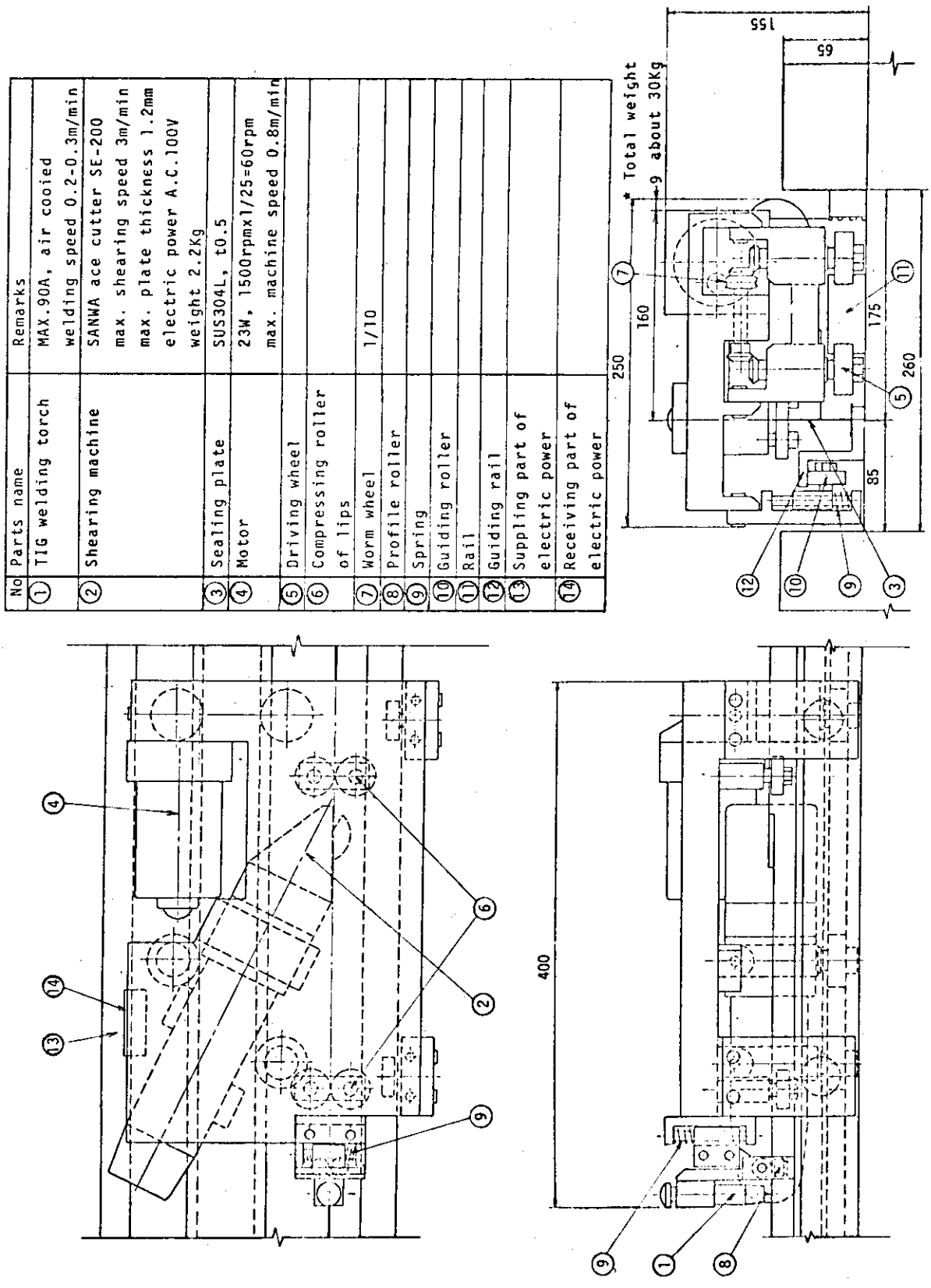

No	Parts name	Remarks
①	TIG welding torch	MAX.90A, air cooled welding speed 0.2-0.3m/min
②	Shearing machine	SANWA ace cutter SE-200 max. shearing speed 3m/min max. plate thickness 1.2mm electric power A.C.100V weight 2.2Kg
③	Sealing plate	SUS304L, t0.5
④	Motor	23W, 1500rpmx1/25=60rpm
⑤	Driving wheel	max. machine speed 0.8m/min
⑥	Compressing roller of lips	
⑦	Worm wheel	1/10
⑧	Profile roller	
⑨	Spring	
⑩	Guiding roller	
⑪	Rail	
⑫	Guiding rail	
⑬	Suppling part of electric power	
⑭	Receiving part of electric power	

Fig. 10.4.1 Automatic Welding Machine

10.5 Design Problems

Design problems in repair and maintenance are follows.

1) Electrical insulation of large belljar.

2) Vacuum seal of large belljar, especially the seal between base anchors and liners and the seal of electrical insulation of belljar base mat.

3) Large space for repair and maintenance.

4) Concentration of atmospheric load and weight of belljar to belljar base.

11. Repair and Maintenance of the Reactor (Concept B)

Special emphasis has been put on reactor maintenance in design study of the reactor system B. In this chapter, the general maintenance concept in the reactor system B is described in Sec. 11.1. Then Sec. 11.2 describes the design of the blanket structure with respect to the removable blanket scheme, maintenance procedure of the blanket structure, and blanket handling machines. Section 11.3 describes the way how to form the vacuum boundaries for the plasma chamber and for the superconducting magnets, and welding and cutting machines for the vacuum boundaries. The concept of the reactor building is reported in Sec. 11.4 which is followed by the discussion of design problems.

11.1 Concept of Reactor Maintenance

It is expected that two stages of operation will be carried out in INTOR, they are hydrogen discharge operation, and D-D and D-T discharge operation. During hydrogen operation, men can reach the reactor to repair failure parts, since the reactor is not radioactive yet. On the other hand, in D-D and D-T discharge operation the level of radioactivity in the inside of the shielding structure is so high that remote handling techniques are required for reactor maintenance when the shielding structure is removed. The failure, which can be expected in the inside of the shielding structure, should be well examined before the D-D and D-T operations are initiated. It should be emphasized that plasma control techniques need to be well established before D-D and D-T operation.

The following two categories can be thought concerning reactor maintenance. The one is routine replacement of the protection wall and the blanket structures based on predicted material life. The other concerns failure of an individual structure, requiring replacement of the single unit. In this case, the failure part has to be identified before that part is replaced. Failure indication systems will have to be designed in is replaced.

In this section, we report replacement procedures of each system component in the reactor system B. Since the blanket structures can be replaced without removing the toroidal field magnets and the shielding structures, shut down time of the reactor during the process of repair and maintenance may be minimized.

(1) Protection wall

Two replacement concepts are proposed. The NBI ports are used to reach the protection wall in both concepts. In the first concept, maintenance machines are attached to the shielding wall of the main vacuum system after the NBI system is removed. The transfer of heavy structures such as NBI may be a demerit of this concept. The second concept requires the transfer of one of the poloidal field magnet. Maintenance machines are inserted inside the plasma chamber through the hatch situated on the upper side of the shielding structure between the reactor and the main vacuum system. Maintenance procedures in the two concepts are listed as follows. These concepts will be studied in detail by designing maintenance machines in future.

Concept I

1. Unseal the plasma vacuum boundary in NBI and disconnect the helium, water, and electric lines in NBI.
2. Equipment of the heavy carrier under NBI.
3. Draw back NBI to the NBI room.
4. Attachment of the maintenance machine to the shielding wall of the main vacuum system.
5. Removal of protection wall.
6. Transfer of the protection wall to the radioactive storage area.
7. Install the new protection wall.

Concept II

1. Removal of the poloidal field magnet.
2. Removal of the hatch.
3. Equip the maintenance machine inside the shielding structure.
4. Removal of the protection wall.
5. Install the new protection wall.

(2) Divertor plates

A maintenance concept of the divertor plates is described in detail in Chap. 12. In this method, the neutral beam injector is removed, and maintenance machines are attached to the shielding wall of the main vacuum system, when the divertor plates are replaced. In the reactor system B, the large hatches to be used for blanket replacement are located on the upper side of the torus shielding structure.

Blanket handling machines reported in 11.2.3 have manipulators with capability of cutting and welding pipes and other sensitive works. There is a great possibility that the divertor plates can be disassembled *in-situ* by means of the blanket handling machines. Since the divertor plates have not been designed in detail in the reactor system B, the divertor plate replacement concept described here have not been studied in detail yet.

Another possible way to replace the divertor plates is to remove the blanket structure with the divertor plates as will be reported next. The divertor plates can be handled easily by maintenance machines in the reactor room. We will study the last two methods in detail in future.

(3) Blanket structures

The blanket structures can be replaced almost independently in the reactor system B. The details of maintenance procedure for the blanket structure is given in Sec. 11.2. The biggest merit of this planket maintenance is that the toroidal field magnets, main vacuum systems, and NBI systems need not be removed when the blanket structures are replaced. It means that, we can save a significant amount of time to cut and weld the vacuum boundaries for the plasma chamber and for the superconducting magnet. Moreover, the liquid helium temperature of the superconducting magnets is planned to be kept during blanket maintenance, which helps us to save more time.

The two poloidal magnets interfering the path to the hatch for blanket access need to be replaced during blanket maintenance, therefore they are supported on the shielding structure. Maintenance procedure of the blanket structure is detailed in 11.2.2.

(4) Toroidal magnets and shielding structures

The toroidal magnet and shielding structure system consists of six modules, each containing two toroidal magnets and their vacuum chamber. A heavy carrier removes one module to the outer side in the major radius direction after the upper and the lower poloidal magnets are removed to the turn table and to the trenches, respectively. The vacuum boundaries for the plasma chamber and for the toroidal magnets need to be unsealed before the magnet and shielding structure module

is removed. The place requiring unsealing is described in detail in Sec. 12.3.

The replacement procedure of the toroidal magnet and shielding structure module is listed as follows. General schemes of replacement of the toroidal magnet and the shielding structure are shown in Figs. 11.1.1 and 11.1.2, respectively.

1. Remove the upper poloidal magnets by the crane and put them on the turn table.
2. Jack down the lower poloidal magnets to the trenches.
3. Unyeal the vacuum boundaries for the plasma chamber and for the toroidal magnets.
4. Separation of the support structures between magnets.
5. Draw back the main vacuum system and the NBI system to the NBI room by a heavy carrier.
6. Remove the magnet and shielding structure module by the carrier.

Toroidal Magnet	Shielding Structure
7. Removal of the toroidal magnet by the crane.	7. Removal of the toroidal magnets by the crane.
8. Transport of the toroidal magnet by the carrier through the transfer gallery to the radioactive storage area.	8. Transport the shielding structure to the reactor room door by means of a carrier.
	9. Transfer the shielding suruc-ture to the radioactive storage area through the transfer gallery.

Installation of the new toroidal magnet and shielding structure is the reverse of the above-mentioned procedure.

(5) Poloidal field magnets

Replacement procedure depends on the positions of the poloidal magnets. Replacement of the poloidal magnets sitting near the center pole requires removal of all the toroidal magnets and shielding structures. Replacement of other poloidal magnets is relatively simple. Spares of poloidal magnets of large diameters can be located below the floor and on the turn table. The replacement procedure of the poloidal magnets, is listed as follows.

Upper and lower poloidal magnets.

1. Disconnection of the poloidal magnets from the support base.
2. Transfer them to the storage area by means of the crane.
3. Installation of the new magnet.

Poloidal magnets near the center pole.

1. Removal of all the toroidal magnets and the shielding structures.
2. Removal of the poloidal magnets near the center pole by means of the jacks.
3. Installation of the new poloidal magnets.

Figure 11.1.3 shows the schematic view of replacement of the upper poloidal field magnet.

11.2 Blanket Structure

11.2.1 Blanket Design

(1) Removable Blanket Scheme

A particular method is employed to overhaul and repair blankets without disassembling or removing other major components such as toroidal field coils, main components of vacuum system, neutral beam injectors, or the most of primary shields. This method may be called the Removable Blanket Scheme, has many advantages described in Sec.11.1.

The main torus including 12 toroidal field coils is divided into 6 fan shaped modules with 60° angle, which can be removed along the major radius for repair of any toroidal field coil or shielding block.

When it comes to repairing a blanket only, the 60° blanket module is divided further into 5 sectors with 12° each. A hatch is located in the upper part of the shielding structure between two toroidal field coils to yield the opening space for removing the small sector of blanket. Each of the 5 blanket sectors except the one right under the hatch has wheels on the bottom to move in the toroidal direction to the center position of the hatch for access. Figure 11.2.1 shows the hatch in the shielding structure.

It is also necessary to cut off the cooling pipes of blanket to release the connection between 12° sectors before removal. All tasks,

except opening the hatch in the shield (i.e. except removing the tie bolts, breaking the vacuum seal) are performed with remote handling machines.

(2) Blanket support structure

Blanket support structure is shown in Fig. 11.2.2. The blanket structure in torus consists of six modules. Each module has five sectors connected each other with flanges and bolts. No connector is furnished on both sides of single module so that the required one turn electric resistance can be achieved.

The blanket sector is sustained by the wedges on adjustable leveling devices as shown in Fig. 11.2.2, hence no weight is placed on the wheels during normal operation. A tandem connected shaft with universal joints, which is driven by a remote handling machine, adjusts the wedge level to lower the blanket sector when disassembly is necessary, and to put the whole wheels on the running streets. The wheels run on concentric circles with synchronized speed.

Cooling system for blanket modules includes inlet, outlet main headers at most outer blanket surface, and sub headers at upper and lower blanket surface. The cooling water enters the inlet header, goes through the inlet sub header on lower part then to the blanket interior. The heated coolant comes out from the outlet headers on the upper blanket structure. Remote pipe cutting tool cuts or welds cooling main header at four points along the torus direction, and the cooling main pipe at two points as shown in Fig. 11.2.3.

11.2.2 Maintenance procedure

(1) Disassembling procedure

Disassembling procedure for blankets is described as follows:

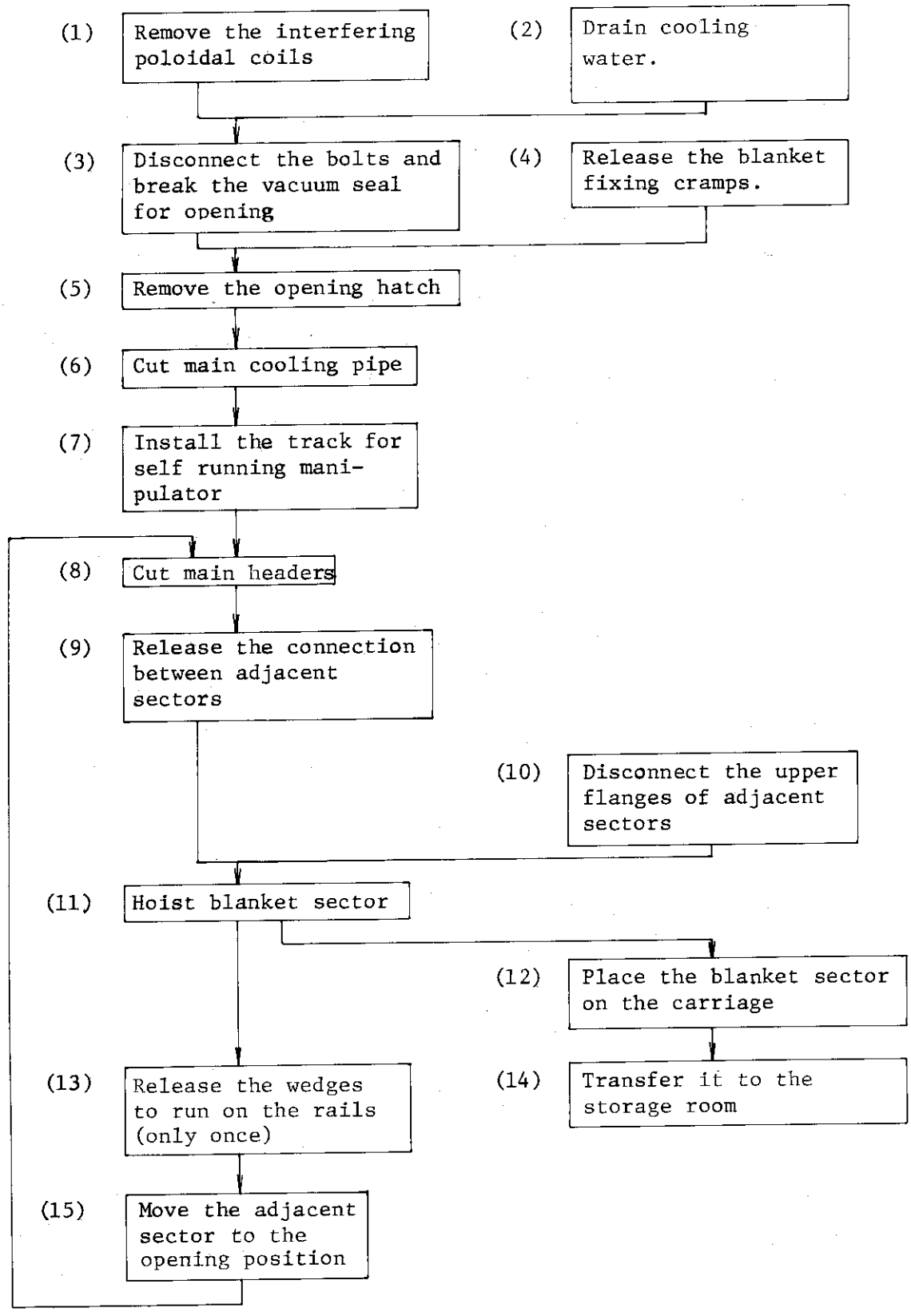

(2) Detailed procedures for disassembling

(a) Steps from (1) to (5), releasing the various connector bolts around the reactor, are carried out by man's hands.

(b) Step (6) removes small part of main pipe to provide enough space for moving the blanket module.

(c) Step (7) inserts the track by the overhead crane, then fixes it inside the shield.

(d) Step (8) cuts cooling headers between sectors, carried out by a manipulator running on the track.

(e) Step (9) and (10) release the bolts connecting the sector under the opening hatch with the adjacent one.

(f) Step (11) hoists the free blanket sector with the overhead bridge mounted machine.

(g) Step (12) places the blanket on the carriage which waits on the reactor room floor.

(h) Step (13) removes the wedges which raise the sectors and wheels.

(i) After step (14) the blanket sector is transferred to the storage area.

(j) Step (15) does move two sectors together to the central position with help of the overhead bridge mounted machine.

(3) Assembling

Assembling the blanket module can be almost done on reverse steps of disassembling. Welding pipes and headers is an additional major task in the assembling, which may be broken down into the following procedures:

(a) Positioning blanket sectors for connection,

(b) Welding the cooling headers and pipes,

(c) Non-destructive inspection on welding spot, and

(d) Cleaning inside of the shielding.

11.2.3 Maintenance machines

(1) Wall mounted manipulator

The function of this manipulator is to cut (weld) the cooling headers and to release (fasten) the tie bolts of flanges. It runs on the track placed inside the shielding wall with remote control.

Figure 11.2.4 shows some features of the manipulator. It has 7

degrees of freedom which is supplied by movements of a trolly and arms. The arm has maximum 1 m length which covers central section of outer blanket flanges on both side and cutting positions on the cooling pipes when the manipulator runs by hydraulic drive on the vertical track. The trolly is equipped with hydraulic drive units, running devices, monitoring TV cameras, magazine to pack various tools, and parts box to store the unfastened bolts. The arm has multi-joints whose tips can mount various tools remotely. At the wrist position of the arm there is a TV camera to watch tasks.

Although remote operations are done with visual information through TV camera, the manipulator execute the pre-programmed procedures in order to shorten the machine down-time. In the pre-programmed procedure a coarse position (±5 mm) is searched by the manipulator, then the final fine working position is determined by the positioning mechanism on each tool. The maximum running speed is 2 m/min, and the arm swings at the rate of 60 °/min. Its weight is about 400 kg.

The track has remote controlled cramps at the bottom and at the upper portion outside the opening. They grip the supporting ports on the inner shielding structure and outside the opening section, respectively.

The upper portion of the track outside the opening hatch has ample length to rest the manipulator. When the blanket sector is pulled out, this part of track with the manipulator are bent back to yield access room for hoisting blanket.

(2) Overhead bridge mounted manipulator

This manipulator cuts (welds) the main cooling pipes by approaching from the opening hatch of the shield, and releases (fastens) the tie bolts of flange in upper portion. Figure 11.2.5 illustrates the manipulator. It consists of a trolly running over the bridge, a support pole extending like a telescope, and a maltijoint arm at the top.

It has 8 degrees of freedom together with trolley movement on the rails. The arm has max. 3.6 m length, and cover all over the inner shield surface when inserted from the opening hatch. The telescopic pole is driven by a winch, while the arm gear for rotation and the joint gear for free movement is functioned by hydraulic devices. The tip of arm has similar mechanical and electrical structures as the wall

mounted manipulator so that it also exchanges the tool remotely. All remote control are conducted by the visual information through TV camera.

Other capabilities: Arm raises at the rate of 3 m/min speed, revolves at the rate of 45 °/min, maximum carrying load (including tools) is 60 kg.

(3) Blanket module handling machine

This machine pull the blanket sectors to the center position, then remove the sector from the hatch. Figure 11.2.5 shows the structure of the machine. This machine uses the same trolly with the overhead bridge mounted machine. When the handling machine is inserted into the shield, the telescopic pole positions the machine at first, then the tip of handling machine rotates itself for fine positioning. After the handling machine hooks the blanket sector, the telescopic pole is retracted upwards and the blanket sector is hoisted by wires.

In order to pull the blanket sectors exactly under the opening hatch, the handling machine is fixed at the opening edge by jacks on the machine sides. Two arms are extended to circular direction to catch the blanket sectors at a distance, then they pull the blanket sectors to the center. All devices except the elevator are driven by hydraulic units. Other capabilities; maximum carrying load is 36 tons, elevation speed is 1 m/min, arm extention speed is 0.3 m/min, own weight is about 3 tons.

(4) Pipe cutting (welding) tool

Figure 11.2.6 shows the main features of this tool which consists of a circular frame and a running device. Part of the frame opens to catch a cooling pipe. The runner moves on a guiding rail along a circular groove on the fixed frame side. A position sensitive devices on the frame searches the desired position measuring the exact distance from the referencial plane on the flange. This makes possible to locate the welding tool at the exact position. The runner carries plasma torch and TV camera, the former is supported by a torch holder with 2 degrees of freedom, i.e. up-down and left-right directions. A T.I.G. torch or a non destructive test probe is mounted on the runner. Opening and positioning the frame require hydraulic drive unit while

other tasks are done by small DC motors.

In order to set a tool at exact location, two flanges with 20 mm width, 20 mm height are fixed on a pipe surface 150 mm away from each cutting line in both directions.

(5) Overhead crane and carriage

The overhead crane carries the upper poloidal field coils to the turn table. The carriage transport the blanket sector to the storage area through the transfer gallery.

11.3 Shielding Structure and Toroidal Field Magnet

11.3.1 Plasma chamber vacuum boundary

(1) Shielding structure

The complete shielding structure is divided into 6 parts as well. Four modules among them have opening ports to neutral beam injectors, as is shown in Fig. 11.3.1. Flanges for module connection, flare seals for welding, bellows for one turn electrical resistance, and the opening hatch for blanket hoisting are the features of the shielding module. The shield is constructed with thick stainless steel rib structures and with stainless steel filling blocks. Cooling water pipes are installed in the thick ribs and filling blocks.

Mechanical connection between the shielding modules is done by tie bolts in the flanges located on the outer shield surface as shown in Fig. 11.3.1. Flanges are formed only on the outer side in the major radius direction where ample working space is available. Welded flare seals make the vacuum boundary for plasma. These flare seals on the outer shield surface go around the torus in poloidal direction. When the seal goes inward in the major radius direction, it intersects with the vacuum boundary of cryogenic chamber for the toroidal and poloidal field magnets. The difficulties of welding the flare seals at intersections are avoided by the method in which an additional cover over the flare seals and connecting flanges is installed to form the part of the cryogenic vacuum boundary. This cover is dismantled in case of welding or cutting the flare seals. Remote operation of welding and cutting seals is mentioned later.

(2) Plasma chamber vacuum boundary

Inner surface of the shielding structure which is also made of thick stainless steel acts as the vacuum boundary for plasma in principle. The exceptions are found at the connection between two shielding modules, or at the bellows, where the actual vacuum boundary runs outside the shielding structure. Near the center pole, the plasma chamber vacuum boundary is also used for the vacuum boundary of toroidal coils and some poloidal coil.

Most of all one turn electrical resistance (>0.2 mΩ) comes from two places in each shielding module, namely, bellows as shown in Fig. 11.3.2. The two shielding blocks are isolated electrically by

the insulator between them but connected mechanically by the insulated bolts. The bellows are divided into two parts in the poloidal direction in order to make a smooth connection to the cryogenic chamber. This is done by inserting the flat plate between the two parts of the bellows, as shown in Fig. 11.3.2.

11.3.2 Superconducting Magnet Vacuum Boundary

The main subject concerning vacuum boundary for superconducting magnets may be to discuss the vacuum boundary for toroidal field magnets. In this section the following four types of vacuum boundary concepts for toroidal magnets are discussed.

(1) Separate type for each magnet

As is shown in Fig. 11.3.4a, each toroidal field magnet in the outer part in the major radius direction has own vacuum chamber which is welded to a cylindrical plate. This cylinder is welded to the outer side of shielding structure, and it also forms the vacuum boundary for the poloidal field magnets near the center pole. The details are shown in Fig. 6.2.4.

(2) Separate type for every two magnets

Two adjacent toroidal magnets have a single vacuum chamber which is located in the section without the neutral beam injector, as is shown in Fig. 11.3.4b. In this part, the outer side of the shielding structure forms a side of the vacuum boundary for the toroidal field magnets. It means that the outer side of the shielding structure in this part forms the toroidal magnet vacuum boundary continuously in minor cross-section.

(3) Belljar type

All of the reactor systems are located in a belljar type vacuum chamber which forms the vacuum boundary for the superconducting magnets, as is shown in Fig. 11.3.5. The neutral beam injectors are located in the outside of the belljar, while the main vacuum systems are located either in the inside or the outside of the belljar. The vacuum boundary for the plasma chamber needs to be formed continuously through the belljar probably by welding.

(4) Vacuum room type

In this case, the reactor room atmosphere is vacuum for super conducting magnets. It means that all of the reactor system, the main vacuum systems, and the neutral beam injectors are in the same vacuum pressure as the magnet vacuum chamber.

These four types are compared in Table 11.3.1 in view of maintenance of reactor systems, support of the torsion force in the toroidal field magnets, and vacuum pump capacity for evacuating the magnet vacuum chamber. Demerits in each type are summarized as follows.

(1) Separate type for each magnet

The toroidal torsion force in the toroidal field magnets requires the support structures between the toroidal magnets. Since the vacuum boundary for the magnets is separated heavily in this type, the support structures, which can be located between the magnets, are limited. In addition, many places of the magnet vacuum boundary have to be cut when the toroidal field magnet is replaced. We also need to separate the bellows for increasing the loop resistance of the torus shielding structure into two parts in minor cross-section, as is shown in 11.3.1.

(2) Separate type for every two magnets

It appears that supporting of the toroidal torsion force in the toroidal magnets might be only a problem. Better support structure can be put in this type than in the type (1), since wider space exists in the vacuum chamber for the two adjacent magnets.

(3) Belljar type

Two ways to reach the reactor system can be thought in this type. The one is shown by the arrow A in Fig. 11.3.5, meaning that the top cover of the belljar is removed and the reactor system is reached only from the upper side. The other is shown by the arrow B in Fig. 11.3.5, meaning that the belljar is removed from the bottom and the reactor system can be reached from the side as well. In the former case, replacement of the shielding structure and the toroidal field magnets may be difficult, because the shielding structure has to be

disassembled *in-situ* and removed. In the latter case, the same maintenance procedure as reported in Sec. 11.1 is applicable. It however appears that lifting of the belljar may be complicated work, because the vacuum boundary for the plasma chamber needs to be continuous through the side wall of the belljar between the torus and the neutral beam injector.

(4) Vacuum room type

The biggest demerit of this type may be the pump capacity necessary for evacuating the reactor room to some 10^{-3} Pa (10^{-5} Torr). We have to estimate this capacity in detail when we decide to use this concept.

To summarize this section, we conclude temporarily that the separated type for every two magnets is the best way to form the vacuum boundary for the toroidal field magnets as far as the torsion force in the toroidal magnets can be supported.

11.3.3 Maintenance machines

Maintenance procedure for the toroidal magnets and shielding structures is described in Sec. 11.1. Here, we report the matenance machines required.

(1) Repair vehicle (Seal cutting and welding machine)

This vehicle is remotely controlled and runs along the connecting periphery of shielding module to disconnect or weld the flare seals. Figure 11.3.6 illustrates the repair vehicle. The speed is controlled accurately with the aid of chain on the track and sprocket on the vehicle. This is equipped with shear cutter for the flare seal, T.I.G. welding torch and TV camera for surveillance. The repair vehicle on the track can be mounted easily by turning knobs at four corners. The shear cutter corrects its moving direction automatically by detection of flare seal height. The torch height is held constant by means of the tracing mechanism. All kinds of control such as running vehicle, cutting, welding, and etc. are performed remotely.

The repair vehicle weights about 50 kg excluding the cable, the maximum running speed is 3 m/min, and the welding velocity is about 200 mm/min. The auxiliary vehicle transports the welder and shield gas bottles toward the working place.

(2) Retraction vehicle

Remotely controlled vehicle carries the shielding module. Figure 11.3.7 shows the main features of the vehicle.

(3) Overhead crane

It transports reactor components such as upper poloidal field magnets, toroidal field magnets, supporting structures and etc.

(4) Overhead bridge mounted manipulator

It cuts the main cooling pipes to detach the main vacuum system and neutral beam injector. The details are described in 11.2.3.

(5) Jack

Jacks are used to bring down lower poloidal field magnets into the trenches when replacement of the toroidal magnets is necessary.

11.4 Concept of Reactor Building

To design the reactor building of INTOR, it is most important that the reactor building has the capability to accept the concept of repair and maintenance shown in Sec. 11.1. First, we discuss what kind of area is necessary to proceed the reactor maintenance in the reactor system B. Second, the way how to transport the replaced structures is discussed. These area and transport concepts give us a concept of the reactor building concerning the reactor system B. The vertical and plane views of the reactor building are shown in Figs. 11.4.1 and 11.4.2, respectively.

(1) Area concept

(a) Reactor room

Almost all the parts in the reactor system B except for the shielding structure can be disassembled in the reactor room, which means that the reactor room is somewhat a maintenance room. The reactor room is designed so that almost all the maintenance operations can be carried out remotely in the smallest reactor room space. Giving a clearance of 4 m between the back side of NBI and the reactor room wall, the radius of the reactor room is determined to be 26 m. This clearance appears to be sufficient to allow reliable remote

maintenance for the NBI systems.

To give sufficient room to work on the reactor system, square NBI rooms are located behind the circular reactor room of the radius 26 m. When the four NBI systems and the main vacuum systems are drawn back to the NBI rooms, wide space is prepared to work on the reactor system. The area of the NBI room is determined to be 16 × 14 m which is sufficient to contain the NBI system, main vacuum system and piping structures.

(b) Storage area for radioactive structures

This area is prepared to store the used protection wall, blanket structure and other radioactive structures. If a repair room for radioactive structures have to be prepared, it will be located in the storage area for radioactive materials. In this case, we also have to develop remote handling machines as well as inspection systems to find failure parts in the system to be repaired.

(c) Storage area for maintenance machines and unirradiated structures

This area is prepared for spares of the blanket structures, protection walls, toroidal magnets and shielding structures. This area is also available to locate maintenance machines which are transferred to the reactor room during maintenance. Unirradiated structures can be repaired in this room with sufficient accessibility.

(d) Turn table

During some maintenance operation, the upper poloidal magnets can be placed on the turn table which is located between the crane and the torus. This table can turn together with crane movement so that the crane can reach any place in the reactor room. The turn table is semicircle and has a sufficient area to hold the upper poloidal magnet of the maximum diameter. Some repair may be possible on the turn table especially for unirradiated structures.

(e) Storage area for lower poloidal coils

On the floor of the reactor room, several ring-shaped trenches centering to the torus major axis are arranged. These trenches are used for storage area of the new lower poloidal magnets and for the area to retract the poloidal magnets during maintenance of the reactor

components. In these trenches several jacks are equipped for retraction and elevation of the magnets.

(2) Transportation concept.

Reactor room has a 500 ton crane and blanket handling machines. Several heavy carriers are stored in the storage area for unirradiated structures. 300 ton cranes are equipped in the storage areas. These machines are used for structure transportation in the following way.

(a) Transportation in the reactor room

The relatively light structures such as the poloidal magnets, and toroidal magnets are transported by the 500 ton crane in the reactor room. The heavier structures such as the main vacuum system, NBI system, toroidal magnet and shielding structure module are carried by the heavy carriers. The jacks equipped in the carrier can lift these heavy structures. The carrier can be installed by the crane on the rails which run linearly and circularly with respect to the torus center.

(b) Transportation between the reactor room and the storage area

A transfer gallery, where the rails for the heavy carrier are installed, is located between the reactor room and the storage areas. The carrier can take care of transfer of any reactor component to the storage rooms. A turn table is located near the storage area to change the direction of carrier movement.

(c) Transportation in the storage area

The 300 ton crane is used to transfer any component in the storage area. The structure heavier than 300 ton have to be disassembled so that they can be taken care of by the crane.

11.5 Design Problems

The concept of reactor maintenance appears to be established reasonably well with reference to the Removable Blanket Scheme. Whether this scheme is achievable or not depends strongly on the possibility to develop the maintenance machines required in this scheme. Structural design described

in this section convinces us that we can design the reactor structures in such a way that the maintenance machines can handle replacement of the reactor structure, once the performance of the maintenance machine is decided. Problems will be the time required during maintenance. Thus, the next step to which we should proceed appears to be a reasonably detailed design of maintenance machines.

In almost all of this section, maintenance means replacement of failure parts to the new structures. It may be worthwhile to develop the way to repair the failure parts either *in-situ* or in the storage room. In any case, we have to develop machines both to find failure parts and to repair those parts. Failure modes also may have to be analyzed to determine what kind of failure we need to expect. If all of these works will have been achieved in future, it might be wise to equip multi-purpose repair center in the storage area for radioactive structures.

Table 11.2.1 Time required for maintenance

1) Disassembling

STEPS	TASK	TIME in hours			SEQUENCE
1	Remove the interfering poloidal coils	16			
2	Discharge cooling water	8			
3	Disconnect the bolts and break the vacuum seal for opening	16			
4	Release the blanket fixing cramps	8			
5	Remove the opening hatch	4			
6	Cut main cooling pipes	4			
7	Install the track for the wall mounted manipulator	4			
8	Cut main headers	6	3	-	
9	Release the connection between adjacent sectors	4	3	-	
10	Disconnect upper flanges of adjacent sectors	12	8	-	
11	Hoist blanket sector	4	4	4	
12	Place the blanket sector on the carriage	4	4	4	
13	Lower the remaining sectors to be movable	6	-	-	
15	Move the adjacent sector under the opening	6	6	-	
	TOTAL TIME				120

2) Assembling

No	ADDITIONAL TASKS TO DISASSEMBLING	Total time in hours	
1	POSITIONING BLANKET SECTORS	20	
2	INSERTING BOLTS INTO THE FLANGE	12	
3	WELDING AND TESTING	20	TOTAL ADDITIONAL TIME
4	CLEANING INSIDE OF THE SHIELDING	8	60
	TOTAL TIME		180
	GRAND TOTAL TIME		300

Table 11.2.2 Estimation of toroidal magnet vacuum boundary concepts in the reactor system B

	Maintenance items					Support of torsion force	Vacuum pump capacity
	Protection wall	Blanket structure	Shielding structure	Toroidal Magnet	Poloidal Magnet		
(1) Separate type for each magnet	A	A	A	AB	A	B	A
(2) Separate type for every two magnets	A	A	A	A	A	B	A
(3) Belljar type	A	AB	B	B	A	A	AB
(4) Vacuum room type	AB	AB	A	A	A	A	C

A = Good, AB = Possible, B = Probably possible, C = Uncertain.

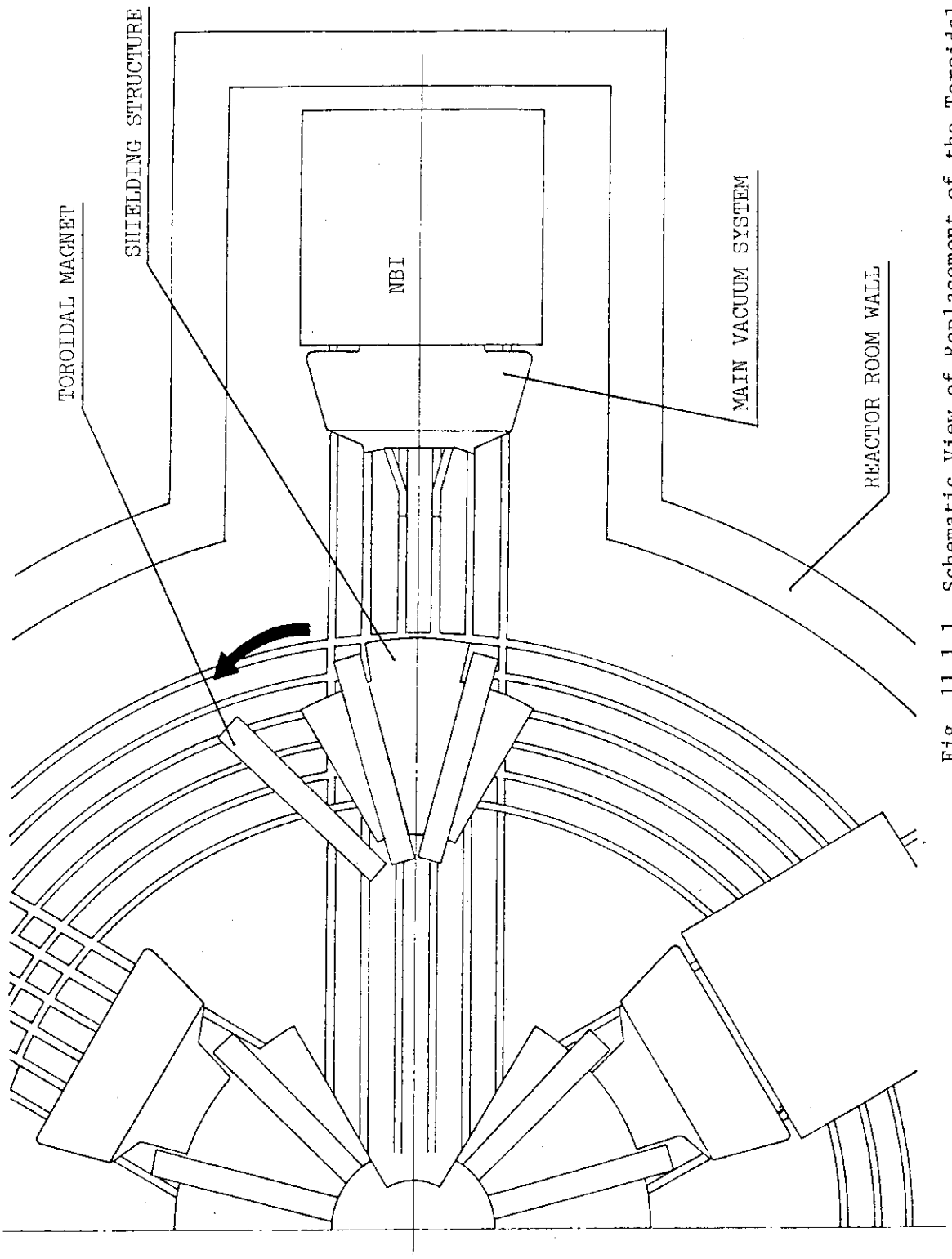

Fig. 11.1.1 Schematic View of Replacement of the Toroidal Field Magnet

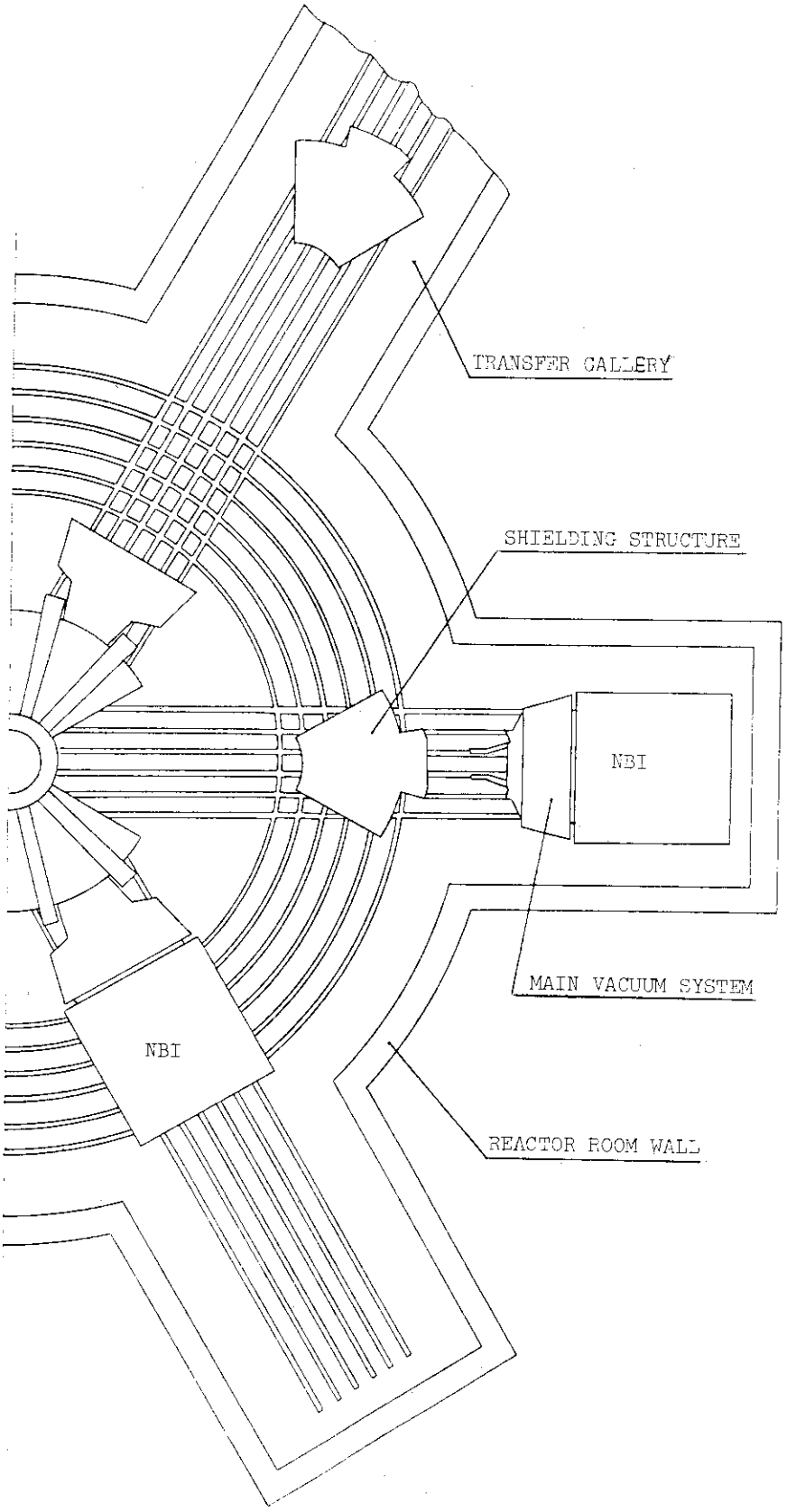

Fig. 11.1.2 Schematic View of Replacement of the Shielding Structure

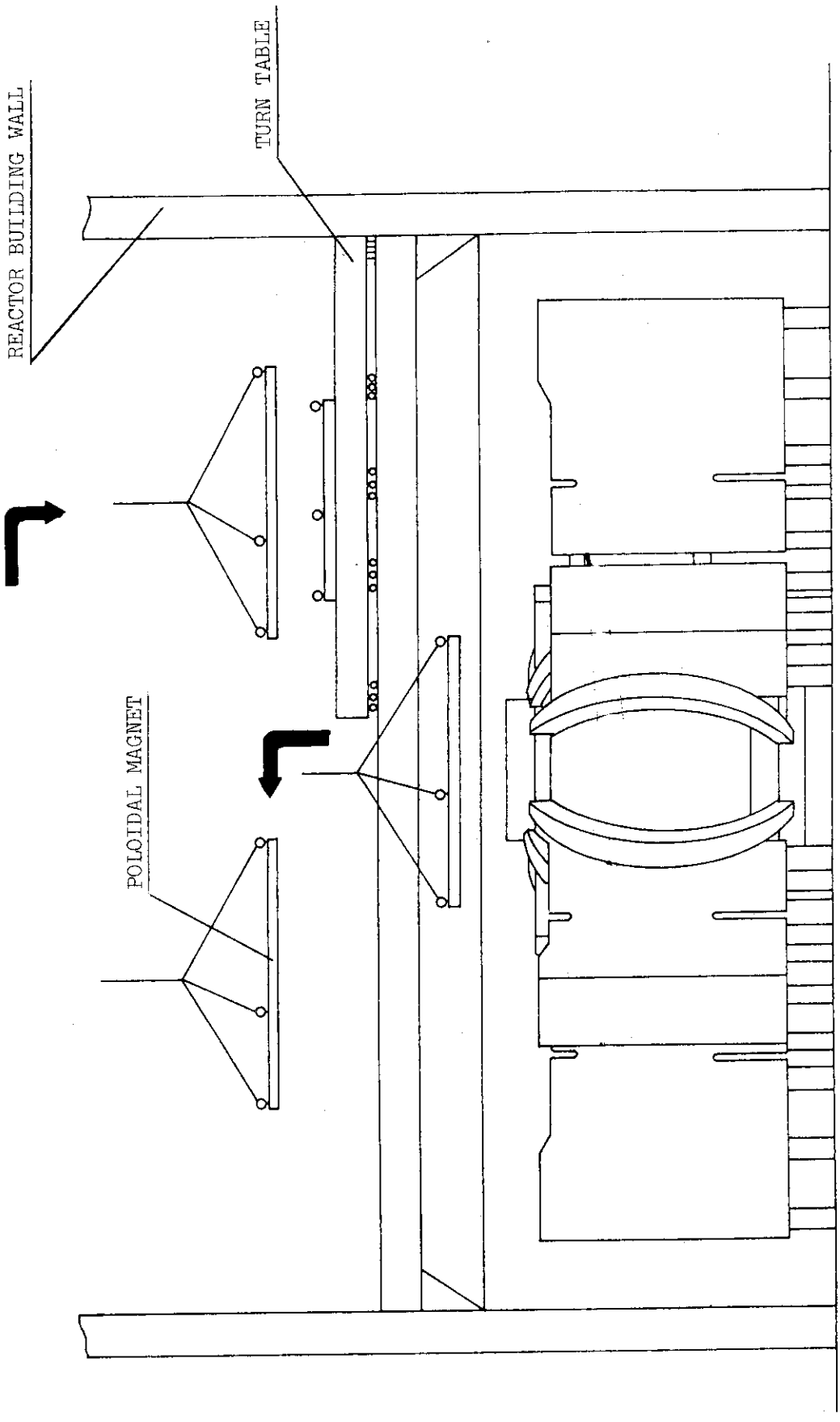

Fig. 11.1.3 Schematic View of Replacement of the Upper Poroidal Field Magnet

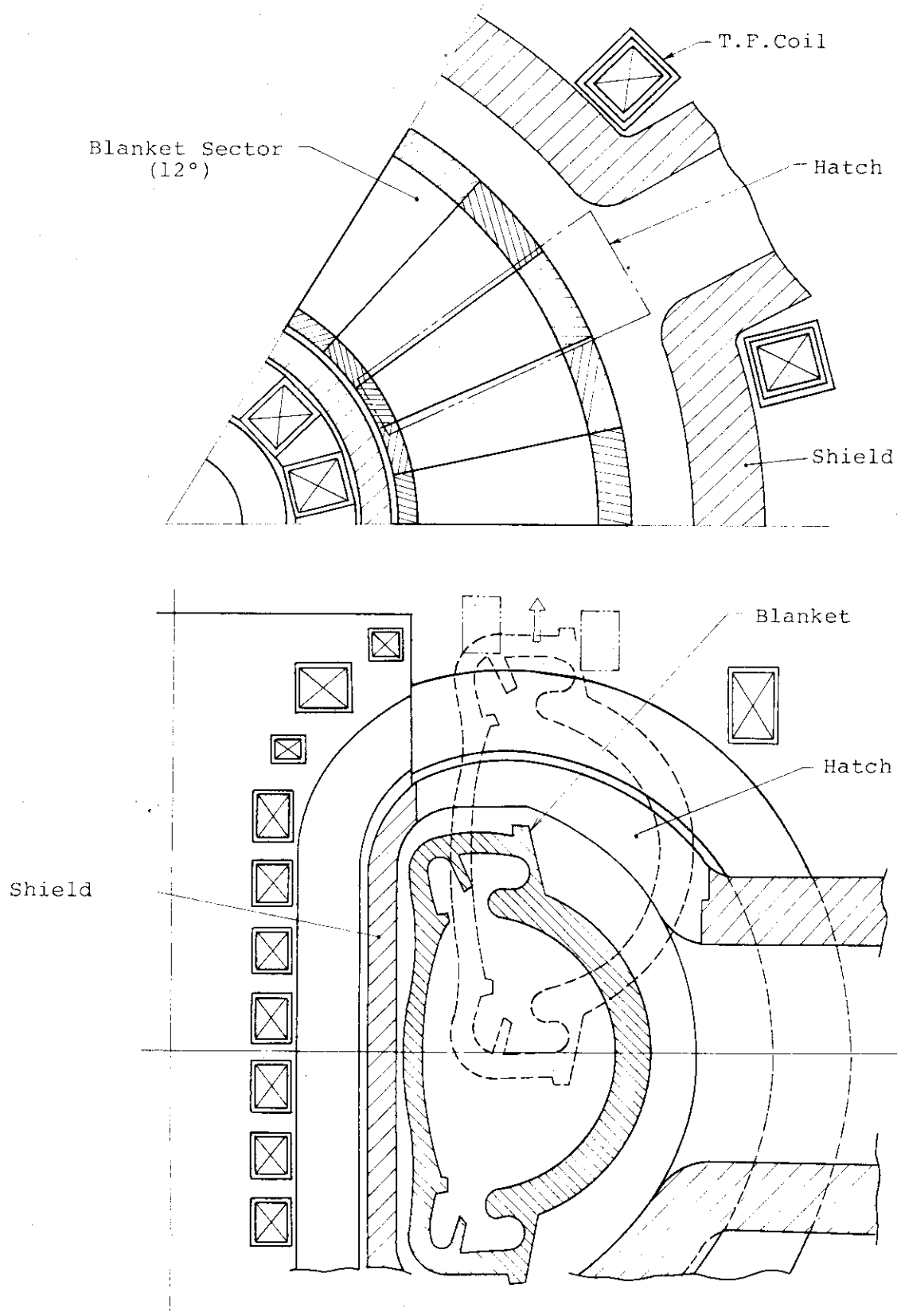

Fig. 11.2.1 Hatch on the Shielding Structure in the Removable Blanket Scheme

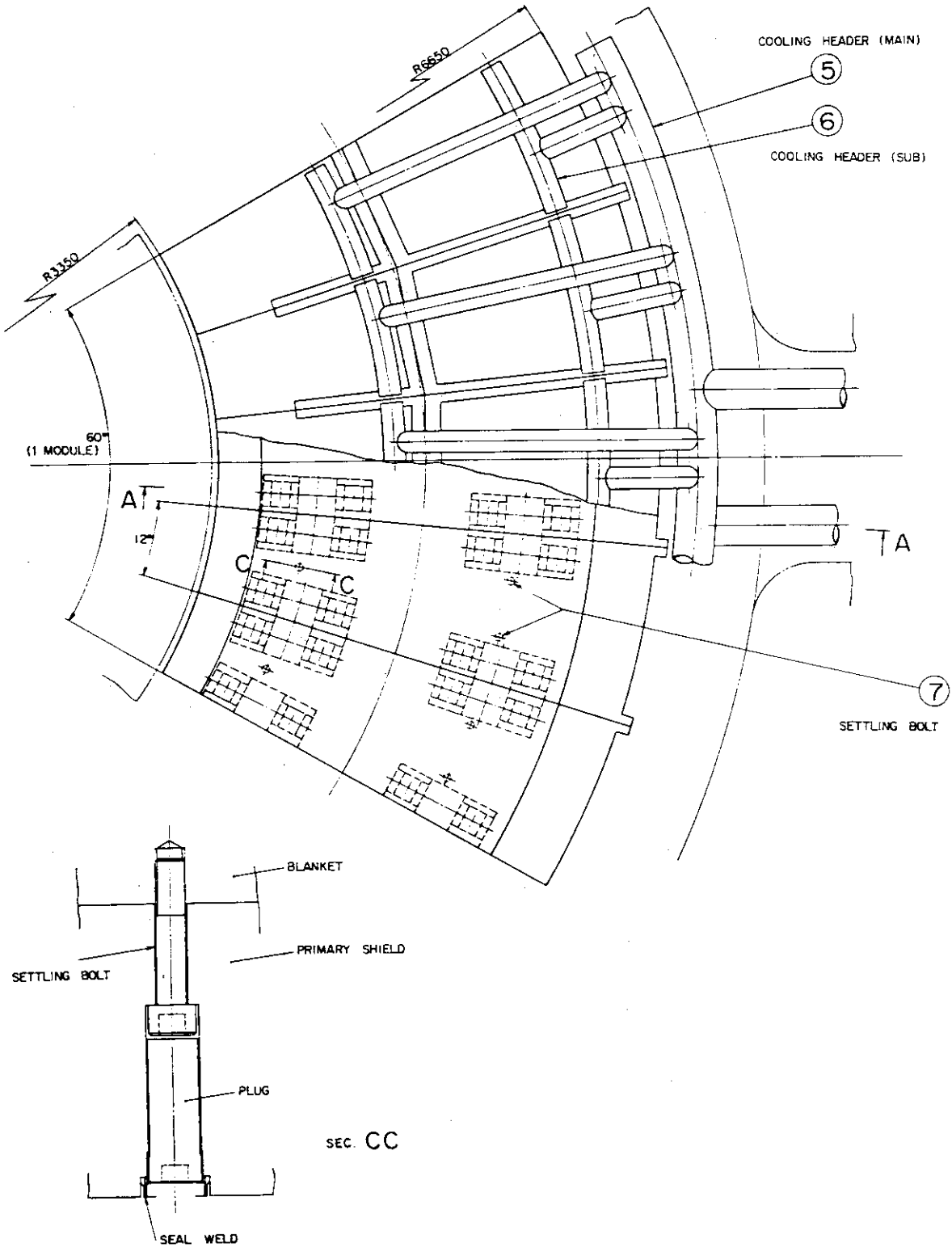

Fig. 11.2.2-a Blanket Structure (horizontal view)

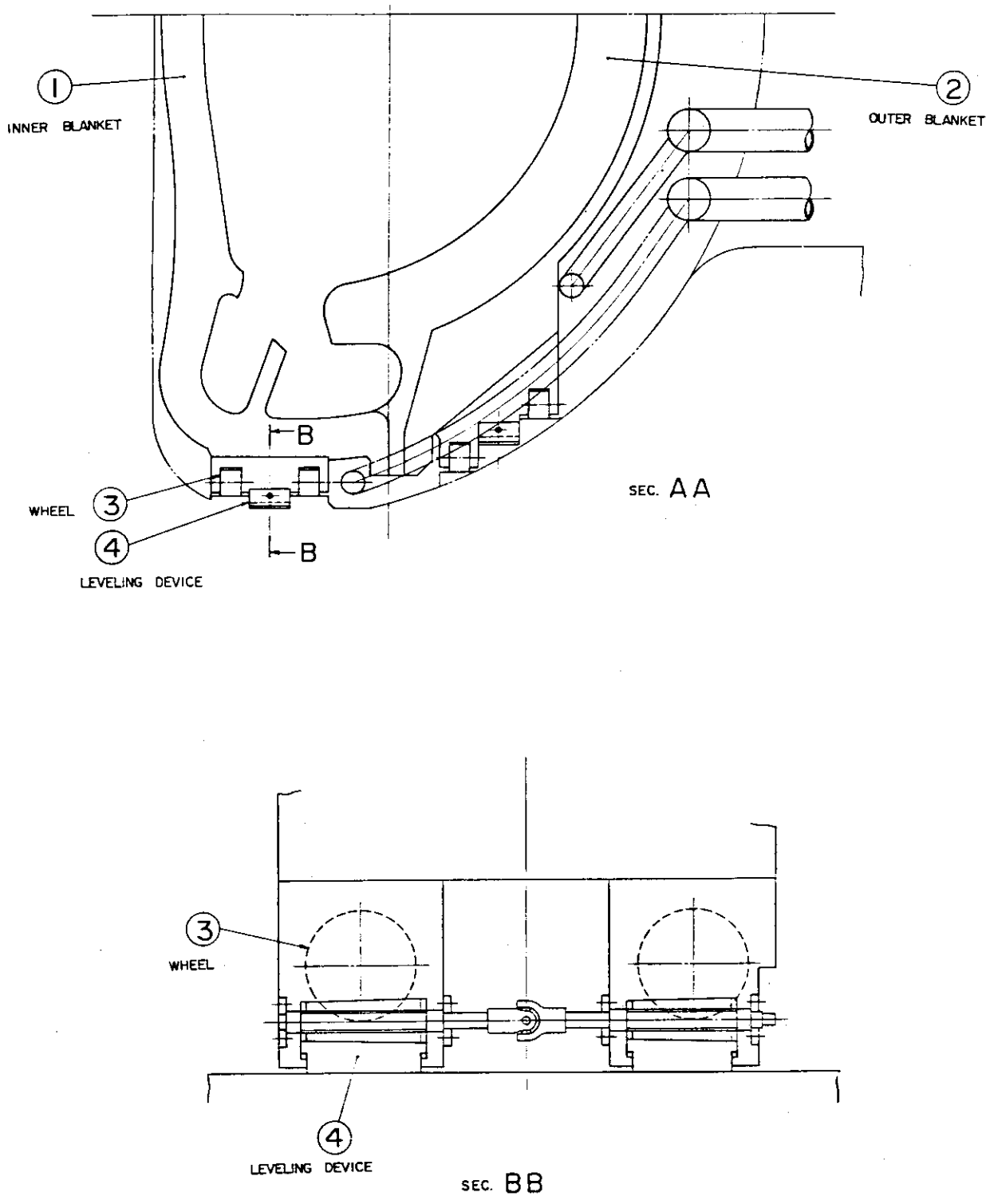

Fig. 11.2.2-b Blanket Structure (vertical view)

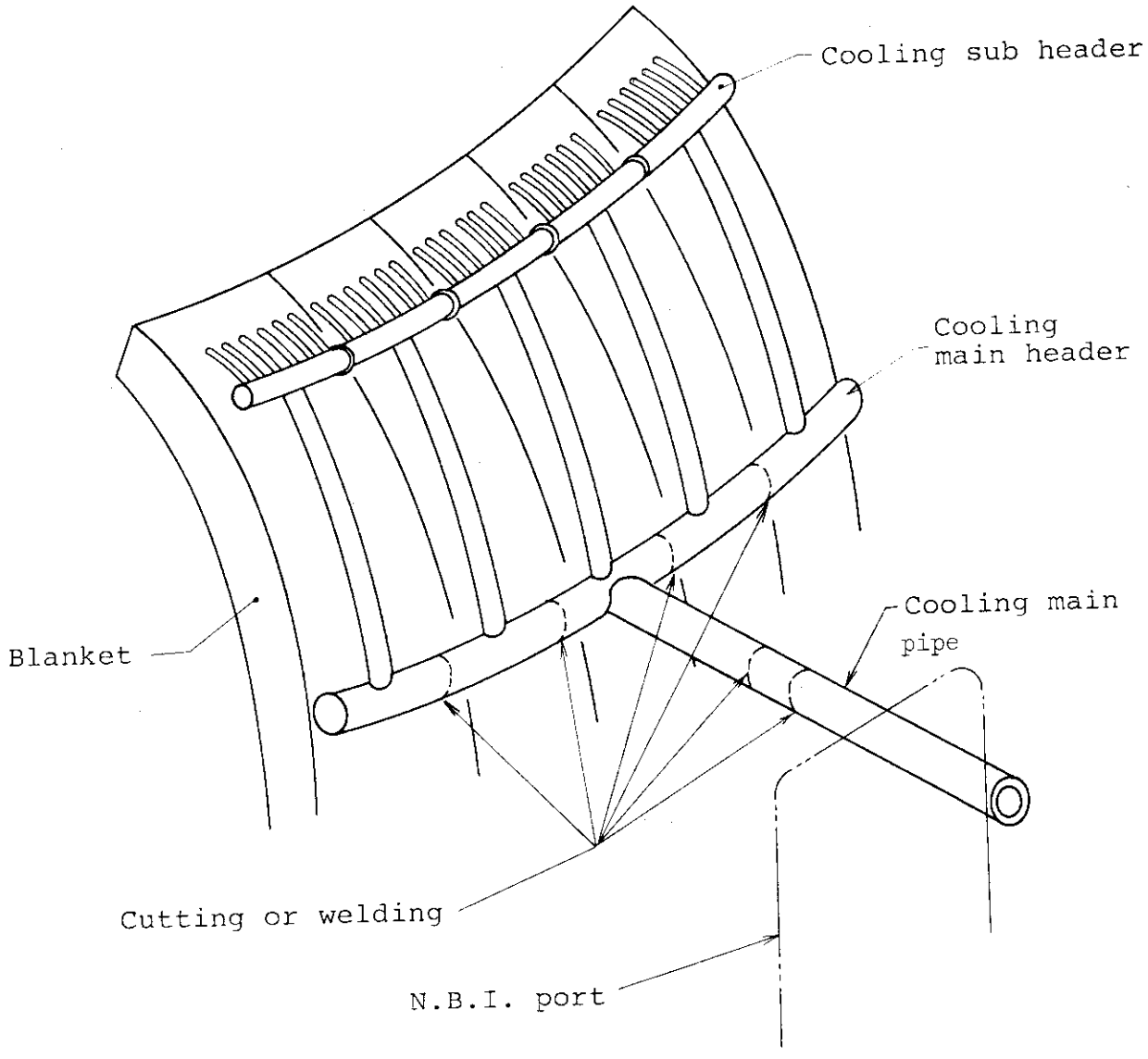

Fig. 11.2.3 Piping Concept for Blanket Cooling

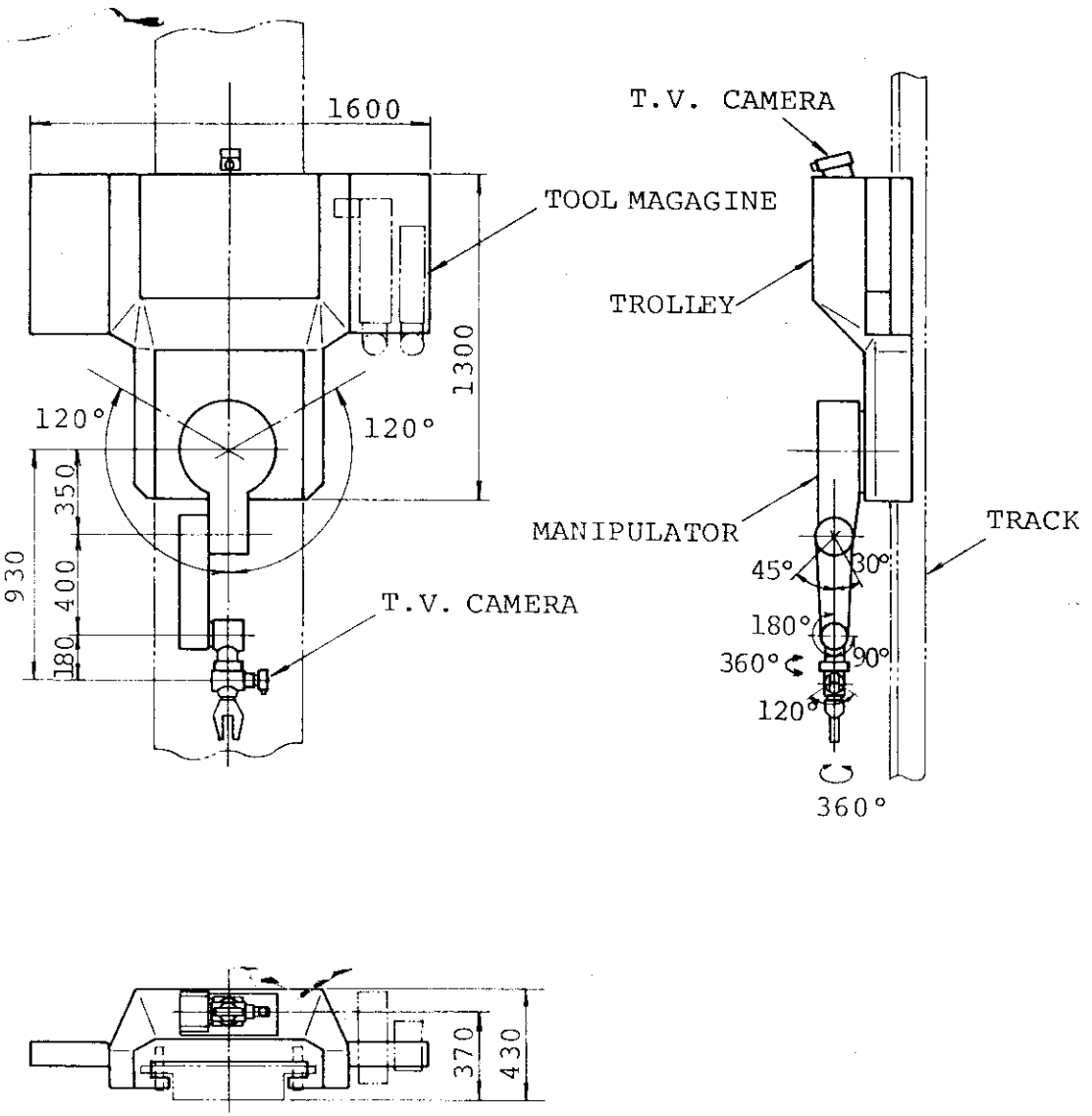

Fig. 11.2.4 Wall Mounted Manipulator

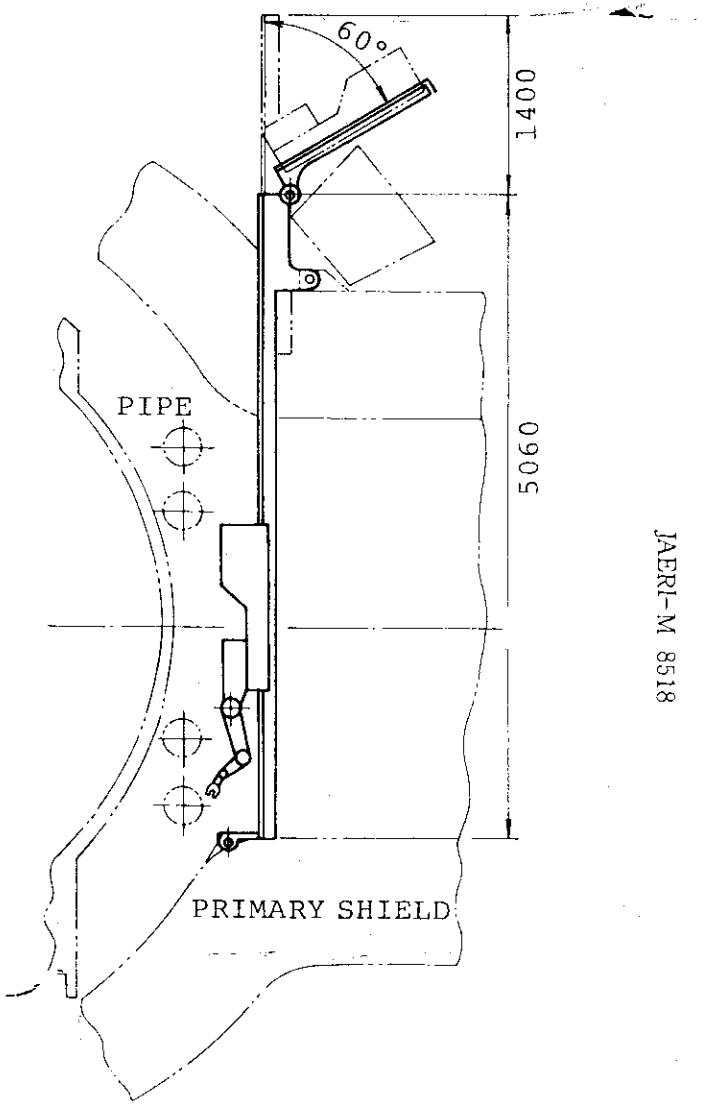

WALL MOUNTED
MANIPULATOR

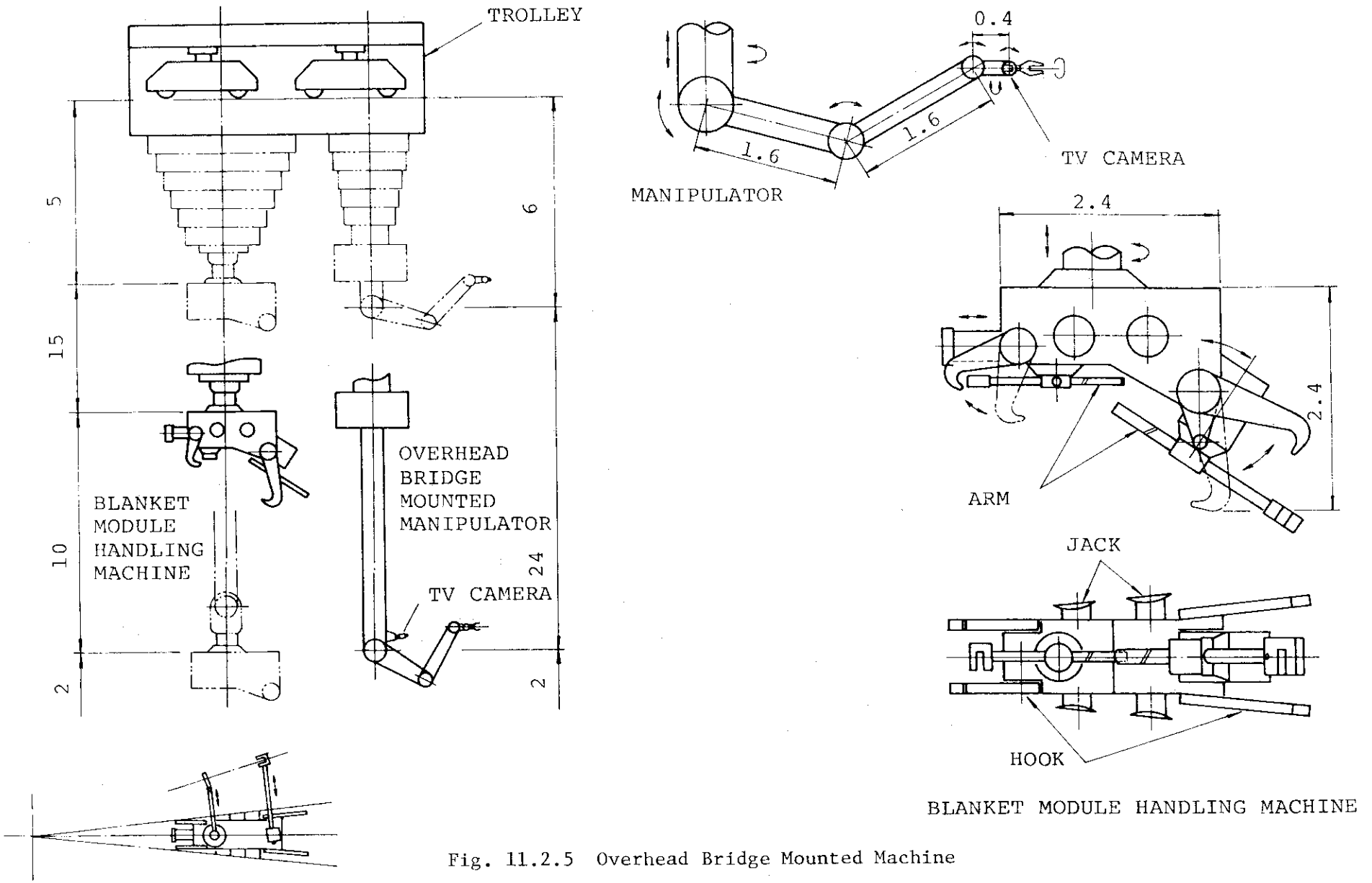

Fig. 11.2.5 Overhead Bridge Mounted Machine

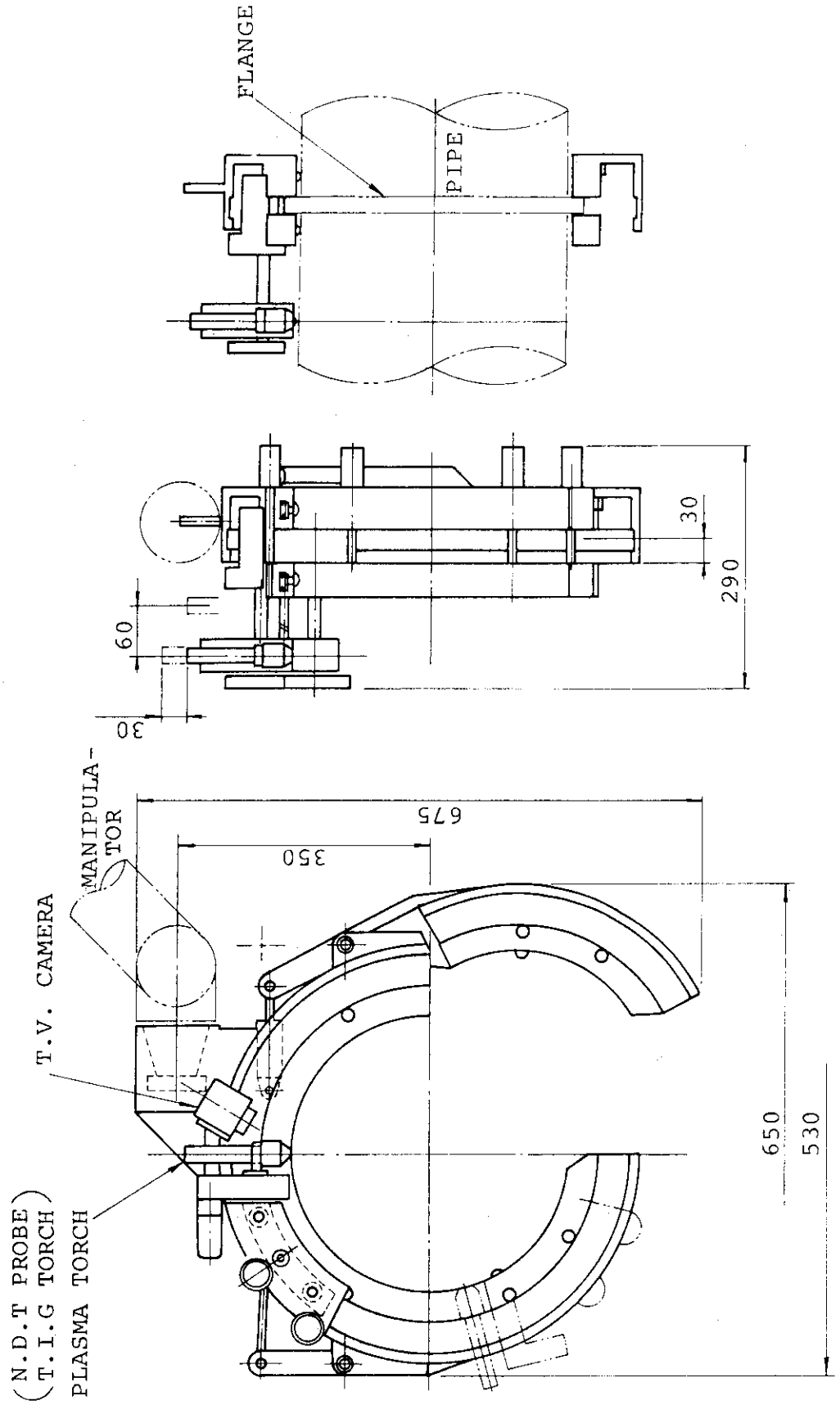

PIPE CUTTING TOOL
(WELDING
TESTING)

Fig. 11.2.6 Pipe Cutting (welding, testing) Tool

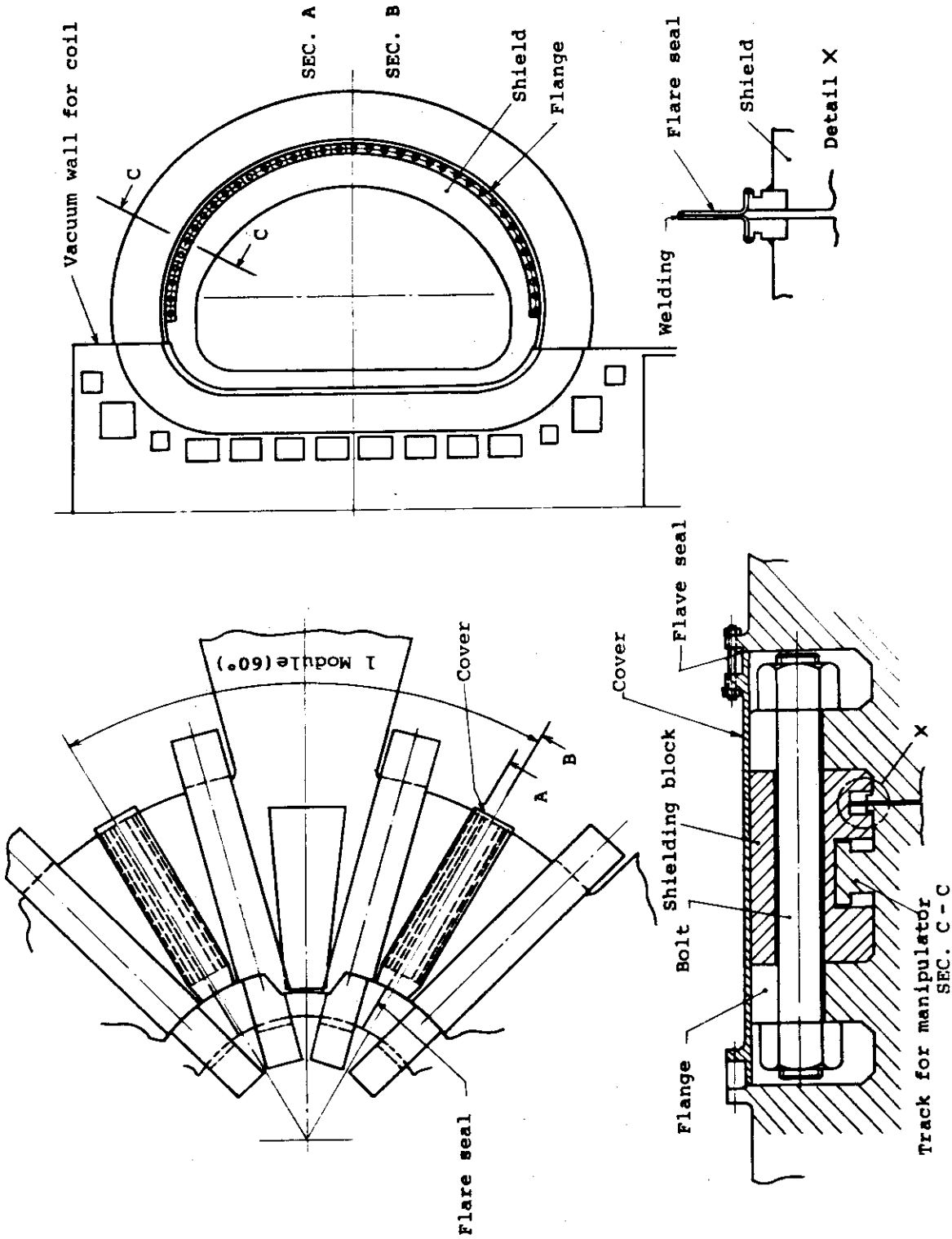

Fig. 11.3.1 Structure of Connecting Flange for Shield

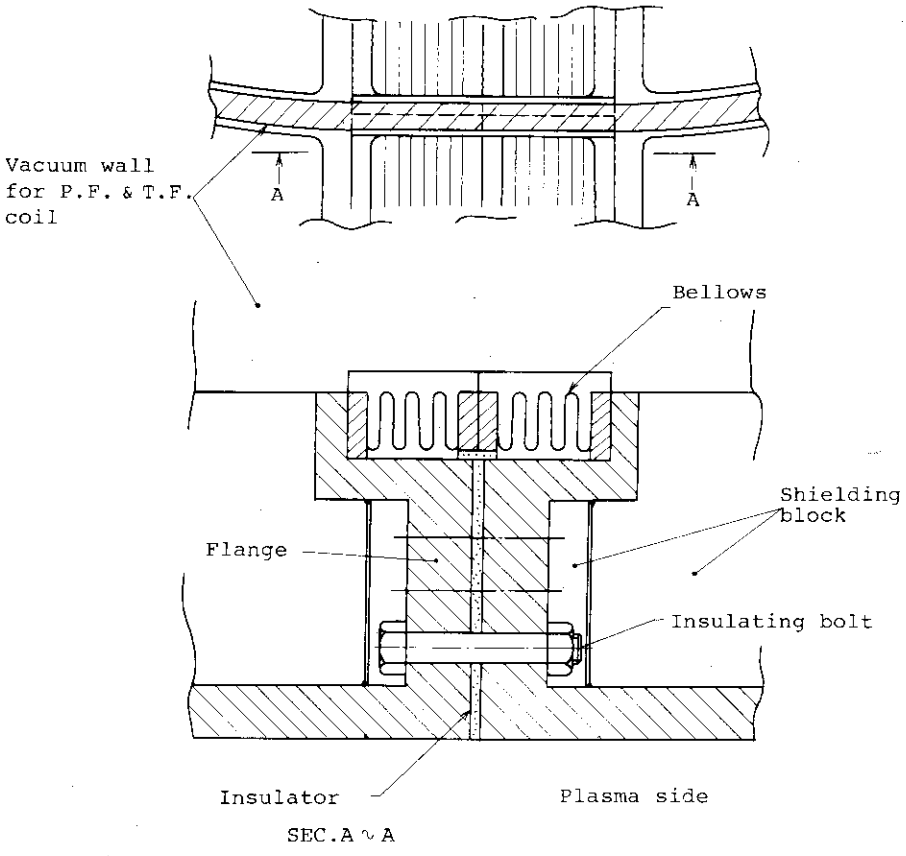

Fig. 11.3.2 Bellows on Shielding Structure

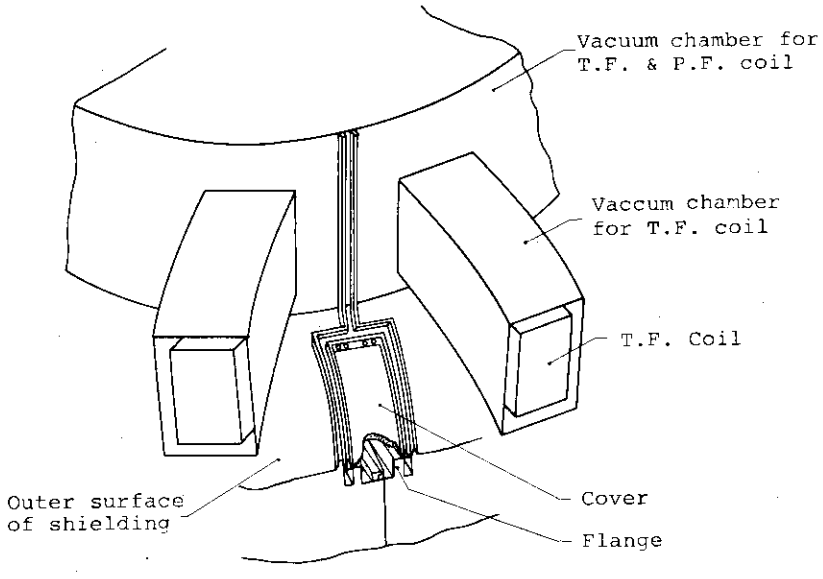

Fig. 11.3.3 Vacuum Boundary of T.F. coil and Plasma Chamber

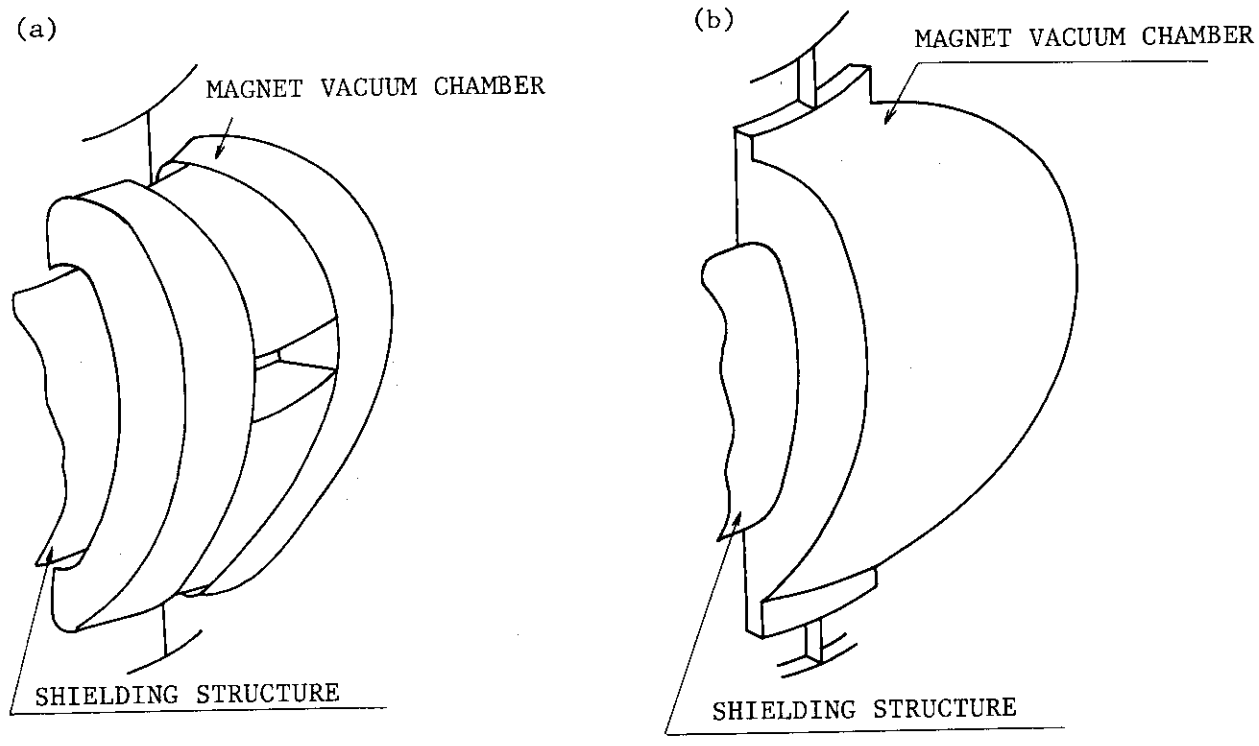

Fig. 11.3.4 Vacuum Boundaries for Superconducting Magnets

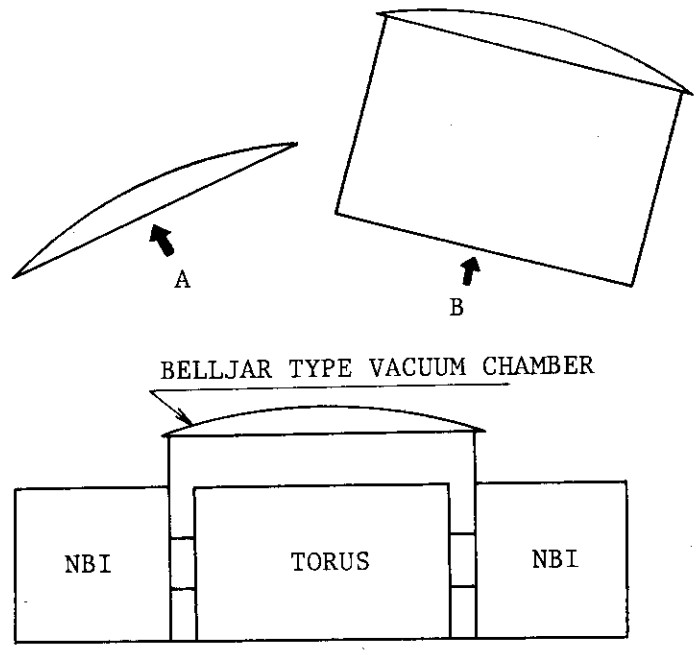

Fig. 11.3.5 Belljar type Vacuum Boundary

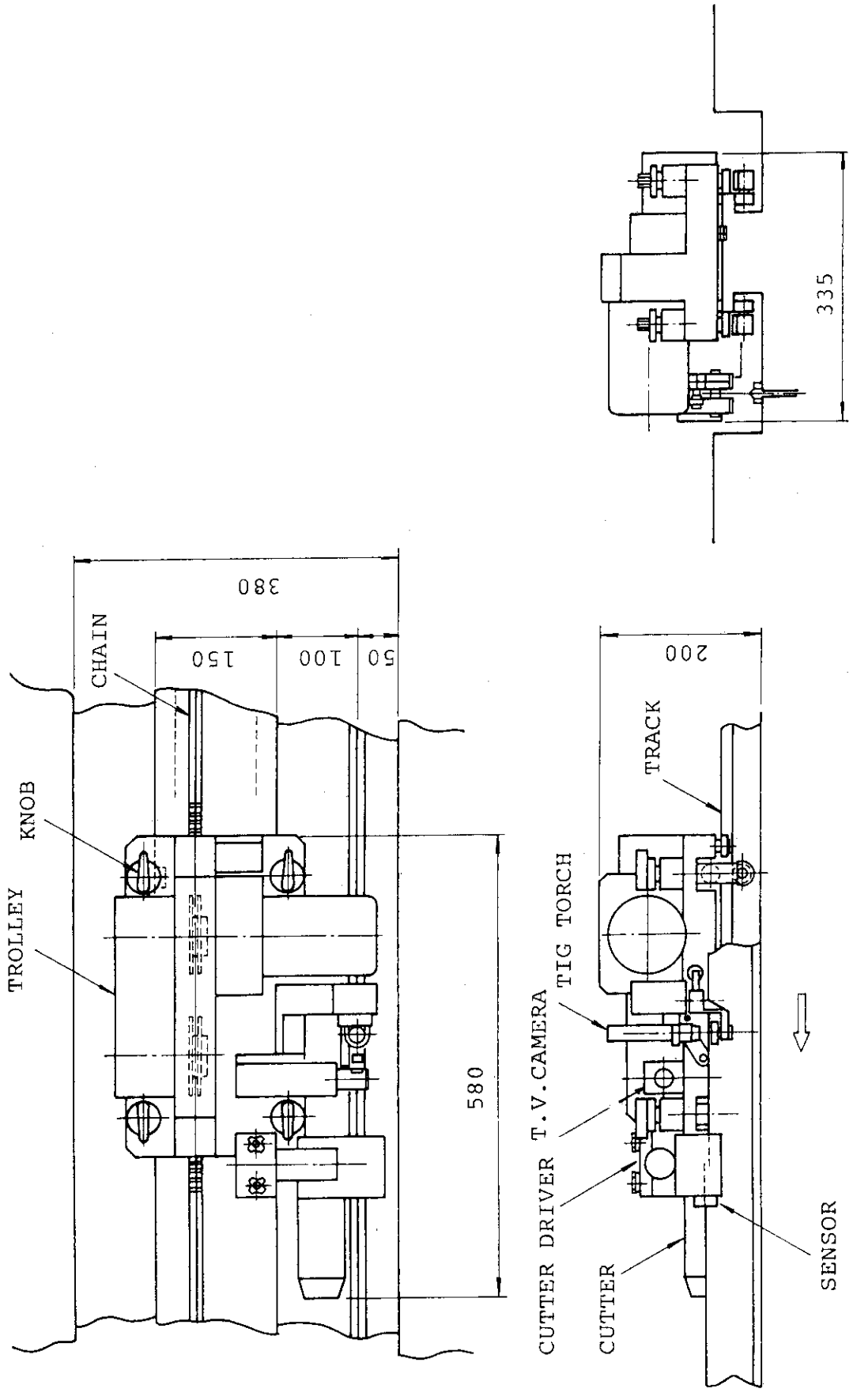

Fig. 11.3.6 Seal Cutting and Welding Machine

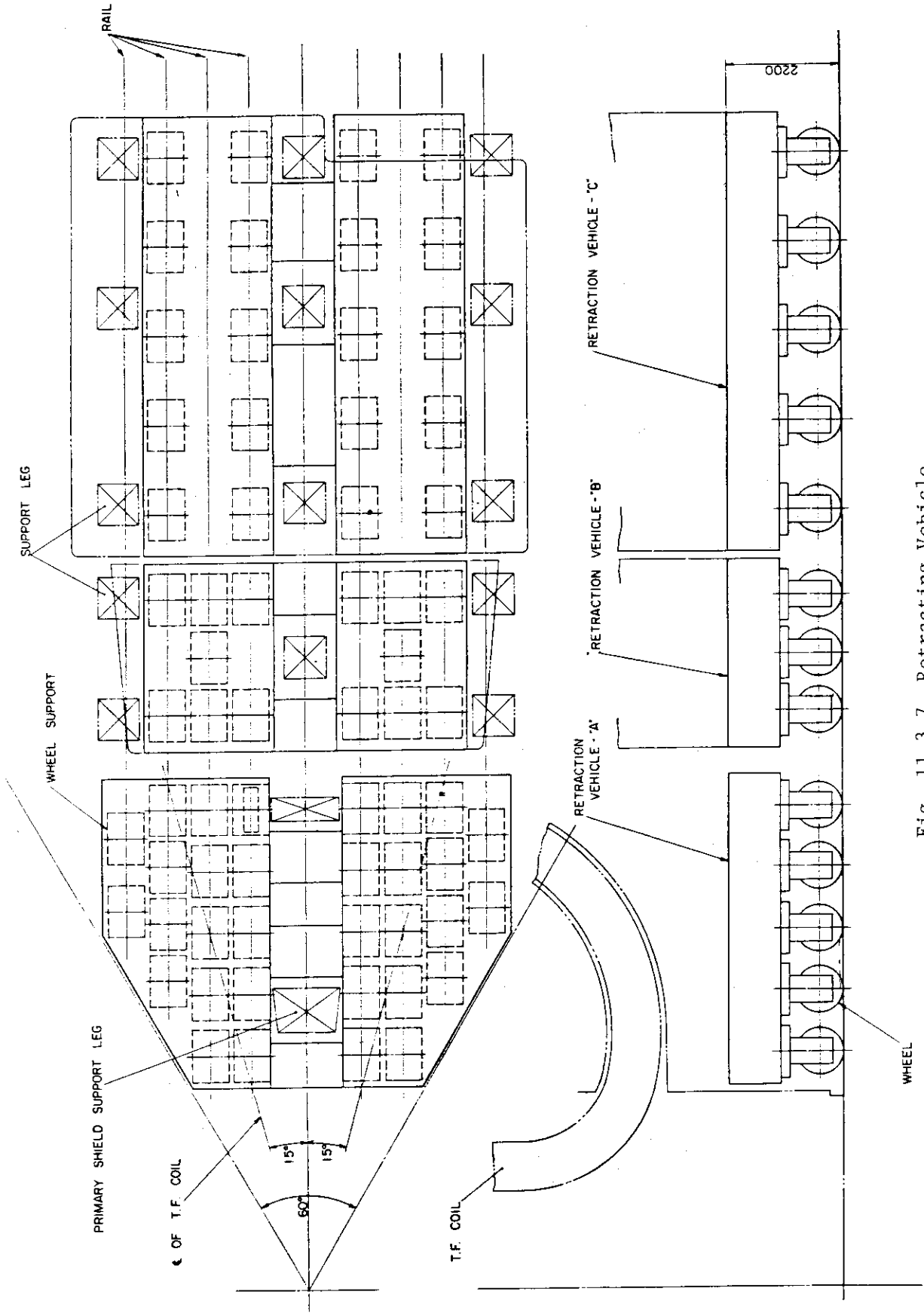

Fig. 11.3.7 Retracting Vehicle

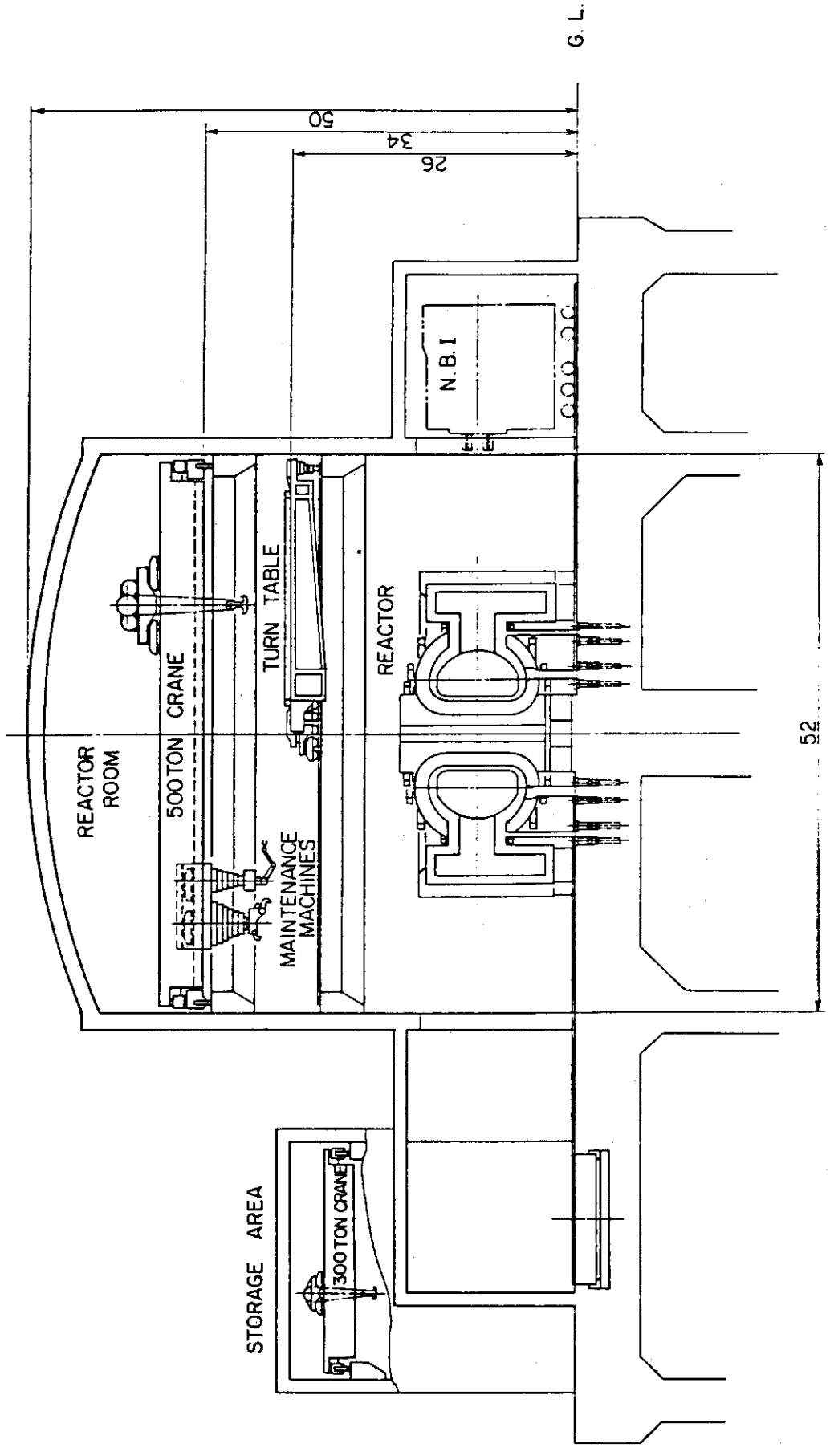

Fig. 11.4.1 Vertical View of the Reactor Building

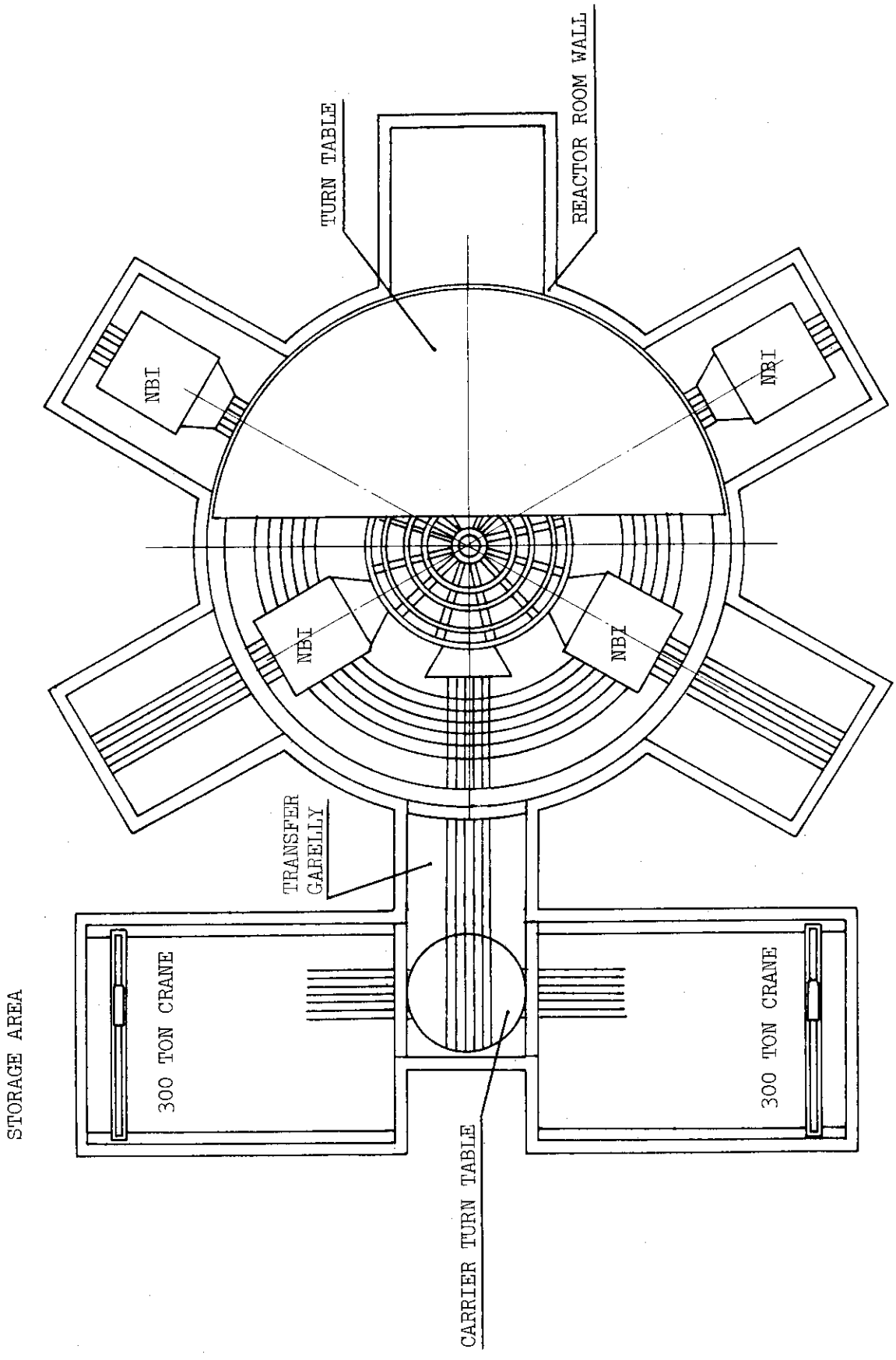

Fig. 11.4.2 Plane View of the Reactor Building

12. Repair and Maintenance of Divertor Plate

The divertor plate is provided to remove the α particles and impurity ions which invade into the plasma by means of the interaction between the plasma-first wall. An ion current of high temperature strikes against the surface of this divertor plate, so there is a possibility that the divertor plate may be damaged by sputtering and heat stress. Therefore, it is necessary to exchange the divertor plate periodically, as well as at an event occurred by the coolant leakage from the divertor plate. On the one hand, after the start, reactor components are strongly activated by fast neutrons, so the Gamma ray will still be strong even after the stop of reactor and it is impossible for people to approach to the reactor.

Accordingly, the exchange and maintenance works must all be carried out by a remote manipulating operation with an automatic equipment, and so the structure of divertor plates must be made suitable for the automation of operations. In this chapter, the exchange and maintenance of divertor plates are investigated inclusive of this point.

12.1 Design Conditions

12.1.1 Structure of Divertor Plate

(1) Configuration

The configuration and dimension, fitting position, material quality of a divertor plate must be determined with heat, electromagnetic field, radiation and other various surrounding conditions, in order that the divertor plate may fulfil its functions. On the one hand, viewing from the standpoint of maintenance and inspection operations by an remote operating equipment, it is necessary to take into consideration the following matters, such as the size and weight of the divertor plate are made to values to be easily handled; the fixing position of divertor plate and the arrangement of cooling piping are selected pertinently; and a clue to fixing means and positioning of maintenance equipments are provided in anticipation within the reactor.

A fitting condition of a divertor plate is shown in Fig. 12.1.1, and a configuration and rough dimension of a divertor plate in Figs. 12.1.2 and 12.1.3.

In this case, the circumferential maximum width of the divertor plate becomes 670 mm which is the size suitable for handling.

In the case of width larger than this, handling and posture conversion at the time of transportation will become difficult in the reactor core, and also the NBI holes (1.5 m × 1.0 m) of the outer blanket for carrying-in and out must be made larger. In case of smaller width, the dimension of header becomes shorter, so many hangers that fix cooling piping and divertor plate will line up closely, and then cutting and welding operations will become difficult. The number of divertor plates to be exchanged for a damage of same area will increase and maintenance time will become longer.

(2) Connection to cooling water piping

The cooling water piping to the divertor plates is connected at the header of divertor plates. In exchange of divertor plates, this piping has to be cut and be connected again. When these works are carried out by a remote equipment, that is, a manipulator provided with tools and a welding machine, it is desirable that the connection of cooling pipe is at the position to which the tools installed on the manipulator can be easily accessible. That is to say, such the position is desirable which will not be shaded by the divertor, viewing from the arm side of the manipulator. It is also desirable that there is no obstacle such as adjacent piping near the connection.

In Fig. 12.1.1 there is shown a cooling water piping and its connection positions. Support (hanger) structures of the divertor plate also have to be designed under the consideration similar to cooling piping.

(3) Weight of divertor plate

The weight of the divertor plate was estimated on considering the strength of the manipulator and a method of transporting the divertor plate. Its configuration was assumed to be two pieces of pipes and trapezoidal plates, and the material is copper.

An outer divertor plate block : 85 kg
An inner divertor plate block : 60 kg

These weights are considerably heavy as articles handled by a remote operation, but they will not be in the range which is incapable of handling.

12.2 Method of Exchanging Divertor Plate

The connecting method of cooling piping must be satisfied with the following condition that no leakage of coolant occurs in high vacuum and, moreover, a structure of connection stands high temperature. In the general, there is a possibility of burning of contact surfaces of metal at high temperature and high vacuum. Accordingly, joints using mechanical connection fittings are suitable, and so cutting and welding joints can be adopted in present designs.

In the exchange of a damaged divertor plate, the weight of the divertor plate must be supported temporarily during cutting or welding of cooling water pipes and hangers. In order to carry out two works of supporting and cutting at the same time, the manipulator has to provide two or more arms moving independently. However, such a composition of manipulator is not suitable for the narrow divertor plate room. As the result, a transportation equipment, that is, a carrier is installed to the damaged divertor plate by fixing temporarily to the hangers. After the removing operation of joint in this state, the carrier is released from the hangers, and then the carrier and the divertor plate in one body are carried out to the outside of the reactor. The damaged divertor plate is released from the carrier and a new divertor plate is fastened to the carrier to be carried into the reactor core. The connection of new divertor plates follows the process opposite to the removal of damaged divertor plates. Thus, this carrier enables one arm of manipulator to operate the removal and connecting of joints, and to transport divertor plates into/out the reactor core.

12.3 Procedure

The outline of repairing procedure of divertor plate by using the manipulator is shown by the flow chart in Fig. 12.3.1. The detail operations in each process are described in the following.

12.3.1 Removal and installation of NBI

Removal and installation of NBI is shown in Fig. 12.3.2. Firstly, an automatic bolt fastening and loosening equipment is lifted up by a crane. Next, this equipment is set to NBI. When this equipment has been secured to NBI by a clamper, a nut runner proceeds and grasps a nut to loosen it.

The nuts pulled out are held in the nut runner. Clamper is released, the bolt fastening and loosening equipment is lifted up again and returned to the origined place. Next, in the same operation, seal weldings between a NBI port and a NBI is cut by the welding equipment. As shown in Fig. 12.3.3, a tow truck is coupled to the NBI and separates the NBI from the reactor.

12.3.2 Setting of working heads

Before installing the manipulator to the NBI Port, a working head is attached to the end of arm of the manipulator. As shown in Fig. 12.3.4 and Fig. 12.3.5, attachment of the working head is carried out by a transporter with a small manipulator. Next, the tow truck is connected to the manipulator and approaches toward the reactor.

12.3.3 Inspection of damaged divertor plates

The inspection is carried out in the following order:

(1) Visual tests
(Detection of deformation and surface damage)
(2) Magnified visual tests
(Detection of trace of coolant leakage and micro-deformation)
(3) Non destructive inspections
(Detection of pin-holes and cracks)

Visual tests are intended to find out comparatively large damages and these damages are observed by using a monitor TV with a ITV camera as shown in Fig. 1213.6.

Operation of the monitor TV in the reactor core is controlled by checking its operational range by means of the pictures of a TV camera, a computer and a senser.

The damaged places of divertor plate which may need fine inspections is recorded for next magnified visual tests. Magnified visual tests implies to investigate in detail the defects found out in the previous coarse inspection by using the magnified visual equipment. In these inspections, the invisible defects as traces of coolant leakage may be easily detected if coolant including a dye is flowed into the divertor plates. The magnified visual equipment, owing to its narrow visual field, should require an aid of a monitor TV supervising operations of this equipment as shown in Figs. 12.3.7 and 12.3.8. The pictures obtained in these inspections also is

recorded on a videotape. In order to survey pin-holes or crocks unable to detect in the above two inspections, there is the non-destructive inspection using the supersonic examination, which has been advanced in comparison with other methods in the automation of operating. In this inspection, positioning technique of a probe on the divertor plate may be required, such as a technique using distance sensor or tactile sensor.

12.3.4 Removal of divertor plate

(1) Attaching of carrier

The procedure of removing operation of the divertor plate is shown in Fig. 12.3.9. First of all, a carrier that prevents dropping of divertor plate must be provided. The carrier transported by a transporter is attached to the arm of manipulator using a small manipulator of the transporter. After installed to the reactor, the manipulator extends its arm and brings the carrier into the reactor core and is positioned to the divertor plate to be removed. Next, with the operation of a big hook, the carrier is secured to the divertor plate. After this operation, a small hook is hung on a lateral bar of a hanger to support weight of carrier itself.

(2) Cutting off pipes

After the arm of manipulator has been released from the carrier and brought out to the outside of the reactor, a pipe cutter is equipped by the small manipulator of the transporter. The manipulator is inst alled in the reactor again, and it performs the cutting operation of cooling water pipes connected to the header of the divertor plate by extending its arm.

(3) Removing off damaged plates

Similarly, connections of the hanger are all cut off. The manipulator which carried out the pipe cutter to the outside of the reactor core is returned to the inside of the reactor again to be connected to the carrier. When the small hook of the carrier is released, the divertor plate is separated from the blanket together with the carrier, so that is carrier out to the outside of the reactor core by operating the manipulator.

12.3.5 Attachment of new divertor plate

Procedure of attachment of a new divertor plate is shown in Fig. 12.3.10. A new divertor plate is attached to the carrier and the carrier in one body with the new divertor plate is attached to the arm of manipulator and carried into the reactor core, and it is temporarily fastened to the hanger.

A welding machine is attached to the arm of manipulator to weld the cooling water pipe and hanger. When the welding of all connections has finished, big hooks and small hooks are disengaged and only a carrier is removed and brought out to the outside of the reactor core.

12.3.6 Inspection of welds

Welded seams must be inspected against defects so that leakage of coolant and break may not happen. The attaching and detaching operation of inspection equipments and procedure of approach to the welded seams are made by the same procedure as in the case of welding.

12.3.7 Procedure for finishing operation

When the damaged divertor plates have been exchanged, a carrier, operating equipments, supervisory equipments, lighting fixture and other equipments in the Vacuum Vessel are carried out to the outside of the reactor. A visual inspection is made about these equipments by ITV camera provided on the transporter to investigate the accidents such as break, falling of parts, etc.

When it has been confirmed that all of the equipments have been completely carried out, the manipulator and carrying equipments are removed, then the NBI is attached as the initial situation. At this stage the repair and maintenance of divertor plates are finished.

12.3.8 Estimation of operating time

In order to improve the load factor of reactor operation, it is necessary to shorten the time needed for exchanging operation of the divertor plates, as much as possible.

The operating time greatly varies according to the operation conditions. The time of every operating step is estimated, then whole operating time are estimated by summing up the time of every step. Whole operation times of several cases under various operation conditions are estimated as shown

Table 12.3.1.

Stationary type and travelling type manipulators are used in the cases of 1 and 2, respectively. In both cases, it is assumed that all divertor plates in one module are inspected and one of them found damaged is exchanged. Assuming that the operation time is 12 hours a day, it takes 4 days for these operation in both cases. It takes more than a half of this time for inspection. If it is possible to specify an unusual cooling piping system by leakage inspection and to limit to range for inspection, the inspection time may be shortened by that much.

In cases 3 and 4, it is supposed that one module containing a damaged plate is not known. It is also supposed that all divertor plates in the reactor are inspected and one plate found damaged is exchanged. In case 3 it takes 22 days for operation by using a stationary manipulator. On the other hand in case 4 it takes 11 days for operation by using a travelling manipulator, because the exchanging operation of manipulator and NBI is required only one time.

In cases 5 and 6, it is supposed that all of the divertor plates are regularly exchanged. In t hese cases no detail inspection is required and an only visual inspection is made. Afterwards all divertor plates are exchanged, and lastly a visual inspection is carried on. In case 5, it takes 90 days for operation by using a s tationary type manipulator. On the other hand, in case 6 it takes 83 days for operation by using a travelling type manipulator. When 6 stationary type manipulators are simultaneously operated, it is expected that the whole operation time may be reduced by 1/6 i.e. to 15 days.

12.4 Maintenance Devices

12.4.1 Stationary type manipulator

Repair and maintenance in the reactor vessel can be performed by using this manipulator without disassembling the reactor into modules. This manipulator is installed instead of the NBI and the operation can be performed by inserting the arm from a neutral beam injector port provided in the outer blanket. This manipulator is operated restrictedly in the area of one module, because the manipulator cannot travel.

This manipulator is shown in Fig. 12.4.1 and Fig. 12.4.2. In order to operate in the divertor chamber, it is necessary that the wrist is always

vertical to the arm, the degree of freedom of the manipulator is required for 10. There is a chuck on the hand of the manipulator in order to connect various kinds of operating devices.

12.4.2 Travelling type manipulator

The manipulator shown in Fig. 12.4.3 travels on the rail laid inside the divertor room and moves to each modules to perform operation. As shown in Fig. 12.4.4, one NBI module is removed, a lifting frame folded double is inserted into a vacuum vessel, and slowly opened to be set to the rail. Next, a small-sized manipulator is carried in and mounted on the lifting frame. This small-sized manipulator receives the divertor plate and operating equipments carried in from the outside of the vessel and moves in the vessel to perform operation. Figure 12.4.5 shows a conveying device which receives devices from this manipulator and delivers them to it.

12.4.3 Carrier

A carrier is used to temporarily support the divertor plate so that the divertor plate may not fall down during exchanging divertor plates. And it is used to transport the plate. Functions required for the carrier are as follows:

(1) Coupling to a divertor plate
(2) Temporary fastening to a hanger and removal
(3) Connection and separation of a manipulator arm
(4) Positioning to an adjacent divertor plate

A carrier that fuflis these functions is shown in Figs. 12.4.6 and 12.4.7. It is provided with two large hooks to fix a divertor plate, four small hooks to be hung on the lateral bar of a hanger and a chuck to be connected to the manipulator. The frame of the carrier is slightly wider than the width of the divertor plate, in order to perform positioning in the adjacent divertor plate.

12.4.4 Automatic cutting and welding devices for piping

Figure 12.4.9 shows the concept of automatic cutting device to remove the coolant piping and hanger from the header of divertor and welding device to connect them to the header. One bend axis is necessary to this device in order to be correctly set to the direction of piping.

A structure of a pipe cutting machine is shown in Fig. 12.4.19.

12.4.5 Inspection equipment

A visual device is shown in Fig. 12.4.10. (a) indicates a visual head for visual inspection. ITV camera and lighting are designed to have the freedom of motions as turning and bending (b) indicates an visual observation header which inspects an object with magnification provided with a lighting lamp. (c) indicates a fiberscope which inspects details. All of them are connected to the hand of the manipulator. For inspecting pinholes and cracks, it is necessary to apply non-destructive inspections shown as follows.

(1) Ultrasonic examination
(2) Eddy current examination
(3) Liquid penetrating examination
(4) Electric resisting examination
(5) Radiographic examination

Methods (1) and (2) are most suitable to automatic detection. (3) is liquid penetrating examination, because of handling an organic solvent, is difficult to be made to automation, and it has a problem that visual inspection devices must be provided to obtain detection resuts. Method (4) cannot give a higher reliability of data. The Radiographic examination of (5) has a problem of making the X ray source smaller and of how to prevent the exposure of film by radiation from the surroundings.

12.4.6 Supervisory system

This device is used under radioactive environments, so no man is allowed to come into the operation position. Therefore, it is required that the device can be manipulated by a remote operation or automatic operation. In order to perform operation without supervisory by operators, it is necessary to prepare sufficiently appropriate supervisory systems so that the following procedures may be made such as understanding the situations i.e. the condition of operating area, works of manipulator, automatic devices, motions of cables and other environmental conditions. It is necessary that pertinent procedures can be taken immediately so that damage may not become larger when emergent situations happen.

A supervisory using ITV is the most effective means. The conceptual status of supervisory device using ITV is shown in Fig. 12.4.11.

12.4.7 Control device

Control using a computer is indispensable to operate a manipulator having many degrees of freedom and sensory functions as this device. Control device roughly consists of a control panel, computers, interfaces and power supply. A operator gives a command to the control device and gets necessary informations from the control device through the control panel. Taking informations, givening instructions and data processing are made by the computers. Other devices such as manipulator, operation devices and sensors are connected to the control device through the interface. It is necessary that the computer has functions such as a conversion of coordinate from the specific coordinate of the manipulator to the cylindrical coordinate of the reactor and its reverse conversion.

An example of operation method of the stationary type manipulator is shown in Fig. 12.4.12. Operation is performed by operating two control levers provided in the control panel. The position of sealing point of the arm and wrist i.e. 4 degrees of freedom of front and rear, right and left, up and down and rotation around the vertical axis, are operated by the control lever for operating arm. The operational direction of the control lever is almost same direction of the movement of the arm.

The composition of the control lever for the wrist is also same as that for the arm. The wrist and control lever are designed to move along polar coordinate system. On the control panel, the motions of manipulators are projected by supervisory devices. An operator can control as looking at them. Another image projects the situation of manipulator axis by a CRT display.

12.5 Design Problems

(1) Influence of gamma ray

Maintenance machines and tools are exposed to strong Gamma ray, so deterioration and change in quality may take place. In the ones subject to the large influence of Gamma ray, optical systems of TV camera, especially glass gets stained and so its transparence will become decrease.

In the glass having a long optical path such as fiberscope, its influence is remarkable. When a semiconductor part is exposed to radiant ray, it produces a noise, so there is a possibility that the quality of TV image may deteriorate. At present, there is no

sufficient data, but the TV camera may become damaged in few hours.

(2) Operational space

To perform the exchanging operation of a divertor plate, sufficient spaces are required around the divertor plate. In special, it is desirable that the entrance to the divertor room has a sufficient width. However, if this width is large, neutralized particles may invade toward a plasma, so to enhance the performance of divertor, it is desirable that the width is narrow as much as possible. Accordingly, the width must be determined from the above two viewpoints.

(3) Treatment of cables

Many cables for the machinery and tools become necessary in the maintenance operation. When these cables are drawn around inside the reactor, they might be broken by twisting and entangling. In particular, the cables for working heads of the manipulator come into question. By means of signal transmission method of high multiplex capability and, furthermore, when many kind of working head use in common a signal cable provided in the arm of manipulator, the number of cables is reduced greatly. In this case, the arm structure of manipulator may become complicated and large. Figure 12.5.1 shows connection between the chuck of manipulator and a working head.

Table 12.3.1 Working Time Estimation of Divertor Plate Exchanging

Condition	Case 1	Case 2	Case 3	Case 4	Case 5	Case 6
No. of Modules for Inspection	1	1	6	6	6	6
No. of Plate for Exchange	1	1	1	1	192	192
Manipulater Type	Fixed	Travelling	Fixed	Travelling	Fixed	Travelling
Removal of NBI	4.0 hrs	4.0 hrs	4.0×6 hrs	4.0 hrs	4.0×6 hrs	4.0 hrs
Setting of Manipulator	4.5	8.0	4.5×6	8.0	4.5×6	8.0
Exchanging of Head	0.5×3	0.5×3	0.5×18	0.5×3		
Visual test	1.7	1.7	1.7×6	7.7	1.7×6	7.7
Magnified Visual Test	8.0	8.0	8.0×6	45.5		
NDI	8.0	8.0	8.0×6	45.5		
Exchanging of Divertor Plate	5.0	5.0	5.0	5.0	5.0×192	5.0×192
Removal of Manipulator	2.5	5.0	2.5×6	5.0	2.5×6	5.0
Setting of NBI	8.0	8.0	8.0×6	8.0	8.0×6	8.0
Total Hours	43.2 hrs	49.2 hrs	260 hrs	130 hrs	1084 hrs	993 hrs
Working Time (12 hr/day)	4 days	4 days	22 days	11 days	90 days	83 days

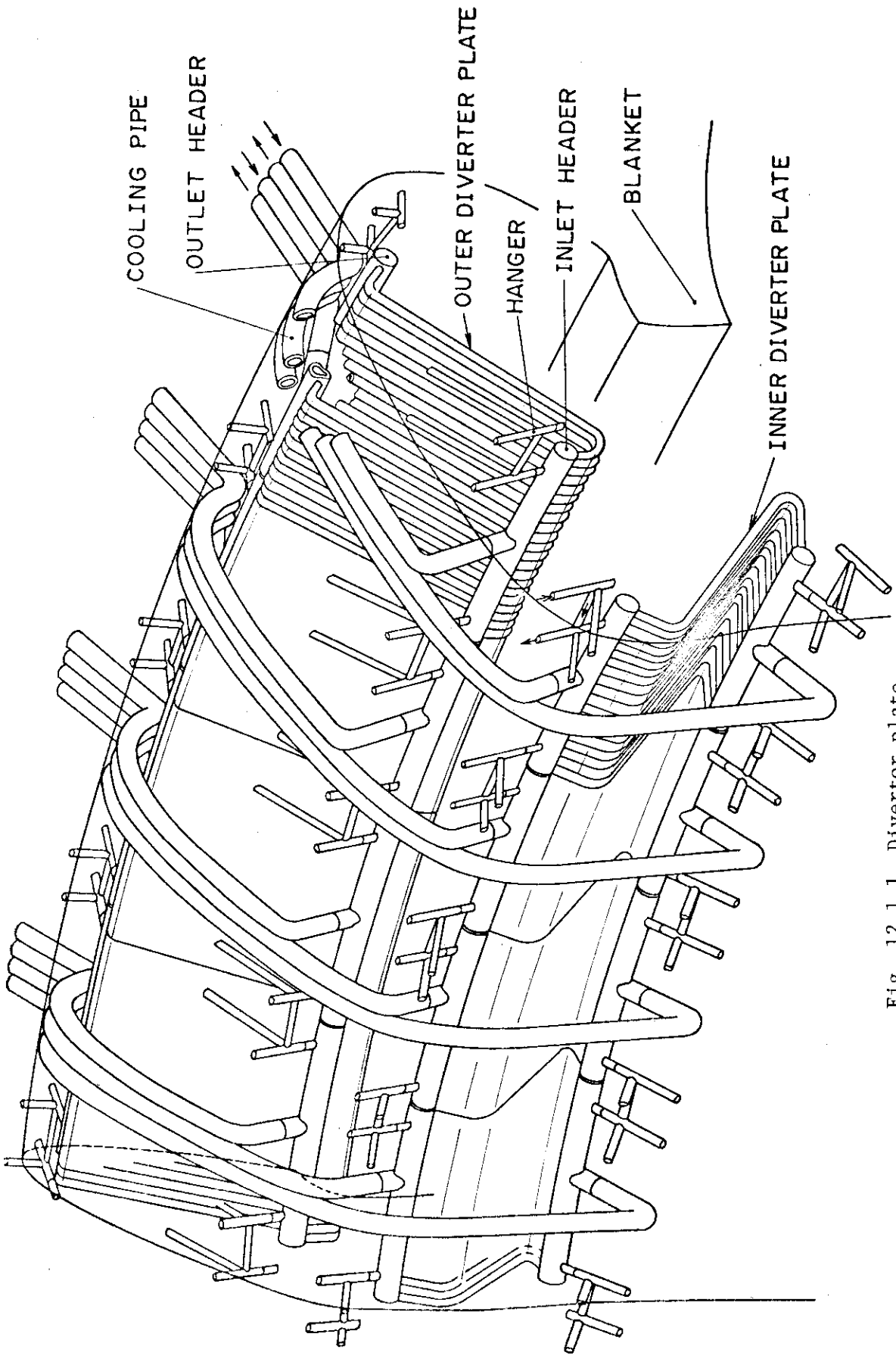

Fig. 12.1.1 Divertor plate

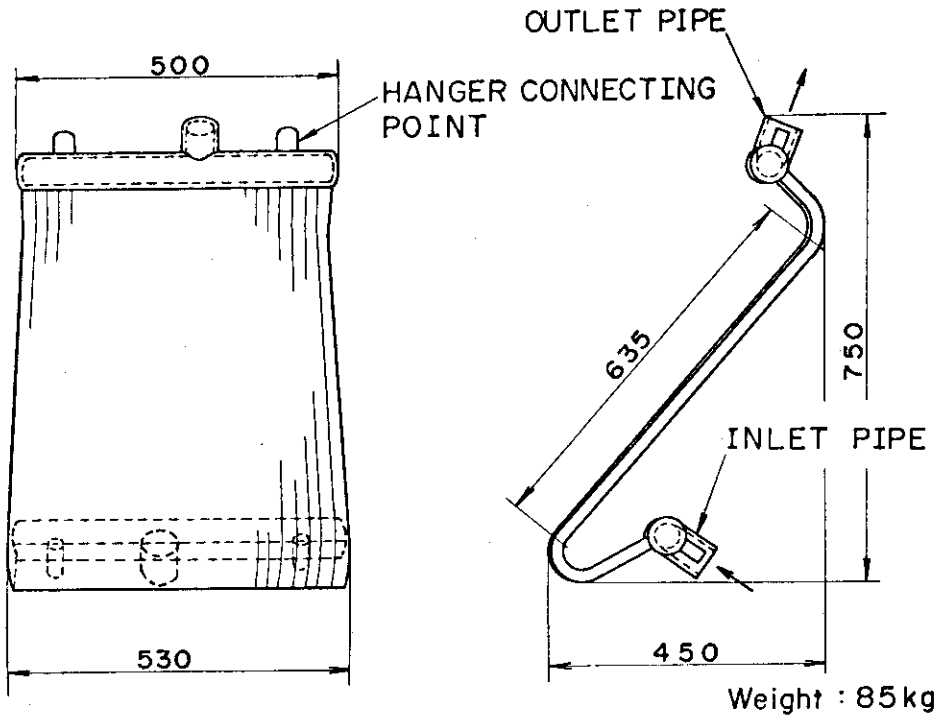

Fig. 12.1.2 Divertor plate A

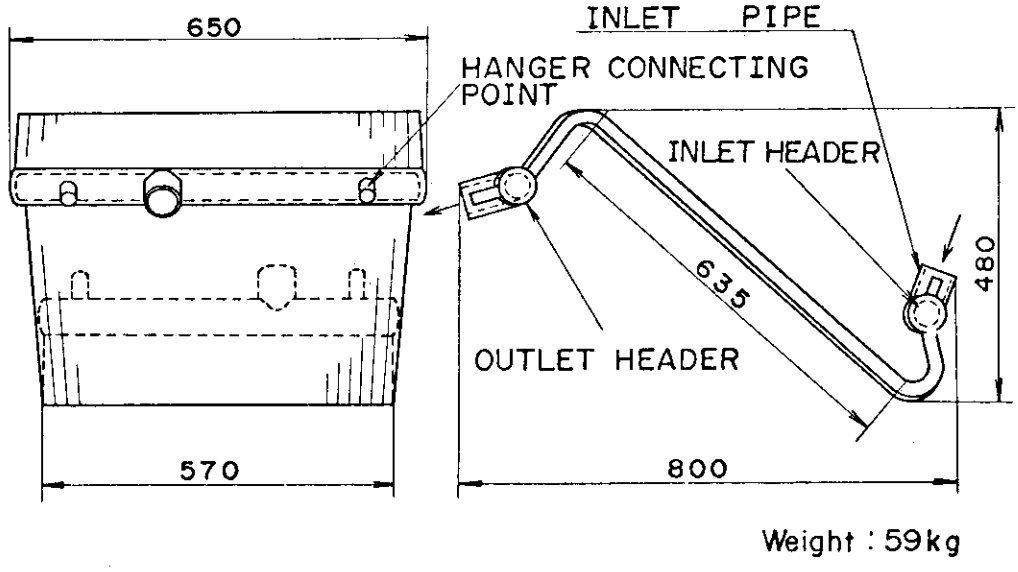

Fig. 12.1.3 Divertor plate B

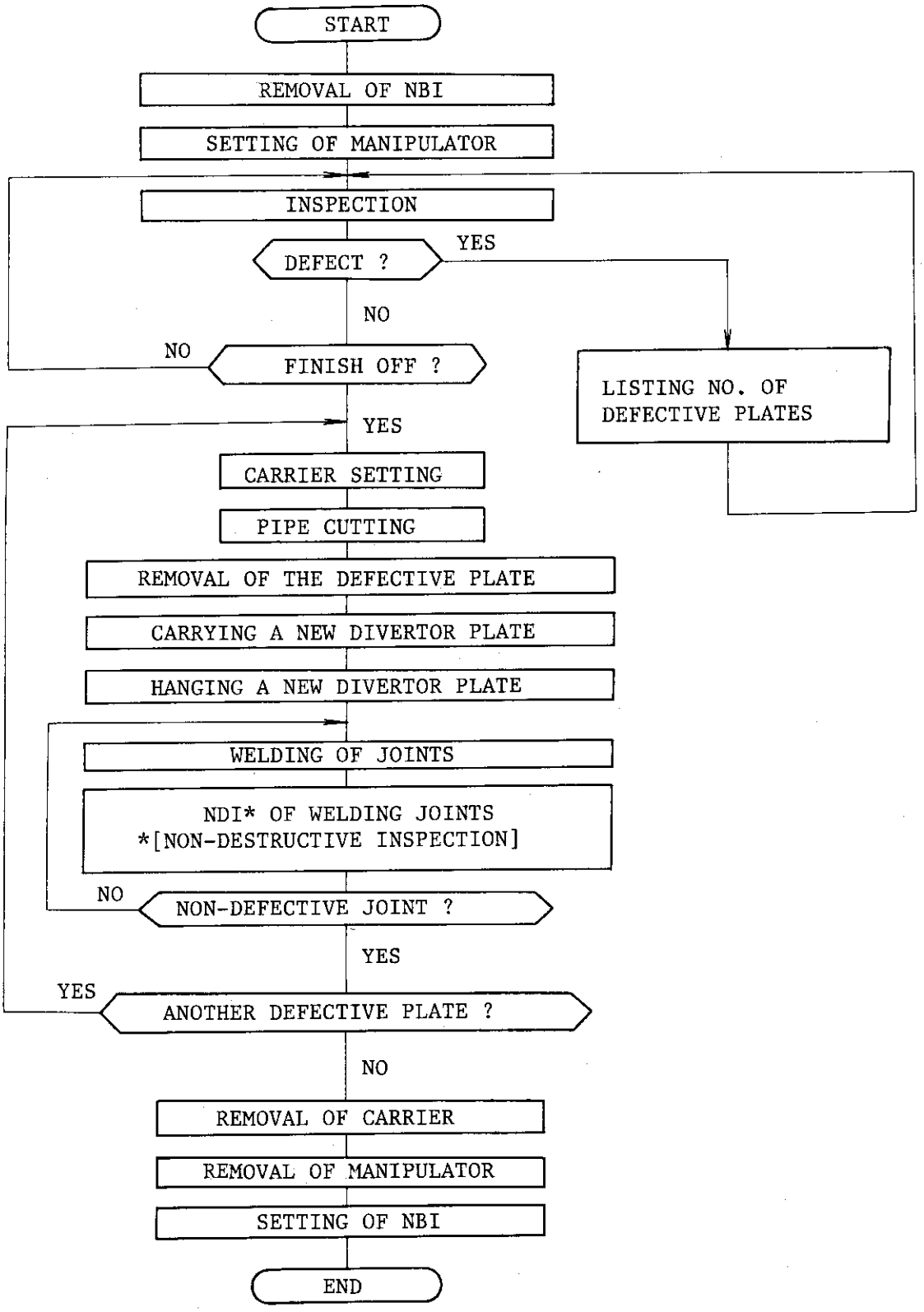

Fig. 12.3.1 DIVERTOR PLATE EXCHANGE PROCEDURE

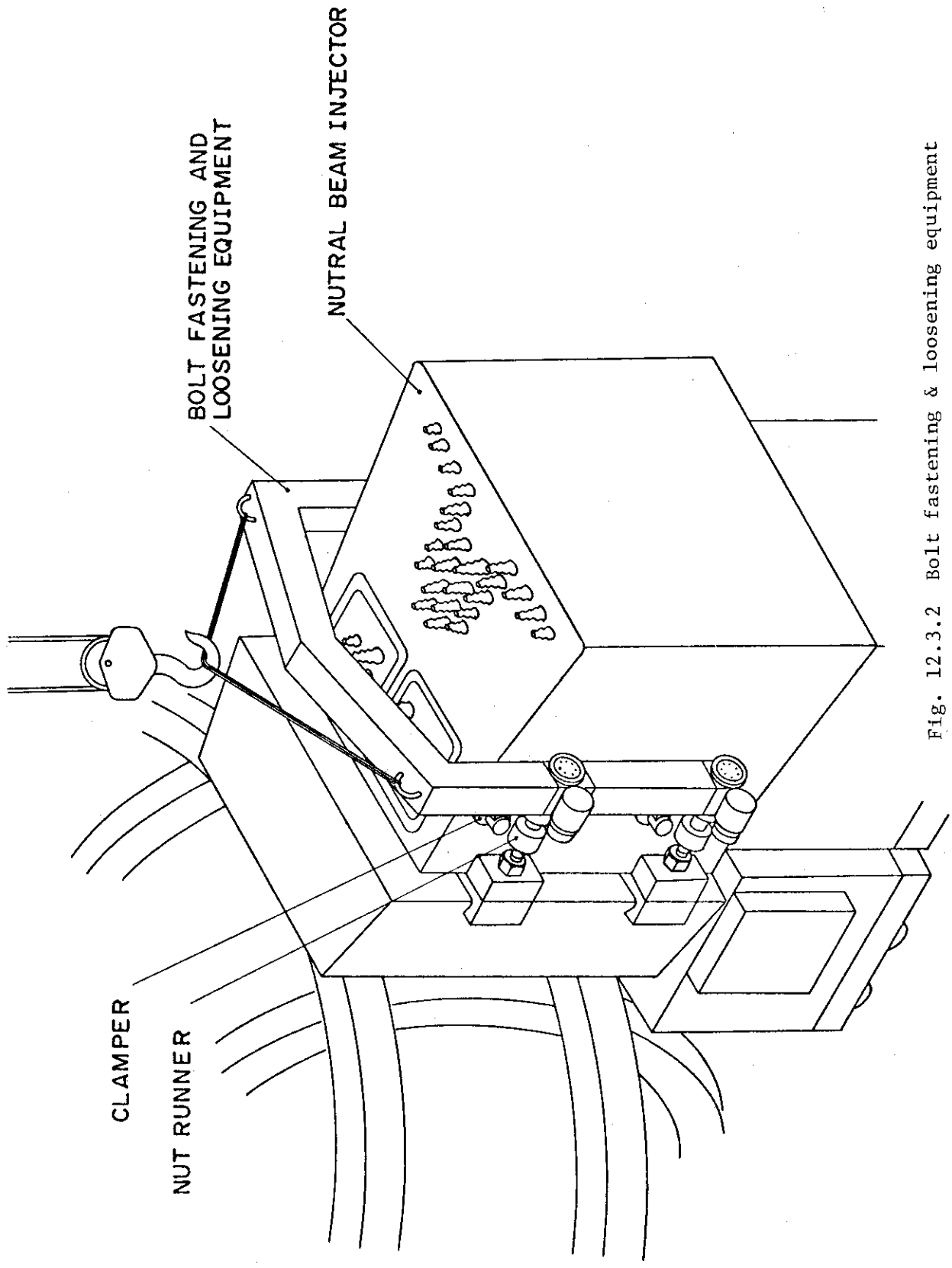

Fig. 12.3.2 Bolt fastening & loosening equipment

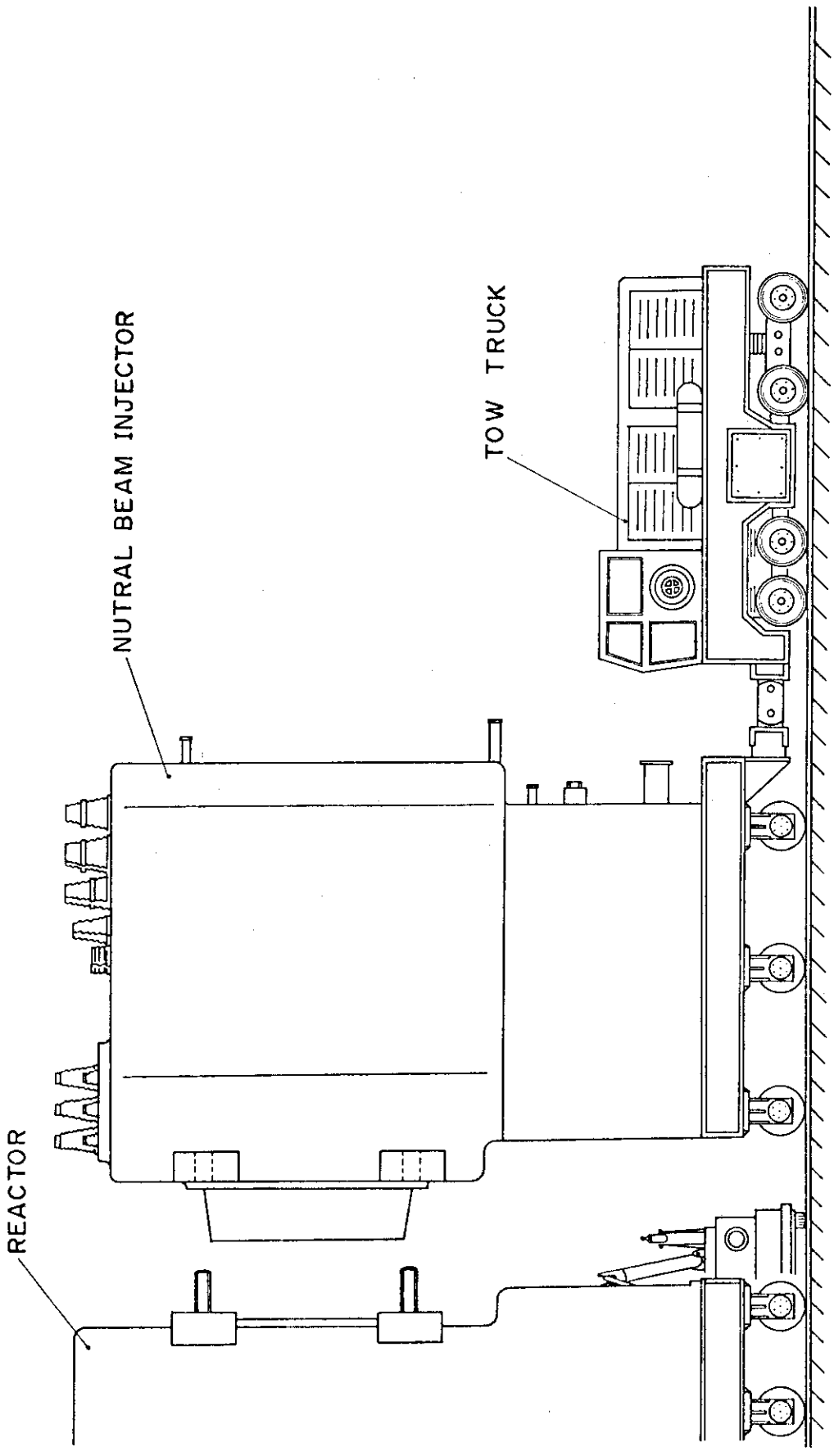

Fig. 12.3.3 Tow truck

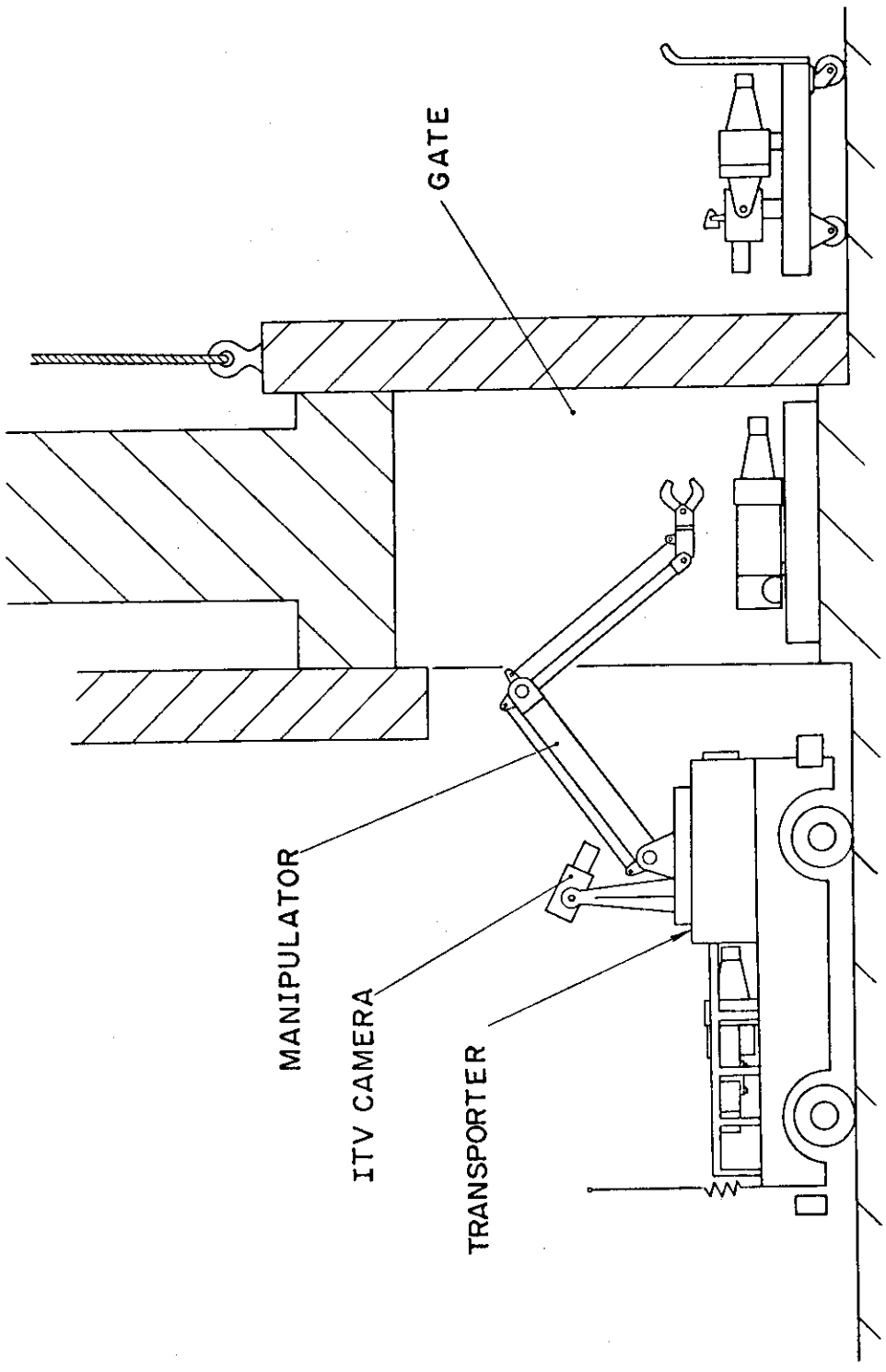

Fig. 12.3.4 Carrying of working head

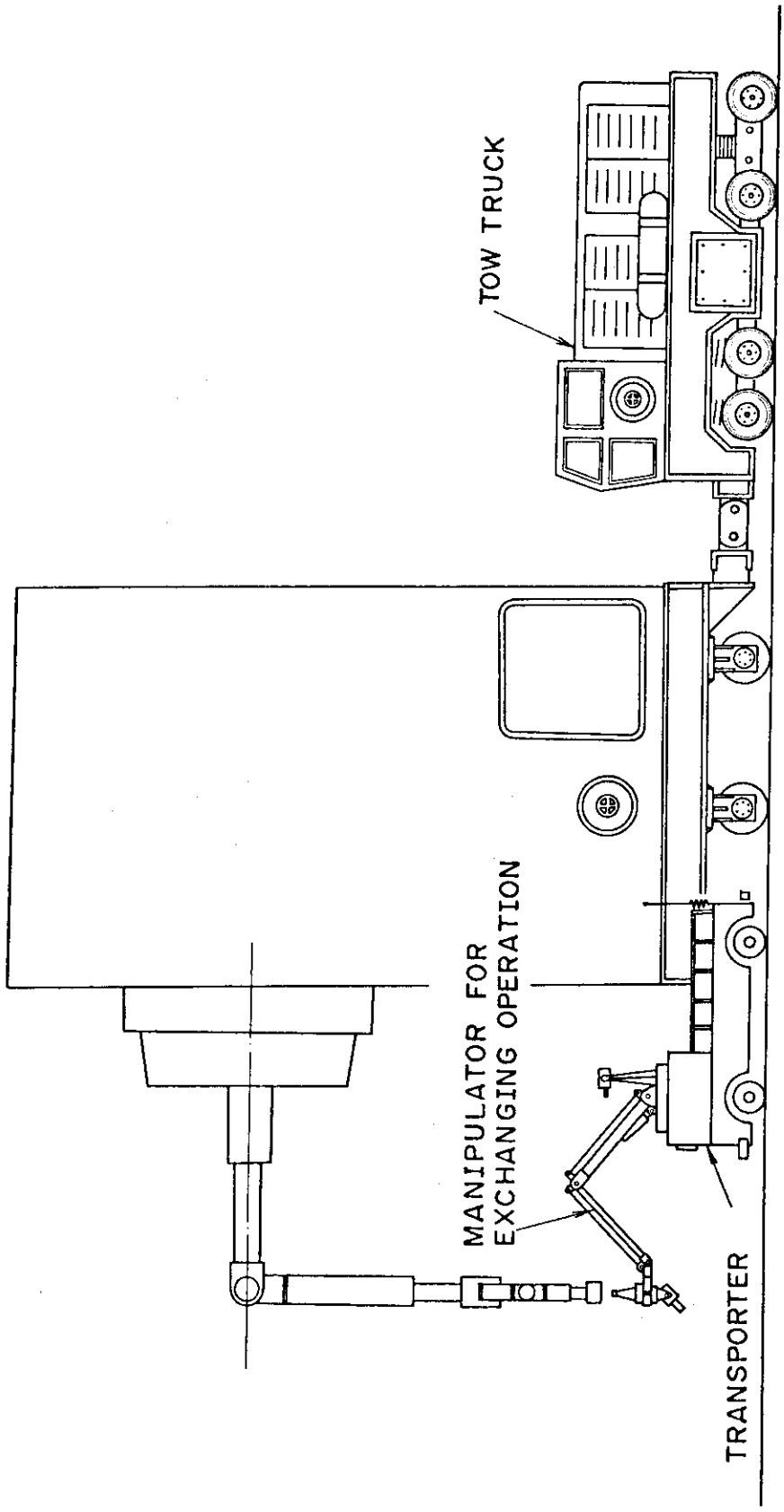

Fig. 12.3.5 Chucking of working head

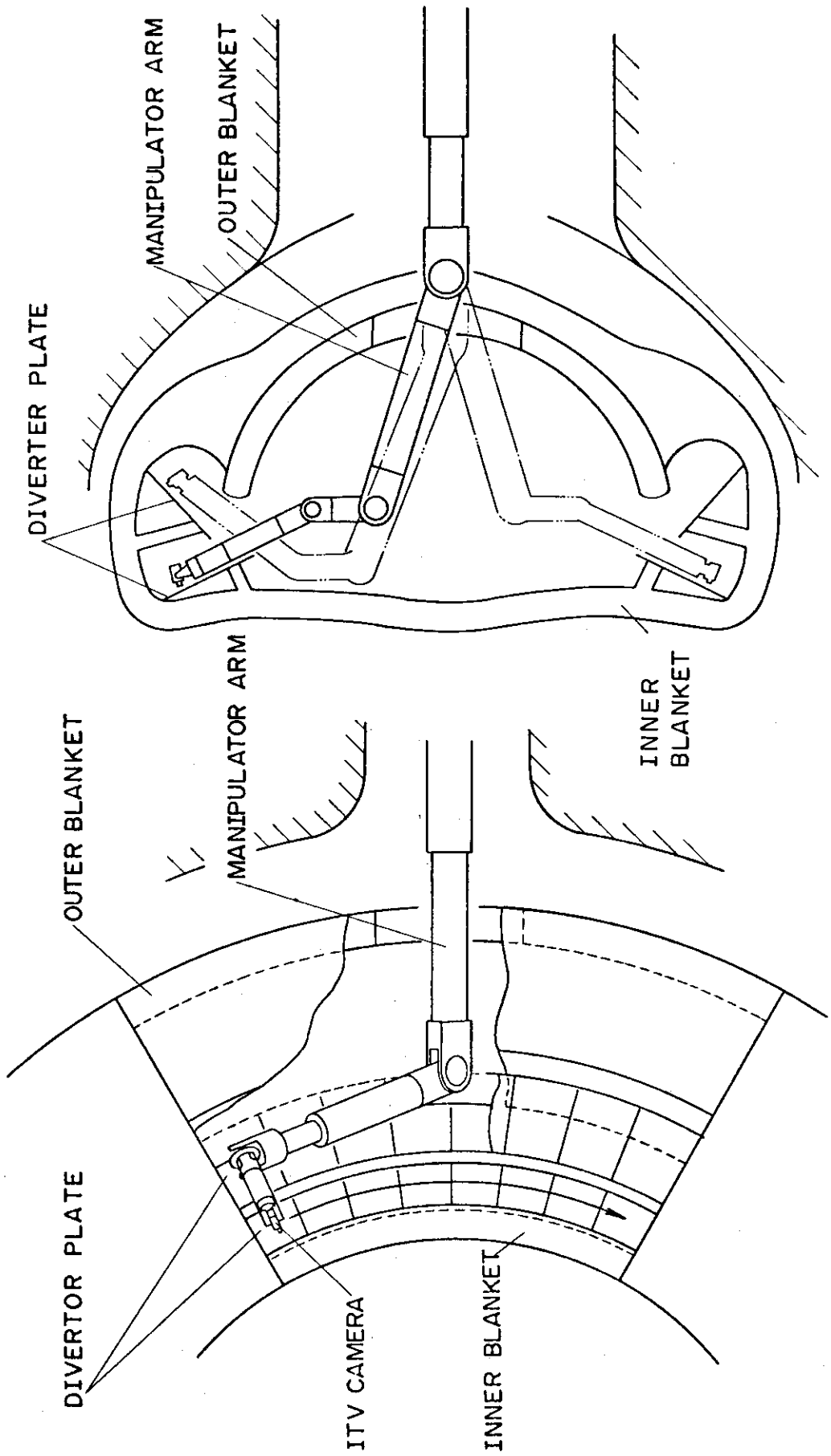

Fig. 12.3.6 Manipulator operation in reactor

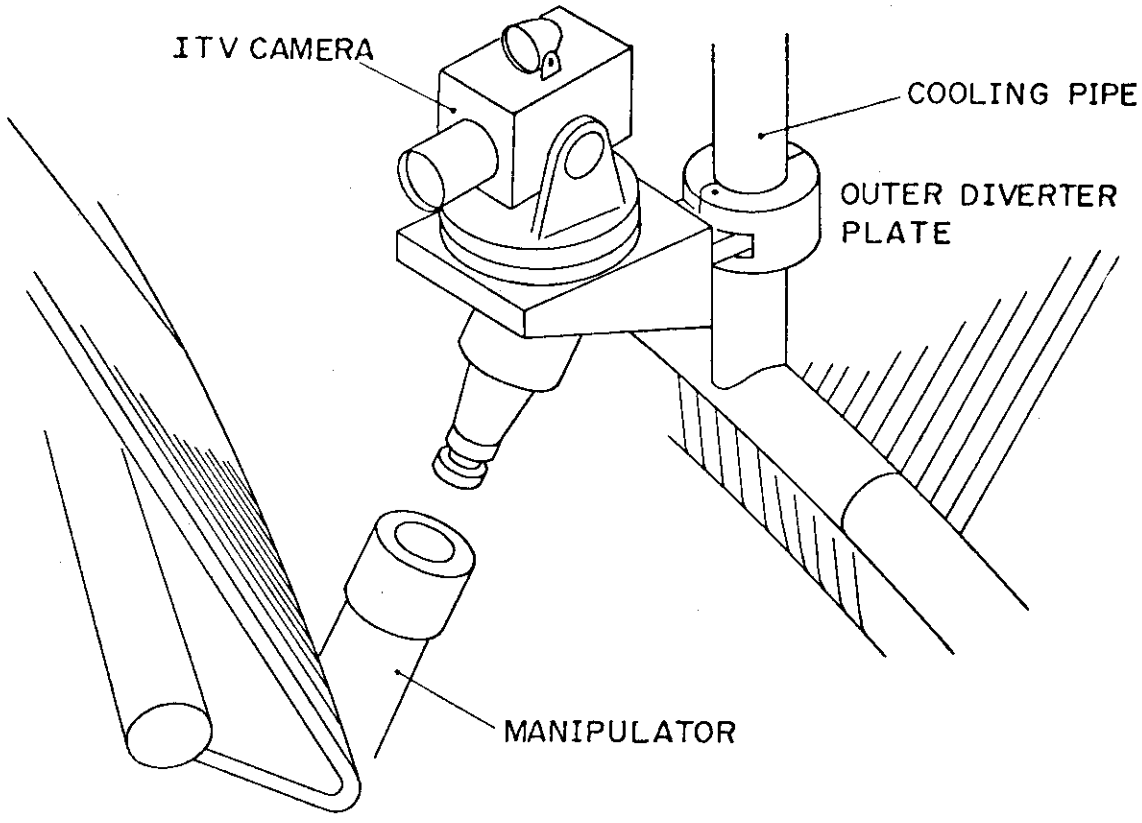

Fig. 12.3.7 Setting of ITV camera

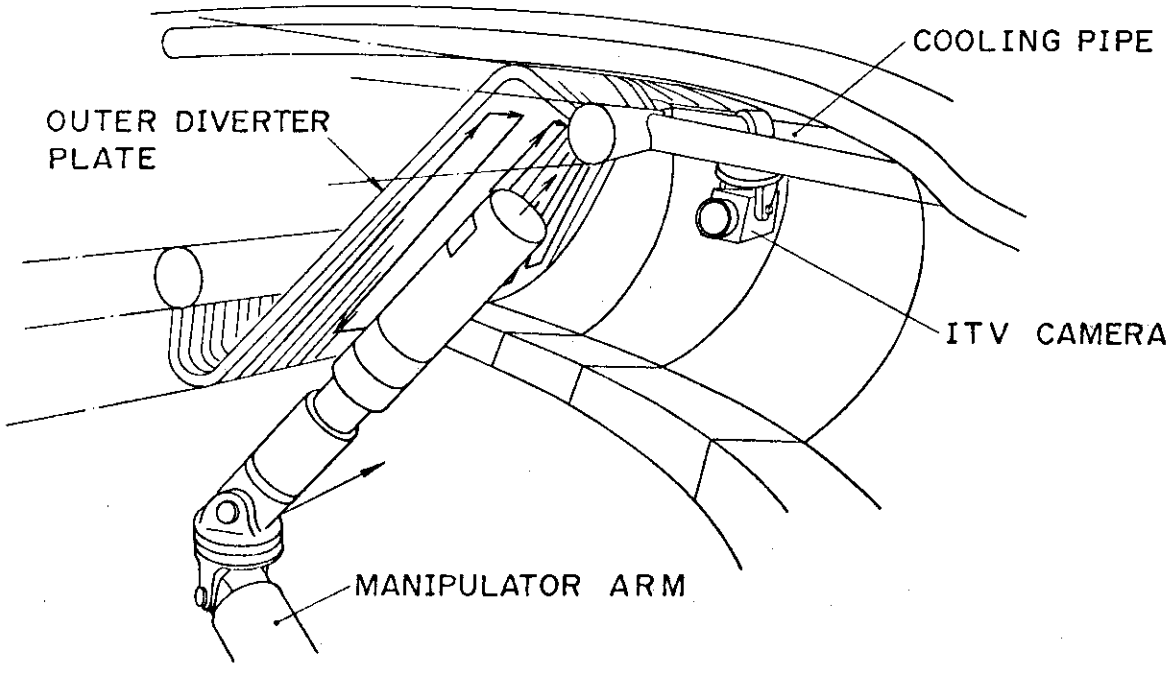

Fig. 12.3.8 Monitoring with ITV camera

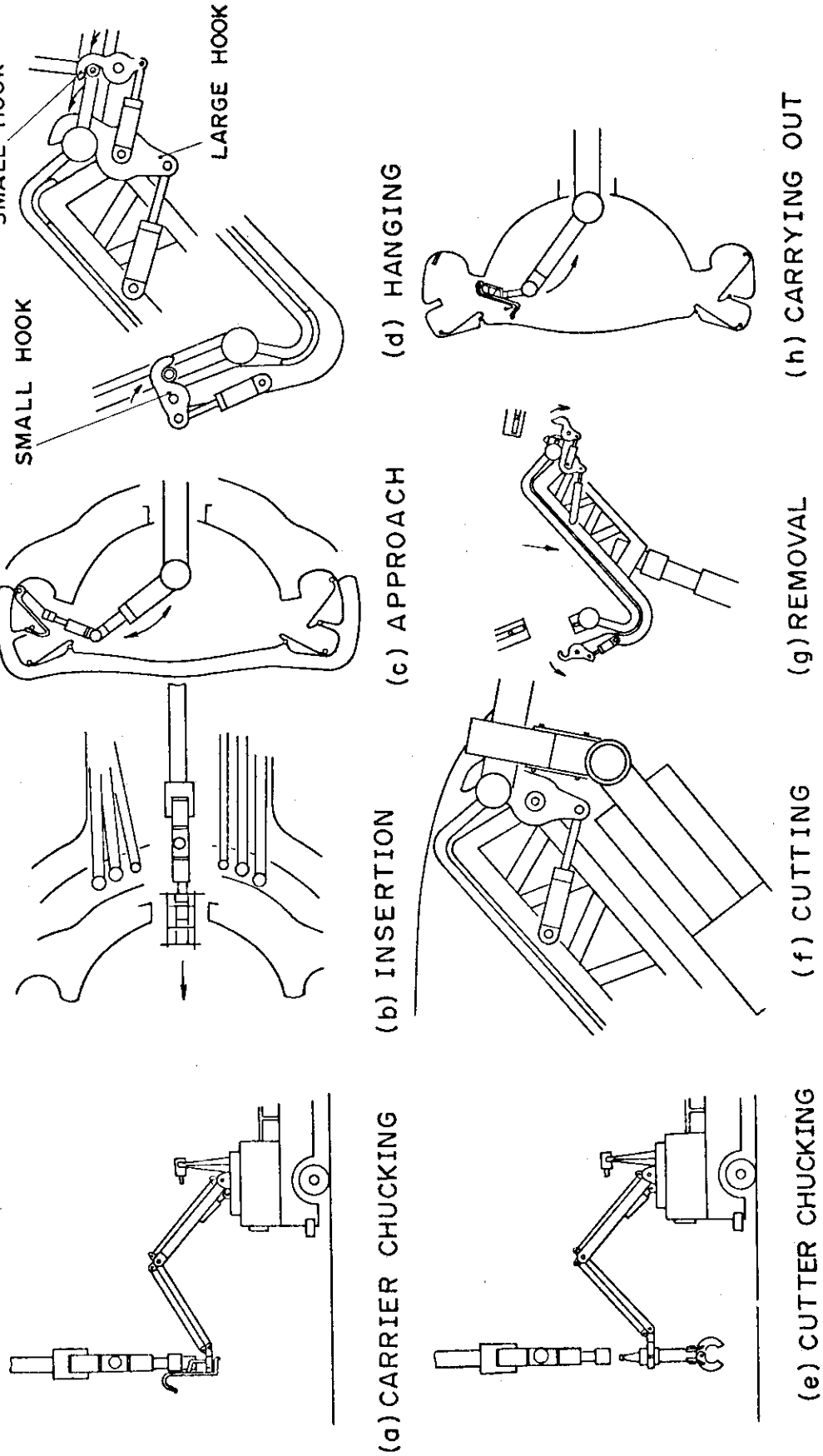

Fig. 12.3.9 Removal of divertor plate

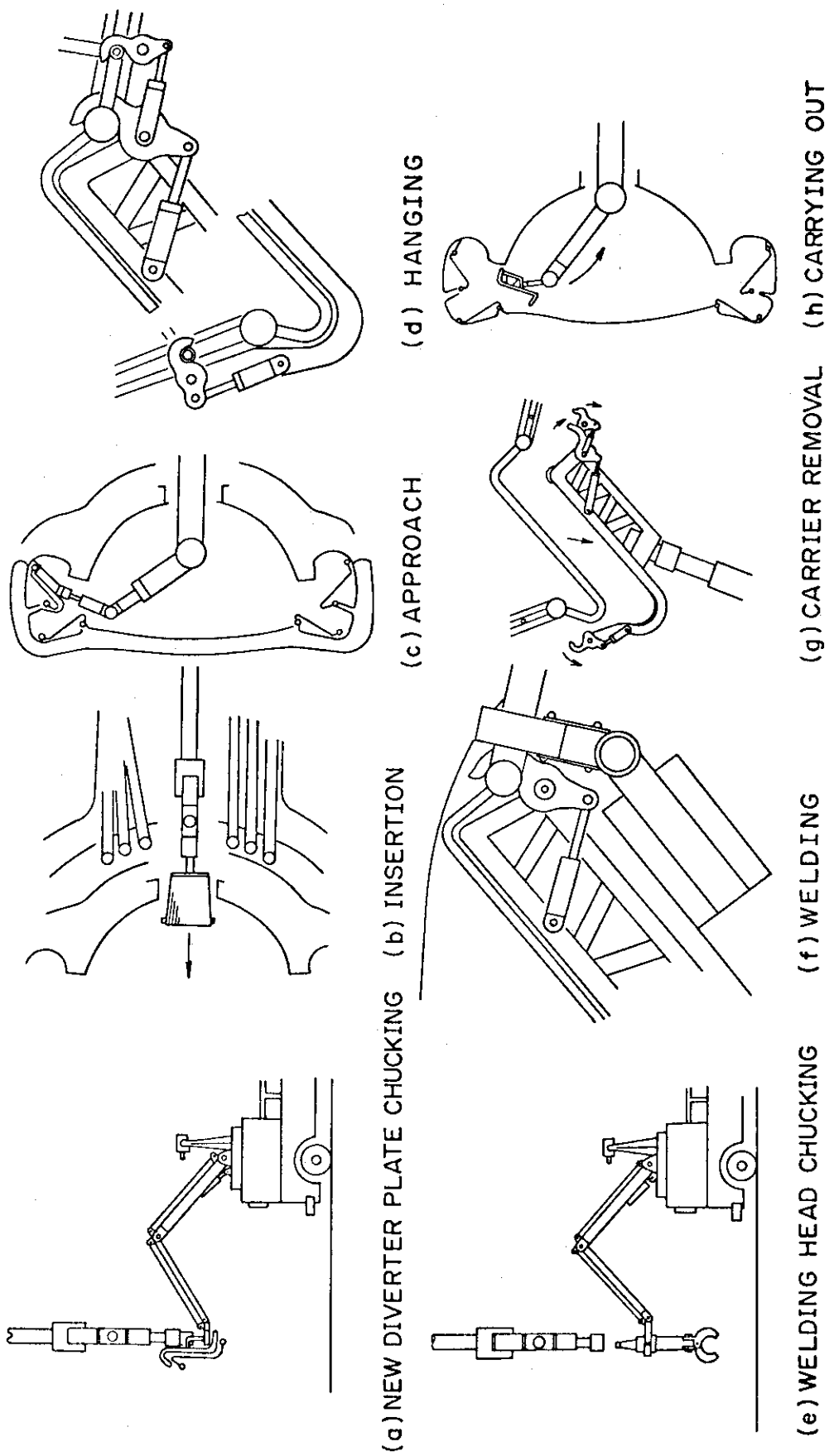

Fig. 12.3.10 Welding of new divertor plate

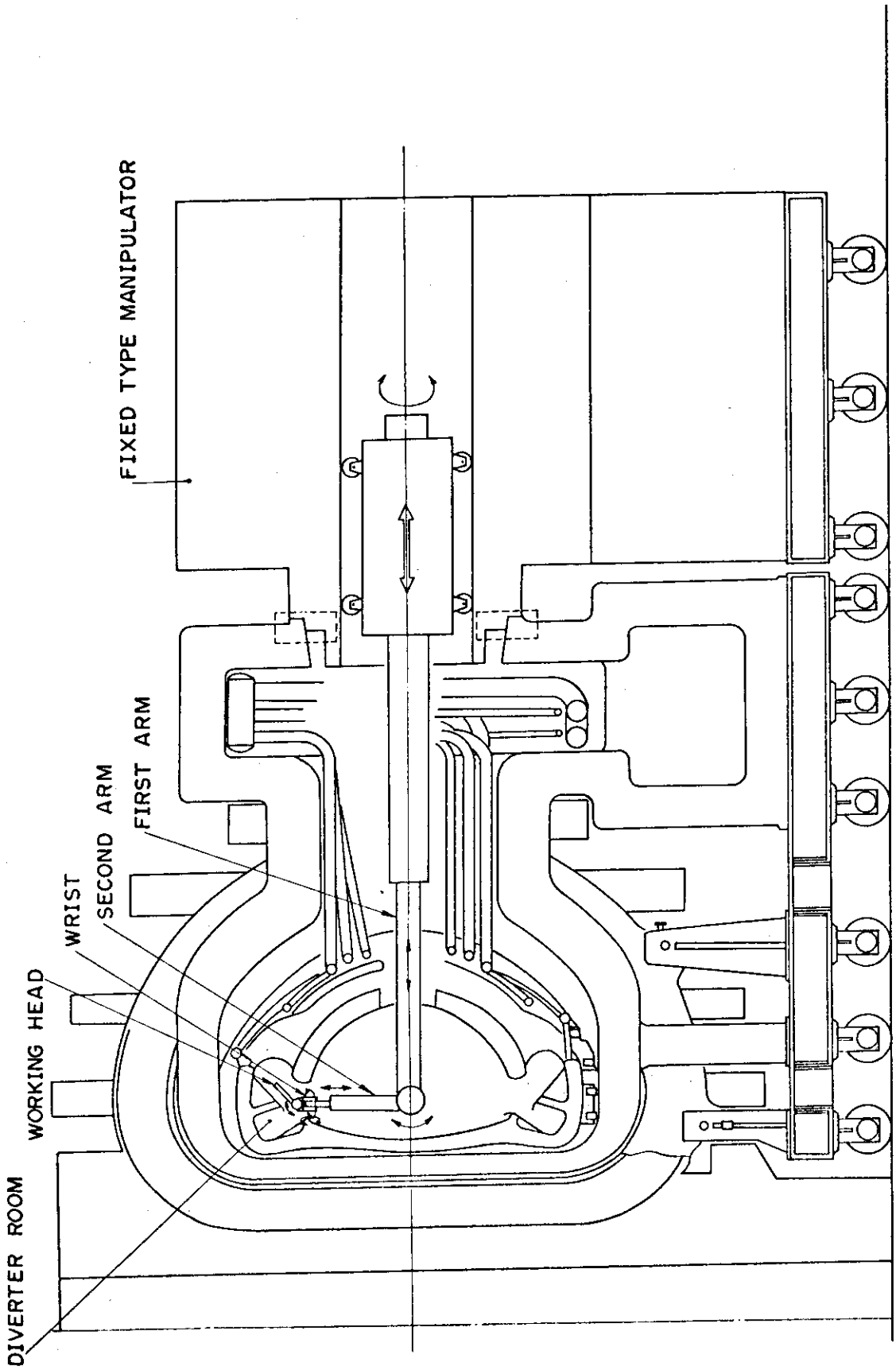

Fig. 12.4.1 Fixed type manipulator

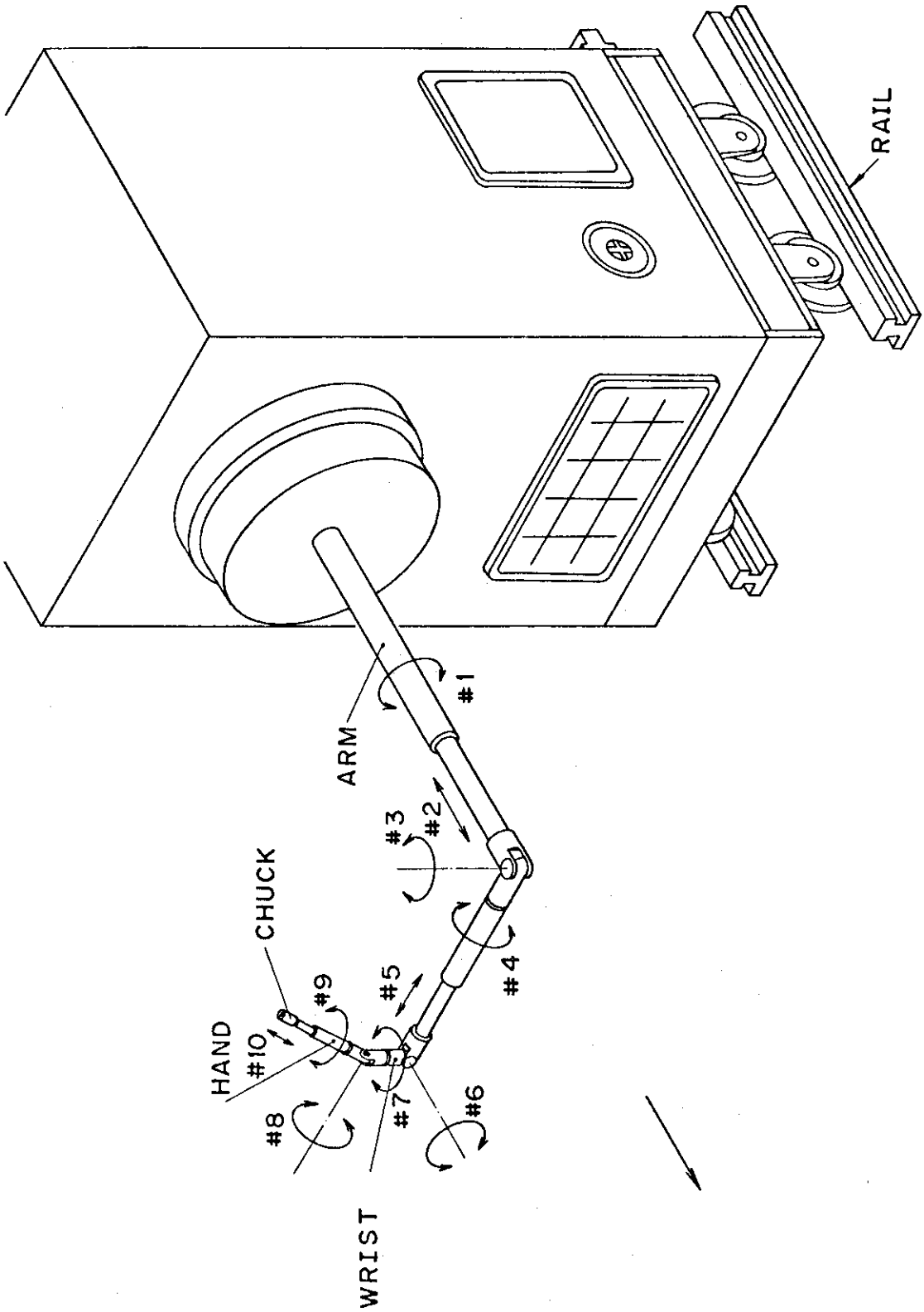

Fig. 12.4.2 Degree of freedom of motion

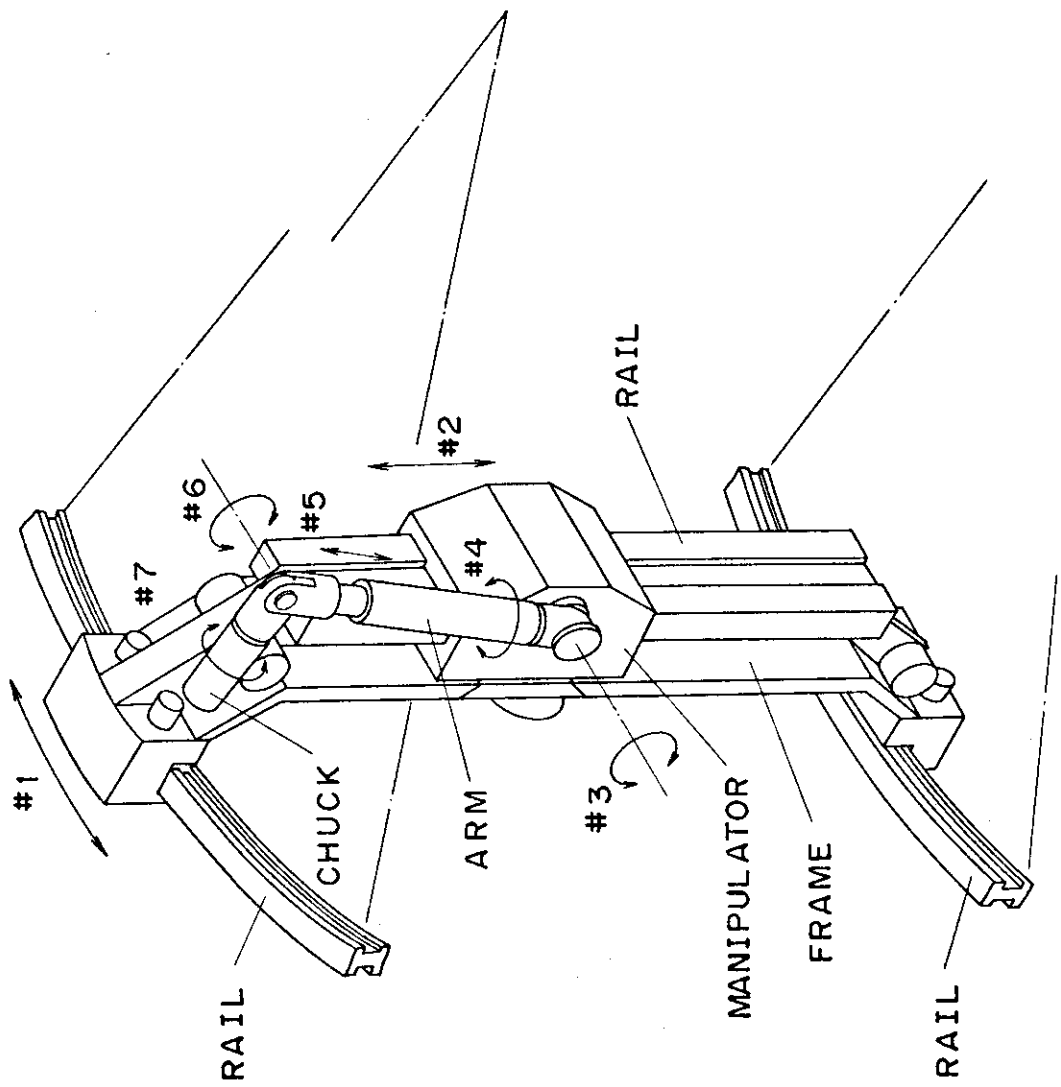

Fig. 12.4.3 Travelling type manipulator

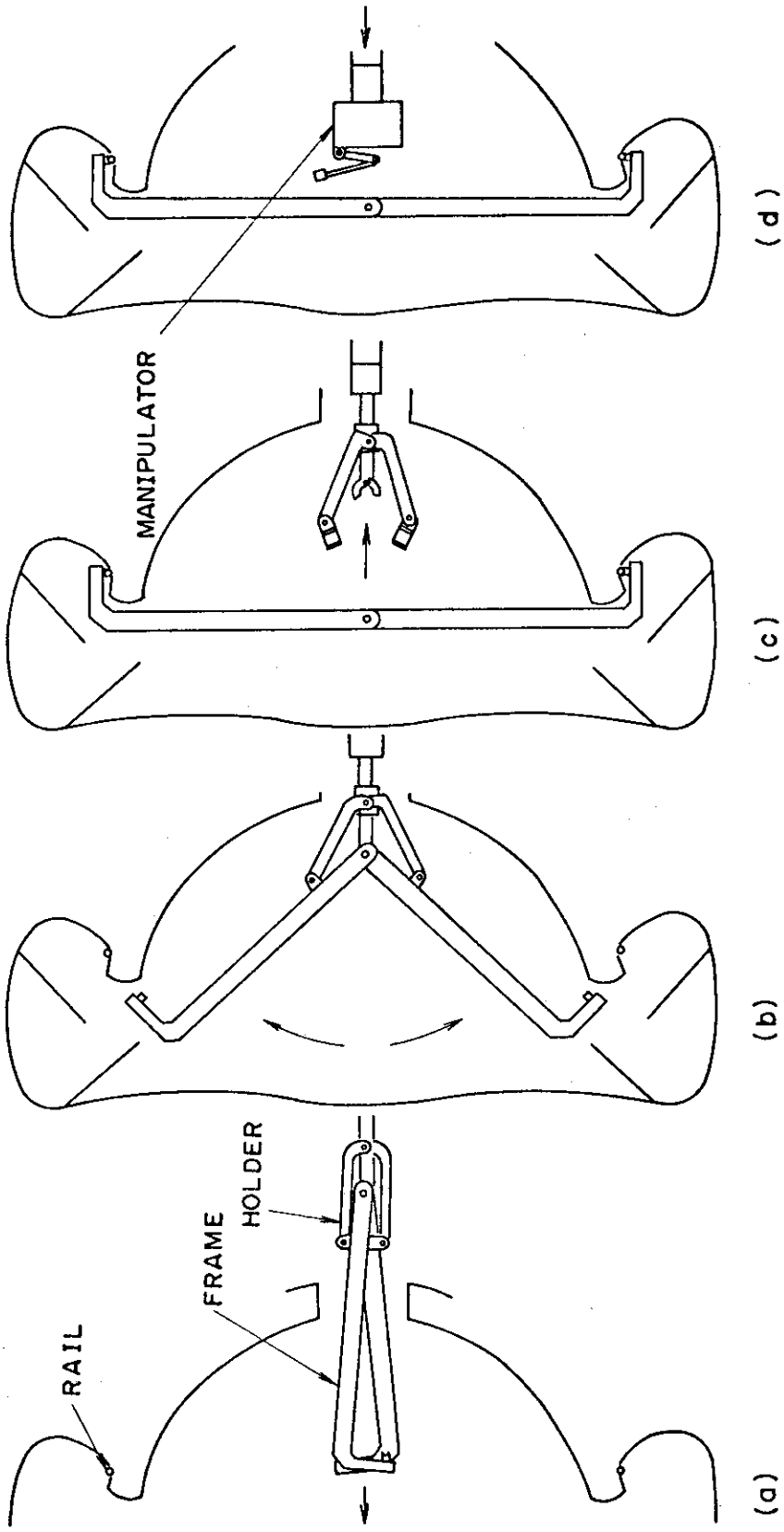

Fig. 12.4.4 Setting & working of travelling type manipulator

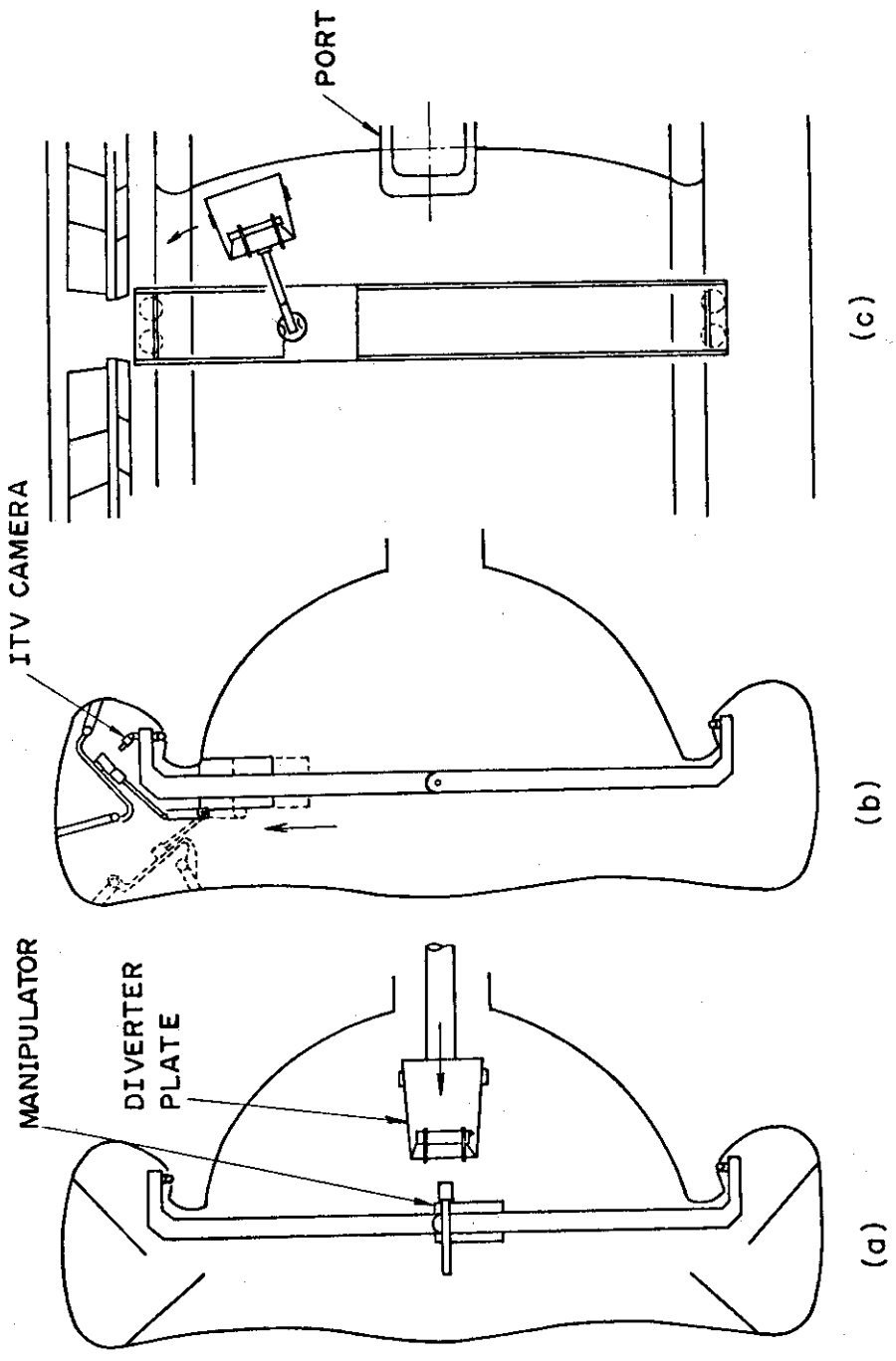

Fig. 12.4.4 Setting & working of travelling type manipulator (continued)

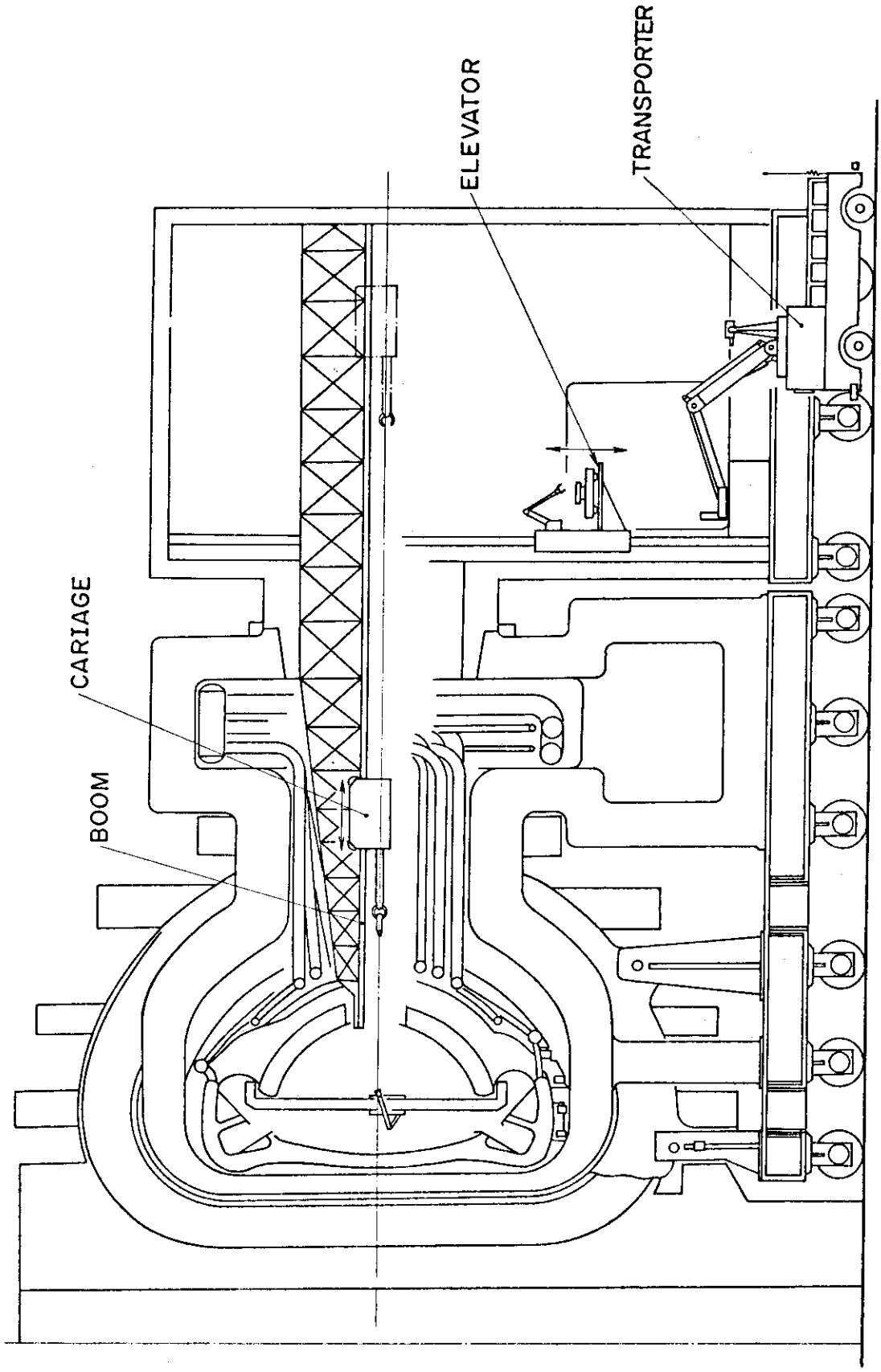

Fig. 12.4.5 Loader

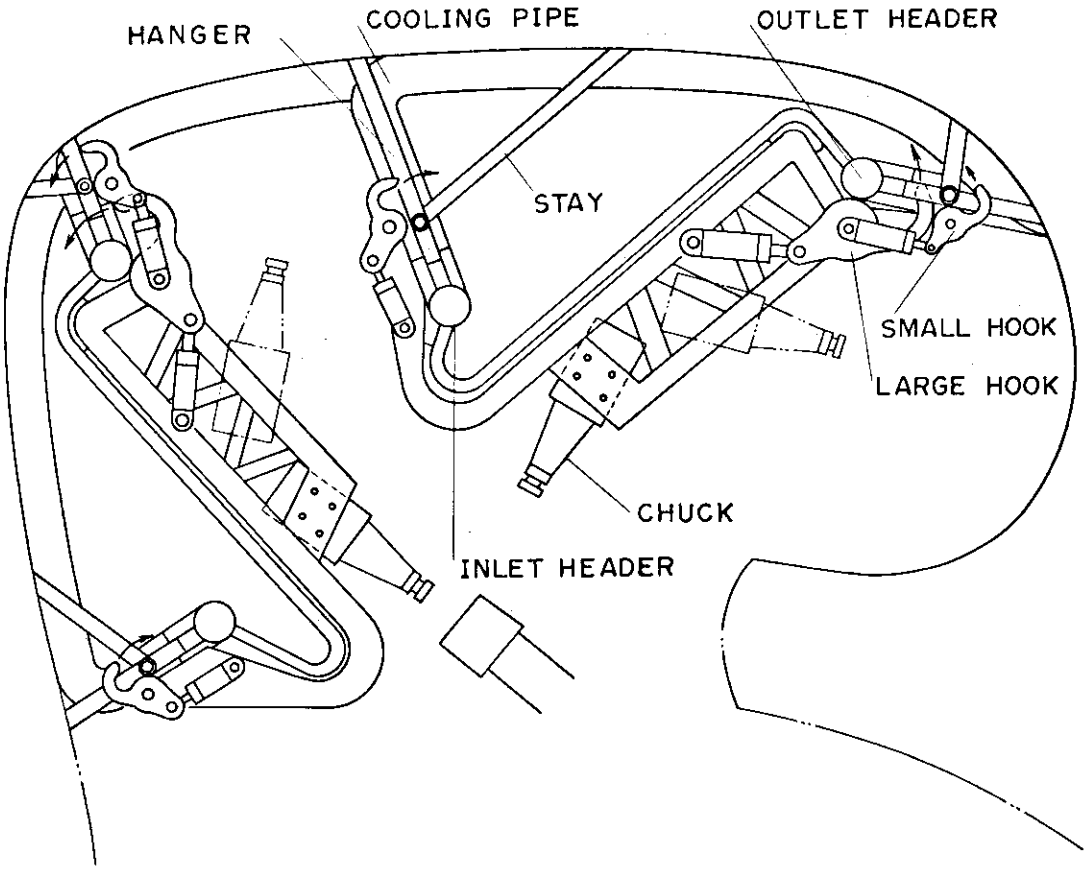

Fig. 12.4.6 Application of carrier

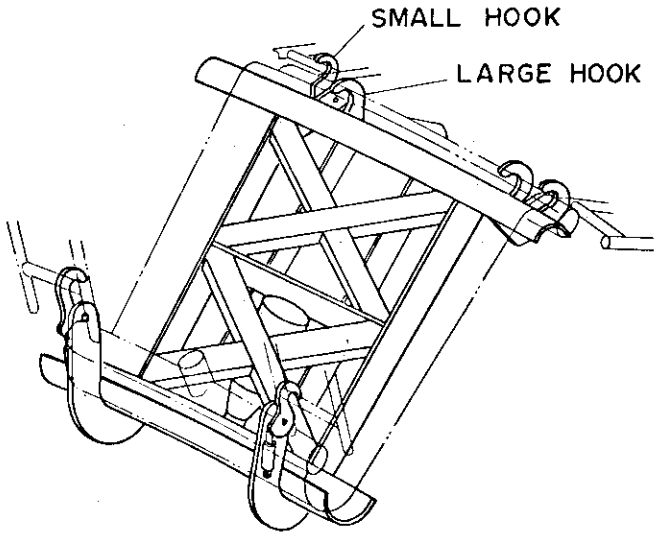

Fig. 12.4.7 Carrier

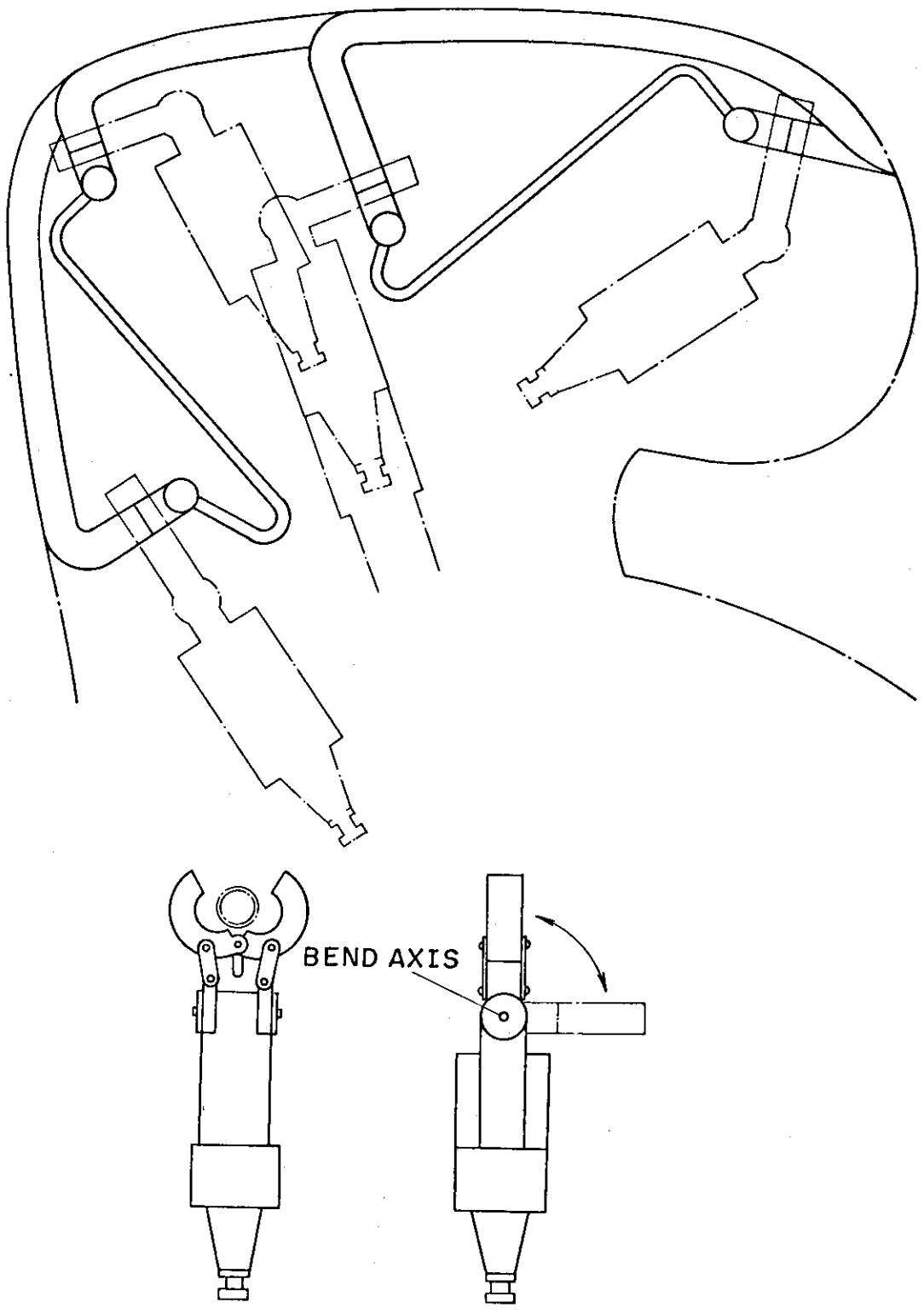

Fig. 12.4.8 Pipe cutting & welding head

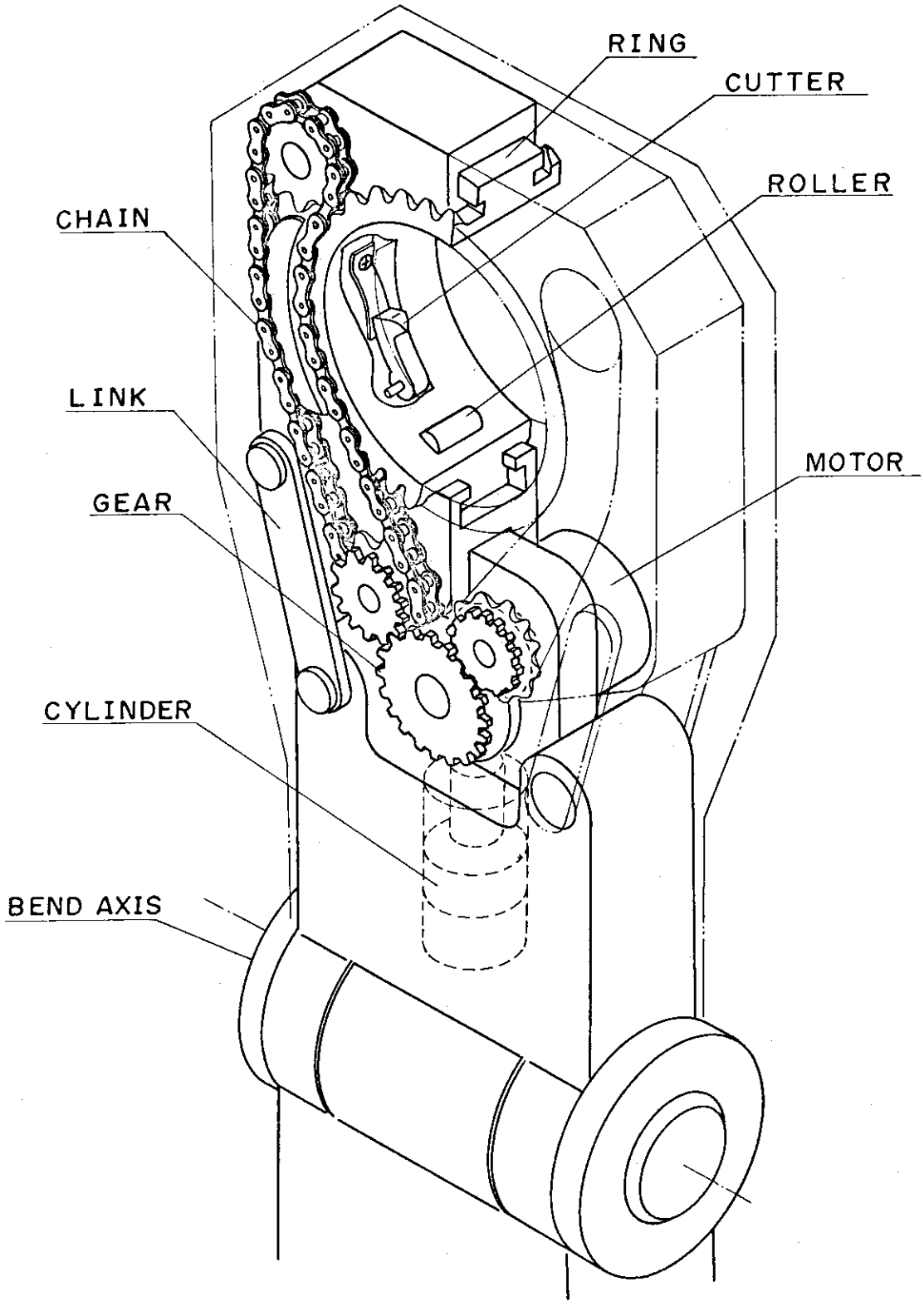

Fig. 12.4.9 Pipe cutting head

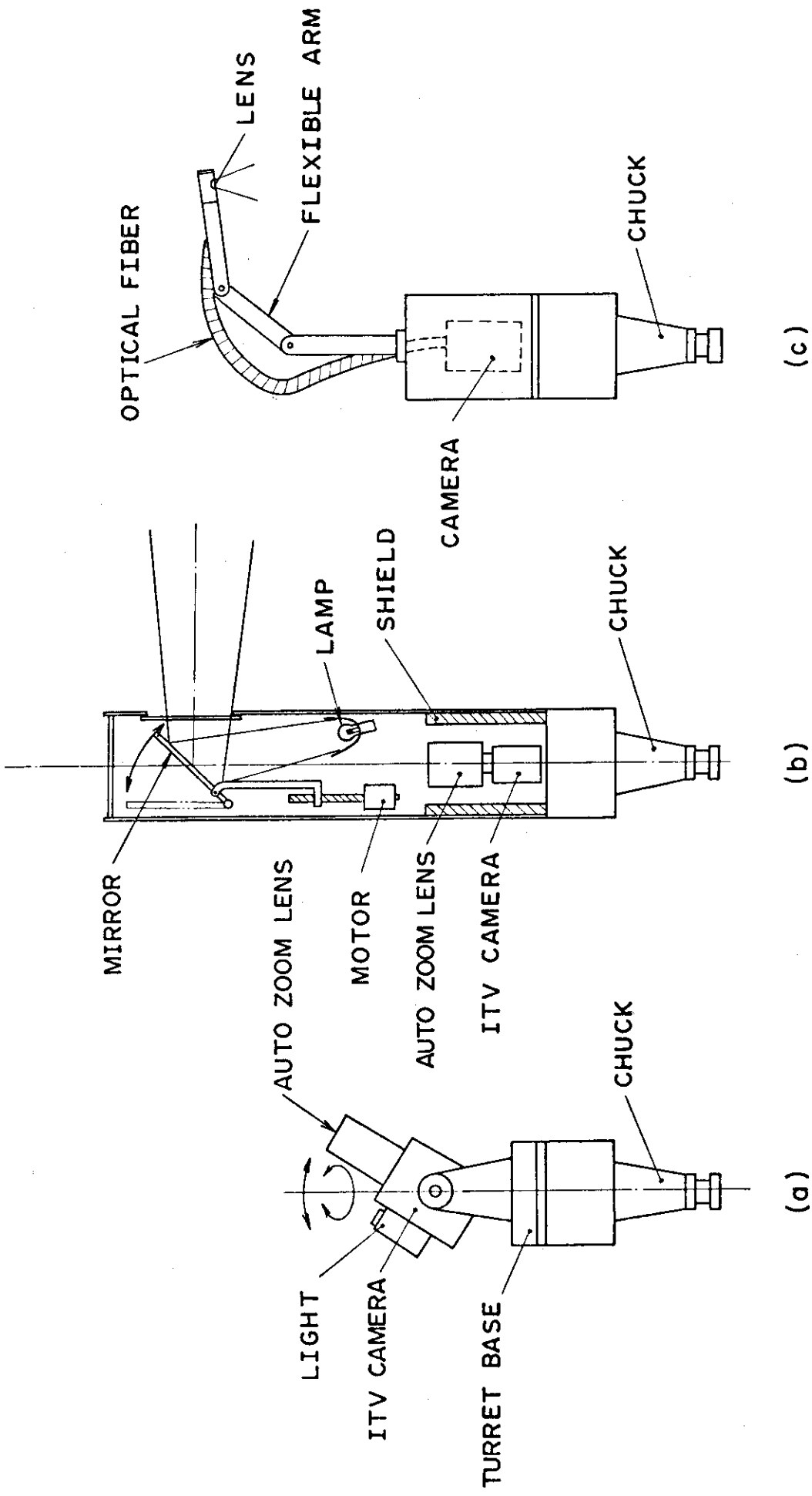

Fig. 12.4.10 Optical head

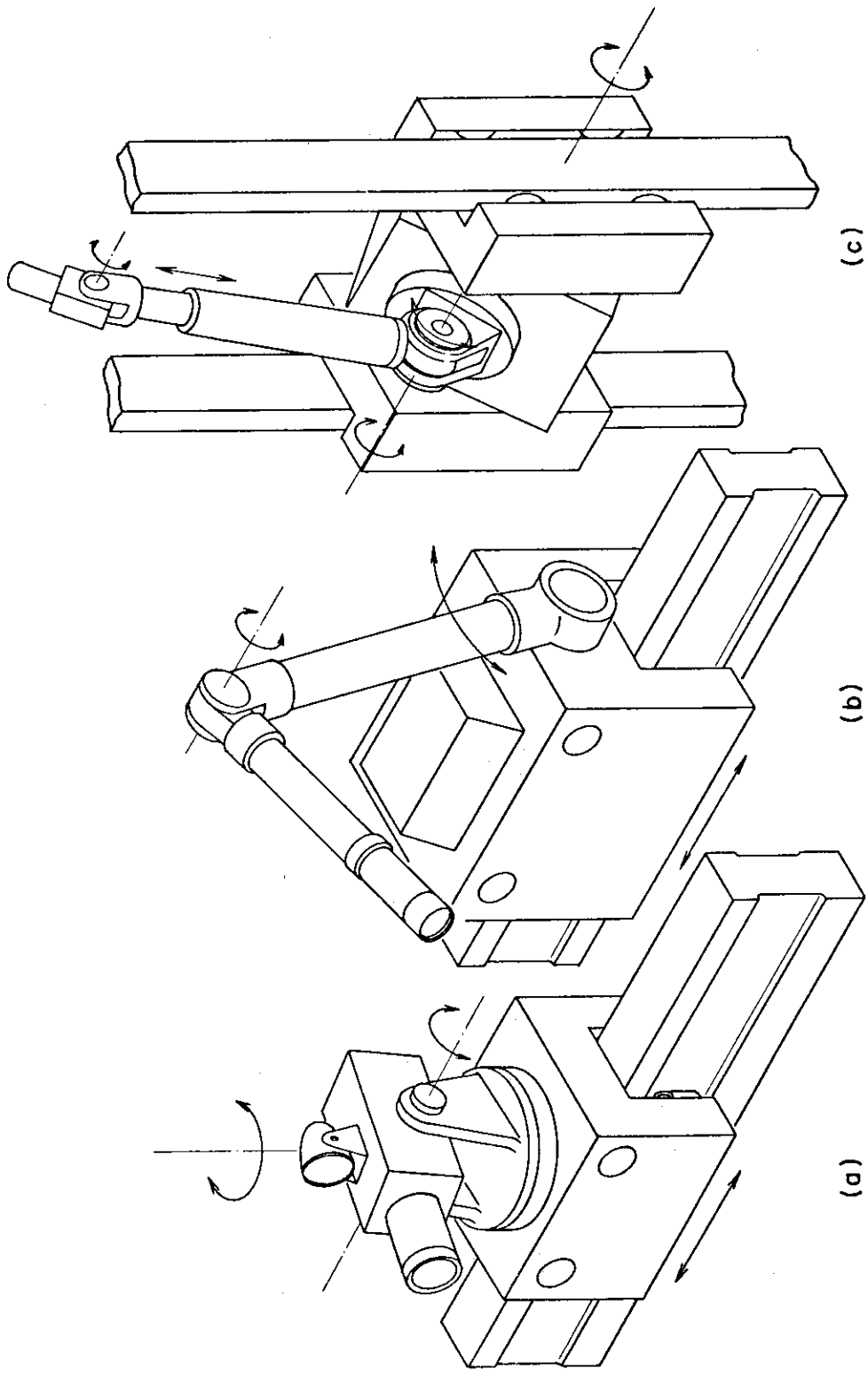

Fig. 12.4.11 Monitor head

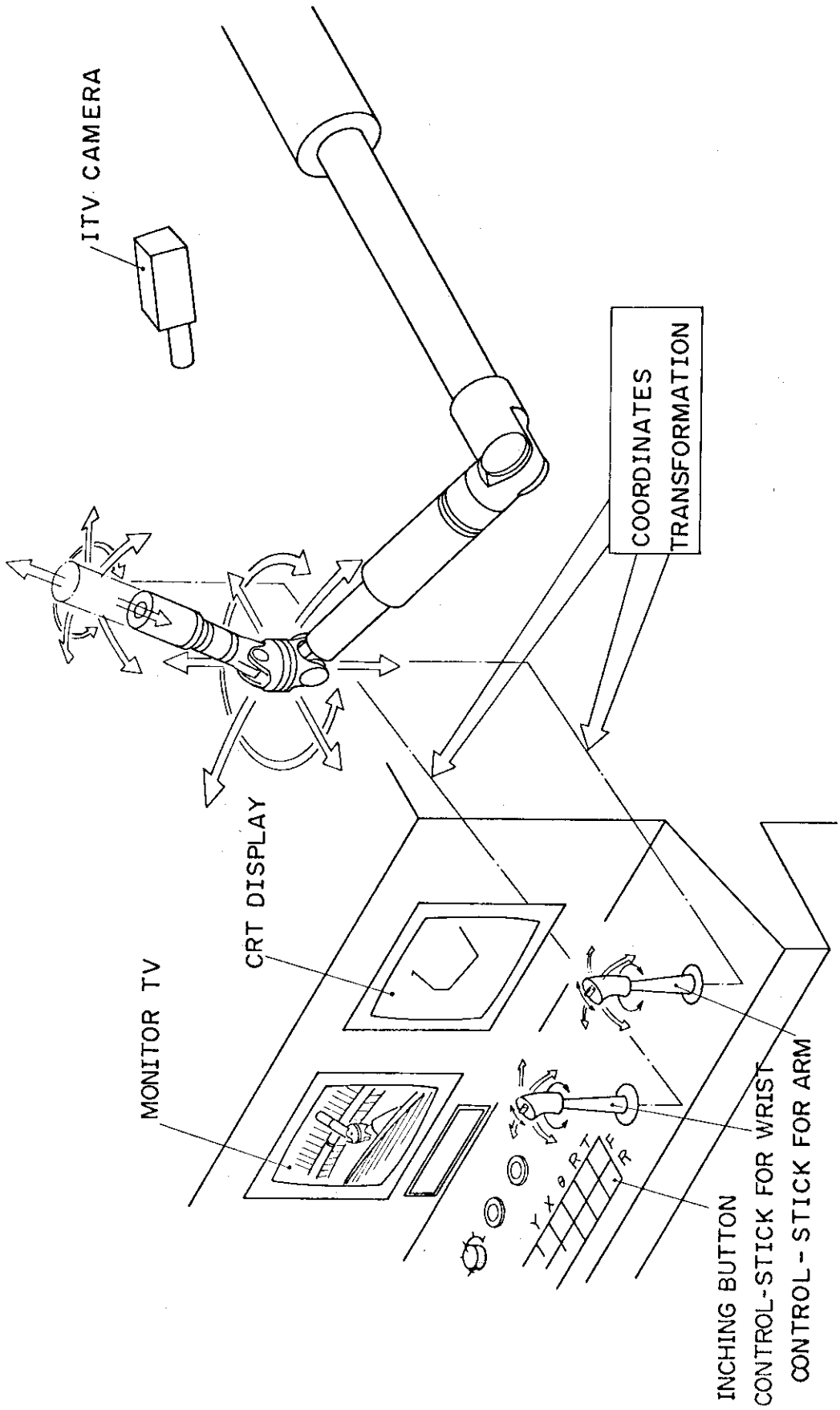

Fig. 12.4.12 Manipulator control

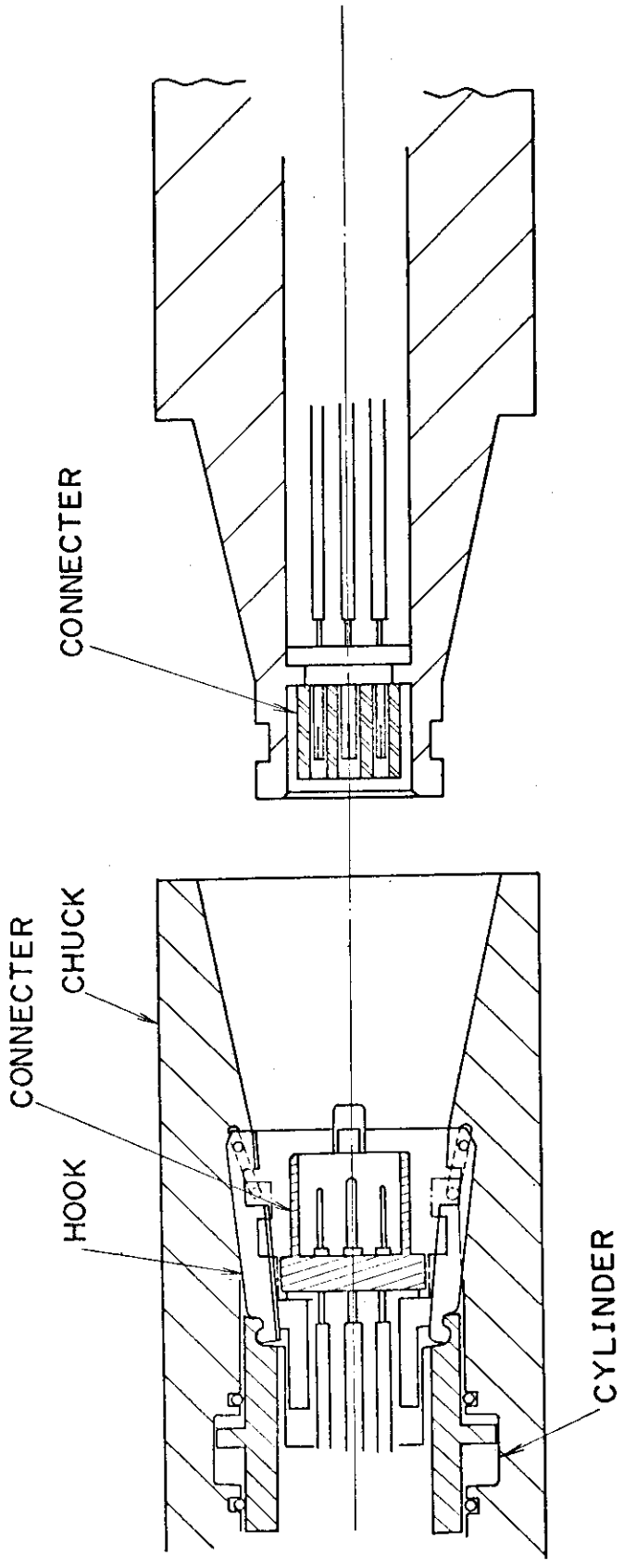

Fig. 12.5.1 Chucking mechanism with connector

13. Reactor Cooling System

The design of the reactor cooling system without divertor is described in this section. In the case of the reactor cooling system with divertor, the thermal energy (heat flux) is devided into the cooling tube and the divertor plate, but there is no basic difference between the reactor cooling systems with and without divertor.

The reactor cooling system is formed with three systems which cool the outer blanket, the inner blanket and the cooling panel. The cooling system has two lines at the outside of the reactor. The coolant of above three systems is once collected in the common header and then distributed to the two lines.

Electric power is not generated in the reactor cooling system.

A secondary loop is provided in order to prevent the environmental release of tritium.

13.1 Design Conditions

(1) The coolant is pressurized water. The pressure of the secondary loop is a little higher than that of the primary loop.
(2) An intermediate loop to prevent a tritium release is provided in the cooling system.
(3) See water is used in the last stage.

The design parameters are shown in Table 13.1.1.

13.2 Heat and Mass Balance

Fig. 13.2.1 shows the heat and mass balance of the reactor cooling system.

13.3 Tritium Problems

In order to prevent strenously the permeation of tritium into the coolant, the temperature of the coolant is restricted to be low. Moreover, a water purification system is also prepared to remove and recover the tritium permeating in the coolant.

Table 13.1.1 Design Parameters of Reactor Cooling System
(Non-breeding)

Thermal Power		
Outer Blanket	:	214 MW
Inner Blanket	:	71 MW
Cooling Panel	:	130 MW
Total	:	415 MW
Duty Factor	:	0.8
Number of Lines	:	2
Coolant (primary/secondary)	:	H_2O/H_2O
Primary Coolant Temperature (inlet/outlet)	:	50/90 °C
Coolant Pressure (primary/secondary)	:	5/7 ata
Temperature of Condenser Cooling water (Sea Water)	:	20 °C

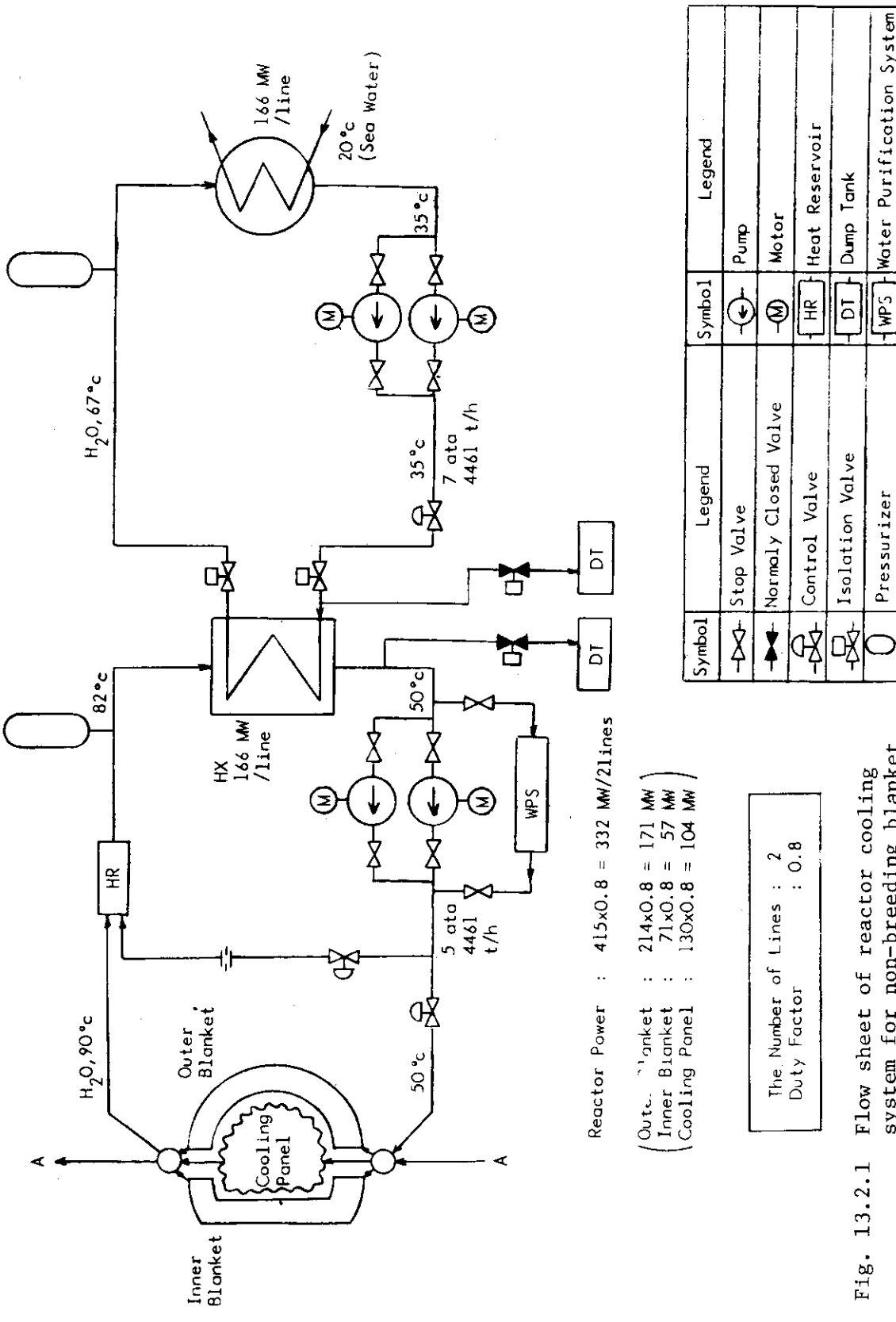

Fig. 13.2.1 Flow sheet of reactor cooling system for non-breeding blanket

14. Blanket Test Section

14.1 Test Module

The design of the blanket test section has been carried out.

For one reactor module, the test rig has two test sections and its size is 1 m × 1 m. Four test sections may be experimented by using two pieces among the 6 reactor modules. The design of the test rig, which is cooled by helium gas, to experiment a tritium breeding is described in this section.

The test rig consists of an insertion tube and a cooling system which includes a primary cooling system and a tritium recovery system.

14.1.1 Design conditions

(1) Each country can use one of the four test sections independently.
(2) The package type test rig reduces the interference which affects all over the reactor system.
(3) The repair in case of accident may be performed easily.
(4) The cooling conditions are similar to A.1.1.4.
(5) The insertion tube is a vacuum boundary.
(6) The insertion tube is kept inserted while the test is not performed.
(7) The insertion tube has another cooling system which is independent from the cooling system of the test section blanket.
(8) The thermal energy of 4 test section blankets is assumed to be 0.5 MW in this design.
(9) The primary cooling system and the exchange equipment of the test rig are prepared on the removal carriage which is similar to that of NBI system.

14.1.2 Test rig

(1) Test blanket

The test blanket serves for a tritium breeding purpose and is cooled by helium gas (see A.1.1). The diameter and height of the test section blanket are 350 mm and 500 mm, respectively.

(2) Insertion tube

The insertion tube is put in and drawn out through the NBI port, sliding on the insertion tube support as shown in Figs. 14.1.1 ∿ 14.1.4.

After the insertion tube is put in, the seal welding for a vacuum is performed between the vacuum wall of the shielding and the test rig.

The cooling panel with a protection wall is prepared at the plasma side of the insertion tube. The top of the insertion tube shown in Fig. 14.1.4 is a double-walled structure and the coolant of water flows between the ribs which is provided in the inside surface of the outer wall.

A guide rail for the mounting carriage is prepared at the lower side of the insertion tube.

The pipings of the cooling system for the cooling tube and the insertion tube penetrate the insertion tube basement.

(3) Mounting carriage

The mounting carriage is put in the insertion tube from the inside of the carriage strage space for the test section, sliding on the rail with the transfer equipment. Four test section blankets are installed at the front of the mounting carriage. At the back of the mounting carriage, a shielding block is installed to prevent the radiation streaming.

(4) Cooling system of test section

The test rig shown in Figs. 14.1.5 and 14.1.6 will be operated after connecting the cooling facility of the test section to the back of the insertion tube. The cooling facility of the test section is a building of three stories.

The components of the primary cooling loop are installed in the first floor, the second floor is the carriage storage space of the mounting carriage. A tritium recovery system (TRS) for the primary cooling system, a jacket tritium processing system (JTPS) and the components of the primary helium dump system are installed in the third floor.

In order to prevent a tritium release through the high temperature piping and components of the primary system, the jacket system, which is a coaxial tube and a double wall structure, is provided from the outlet of the test section blanket to the inlet of IHX. A sweep gas of helium is flown in the outside tube of the coaxial tube and the tritium permeating through the tube wall is removed by the JTPS.

During operation, the inside of the cooling facility and the insertion tube is filled with helium gas.

(5) Setting procedure of the test rig

The setting procedure of the test rig is shown in Fig. 14.1.7.

The outline of the setting procedure in the case where the test rig is put in or drawn out is described as follows.

1. Setting the test rig in the reactor room with the transfer carriage (Position A).
2. Connecting the building of the primary cooling system to the shielding of the blanket module (Position B).
3. Bolting and seal welding the connecting flange.
4. Inserting the test section blanket into the insertion tube.
5. Connecting the cooling tube.
6. Exchanging air for helium gas in the test rig.
7. Operating (Position C)

The test rig is unsetted after the operation in the inversed procedure to the setting one mentioned above.

14.1.3 Design analysis

See Appendix A.1.1.3.

14.1.4 Cooling system

The cooling system of the test rig is formed with the cooling system of the test section blanket and that of the insertion tube. Each system has one cooling line.

(1) Design conditions

Power generation

Electric power will be generated only in the cooling system of the test section blanket. The coolant of the test section blanket is helium gas, but the coolant of the insertion tube is pressurized water. The intermediate loop is provided in the cooling system of the test section to protect the environmental release of tritium.

The design parameters are shown in Table 14.1.1.

Non power generation

The primary loops of the cooling system for the test section and the insertion tube are similar to those of the power generation system. The coolant of the secondary loop for the test section is water at normal pressure.

The design parameters are shown in Table 14.1.2.

(2) Heat and mass balance

Power generation

Figure 14.1.8 shows the heat and mass balance of the cooling system for the power generation.

Non power generation

Figure 14.1.9 shows the heat and mass balance of the cooling system for the non power generation.

(3) Tritium problems

Power generation

In the primary and secondary loops of the cooling system for the test rig, the tritium recovery system is provided in order to remove tritium containing in a coolant. At the high temperature piping system, the jacket system is provided in order to recover a tritium permeating through the tube wall. The primary loop and flow sheet of the jacket system corresponds to Figs. A.1.1.15 and A.1.1.16 in Appendix A.1. In case of the cooling system for the insertion tube, the coolant is kept to be a low temperature to prevent the tritium permeation into the coolant and the water purification system shown in Fig. A.1.1.17 in Appendix A.1 is prepared to remove and recover the tritium permeating into the coolant.

Non power generation

The tritium recovery system of the primary loop and other systems are similar to the power generation system mentioned above.

14.1.5 Design problems

See A.1.1.5 in Appendix A.1.

14.2 Test Segment

The operation of the test segment will be performed by one reactor module. The design conditions are similar to Appendix A.1.1, but the thermal energy to remove with the cooling system is different from Appendix A.1.1.

Table 14.1.1 Design Parameters of Test Rig Cooling System
(Power Generation)

Thermal Power (4 test blankets)	:	0.5 MW
Duty Factor	:	0.8
Number of Lines	:	1
Coolant (primary/secondary/tertiary)	:	He/He/H_2O
Primary Coolant Temperature (inlet/outlet)	:	250/550 °C
Coolant Pressure (primary/secondary/tertiary)	:	30/-/- ata
Temperature of Condenser Cooling Water (Sea Water)	:	20 °C
Condensate Temperature/pressure	:	33°C/0.05ata
Turbine Efficiency	:	-
(Power Transfering Efficiency) x (Generator Efficiency)	:	-
Electric Power (Gross)	:	-
Circulator Power	:	-

Table 14.1.2 Design Parameters of Test Rig Cooling System
(Non-power Generation)

Thermal Power (4 test blankets)	:	0.5 MW
Duty Factor	:	0.8
Number of Lines	:	1
Coolant (primary/secondary)	:	He/H_2O
Primary Coolant Temperature (inlet/outlet)	:	250/550 °C
Coolant Pressure (primary/secondary)	:	30/1 ata
Temperature of Condenser Cooling Water (Sea Water)	:	20 °C

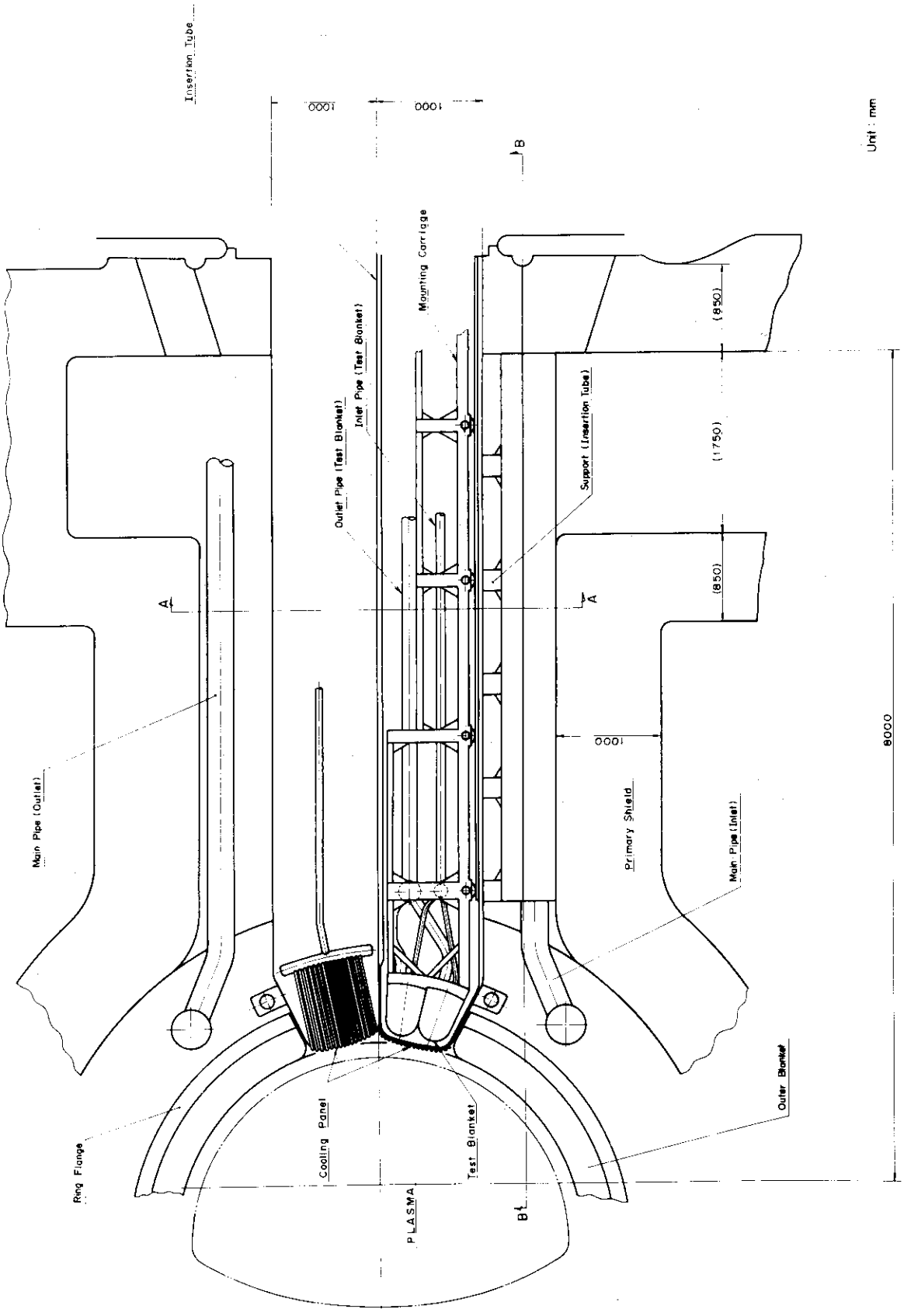

Fig. 14.1.1 Cross Sectional View of Insertion Tube

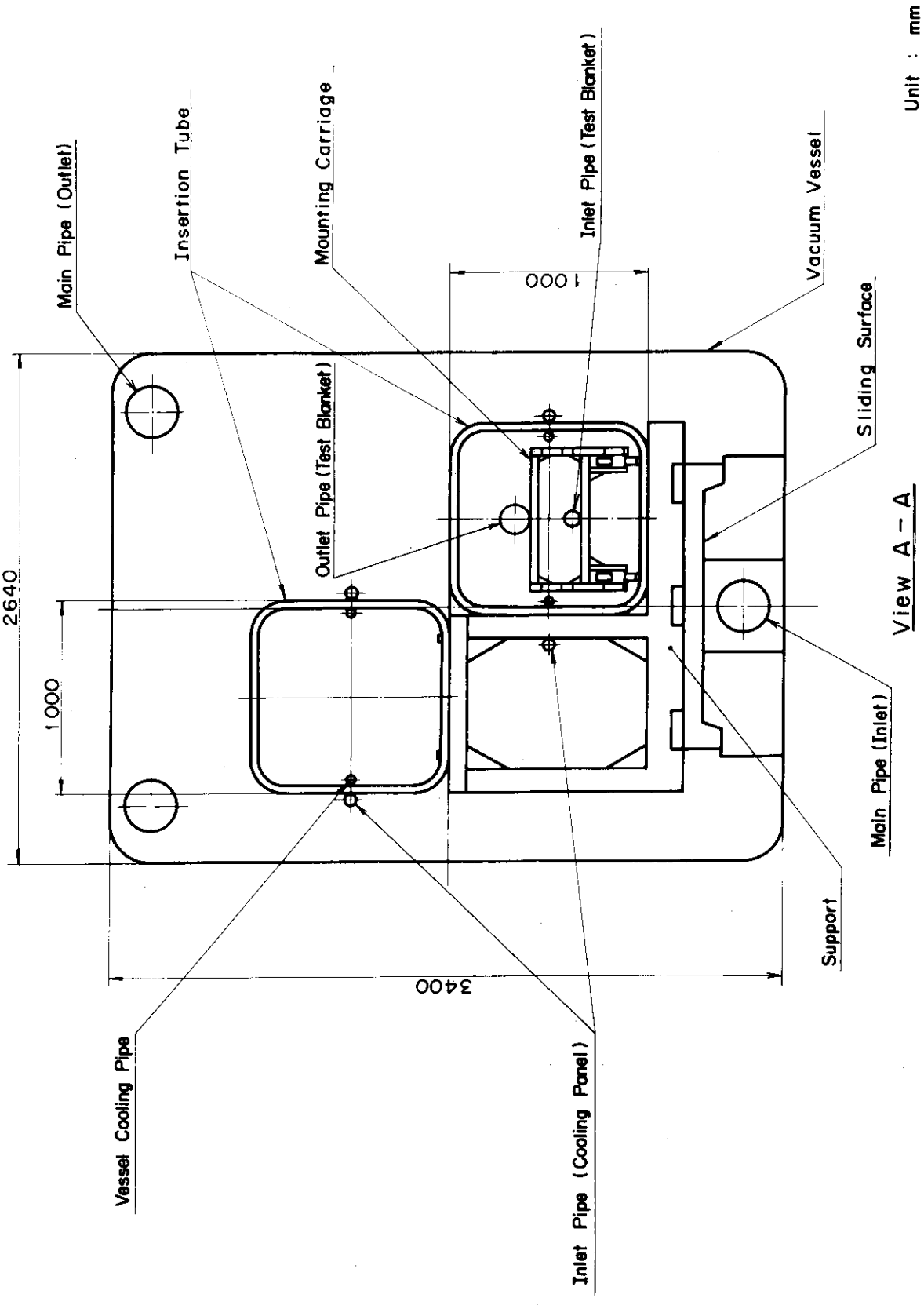

Fig. 14.1.2 A-A View in Fig. 14.1.1

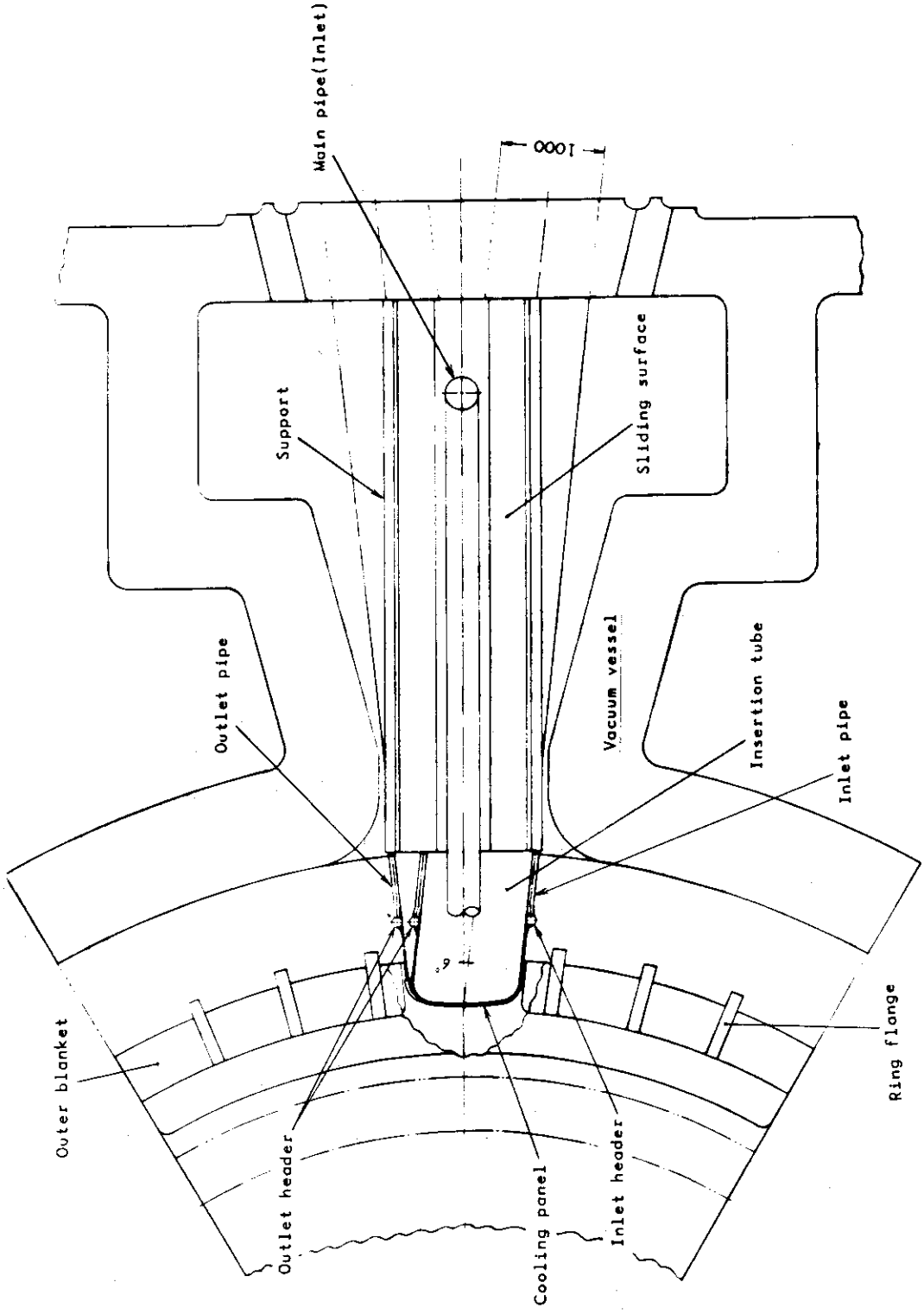

Fig. 14.1.3 B-B View in Fig. 14.1.1

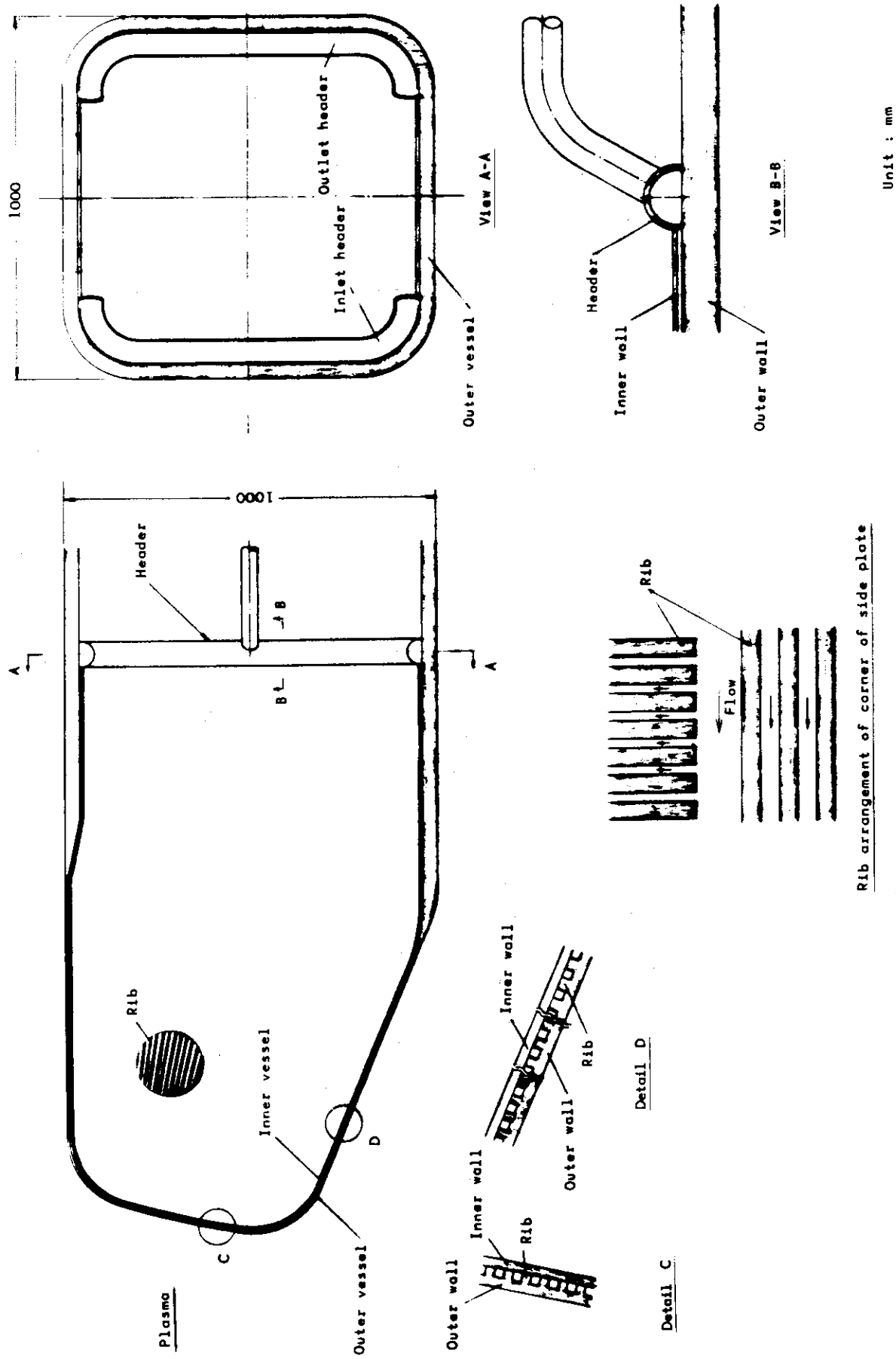

Fig. 14.1.4 Details at the Top of Insertion Tube

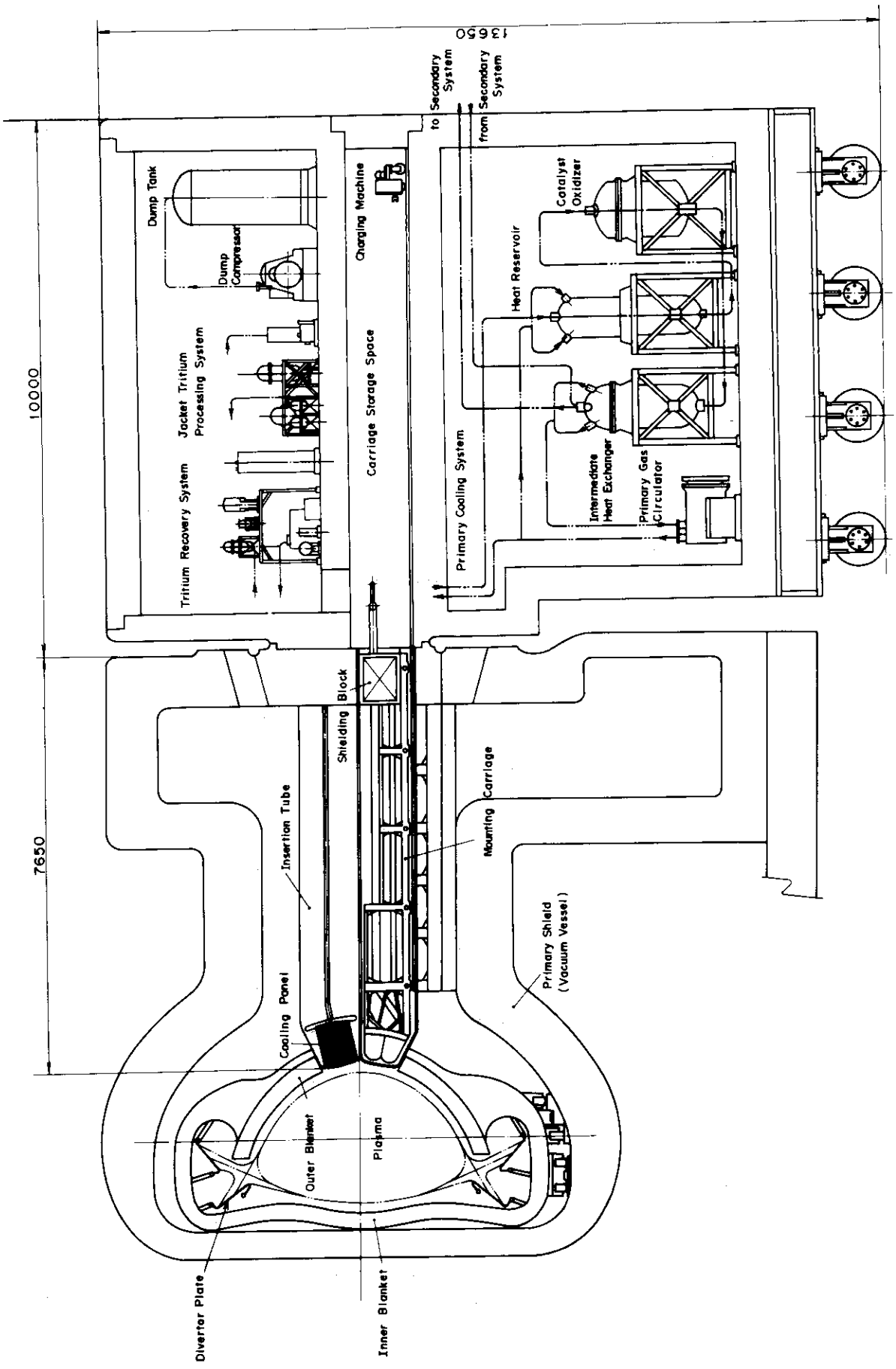

Fig. 14.1.5 Side View of Test Rig

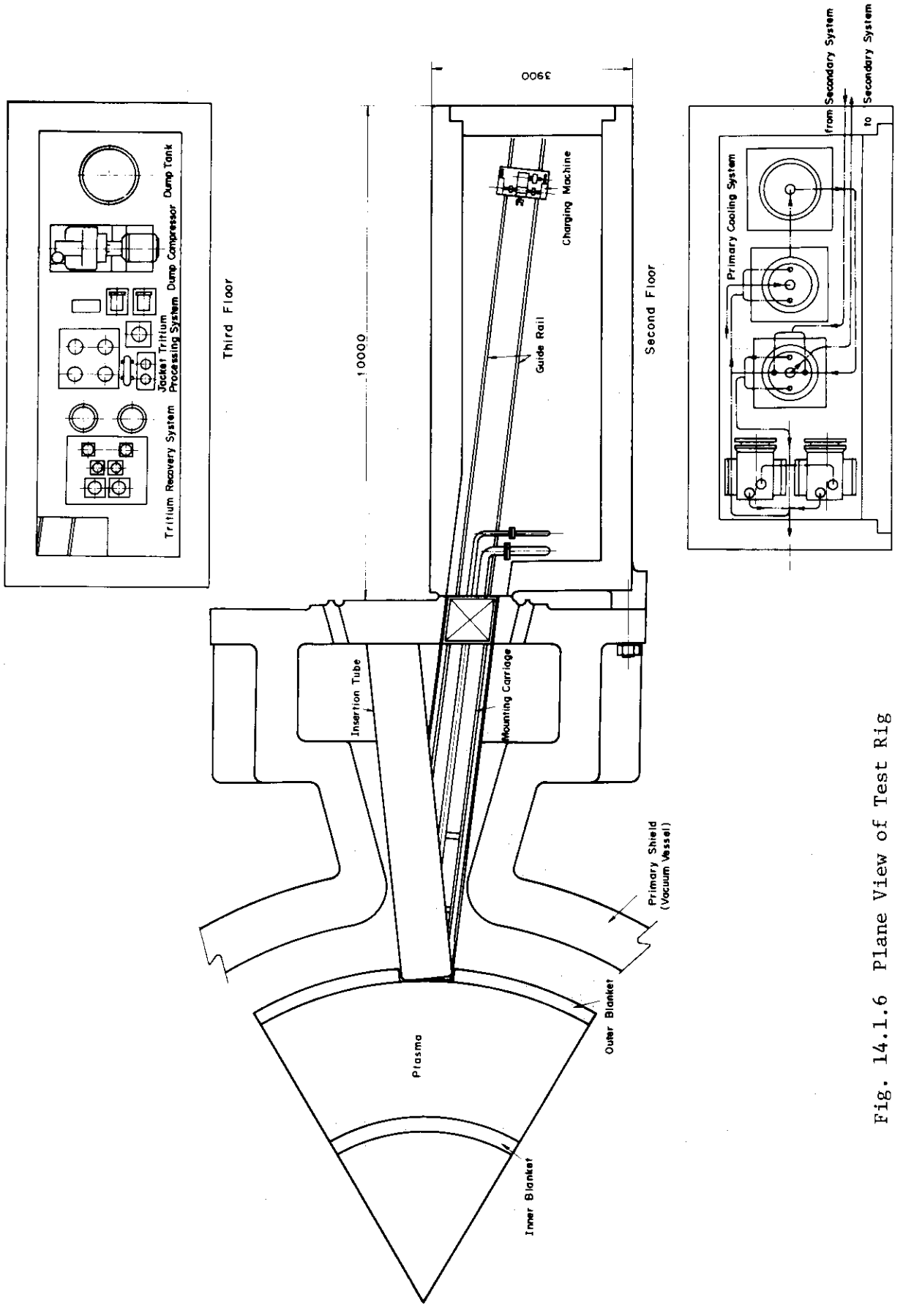

Fig. 14.1.6 Plane View of Test Rig

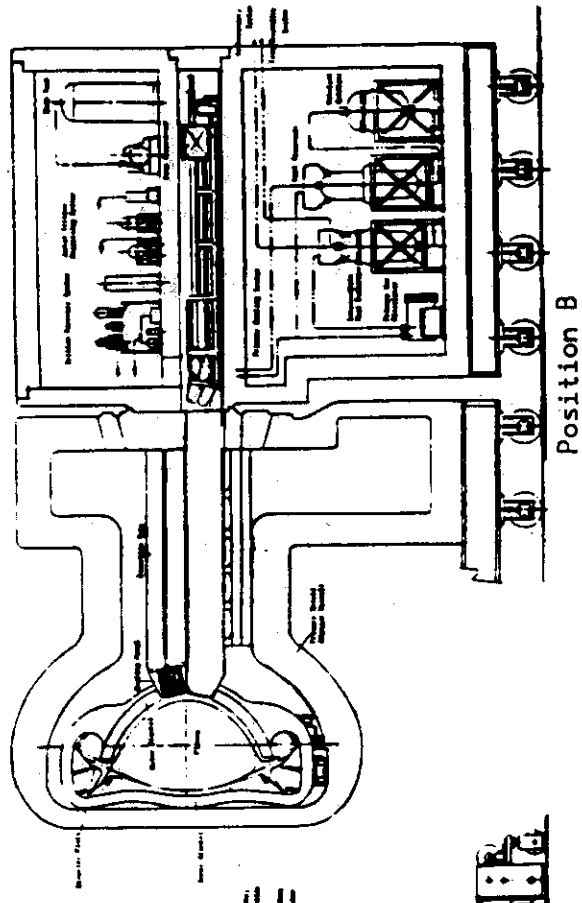

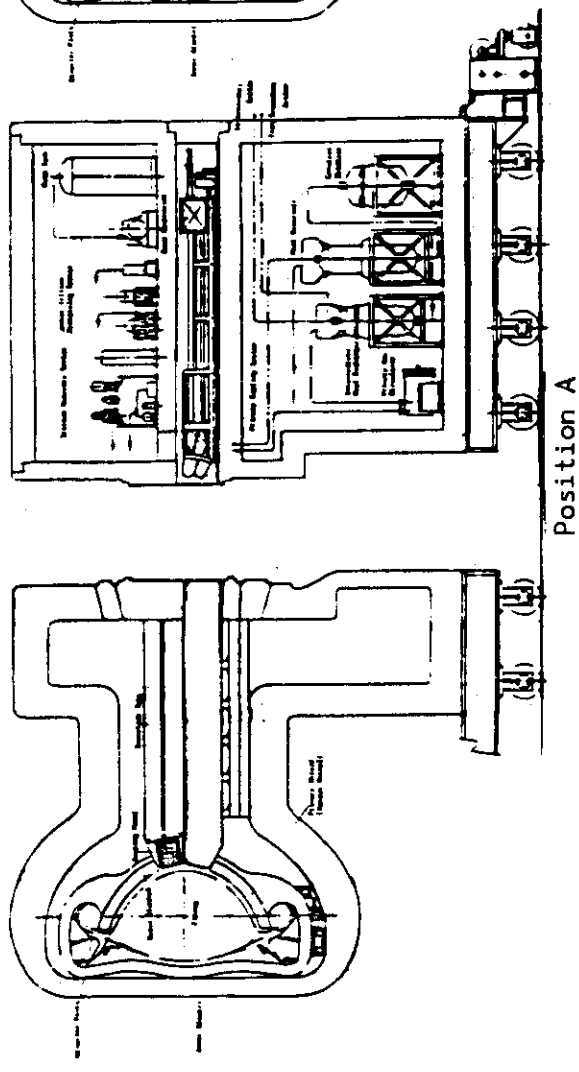

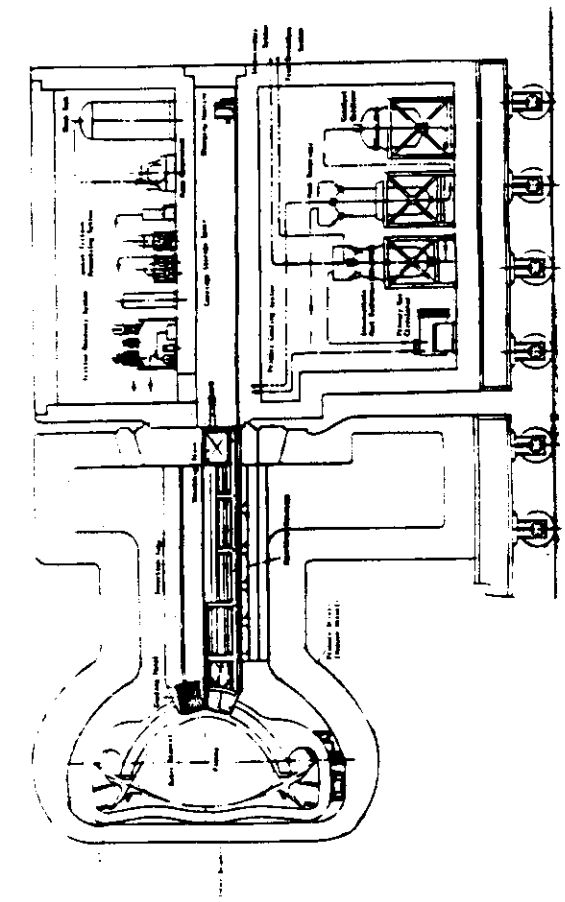

Fig.14.1.7 Setting Procedure of Test Rig

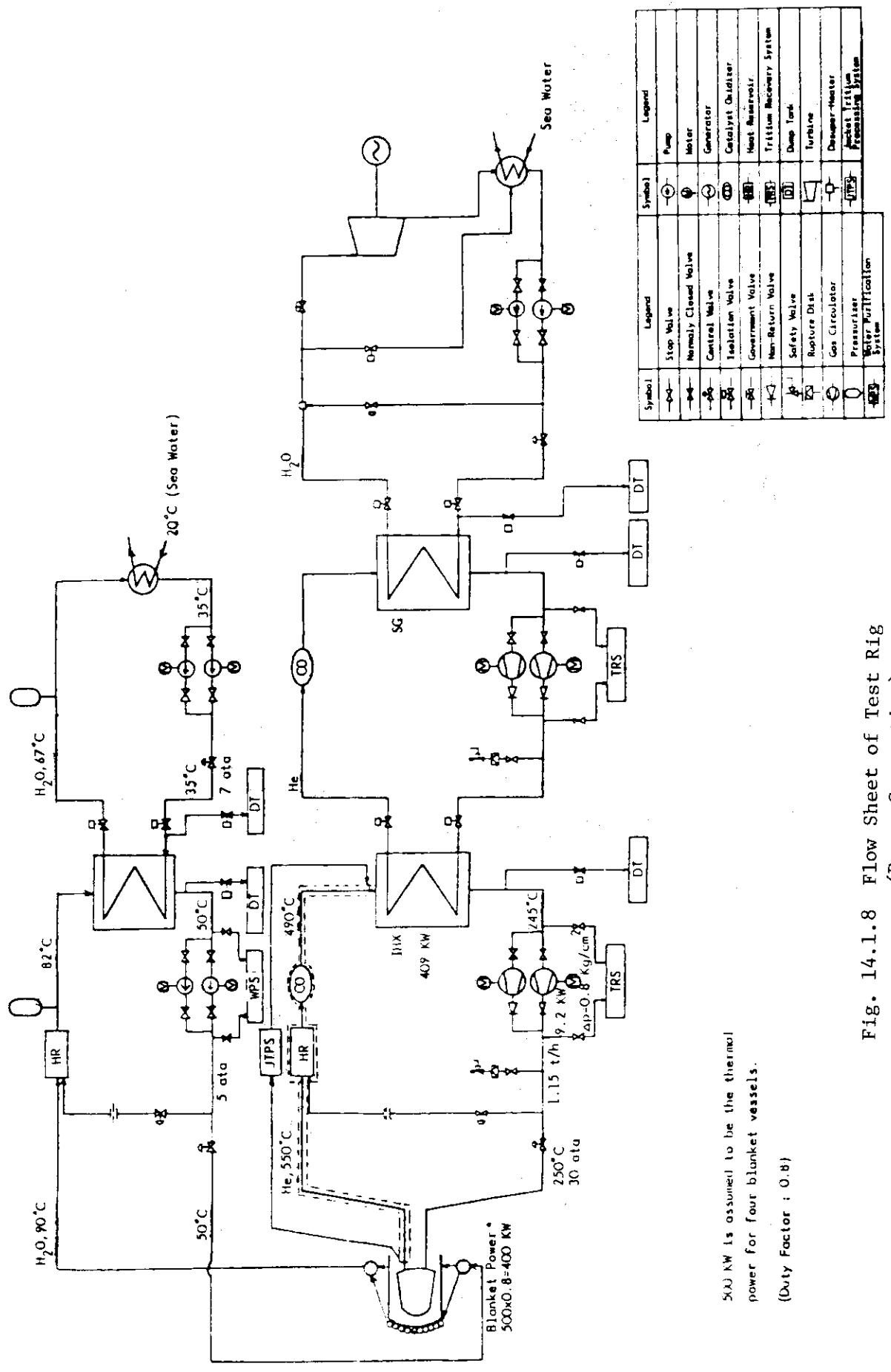

* 500 KW is assumed to be the thermal power for four blanket vessels.
(Duty Factor : 0.8)

Fig. 14.1.8 Flow Sheet of Test Rig (Power Generation)

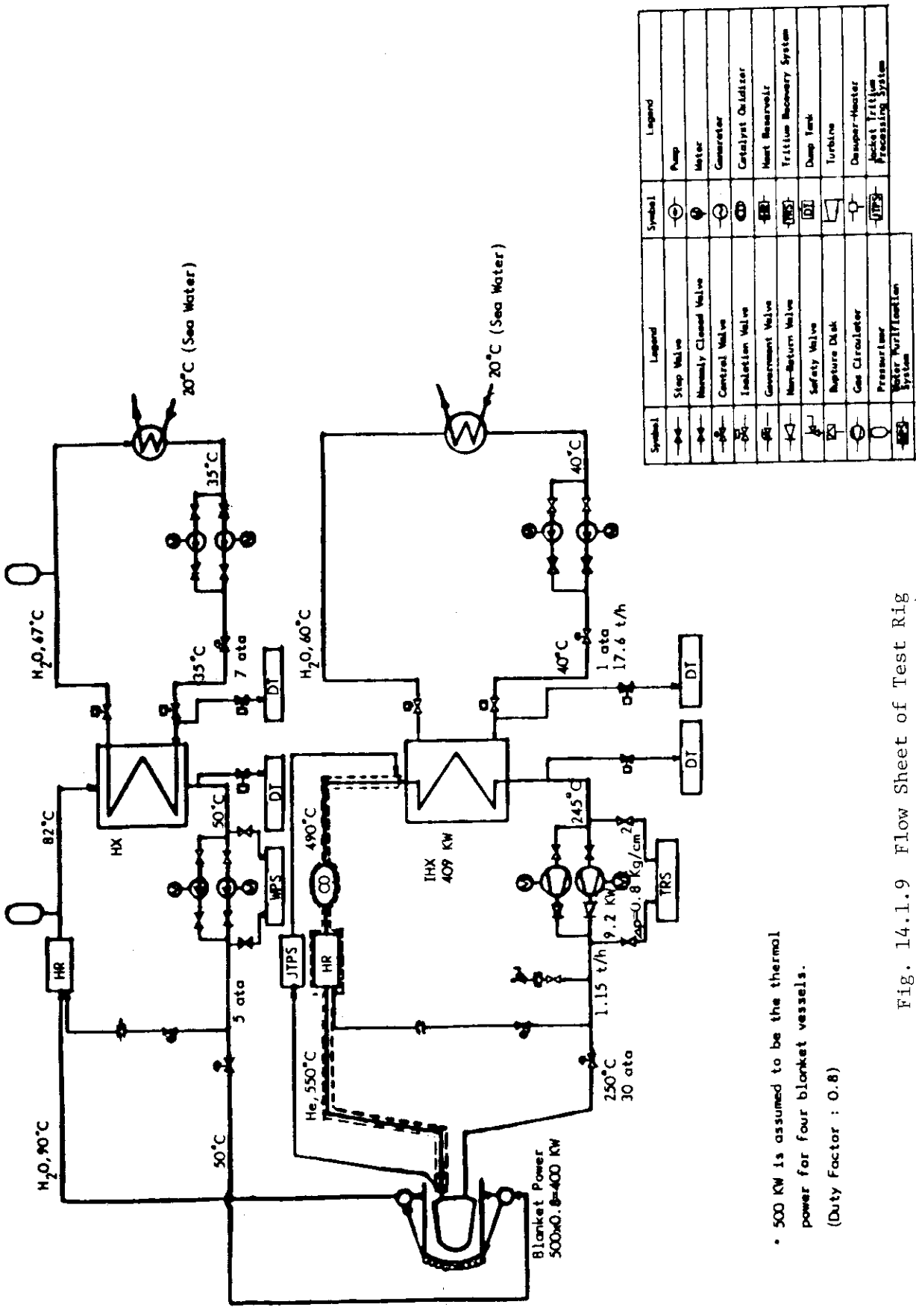

• 500 KW is assumed to be the thermal power for four blanket vessels.
(Duty Factor : 0.8)

Fig. 14.1.9 Flow Sheet of Test Rig (Non-Power Generation)

15. R&D Items

15.1 General

The R&D items required for INTOR construction are classified and discussed in the following sections. Though some of them are not sufficiently reviewed because of lack of time, they seem to be useful for making detail plan of INTOR component's R&D since they are made based upon the systematic design study for INTOR.

15.2 Neutronics

The proposal for the R & D schedule for fusion reactor neutronics in JAERI for the next five years is given in Table 15.1.

15.3 Blanket

Research and development program to fabricate the INTOR fusion reactor satisfactorily is as follows;

(1) Development of compact non-filler TIG orbital welding machine for small-sized tube
(2) Establishment of automatic brazing technique for cooling tube and block
(3) Development of electron beam welder for double-wall outer blanket
(4) Development of vacuum system and commercialization of compact portable-type electron beam gun for partial-vacuum electron beam welder
(5) Consideration of electron beam deflection technique for full-vacuum electron beam welder
(6) Feasibility study for fin tube production
(7) Development of fully automatic welding machine and nondestructive testing technique

15.4 Shielding Structure

(1) Development of Construction of heavy concrete structure at narrow part
(2) Study of aggregate's material and its ratio in the concrete
(3) Study of fine chips material and it's ratio of mortar
(4) Development of material of thin electrical insulation
(5) Development of automatic welding and cutting machine

15.5 Divertor

(1) Repetitive thermal stress due to pulsive operation of the reactor might lower the life time of the divertor plate to 3 to 4 months.

(2) Radiation damage of the plate due to 14-MeV-neutron irradiation, especially swelling of copper, could be a serious problem. But, it is difficult to evaluate its effect on the life time of the plate due to lack of data for radiation damage.

(3) Enrichment and exhaustion of α particles and impurities in divertor chamber must be simulated as accurately as possible.

15.6 Toroidal Field Magnet

(1) Detailed design study

(2) Basic R&D items
  (a) Development of large current Nb_3Sn cable at high magnetic field
  (b) Development of electrical insulation
  (c) Fatigue test of structural materials under Liq. He temperature
  (d) Development of jointing structure of cable
  (e) Development of winding and annealing process of cable

(3) Some scale model test for magnet systems to confirm fabrication processes and integrity of coil support structure

(4) Trial fabrication and test of full size coil

(5) Development and test of economical large liquid helium system

(6) Development of magnet protection systems

15.7 Poloidal Field Magnet

(1) R&D for AC effects
The other R&D items are similar to those of toroidal field magnet as mentioned above

15.8 Neutral Beam Injector

(1) Single unit of full scale test including the hollow cathode ion source, 200 kV acceleration grids, and direct energy converter.

(2) New idea for neutralization of ion beams such as metal vapor and ice cluster methods.

15.9 Main Vacuum Pump

(1) Development of large diameter gate valve

(2) Development of reliable cryo-sorption pump

15.10 Repair and Maintenance of Reactor (Concept A)

(1) Design study of remote handling systems and equipments

(2) Development of devices for assembling and disassembling
   1) Automatic welding machine
   2) Tug barrow
   3) Car mounted crane
   4) Manipulator with bolting and unbolting machine on crane having shielding cab.
   5) Manipulator with bolting and unbolting machine on vehicle mounted shield operation room
   6) Manipulators for maintenance room

(3) R&D devices for inspection
   1) Manipulator with inspection apparatus mounted on bell jar cylinder
   2) Manipulator with inspection apparatus mounted on bell jar dome
   3) Manipulator with inspection apparatus mounted on movable base
   4) Movable manipulator with inspection apparatus

15.11 Repair and Maintenance of Reactor (Concept B)

(1) Small scale model of blanket handling machines, a torus segment, and blanket and shielding structures including blanket transport mechanisms.

Accessibility of the blanket handling machine from the crane rails, also needs to be simulated.

(2) Full scale model of welding and cutting machines for plasma chamber vacuum boundary including transport mechanisms of those machines.

Some part of the shielding structure need to be made to test the feasibility of the vacuum boundary concept and to test the cutting and welding machine.

15.12 Repair and Maintenance of Divertor Plate

- R&D of glass and fiberscope which are hardly damaged by radiation such as γ-ray and neutron.
- R&D of light and stiff materials in order to make the size of devices small and to lift and carry heavy equipments.
- R&D of soft and hard wares to control the devices with multi-degrees of freedom of motions as these manipulators presented in this report.

Table 15.1 Proposed R & D Schedule for Fusion Reactor Neutronics in JAERI

FY1980 = April, 1980 ~ March, 1981

Items, descriptions	FY 1980	FY 1981	FY 1982	FY 1983	FY 1984
(1) Blanket neutronics experiments					
o Blanket benchmark experiments	Lithium benchmark →				
	Li_2O benchmark →				
o Neutronically optimized blanket		Optimized blanket assembly →			
o Blanket mockup experiments				EPR blanket mockup →	
o Measurement technique development	Tritium breeding rate,	Nuclear heating rate,		New methods →	
(2) Induced acivity experiments	Short-life induced nuclides decay heat	Medium-lifetime induced nuclides relevant to personnel dose		Long-lifetime induced nuclides for rad-waste evaluation →	
(3) Shielding neutronics experiments					
o Streaming experiments	Around blanket	NBI port	Penetration thru primary shield	Mockup exp. →	
o SCM neutron irradiation			Neutron damage evaluation exp. →		
o Skyshine measurements	Near the FNS	Far from the FNS →			
(4) Analysis, data and methods development					
o Integral transport calculation method for deep penetration problem (rigorous treatment of inelastic neutron anisotropy)	1D code and input data	2D code and input data	3D code development →		
o Reactor design codes	$2DS_N$-Monte Carlo coupling, Advanced Monte Carlo Code →				
	3d-induced activity calculation →				

ACKNOWLEDGEMENT

The authors are greatly indebted to Drs. S. Mori and Y. Obata for their encouragement. They also thank deeply to the people in JAERI who participated in the INTOR-J program, especially to Drs. T. Hiraoka and T. Tazima for valuable discussions.

Special thanks are extended to Drs. Y. Shimomura, S. Shimamoto, H. Shirakata and K. Shiraishi for valuable discussions and comments on divertor, SC magnets, NBI and Material, respectively.

A. Appendices

A.1 Tritium Breeding Blanket

Two kinds of tritium breeding (outboard only) with electricity production have been studied. They are:

(1) He-cooled Li_2O blanket (pressure vessel type)

(2) Water cooled Li_2O blanket (Tube-in-shell type)

Dusign of He-cooled Li_2O blanket with tube in shell type is also in progress

In case of non divertor concept the breeding ratio of the above blanket systems are as follows:

(1) 0.61

(2) 0.74

Details are described in Appendix A.2.

In case of segment test, 1/6 of the reactor is used for tritium breeding.

A.1.1 Pressure Vessel Type

The design of the reactor cooling system without divertor is described in this section. In the case of the reactor cooling system with divertor, the thermal energy (heat flux) is devided into the cooling panel and the divertor plate, but there is no basic difference between the reactor cooling systems with and without divertor.

A blanket structure shown in Fig. A.1.1.1 consists of six blanket modules and is placed in a vacuum vessel. Each module is formed with 16 blanket rings and is assembled with inner blanket (non tritium breeding), outer blanket (tritium breeding), cooling panel with a protection wall, piping system and support structure.

A.1.1.1 Design Conditions

Blanket Cell

(1) The blanket cell is cooled by helium gas at 30 kgf/cm^2 during operation.

(2) The coolant flows helically between inner and outer wall and arrives at the plasma side.

(3) The coolant enters from the inlet duct at 250 °C, becomes

about 340 °C at the top of the dome and exits from outlet duct at 550 °C being heated in the inner part (Li_2O) of the blanket cell.

(4) The temperature on the top of the some is about 370 °C (See Fig. A.1.1.5).

Cooling Panel

(1) The cooling panel is cooled by helium gas at 70 kgf/cm^2.

(2) The coolant enters from the inlet header which is provided at the lower part of the torus, flows through the inside and outside surface of the torus and is collected with the outlet header at the upper part.

(3) The inlet and outlet temperature of the coolant are 200 °C and 300 °C, respedtively and the maxiumu temperature of the structural material (pressure boundary) is about 400 °C.

A.1.1.2 Blanket Structure

Outer Blanket (Blanket Cell)

Fig. A.1.1.2 shows a typical blanket cell. The blanket vessel is a double-walled and truncated conical thin shell made of Type 316 stainless steel with a spherically domed surface at the plasma side. A thick cover plate, to which inlet and outlet coaxial duct attaches, is placed at the opposite side of the plasma. Ribs (5 × 5 mm) for the coolant channel are provided between inner and outer wall. For tritium breeding, the blanket cell contains pebbles and blocks of lithium oxide (Li_2O) which are packed in the stainless steel canning to prevent their deformations.

The blanket cells are in a triangular arrangement in this design and are fixed with two ring flanges welded to the outside of the cover plate.

There are two kinds of the blanket rings for the sake of the trianglar arrangement and they are assembled alternately. However, the two blanket rings which have a neutral beam injection hole is not in a triangular arrangement. Moreover, as the both end rings of the blanket module separate from the adjacent blanket modules, the triangular arrangement is not taken in between the end rings of the adjacent blanket modules.

The blanket cell are fixed with two pieces of ring flanges welded to the outside of the cover plate as shown in Fig. A.1.1.2.

The inner and outer blanket module are formed with ring units. The inner and outer blanket ring are connected with each ring flange to increase the strength of the blanket structure due to the unification of two ring flanges.

Cooling Panel

Fig. A.1.1.3 shows a cooling panel. The cooling panel is provided in front of the inner and outer blanket surrounding a plasma in order to remove all thermal radiation which comes from the plasma and a part of nuclear heating. The cooling panel consists of 6 cooling panel modules and each module is formed with 16 cooling panel rings.

The cooling panel is a membrane wall structure which is assembled with a lot of fin-tubes having a small diameter made of Type 316 stainless steel. It is sustained with some supporting bars which is attached to the blanket flanges.

The cooling panels at the inbored and outbored section are formed with the arrangement of many fin-tube. At the inbored section, as the variation of the pitch to arrange the fin-tube is small, the fin-tubes do not overlap. However, at the lower and upper part of the outbored section, the variation is large and the fin-tubes overlap. If the cooling panel at the outbored is horizontally arranged to prevent the overlap, it is difficult to install the support structure of the cooling panel in the case of the pressure vessel blanket type. Therefore, the arrangement of the outbored section is similar to the inbored.

A protection wall, which is made of TZM, is attached to the plasma side of the cooling fin-tube so that the plasma does not directly contacts with the surface of the cooling fin-tube. The shape of the protection wall is a semi-cylindrical shell which is determined from the following requirements, (1) to moderate the thermal radiation to the cooling panel and (2) to transfer the thermal radiation to the backside of the cooling panel.

Piping System

A piping system for the outer blanket is formed with a lot of

blanket pipes, some collection manifolds, some inlet and outlet headers and main coolant pipes. The former two components are made of coaxial pipes with the hot outlet pipe inside the inlet pipe so that the piping arrangement becomes simple and the temperature of the blanket structure becomes low. The thermal insulator is attached to the inside surface of the outlet pipe in order to avoid the thermal expansion of the outlet pipe and the heat exchange between inlet and outlet pipe.

Repair and Maintenance

In case of repair and maintenance, the blanket module will be withdrawn in the toroidal direction by using a wheel which is set on the lower part of the blanket module. In this case, the main pipe will be disconnected by automatic cutting machine. During operation, however, the blanket module will be supported with the support block which is set under the blanket module support.

The weights of the each component are as floolws;

a.	blanket cell	55 ton/module
b.	inner blanket	32 ton/module
c.	cooling panel	5 ton/module
d.	piping header	34 ton/module
e.	ring flange	47 ton/mocule
f.	support structure	10 ton/module
	total	183 ton/module

A.1.1.3 Design Analysis

Stress Analysis of Blanket Vessel

The stress analysis of the blanket vessel which forms the outer blanket module for tritium breeding has been carried out.

The blanket vessel is a double-walled and truncated conical thin shell with the spherical dome at the plasma side made by Type 316 stainless steel. The blanket vessel is cooled by helium gas at 30 kgf/cm^2 during operation. The inlet and outlet temperature of the coolant are 250 °C and 550 °C, respectively. The maximum nuclear heating ratio is 11 W/cc at the top of the dome.

Fig. A.1.1.4 shows the calculational model for the outer wall of the blanket vessel. Two-dimensional axisymmetric finite element

was employed for the elastic and thermal stress analysis. The thickness of the body is 12 mm and the thickness of the dome is 6 mm at the top. The height for the coolant channel (5 mm) and the thickness of the inner wall (5 mm) were excluded from the those thickness and the thick cover plate was not considered in this analysis.

We carried out the stress analysis under internal pressure 30 kgf/cm^2 taking account of temperature distribution of the blanket vessel during burn time. The temperature distribution employed in this analysis was obtained from a steady state heat transfer analysis with two-dimensional model using above conditions, assuming that the temperature was constant in the circumferential direction of the outer wall. The temperature distribution is shown in Fig. A.1.1.5. The material properties of Type 316 stainless steel at 400 °C were used in this analysis. The Young's modulus E, Poisson's ratio ν and mean coefficient of thermal expansion α are 17200 kgf/cm^2, 0.3 and 1.8×10^{-5}/°C, respectively.

The pre and post deformations of the blanket vessel is shown in Fig. A.1.1.6. The distribution of the stress intensities at the inside and outside surface are shown in Fig. A.1.1.7. The maxima of the stress intensities at the inside and outside surface were 11.7 kgf/mm^2 and 6.5 kgf/mm^2, respectively.

Assuming that those stress intensities are taken for P_L+P_b+Q in ASME. Boiler and Pressure Vessel Code Sec. III, they are smaller than 3 Sm (Sm is an allowable stress and is 11.3 kgf/mm^2 of Type 316 stainless steel at 400 °C). Therefore, the blanket vessel has an enough margin against the thermal fatique failure.

Thermal Analysis

The heat flux to the first wall from plasma is 25 W/cm^2 on the average and the nuclear heating is 12 W/cm^3. Assuming heat flux of 30 W/cm^2 and nuclear heating of 12 W/cm^3, the transient behavior of the temperature distribution of cooling tube and protection wall has been analyzed by two-dimensional calculations. Cooling tube configuration and analytical conditions used are shown in Fig. A.1.1.8. Temperature changes after start up are shown in Fig. A.1.1.9. Temperature distributions in the cooling tube and protection wall are shown in Fig. A.1.1.10.

The temperature distribution becomes more uniform by the addition of the copper liner. But the integrity of the liner must be demonstrated experimentally. A disign accomodating the heat flux of 30 W/cm^2 is feasible but the fabrication of practicable panel is not easy. The design of cooling panel will be eased in case of the divertor concept owing to the reduced heat flux.

Stress Analysis of Cooling Tube

The stress analysis of the cooling tube with a copper liner on the inside surface was carried out under internal pressure and temperature distribution shown in Fig. A.1.1.10.

Two-dimensional finite elements of plane strain and plane stress conditions were employed for the elastic and thermal stress analysis. The thickness and outside radius of the cooling tube are 2.0 mm and 10.0 mm, respectively.

Fig. A.1.1.11 shows the shape of the deformation and the displacements of the cooling tube for the two conditions.

Fig. A.1.1.12 shows the distribution of the stress intensity in the plane strain condition and Fig. A.1.1.13 shows in the plane stress condition.

The results obtained from this stress analysis shows that the thermal stress depending upon the temperature difference between the sides with fin and without fin results from only the stress of the longitudinal direction. The large thermal stress of the direction generated in the area of the fin will reduce if the several cuts are given in the longitudinal direction of the fin. The reasonable deformation and stress of the cooling tube will be present between the results of plane strain and plane stress conditions. In future, it is necessary to carry out a detailed stress analysis with three-dimensional model.

A.1.1.4 Cooling System

The design of the reactor cooling system without divertor is described in this section. In the case of the reactor cooling system with devertor, the thermal energy (heat flux) is devided into the cooling panel and the divertor plate, but there is no basic difference between the reactor cooling systems with and without divertor.

The reactor cooling system is formed with three systems which cool outer blanket (tritium breeding), inner blanket (non-breeding) and cooling panel. The outer blanket cooling system has 2 lines, the inner blanket cooling system has 1 line and the cooling panel has 2 lines.

An electric power will be produced in the outer blanket cooling system and cooling panel, but not in the inner blanket cooling system. Intermediate loops to protect a tritium release are provided in each system.

Design Conditions

(1) Helium gas is used for the cooling system of the outer blanket (primary and secondary loops) and the cooling panel (primary and secondary loops).
(2) Pressurized water is used for the cooling system of the inner blanket.
(3) Design parameters of the reactor cooling system and heat load of each system are shown in Table A.1.1.1.

Heat and Mass Balance

The heat and mass balance of the cooling system is shown in Fig. A.1.1.14.

Tritium Problems

A tritium recovery system in the coolant is provided in the primary and secondary loops of the cooling system for the outer blanket and cooling panel, (He coolant). A jacket system is also provided to recover the tritium which permeates throuth the pipe wall around the high temperature piping of each primary cooling loop at the outside of the vacuum vessel wall.

The flow sheets of the tritium recovery system at each primary and secondary loop are shown in A.1.1.15. The flow sheet of the jacket system is shown in Fig. A.1.1.16.

The coolant temperature of the inner blanket cooling system is restricted to be low to prevent the tritium permeation into the coolant (water). Water purification system shown in Fig. A.1.1.17 is also prepared to remove and recover the tritium permeating in the coolant.

A.1.1.5 Design Problems

INTOR structures include many complicated components where difficulties are encountered in the fabrication. Therfore. Therefore, some of the most problematical fabrication techniques required are herein picked up and explained in brief.

(1) Welding of Outer Nozzle and Connecting Pipe

This welding is to be carried out in all positions at the workshop. Furthermore, the gap between outer nozzle and inner one is strictly limited and the integrity of the welds must be assured. From this standpoint, automatic orbital TIG welding process is employed by means of controlling system of welding conditions of each welding position.

(2) Welding of Cooling Tube and Stub

Both cooling tube panel and inner blanket are small sized in the outside diameter and closely spaced. Therfore, welding of cooling tube and stub should be automatically carried out without filler metal. Meanwhile, the welds of these small-sized tubes are apt to accompany concavity on the outside surface resulting from the relation between the gravity of molten metal and its surface tension.

In this sense, automatic orbital TIG welding should be conducted by controlling device of shield gas pressure which can give slight pressure difference between inside and outside of the tube.

(3) Welding of Non-destruction Testing of Coolant Pipe

In the welding of coolant pipe, accessibility and vigibility during welding is not insured especially at the site. Furthere, the best quality of the welds must be assured. Therefore, welding performance should be remotely controlled and its non-destructive testing is to be automatically carried out either.

Table A.1.1.1 Design Parameters of the Reactor Cooling System
(Tritium Breeding, Pressure Vessel Type)

Thermal Power		
Outer Blanket	:	214 MW
Inner Blanket	:	71 MW
Cooling Panel	:	130 MW
Total	:	415 MW
Duty Factor	:	0.8
Number of Loops		
Outer Blanket	:	2
Inner Blanket	:	1
Cooling Panel	:	2
Coolant		
Outer Blanket (primary/secondary/tertiary)	:	$He/He/H_2O$
Inner Blanket (primary/secondary)	:	H_2O/H_2O
Cooling Panel (primary/secondary/tertiary)	:	$He/He/H_2O$
Inlet and Outlet Helium Temperature of Outer Blanket Cell	:	250/550 °C
Inlet and Outlet Helium Temperature of Cooling Panel	:	200/300 °C
Inlet and Outlet Water Temperature of Inner Blanket	:	43/100 °C
Helium Pressure of Outer Blanket (primary/secondary; 40ϕ pipe)	:	30/50 ata
Helium Pressure of Cooling Panel (primary/secondary; 14ϕ tube)	:	70/75 ata
Water Pressure of Inner Blanket (primary/secondary; 10ϕ tube)	:	5/7 ata
Condensing Temperature and Pressure*	:	33°C,0.05ata
Turbine Efficiency	:	80 %
Power Transfering Efficiency x Generator Efficiency	:	95 %
Electric Power (Gross)	:	79.3 MW
Circulator Power	:	12.0 MW

*) Using a sea water cooling condensor

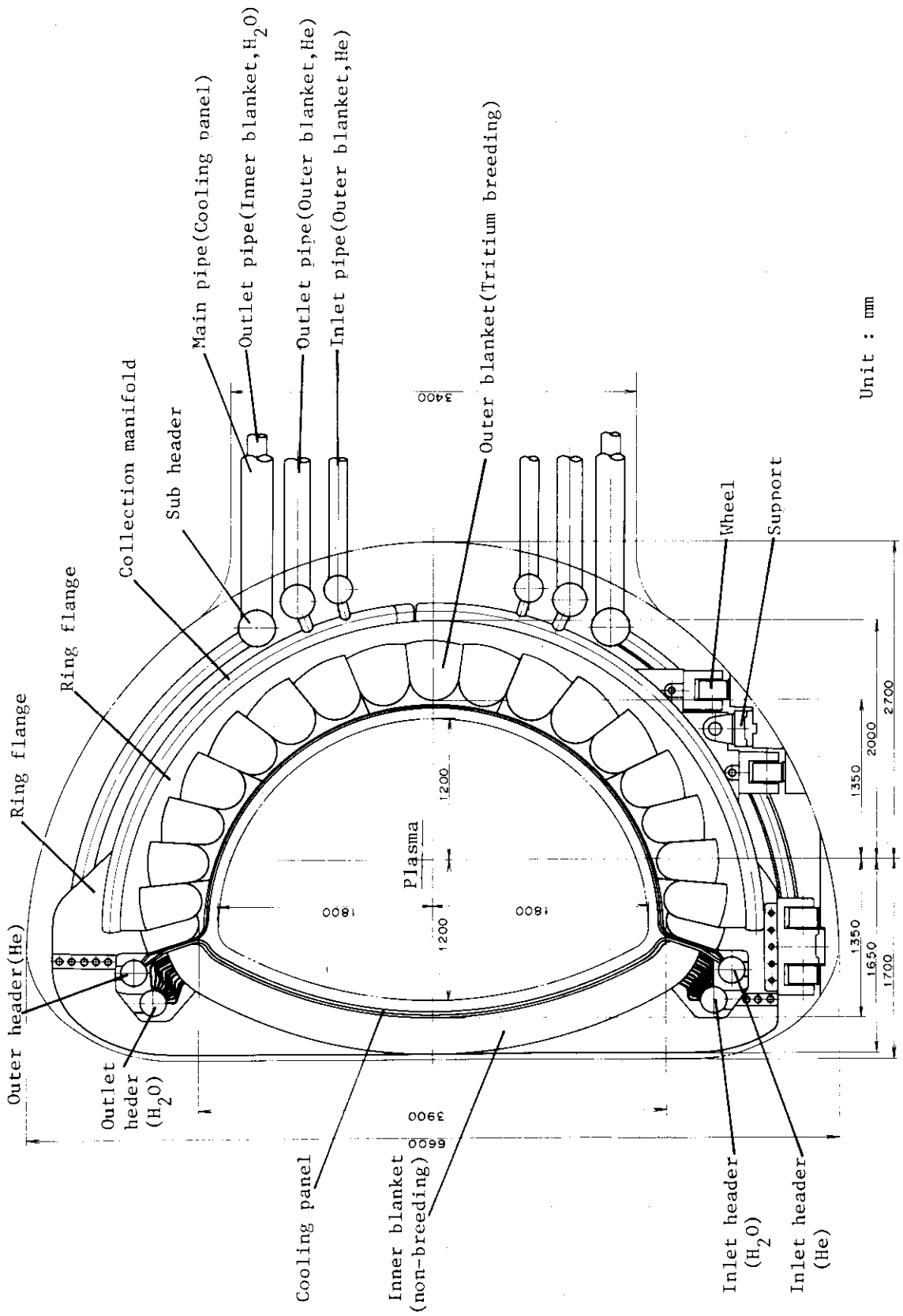

Fig. A.1.1.1 A Side View of Blanket Structure

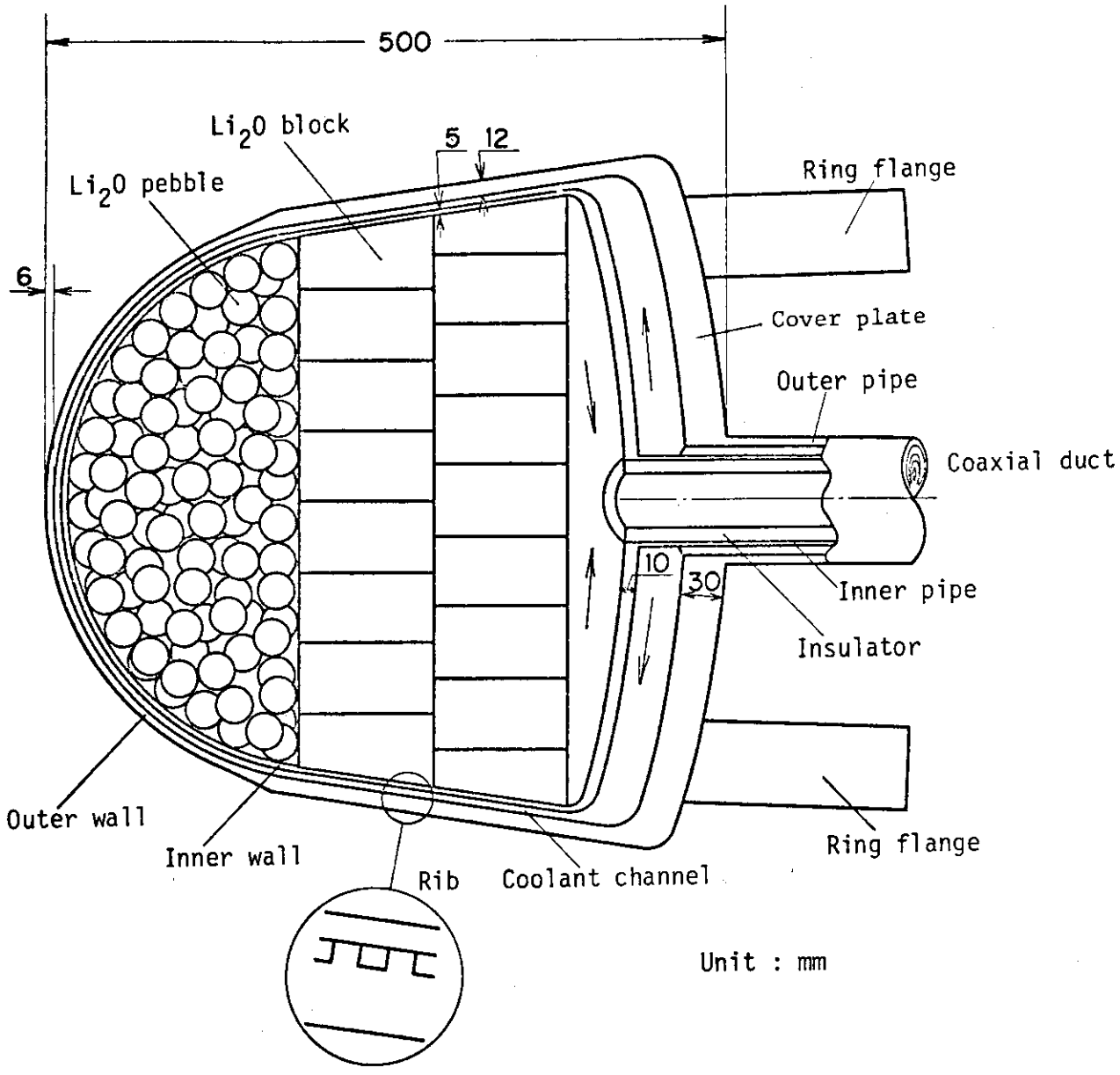

Fig. A.1.1.2 A Typical Blanket Cell

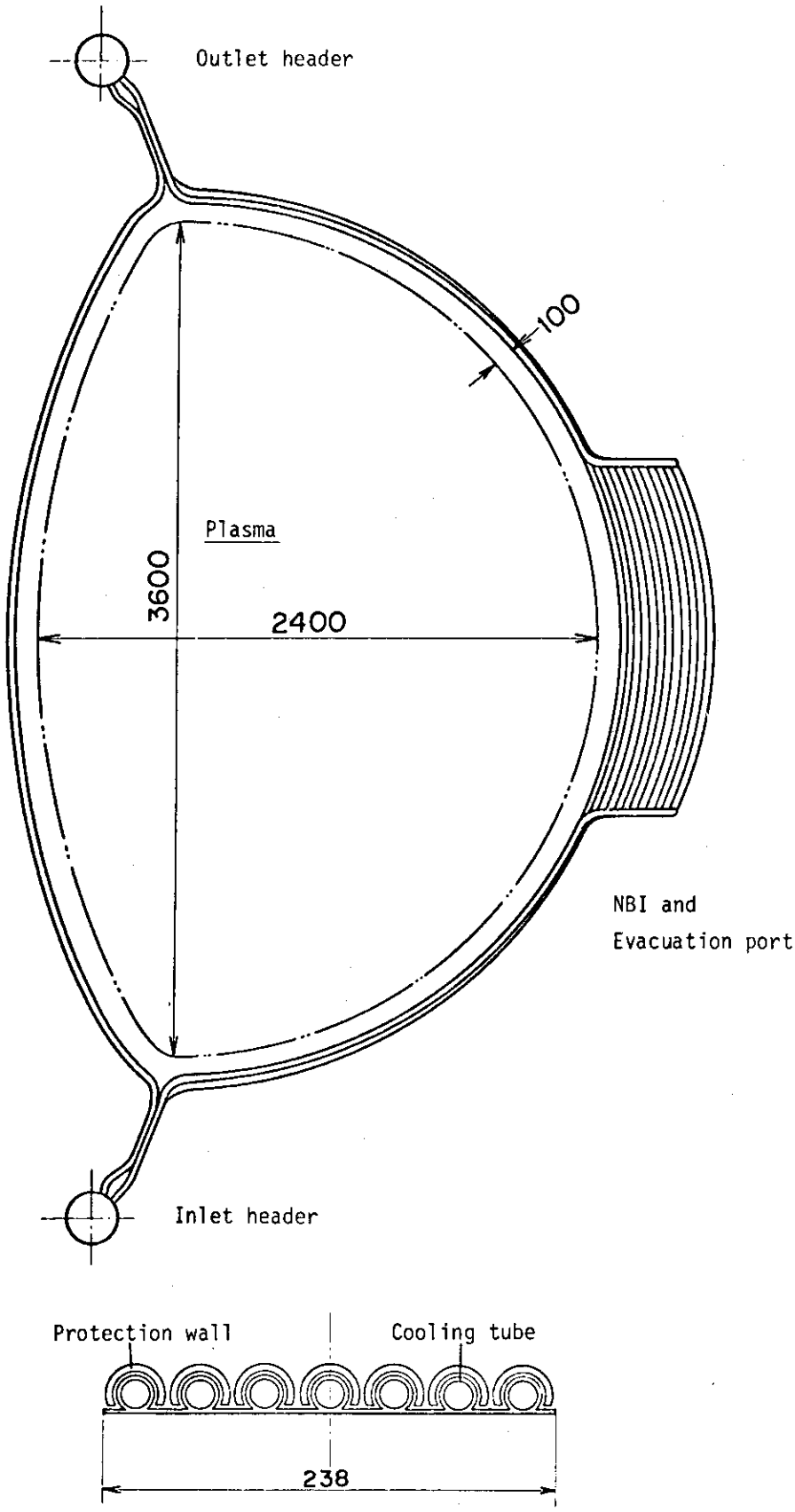

Fig. A.1.1.3 A Conceptual Structure of Cooling Panel

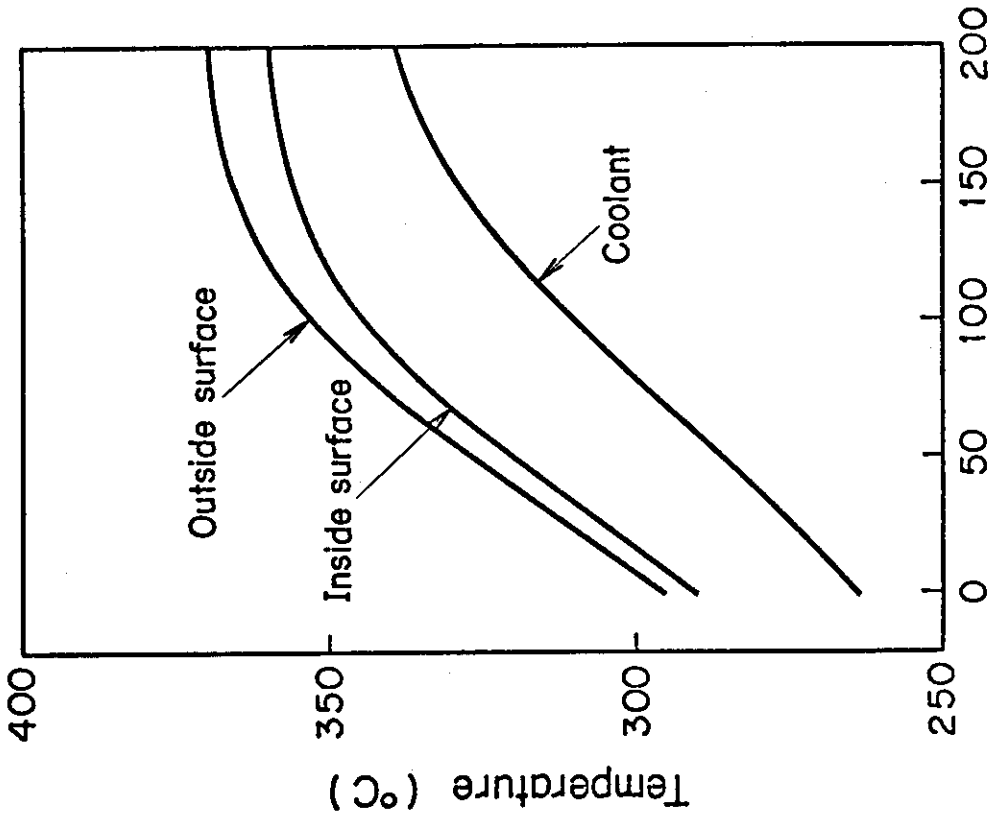

Fig. A.1.1.5 Temperature Distribution at The Dome of The Blanket Vessel

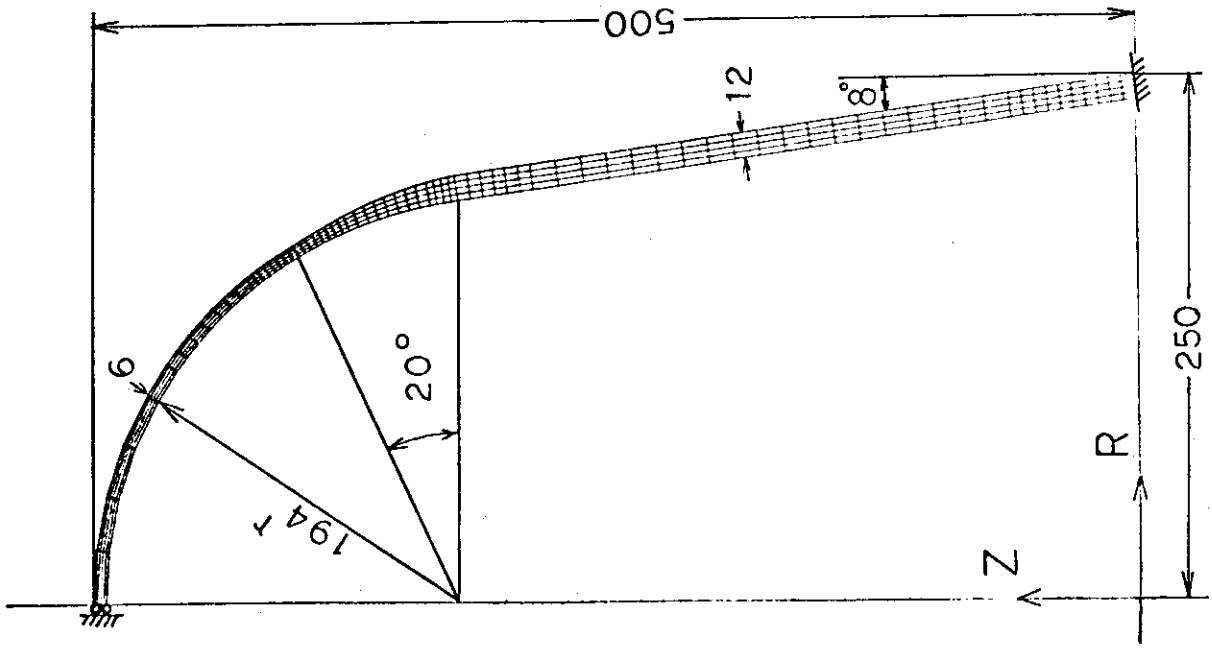

Fig. A.1.1.4 Calculational Model and Finite Element Mesh of The Blanket Vessel

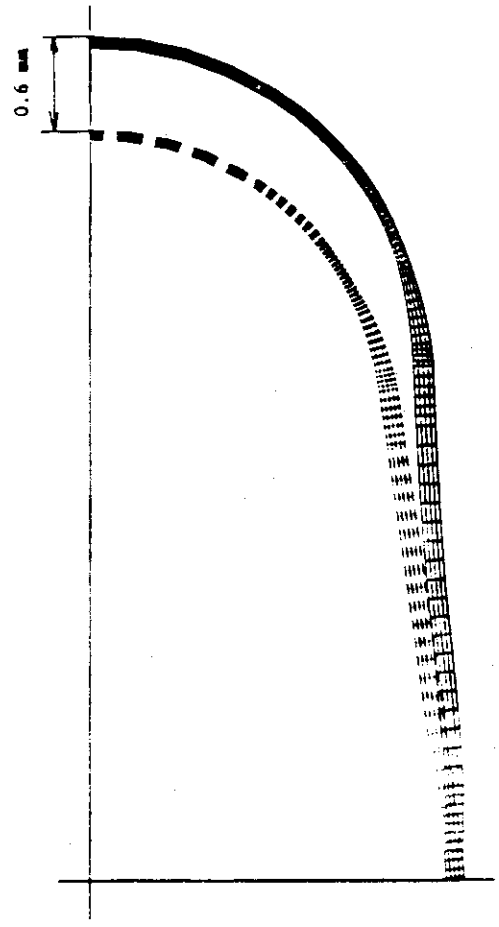

Fig. A.1.1.6 Exaggerated Deformation Shape of The Blanket Vessel

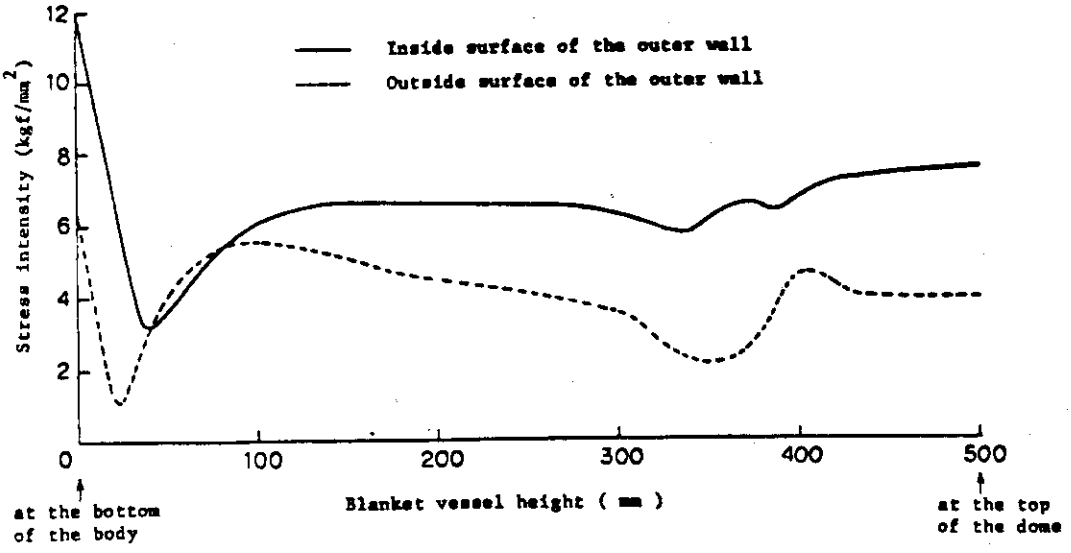

Fig. A.1.1.7 Distributions of The Stress Intensities of The Blanket Vessel under Internal Pressure and Temperature Distribution

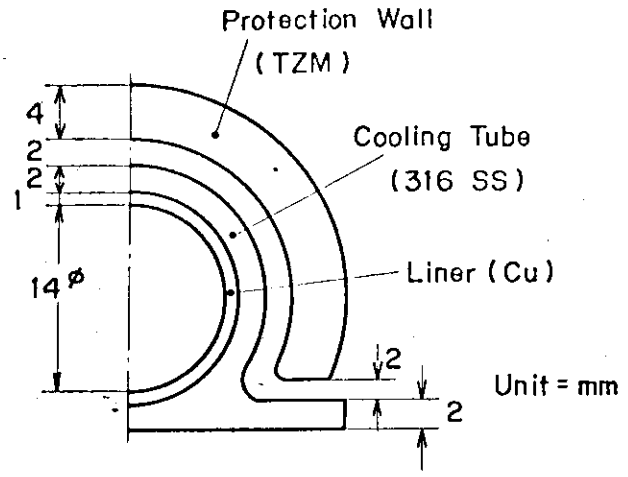

Type B

Cp_{TZM} = 0.068 cal/g °C
Cp_{316SS} = 0.13 cal/g °C
Cp_{Cu} = 0.8 cal/g°C
ρ_{TZM} = 10.2g/cc
ρ_{316SS} = 8.0g/cc
ρ_{Cu} = 8.96g/cc
h = 0.130 cal/cm^2 s °C
He Temp. = 300°C

Fig. A.1.1.8 Cooling Tube Configulation and Analytical Conditions

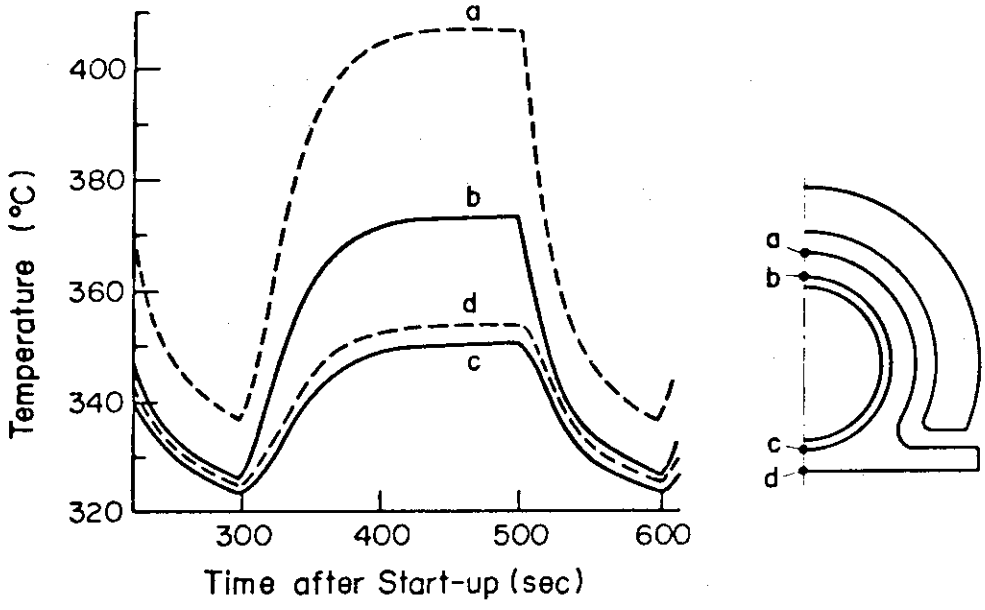

Fig. A.1.1.9 Temperature Change of Cooling Tube after reactor start up

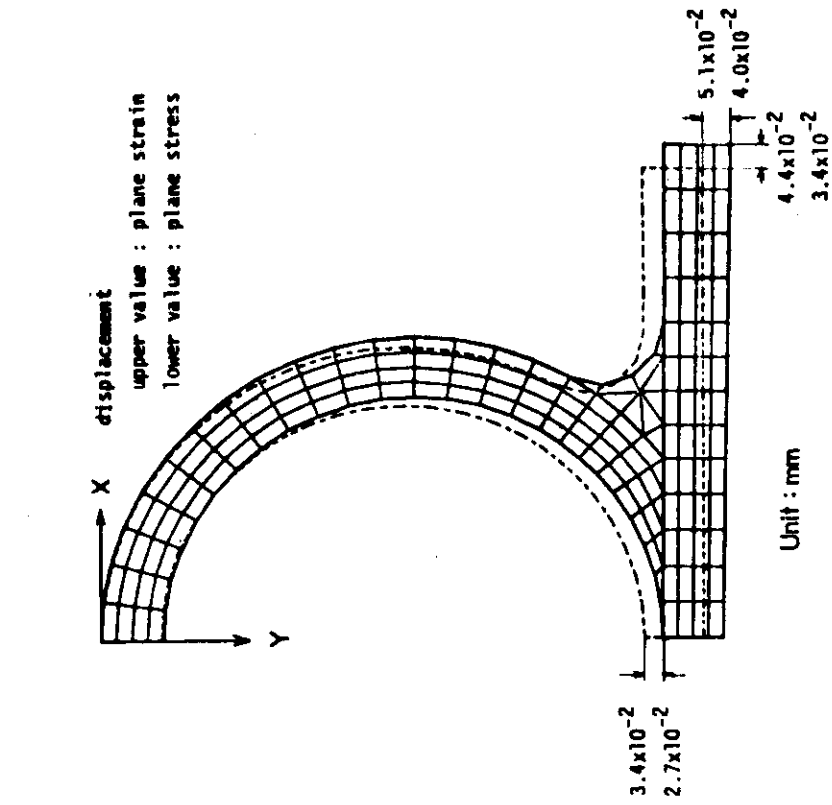

Fig. A.1.1.11 Shape of Deformation and Displacements of The Cooling Tube for Two Conditions

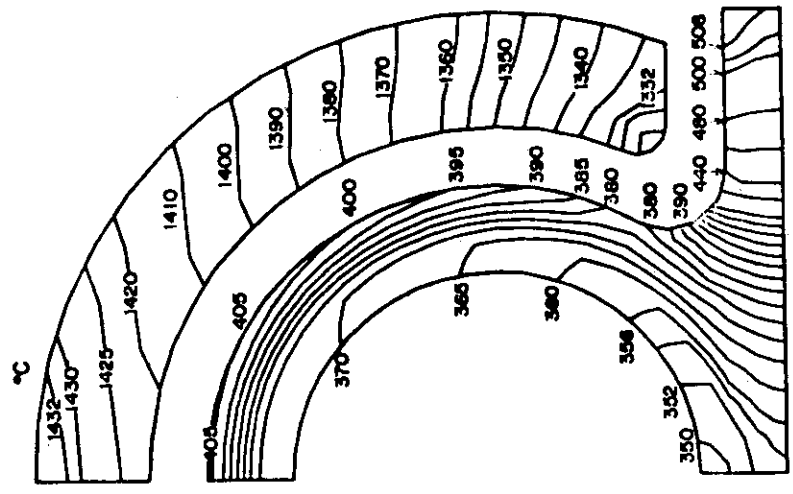

Fig. A.1.1.10 Temperature Distribution in The Cooling Tube and Protection Wall

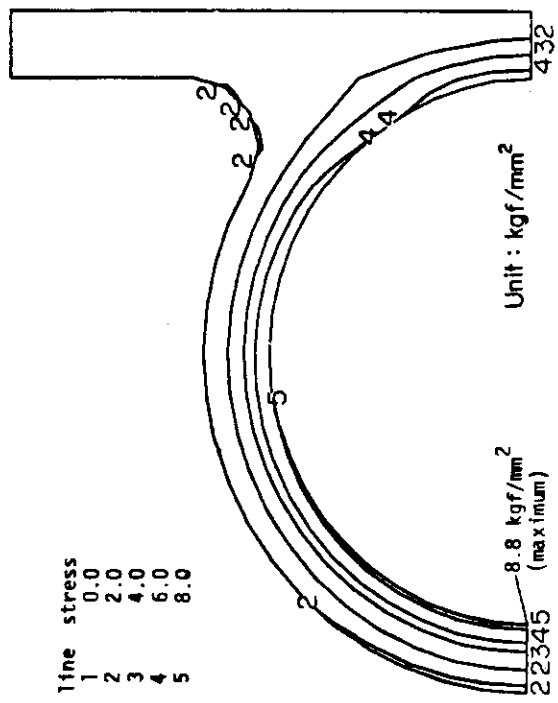

Fig. A.1.1.13 Distribution of Stress Intensities for Plane Stress Condition

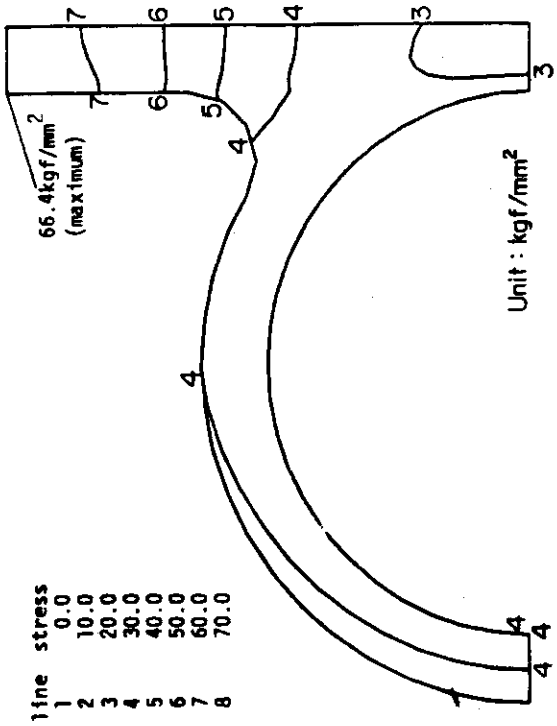

Fig. A.1.1.12 Distribution of Stress Intensities for Plane Strain Condition

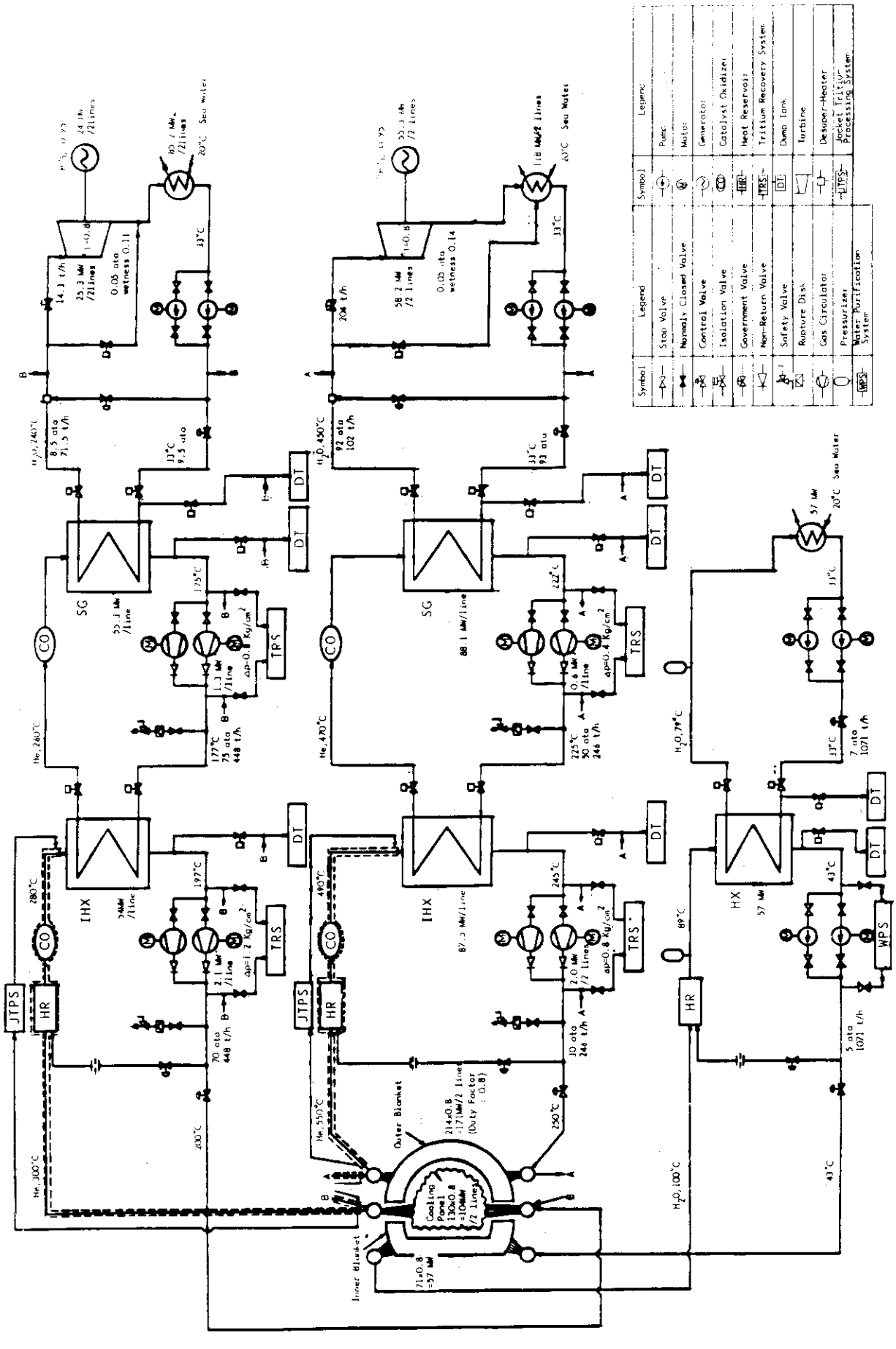

Fig.A.1.1.14 Flow Sheet of Tritium Breeding System (Pressure Vessel Type)

BL-1,2	Blower	SMS-1,2,3	Small Molecular Sieve Tower
HX-1,2	Heat Exchanger	CT-1,2	Cold Trap
CL-1	Cooler	EC-1,2	Electric Cell
DS-1,2	Dust Separater	PM-1,2	Pd Membrane Permeater
LMS-1,2	Large Molecular Sieve Tower	ISS	Isotope Separation System
ACT-1,2	Adsorptive Cold Trap	TT-1,2,3	Tritium Storage Tank
ST-1,2	Surge Tank		

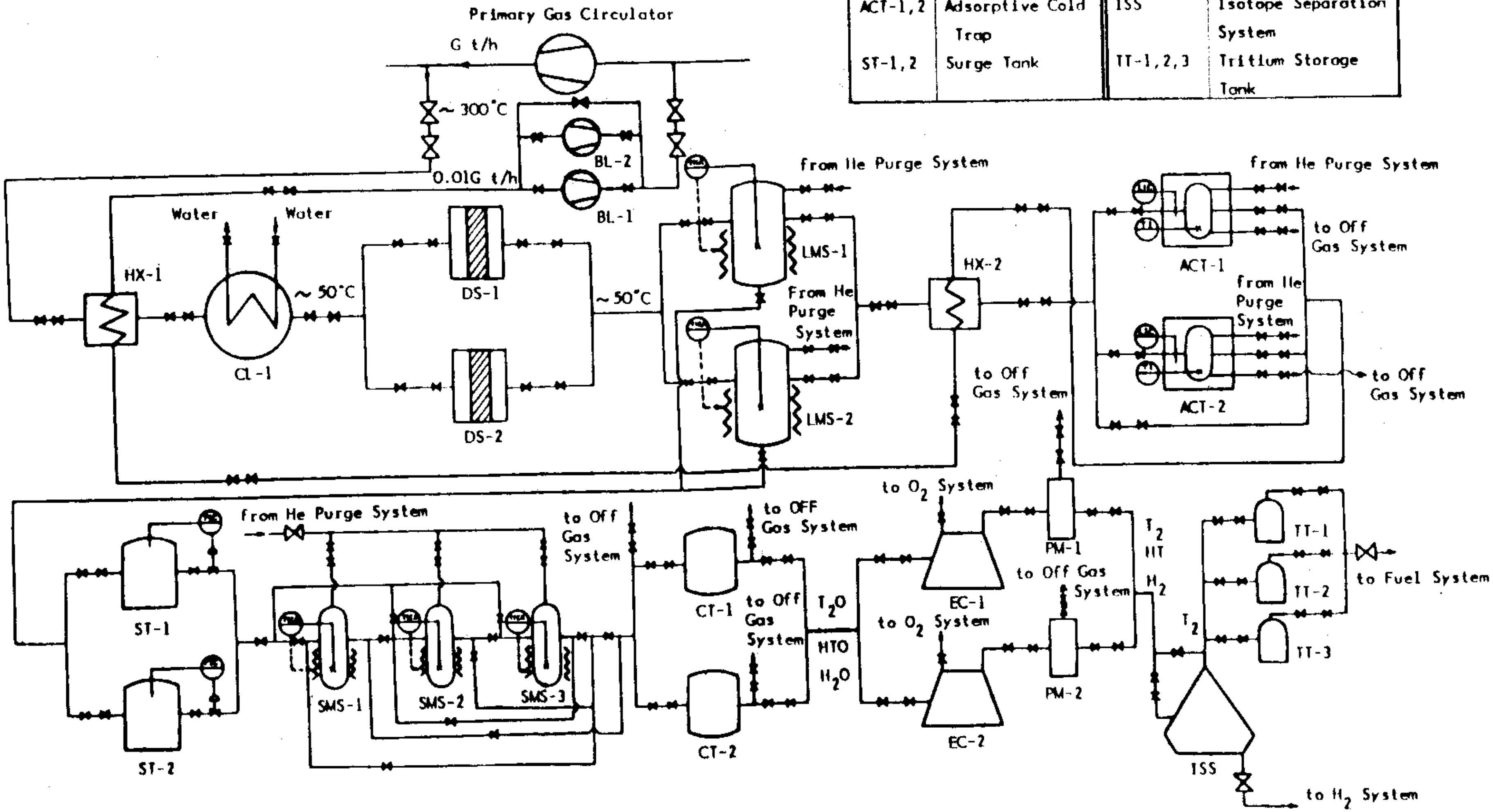

Fig.A.1.1.15 Flow Sheet of Tritium Recovery System

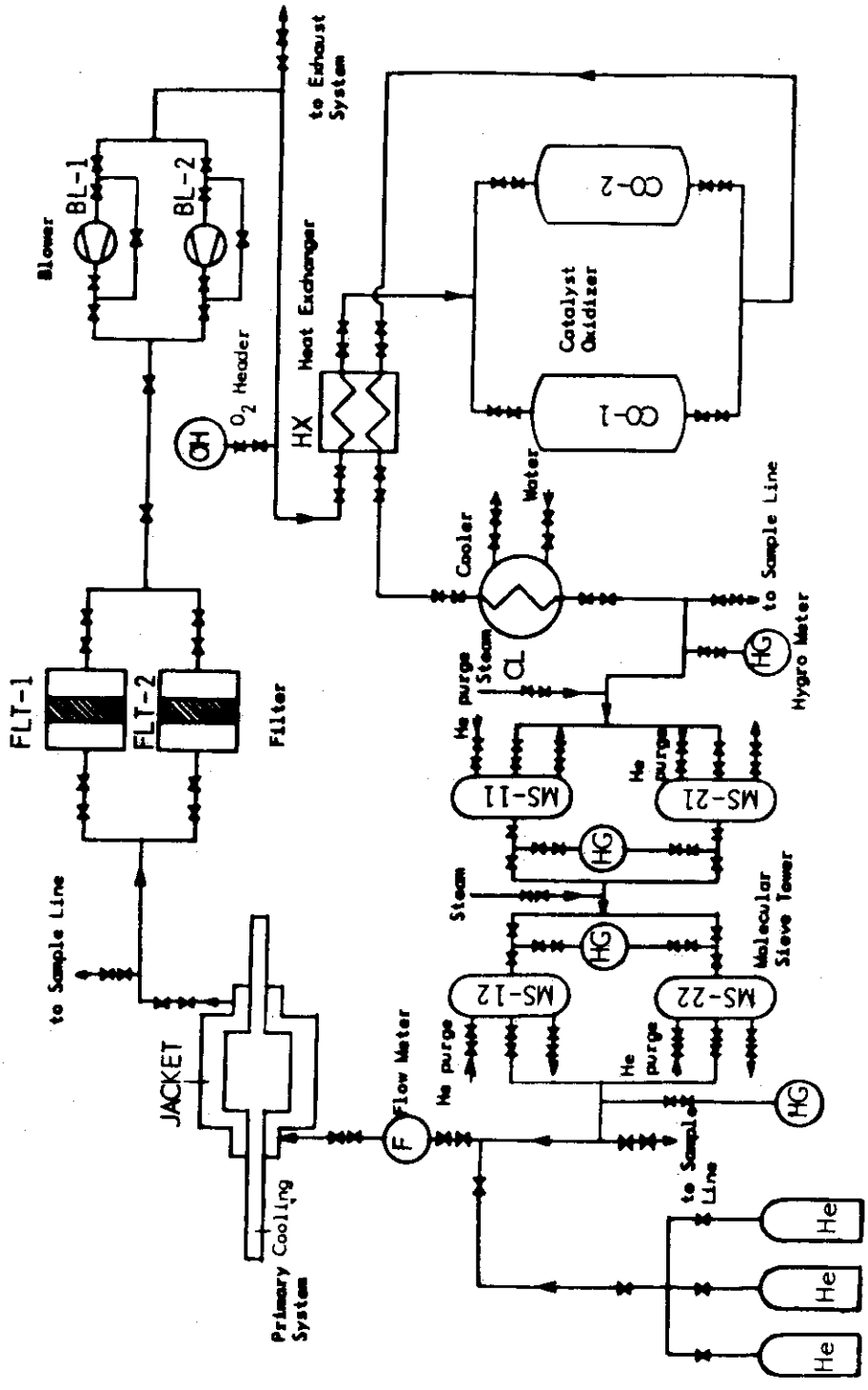

Fig.A.1.1.16 Flow Sheet of Jacket Tritium Processing System

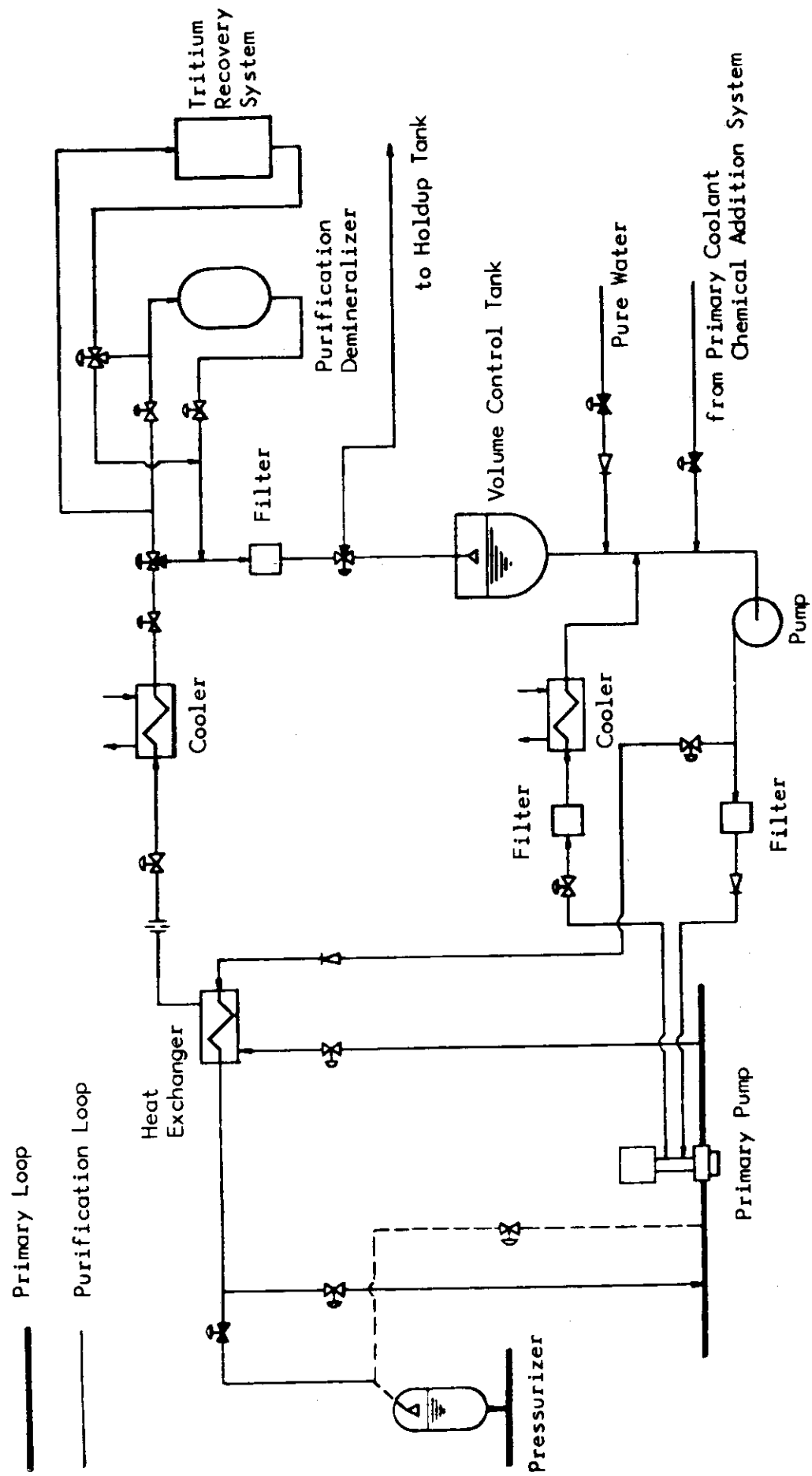

Fig. A.1.1.17 Flow Sheet of Water Purification System

A.1.2 Tube in Shell Type

The blanket structure of the tube in shell type consists of six blanket modules. As concerns with the outer blanket of each module, the cooling tubes are arranged in the blanket shell and Li_2O pebbles are filled around the cooling tubes. The cooling panel is provided at the plasma side of the blanket shell. The tritium, which is produced in Li_2O pebbles, is recovered by helium purge gas.

Both water and helium gas may be used as the coolant in the tube, but the design of the cooling system cooled by water is described in this section.

A.1.2.1 Design Conditions

Outer Blanket

(1) The outer blanket for tritium breeding is cooled by pressurized water at 100 kgf/cm^2.
(2) The coolant flows horizontally in the cooling tube from one end of the blanket module to the other end.
(3) The inlet and outlet temperatures of the coolant are 290 and 305 °C, respectively.

Inner Blanket

(1) The inner blanket for non-breeding is cooled by pressurized water at 100 kgf/cm^2.
(2) The coolant flows from the lower side of the inner blanket to the upper side.
(3) The inlet and outlet temperatures of the coolant are 290 and 305 °C, respectively.

Cooling Panel

The cooling panel with a protection wall is prepared in front of the plasma side of each blanket and the cooling conditions are similar to each blanket cooling system.

He Purge System

The purge gas to recover tritium is helium at 1 kgf/cm^2.

Power Generation

The cooling conditions of each coolant are completely similar.

Each coolant is collected in the common header and then is led to the power generation system.

Heat Flux and Nuclear Heating Rate

(1) The maximum heat flux is 30 W/cm^2.

(2) The maximum nuclear heating rate is 12 W/cc.

A.1.2.2 Blanket Structure

The outer blanket is a double-walled shell made of stainless steel which is 5 mm in thickness at the plasma side. A lot of cooling tubes, which is 30 mm in O.D. x 5.0 mm in thickness, are horizontally arranged.

The pitch in the area close to the plasma is small and the one in the area far from the plasma is large so that the temperature of Li_2O pebbles becomes entirely constant in the blanket.

As the nuclear heating rate at the plasma side of the blanket shell is especially large (about 12 W/cc), ribs fcr the forced cooling are provided in the inside of the blanket shell in order to restrict the temperature of the wall within the allowable limitation. Moreover, as the helium of high temperature is in contact with the neighborhood of the outlet for the helium purge gas, the neighborhood is so cooled that the wall temperature of the blanket shell becomes low.

The structures of the inner blanket and the cooling panel are similar to Chapter 3.1.

The coolant (water) of the cooling panel and each blanket is collected in the common header, is distributed two loops and then is led to power generation system.

Fig. A.1.2.1 shows the conceptional structure of the blanket for water cooling and tube in shell type.

Fig. A.1.2.2 shows the cross section of the outer blanket.

A.1.2.3 Design Analysis

Maximum Temperature of Li_2O

(1) Analytical Model

The thermal energy generated in Li_2O is removed with a lot of Cooling tubes which are arranged in the blanket shell. As the model of the simple analysis, the cooling area of one cooling tube is regarded as one-dimensional model shown in these figures.

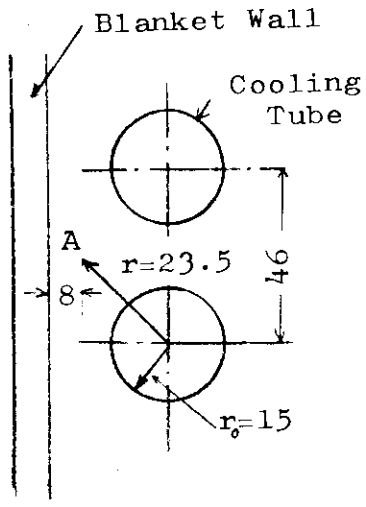

Analytical Unit

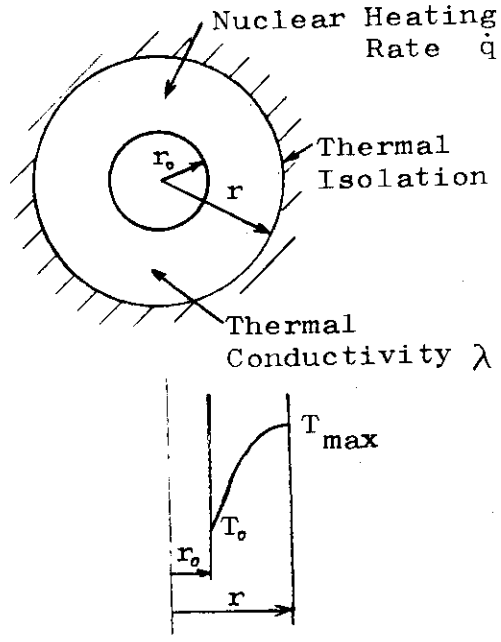

Analytical Model

It seems that the maximum temperature is indicated at point A which is far from the cooling tube.

(2) Analytical Method

The maximum temperature which is obtained from that model is given by the following equation.

$$T_{max} - T_o = \frac{\dot{q}}{\lambda} \left(\frac{r^2}{2} \ln \frac{r}{r_o} - \frac{r^2 - r_o^2}{4} \right) \qquad (1)$$

where, T_{max} : Maximum temperature of Li_2O which is generated at the adiabatic boundary

T_o : Nuclear heating rate of Li_2O

: Equivalent thermal conductivity of Li_2O

$\dot{q}$: Outside radius of Li_2O

λ : Inside temperature of Li_2O which is in contact with

r the cooling tube

r_o : Inside radius of Li_2O

(3) Analytical Results

The nuclear heating rate at the point which is 8 mm away from the wall of the blanket shell is as follows;

$$\dot{q} = 6.75 \exp(-x / 20.7) \quad W/cc$$

In order to calculate the equivalent thermal conductivity of

Li_2O, it is assumed that Li_2O of which theoritical density is 85 % occupies the space of 75 % and each layer (Li_2O and helium) is arranged in a row or in a series.

$$\lambda_{row} = 0.75\ \lambda_{Li_2O} + 0.25\ \lambda_{He} = 6.06\times10^{-3}\ \text{cal/cm s °C}$$

$$\lambda_{series} = \frac{1}{\frac{0.75}{\lambda_{Li_2O}} + \frac{0.25}{\lambda_{He}}} = 2.64\times10^{-3}\ \text{cal/cm s °C}$$

The true thermal conductivity will exist in the middle of above values.

The results obtained from those values above mentioned is shown in a following table.

λ (cal/cm s °C)	6.06×10^{-3}	2.64×10^{-3}
T_{max} (°C)	849	1514

In this analysis, the inside temperature of Li_2O (T_o) is assumed 335 °C.

A.1.2.4 Cooling System

The design of the cooling system without divertor is described here.

The cooling system is formed with four systems which cool the outer blanket (tritium breeding), the first wall of the outer blanket (rib), the inner blanket (non-breeding) and the cooling panel. The cooling system has two loops at the outside of the reactor. The coolant is once collected in the common header and then is again distributed. The power generation system has one loop.

Design Conditions

(1) The coolant of the primary system is pressurized water.
(2) The thermal energy in the reactor is used to generate electric power.
(3) In order to generate the electric power, the existing PWR conditions are adapted to the power generating system.
(4) The indirect steam generator is prepared to protect a tritium release.
(5) The design parameters of the cooling system are shown in Table A.1.2.1.

Heat and Mass Balance

Fig. A.1.2.3 shows the heat and mass balance of the cooling system.

Tritium Problems

A water purification system is prepared to remove and recover the tritium permeating in the coolant.

A.1.2.5 Design Problems

Piping System

Site welding of pipe must be carried out in the limited space. These welded joint of pipe must be defect-free lest leakage should occur during operation. In this sense, welding should be automatically perfomed with high reproducibility by unmanned welding machine which enables supervisory and remote control. Furthermore, nondestructive testing must be also automatically carried out by remote handling to assure the integrity of the welds.

Outer Blanket

When double-wall structure is introduced, inner and outer shell are joint by electron beam welding process, and later cover plate is assembled to the shell. Cooling tube bundle penetrates this cover plate and is closely spaced in the inner shell.

As far as it concerns with electron beam welding, it is most desirable welding process for this kind of joint between inner and outer shell in view of less weld deformation in itself. Partial-penetration electron beam welding is conducted from inside of inner shell, and its accessibility is very much limited in welding procedure. Therefore, it is required that welding is carried out by compact portable-type partial-vacuum one with beam deflection mechanism.

Meanwhile, TIG welding of small-sized tube is mentioned afore in inner blanket in Chapter 3.5.

Table A.1.2.1 Design Parameters of the Reactor Cooling System
(Tritium Breeding, Tube in Shell Type)

Thermal Power		
Outer Blanket	:	214 MW
Inner Blanket	:	71 MW
Cooling Panel	:	130 MW
Total	:	415 MW
Duty Factor	:	0.8
Number of Loops	:	2
Coolant (primary/secondary)	:	H_2O/H_2O
Primary Coolant Temperature (inlet/outlet)	:	290/305 °C
Coolant pressure (primary/secondary)	:	100/15 ata
Temperature of Condenser Cooling Water (Sea Water)	:	20 °C
Condensate Temperature/Pressure	:	33°C/0.05ata
Eletric Power (Gross)	:	111 MW

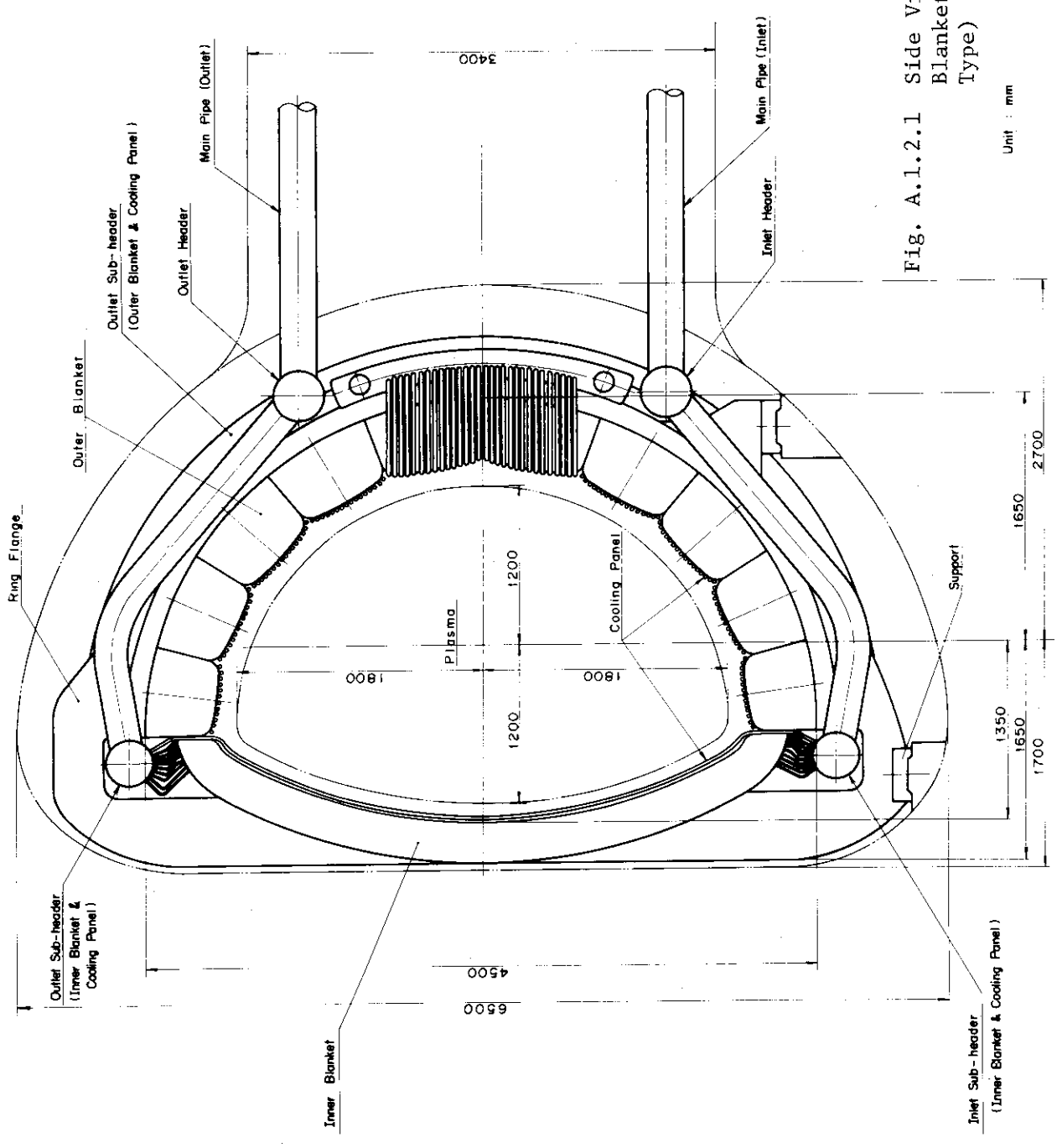

Fig. A.1.2.1 Side View of Breeding Blanket (Tube in Shell Type)

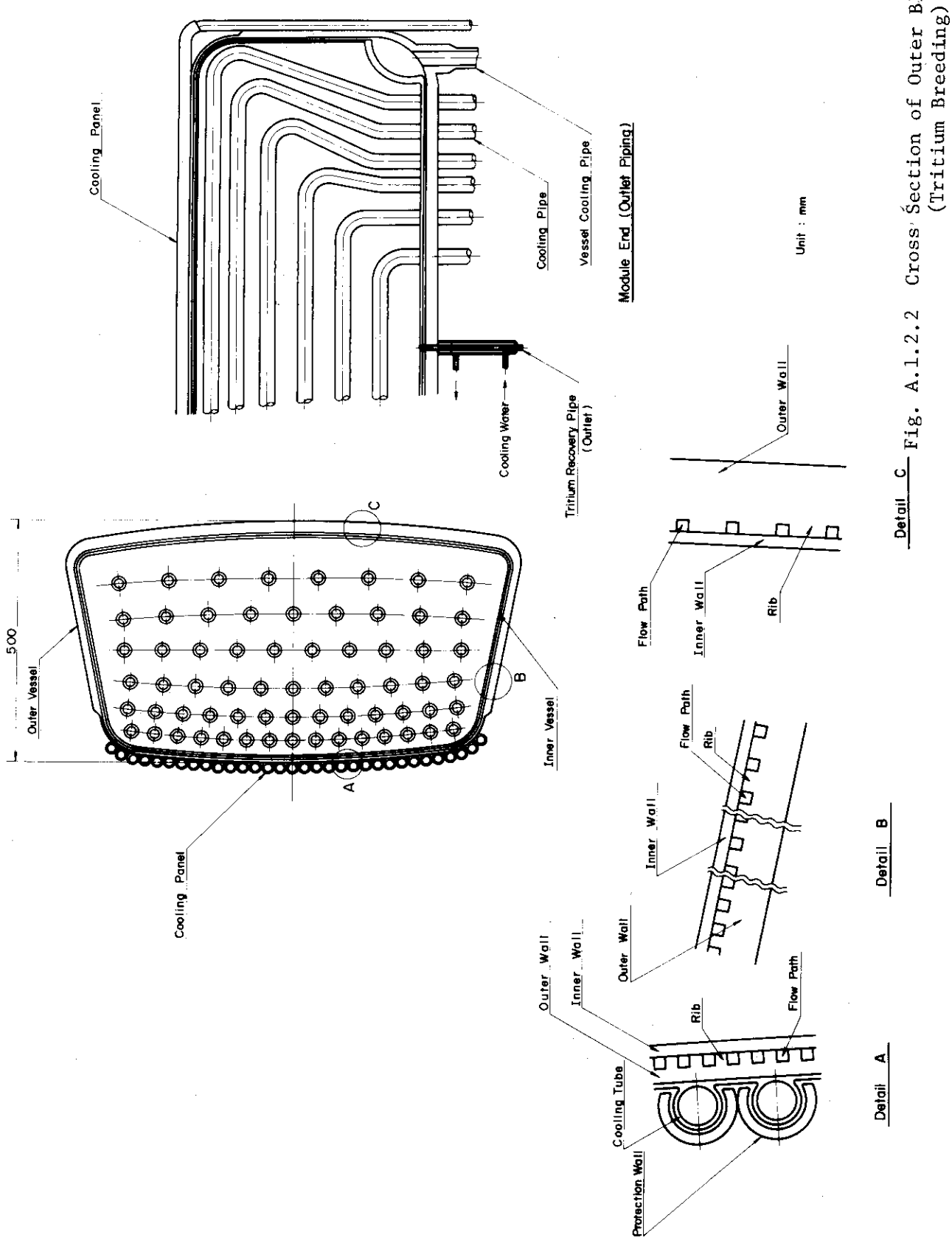

Fig. A.1.2.2 Cross Section of Outer Blanket (Tritium Breeding)

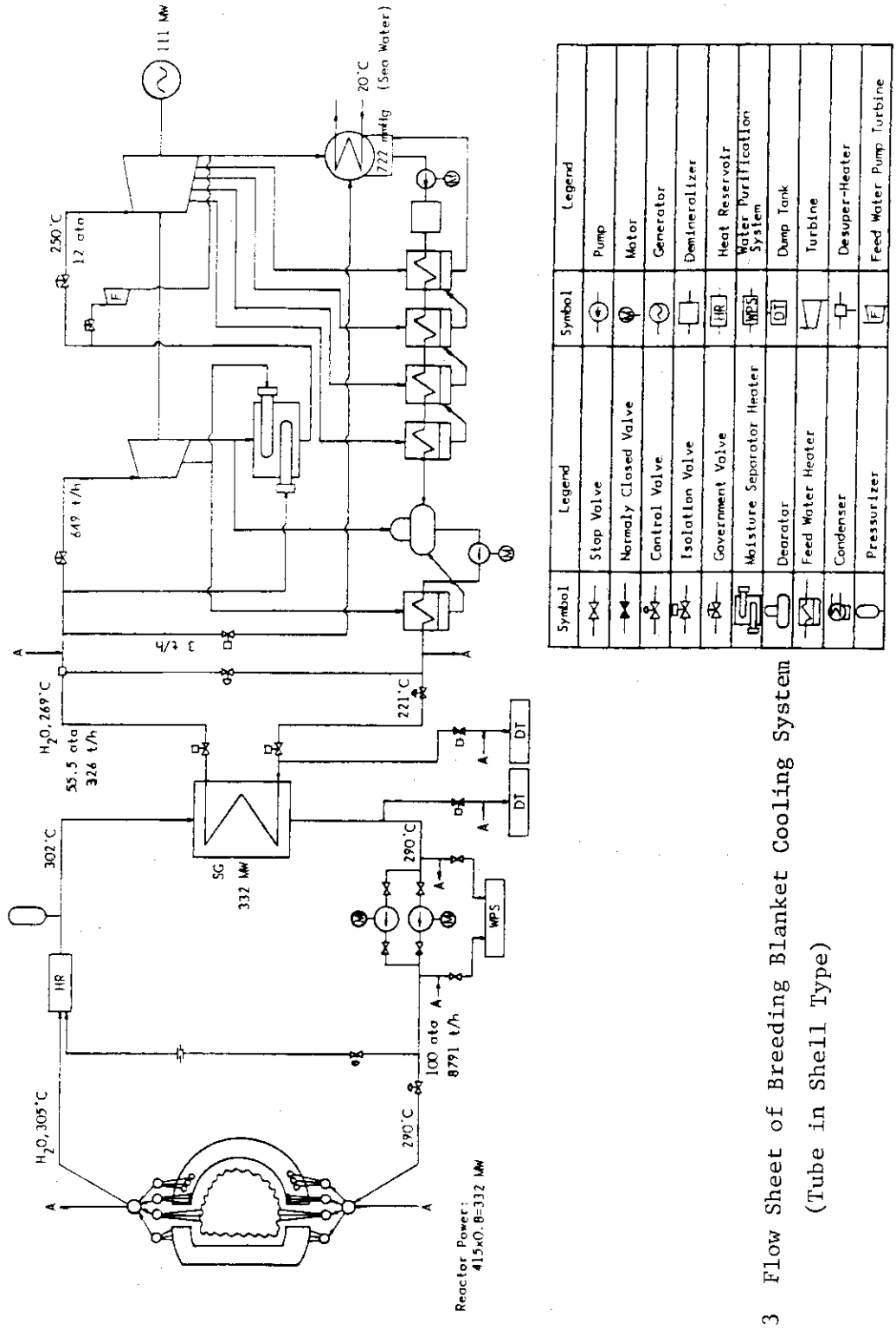

Fig. A.1.2.3 Flow Sheet of Breeding Blanket Cooling System (Tube in Shell Type)

A.2 Neutronics Calculations for Tritium Breeding Blanket

A.2.1 Tritium breeding ratio

(1) Pressure vessel type blanket

To estimate tritium breeding ratio of pressure vessel type blanket mentioned in A.1.1 three cases of calculation are carried out.

Figure A.2.1.1 shows the calculational model of case 1 which is performed by using one-dimensional Sn transport code ANISN. Figure A.2.1.2 shows the triton production distribution obtained by this code. The case 2 and case 3 are three-dimensional calculations by Monte Carlo transport code MORSE-I. Figure A.2.1.3 shows the calculation model of the case 2. In this case, torus geometry of plasma, blanket and shield, neutron source density distribution and the difference between the compositions of inner and outer blankets are taken into account while in one-dimensional calculation they are not. The case 3 is a three-dimensional blanket cell model which takes account of heterogeneity of the cell. Figure A.2.1.4 and 5 show the calculational model of the case 3. Table A.2.1.1 shows tritium breeding ratios estimated in the three cases. The case 1 and the case 3 give almost same value of tritium breeding ratio, so the effect of blanket cell heterogeneity must be very small in this case. The tritium breeding ratio for the case 2 is about two thirds of that for the case 1. It is because the case 2 takes account of the fact that the inner blanket does not contain breeding materials. It is almost impossible to load breeding materials in the inner blanket of a small-sized tokamak reactor such as INTOR because the inner blanket is required to be a high energy neutron shield rather than tritium breeding blanket. The tritium breeding ratio of INTOR with blanket cells as shown in Figure A.1.1.1 is estimated to be about 0.6 according to the case 2 calculation.

Table A.2.1.1 Tritium breeding ratios of pressure vessel type blanket

	Tritium Breeding Ratio		
	^{7}Li	^{6}Li	Total
Case 1	0.157	0.751	0.908
Case 2	0.127	0.487	0.614
Case 3	0.158	0.734	0.892

Neutron source distribution in three dimensional calculation

Neutrons are emitted isotropically from sources which distribute proportionally to fusion power density.

The power density distribution is obtained by the following process. In the MHD equilibrium, plasma pressure is expressed with the flux function Ψ as follows:

$$P = P_0 \, \psi^{\zeta}$$

Then ion temperature and density distributions are assumed as follows:

$$T = T_0 \, \psi^{\eta}$$

$$n = n_0 \, \psi^{\xi}$$

$$\eta + \xi = \zeta$$

In the case of INTOR, the value of ζ is 1.48, and η is assumed to be 1.0 for this calculation.

The fusion power dnesity is given by

$$P_f = \frac{< \sigma v > n^2}{4} \cdot Q$$

Figure A.2.1.6 shows the fusion power density distribution when the average ion temperature $\bar{T}$ is 10 keV. Where $\bar{T}$ is defined as

$$\bar{T} = \frac{\int nT \, dv}{\int n \, dv}$$

The fusion reaction cross section used in this calculation is

$$< \sigma v > = 370.0 \exp(-20 \times Ti^{-\frac{1}{3}}) \; / \; ((1+(Ti/70)^{1.3}) \times Ti^{\frac{2}{3}}) \quad 8)$$

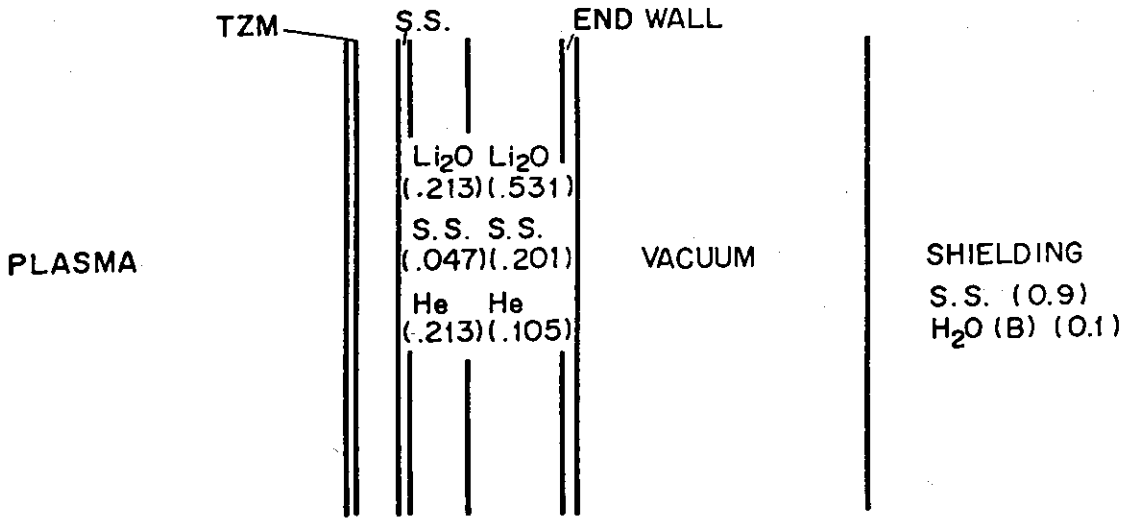

Fig. A.2.1.1 One-dimensional Calculation Model of INTOR-J

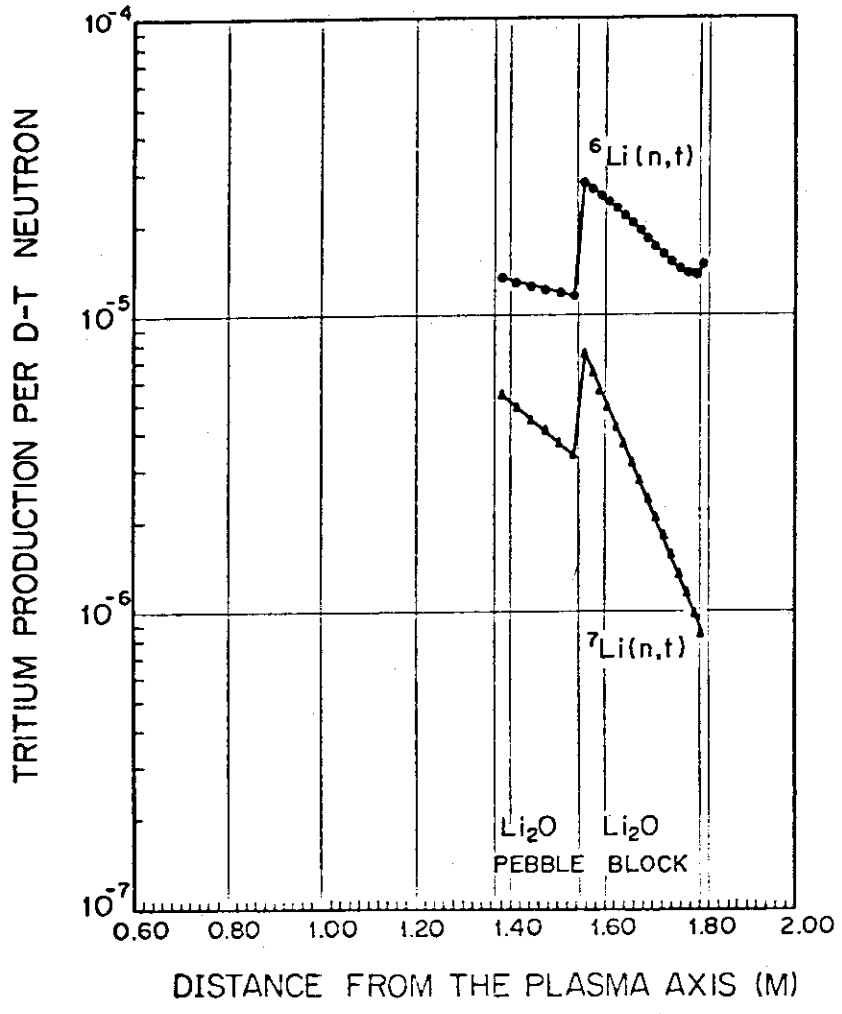

Fig. A.2.1.2 Tritium production distribution in outboard blanket

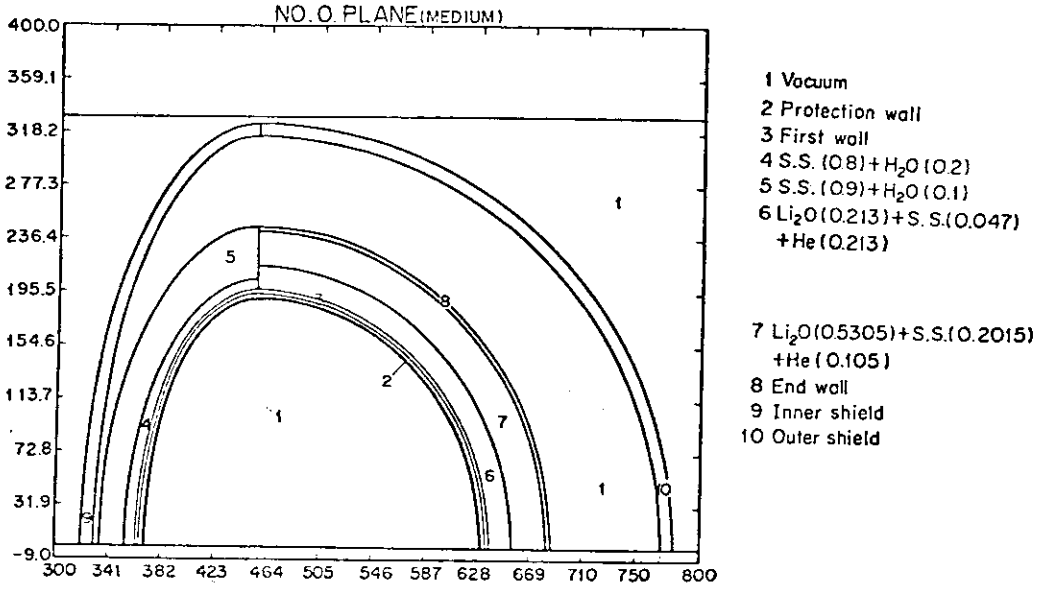

Fig. A.2.1.3 Three-dimensional Calculation Model of INTOR-J

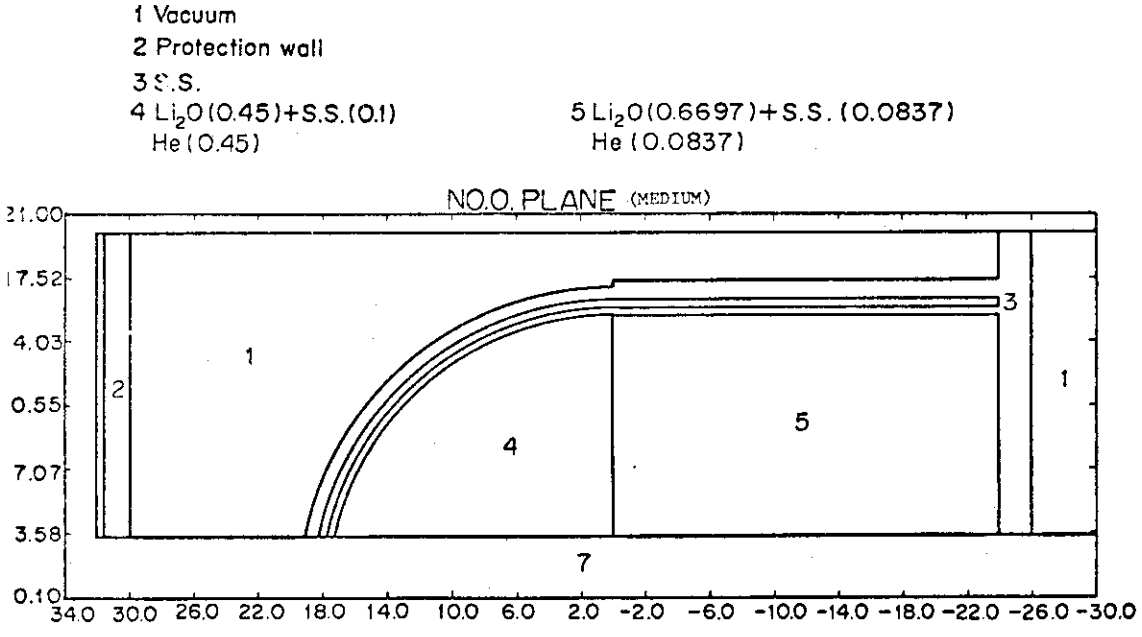

Fig. A.2.1.4 Three-dimensional Calculation Model of Pressure Vessel Type Blanket Cell

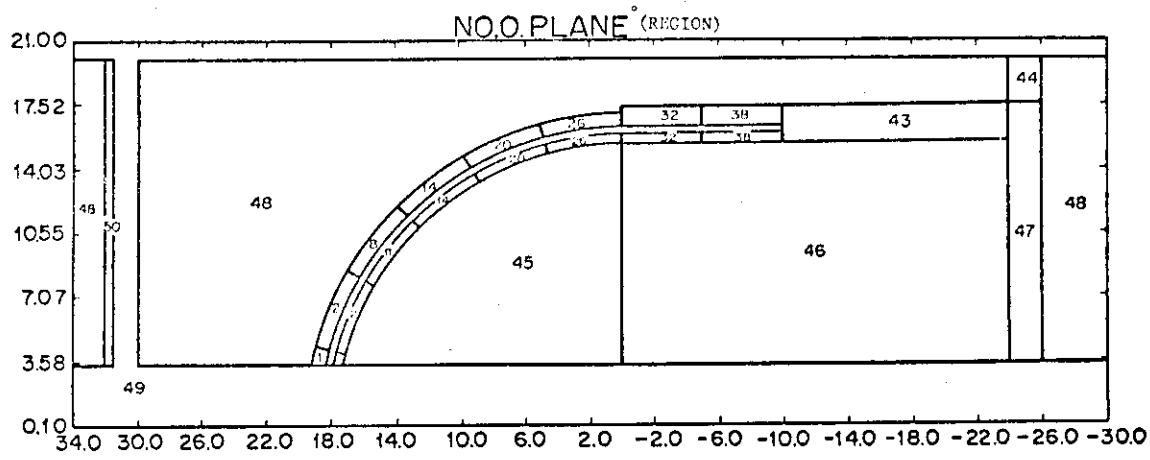

Fig. A.2.1.5 Nuclear Heating Density Editing Region for Pressure Vessel Type Blanket Cell

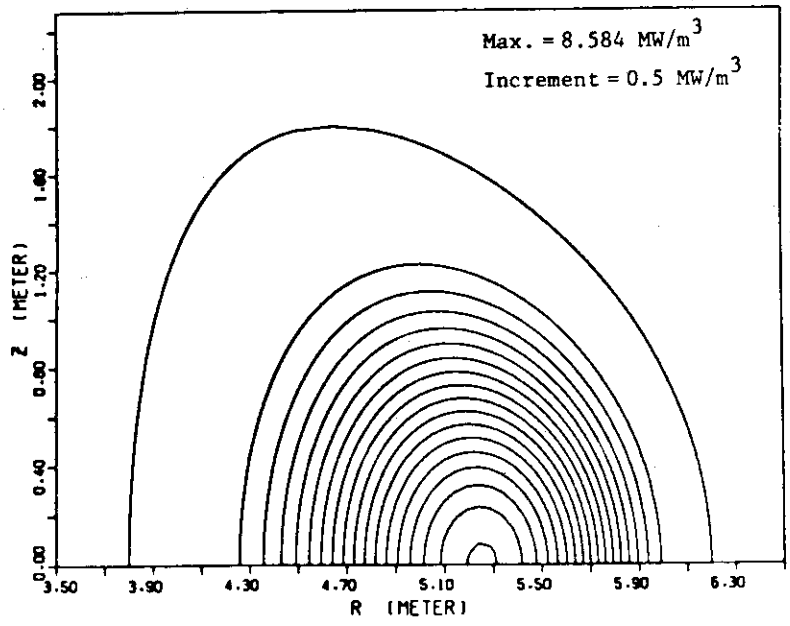

Fig. A.2.1.6 Power Density Contour

(2) Tube in shell type blanket

Figure A.2.1.7 shows schematic layout of one dimensional calculation model of tube in shell type blanket. The tritium breeding ratio with this blanket placed fully around the plasma is calculated to be 1.10. When this blanket is placed only on the outboard of torus tritium breeding ratio can be estimated to be 0.74 considering the ratio of tritium breeding ratios of case 1 and 2 in Table A.2.1.1 is 0.676.

The tritium breeding ratio of the tube in shell type blanket with helium cooling in place of water cooling will be nearly same as above if the volume ratio of stracture is not changed.

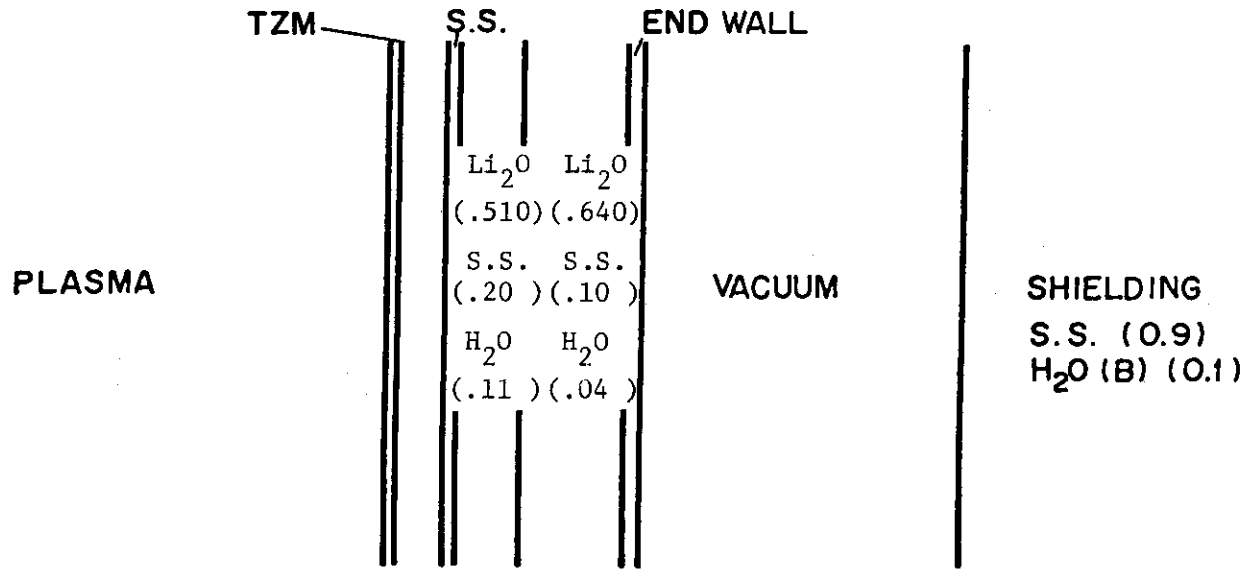

Fig. A.2.1.7 One-dimensional Calculation Model of Tube in Shell Type Blanket

(3) Test module

The tritium produced in a test module (area of 1 m^2) shown in Fig. 14.1.1 is expected to be 4 g/y. If the test cell is tube in shell type larger space factor (0.6 ; twice of the pressure vessel type), and hence larger tritium production rate, will be obtained.

(4) Test segment

The tritium of about 900 g will be produced in a test segment.

A.2.2 Nuclear Heating Rate

The detail nuclear heating rate distribution in the dome of pressure vessel type blanket is calculated by Monte Carlo code. The calculational model is the same as case 3 in A.2.1 (see Fig. 2.1.4 and 5).

The calculational result is shown in Fig. A.2.2.1. The peak of the heating rate at the top of dome is about 10 w/cc which agrees well with the one dimensional calculation.

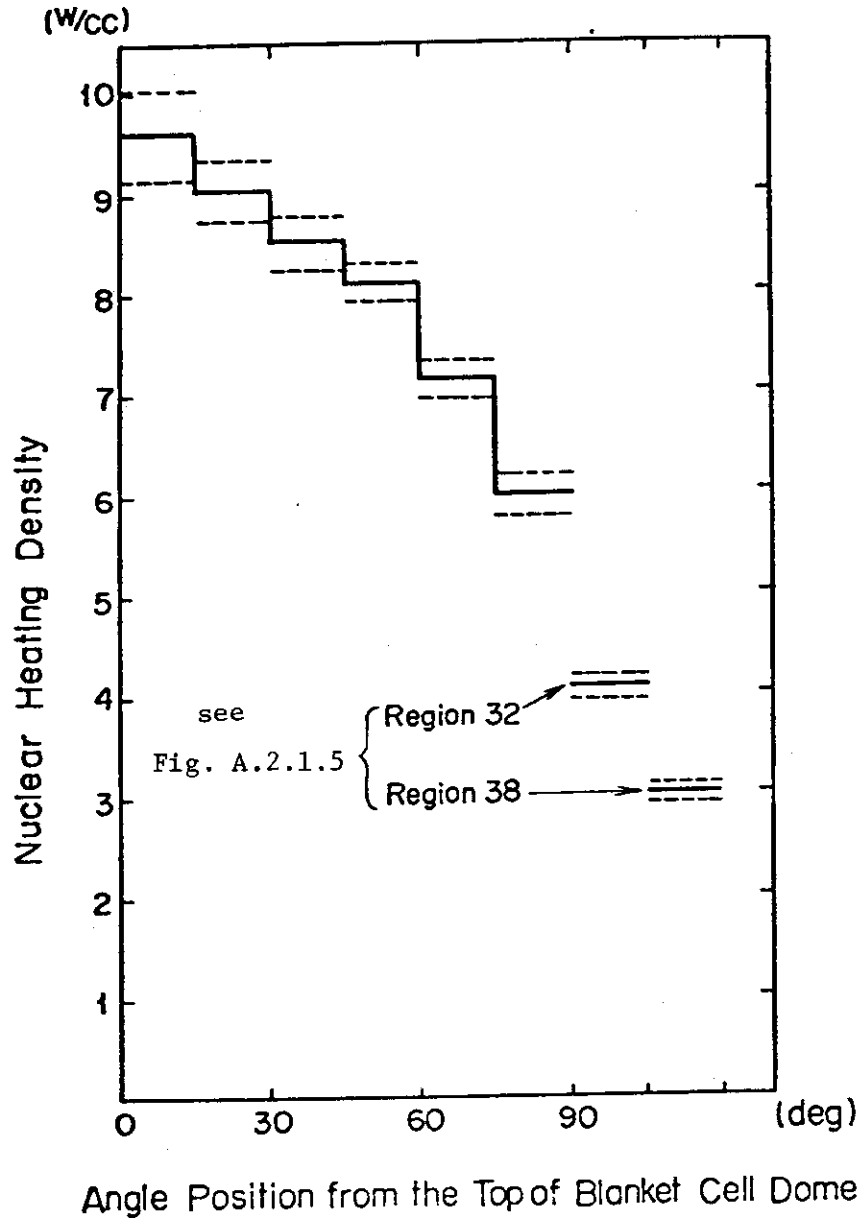

Fig. A.2.2.1 Nuclear Heating Density Distribution on the Blanket Dome

A.3 Minimum Thickness of the Inboard Shield

Shield must be fabricable as well as have sufficient radiation shielding capability. Next, the price must be reasonable and affordable.

Due to the short time available for preparing the report, a limited number of material composition change was considered in a parametric survey. At the same time a shielding structural design taking account of fabrication was performed. The structural design and the results of the parametric survey are described in 4.2 and 2.3, respectively.

From the requirement from the repair and maintenance design, the shield must be modularized and as a result the neutron streaming through the inevitable gap between the adjacent modules becomes a problem. Also required in the shield is the space in the shape of a gutter where auto-welding and cutter machines move. According to the designs of such machines, the required depth of the gutter was estimated to be small enough not to cause problematic radiation streaming. The minimum bulk sheild thickness was calculated to be about 80 cm with the use of tungsten and 90 cm without it. The actual space from the first wall to the surface of SCM conductor including the gaps were estimated to be 110 cm for the former and 120 cm for the latter.

A.4 Vacuum Boundary of SCM

Design of the vacuum boundary for SCM is closely related to reactor system design, and affected especially the repair and maintenance scheme. Therefore the vacuum boundary scheme should be selected in the course of the detailed repair and maintenance design. As described in Chapters 11 and 12, the Belljar type seem to be suited to Modular Concept (Concept A) and Sperated type to fit well with the In-Situ Concept (Concept B). At present both the Belljar and Separated types look promising.

A.5 Repair and Maintenance

The parts of the components with short expected life time such as divertor plates must be replaceable or repairable without excessive disassembly of the reactor. Many ideas have been proposed for the repair and maintenance of blanket and cooling panel. Two of the most promising concepts, namely Modular Concept (Concept A) and In-Situ Concept (Concept B) have been disigned and investigated in this report.

Both concepts seem to be difficult but feasible and both have merits and demerits. At present not knowing the frequency of the blanket failure, the one out of two selection is difficult. It should be determined after more detailed design and detailed failure analysis. The repairing method, step and required time etc. are discribed in Chapters 11 and 12.

A.6 Structure of SCM

The best choice for TF coil is copper stabilized Nb_3Sn filaments and for PF coil, copper stabilized NbTi filaments. The partial use of copper normal conductor for PF coils is feasible.

The selection between the Disk type (Concept A) or Pancake type (Concept B) structures for TF coil is very important. It should be decided after detailed designs and seeing the results of large scale R & D such as LCT. The selection for the cooling method between pool boiling and forced convection is also inportant and should be resolved in the same manner. Another important problem is the ambiguity in defining the allowable stress.

A.7 Estimation of Heat Load and Refrigeration Requirement for SC Magnet

For different two types of designs, estimation of heat load and refrigeration requirement for SC magnet is carried out. Values obtained for two types of designs are similar in spite of different design. Heat load at liquid helium and liquid nitrogen temperature is about 40 KW and 20 KW respectively. The electric power for above cryogenic requirement is estimated about 20 MW.

A.7.1 Estimation for Concept A

For Concept A, values of heat load, refrigeration requirement, electric power requirement, refrigeration efficiency and cool down and warm up time are given as follows. Also schematic diagram of cooling system is shown in Fig. A.7.1.

1. Heat load

(1) 4.5°k load

TF coil		7.2 kW
PF coil		15.2 kW
Cryostat		7.8 kW
	Total	30.2 kW

(2) 80°k load

Thermal shield		10.5 kW
Thermal anchor		5.9 kW
	Total	16.4 kW

2. Refrigeration requirement

Multiplying above heat load by 1.2

(1)	4.5°k Refrigeration capability	36	kW
(2)	80°k Refrigeration capability	20	kW

3. Electric power requirement

Helium Liquefier	11,300	kW
Nitrogen Liquefier	3,000	kW
Control system	100	kW
Total	14,400	kW

4. Systemrefrigeration efficiency

$$\left(\frac{Wc}{Q}\right)_{\text{actual}} = \frac{14,400}{36} = 400$$

$$\%\ \text{carnot} = \frac{(Wc/Q)\ \text{carnot}}{(Wc/Q)\ \text{actual}} \times 100 = \frac{65.66}{400} \times 100 = 16.4$$

5. Cool down time and warm up time

Cooling capability	36	kW ($^{4.5\ k}_{\text{Refrigerator}}$)
Cool down weight	6,000	ton
Mass flow rate He	3,000	g/s
Cool down time	∿ 400	hr. (16.7 days)
Warm up time	∿ 320	hr. (13.4 days)

A.7.2 Estimation for Concept B

Heat load considered here for the system includes static load as well as pulsive load which will be generated in the toroidal field magnets, poloidal field magnets, supporting structures and others. The total heat load amounts to about 45 kW at 4.2°K and 20 kW at 80°K as described below. It is well known that the dominating heat load is caused by the eddy current in structures. The eddy current loss could be further reduced by insulation cuts, while this matter must be considered in conjunction with structual intergrity.

1) Static load at 4.2°K

(a)	Conduction and radiation loss	0.7 kW
(b)	Power load	2.5
(c)	Piping	0.2

2) Pulsive load at 4.2°K

(a)	Toroidal field magnets	13.7 kW
(b)	Poloidal field magnets	5.0
(c)	Structures	22.6

3) Total heat load

(a)	Heat load at 4.2°K	45 kW
(b)	Heat load at 80°K	20

The electric power for above cryogenic requirement totals to about 20 MW.

More detailed pulsive loss is shown below.

1) Toroidal field magnets

(a)	Hysteresis loss	0.3 kW
(b)	Eddy current loss	10.6
(c)	Coupling loss	2.8

2) Poloidal field magnets

(a)	Hysteresis loss	2.0 kW
(b)	Eddy current loss	1.6
(c)	Coupling loss	1.4

3) Structures

(a)	Helium vessel	15.2 kW
(b)	Torque beam	1.6
(c)	Cylinder post	2.1
(d)	Support base	2.6
(e)	Support ring	1.1

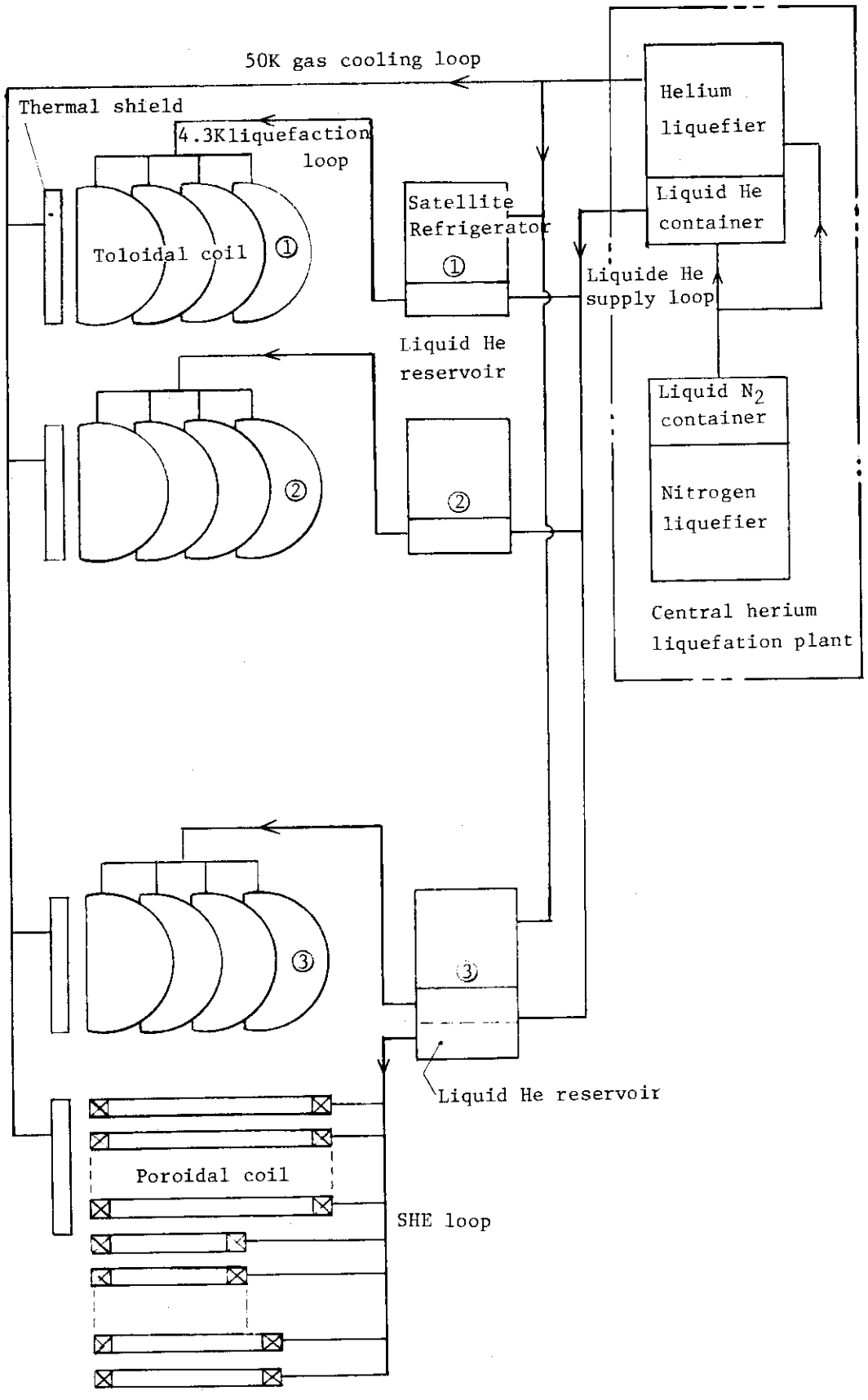

Fig. A.7.1 Schematic Diagram of Cooling System

A.8 Blanket Structure for Divertor Concept

Figures A.8.1 and A.8.2 show an example of the blanket structure for divertor concept. The repair and maintenance procedure is taken into consideration in the same way as the blanket structure for non-divertor concept described in Chapter 3.

The cross sections of the inner and outer blanket are similar to those shown in Figs. 3.2.3 and 3.2.4.

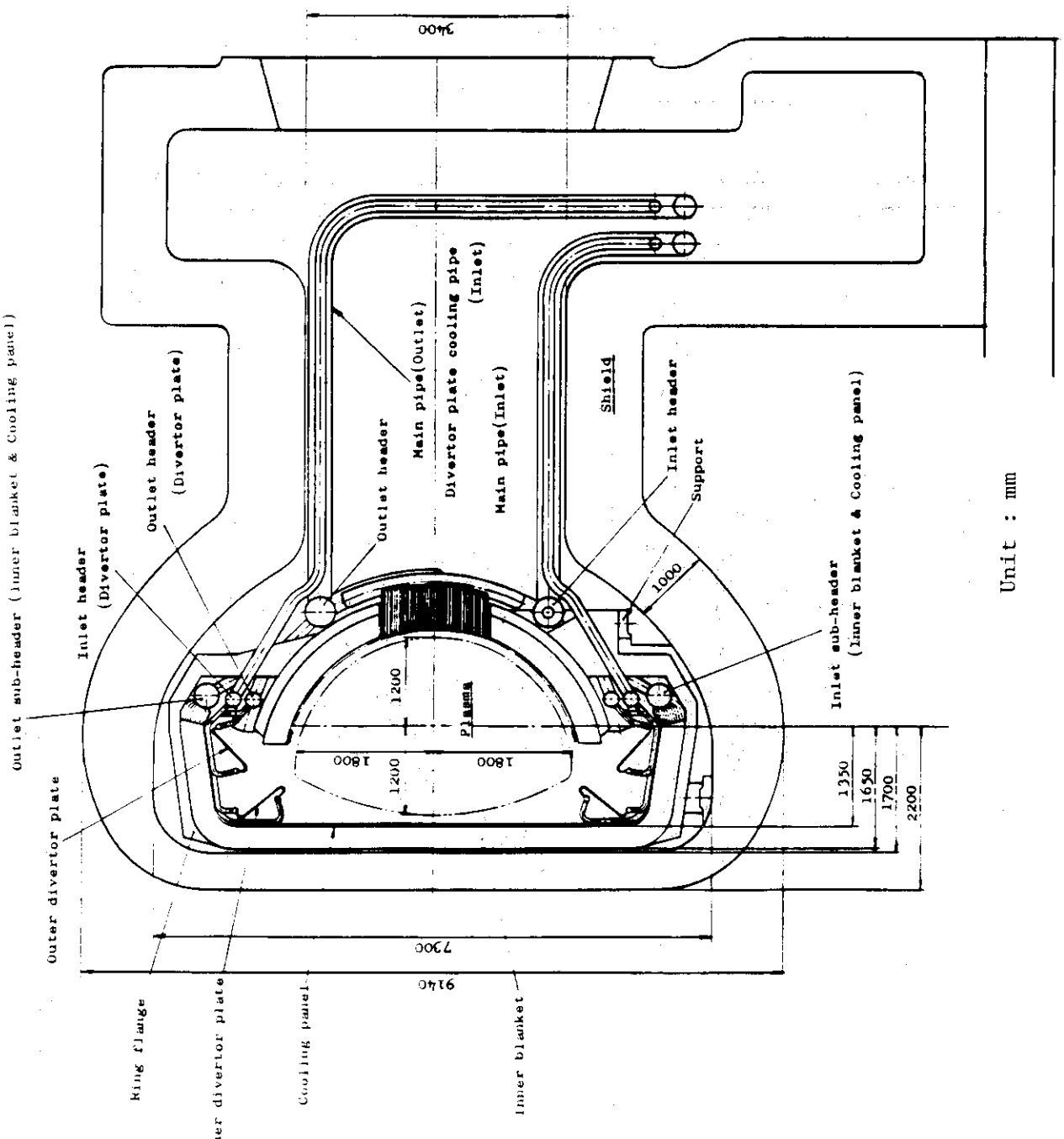

Fig. A.8.1 Side View of Blanket Module for Divertor Concept

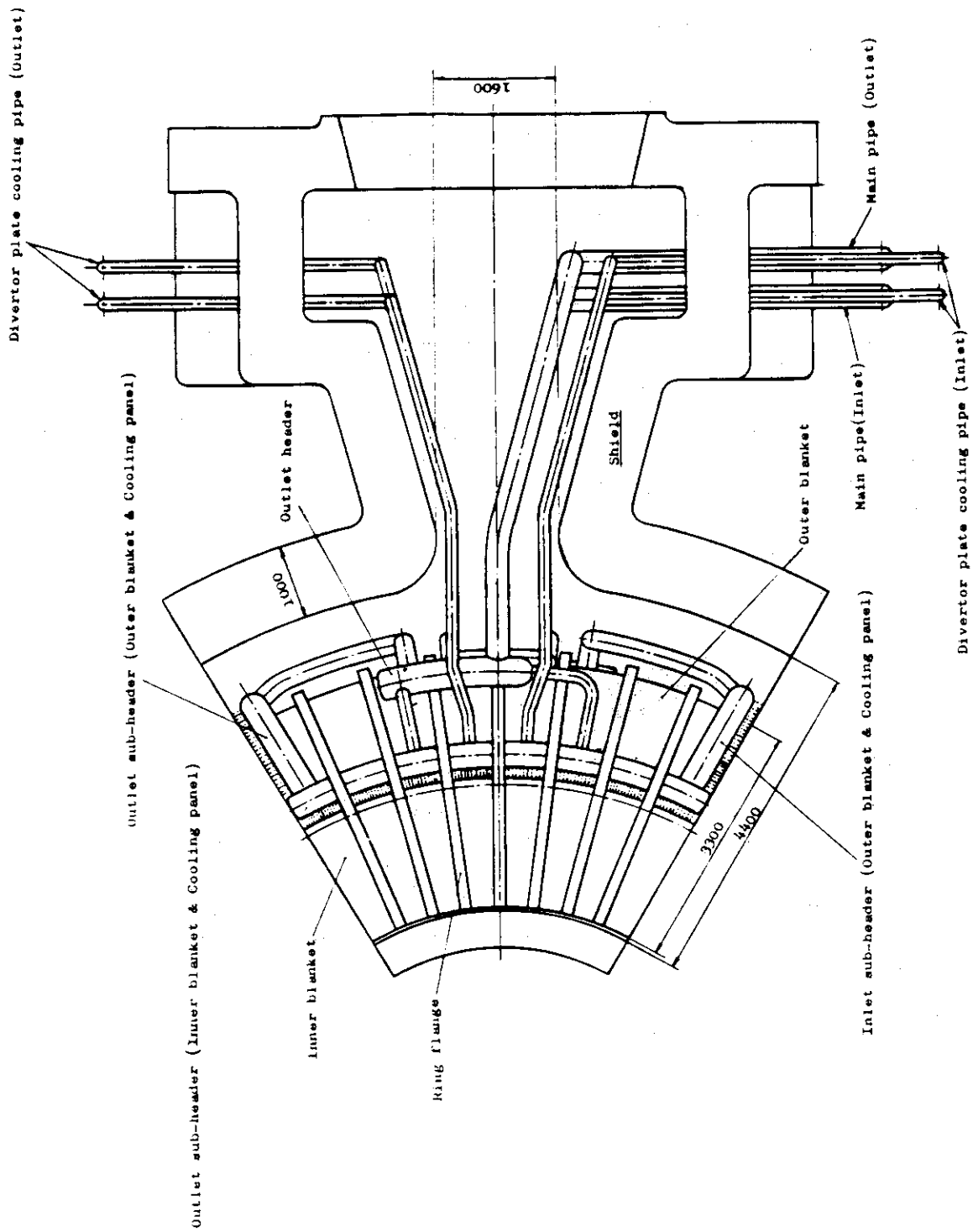

Fig. A.8.2 Plane View of Blanket Module for Divertor Concept